論　文　集

IEEE TRANSACTIONS ON APPLIED SUPERCONDUCTIVITY, VOL. 26, NO. 3, APRIL 2016 5400504

Circulation Test of Liquid Nitrogen for Long Superconducting DC Power Transmission Lines

Hirofumi Watanabe, Yury V. Ivanov, Makoto Hamabe, Noriko Chikumoto, Toshio Kawahara, Hirohisa Takano, and Satarou Yamaguchi

***Abstract*—The pressure drop during circulation of the refrigerant limits the distance for superconducting power transmission. Evaluation of the pressure drop with respect to the flow rate of the refrigerant is crucial, particularly for long transmission lines. A circulation test, including pressure drop measurements, was performed in the sixth cooling test with the 200-m-class superconducting dc power transmission system at Chubu University (CASER-2). Pressure drops were measured in the high-flow-rate region, up to 31 L/min, to simulate 1-km-class systems, unlike those used in the first five cooling tests. A pressure drop of 12 kPa at 31 L/min for the 200-m cryogenic pipe was obtained. The obtained results were compared with the calculated results and showed good agreement. The model used for the calculation can predict the pressure drop with sufficient accuracy, making the prediction for the pressure drop for long transmission lines possible.**

***Index Terms*—Circulation of refrigerant, cryogenics, DC power transmission, high-temperature superconductors, pressure drop.**

I. Introduction

SUPERCONDUCTING power transmission is an efficient way to transport electricity, in particular, for long distances. In recent years, km class superconducting power transmission lines were planned and constructed around the world [1]–[3]. In Japan, a new project for the construction and operation of 500 m and 1 km class superconducting DC power transmission lines was launched in the Ishikari area [3]. This project is called the Ishikari project. A high-temperature superconducting cable for power transmission is installed in a cryogenic pipe for thermal insulation and cooled by the flow of a refrigerant, such as liquid nitrogen, to achieve superconducting state. The current characteristics of the cable core strongly relay on the temperature of the refrigerant and the temperature of the refrigerant should be lower than that required for the specification of the cable core. Therefore, from this point of view, the flow rate of the refrigerant should be high enough to limit temperature rise along the cable core. However, frictional resistance between the refrigerant and the inner surface of the pipe manifests as a pressure drop in the circulation. This pressure drop increases with increasing flow rate, and this affects the pumps that circulate the refrigerant and the structures of the cryogenic pipes, such as their diameter. Therefore, the evaluation of the pressure drop with respect to the flow rate is indispensable for the design of superconducting power transmission systems, in particular, over long distances.

We have performed six cooling tests since 2010 at the 200 m class superconducting DC power transmission system at Chubu University, called CASER-2 [4]–[8]. In the first four cooling tests, the heat leak of the cryogenic pipe was tested [4]–[6], and the pressure drop in the circulation of the refrigerant was measured in the second and third cooling tests [9], in addition to the current feeding tests. Up to the fifth cooling test, the experiments have been performed with a flow rate of approximately 10 L/min. At this flow rate, the temperature rise was approximately 1 K, which is low enough for the cable of CASER-2 [5]. However, because the flow rate in a km class transmission system would be several times higher than that in our experiments, the behavior of the pressure drop may also be different. To estimate the pressure drop in the higher flow rate region, the cooling and pumping system of CASER-2 was recently modified to meet the conditions of the Ishikari project. This modification made experiments with flow rates twice as high as previous measurements possible. The circulation test, including pressure drop measurements, was performed in the sixth cooling test. The results of the pressure drop were compared to a calculation based on a previously presented model [9], [10].

II. CASER-2

The layout of CASER-2, consisting of a cryogenic pipe installing a cable, two terminals, and a cooling and pumping system is shown in Fig. 1. The terminals are installed side-by-side in the laboratory, and the cryogenic pipe that is connected to the terminals stretches out from the laboratory to the outdoors with an L-shaped configuration for approximately 200 m. The cooling and pumping system is located beside the terminal A.

The model of the cryogenic pipe used in CASER-2 is shown in Fig. 2. The diameter of the outer pipe is 216.3 mm and that of the inner pipe is 60.5 mm. The inner pipe is wrapped in multi-layer insulation to reduce heat leak from the outer pipe. In superconducting power transmission, corrugated pipes are commonly used for the cryogenic pipes [11], [12]. For CASER-2,

Manuscript received September 8, 2015; accepted January 25, 2016. Date of publication January 28, 2016; date of current version February 16, 2016. This work was supported by the Ministry of Education, Culture, Sports, Science and Technology through the Strategic Research Foundation Grant-aided Project for Private Universities.

The authors are with Chubu University, Kasugai 487-8501, Japan (e-mail: h_watanabe@isc.chubu.ac.jp; ivanov@isc.chubu.ac.jp; hamabe@isc.chubu.ac.jp; nchiku@isc.chubu.ac.jp; toshi@isc.chubu.ac.jp; hirohisa_takano@isc.chubu.ac.jp; yamax@isc.chubu.ac.jp).

Color versions of one or more of the figures in this paper are available online at http://ieeexplore.ieee.org.

Digital Object Identifier 10.1109/TASC.2016.2523249

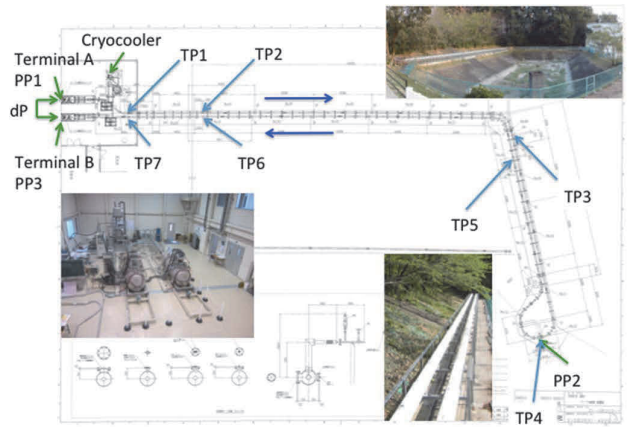

Fig. 1. Layout of CASER-2. TP1-TP7 and PP1-PP3 are the positions of the temperature and pressure measurements of liquid nitrogen.

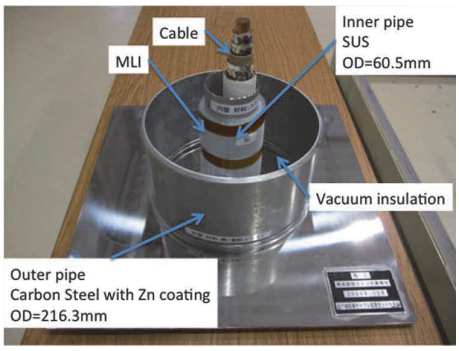

Fig. 2. Cross-sectional model of the cryogenic pipe of CASER-2.

TABLE I
COOLING AND PUMPING SYSTEM OF CASER-2

Cryocooler	Stirling type
Cooling power	1 kW @ 77 K
Pump	Centrifugal
Max. flow rate	31 L/min
Max. discharge pressure	0.11 MPa
Flowmeter	Coriolis type
Volume of tanks	200 L each

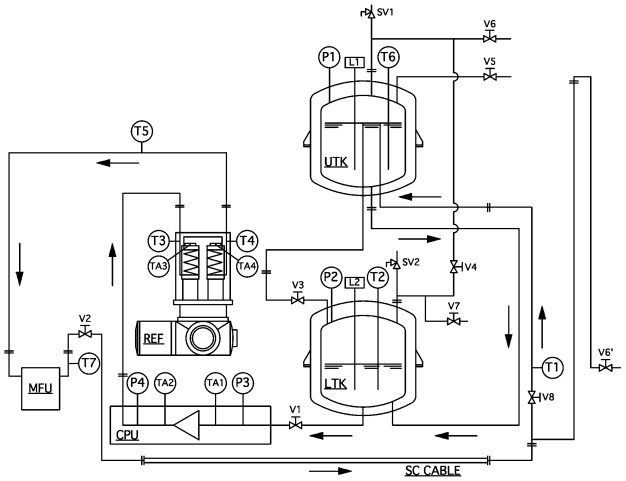

Fig. 3. Schematic diagram of the cooling and pumping system after modification.

a smooth pipe, in part bellows to compensate for thermal shrinkage, is used for the inner pipe to reduce pressure drop for circulating the liquid nitrogen. Similar types of smooth cryogenic pipes are used in the Ishikari project [3].

The diameter of the cable core is approximately 35 mm and its outer surface is wrapped with fabric tapes, which may cause pressure drop significantly. The cable core has coaxial two layers of BSSCO wires for bipolar operations. The rated current and voltage are 2 kA and $\pm$10 kV, respectively.

The cooling and pumping system consists of a Stirling-type cryocooler with a cooling power of 1 kW at 77 K, a centrifugal pump, a Coriolis-type mass flowmeter, an upper tank (UTK), a lower tank (LTK), and pipes connecting these elements. The specification of the system is summarized in Table I. Until the fifth cooling test, the maximum discharge pressure of the pump and the maximum flow rate of the liquid nitrogen have been limited to 0.028 MPa and 16 L/min, respectively. We assumed that these limitations originated from cavitation in the pump, because they were improved by increasing the pressure of the liquid nitrogen. To increase the flow rate, the piping was altered to increase the net positive suction head available at the pump inlet. The schematic diagram of the cooling and pumping system after the alteration is shown in Fig. 3 and the original design can be found in a previous paper [7]. This alteration includes changing the connection from the UTK outlet, which had been connected to the cable system, to the inlet of the circulation pump unit (CPU) via LTK to use the head of the upper tank. In addition, the flow channels in the impeller of the pump were increased to reduce the pressure drop, and balance holes were made in the impeller to cancel the force originating from the increased flow rate. Fig. 4 shows the discharge pressure, i.e., the pump head, with respect to the flow rate. The pump input power is also shown for reference. The system head curve, including the cable system, is also shown in the figure. The maximum discharge pressure was improved from 0.028 MPa to 0.11 MPa and, consequently, the maximum flow rate rose from 16 L/min to 31 L/min. This allows for experiments to simulate the flow in long transmission lines, such as in the Ishikari project.

III. CALCULATION OF PRESSURE DROP

We calculated the pressure drop in the cryogenic pipe in which the cable core is installed [9], [10]. In the calculation, the Darcy-Weisbach equation,

$$\Delta p = f \frac{L}{D_h} \frac{\rho v^2}{2} \tag{1}$$

was used, where f is the friction factor, Δp is the pressure drop, L is the length of the cryogenic pipe, D_h is the hydraulic diameter, ρ is the density, and v is the flow velocity. In the calculation, it was assumed that the friction factors for both the

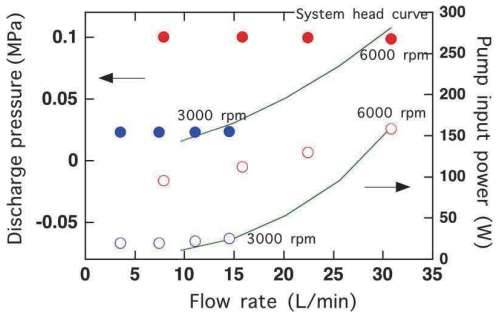

Fig. 4. Discharge pressure and input power of the pump for the rotational speed of 6000 and 3000 r/min with respect to the flow rate. The system head curve, including the cable system, is also shown.

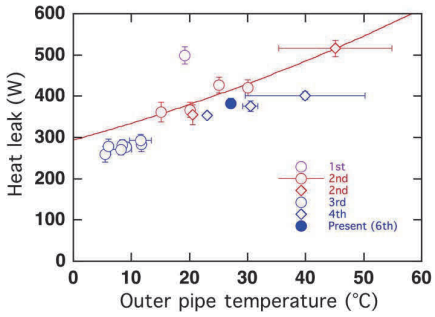

Fig. 5. Results of the heat leak measurements obtained in the first to sixth cooling tests arranged to the outer pipe temperature of the cryogenic pipe. The values are for the 175-m part of the cryogenic pipe. The values from the first to fourth cooling test were previously reported [6].

inner surface of cryogenic pipe and the surface of the cable core for the laminar flow region followed:

$$f = \frac{\mathrm{Re}}{64} \tag{2}$$

and those for the turbulent flow region followed the Colebrook-White equation

$$\frac{1}{\sqrt{f}} = -2\log\left(\frac{\varepsilon}{3.7D_h} + \frac{2.51}{\mathrm{Re}\sqrt{f}}\right) \tag{3}$$

for circular pipes. Here, ε is the mean height roughness (0.1 mm for the inner pipe surface [13] and 1 mm for the cable core surface) and Re is the Reynolds number. The friction factor (f) was calculated as the weighted sum of the friction factors for the inner surface of the cryogenic pipe and the surface of the cable core using their wetted perimeters [9]. The influence of the cable core lying in the cryogenic pipe was considered by introducing correction factors to the friction factor [10], [13], which reduced the friction factor by approximately 20%. The effect of the bellows sections of the inner pipe was not considered because the bellows are hidden by moveable smooth pipes and are not exposed to the flow of the liquid nitrogen.

IV. Results and Discussion

The amount of the heat leak under the present experimental condition was measured and is presented in Fig. 5. The previously reported results [6] measured in the first to fourth cooling tests are also shown in the figure. The values of the heat leak in the figure are for the 175 m part of the cryogenic pipe and obtained from the temperature rise measured using the platinum resistance temperature detectors at TP1 and TP7 shown in Fig. 1. The heat leak increases with an increase in the outer pipe temperature. Between the second and third cooling tests, the heat leak was significantly reduced by the modification of the cryogenic pipe structure [5]. The heat leak affects both the efficiency of the entire system from the energy needed to pump out the heat by the heat leak and the pressure drop, because the pressure drop can be written from (1) as

$$\Delta p = f\frac{L}{D_h}\frac{\rho}{2}\left(\frac{qL}{\rho A C_p \Delta T}\right)^2 \tag{4}$$

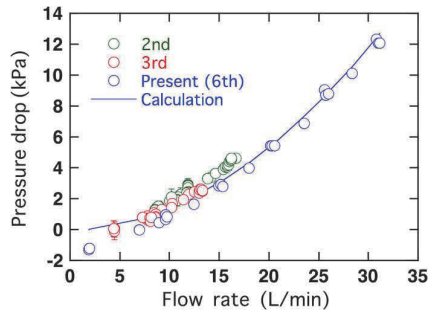

Fig. 6. Results of the pressure drop measurements and calculations with respect to the flow rate. The data obtained in the second and third cooling tests are also shown [9].

where q is the heat leak, A is the cross section of the channel and ΔT is the temperature rise. Therefore, the reduction of the heat leak is important for reducing the pressure drop.

Fig. 6 shows the results of the pressure drop measurements. The experimental results below 8 kPa were measured with a differential pressure gauge (the pressure difference between the terminals). Over 8 kPa, the pressure drop was obtained by taking the difference of the pressures measured at the terminals using pressure gauges. The separation between the terminals is 200 m. Therefore, the values are the pressure drop per 200 m of the cryogenic pipe in CASER-2. As seen in the figure, in the low flow rate region below 5 L/min, the pressure drop takes negative values because of the thermosiphon effect [14]. This means that the circulation can be driven without a pump. In the sixth cooling test, the pump was stopped for tens of hours and the continuation of the circulation was confirmed. As the flow rate increases, the pressure drop increases. The present data below 17 L/min are consistent with previously reported data [9]. The pressure drop reaches 12 kPa at 31 L/min for the 200 m cryogenic pipe of CASER-2. If the cryogenic pipe of CASER-2 is extended to 1 km, the pressure drop would be 60 kPa at 31 L/min. Therefore, we expect that the pump of CASER-2, whose maximum discharge pressure is 0.11 MPa, can be used for the 1 km line of the Ishikari project.

The results of the calculated flow rate and pressure drop are shown in Fig. 6. In the low flow rate region, the calculated results are a little larger than the experimental values. In this region, the thermosiphon effect is effective, which was not included in

the calculation. The thermosiphon effect reduces the pressure drop, and the exclusion of this effect makes the calculated results larger than the experimental ones [14]. Except for this, the calculated results reproduce the experimental results well, in particular, in the high flow rate region. This indicates that our model, using the friction factors for circular pipes and approximating the effect of the cable position in the pipe, reproduces the pressure drop in the cryogenic pipe for the low flow rate region reported previously [9] and the high flow rate region presented here. From this result, we can estimate the pressure drop in the Ishikari project, which uses similarly smooth cryogenic pipes.

V. Conclusion

We have performed a sixth circulation test with CASER-2. Prior to the test, the cooling and pumping system was modified enabling experiments with higher flow rates, up to 31 L/min, and with a higher pressure drop, up to 0.11 MPa. This makes experiments simulating the flow in long transmission lines, such as in the Ishikari project, possible. The pressure drop was found to be 12 kPa at 31 L/min for the 200 m cryogenic pipe with a smooth pipe. The calculation of the pressure drop was performed and the results reproduced the experimental findings well, except for a small difference in the low flow rate region, where the thermosiphon effect was significant. In conclusion, our model can predict the pressure drop in smooth cryogenic pipes for long distances with sufficient accuracy, within in the range of the measurements.

Acknowledgment

The authors would like to thank Dr. A. Iiyoshi, Chancellor of Chubu University, for his continuous encouragement for this work and Dr. H. Fujiwara for his support for our project. The authors would also like to thank JFE Steel Corporation for supplying carbon steel pipes for the construction of the cryogenic pipe of CASER-2.

References

[1] M. Stemmle, F. Merschel, M. Noe, and A. Hobl, "AmpaCity—Installation of advanced superconducting 10 kV system in city center replaces conventional 110 kV cables," in *Proc. IEEE ASEMD*, 2013, pp. 323–326.

[2] V. E. Sytnikov *et al.*, "Status of HTS cable link project for St. Petersburg grid," *IEEE Trans. Appl. Supercond.*, vol. 25, no. 3, Jun. 2015, Art. ID 5400904.

[3] H. Watanabe *et al.*, "Thermal insulation test of new designed cryogenic pipes for the superconducting DC power transmission system in Ishikari, Japan," *Phys. Procedia*, vol. 67, pp. 239–224, 2015.

[4] H. Watanabe *et al.*, "Cooling test of the 200 m superconducting DC transmission power cable system at Chubu University," *Phys. C, Supercond.*, vol. 471, no. 21/22, pp. 1304–1307, Nov. 2011.

[5] H. Watanabe *et al.*, "Heat leak measurement of the 200 m superconducting DC power transmission system at Chubu University," *Phys. Procedia*, vol. 36, pp. 1366–1371, 2012.

[6] H. Watanabe *et al.*, "Cooling of the 200 m superconducting DC power transmission system at Chubu University," *Phys. Procedia*, vol. 27, pp. 376–379, 2012.

[7] M. Hamabe *et al.*, "Status of a 200-Meter DC superconducting power transmission cable after cooling cycles," *IEEE Trans. Appl. Supercond.*, vol. 23, no. 3, Jun. 2013, Art. ID 5400204.

[8] M. Hamabe, H. Watanabe, J. Sun, T. Kawahara, and S. Yamaguchi, "Long term operation in 200 m class superconducting DC power transmission test facility in Chubu University," *J. Phys. Conf. Ser.*, vol. 507, no. 3, May 2014, Art. ID 032020.

[9] Y. Ivanov *et al.*, "Design study of LN2 circulation in long SC power transmission lines," *Phys. Procedia*, vol. 36, pp. 1372–1377, 2012.

[10] Y. V. Ivanov, M. A. Romashov, S. E. Bemert, and V. E. Sytnikov, "Choice of flexible cryostat for 2.5 km DC HTS cable to be laid in St. Petersburg," in *Proc. AIP Conf.*, 2014, vol. 1573, pp. 887–892.

[11] T. Masuda *et al.*, "Fabrication and installation results for Albany HTS cable," *IEEE Trans. Appl. Supercond.*, vol. 17, no. 2, pp. 1648–1651, Jun. 2007.

[12] H. Yumura *et al.*, "Update of YOKOHAMA HTS cable project," *IEEE Trans. Appl. Supercond.*, vol. 23, no. 3, Jun. 2013, Art. ID 5402306.

[13] E. Fried and I. E. Idelchik, *Flow Resistance: A Design Guide for Engineers*. Bristol, PA, USA: Hemisphere, 1989.

[14] Y. Ivanov *et al.*, "Observation of the thermosiphon effect in the circulation of liquid nitrogen in HTS cable cooling system," *Phys. Procedia*, vol. 27, pp. 368–371, 2012.

Current Imbalance and AC Losses of Long Distance DC HTS Cable

Yury Ivanov, Vladimir Vyatkin, Hirofumi Watanabe, Noriko Chikumoto, Makoto Hamabe, Jian Sun, Hirohisa Takano, Satarou Yamaguchi, and Edmund Otabe

***Abstract*—Despite intensive research in the field of applied superconductivity only now we start to use of this phenomenon for the most obvious application, namely, power transmission. At present, it can be seen an explicit shift from AC to DC HTS cable systems due to the many advantages of the DC ones. However, even at direct current transmission line is subjected to current fluctuations and, consequently, AC losses. One more reason for reducing the efficiency of HTS lines is current imbalance. It is associated with the presence of electrical resistance at the soldered connections of the superconducting tapes. Although these resistances are very low, but against the background of zero resistance of the rest of the superconductor they determine the individual currents in tapes and introduce essential nonlinearity into the dependence of these currents on the total current. A large national project on DC HTS power transmission was launched in Japan in FY 2013. Within the framework of the project, two HTS cables were laid in Ishikari (Hokkaido) for commercial and research purposes. Since the novel design of the thermal insulation is used, it becomes important to carefully consider the contribution of internal heat generation. In order to estimate AC losses, the frequency characteristics of the ripple current were calculated taking into account current imbalance in the cable.**

***Index Terms*—DC HTS power transmission cable, ripple current, current imbalance, AC loss.**

I. Introduction

THERE are several more or less successful large cable systems in the world created in order to develop technology of energy transmission by means of superconductors. Now it is clearly seen a shift from the AC superconducting cables to the possessing higher usability and efficiency DC ones. Ideally, in DC HTS cable there are no hysteresis and other losses native to AC, which significantly reduce the efficiency of the power transmission line [1] and complicate the design of HTS tapes and cables. However, the current fluctuations as because of the harmonics generated by AC/DC converters (rectifiers), and because of change in the load operating modes are superimposed on DC. These fluctuations produce AC loss. The spectrum of the ripple current depends on the type of rectifier.

Manuscript received December 21, 2015. This work was supported in part by the Japanese Ministry of Economy, Trade and Industry (METI).

The authors are with the Center of Applied Superconductivity and Sustainable Energy Research, Chubu University, Kasugai, Aichi 487-8501, Japan (e-mail: ivanov@isc.chubu.ac.jp).

E. Otabe is with the Dept. of Computer Science and Electronics, Kyushu Institute of Technology, Iizuka 820-8501, Japan.

When discussing AC cables made of many HTS tapes, significant attention is paid to the current imbalance. The analysis is carried out by taking into account self- and mutual inductances [2]-[4]. In the case of DC cables, the resistances define the current distribution. Each end of the tape is connected to the output terminal or to the connecting bus. It is technically feasible to make the resistance of these solder joints sufficiently low. Furthermore, manufacturer-supplied HTS tapes have randomly distributed splices. Whereas the splices are limited in size, the contact area is not enough to support low resistance. For example, according to the specification of Type HT-CA BSCOO tape available from Sumitomo Electric Industries, Ltd., the balance between the splice resistance and the stiffness at the splice point selects the length of splices, and the resistance does not exceed 90 nΩ. A reel contains 450 m of the tape. Although the splices' resistances are very low, but against the background of zero resistance of HTS they define the individual currents in the tapes. The current through the tape with splice becomes non-vanishing only when the current through the parallel tape without splice approaches the critical value and the tape becomes resistive. Obviously the longer the tape (cable), the stronger the influence of the resistive state, and current imbalance will be suppressed. In the presence of this nonlinearity ripple current causes the occurrence of additional higher harmonics. Therefore, AC losses in the DC HTS power cable are distributed in a complicated manner.

II. Theory

Let us consider the current imbalance in DC HTS cable using the standard representation for the current-voltage characteristic

$$E = E_0 \left(\frac{I}{I_c} \right)^n , \tag{1}$$

where E is the electric field, μV/cm; E_0 is the conventional value of electric field at critical current, 1 μV/cm; I is the current, A; I_c is the HTS tape critical current, A; and n is the dimensionless index of voltage-current curve of the superconductor. The non-linear current divider problem for any number of tapes in the cable can be easily solved by the iteration method. In the simplest case of two HTS tapes with one splice and zero resistance at the terminals, we have a distinct picture of currents imbalance (Fig. 1), which persists

with increasing complexity of the circuit (Fig. 2). In all calculations, the critical current is 180 A and n=15. If the operating point of i-th tape is near non-linear part of the I_i-I_{total} curve, the waveform of the ripple current superimposed on the high transport DC will be distorted and additional higher harmonics will arise, that give a significant change in the pattern of AC loss.

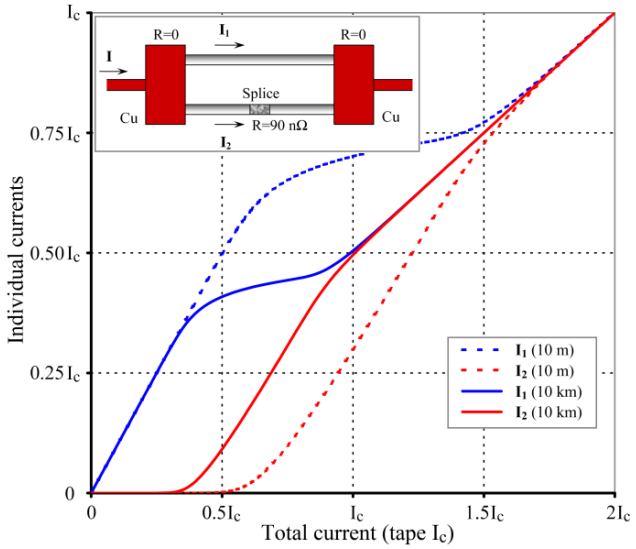

Fig. 1. Direct current imbalance in two HTS tapes.

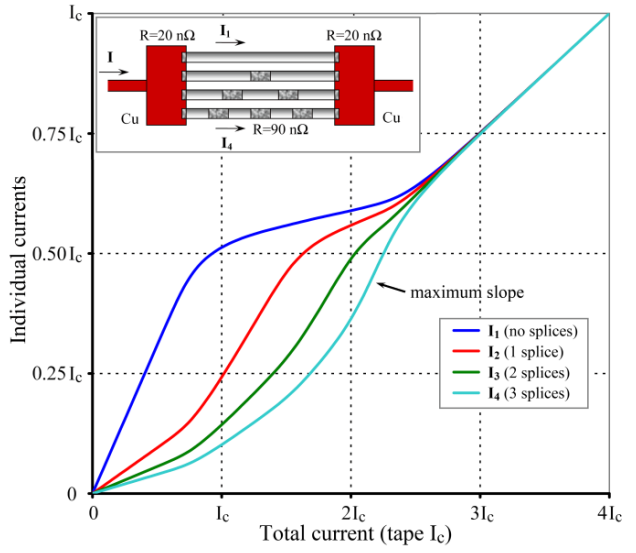

Fig. 2. Direct current imbalance in four HTS tapes.

The current at the output of the p-pole rectifier can be written [5] as

$$I_p(t) = I_0 \cos\left(\omega t - \frac{2m\pi}{p}\right), \quad (2)$$

where m is integer, and $\left|\omega t - \frac{2m\pi}{p}\right| < \frac{\pi}{p}$.

This function can be expanded into a Fourier series as

$$I_p(t) = I_0 \frac{p}{\pi}\sin\frac{\pi}{p} - 2I_0 \frac{p}{\pi}\sin\frac{\pi}{p}\sum_{k=1}^{\infty}\frac{(-1)^k}{p^2k^2-1}\cos(pk\omega t), \quad (3)$$

where t is time, s; and ω is the angular frequency of AC, s^{-1}.

The first term is the DC component with amplitude is slightly lower than I_0. The ripple current waveform for 6-, 12- and 24-pulse rectification, as well as the amplitudes of the first three harmonics for 6-pulse rectification are shown in Fig. 3 in arbitrary units. More harmonics arising from the above-described distortion of the oscillation can be readily found numerically, e.g., by five ordinates method.

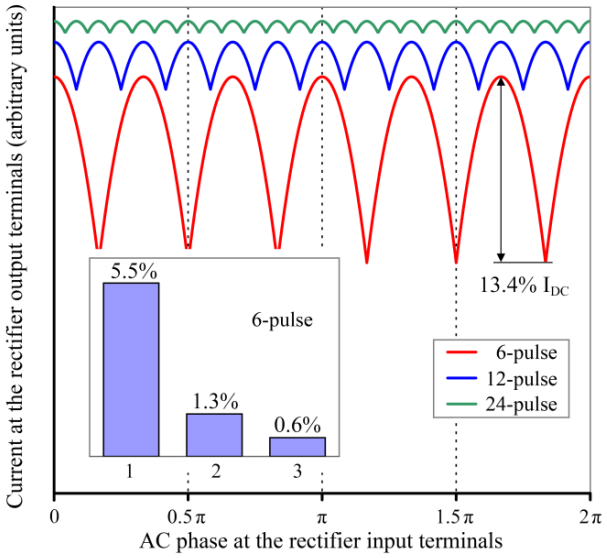

Fig. 3. Ripple currents at the output of 6-, 12-, and 24-pulse rectifies.

It was found that the AC losses with and without DC were the same when the magnetic field dependence of critical current density was ignored [6]. The AC losses consists of the hysteresis loss and coupling loss. It is shown in [5] that in DC cable of the type under consideration at low frequencies cooperative loss is negligible. Expression for the hysteresis loss per cycle per unit length of the elliptic-sectioned wires, Q, was proposed by Norris [7]. It should be mentioned that the expression does not depend on the ellipticity.

$$Q = Q_0\left[(1-F)\ln(1-F) + (2-F)F/2\right], \quad (4)$$

where $Q_0 = \mu_0 I_c^2/\pi$; $F = I/I_c$; and μ_0 is the vacuum permeability, $4\pi\cdot10^{-7}$ H/m.

Total hysteresis loss per unit length of the cable made of N tapes, can be obtained by summing all of the tape losses at all corresponding frequencies. As was also mentioned above, amplitudes of the harmonics at the output of the rectifier should

be corrected to take into account the non-linearity of the "transfer characteristics" I_i-I_{total}. Calculations show (see Fig. 4) that even in the case of the 6-pulse rectifier distortion of the sinusoidal component will not be significant. Obviously, peaks correspond to areas of maximum curvature of the I_i-I_{total} curves. Here, we defined a distortion factor K_h as

$$K_h = \frac{\sqrt{A_2^2 + A_3^2 + A_4^2}}{|A_1|}, \quad (5)$$

where A_1-A_4 are the amplitudes of the first four harmonics.

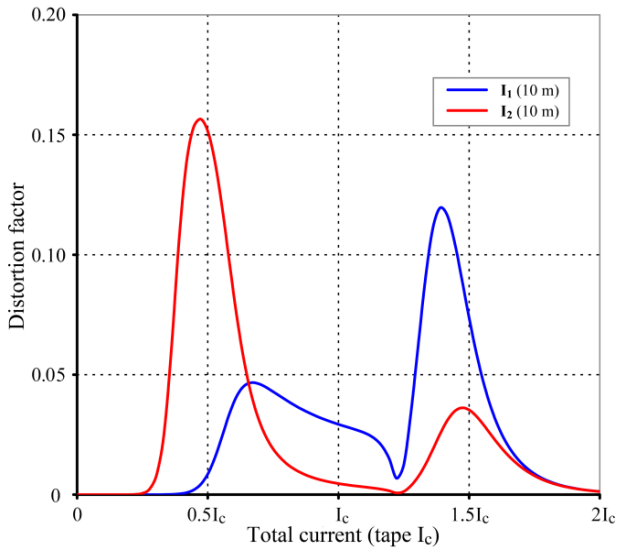

Fig. 4. The distortion factors of the first harmonic of the 6-pulse rectifier in the case of parallel connection of two HTS tapes as shown in the inset in Fig. 1. In the real HTS cable, resistances at the terminals will decrease these peaks.

Since the relative amplitudes of the harmonics are small (F<<1), expression (4) for the hysteresis loss can be rewritten as

$$Q = Q_0 \frac{F^3}{6}, \quad (6)$$

As can be seen, the higher harmonics can be neglected. Therefore, for the calculation of AC loss it is sufficient to take into account only the first harmonic, and its amplitude in each HTS tape should be corrected using corresponding I_i-I_{total} curve. Harmonic frequency is fp, where f is the rated frequency.

III. Results and Discussion

A clear picture of the current imbalance is given in Fig. 1. In the case of the constant local resistances the longer the tapes, the stronger relative contribution of the resistive state, and the range of current imbalance will scaled down, but not as strong as it could be imagined. According to Fig. 1, the change in tape lengths from 10 m to 10 km leads to only 39 % change in the range width (from 0-0.81 to 0-0.49 of the two-tape cable critical current), which is associated with the high value of parameter n.

"Cable" shown in Fig. 2 is composed of four HTS tapes of 450 m standard length with a different number of splices and 20 nΩ resistances at terminals. It is clearly seen that at the conventional operating current equals to about 70 % of the cable I_c, the imbalance is negligibly small.

Fig. 5 shows the AC loss in the same four-tape cable in the approximations of equal and imbalanced currents in the worst case of 6-pulse rectification. Rated frequency is 60 Hz. Calculations using imbalanced currents model reveal pronounced peak of AC loss at about 0.5-0.6·(cable I_c) and weak peaks at the lower currents. If we consider similar 450 m 2.5 kA DC cable made of 20+20 HTS tapes with 0-3 splices each, the hysteresis loss at operating current is about 0.30 mW/m, but at lower current of 2 kA it is 0.45 mW/m.

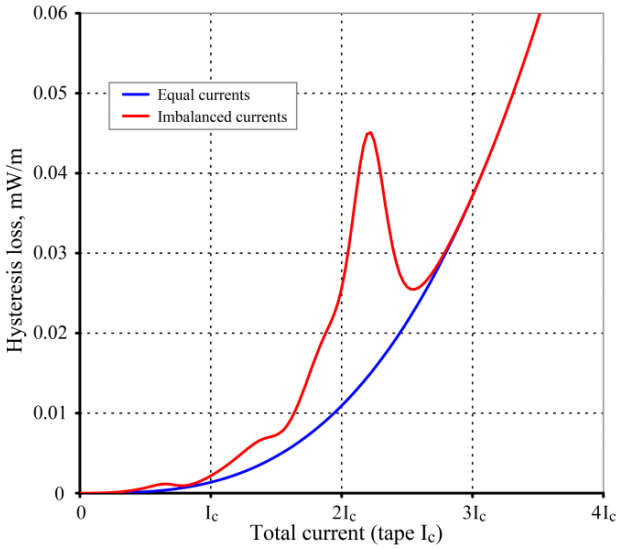

Fig. 5. Hysteresis loss obtained by different approximations.

The existence of this large peak can be easily explained by means of Fig. 2. The point on the I_i-I_{total} curve determines DC component in the tape whereas the slope of the curve at the corresponding point, i.e. derivative, determines amplitude of the small oscillations superimposed on DC. In areas where the curve is flat, the oscillations are suppressed, and where is rapid, the oscillations are amplified. At the high total current near the area of mutual approach, lower curves in the bindle will have the maximum slope. These curves correspond to the HTS tapes with higher joint resistance. Since the dependence of the AC loss on the harmonic amplitude is cubic (6), then amplitude imbalance will drastically increase Q.

IV. Conclusions

The current imbalance in DC HTS cables arising due to the significant differences in soldered joint resistances of individual HTS tapes and its impact on the hysteresis loss due to the ripple current were discussed. It was found that current imbalance at conventional operating current which is about

70 % of the cable critical current is insignificantly small.

Change in the amplitudes of the higher harmonics of the ripple current due to the nonlinearity of I_i-I_{total} curves was estimated as has no effect on the AC loss.

The nonlinearity of I_i-I_{total} curves causes peak of the hysteresis loss at currents noticeably lower than operating. The loss in 2.5 kA DC HTS cable is small compared with the external heat load and can be neglected even in the worst case of 6-pulse rectification.

ACKNOWLEDGMENT

We acknowledge to Professor A. Iiyoshi, the President of Chubu University for his continuous encouragement.

REFERENCES

[1] M. Hirose, T. Masuda, K. Sato, and R. Hata, "High-Temperature Superconducting (HTS) DC Cable," *SEI Technical Review*, vol. 61, pp. 29-35, Jan. 2006.

[2] N. Amemiya, "Overview of current distribution and re-distribution in superconducting cables and their influence on stability," *Cryogenics*, vol. 38, pp. 545-550, May 1998.

[3] V. E. Sytnikov, P. I. Dolgosheev, G. G. Svalov, N. V. Polyakova, and D. I. Belij, "Influence of the multilayer HTS-cable conductor design on the current distribution," *Physica C*, vol. 310, pp. 387-391, Dec. 1998.

[4] V. E. Sytnikov, N. V. Polyakova, and V. S. Vysotsky, "Current distribution and voltage-current relation in multi-layered LTS and HTS power cable core: a review," *Physica C*, vol. 401, pp. 47-56, Jan. 2004.

[5] K. Yoshitomi, E. S. Otabe, V. S. Vyatkin, M. Kiuchi, T. Matsushita, M. Hamabe, S. Yamaguchi, and R. Inada, "AC loss of ripple current in superconducting DC power transmission cable," *Physics Procedia*, vol. 58, pp. 326-329, 2014.

[6] E. S. Otabe, K. Ohashi, M. Kiuchi, T. Kawahara, and S. Yamaguchi, "Estimation of AC loss in cylindrical superconductor with ripple current," *Physics Procedia*, vol. 27, pp. 248-251, 2012.

[7] W. T. Norris, "Calculation of hysteresis losses in hard superconductors carrying ac: isolated conductors and edges of thin sheets," *Journal of Physics D: Applied Physics*, vol. 3, pp. 489-507, Apr. 1970.

Special Submission Instruction and Guideline for ASEMD2015 Authors

Duplication and Proper Attribution

Submissions to the Special Issue can not be duplicated to the papers which have been submitted to the ASEMD2015.

Duplication to the ASEMD2015 submissions is not acceptable at ANY level unless there is direct attribution, e.g. "we re-state what we wrote in our previous manuscript [ref]: <duplicated content>", or "the <project> will require a <performance parameter> of <specification> [ref]". Proper attribution means, for example, "in this figure, we re-plot data originally presented in [ref], and we include our new measurements", or "this diagram, shown previously in [ref], outlines the configuration of the magnet system". (Title can be the same as the ASEMD2015 conference paper's, but suggested to reword while keeps the same meaning; Figures can have one from the ASEMD2015 conference two-page paper, however in any case no more than two from the ASEMD2015 conference two-page paper, redrawing will not be recognize as the same in general; total text duplication is less than 20%)

-- Manuscripts must be original. Manuscripts that present small increments relative to previous work published or submitted for publication by the same author might not be considered as sufficiently original to merit publication.

-- Manuscripts submitted for publication should not also have been submitted for consideration by another publication.

-- Manuscripts may not re-use previously published material without proper attribution. This applies to both text and figures. IEEE conducts a mandatory and automatic check for re-use of material for all submitted manuscripts.

-- If authors choose to prepare their manuscript by using a previous manuscript as a template, authors must ensure that the new manuscript does not improperly re-use material from the previous manuscript, and that the new manuscript conforms to the style and formatting requirements in the latest template for IEEE Trans. Appl. Supercond.

-- If authors choose to re-use graphics in figures, they should inform the editor and provide proper attribution to the original source of the figure in the text.

-- Manuscripts that re-use more than 1 graphic figure may be closely examined for original content.

EUCAS-15_1A-LS-P-04.05

Thermosiphon effect during cooling test of a 200 m DC HTS cable facility

Yury V. Ivanov, Hirofumi Watanabe, Noriko Chikumoto, Makoto Hamabe, Hirohisa Takano, Jian Sun, and Satarou Yamaguchi

Abstract—**Industrial application of HTS cables for power transmission is largely constrained by the imperfection of the cryogenic pumps which are expensive apparatuses providing additional heat load. Temperature and, consequently, density of the liquid cryogen change while it flows through the channel. If the cryogenic pipe route has enough elevation difference, this will lead to natural circulation. As a result, it may be not necessary to use pump and the system cost and complexity will reduce significantly. The feasibility of the given approach was confirmed theoretically for various system configurations. Preliminary experiments were also carried out using 200-meter DC HTS facility at Chubu University during 3rd and 4th cooling tests. Recently, during 6th cooling test the cryogenic pump was stopped intentionally. Meanwhile, the natural circulation of the liquid nitrogen was observed at flow rate of about 2 l/min, and the cable temperature remained low.**

Index Terms—**Power transmission, HTS power cables, liquid nitrogen, cooling system, thermosiphon effect.**

I. Introduction

THE important components of the ecological stress are the energy mining activity and energy transportation. The pass to renewable energy sources, energy loss reduction, and optimization of delivery systems can improve considerably the ecological situation on the Earth. It is considered that technologies on the basis of effect of superconductivity are one of the optimal approaches to solve these problems. Centenary period of research in superconductivity has come to the end with creation of experimental high temperature superconducting power transmission (HTS PT) lines of several hundred meter class. Projects of HTS PT lines of kilometer class, which will be established in really operating urban networks, are under consideration [1]-[3] and construction [4] now. Unfortunately, high cost and complexity of HTS cable cooling systems restrain a rapid progress in the field of large-scale application of HTS. Several years ago, a proposal to use a thermosiphon effect to keep HTS cable at low temperature was made. The density of cryogen changes from point to point because it naturally heats up while flows through the cryogenic channel accumulating heat load. Therefore, a low hydraulic resistance and sufficient cryogen level difference will lead to natural circulation. Ideally, HTS PT line may not contain a cryogenic pump. This approach can reduce the cost of the system making it more simple and stable. Existing test HTS PT lines are constructed using corrugated cryogenic pipes, which exhibit very high hydraulic resistance in comparison with straight pipes. Therefore, possible thermosiphon effect could not be observed against the background of a large pressure loss and did not attract the attention of researchers.

Authors are with the Center of Applied Superconductivity and Sustainable Energy Research, Chubu University, Kasugai, Aichi 487-8501, Japan (e-mail: ivanov@isc.chubu.ac.jp).

The feasibility of this given approach was confirmed theoretically for various system configurations [5], [6]. Preliminary experiments were carried out using 200-meter DC HTS facility at Chubu University during 3rd cooling test [7]. The facility is distinguished from other experimental lines by several important innovations. In particular, cryogenic channel is composed of smooth pipes in order to decrease the hydraulic resistance. The experimentally obtained pressure drop versus effective temperature difference behavior at flow rate of about 8 l/min obviously show the presence of thermosiphon effect which is in the qualitative agreement with the theory [7]. Before the 4th cooling test the facility was upgraded with the installation of a new differential gauge to improve accuracy of the measurements. A new series of the experiments was carried out at a flow rate of 6 l/min. The quantitative agreement between the experimental data and the theory was noticed. It was very important that the overall pressure drop between terminals vanished at a certain artificial heat load.

TABLE I
Brief Information about Experiments

Cooling test	Flow conditions	Results	Ref.
3rd	7.9 l/min (forced circulation)	Effect was observed qualitatively	[7]
4th	5.9 l/min (forced circulation)	Effect was observed quantitatively; zero pressure drop was achieved	present paper
6th	2.0 l/min (natural circulation)	Pure natural circulation was observed	present paper

Final measurements were performed during 6th cooling test in 2014. The experiments began with the liquid nitrogen (LN_2) flow rate of about 11 l/min. After a short-time preheating of (LN_2), cryogenic pump was turned off. Decaying positive oscillations of the flow rate were observed. In the longest experiment, the steady state at 2 l/min was achieved after about 40 min. The experiment lasted more than 6 hours without accidents, and then the cryogenic pump was started again. The maximum outlet temperature was 80.3 K. Although the LN_2 level difference was rather small, the effect was

strong enough to keep HTS cable temperature at an acceptable level. Brief information about the experiments is summarized in Table 1.

II. Experiment

The construction of 200-meter experimental DC HTS cable facility at the Chubu University was started in 2009 and completed in 2010. One of the goals of this facility was to develop new technologies to achieve a record cooling length of the HTS cable and minimum cost of installation. The level difference of the cryogenic pipes of 2.58 m and low hydraulic resistance caused by using direct smooth pipes create together favorable conditions for the observation of the thermosiphon effect. LN_2 flows through a narrow space between the HTS cable of 35 mm diameter and the inner surface of cryogenic pipe (inner diameter of 57.2 mm). Several pairs of platinum resistance thermometers located at different positions measured the actual distribution of temperature inside the cryogenic flow channel. The overall pressure drop between terminal units was measured by means of a differential gauge. In order to simulate natural heat load and thus vary the density of LN_2, the system was supplied with heaters of capacity of up to 350 W, two of which are located at the downflow and upflow sections of the cryogenic pipe. The measured data were recorded at time interval of 3 s [8], [9]. The locations of heaters and sensors used in experiment are shown in Fig. 1.

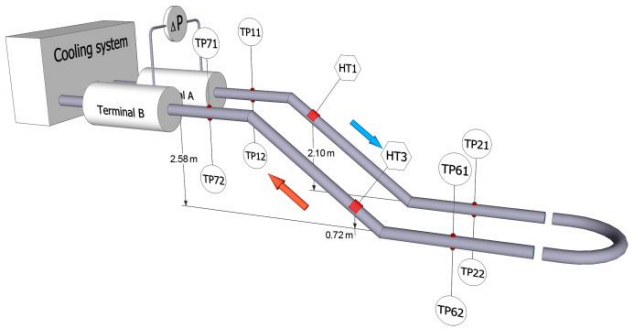

Fig. 1. Sketch of the 200 m DC HTS cable facility at the Chubu University. Only terminal units, cryogenic pipes, differential gauge (ΔP), selected thermometers (TP) and heaters (HT) are shown in the picture. Level difference is 2.6 m.

III. Results and Discussion

In our case, the value of the additional change of the pressure drop caused by thermosiphon effect is defined by two parameters. There are 1) the temperature difference (or the overall heat load) between the inclined segments of the cryogenic pipe, and 2) the level difference. The pressure drop versus LN_2 flow rate dependence at approximately constant ambient heat load of about 300 W is shown in Fig. 2. The flow rate ranged from 3 to 11 l/min that corresponded to the flow velocities ranged from 0.03 to 0.11 m/s and to the Reynolds numbers ranged from 3200 to 11700 (transient and turbulent flows). The temperature difference was within the range of 1.0-3.6 K. Points in Fig. 2 represent data averaged over 10 min (200 readouts). Design curve was calculated using formulae summarized in [10] taking into account pipe and cable jacket surface roughnesses, and cable displacement from the center of the cryopipe. Remarkable feature of the experimental dependence is that at the flow rate of about 4.5 l/min pressure drop vanishes, that means the hydraulic friction is fully compensated by the thermosiphon effect. As can be seen, experimental points at the low flow rates lie considerably lower than the design curve. This can be explained by the low accuracy of the flowmeter and pressure gauge in this area. Besides that, there is some additional 40 cm slope of the horizontal part of the cryogenic pipe, which a little strengthens the thermosiphon effect.

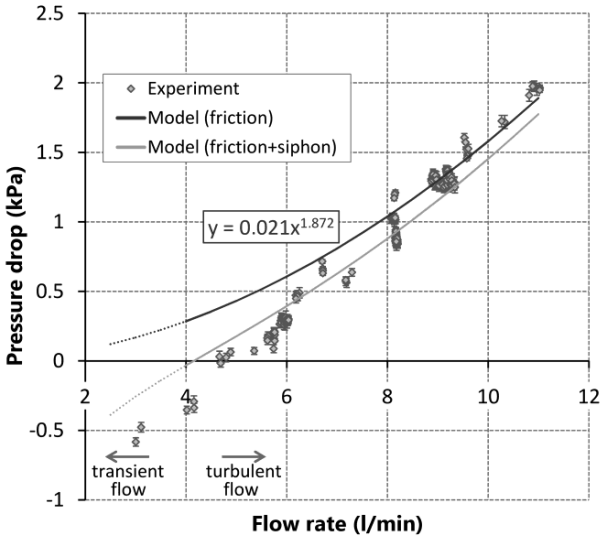

Fig. 2. Pressure drop as a function of LN_2 flow rate at constant heat load. Design curve is shown in black. Grey curve is the design curve corrected for the natural thermosiphon effect. Experimental points represent averaged over 10 min data.

The dependence between the pressure drop and the temperature difference at constant flow rate was measured during next part of our work. In comparison with the preliminary experiment described in [7], the measurements were carried out at lower flow rates of 5.87-6.0 l/min in order to decrease background value of the pressure drop. Unfortunately, we were not able to maintain lower values of the flow rate that is 3-5 l/min long enough to complete data recordings because of the unstable operation of the cryogenic pump. The power rates of heaters HT1 and HT3 were varied stepwise from 0 to 300 W. Consequently, the temperature difference intentionally decreased with heating of HT1, and increased with heating of HT3. The driving force in the typical single-phase closed thermosiphon is proportional to the difference between upflow and downflow temperatures (1).

$$\Delta p \propto \Delta T \qquad (1)$$

In our case, the temperature difference at a constant flow rate is determined by combination of distributed ambient heat load and local heat load provided by heaters. Ambient heat

load can be considered as constant because the experiments were carried out under similar weather conditions. Therefore, the constant driving force always exists regardless of the state of heaters, and corresponding experimentally determined constant should be introduced in the right-hand side of (1). The actual temperature of LN2 in the inclined sections can be estimated by interpolation of the values obtained by two pairs of thermometers TP11/TP12 and TP21/TP22 for downflow, and by TP61/TP62 and TP71/TP72 for upflow. Because of asymmetric arrangement of thermometers, formula (1) becomes more complicated. Furthermore, the heaters are arranged so that they can change the temperature of LN2 only inside the part of the corresponding inclined segment (see Fig. 1). This fact also requires the introduction of appropriate correction coefficients. To simplify the analysis, the resulting complex expression can be linearized by introducing an effective temperature difference ΔT_{eff}. This parameter takes into account piecewise-linear shape of the temperature distribution during heater experiment. Since heaters were not used simultaneously, for simplicity we can write two separate expressions for HT1 and HT3 as follows:

$$\Delta p = A\Delta T_{eff} + B \tag{2}$$

where for HT1

$$\begin{aligned} \Delta T_{eff} &= \left(TP_7 - TP_1\right) - \varepsilon_{HT1}\left(TP_2 - TP_1\right) \\ A &= gH\gamma \\ B &= A\left(a\varepsilon_{HT1} - c\right)/J \end{aligned} \tag{3}$$

and for HT3

$$\begin{aligned} \Delta T_{eff} &= \left(TP_7 - TP_1\right) + \varepsilon_{HT3}\left(TP_6 - TP_1\right) \\ A &= gH\gamma \\ B &= A\left(b\varepsilon_{HT3} - c\right)/J \end{aligned} \tag{4}$$

where g is the gravitational acceleration, 9.81 m/s^2; H is the difference in elevation between the highest and the lowest points of the cryogenic pipe, 2.58 m; h_{HT1} and h_{HT3} are the difference in elevation between heaters HT1 and HT3, and lowest point of cryogenic pipe, 2.10 and 0.72 m, correspondingly; J is the volume flow rate, l/min; Δp is the pressure drop, Pa; TP_1, TP_2, TP_6, and TP_7 are the average temperatures measured by pairs of thermometers TP11/TP12, TP21/TP22, TP61/TP62, and TP71/TP72, correspondingly, K; ΔT_{eff} is the effective temperature difference, K; $\varepsilon_{HT1}=h_{HT1}/H$ and $\varepsilon_{HT3}=h_{HT3}/H$ are the relative difference in elevation between heaters HT1 and HT3, and lowest point of cryogenic pipe; and γ is the thermal expansion coefficient of the liquid nitrogen, 4.4 kg/m^{3}K.

Experimentally obtained constants a=2.66, b=1.95, and c=0.25 have a dimension of K·l/min. These constants give us correctional values for the additional ambient heating of LN_2 that occurs at sites between thermometers TP11/TP12 and TP21/TP22, and TP61/TP62 and TP71/TP72. The constants differ from those published in the description of the preliminary experiments [7] because the upgrade caused a change in thermal insulation.

Results of measurements are presented in Fig. 3. Straight lines show the theoretical behavior. The key parameter of the thermosiphon is the slope coefficient A. It is evident that results agree satisfactorily with the theory. Vertical shift of the points reflects complexity of exact calculation of the background pressure drop taking into account complicated eccentric configuration with different roughnesses of the internal surface of the cryogenic pipe and cable jacket.

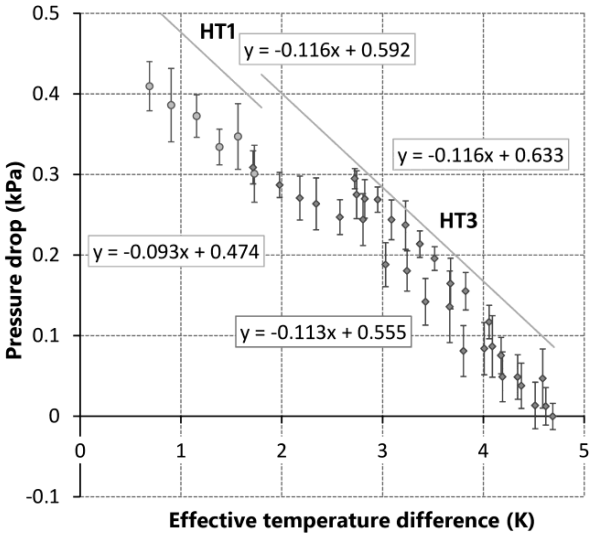

Fig. 3. Pressure drop as a function of the effective temperature difference between the inclined segments of the cryogenic pipe varied by the heaters HT1 and HT3. Flow rate is fixed at 5.94±0.07 l/min. The data are averaged over 4 min. Equations are the explicit form of (2) correspond to the theoretical behavior obtained by (3), (4) (see top right), and to the experimental data with coefficients obtained by least square method (see bottom left).

After confirmation of the existence of thermosiphon effect, it was decided to carry out the final direct experiments. The experiment was repeated four times. At the conventional flow rate of about 11 l/min the temperature difference was only 1 K, the heater HT3 was switched on for a short time just before shutting down the cryopump in order to initiate the natural circulation. LN_2 flow oscillations without changing the direction of the flow were observed for up to two hours after switching off the cryopump. This oscillatory instability of single-phase flow in a closed siphon is well known and has a theoretical description [11], [12]. Taking into account the design of the cryogenic pipe, it can be assumed that the specific source of the instability is local LN_2 boiling at low flow rate in the areas near heat bridges. It should be particularly noted that the measured temperatures of LN_2 in all points were always a few degrees below the boiling point at a given pressure. Therefore, the flow was single-phase liquid. The steady natural circulation was achieved at a flow rate of about 2 l/min. Time dependences of the flow rate, temperature

difference, downflow and upflow temperatures, and heaters' power during selected experiment are presented in Fig. 4.

It is interesting to note that the facility can be characterized by two time constants. The first one corresponds to the turbulent flow regime, and the second one to the laminar flow regime. Numerical computation gives values of 25 s and 270 s, correspondingly. Therefore, it will take about 200 s to reduce the flow rate from 10 to 1 l/min, and about 830 s to reduce from 10 to 0.1 l/min.

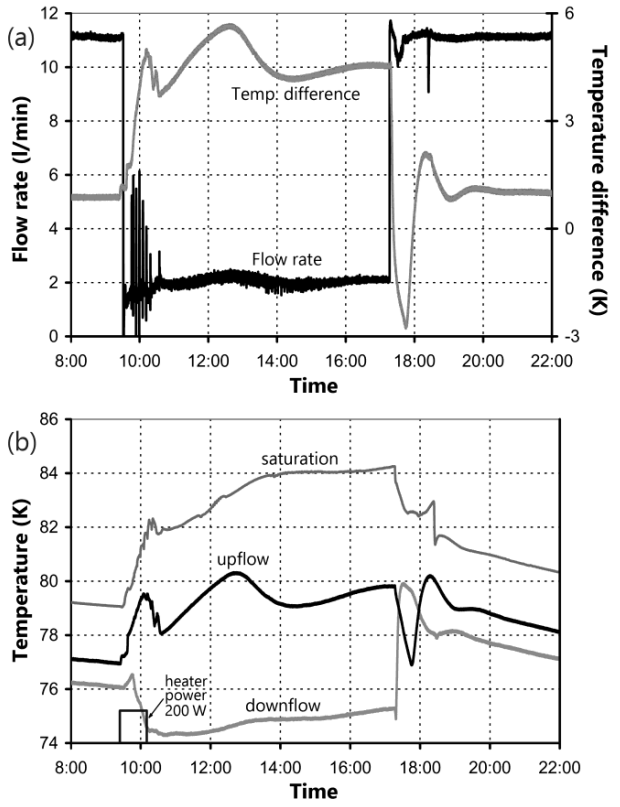

Fig. 4. (a) Time dependences of the flow rate and temperature difference, and (b) downflow and upflow temperatures, and heaters' power during thermosiphon experiment. Cryogen boiling temperatures are also shown.

The duration of the natural circulation during each of four 1-day experiments was from 4 to 6 hours. The maximum recorded temperature difference was 6 K. The most important fact to be considered was that the outlet temperature of the cable channel did not exceed 81 K even at high enough inlet temperature of 74-75 K. Therefore, for the first time the possibility of cooling long HTS cable without the use of forced circulation of the cryogen was experimentally confirmed.

IV. Conclusion

The thermosiphon effect arising in the real 200 m HTS cable cooling system in the presence of the level difference was investigated experimentally. The thermosiphon effect was observed satisfactorily in quantitative agreement with theory even though the level difference was rather small. This was achieved with low background pressure drop by using smooth cryogenic pipes and low flow velocity of LN_2. Zero value of the overall pressure drop was recorded with additional heat load of 300 W. It means that the thermosiphon effect can compensate the hydraulic friction in the cryogenic pipe when conditions for natural circulations were created.

After these preliminary experiments, the cryogenic pump was stopped. Meanwhile, the steady natural circulation was observed for a long time, and HTS power cable temperature remained low enough to keep superconducting state.

The authors felt that a special research using adopted experimental facility should be undertaken in order to investigate the instability problem of LN_2 flow.

Acknowledgment

The authors thank Dr. Atsuo Iiyoshi, the Chairman of the Board of Trustees and the Chancellor of Chubu University, for his encouragement during the course of this work.

The authors acknowledge Dr. Hiroshi Fujiwara for his support of our project.

References

[1] I. Melnik, A. Geschiere, D. Willén, and H. Lentge, "Long length HTS cable with integrated FCL property," *J. Phys. Conf. Ser.*, vol. 234, 2010, Art. ID. 032037.

[2] S. Kopylov *et al.*, "HTS DC transmission line for megalopolis grid development," *J. Phys. Conf. Ser.*, vol. 507, 2014, Art. ID. 032047.

[3] V. E. Sytnikov *et al.*, "Status of HTS cable link project for St. Petersburg grid," *IEEE Trans. Appl. Supercond.*, vol. 25, no. 3, Jun. 2015, Art. ID. 5400904.

[4] S. Yamaguchi, H. Koshizuka, K. Hayashi, and T. Sawamura, "Concept and design of 500 meter and 1000 meter DC superconducting power cables in Ishikari, Japan," *IEEE Trans. Appl. Supercond.*, vol. 25, no. 3, Jun. 2015, Art. ID. 5402504.

[5] Y. Ivanov, H. Watanabe, T. Kawahara, M. Hamabe, J. Sun, and S. Yamaguchi, "Superconducting power transmission line cooled with naturally circulating LN_2," in *Proc. 23 Int. Cryog. Eng. Conf. Int. Cryog. Mater. Conf. 2010*, 2011, pp. 1017-1022.

[6] Y. Ivanov *et al.*, "Compact counter-flow cooling system with subcooled gravity-fed circulating liquid nitrogen," *Physica C*, vol. 470, no. 20, Nov. 2010, pp. 1895-1898.

[7] Y. Ivanov, H. Watanabe, M. Hamabe, T. Kawahara, J. Sun, and S. Yamaguchi, "Observation of the thermosiphon effect in the circulation of liquid nitrogen in HTS cable cooling system," *Phys. Procedia*, vol. 27, 2012, pp. 368-371.

[8] S. Yamaguchi *et al.*, "Design and construction of 200-meter high temperature superconducting DC power cable test facility in Chubu University," in *Proc. 23 Int. Cryog. Eng. Conf. Int. Cryog. Mater. Conf. 2010*, 2011, pp. 1041-1047.

[9] Y. V. Ivanov, H. Watanabe, M. Hamabe, J. Sun, T. Kawahara, and S. Yamaguchi, "Circulation pump power for 200 m cable experiment," *Physica C*, vol. 471, no. 21-22, Nov. 2011, pp. 1308-1312.

[10] I. E. Idel'chik, *Flow resistance: a design guide for engineers*, E. Fried, Ed. New York, Washington, Philadelphia, London: Hemisphere Publ. Corp., 1989, pp. 5-42.

[11] P. Welander, "On the oscillatory instability of a differentially heated fluid loop," *J. Fluid. Mech.*, vol. 29, part 1, 1967, pp. 17-30.

[12] J. E. Hart, "A new analysis of the closed loop thermosyphon," *Int. J. Heat Mass Transfer*, vol. 27, no. 1, 1984, pp. 125-136.

This article has been accepted for publication in a future issue of this journal, but has not been fully edited. Content may change prior to final publication. Citation information: DOI 10.1109/TASC.2016.2535135, IEEE Transactions on Applied Superconductivity

Study of 2D residual current density profiles of BSCCO and YBCO HTS tapes by means of 3D Hall probe system

Mohamed Tallouli, Jian Sun, Oleg Shyshkin, Makoto Hamabe, Hirofumi Watanabe, Noriko Chikumoto, Samia Charfi Kaddour, Sataro Yamaguchi, *Member, IEEE*

***Abstract*— The residual current distribution in the high temperature superconducting (HTS) tapes effects the operation of power cables, superconducting magnets and other devices built using these tapes. This effect is crucial for restarting procedure of the devices after either emergency or scheduled shutdown or after the short circuit. Furthermore, current distribution along and across the HTS tape provides us with the information about the quality of the tape performance. In present paper we examine 2D residual current density distribution in different BSCCO and YBCO tapes by means of 3D Hall probe system after the emergency shutdown of the 100 A direct current. After the experimental measuring of the self-magnetic field near the tape inducted by residual current, the inverse problem solver aim at calculation of current density distribution throughout the tape is applied. The results of calculation show the strong asymmetry and vortex-like structure of 2D residual current flow in BSCCO tape while the current flow in YBCO tapes has a tendency to the symmetry about the center of the HTS tape. The significant difference in shape and amplitude of the residual current density profiles is observed as well.**

***Index Terms*—2D current density distribution, HTS tape, inverse problem solution, self-magnetic field, residual current.**

I. Introduction

The homogeneity of the HTS tapes plays a key role in current carrying properties of power cables, superconducting magnets and other devices built with use of these tapes. The reason is that the homogeneity results in the current density distribution along and across the tape for either transport or residual currents. The redistribution of residual current throughout the HTS tape is crucial for the restarting procedure of the devices after either emergency, scheduled shutdown or after short circuits. One should be aware of the shape and the amplitude of the residual current distribution that defines the value of stored electric energy in HTS tapes after the shutdown phase. Furthermore, residual current density distribution provides us with the information about the quality of the tape performance.

Solving the inverse problem to obtain the current density distribution from measurements of self-magnetic field is a widely demanded task for current-carrying flat surfaces including HTS tapes [1]-[6]. Some algorithms presented in earlier papers, which include two-dimensional Fourier transforms of magnetic fields, current densities and weight functions [3], are more suitable to calculate localized current loops in limited in size conductors [4]. Such technique usually could not be used for a long HTS tape because of long scanning time.

We present in this paper methods that are suitable for examination of current density distribution in long HTS tapes. One is the solution of the set of linear equations issued from the Biot-Savart law and the other is the method of least squares. These two methods are the extended versions of the previous ones [2], [5]. It was found that the combination of both methods would be beneficial. The new combined algorithm is discussed and applied for calculations.

We examine 2D residual current density distribution in different BSCCO and YBCO tapes by means of 3D Hall probe system after the emergency shutdown of the 100 A direct current. In order to obtain the current density distribution we use a 3D Hall probe to scan three components of self-magnetic field induced by the residual current above the tape. And then this dataset is used to solve the inverse problem aimed at calculating 2D current distribution [1], [7]-[11].

II. Experiment

A. Samples and experiment set up

The experimental device consists of an open cryostat in which different devices are mounted: 3D Hall probe scanning system, two stepping motors, and HTS tape fixed on a FRP (fiber reinforced plastic) plate. See Fig. 1 (a). We use three different tapes, one BSCCO tape and two coated YBCO tapes made by three different companies.

Template version 5.2, January 6, 2014.
Manuscript received September 8, 2015.

Mohamed Tallouli, Jian Sun, Makoto Hamabe, Hirofumi Watanabe, Noriko Chikumoto, Sataro Yamaguchi are with Center of Applied Superconductivity and Sustainable Energy Research, Chubu University, Aichi, Japan, phone: +81-568-51-9419; fax: +81-568-51-9413; e-mail: yamax@isc.chubu.ac.jp

Oleg Shyshkin, is with V.N.Karazin National University, Kharkov, 61022, Ukraine, phone: + 380-57-335-35-59; fax: + 380-57-335-15-62; e-mail: oleg.shyshkin@gmail.com

Samia Charfi Kaddour is responsible of condensed matter team in El Manar University, 1060 ,Tunis, Tunisia, phone: +216-71-872-600; fax: +216-71-855-073 e-mail <s.charfikaddour@gmail.com.

This article has been accepted for publication in a future issue of this journal, but has not been fully edited. Content may change prior to final publication. Citation information: DOI 10.1109/TASC.2016.2535135, IEEE Transactions on Applied Superconductivity

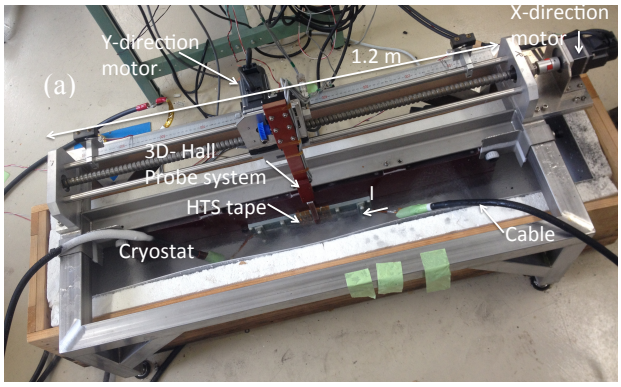

(b)

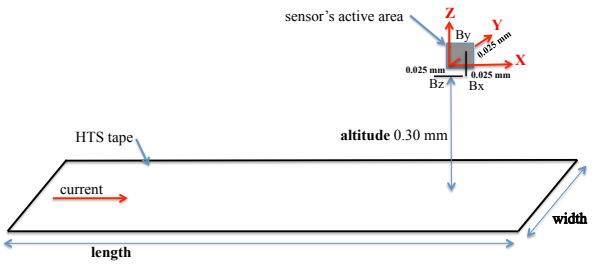

Fig. 1. (a) Photo of Experimental device. (b) Experimental configuration.

Table I describes the characteristics of each HTS tape including: size, architecture, fabrication processing and critical current.

TABLE I
HTS TAPES CHARACTERISTICS

HTS tape	BSCCO (Sumitomo) [12]	YBCO (AMSC) [13]	YBCO (Fujikura) [14]
Critical current @77K	200 A	300 A	572 A
Width	4.5 mm	12 mm	10 mm
Tape thickness	0.35 mm	0.2 mm	0.2 mm
Architecture	BSCCO filaments (10 µm x 250 µm) Ag matrix (0.25 mm) Two Cu reinforced alloys (50 µm)	Two Cu stabilizer strips (~50 µm) Ag layer (~3 µm) YBCO HTS layer (~ 0.8 µm) Buffer layer: [Y_2O_3, etc.] (~ 0.2 µm) NiW(5 at.%) texture (75 µm ~ 100 µm)	Cu stabilizer layer (75 µm ~ 100 µm) Ag layer (~2 µm) GdBaCuO HTS layer (~ 2 µm) Buffer layer: [MgO, etc.] (~ 0.7 µm) Hastelloy texture (75 µm ~ 100 µm)
Processing	Powder in tube	RABIT/MOD	*IBAD/PLD*

The 3D Hall probe system consists of 3 Hall probe sensors with 0.05 x 0.05 mm^2 active areas. It moves across the tape in Y direction (tape's width) and in X direction (tape's length) at 0.3 mm altitude from the tape surface as shown in Fig. 1 (b). The distance between sensors is 0.025 mm and its altitude shift was taken into account in data plotting. The Hall probe current is set to be 10 mA for each sensor.

The stepping motors are controlled by Labview environment synchronously with the data acquisition system. Each increment in both X and Y directions is controlled by the stepping motor system.

B. 3D magnetic field scanning

Transport DC current of 100 A was applied to each HTS tape during 20 minutes. After 20 minutes we switch off the DC current in 0.15 ms [1] and then start scanning three components (Bx, By and Bz) of self-magnetic field of each HTS tape along the Y direction with 0.1 mm step as shown in Fig. 2.

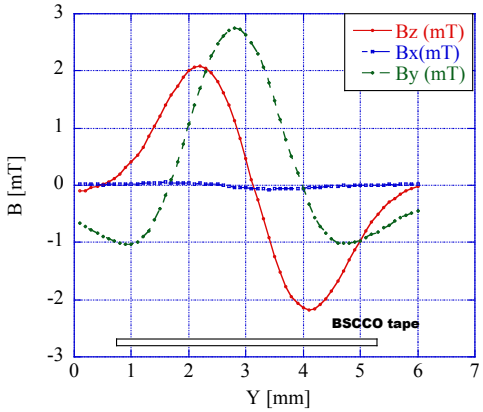

Fig. 2. Three components of the residual magnetic field (BSCCO tape).

Afterwards we change the longitudinal location (X coordinate) of 3D-Hall probe system by 0.1 mm and repeat scanning in Y direction again. Total scanning distance along the X direction is almost 1 cm for each HTS tape. We got 3D self-magnetic field maps. We show for examples three maps in Figs. 3, 4 and 5.

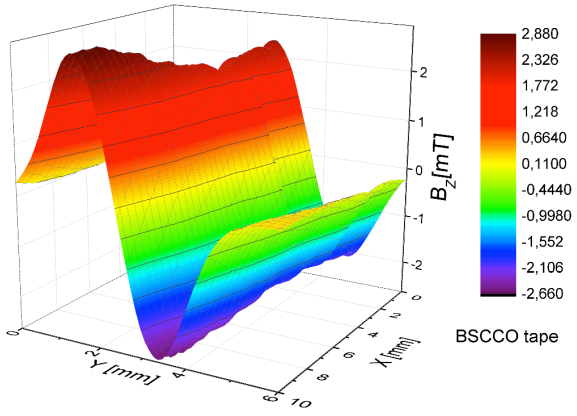

Fig. 3. B*z* components of the 3D self-magnetic field map (BSCCO tape).

This article has been accepted for publication in a future issue of this journal, but has not been fully edited. Content may change prior to final publication. Citation information: DOI 10.1109/TASC.2016.2535135, IEEE Transactions on Applied Superconductivity

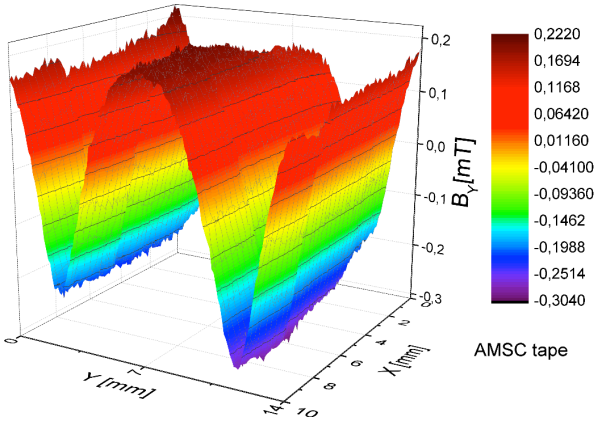

Fig. 4. B*y* components of the 3D self-magnetic field map (AMSC tape).

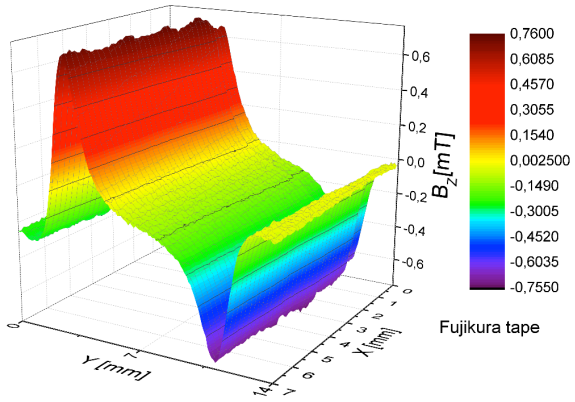

Fig. 5. B*z* components of the 3D self-magnetic field map (Fujikura tape).

During the experiment we keep the HTS tape and the Hall probe sensors in liquid nitrogen continuously by refilling the open cryostat.

III. Experiment Analysis

A. Inverse problem technique

To calculate the magnetic field above the HTS tape in an arbitrary position $\mathbf{r}_d$ the Biot-Savart law in general form is used

$$\mathbf{B}(\mathbf{r}_d) = \frac{\mu_0}{4\pi}\int_{\Sigma}\frac{[\mathbf{j}\times\mathbf{R}]}{R^3}dS, \qquad (1)$$

where $R=\sqrt{R_x^2+R_y^2+z_d^2}$ is the distance between the segment on the tape and detector position. All notations are shown on Fig. 6.

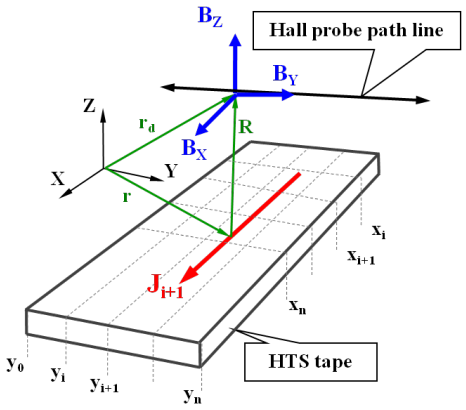

Fig. 6. The schematic representation of the experimental layout together with the HTS tape discretization used for the inverse problem solution algorithm.

The integration in equation (1) is performed through the surface of the tape $dS=dx\,dy$, which is limited in Y direction by the width of the tape, and in the X direction it could be either limited or performed in the range $(-\infty,\infty)$. The fact that the magnetic field decreases as $\sim 1/R^2$ makes the contribution of currents running on large distances negligible.

After the integration in Cartesian coordinates including the fact of fast magnetic field decreases with the distance and assuming the local symmetry of the current J_Y about the center of integration segment, we obtain the next set of linear equations

$$\mathrm{B}_X(\mathbf{r}_d) = 2\cdot 10^{-7}\sum_{i=1}^{n} J_{Yi}\left(\arctan\frac{y_d-y_i}{z_d}-\arctan\frac{y_d-y_{i-1}}{z_d}\right), \qquad (2)$$

$$\mathrm{B}_Y(\mathbf{r}_d) = -2\cdot 10^{-7}\sum_{i=1}^{n} J_{Xi}\left(\arctan\frac{y_d-y_i}{z_d}-\arctan\frac{y_d-y_{i-1}}{z_d}\right), \qquad (3)$$

$$\mathrm{B}_Z(\mathbf{r}_d) = 10^{-7}\sum_{i=1}^{n} J_{Xi}\ln\frac{(y_d-y_{i-1})^2+z_d^2}{(y_d-y_i)^2+z_d^2}. \qquad (4)$$

The equation (4) fits to that used for calculations of 1D current distribution in previous papers [1], [2]. These equations have the compact form

$$B_{Xk} = \sum_{i=1}^{n} A_{ki}\,J_{Yi},$$

$$B_{Yk} = \sum_{i=1}^{n} B_{ki}\,J_{Xi}, \qquad (5)$$

$$B_{Zk} = \sum_{i=1}^{n} C_{ki}\,J_{Xi},$$

where A_{ki}, B_{ki} and C_{ki} are the components of the matrixes representing distances between the segment with the current and detector position.

The set of equations (5) should be enhanced with the additional equation that goes from the constraint on the total current value. For the case of residual current I_{tot}=0. Afterwards, the equations will be solved by Cramer's rule, which is more stable for our case.

This article has been accepted for publication in a future issue of this journal, but has not been fully edited. Content may change prior to final publication. Citation information: DOI 10.1109/TASC.2016.2535135, IEEE Transactions on Applied Superconductivity

The advantages of this method are the fast calculation and low error level. The disadvantage of this method is the limited number of the resolved data points caused by the fact that the determinants of the matrixes consisting of elements A_{ki}, B_{ki} and C_{ki} approach to zero value with the increasing of number of data points.

To avoid these problems the method of least squares is used. The idea of the method of least squares is to minimize the value of the error function by varying the model of the current density profile

$$err = \sum_{i} \sqrt{\left(B_{exp}\left(y_i\right) - B_{calc}\left(y_i\right)\right)^2}. \quad (6)$$

Here $B_{exp}(y_i)$ is the experimentally measured profile of the magnetic field, and $B_{calc}(y_i)$ is the magnetic field calculated from the model current density profile by means of Biot-Savart law. The algorithm of this method is as described further. Firstly, we scan the magnetic field above the tape and convert it in data array $B_{exp}(y_i)$. After that we define an arbitrary shape of the current density profile in HTS tape and calculate the self-magnetic field $B_{calc}(y_i)$ exactly in the same points where the experimental magnetic field is measured. The arbitrary current density profile is presented as an array with each element equal to the current density value in segment J_i as shown on Fig. 6. Varying the values of current density in different segments we modify the magnetic field profile $B_{calc}(y_i)$. When the calculated profile approaches to the measured profile, the error function value (6) reaches its minimum. That value is prescribed at the beginning of calculation. Hence, we obtain the current density profile in HTS tape with the error defined in advance, equal in our calculation 1% of $B_{exp}(y_i)$. The crucial point of the method is to present the initial model current density profiles that will be used to initiate calculation. The initial shape of the profile could be an arbitrary, but in some cases, it will affect the result of calculation.

In the combined method as the first step, the solution of the set of linear equations is applied. It gives the preliminary profile, which is used as an input current density profile in the method of least squares. This combination of two methods provides us with faster, more detailed and accurate analyze of current density distribution. This is the method we use for the calculation of 2D current density distribution in different HTS tapes.

B. Current density profiles

We used the inverse problem technique discussed above to calculate 2D residual current density map for each HTS tape. We show the residual current distribution in the HTS tapes using a map of (*Jx, Jy*) current vectors with amplitude proportional to the residual current, as in Figs. 7, 8 and 9.

The edge thickness of BSCCO silver matrix (~200 μm) is considered in Fig. 7 to present the 2D residual current vectors. However, for YBCO tapes the 2D residual current vectors are distributed for almost whole tapes width.

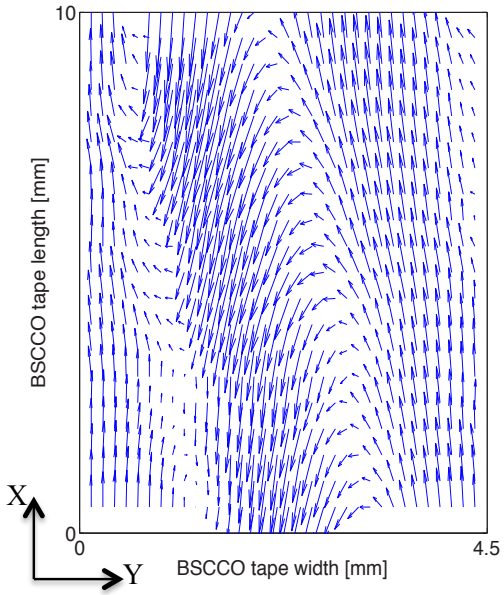

Fig. 7. Two-dimensional residual current density profiles in BSCCO tape.

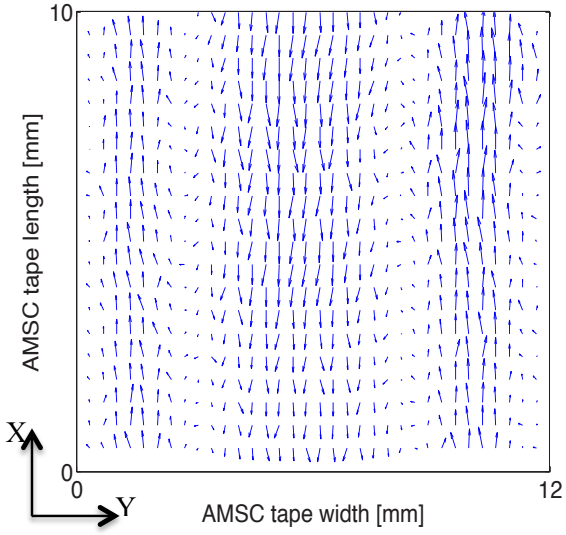

Fig. 8. Two-dimensional residual current density profiles in AMSC tape.

This article has been accepted for publication in a future issue of this journal, but has not been fully edited. Content may change prior to final publication. Citation information: DOI 10.1109/TASC.2016.2535135, IEEE Transactions on Applied Superconductivity

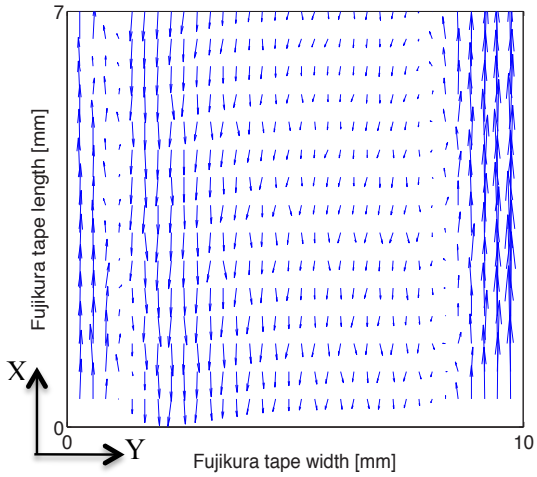

Fig. 9. Two-dimensional residual current density profiles in Fujikura tape.

IV. Discussion and Conclusion

Three components of self-magnetic field and corresponding 2D residual current density profiles for three types of HTS tapes are demonstrated in this paper.

For the BSCCO tape, we observe different 3D magnetic field maps along the tape. In fact, non-identical B*z* profiles along 10 mm of the tape length were observed. That predicts an inhomogeneity of current density distribution and might depend on the manufacturing of this tape.

In Fig. 7 the 2D residual current density distribution shows a high density of superconducting filaments at the center and two directions of the current. One direction is via the tape's edges and the second direction via the tape's center. The residual current density at the edges is not symmetric, which proves that the quality of the superconductor filaments is not same. Our observation might indicate a defection of the BSCCO tape observed in the 2D residual current density distribution.

On the other hand, the residual current flow at the center is not parallel to the tape's length direction. The superconductor filaments inside the BSCCO tape might be over lapped due to fabrication procedure. The quality of superconducting filaments is then not homogenous.

We can observe also in Fig. 7 a vortex-like structure of current density vectors inside the BSCCO tape.

For the YBCO tapes, the 3D self-magnetic field scans are almost the same along the tape longitudinal direction, indicating a high homogeneity. We show in Figs. 4 and 5 the B*y* components of the AMSC tape self-magnetic field and the B*z* components of Fujikura tape self-magnetic field.

In the 2D residual current density profiles shown in Figs. 8 and 9 we observe also two directions of the current via tape's edges and center.

For the AMSC tape, the residual current density at the edges is almost symmetric along the X direction and penetrates to the tape's center (see Fig. 8). However for Fujikura tape, the residual current density profiles are not symmetric along edges (see Fig. 9).

As shown in Table I, the critical current of Fujikura tape is more than five times higher than the transport current before switch off. And the critical current of AMSC tape, which is wider than Fujikura tape, is three times higher than the transport current before switch off.

Residual current density profiles show lower penetration to the Fujikura tape's center comparing to the AMSC tape.

The results of present research demonstrate the strong asymmetry and vortex-like structure of 2D residual current density profile in BSCCO tape while the current flow pattern in YBCO tapes is symmetric about the center of the tape. That could be explained by the manufacturing specifics of the BSCCO tape that results in filament structure of it while the structure of YBCO tape is uniform. The significant difference in the shape and amplitude of the residual current density profiles is observed as well.

Acknowledgment

The authors thank Prof. Atsuo Iiyoshi, Chancellor of Chubu University for his continuous encouragement through this work. The authors thank also all the staff of Center of Applied Superconductivity and Sustainable Energy (CASER) specially Mr. Koji Yoshimura for their help to preform the experiment and constant encouragement.

References

[1] M. Tallouli, J. Sun, O. Shyshkin, A. Ninomia, M. Hamabe, H. Watanabe, N. Chikumoto, S. Charfi Kaddour, and S. Yamaguchi, "Residual Magnetic field measurement of BSCCO and YBCO tapes by a Hall probe," *IEEE Trans. Appl. Supercond.,* vol. 25, p. 8000704, 2015, (4pp).

[2] M. Carrera, X. Granados, J. Amoros, R. Maynou, T. Puig, and X. Obradors, "Current distribution in HTSC tape obtained by inverse problem calculation", *J. Phys: Conf. Series,* vol. 234, p. 012009, 2010. [*9th Europ. Conf. Appl. Supercond,* 2009].

[3] B. J. Roth, Nestor G. Sepulveda and J. P. Wikswo, "Using a magnetometer to image a two-dimensional current distribution*", J. Appl. Phys.,* vol. 65, p. 361, 1989.

[4] R. J. Wijngaarden, K. Heeck, H. J. W. Spoelder, R. Surdeanu, and R. Griessen, "Fast determination of 2D current patterns in flat conductors from measurement of their magnetic field", *Physica C*, vol. 295, pp. 177-185, 1998.

[5] B. Dutoit, J. Duron, S. Stavrev, and F. Grilli, "Dynamic Field Mapping for Obtaining the Current Distribution in High-Temperature Superconducting Tapes", *IEEE Trans. Appl. Supercond.* vol. 15, NO. 2, JUNE 2005.

[6] J. Sun, M. Tallouli, O. Shyshkin, M. Hamabe, H. Watanabe, and N. Chikumoto, and S. Yamaguchi "Residual magnetic field profiles and their current density profiles of coated conductors for fast and slow cut-off current operations", *Progrs. Supercond. Cryog.,* vol. 17, pp. 17-20, 2015.

[7] R. Inada, T. Makihara, Y. Araki, S. Bab, Y. Nakamura, A. Oota, S. Sakamoto, C.S. Li, and P.X. Zhang, "Non-Destructive evaluation for twisted Bi2223 tapes using scanninf Hall-probe microscopy," *Physica C,* vol. 470, pp. 1392-1396, 2010

[8] J. Amoros, M. Carrera, and X. Granados "An effective model for fast compultion of current distribution in operating HTS tapes from magnetic field measuremnts in non-destructive testing," *Supercond. Sci. Technol.,* vol 2, pp. 104005-104013, 2012.

[9] P. Usak, M. Polak, and P. Mozola, "Measurement of the lateral Transport Current Distribution in YBCO Tape," *IEEE Trans. Appl. Supercond.,* vol 19, pp. 2839-2842, 2009.

[10] Y. Honda, K. Higashikawa, M. Inoue, T. Kiss, N. Ayai, M. Kikuchi, K. Hayashi, and K. Sato "Study on the critical current distribution in CT-OP Bi-2223 tape based on the Hall probe magnetic miroscopy," *Physica C,* vol. 470, pp. 1377-1379, 2010.

[11] M. Carrera, J. Amoros, X.Granados, R. Maynou, T. Puig, and X. Obradors, "Computation of Current Distribution in YBCO Tapes With Defects Obtained From Hall Magnetic Mapping by Inverse Problem Solution," *IEEE Trans. Appl. Supercond.*, vol. 21, pp. 3408-3412, 2011.

This article has been accepted for publication in a future issue of this journal, but has not been fully edited. Content may change prior to final publication. Citation information: DOI 10.1109/TASC.2016.2535135, IEEE Transactions on Applied Superconductivity

[12] N. Ayaki, K. Yamazaki, M. Kikuchi, G. Osabe, H. Takaaze, H.Takayama, S. Kobayashi, J. Fujikami, K. Hayashi, K. Sato, K. Osamura, H. Kitaguchi, S. Matsumoto, T. Kiyoshi, and J. Shimoyama, "Electrical and Mechanical Proprties of DI-BSCCO Type HT Reinforced With Metallic Sheathes," *IEEE Trans. Appl. Supercond.,* vol 19, pp. 3014-3017, 2009.

[13] M. W. Rupich, X. Li, S. Sathyamurthy, C.L.H. Thieme, K. DeMoranville, J. Gannon, and S. Fleshler, "Second Generation Wire Development at AMSC," *IEEE Trans. Appl. Supercond*., vol. 23, p. 6601205, 2013, (5pp).

[14] Y. Iijima, "High-Performance Y-based Superconducting Wire and Their Applications," Fujikura Technical Review, Superconductor Business Development Department, pp. 117-121, 2013.

IEEE TRANSACTIONS ON APPLIED SUPERCONDUCTIVITY, VOL. 25, NO. 3, JUNE 2015 8000404

Critical Current Enhancement of BSCCO Tapes in Stacked Conductors With Ferromagnetic Sheets

Hisato Ohara, Jiàn Sūn, Makoto Hamabe, Toshio Kawahara, and Satarou Yamaguchi

***Abstract*—A 200-m-long high-temperature superconducting (HTS) cable for dc power transmission, called CASER-II, was constructed at Chubu University using BSCCO tapes in 2010. The critical current of HTS tapes has been extensively studied against their layouts to improve the performance of HTS tapes in the cable. The multilayer structure of the tapes is needed to obtain a high current capacity. In the stacked tape conductors, the critical current of BSCCO tapes shows strong dependence on the current feeding directions between the tapes. The critical current is improved when the opposite-direction current is applied to them and reduced for the same-direction current feeding mode because of the strong magnetic field interaction between them. By using the ferromagnetic sheets, self-field of HTS tapes will be affected and may improve their critical currents. This technical paper presents the measurements of the critical currents of BSCCO tapes in the stacked conductors covered with the ferromagnetic sheets under different current feeding modes. We will present effects on the critical current of HTS tapes of the magnetic field from the currents applied to the neighboring tapes and the ferromagnetic sheets through the magnetic field analysis.**

***Index Terms*—BSCCO, critical current, dc power transmission, dc superconducting cable, high-temperature superconductor.**

I. Introduction

RESEARCH studies on dc superconducting power transmission (SC-PT) applications by using HTS tapes were studied around the world because of its higher efficiency than AC systems [1]–[4]. As for a dc power system, improvement of current capacity of the cable is most important because of free from ac losses and the critical current of HTS tape is a key parameter for power cable applications. After combining HTS tapes into SC conductor in a power cable, self-field of each HTS tape is affected by the other tapes and its critical current will be changed while the transport current is applied to the cable.

A 200 m dc SC-PT system, called as CASER-II, was constructed at Chubu University by using BSCCO tapes in 2010 [5]. Fig. 1(a) and (b) presents a photo of the coaxial cable and a scheme of a three-layer structure used for the CASER-II. The critical current of HTS tape has been extensively studied with respect to their layout to improve their performance of HTS tapes in the cable [6]. The multi-layer structure of HTS tapes is needed to obtaining a high current capacity as in Fig. 1(b).

Manuscript received August 11, 2014; accepted November 8, 2014. Date of publication November 20, 2014; date of current version February 6, 2015. This work was supported by the Ministry of Education, Culture, Sports, Science, and Technology as "Collaboration with Local Communities" Project for Private Universities.

The authors are with Chubu University, Kasugai 487-8501, Japan (e-mail: j_sun@isc.chubu.ac.jp).

Color versions of one or more of the figures in this paper are available online at http://ieeexplore.ieee.org.

Digital Object Identifier 10.1109/TASC.2014.2373657

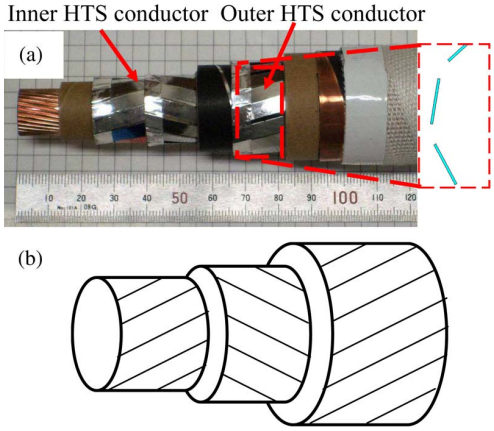

Fig. 1. (a) Photo of a dc coaxial power cable composed of DI-BSCCO tapes as two SC conductors for bipolar dc power transmission and a sketch of the gap. (b) Scheme of a three-layer structure used for the CASER-II cable.

In the stacked tape conductors, the critical currents of BSCCO tapes show strong dependence on the current feeding directions between the tapes. The critical current is improved when the opposite-direction current applied to them and reduced for the same-direction current feeding mode because of strong magnetic field interaction between them [7].

By using the ferromagnetic sheets, self-field of HTS tapes will be affected and may improve their critical current in the cable. Several works have shown performance improvement of single tape due to ferromagnetic covers on the edges. By introducing nickel coating near the tape edges, about 11% increment of the critical current is observed for a single Bi-2223/Ag tape [8]. Gömöry groups reported the improvement of the critical current and reduction of AC loss for a common multifilamentary Bi-2223/Ag tape with thin nickel layer electroplated at the edges [9]. While forming a stacked tape conductor, the processes of magnetic field interaction between the ferromagnetic sheets and the tapes become different from a single tape with ferromagnetic materials. This technical paper will present the measurements of the critical currents of BSCCO tape in the stacked conductors covered with the ferromagnetic sheets under different current feeding modes. We will present effects on the critical current of HTS tape of the magnetic field from the currents applied to the neighboring tapes and the ferromagnetic sheets through the magnetic field analysis.

II. Samples and Experimental Procedures

BSSCO tapes (Type HT-CA) are from Sumitomo Electric Industries [10] and are laminated with 0.05 mm Cu-alloy layer on both sides. The critical current of the BSCCO tape is 200 A in

TABLE I
SPECIFICATIONS OF HTS TAPES AND FERROMAGNETIC SHEETS

Items	BSCCO tape	Ferromagnetic sheets
Width	4.5 mm	3.0 mm / 5.0 mm
Thickness	0.35 mm	0.30 mm
Length	27 cm	15 cm

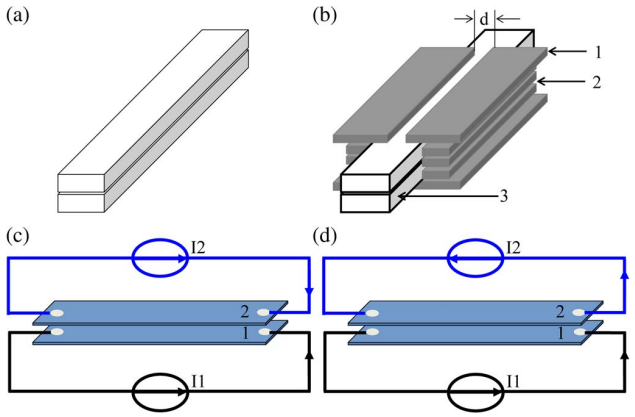

Fig. 2. Schemes of the two-layer stacked tape conductor (a) without and (b) with ferromagnetic sheets. 1: 5-mm-wide FMS; 2: 3-mm-wide FMS; 3: HTS tape. d is the gap distance between FMSs. Schematic layouts of circuit loops for the (c) same-direction ($\uparrow\uparrow$) and (d) opposite-direction ($\uparrow\downarrow$) current feeding modes.

self-field at 77 K. The ferromagnetic sheets are grain-oriented steel provided by JFE-Steel (Japan) [11]. The specifications of BSCCO tapes and ferromagnetic sheets (FMS) are shown in Table I. In the experiment, several FMSs with different width of 3 and 5 mm are used to cover the stacked tape conductors. Two BSCCO tapes are used to form a stacked tape conductor as in Fig. 2(a) and covered with six 3-mm-wide and four 5-mm-wide FMSs at the edges as in Fig. 2(b). d denotes the space gap distance between FMSs.

Critical current measurements are performed at 77 K by immersing the samples into liquid nitrogen [6]. The critical current of HTS tape is measured by the four probe method. Three voltage taps are soldered on each tape with spaces of 8 cm and 10 cm, respectively. The voltage signals are measured by a KEITHLEY 2700 multimeter with sensitivity of 0.1 μV/cm. The transport currents are measured by a 0.125 mΩ current shunt resistor. The current feeding mode is controlled by using two power supplies as shown in Fig. 2(c) and (d). The critical current of the tape #1 in the stacked tape conductor is measured against the current ($I2$) applied to tape #2. V–I characteristics are measured for the stacked tape conductor with and without FMS for different current feeding modes and their E–I characteristics are obtained by normalizing the voltages to the distance between the voltage taps.

III. RESULTS AND DISCUSSION

A. Critical Current for Stacked Tape Conductor Without Ferromagnetic Sheets

Fig. 3 presents a typical E–I curves of BSCCO tape in a stacked tape conductor without FMS in comparison with that of a single one. The neighboring current $I2$ is $\pm$100 A and $\pm$160 A. The negative current denotes the opposite-direction

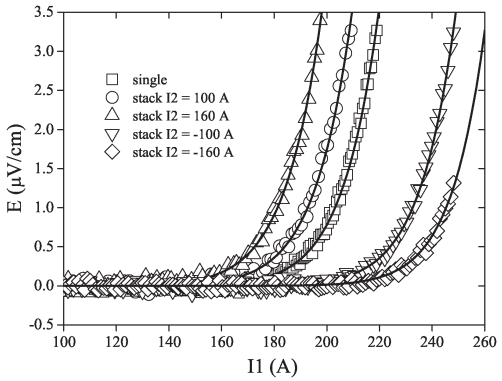

Fig. 3. E–I curves of BSCCO tape #1 for single- and two-layer stacked tape conductors with different neighboring current $I2$ of $\pm$100 and $\pm$160 A.

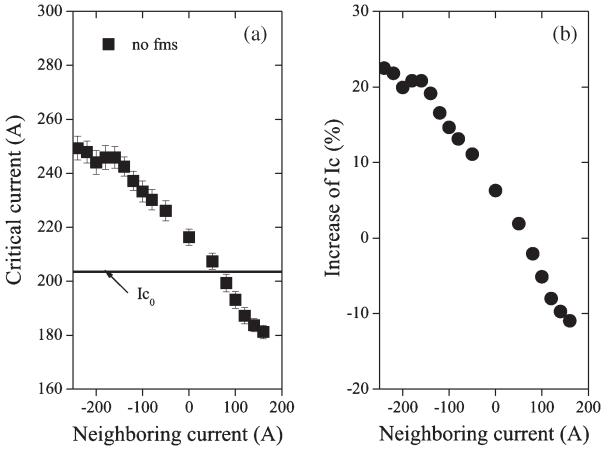

Fig. 4. (a) Critical current of BSCCO tape #1 with respect to the neighboring current in tape #2 for a two-layer stacked tape conductor without FMS. (b) Increase of the critical current with respect to the neighboring current.

($\uparrow\downarrow$) current feeding mode. E–I curves shows strong difference for different neighboring current.

Fig. 4(a) summarizes the critical currents of BSCCO tape with respect to neighboring current for the stacked tape conductor. The critical current is determined at the electric field criterion of 1 μV/cm through power line fitting in E–I curves [7]. The critical current of a single tape is measured to be 203.5 A for the tape #1. Fig. 4(b) shows the increase of the critical current with respect to neighboring current. Different performances are shown for the current feeding mode with opposite ($\uparrow\downarrow$) and same direction ($\uparrow\uparrow$). As for the opposite-direction current feeding mode, the critical current increases with decrease of the neighboring current $I2$. When the transport currents are applied to two tapes with the same-direction, the critical current decreases with increasing the neighboring current. While the $I2$ is zero, the increment about 5% of the critical current is observed resulting from the shielding effects of HTS tape #2 itself [7]. When the neighboring current $I2$ is larger than 80 A, the critical current becomes smaller than that of a single one.

B. Critical Current for Stacked Tape Conductor Covered With Ferromagnetic Sheets

As shown in Fig. 2(b), the critical currents for a two-layer stacked tape conductor covered with FMSs are measured for

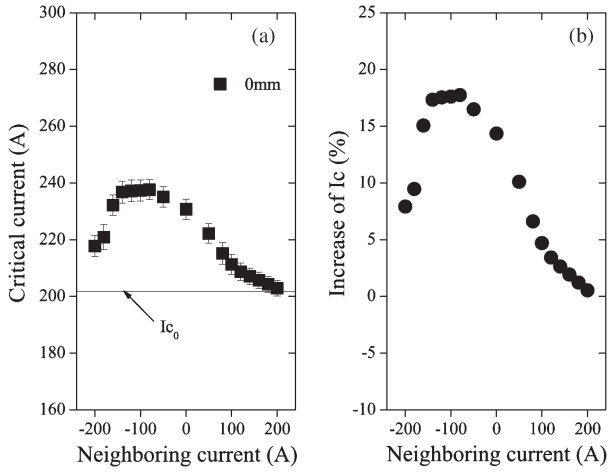

Fig. 5. (a) Critical current of BSCCO tape #1 with respect to the neighboring current in tape #2 for a two-layer stacked tape conductor fully covered with ferromagnetic sheets. (b) Increase of the critical current with respect to the neighboring current.

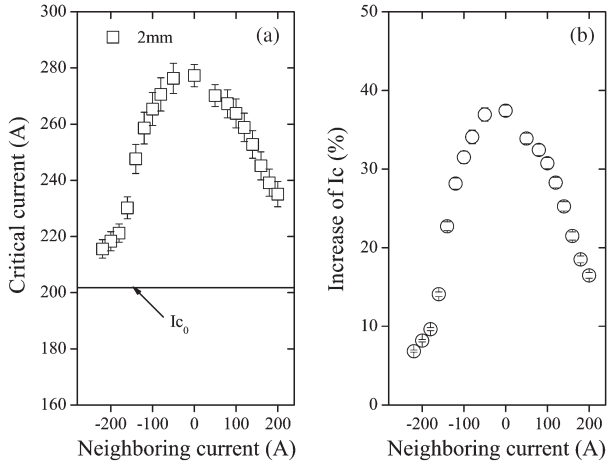

Fig. 6. (a) Critical current of BSCCO tape #1 with respect to the neighboring current in tape #2 for a two-layer stacked tape conductor covered with FMSs. The gap d is 2.0 mm. (b) Increase of the critical current with respect to the neighboring current.

different current feeding modes. Fig. 5(a) shows the critical current of BSCCO tape in a stacked tape conductor fully covered with FMSs, i.e., the gap $d = 0$ mm. The profile of the critical current is different from those in Fig. 4(a).

1) The critical current becomes not less than that of a single one when the transport current of less than 200 A is applied to the neighboring tape #2 as in Fig. 5(b).
2) None degradation of the critical current is observed for fully covered stacked tape conductor, which is different from that of single one as stated in [9].
3) When the opposite currents are applied to two tapes, peak of the critical current appears at the neighboring current of ∼100 A.

More improvement of the critical current are presented in Fig. 6(a) and (b) for a two-layer stacked tape conductor covered by FMSs with a gap of 2 mm above both sides of the tape

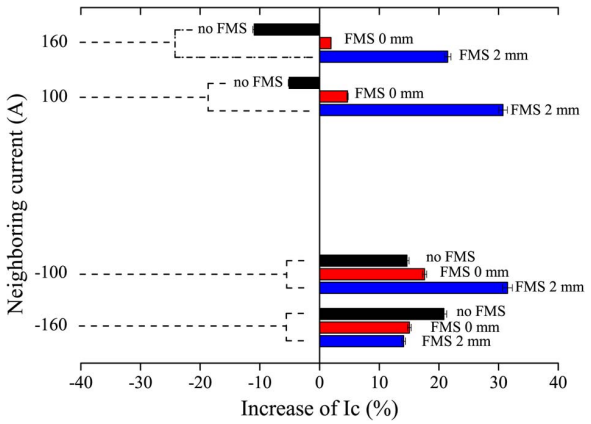

Fig. 7. Comparison of performance improvement of the critical current for the two-layer stacked tape conductor with and without ferromagnetic sheets.

surface. Profile of the critical current for the stacked tape conductor covered by FMSs with a 2 mm gap is similar with that of fully covered. Fig. 7 shows comparison of performance improvement of the critical current for a two-layer stacked tape conductor covered with and without FMS for the neighboring current of ±100 A and ±160 A. When the neighboring current is −160 A, the critical currents are improved to more than 13% for the stacked tape conductor in spite of with and without FMSs. Difference is shown when the same-direction (↑↑) currents are applied to two tapes as seen in Fig. 7. Therefore, by assembling the stacked tape conductor with ferromagnetic sheets, the critical current of BSCCO tape can be enhanced for different current feeding mode especial when a gap of 2 mm exists between FMSs.

C. Effect of Ferromagnetic Sheets and Magnetic Field Interactions on the Critical Current

To study the effects of ferromagnetic sheets and magnetic field interaction in the stacked conductors, a commercial finite element code (ANSYS) [12], [13] is used to analyze the magnetic field with nonlinear $B - H$ characteristics of FMS [14]. The calculation is done by an assumption of uniformly distributed transport current of 200 A in the cross section of BSCCO filaments area, i.e., the cross section of the transport current area is 4.5 mm × 0.25 mm [6]. Fig. 8(a)–(c) presents the magnetic flux when same-direction currents (↑↑) of 200 A are applied to two tapes in the stacked tape conductor without FMS, with fully covered by FMS and covered by FMS with a gap of 2.0 mm, respectively. The lowest critical current as in Fig. 4 is due to the strongest perpendicular magnetic component as Fig. 8(a). The magnetic flux are through the area when the FMS are used, which results in the reduction of the magnetic field at the HTS area as in Fig. 8(b) and (c). Therefore, the critical currents are improved for the stacked tape conductor covered with FMS as in Figs. 5 and 6. The neutral zone of magnetic field is formed as in Fig. 8(c)–(g) which leads to improvement of the critical current in their configurations as in Fig. 7. When the opposite-direction currents (↑↓) of ±200 A are applied to two tapes in the stacked tape conductor, the magnetic flux are

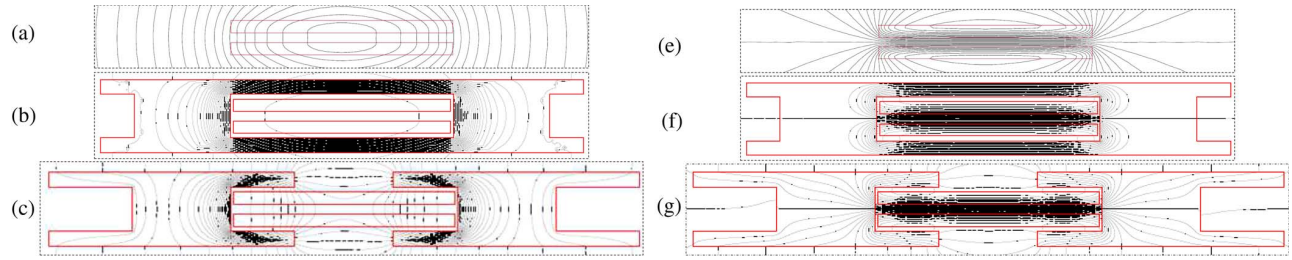

Fig. 8. (Left) Calculated magnetic flux for same-direction current applied to two tapes (a) uncovered (b) fully covered by FMS and (c) covered by FMS with a gap of 2.0 mm. (Right) Calculated magnetic flux for opposite-direction current applied to two tape (e) uncovered (f) fully covered by FMS and (g) covered by FMS with a gap of 2.0 mm. The solid line of the square area shows the cross-sectional image of the stacked conductor and FMSs as in Fig. 2(a) and (b).

concentrated between two tapes as shown in Fig. 8(e)–(g). When the FMSs are used to cover the edges of the stacked tape conductors, the magnetic flux are attracted to the area of the HTS tapes. Therefore, the enhancement ($\sim$8%) of the critical current for the stacked conductor with FMS becomes smaller than that ($\sim$20%) of uncovered ones.

IV. Conclusion

We have measured the critical current of BSCCO tapes in the stacked tape conductors with and without ferromagnetic sheets. Dependence of the critical current of BSCCO tapes on current feeding mode shows that the critical current is improved when the opposite-direction currents are applied and degraded for same-direction current feeding mode. Mutual interaction of the ferromagnetic materials and current feeding leads to no degradation of the critical current of BSCCO tape in the stacked tape conductors. Employing the ferromagnetic sheets could be one way to suppress the effects of same-direction ($\uparrow\uparrow$) current feeding on the critical current of HTS tapes in the stacked conductor for cable applications.

Acknowledgment

The authors would like to thank Dr. A. Iiyoshi, Chairman of the Board of Trustees and Chancellor of Chubu University, for his continuous encouragement throughout this work, as well as Dr. H. Fujiwara, a Professor of Keio University and the President of Nano-Opt Energy Corporation, for his financial support on the 200-m cable system construction.

References

[1] M. Ichikawa *et al.*, "Thermomechanical characteristics of 500-m HTS power cable," *IEEE Trans. Appl. Supercond.*, vol. 15, no. 2, pp. 1771–1774, Jun. 2005.

[2] S. Dai *et al.*, "The three-phase 75 m long HTS power cable," *Cryogenics*, vol. 27, no. 7/8, pp. 402–405, Jul./Aug. 2007.

[3] J. Lim *et al.*, "Performance test of 100 m HTS power cable system," *IEEE Trans. Appl. Supercond.*, vol. 19, no. 3, pp. 1710–1713, Jun. 2009.

[4] R. Soika, X. Garcia, and S. Nogales, "ENDESA supercable, a 3.2 kA, 138 MVA, medium voltage superconducting power cable," *IEEE Trans. Appl. Supercond.*, vol. 21, no. 3, pp. 972–975, Jun. 2011.

[5] S. Yamaguchi *et al.*, "Experiment of 200-meter superconducting DC cable system in Chubu University," *Phys. C, Supercond.*, vol. 471, no. 21/22, pp. 1300–1303, Nov. 2011.

[6] J. Sun *et al.*, "Critical current measurements for design of superconducting DC transmission power cable," *Phys. C, Supercond.*, vol. 471, no. 21/22, pp. 1313–1316, Nov. 2011.

[7] J. Sun *et al.*, "Critical current behavior of a BSCCO tape in the stacked conductors under different current feeding mode," *Phys. C, Supercond.*, vol. 494, pp. 297–301, Nov. 2013.

[8] A. K. M. Alamgir, C. Gu, and Z. Hán, "Experiment of enhancing critical current in Bi-2223/Ag tape by means of ferromagnetic shielding," *Phys. C, Supercond.*, vol. 432, no. 3/4, pp. 153–158, Nov. 2005.

[9] F. Gömöry *et al.*, "Performance improvement of superconducting tapes due ferromagnetic cover on edges," *IEEE Trans. Appl. Supercond.*, vol. 17, no. 2, pp. 3083–3086, Jun. 2007.

[10] N. Ayai *et al.*, "Electrical and mechanical properties of DI-BSCCO type HT reinforce with metallic sheathes," *IEEE Trans. Appl. Supercond.*, vol. 19, no. 3, pp. 3014–3017, Jun. 2009.

[11] H. Inoue and S. Okabe, "Magnetic properties of grain oriented electrical steel in model transformer under direct current-biased magnetization," *J. Appl. Phys.*, vol. 115, no. 17, pp. 17A332-1–17A332-3, May 2014.

[12] ANSYS Academic Teaching Advanced, Release 12.1. [Online]. Available: www.ansys.com

[13] S. Farinon, P. Fabbricatore, and F. Gömöry, "Critical state and magnetization loss in multifilamentary superconducting wire solved through the commercial finite element code ANSYS," *Supercond. Sci. Technol.*, vol. 23, no. 11, 2010, Art. ID. 115004.

[14] S. E. Zirka *et al.*, "Generalization of the classical method for calculating dynamic hysteresis loops in grain-oriented electrical steels," *IEEE Trans. Magn.*, vol. 44, no. 9, pp. 2113–2126, Sep. 2008.

Residual magnetic field measurement of BSCCO and YBCO tapes by a Hall probe

Mohamed Tallouli, Jian Sun, Oleg Shyshkin, Akira Ninomia, Makoto Hamabe, Hirofumi Watanabe, Noriko Chikumoto, Samia Charfi Kaddour, Sataro Yamaguchi, *Member, IEEE*

***Abstract*— A serious damage can happen to the power cable manufactured from the high temperature superconducting (HTS) tapes due to overcurrent conditions or because of technical errors during the cable assembling. To avoid the cable damage in any urgent case a quick interruption of the transport current is necessary. Comprehensive understanding of the current cut off time of HTS tape is required to restart the operation of power transmission line. In this study we applied 100A transport current to BSCCO and YBCO tapes. After interrupting the current we measured the magnetic field profiles of each HTS tapes. We compare the magnetic field profiles for the fast and slow cut of the current. The cut off time is 0.15 ms for the fast cut and 100 s for the slow one. The current density profiles are obtained by solving the inverse problem. Our results show that the magnetic field profiles are quite different from each experimental condition and HTS tapes, which are related to the hysteresis of HTS tape characteristics.**

***Index Terms*—Superconductor tapes, Magnetic field measurement, Current measurement.**

I. Introduction

High Temperature superconductor (HTS) tapes are a key issue of superconducting technologies such as power cables [1]. Power grid assembled from the HTS power cables can have problems caused by short circuit or overcurrent [2], [3]. Therefore a quick interruption is required in such fault conditions to protect superconductor cable. To restart the system, we should consider the residual current density profiles after the transport current cut-off. These residual current density profiles affect the performance of the cable and depend on the transport current cut-off speed. Scanning Hall probe measurement of residual magnetic field followed by a current density calculation constitutes a direct tool to study such characteristic [4]-[6]. In order to improve the understanding of this topic, we studied two different scenarios of transport current cut-off for two types of HTS tapes i.e., BSCCO and YBCO used in power cable manufacturing. One scenario is the rapid transport current cut-off during the 0.15 ms, and the other scenario is the slow decreasing of the current during 100 seconds. In order to calculate the residual current density in the HTS tapes, basing on the Hall probe measurements of the residual magnetic field, the inverse problem solution technique was applied.

A. Experiment set-up

In this experiment we use two different kinds of HTS tapes: BSCCO tape made by SUMITOMO [7] and YBCO tape made by American Superconducting Corp (AMSC) [8].
Table I describes the characteristics of each HTS tape include their dimensions and critical currents.

TABLE I
HTS Tape Characteristics

HTS tapes	BSCCO (Sumitomo)	YBCO (AMSC)
Critical Current @77K	200 A	300 A
Width	4.5mm	12mm
Thickness	0.35mm	0.2mm

The experimental layout is shown in Fig. 1 (a) and (b). We fix the HTS tape on a plate for the measurement, and the Hall probe with 0.05×0.05 mm^2 active area [4] and with the controlled positions moves above the tape at 0.3 mm altitude. The Hall probe is operated by 10 mA and the data was acquired by a 4000 data per second acquisition system while the magnetic field was deduced from the Hall probe measurements by 49 mT/μV sensitivity with 1nV accuracy.

A step motor with 0.05 mm step and 0.0025 mm acquisition controls the Hall probe position. This step motor is connected to computer and its position is fixed by a soft. The Hall probe supporter with the step motor constitutes the scan system. We placed the HTS tapes in an open cryostat filled with liquid nitrogen LN2 at 77 K.

Template version 5.2, January 6, 2014.
Manuscript received August 10, 2014.
Mohamed Tallouli, Jian Sun, Makoto Hamabe, Hirofumi Watanabe, Noriko Chikumoto, Sataro Yamaguchi are with Center of Applied Superconductivity and Sustainable Energy Research, Chubu University, Aichi, Japan, phone: +81-568-51-9419; fax: +81-568-51-9413; e-mail: yamax@isc.chubu.ac.jp
Oleg Shishkin, is with V.N.Karazin National University, Kharkov, 61022, Ukraine, phone: + 380-57-335-35-59; fax: + 380-57-335-15-62; e-mail: oleg.shyshkin@gmail.com
Akira Ninomia, Seikei University, Tokio, 180-8633 Japan, phone: +81-422-37-3739; fax: +81-422-37-3871; e-mail: ninomia@st.seikei.ac.jp
Samia Charfi Kaddour is responsible of condensed matter team in El Manar University, 1060 ,Tunis, Tunisia, phone: +216-71-872-600; fax: +216-71-855-073 e-mail <s.charfikaddour@gmail.com.

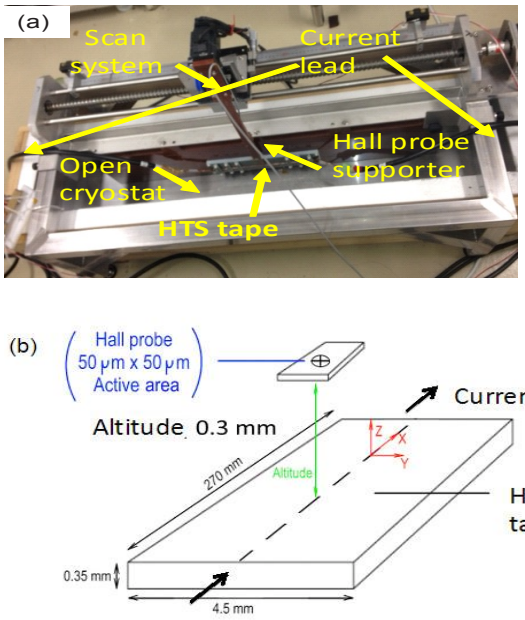

Fig. 1. Experiment set-up, (a) photo of the experiment device, (b) configuration to measure the magnetic field.

B. Residual magnetic field scanning

The transport DC current of 100 A was applied to each HTS tapes during 10 minutes. After 10 minutes we switch off the DC current by two operations; first operation is a quick switch off by just switching off the electric switcher manually (Fast op.). Second operation is by decreasing the current manually by 1A/s (Slow op.) Fig .2.

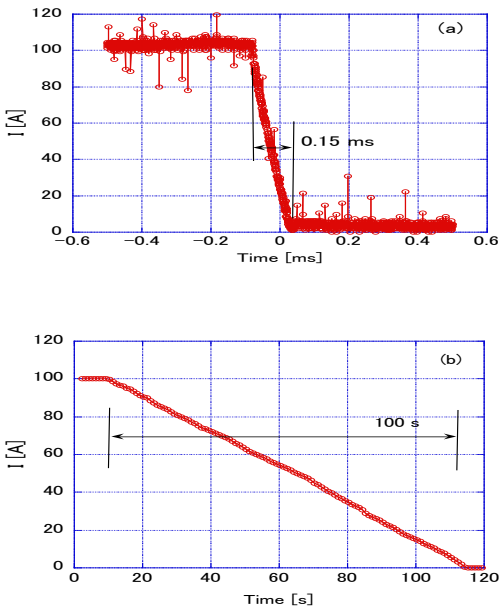

Fig. 2. The current cut-off scenarios, (a) rapid cut-off (Fast op.), (b) 1A/s decreasing (Slow op.).

Then, we start scanning the perpendicular component of the residual magnetic field of each HTS tape along the Y direction to cover the tape width. We change then the X position along the longitudinal direction. We repeat these measurements for both current operations. During the experiment we keep the constant level of LN2 in the open cryostat.

The perpendicular component of the residual magnetic field of BSCCO tape was scanned at three positions along the X direction with 10 mm distance separate each (See Fig. 3). The perpendicular component of the residual magnetic field of YBCO tape was scanned also at three X positions with 10 mm separate each (See Fig. 4).

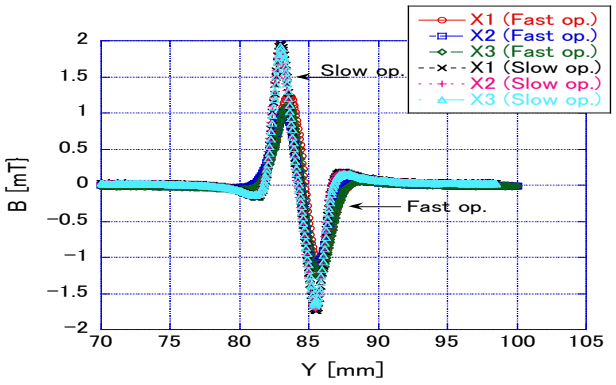

Fig. 3. Vertical components profiles of the residual magnetic field of BSCCO tape measured for the operation 1 and 2 on three X-axis positions.

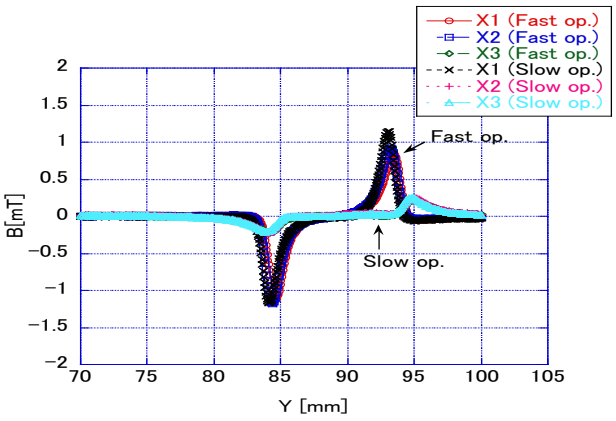

Fig. 4. Vertical components profiles of the residual magnetic field of YBCO tape measured for the operation 1 and 2 on three X-axis positions.

II. Experiment Analysis

A. Inverse problem technique

As it was described above, in order to measure the perpendicular component of the magnetic field of the HTSC tape, the detector i.e., the Hall probe moving on the specified altitude above the tape is used. In this section we present the inverse problem solution algorithm that allows us to calculate the current density profile in HTS tape basing on the measurements of the magnetic field above the tape.

As in Fig. 2 the schematic representation of the experimental layout for the B_z measurements is shown. We put the HTSC

tape in Cartesian coordinates, which are used for the calculations, along the X axis, in the plane $Z=0$ so that Y axis crosses the tape. The Hall probe path line goes parallel to Y axis on the defined altitude z_d above the tape.

Here we have to make several assumptions to simplify the analytical treatment of this problem and speed up the numerical calculations. Firstly we assume the thickness of the tape to be infinitesimal so that all the current running within the tape could be considered as a surface current presented through the surface current density $\mathbf{J}$ (see Fig. 2). Further we suppose that all the current is running along the tape so that the only X-component of the current density exists. The current density doesn't depend on X coordinate and is a function only of Y coordinate $J=J_x(Y)$. In this case we can make a discretization of the tape (i.e., divide the tape into a number of sub-tapes) with the fixed current density value J_i in each sub-tape.

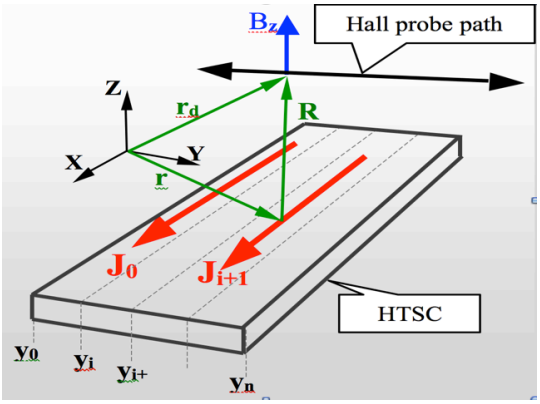

Fig. 5. HTS tape discretization used for the inverse problem solution algorithm of the inverse problem.

The perpendicular component of the magnetic field B_z (blue arrow on Fig. 5) is measured by detector in position $\mathbf{r}_d \equiv (x_d, y_d, z_d)$. Vector $\mathbf{r}=(x,y,z)$ determines the coordinates of each current element on HTSC tape. The distance between the separate current element and arbitrary coordinate of detector is presented by vector $\mathbf{R}=\mathbf{r}_d-\mathbf{r}$ with its absolute value $R=\sqrt{R_x^2+R_y^2+z_d^2}$ where $R_x=x_d-x$ and $R_y=y_d-y$. All these notations will be used throughout further treatment.

Generally the magnetic field $\mathbf{B}$ at an arbitrary position $\mathbf{r}_d$ could be calculated by means of Biot-Savart equation

$$\mathbf{B}(\mathbf{r}_d)=\frac{\mu_0}{4\pi}\int_{\Sigma}\frac{\mathbf{J}\times\mathbf{B}}{R^3}\mathrm{dS}. \qquad (1)$$

The integration in Equation (1) is performed through the surface Σ of the tape $\mathrm{dS}=\mathrm{dx\,dy}$, which is limited in y -direction by the width of the HTSC tape and in the x -direction it could be either limited manually or the integration could be performed in the range $(-\infty, \infty)$. The fact that the magnetic field decays as $\sim\frac{1}{R^2}$ makes the impact of currents running on the large distances negligible.

Including the mentioned above assumptions the Biot-Savart equation (1) after the integration along x -direction in the range $(-\infty, \infty)$ could be written as following

$$B_z(r_d)=\frac{\mu_0}{2\pi}\sum_{i=0}^{n-1}\int_{y_i}^{y_{i+1}}\frac{R_y J_i}{R_y^2+z_d^2}\mathrm{dy}. \qquad (2)$$

The summation in expression (2) should be done over all sub-tapes with the current density elements. After the integration along y -direction we obtain the final formula used for the inverse problem solution

$$B_z(\mathbf{r}_d)=\frac{\mu_0}{4\pi}\sum_{i=0}^{n-1}J_i\ln\frac{(y_d-y_i)^2+z_d^2}{(y_d-y_{i+1})^2+z_d^2}. \qquad (3)$$

This expression is similar to that presented and justified by M. Carrera ET. Al. [9]. For a number of measurements of the vertical components of the magnetic field the expression (3) gives a system of linear equations with known magnetic field B_z and unknown current density elements J_i. We developed MATLAB code to solve this system of linear equations by means of Cramer's rule. As a result of inverse problem solution we obtain the current density profiles, which are presented further.

B. Current density profiles

We used the inverse problem technique discussed above to calculate the current density profiles corresponding to each HTS tape measured at the different X positions.

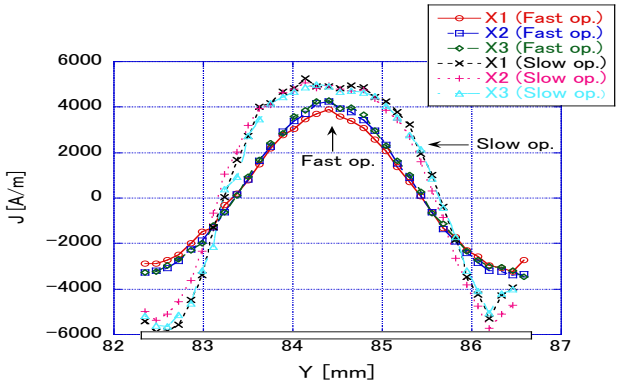

Fig. 6. Current density profiles of the BSCCO tape at different longitudinal positions.

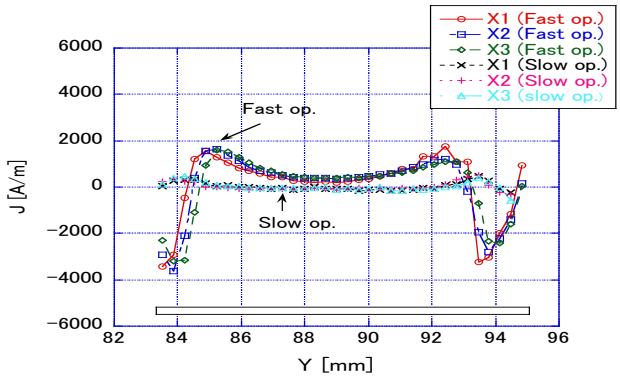

Fig. 7. Current density profiles of the YBCO tape at different longitudinal positions.

From each vertical component of the residual magnetic field we calculated the current density profile. For the BSCCO tape and he YBCO tape we got six current densities. For both cut off operations we got three current density profiles corresponding to X-axis positions along the HTS tape as in Fig .6 and Fig .7.

III. Discussion and Conclusion

The profiles of the residual magnetic fields in BSCCO tape are almost the same on the direction of transport current. Therefore, their current density profiles along this direction are almost the same. They are almost symmetric for the center of the tape, which means that the uniformity of the BSCCO tape is high. In the case of YBCO tape, the residual magnetic fields are different for different coordinates along the tape that is the evidence of the inhomogeneity of the YBCO tape. This is the fundamental difference between these two tapes in the present samples.

The peak current density is higher for the slow cut-off operation as compared with the fast cut-off operation for BSCCO tape, and this tendency is reverse of the resistive materials, such as copper. The reason would be the shielding effect of the matrix material. The copper and silver are used as the matrix materials for BSCCO, and these materials would consume high electric energy before it comes to the superconductor filaments. In case of 1A/s decreasing operation, high electric field can penetrate into the HTS tape, and induce the permanent current.

Different magnetic field profiles can be observed for YBCO tape. They are not high uniform like the BSCCO ones. The amplitude of current densities in fast cut-off operation is almost four times higher than these of the slow cut-off operation.

The quality of the BSCCO filaments near the edge would be lower than the center's. This is one of the reasons why the current density profile is peaked at the center, which is not true for YBCO. We should consider the shielding effect of the superconducting filaments and the matrix materials, such as copper and silver. These resistive materials can consumes electric power. On the other hands, the quality of the superconducting layer of the YBCO tape would be the same all over the tape. This is the reason that the current density is high near the edge.

Since the behaviors of the YBCO and BSCCO tapes are different each other for the fast and slow current cut-off operations, we should consider these phenomena for HTS cable applications.

Acknowledgment

The authors thank Prof. A. Iiyoshi, Chancellor of Chubu University for his continuous encouragement through this work. The authors thank also all the staff of Center of Applied Superconductivity and Sustainable Energy (CASER) specially Mr. K. Yoshimura for their help to prepare the experimental devices.

References

[1] J. Sun, S. Yamaguchi, M. Sugino, H. Watanabe, M. Hamabe, and T. Kawahara, "Critical current distributions of BSCCO tapes in the multi-layer HTS conductors," *Physica C,* vol. 471, pp. 1313-1316, 2011.

[2] S. Torii, H. Kado, M. Ichikawa, H. Suzuki, M. Yagi, and S. Mukoyama, "Short Circuit Test of HTS Power Cable," *IEEE Trans. Appl. Supercond,* vol. 17, 2007.

[3] K.jensen, C.Traeholt, E. Veje,, M. Daumling, C. Rasmussen, D. A.Willen and O. Tonnesen, "Overcurrent Experiments on HTS tape and cable Conductor," *IEEE Trans. Appl. Supercond,* vol. 11, pp. 1781-1784, 2001.

[4] C. Gu, Timing Qu, and Z. Han, "Measurement and calculation of residual magnetic field in a Bi2223/Ag Magnet," *IEEE Trans. Appl. Supercond.,* vol. 17, pp. 2394-2397, 2007.

[5] R. Inada, S. Baba, R. Ohtsu, T. Makihara, S. Sakamoto, and A. Oota, "Longitudinal Uniformity of Commercial Bi2223 Characterized by Scanning Hall-Probe," *IEEE Trans. Appl. Supercond,* vol. *21, pp. 2816-2819, 2011.*

[6] P. Usak, M. Polak, and P. Mozola, "Measurement of the lateral Transport Current Distribution in YBCO Tape," *IEEE Trans. Appl. Supercond.,* vol. 19, pp. 2839-2842, 2009

[7] N. Ayaki, K. Yamazaki, M. Kikuchi, G. Osabe, H. Takaaze, H. Takayama, S. Kobayashi, J. Fujikami, K. Hayashi, K. Sato, K. Osamura, H. Kitaguchi, S. Matsumoto, T. Kiyoshi, and J. Shimoyama "Electrical and Mechanical Proprties of DI-BSCCO Type HT Reinforced With Metallic Sheathes," *IEEE Trans. Appl. Supercond*, vol. 19, pp. 3014-3017, 2009.

[8] U. Schoop, M. W. Rupich, C. Thieme, D. T. Verebelyi, W. Zhang, X. Li, X. T. Kodenkandath, N, Nguyen, E. Siegal, L. Civale, T. Holesinger, B. Maiorov, A. Goyal, and Paranthaman, "Second Generation HTS Wire Based on RABiTS Substrates and MOD YBCO," *IEEE Trans. Appl. Supercond.,* vol. 15, pp. 2611-2616, 2005.

[9] M. Carrera, X. Granados, J. Amoros, R. Maynou, T. Puig, X. Oborados, "Current distribution in HTSC tapes obtained by inverse problem calculation, " *Journal of Physics: Conference Series* **234** (2010) 012009.

11th European Conference on Applied Superconductivity (EUCAS2013) IOP Publishing
Journal of Physics: Conference Series **507** (2014) 032020 doi:10.1088/1742-6596/507/3/032020

Long term operation in 200 m class superconducting DC power transmission test facility in Chubu University

M Hamabe, H Watanabe, J Sun, T Kawahara and S Yamaguchi
Center of Applied Superconductivity and Sustainable Energy Research, Chubu University, Kasugai, Aichi, 487-8501, Japan

E-mail: hamabe@isc.chubu.ac.jp

Abstract. We constructed the 200 m class superconducting DC power transmission test facility (CASER-2) in 2010, and have carried out the cooling down and operation test. The 5th cooling down and operation test was carried out from August to November 2012. Long term current feeding was tested for a month with various currents and temperatures in the 5th test. From the long term current feeding test, the LN2 circulation was clearly affected by the operation of the cryogenic system and the atmosphere, not only by the operation DC current. It was also confirmed that the Peltier current leads worked effectively for the reduction of heat leak at the cable terminal.

1. Introduction

Recently, superconducting DC (SC-DC) power transmission is one of the attractive themes in commercial use of superconductivity, since the SC-DC power transmission is theoretically free from the AC losses, and is able to design the very large current cable for the power transmission. As a practical use, a 380 m/10 kA SC-DC cable was installed in the aluminum electrolysis system of Henan Zhongfu Industrial Co., in China[1]. The Electric Power Research Institute (EPRI) finished a design study of 10 GW SC-DC power transmission over 1000 km in U. S.[2]. Railway Technical Research Institute (RTRI) in Japan started a project to develop SC-DC power transmission system for railways[3].

In Chubu University, the first SC-DC power cable test facility (CASER-1) with a cable length of 20 m was constructed in 2006[4]. Since the first cooling down in October 2006, six cycles of cooling-down were carried out in CASER-1. The performance of the SC-DC cable showed no degradation through these cycles in that the critical currents of the HTS tapes in CASER-1 cable were in the same temperature dependence[5]. Based on the experiments in CASER-1, Chubu University constructed a new test facility of 200 m SC-DC power transmission (CASER-2) in 2010 to establish a power transmission system of a low total cryogenic energy loss[6]. This CASER-2 also has experienced cooling cycles repeatedly, and the 5th cooling cycle of the CASER-2 was carried out from August to November 2012. In this paper, we will describe the results of long term current feeding test for a month with various currents and temperatures in the 5th cooling cycle.

2. Specification of CASER-2

Table 1 shows the electric properties of CASER-2, and Table 2 shows the cryogenic properties to circulate liquid nitrogen (LN2). Figure 1 shows a photograph of a cut-model of a SC-DC cable core fabricated by Sumitomo Electric Industries, Ltd The cable consisted of co-axial three layers of DI-

11th European Conference on Applied Superconductivity (EUCAS2013) IOP Publishing
Journal of Physics: Conference Series **507** (2014) 032020 doi:10.1088/1742-6596/507/3/032020

BSCCO® HTS tapes; one outside layer of 16 tapes and two inside layers of 23 tapes were insulated by polypropylene laminated paper (PPLP®) for bipolar current feed with an insulation voltage of 20 kV in LN2. All HTS tapes were also insulated by PPLP® from the copper former and shield in the earth potential with an insulation voltage of ±10 kV. Designed total current of the cable was 2 kA at 78 K.

One of the features of CASER-2 is that the cable core was placed in the smooth cryogenic pipe with vacuum insulation[6]. Compared with the corrugated pipe, which is widely used for the cryogenic pipes of superconducting cables, the smooth pipe has the advantage to reduce the pressure drop of LN2 flow[7,8]. Moreover, we employed a zinc-coated carbon-steel pipe (216 mm in outside diameter and 5.8 mm in thickness) as the outside pipe, since the outside pipe is used in the atmosphere to keep the vacuum insulation and an expensive stainless-steel pipe is not necessary. As the inside pipe, a stainless-steel pipe (60.5 mm in outside diameter and 1.65 mm in thickness) was employed from the viewpoint of the low-temperature brittleness in a LN2 temperature. Figure 2 shows a photograph of the cryogenic system of CASER-2. Due to the employment of the smooth cryogenic pipe, low pressure drop along the 200 m cable was achieved; consequently, one Stirling type refrigerator and one LN2 pump are sufficient in CASER-2 to circulate the LN2 along the 200 m cable length.

Table 1. Electric specification of CASER-2

	Specification
Current	DC 2 kA at 78 K
Voltage	DC ± 10 kV
Cable structure	Coaxial, bipolar current feed
SC tape	39 DI-BSCCO® HTS tapes (23 tapes in inside HTS layer, and 16 tapes in outside HTS layer)
Current leads	72 Peltier current leads (46 leads in inside HTS layer and 26 leads in outside HTS layer), and 6 copper leads (all in outside HTS layer)

Table.2 Cryogenic specification of CASER-2

	Specification
Cryogenic system	Coolant is subcool LN2 LN2 was circulated by 1 LN2 pump and cooled by 1 Stirling type refrigerator
Cooling power	1 kW @ 77 K (COP=0.083 @ 77K)
Cryogenic pipe	Vacuum insulated double pipe Outside pipe: Zn-coated steel pipe / Inside pipe: stainless-steel pipe Smooth pipes with several bellows

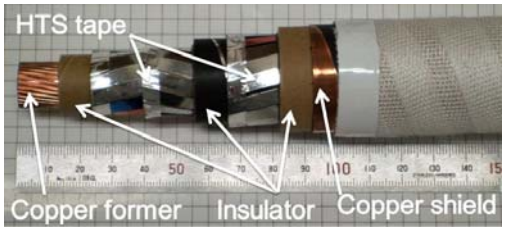

Figure 1. A cut-model of DC superconducting power cable core of CASER-2


Figure 2. Cryogenic system in CASER-2

11th European Conference on Applied Superconductivity (EUCAS2013) IOP Publishing
Journal of Physics: Conference Series **507** (2014) 032020 doi:10.1088/1742-6596/507/3/032020

3. Experimental results in long term operation test

We carried out the 5th cooling down test from August to November in 2012. During the 5th cooling down, we continuously fed the current to the SC cable from September 20th to October 22nd as a long term operation test of CASER-2. We varied operation current and temperature setting of refrigerator as parameters, and kept the speed of the LN2 pump constant, during this long term operation test. Note that the current was limited to 1200 A for the inside layer of the coaxial SC cable and to 600 A for the outside layer, because of the trouble in the connection between the current lead and the power supply.

Figure 3 shows the time evolution of (a) operation current, (b) LN2 temperatures in cryogenic system for the various temperature settings of refrigerator, (c) LN2 flow rate, (d) temperature rise along the 200 m cryopipe as cable line, (e) heat leak on the 200 m cryopipe, (f) temperature rise in and out of the cable terminal B, and (g) heat leak on the terminal B.

From the comparison of figures 3 (a)~(c), the LN2 temperature decreased due to the decrease of refrigerator setting, and increased due to the increase of the operation current. The decrease of LN2 temperature leads to the decrease of the viscosity of LN2. Therefore, the LN2 flow rate also varied following the variation of the LN2 temperature, despite of the constant LN2 pump speed. When the heat leak is stable, the temperature rise along the cryopipe and the cable terminal is inversely proportional to the LN2 flow rate. In figures (d) and (f), the temperature rises shows the undulating

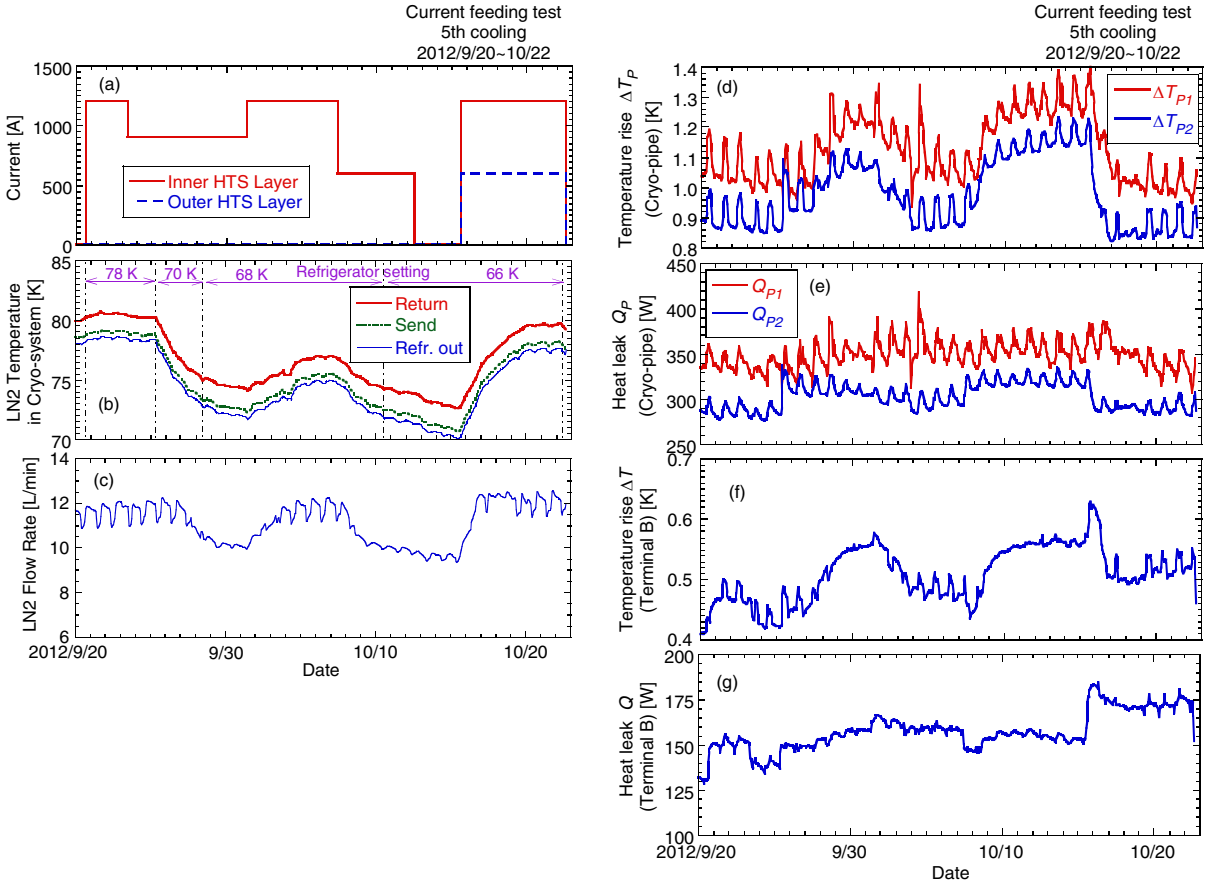

Figure 3. Time evolution of (a) operation current, (b) LN2 temperatures in cryogenic system (refrigerator out, send into and return out of the cable) for the various temperature settings of refrigerator, (c) LN2 flow rate, (d) temperature rise and (e) heat leak along the 200 m cryopipe as cable line, (f) temperature rise and (g) heat leak on the terminal B. In (d) and (e), suffixes 1 and 2 show the data derived from the temperatures of the top and bottom of the cryopipe, respectively.

time evolutions inversely following the variation of the LN2 flow rate.

Figures 3 (c) ~ (g) also shows the spike-like variations with the cycles of 1 day, in particular for (d) and (e). In CASER-2, 80% of the cryopipe was placed outside of the building, and then the temperature of the cryopipe surface was affected by temperature of atmosphere. This variation of the cryopipe temperature led to the daily variation of the heat leak into the cryopipe, in particular as the radiation heat, and also affected to the temperatures of terminals and the LN2 flow rate; consequently, they showed the spike-like daily variations.

The heat leak in the terminal B (figure 3 (g)) slightly increased when only the inside HTS layer operated with a current to 1200 A. This is because the Peltier heat of the Peltier current leads (PCLs) [9] in the cable terminal (Table 1) suppressed the Joule heating due to the operation current. Contrastingly, the heat leak in the terminal B clearly increased when a 600 A current was fed to the outside HTS layer. This was because the current leads in the outside HTS layer included 6 copper leads and Joule heating of copper leads led to the increase of the heat leak in the cable terminal.

4. Conclusion

We carried out the 5th cooling down in 200 m class SC-DC power transmission test facility（CASER-2) from August to November in 2012. During the 5th cooling down, a long term current feeding test was continued for 1 month with varying the operation current and the temperature setting of the refrigerator in the cryosystem. This long term operation clearly showed the relationship of the operation current, the operation temperature of the cryogenic system and the LN2 circulation. In addition, the LN2 circulation was affected by the atmosphere, in particular in the heat leak at the cryopipe; therefore, the LN2 circulation showed the daily variations. It was also confirmed that the PCLs worked effectively to suppress the heat leak at the cable terminal.

Acknowledgement

Parts of this work were supported by a grant of Strategic Research Foundation Grant-aided Project for Private Universities, by Ministry of Education, Culture, Sports, Science and Technology (MEXT).

References

[1] Liang XM, Dai ST, Gao ZY, Song NH, Wang YS, Zhang D, et al., 2010 Design of a 380 m DC HTS power cable. *IEEE Trans. Appl. Supercond.* **20** 1259–62.

[2] Hassenzahl W, Daneshpooy A, Eckroad S, Grant P, Gregory B, Nilsson S 2009 Program on Technology Innovation: A Superconducting DC Cable. *EPRI Report 2009*; 1020458.

[3] Tomita M, Suzuki K, Fukumoto Y, Ishihara A, Muralidhar M 2011 Next generation of prototype direct current superconducting cable for railway system. *J. Appl. Phys*. **109** 063909.

[4] Yamaguchi S, Hamabe M, Yamamoto I, Famakinwa T, Sasaki A, Iiyoshi A, et al., 2008 Research activities of DC superconducting power transmission line in Chubu University. *Jour. of Phys.: Conf. Ser.* **97** 012290.

[5] Hamabe M, Fujii T, Sugino M, Sasaki A, Sugimoto T, Watanabe H, et al., 2010 Cooling cycle test of DC superconducting power transmission cable. *Jour. of Phys.: Conf. Ser.* **234** 032019.

[6] Yamaguchi S, Kawahara T, Hamabe M, Watanabe H, Ivanov Yu, Sun J, et al., 2011 Design and construction of 200-meter high temperature superconducting DC power cable test facility in Chubu University. *Proc. the 23 Int. Cryogenic Eng. Conf. and Int. Cryogenic Mat. Conf. (Wroclaw, Poland, 18-23 July 2010)*, (Wrocław: Oficyna Wydawnicza Politechniki Wrocławskiej) 1041-47.

[7] Weisend II JG, Van Sciver SW 1990 Pressure drop from flow of cryogens in corrugated bellows. *Cryogenics* **30** 935-941

[8] Sasaki A, Hamabe M, Famakinwa T, Yamaguchi S, Radovinsky A 2008 A Numerical Analysis in LN2 Channel for DC-SC Power Transmission Line *Adv. in Cryogenic Eng.* **53A** 75-82

11th European Conference on Applied Superconductivity (EUCAS2013) IOP Publishing
Journal of Physics: Conference Series **507** (2014) 022038 doi:10.1088/1742-6596/507/2/022038

Critical current measurement of HTS tape relating with cable structure for a DC power cable

Jian Sun[1], Hirofumi Watanabe[1], Makoto Hamabe[1], Toshio Kawahara[1] and Satarou Yamaguchi[1,2]

[1]Center of Applied Superconductivity and Sustainable Energy Research, Chubu University, 1200, Matsumoto-cho, Kasugai, Aichi 4878501, Japan
[2]Department of Electrical Engineering, Chubu University, 1200, Matsumoto-cho, Kasugai, Aichi 4878501, Japan

E-mail: j_sun@isc.chubu.ac.jp

Abstract.

In the 200 m high temperature superconducting (HTS) cable test facility at Chubu University, a coaxial power cable is used and composed of two BSCCO (Bi-2223) superconducting layers. The tapes are wound closely to reduce effects on the critical current of BSCCO at self-field. Accordingly, each superconducting layer has a different number of BSCCO tapes. Previously, we have investigated dependence of the critical current (I_c) on the gap in order to optimize the HTS DC cable design. We have been studying the effect on the performance of HTS tapes for the superconducting DC power cables by critical current measurements. In the present experiments several HTS tapes are used and set as a similar structure in the cable with a two-layer structure. The critical current of HTS tapes are measured against the gap between the tapes in the same layer. The experiments show the improvement of the critical current by optimizing the tape arrangements due to magnetic field interaction between the tapes. We will present the experimental results and discuss the design of the HTS DC cable.

1. Introduction

DC superconducting power transmission system has been studied at Chubu University by using HTS tapes [1]. In the 200 m HTS cable system, called as CASER-2, a coaxial cable is used as shown in Fig. 1, which is made of BSCCO tapes by Sumitomo Electric Industries (SEI) [2]. There are 23 tapes with a two-layer structure for the inner HTS conductor and 16 tapes with a mono-layer structure for the outer one in consideration of the gap effect on the critical current of the tapes in the cable, which affects the rated current of the cable. In order to optimize the structure of a HTS power cable, we have been studying the effects of tape arrangements on the critical current to improve the superconductivity characteristics of HTS tape in the cable. Previous study shows strong dependence of the critical current of BSCCO tape on the gap. The critical current of the middle tape in three straight tapes in parallel increases by 10% for a two-layer structure [3].

We continue to measure the critical currents of BSCCO tape due to HTS tape arrangements to study the effect on the performance of BSCCO tapes for the superconducting DC power cables relating with cable structure [4]. As shown in Fig. 1b, the tapes are wound crossly and there are small gaps due to the shape of the former which may degrade the performance of the

11th European Conference on Applied Superconductivity (EUCAS2013) IOP Publishing
Journal of Physics: Conference Series **507** (2014) 022038 doi:10.1088/1742-6596/507/2/022038

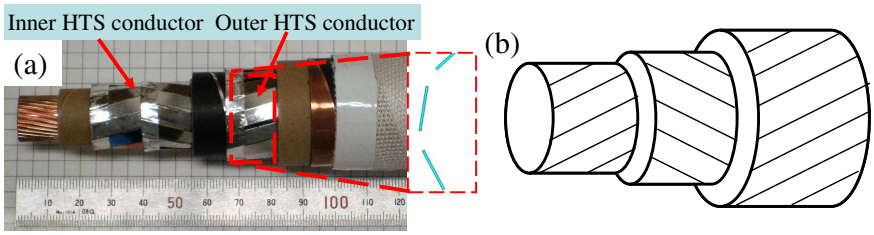

Figure 1: (a) The coaxial HTS power cable for CASER-2 and (b) A diagram of the tapes winding arrangement in the CASER-2 power cable. The insert of (a) shows gaps between HTS tapes.

tape. In this work more HTS tapes are set as a similar structure in the cable with a two-layer structure by considering the winding directions. This paper presents the I_c measurements of BSCCO tape relating with the cable structure by varying the transport current independently.

2. Experiments

BSCCO tapes are used with a cross section of 4.5 mm wide and 0.35 mm thick by SEI [5],[6]. The I_c of BSCCO tape is about 160 A at 77 K, self field. Figure 2a shows the tape arrangements with a two-layer structure for different winding directions. d is the lateral space gap between the tape edges in the same layer. The gaps are set to be 0.4 mm and 2.0 mm. Five tapes are used with a length of 27 cm and are insulated from each other by an insulating tape. Figure 2b shows a current loop applied to the five tapes conductor. Different currents are applied to the tapes by two power-supplies. The critical current of the middle tape #3 in the lower layer is measured by changing the lateral space gaps for different transport current in the neighboring tapes.

The experimental setup for the critical current measurement is similar to previous experiment [3] in which the tapes are immersed into liquid nitrogen at 77 K. Three voltage taps are attached on BSCCO tapes with distance of 8 cm and 10 cm for parallel tape conductor and 2 cm and 3 cm for cross tape conductor. The transport current is measured by a current shunt resistor. The voltage signals are measured by a KEITHLEY 2700 digital multimeter. The V - I characteristics of HTS tapes are obtained by the four-probe method.

3. Results and discussion

Figure 3 shows E-I curves of middle tape #3 for single and five parallel tape conductors with different gaps by dividing the measured voltages to the distance between the voltage taps. The

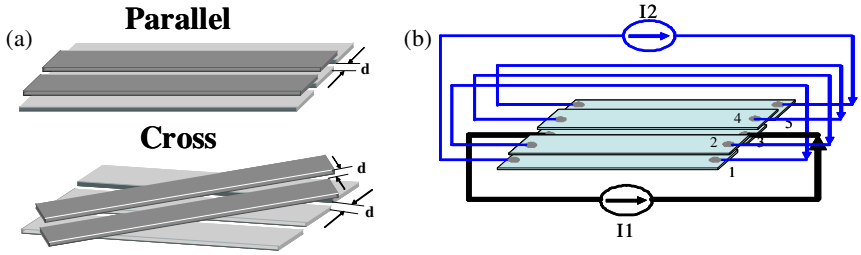

Figure 2: (a) A schematic diagram of the experimental setup for the parallel and cross tape conductors and (b) Circuit loop for the current applied to five tapes conductors. Power supply I1 is applied to tape #3 and I2 to other tapes in series mode.

11th European Conference on Applied Superconductivity (EUCAS2013) IOP Publishing
Journal of Physics: Conference Series **507** (2014) 022038 doi:10.1088/1742-6596/507/2/022038

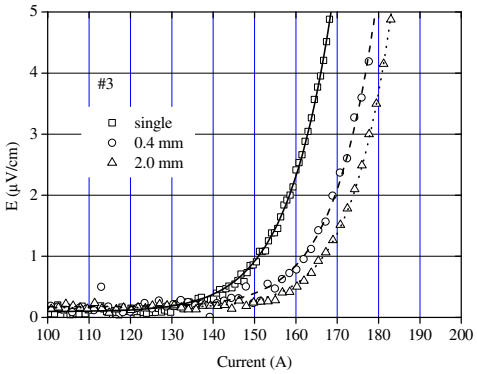

Figure 3: *E-I* curves of middle BSCCO tape in five tapes conductor with different gaps. The neighboring current $I2$ is 120 A.

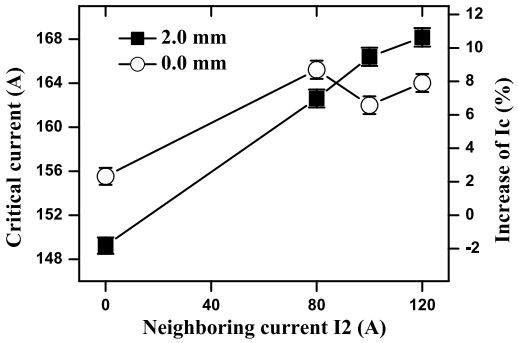

Figure 4: Dependence of the critical current of middle tape #3 in five parallel tapes conductor on the neighboring current $I2$.

transport currents in the neighboring tapes are 120 A. *E-I* curves are quite different between small and large gaps and the critical current of tape #3 in the five tapes is larger than that of a single tape. The critical current is determined on the criterion of 1 μV/cm. Figure 4 presents the dependence of the critical current of middle BSCCO tape #3 in five parallel tapes conductor on the neighboring current $I2$. When the neighboring current is larger than 80 A, the critical current becomes larger than that of a single tape. When the neighboring current is larger than 100 A, the critical current for large gap of 2.0 mm becomes larger than that for small gap of 0.4 mm. The measured critical currents of middle tape #3 increases 10% for 2.0 mm gap in the five parallel tapes arrangement and thus the critical current of BSCCO tape is improved when there are gaps between the tapes in the same layer.

We calculate the magnetic field distribution by the commercial finite element method code (ANSYS) [4, 7, 8]. Figure 5a-f present the magnetic flux lines around the five tape conductors with increasing gaps between the tapes. The transport current of 160 A is assumed to be uniformly distributed in the BSCCO filaments area. The cross section of the transport current area is assumed to be 4.5 mm × 0.25 mm for BSCCO tape by subtracting the reinforcing copper layer [6] and thus the current density is 142 A/mm^2. The magnetic flux density in the BSCCO filament area is reduced by increasing the gaps between the tapes. When the gap is 2.0 mm, about half of the tape width, neutral zone is formed in the intermediate tape in the second layer as in Fig. 5f. Therefore, the critical current in the five tape conductors is improved when there exists a gap of 2.0 mm as shown in Fig. 3 and 4.

As shown in Fig.1b, the tapes for HTS conductor are wound crossly between each layer. Five long tapes are wound around a supporter with a similar pitch as the CASER-2 power cable. Figure 6 presents the dependence on the gaps of the increase of I_c and the n-value of BSCCO tape in the five tapes conductor for different neighboring currents by comparison of the parallel and cross arrangements. The I_c of BSCCO tape is measured to be 161 A. The I_c and the n-value of BSCCO tape become larger than those of the single one. The increased I_cs of BSCCO tape by about 10% is measured for the parallel arrangement. However, the cross arrangement leads to the decrease of the I_c and the n-value of BSCCO tape. Therefore, the performance of HTS power cable can be improved by the parallel arrangement.

4. Conclusion

We investigated the critical current of BSCCO tape relating with the cable structures of gaps and winding methods for the five tapes conductor with a two-layer structure. The critical current

11th European Conference on Applied Superconductivity (EUCAS2013) IOP Publishing
Journal of Physics: Conference Series **507** (2014) 022038 doi:10.1088/1742-6596/507/2/022038

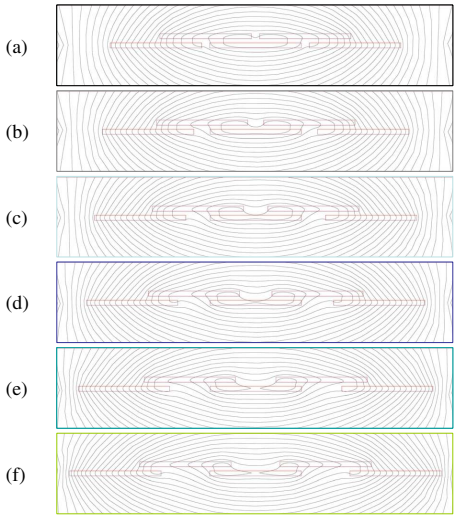

Figure 5: Magnetic flux lines around five tape conductors with increasing gaps between 0.4 mm (a) and 2.4 mm (f) by a step of 0.4 mm.

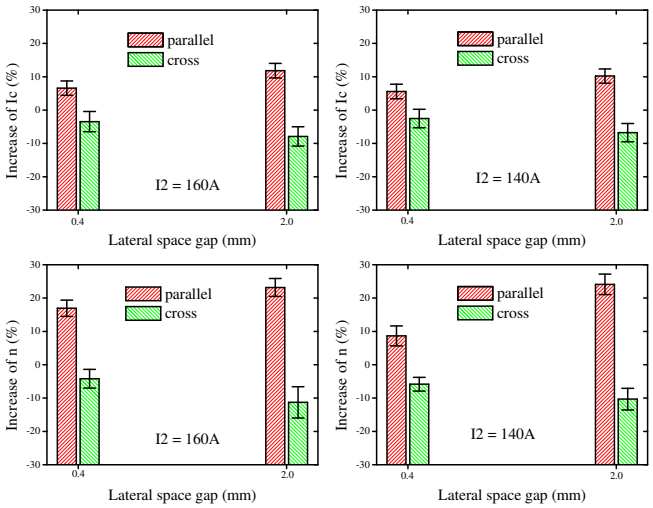

Figure 6: The dependence of increase of I_c and n-value of BSCCO tape on the gaps between the tapes for parallel and cross tapes conductor. Left: $I2 = 160$ A; Right: $I2 = 140$ A.

of BSCCO tape is improved when gaps exist for the five parallel tape conductor. The critical current and the n-value of BSCCO tape for the parallel arrangement become larger than those for the cross arrangement. Therefore fewer BSCCO tapes can be wound in parallel with gaps for a DC power cable with a two-layer structure.

Acknowledgments
The authors thank Dr. Atsuo Iiyoshi, Chancellor of Chubu University for his continuous encouragement through this work. We acknowledge Dr. Hiroshi Fujiwara for his support on the construction of 200 m superconducting facilities of CASER-2. Parts of this work were supported by a grant of Strategic Research Foundation Grant-aided Project for Private Universities, by Ministry of Education, Culture, Sports, Science and Technology (MEXT).

References

[1] Yamaguchi S, Hamabe M, Yamamoto I, Famakinwa T, Sasaki A, Iiyoshi A, Schultz J, Minervini J, Hoshino T, Ishiguro Y and Kawamura K 2008 *J. Phys.: Conf. Series* **97** 012290
[2] Yamaguchi S, Kawahara T, Hamabe M, Watanabe H, Ivanov Y, Sun J and Iiyoshi A 2011 *Phyica C: Superconductivity* **471** 1300–3
[3] Sun J, Yamauchi S, Sugino M, Watanabe H, Hamabe M, Kawahara T and Yamaguchi S 2011 *Physica C: Superconductivity* **471** 1313–6
[4] Sun J, Watanabe H, Hamabe M, Kawahara T, Iiyoshi A and Yamaguchi S 2012 *Phys. Proc.* **36** 372–5
[5] Kikuchi M, Ayai N, Fujikami J, Kobayashi S, Yamazaki K, Yamada S, Ishida T, Kato T, Hayashi K, Sato K, Hata R, Iihara J and Yamaguchi K, Kumakura H, Kitaguchi H, Osamura K and Shimoyama J 2008 *AIP Conf. Proc.* **986** 407–15
[6] Ayai N, Yamazaki K, Kikuchi M, Osabe G, Takaaze H, Takayama H, Kobayashi S, Fujikami J, Hayashi, Sato K, Osamura K, Kitaguchi H, Matsumoto S, Kiyoshi T and Shimoyama J 2009 *IEEE Trans. Appl. Supercond.* **19** 3014–7
[7] ANSYS® Academic Teaching Advanced, Release 12.1 ANSYS Inc. www.ansys.com
[8] Farinon S, Fabbricatore P and Gömöry 2010 *Supercond. Sci. Technol.* **23** 115004

GRAND RENEWABLE ENERGY 2014 Proceedings
27 July - 1 August, 2014
Tokyo Big Sight, Tokyo Japan

P-Pe-3-5

DEVELOPMENT OF THE SUPERCONDUCTING DC POWER TRANSMISSION SYSTEM FOR THE RENEWABLE ENERGY

Hirofumi Watanabe[1], Yury V. Ivanov[1], Makoto Hamabe[1], Noriko Chikumoto[1], Toshio Kawahara[1], Hirohisa Takano[1], Satarou Yamaguchi[1], Kenji Itaka[2], Yasubumi Furuya[2] and Hideomi Koinuma[3]

[1]Chubu University, Kasugai, 487-8501 Japan
[2]Hirosaki University, Aomori, 030-0813 Japan
[3]University of Tokyo, Kashiwa, 277-8561 Japan

The superconducting DC power transmission is an efficient way to send electricity for a long distance, which is ideal for the transmission of the electricity generated by the renewable energies. For the long distance superconducting DC power transmission, the reduction of the heat leak of the cryogenic pipe and that of the pressure drop of the circulating refrigerant are particularly important. A 200 m class superconducting DC power transmission test facility has been constructed at Chubu University. The heat leak and pressure drop measurements, recently performed, were promptly reported together with the results performed previously.

Keywords: superconducting DC power transmission, superconductivity, renewable energy

INTRODUCTION

The shortage of natural resources producing energy such as oil, natural gas and so on near the future has been recognized as an urgent problem to be solved in recent years. Moreover, the use of the fossil fuels emits the carbon dioxide and a lot of the use of them is considered to cause a global warming problem, which leads to the change of climate drastically. It is considered that we have to make a society which does not rely on the fossil fuels too much. One of the resolutions for these problems is the use of the renewable energies. The renewable energies will not be exhausted and does not emit the carbon dioxide. However there are several issues to be solved to use the renewable energies. The examples are the unstable output of these energies for their dependence on the weather and the distance from the places which are appropriate for the power generation to the industrial areas and cities which consume the energy a lot. The unstable output can be stabilized by the use of batteries and the other ways of the energy storage. On the other hand, since the weathers of different places are usually different, the unstable output can be stabilized by the exchange of the electricity in the wide range of area. If we look at Europa, for example, the areas appropriate for the wind power generation are offshore of the coast of North Sea and those for the photovoltaic and solar thermal power generations are the desert like the Sahara [1]. These places are far from the industrial areas and cities in the center of the western Europa. Therefore, the long distance power transmission systems with high efficiency will be required for the efficient use of the renewable energies.

The superconducting DC power transmission is one of the resolutions for these issues. Since it uses the property of the superconductivity that the electric resistance is zero, the Joule heat, which is one of the primary origins of the energy loss in the conventional power transmission, is zero. Therefore, the transmission loss of the superconducting power transmission can be reduced significantly in the case of the long distance power transmission. However to utilize the property of the superconductivity, the cable have to be cooled down, at least, to the liquid nitrogen temperature. The heat leak to the low temperature parts can be a main source of the energy loss, because the heat by the heat leak has to be pumped out by a cryocooler and the power required to operate the cryocooler will be the loss of the transmission. Therefore the heat leak reduction of the system is important to make the efficiency of the system higher. In the case of the long distance power transmission, the heat leak of the cryogenic pipe constituting the transmission line becomes relatively large in comparison with the other parts of the system. Therefore the heat leak reduction of the cryogenic pipe is particularly important [2].

The distance of the superconducting DC power transmission can be limited by the pressure drop of the circulating refrigerant [3], which is caused by the friction between the inner surface of the cryogenic pipe and the circulating refrigerant. The pressure drop is proportional to the third power of the transmission distance, provided the temperature rise of the refrigerant between the inlet and the outlet of the cryogenic pipe is the same to keep the temperature of the refrigerant below the critical temperature of the cable. If the pressure drop is large, the large pump with high discharge pressure should be required. Therefore the issues caused by the pressure drop could change the design of the cryogenic pipe and the circulation system. The estimation of the pressure drop is important for the long distance superconducting DC power transmission.

We have been studying the superconducting DC power transmission systems and constructed a 200 m class superconducting DC power transmission test facility at Chubu University, which we call CASER-2 [2, 4]. In this paper we will introduce our research concerning the heat leak and the pressure drop for the development of the long distance superconducting DC power transmission for the use of the renewable energies.

GRAND RENEWABLE ENERGY 2014 Proceedings
27 July - 1 August, 2014
Tokyo Big Sight, Tokyo Japan

200M CLASS SUPERCONDUCTING DC POWER TRANSMISSION TEST FACILITY (CASER-2)

Fig.1 shows the layout of CASER-2, details of which were explained in elsewhere [2, 4, 5]. The distance of transmission, that is the length of the cryogenic pipe, is about 200 m. Terminals are placed side by side in the laboratory, where current leads are installed to feed electricity to the cable. Almost all the cryogenic pipe, which stretches from the terminals, is installed in the outdoors as the L-shaped configuration. The cryogenic pipe runs parallel and there is a turn with the radius of about 2 m at about 100 m from the laboratory.

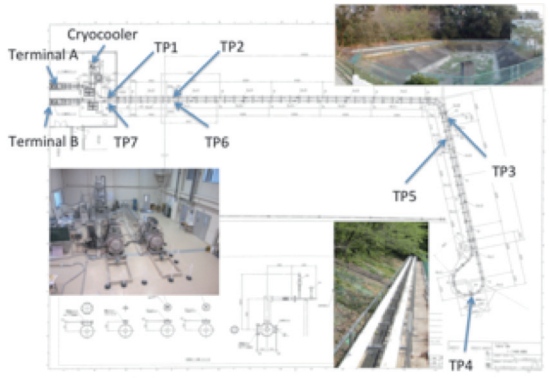

Fig.1: The layout of CASER-2. TP1-TP7 are the positions of the sensors to measure the liquid nitrogen temperature.

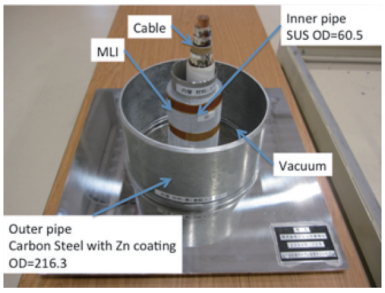

Fig.2: The cross sectional model of the cryogenic pipe of CASER-2.

Fig. 2 shows a cross sectional model of the cryogenic pipe of CASER-2. The cryogenic pipe is double pipes. The space between the double pipes is evacuated for the vacuum insulation. The vacuum is kept below 0.05 Pa to achieve sufficient vacuum insulation [6]. The inner pipe is made of stainless steel pipes with the nominal outer diameter of 60.5 mm and, in part, made of bellows pipes to compensate the thermal shrinkage. The smooth straight pipes are adopted for the inner pipe, which is contrasted with the conventional cryogenic pipes for the superconducting power transmission using corrugated pipes. The adoption of the smooth straight pipes can reduce the pressure drop of the circulating refrigerant [7]. The cable is installed in the inner pipe, which is cooled by the liquid nitrogen flowing in the inner pipe. Multi-layer insulation is wrapped around the inner pipe to reduce the radiative heat transfer. The inner structures are supported by fiber reinforced plastic rods and plates to the outer pipe. The outer pipe is made of carbon steel pipes with the nominal outer diameter of 216.3 mm.

Along the cryogenic pipe and at the terminals, several sensors are equipped, including temperature sensors, pressure gauges and a differential pressure gauge for liquid nitrogen. In Fig. 1 the positions at which temperatures of liquid nitrogen are measured are shown as TP1-TP7. We usually use the sensors at TP1 and TP7 to estimate the heat leak of the cryogenic pipe. The distance between TP1 and TP7 is approximately 175 m. The pressure gauges are installed at the terminals for the measurement of the inlet and outlet pressures of the cryogenic pipe, which are used for the pressure drop measurements. A differential pressure gauge is also installed between the terminals to measure pressure drop accurately.

A cryocooler system is installed in the laboratory beside the terminal A. The system has a pump, a Coriolis flow meter and two reserver tanks. The cryocooler is Stirling type, whose cooling power is about 1 kW at 77 K. The terminal A is equiped with a GM type auxiliary cryocooler with the cooling power of 180 W at 77 K to cool the terminal separately. The pump can circulate liquid nitrogen with the flow rate from 3 to 27 l/min. The maximum discharge pressure of the pump is 0.11 MPa.

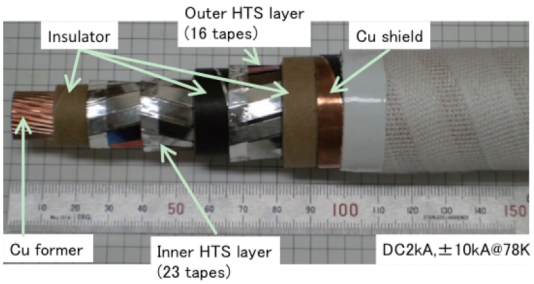

Fig.3: The superconducting DC power transmission cable used in CASER-2.

The cable for the superconducting DC power transmission is shown in Fig. 3. Bismuth based high temperature superconducting (HTS) tapes are used as conductors. The cable is coaxial and bipolar. The inner layer has two layers, which is composed of 23 HTS tapes in total, and the outer HTS layer has one layer, which is composed of 16 HTS tapes. These tapes are wound spirally around the copper former which gives mechanical strength to the cable. The outer and inner layers are insulated mutually and also insulated from the earth. The rated current and voltage of the cable is 2 kA and ±10kV at 78 K.

Peltier current leads (PCLs) are used for the current leads at the terminals. Thermoelectric material of bismuth telluride is used in the PCLs. Low thermal conductivity of bismuth telluride and the Peltier effect at the time when the current is supplied reduce the heat leak in comparison with the conventional copper current leads

RESEARCH TOWARDS THE LONG DISTANCE TRANSMISSION

We completed the construction of CASER-2 and started a cooling test on January 2010. The cooling tests

have been performed five times by the end of 2012. The cooling tests include the tests of the thermal insulation, the current feeding, the liquid nitrogen circulation, the cooling procedure and so on. From this summer of 2014, 6th cooling test was started. Two experiments performed in the 6th cooling test will be promptly reported, to introduce the heat leak and pressure drop measurements.

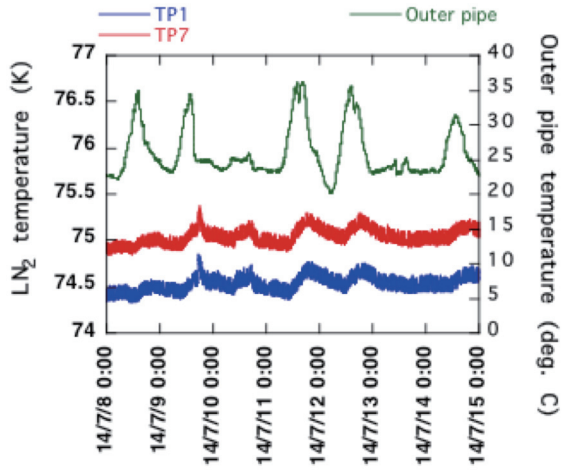

Fig.4: The variation of the liquid nitrogen temperature between TP1 and TP7 in Fig. 1, together with that of the outer pipe temperature.

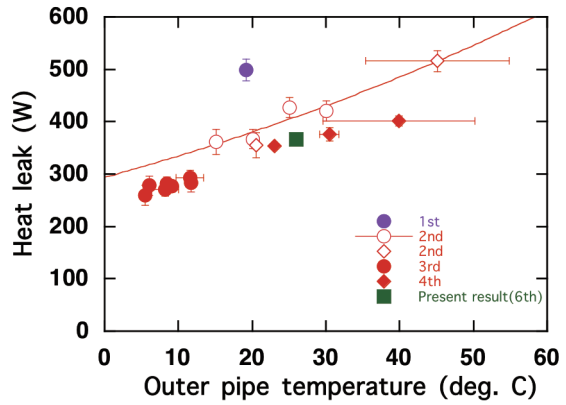

Fig.5: The heat leak measured between TP1 and TP7. The results from 1st to 4th cooling tests were reported by Watanabe et al [2].

Fig. 4 shows the liquid nitrogen temperatures measured at TP1 and TP7 and the outer pipe temperature. As seen in the figure, the variations of liquid nitrogen temperature follows that of the outer pipe temperature, which is due to the change of the heat leak by the outer pipe temperature. The heat leak, ΔQ, is written as

$$\Delta Q = \rho q_v C_p \Delta T \qquad (1)$$

where ρ is the density and C_p is specific heat of liquid nitrogen. q_v is the flow rate and ΔT is the temperature rise, which are obtained from the experiment. The difference of the liquid nitrogen temperature between TP1 and TP7 is approximately 0.51 K during the period shown in the figure and the flow rate was approximately 26 l/min. Therefore the heat leak of this period is estimated to be about 370 W. In Fig. 5 the heat leak measured from 1st to 6th cooling tests are summarized with respect to the outer pipe temperature [2] The heat leak increases with the increase of the outer pipe temperature due to the increase of the radiative and conductive heat transfers. As seen in the figure, the result obtained in the 6th cooling test is consistent with the previous results. From the 1st to 6th cooling tests, the heat leak is notably reduced. This is due to the improvements of the cryogenic pipe performed between the cooling tests. Further reduction of the heat leak is expected for the long distance superconducting DC power transmission. Recently new designs of the cryogenic pipes for the superconducting DC power transmission project started in Ishikari area in Japan were reported, together with the results of the heat leak measurements with test pipes. With the designs, the heat leak was significantly reduced [8].

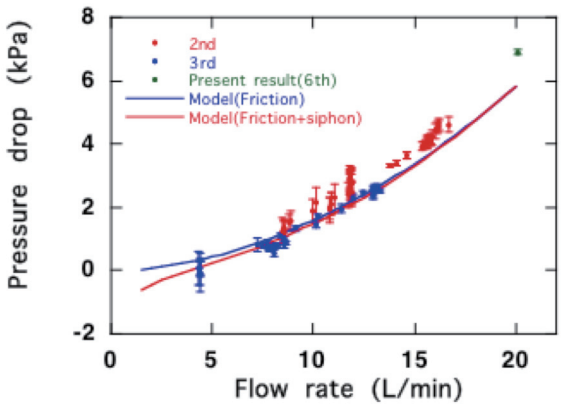

Fig.6: The pressure drop of liquid nitrogen by the circulation from the terminal A to the terminal B. The results in 2nd and 3rd cooling tests and the theoretical results were reported by Ivanov et al [3].

Fig. 6 shows the pressure drops of liquid nitrogen during the circulation in the cryogenic pipe between the terminals. The present result was measured with the differential pressure gauge installed between the terminals. The measurement was performed at the flow rate of 20 l/min. In the figure the results obtained in the 2nd and 3rd cooling tests are also shown together with the theoretical results, the details of which are explained by Ivanov et al [3]. The pressure drops measured previously are the pressure difference of the terminals measured with the pressure gauges. The theoretical results were calculated based on the Darcy-Weisbach formula as

$$\Delta P = f \frac{L}{D_h} \frac{\rho v^2}{2} \qquad (2)$$

where f is the friction factor, D_h is the hydraulic diameter, and v is the flow velocity. The friction factor depends on the flow velocity weakly and on the roughness of the cable surface and the pipe inside surface, which can be calculated with semi-empirical formulae [3].

At the low flow rate region in Fig. 6, the pressure drops are small and even take negative values. This means that the circulation was promoted in the cryogenic pipe. It is considered that the thermal siphon effect was

promoting the circulation in the low flow rate region [9]. The theoretical result considering the thermal siphon effect well explains the behavior of the pressure drop in the low flow rate region. The pressure drop is nearly proportional to the second power of the flow velocity, i.e. the flow rate as shown in eq. (2). The pressure drops increase quickly with the increase of the flow rate. It reaches about 7 kPa at the flow rate of 20 l/min. This value is slightly larger than the theoretical results. This might be originated from the underestimation of the friction between the liquid nitrogen and the structures in the inner pipe of the cryogenic pipe. Accumulation of data in the wide range of the flow rate is expected to predict the behavior of the pressure drop accurately.

SUMMARY

The superconducting DC power transmission is one of the solutions for the efficient use of the renewable energies. We constructed the 200 m class superconducting DC power transmission system, CASER-2, at Chubu University. Several tests have been performed with CASER-2. In this paper the heat leak and pressure drop measurements recently performed were promptly reported. The reduction of the heat leak and the pressure drop of the cryogenic pipe is particularly important for the long distance superconducting DC power transmission.

ACKNOWLEDGEMENTS

The authors thank Dr. Atsuo Iiyoshi, Chancellor of Chubu University, for his continuous encouragement throughout this work. The authors acknowledge Dr. Hiroshi Fujiwara for his financial support for our project. We also thank JFE Steel Corporation for supplying carbon steel pipes for the construction of CASER-2. Parts of this work were supported by a grant from the Strategic Research Foundation Grant-aided Project for Private Universities Ministry of Education, Culture, Sports, Science and Technology, Japan.

References

[1] A. B. Stambouli and H. Koinuma, “A primary study on a long-term vision and strategy for the realization and the development of the Sahara Solar Breeder project in Algeria”, *Renewable and Sustainable Energy Reviews*, 2012, pp. 591-598.

[2] H. Watanabe et al., “Cooling of the 200 m superconducting DC power transmission system at Chubu University”, *Physics Procedia*. **27**, 2012, pp.376-379.

[3] Y. Ivanov et al., “Design study of LN_2 circulation in a long SC power transmission lines”, *Physics Procedia*. **36**, 2012, pp.1372-1377.

[4] S. Yamaguchi et al., “Experiment of 200-meter superconducting DC cable system in Chubu University”, *Physica C*. **471**, 2011, pp.1300-1303.

[5] H. Watanabe et al., “Heat leak measurement of the 200 m superconducting DC power transmission system at Chubu University”, *Physics Procedia*. **36**, 2012, pp.1366-1371.

[6] P. J. Sun et al., “Experimental study of the influences of degraded vacuum on multilayer insulation blankets”, *Cryogenics*. **49**, 2009, pp.719-726.

[7] A. Sasaki et al., “A numerical analysis in LN2 channel for DC-SC power transmission line”, *AIP Conference Proceedings*. **985**, 2008, pp.75-82.

[8] H. Watanabe et al., “Thermal insulation test of new designed cryogenic pipes for the superconducting DC power transmission system in Ishikari, Japan”, *presented at 25th ICEC-ICMC2014*. 2014, Tue-Af-P1.3-18.

[9] Y. Ivanov et al., “Observation of the thermosiphon effect in the circulation of liquid nitrogen in HTS cable cooling system”, *Physics Procedia*. **27**, 2012, pp.368-371.

Materials Science Forum Vols. 778-780 (2014) pp 767-770
© (2014) Trans Tech Publications, Switzerland
doi:10.4028/www.scientific.net/MSF.778-780.767

Effects of machining fluid on electric discharge machining of SiC ingot

Norimasa Yamamoto[1,a,*], Satarou Yamaguchi[2,a], Tomohisa Kato[3,c,d]

[1]Center of Applied Superconductivity & Sustainable Energy Research, Chubu University, 1200 Matsumoto-cho, Kasugai, Aichi 487-8501 Japan

[2] R&D Partnership for Future Power Electronics Technology, Central2, 1-1-1 Umezono, Tsukuba, Ibaraki 305-8568 Japan

[3]National Institute of Advanced Industrial and Technology, Central2, 1-1-1 Umezono, Tsukuba, Ibaraki 305-8568 Japan

[a]yamamoto-no@isc.chubu.ac.jp, [b]yamax@isc.chubu.ac.jp, [c]t-kato@aist.go.jp, *corresponding author

Keywords: electronic discharge machining, ingot slicing, kerf loss

Abstract. Recently, ingots of silicon carbide have been adapted to be sliced by the wire-cut electrical discharge machining. Fast slicing, and the reduction in the loss are important for slicing of the wafer. In this paper, characteristic features of the electric discharge machining in the ion-exchange water and the fluorine-based fluid were compared for these improvement. The discharge was caused by a pulse voltage applied to a ingot of silicon carbide and the wire in machining fluid, and the slicing was proceeded. As a result, improvement of surface roughness and kerf loss was confirmed, for the first time. In addition, the improving methods for fast slicing were considered.

Introduction

In order to slice a silicon carbide material for semiconductor, the wire-cut electric discharge machining (EDM) has been adapted [1-4]. Multi-wire system in the EDM also is developed as with wire saw [3,4]. In general, techniques of low-loss and the speeding-up in a wafer slicing are important. Furthermore, the reduction in the kerf loss and improvement of surface roughness are required. The reduction in kerf loss means that a number of cutout wafers from an ingot are increased. The size of the kerf loss depends on the wire diameter and breakdown distance. By using fine wire, the broadening was strongly reduced [2]. The improvement of surface flatness was confirmed by making polishing process after slicing to be shorter. The slicing speed depends on voltage, discharge current, and these frequency. There is limitation of the slicing speed by the power supply. Therefore, a suggestion in increasing of the slicing speed by adding other effect during discharge is necessary. In fact, the cutting speed depends on kinds of gases in the case of EDM with gas atmosphere. The improvement of the cutting speed was confirmed by gas atmosphere of tetrafluoromethane, CF_4 [5]. CF_4 is a gas that is applied to the dry etching of semiconductor. In this paper, improvement on the kerf loss and surface roughness, and the speeding-up of the cutting speed in fluorine-based fluid are studied.

Experimental

The EDM instrument for experiments is consists of the numerical control part of DWC90G (Mitsubishi co.) and the power supply generating pulse voltage [6]. Pulse voltage value, and the pulse width for the electric discharge were adjusted by the power supply. Copper alloyed wire with diameter of 200 μm or 300 μm were applied to EDM experiment. Feeding velocity of the wire is 6-8 m/min. Silicon carbide ingot of 2-inch diameter was provided from AIST. The ingots were sliced as a wafer with thickness of 2.8 mm. Characteristic features of the EDM were obtained by cutting the wafer as slab as shown in Fig. 1(a). Machining fluid is passed along the line of the wire as shown in Fig. 1(b). Resistivity of ion-exchange water is roughly 10^3 Ωm. As fluorine-based fluid, 3M™ Fluorinert™

FC-3283 is adopted. Property of material is summarized in Table 1. Since breakdown field of Fluorinert is larger than that of ion-exchange water, reduction of in the kerf loss is expected. Improvement on surface flatness also is expected by the high resistivity. Flow rates of machining fluid were 10 ml/min for Fluorinert and 100 ml/min for ion-exchange water, which was an effect to to cooling of the wire by large specific heat. Voltage and discharge current between the wire and the material were measured with an oscilloscope.

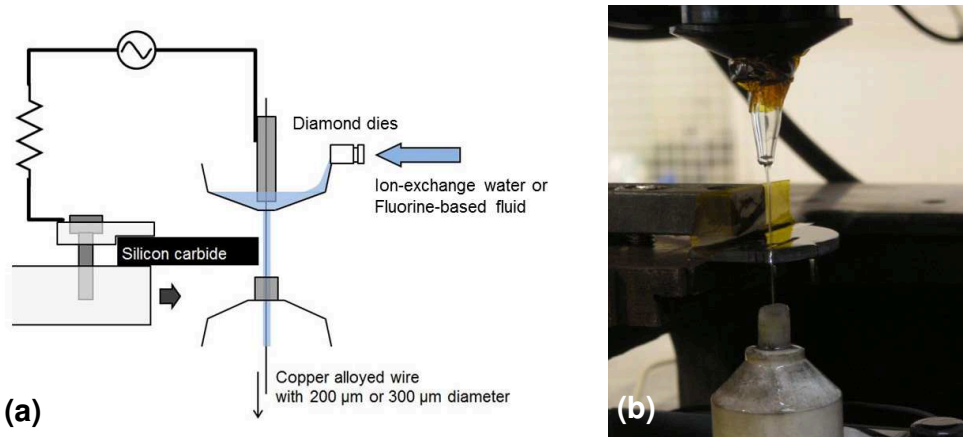

Figure 1. Schematic image (a) and photograph during discharge (b).

Table 1. Summary of specific charactereistics of machining fluid.

Machining fluid	Breakdown field ($kV \cdot cm^{-1}$)	Resistivity ($\Omega \cdot m$)	Specific heat ($J \cdot kg^{-1} \cdot K^{-1}$)	Surface tension ($mN \cdot m^{-1}$)
Fluorinert (FC-3283)	169	$>10^{13}$	1050	73
Ion-exchange water	< 30	$\sim 10^{3}$	4.2	16

Results and discussion

Figure 2 shows the cutting volume a discharge pulse in Fluorinert and ion-exchange water. Current I is proportional to voltage, E. For discharge current up to 3 A, the cutting volume in ion-exchange water is propotional to E^2. On the other hand, the cutting volume in Fluorinert is found to be proportional to E. Therefore, the cutting speed in Fluorinert increased insufficiently. It is considered that it has not been heated to a temperature sufficient to cutting SiC in Fluorinert. The effect of the etching becomes weaker under low temperature. In order to generate high temperature plasma, a large discharge current over 3 A is considered to be required.

Figure 3 shows top-view photograph of a slit. Kerf loss by cutting in ion-exchange water is 253.1 ± 2.4 μm, and that in Fluorinert is 228.3 ± 2.8 μm. In Fluorinert, reduction in 25 μm was found. By large break down field of Fluorinert, the kerf loss is considered to became narrower.

Surface roughness of R_a and R_z are shown in Figure 4. R_a is the calculated average roughness and R_z is the maximum height. In Fluorinert, R_a and R_z were 0.459 ± 0.035 μm and 3.626 ± 0.198 μm, respectively. In ion-exchange water, R_a and R_z were 0.982 ± 0.068 μm and 6.383 ± 0.749 μm, respectively. The surface roughness in Fluorinertis almost half of ion-exchange water. By higher resistivity of Fluorinert, surface roughness is considered to be improved.

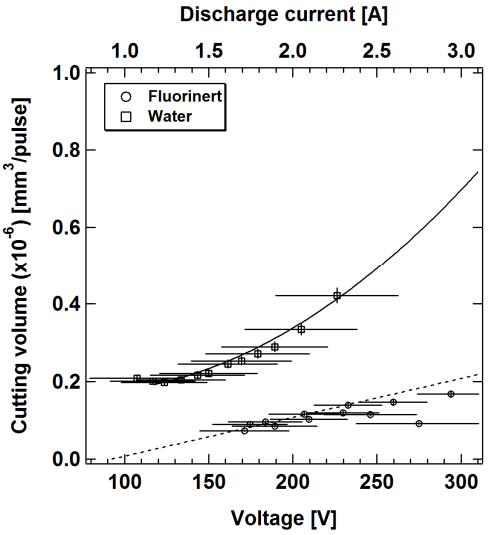

Figure 2. The cutting volume per a discharge pulse for the case of Fluorinert (open circle) and ion-exchange water (open square). Solid and dashed curves are functions to be propotional to E^2 and E, respectively.

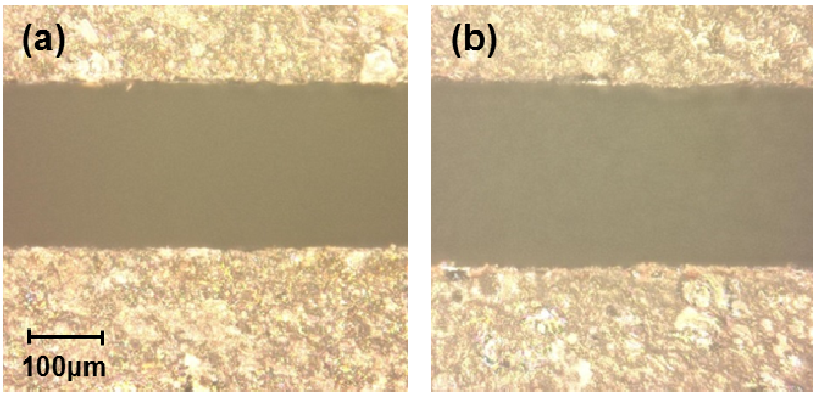

Figure 3. Top view photograph of the slit of SiC material with the optical microscope for the case of Fluorinert (a) and ion-exchange water (b)

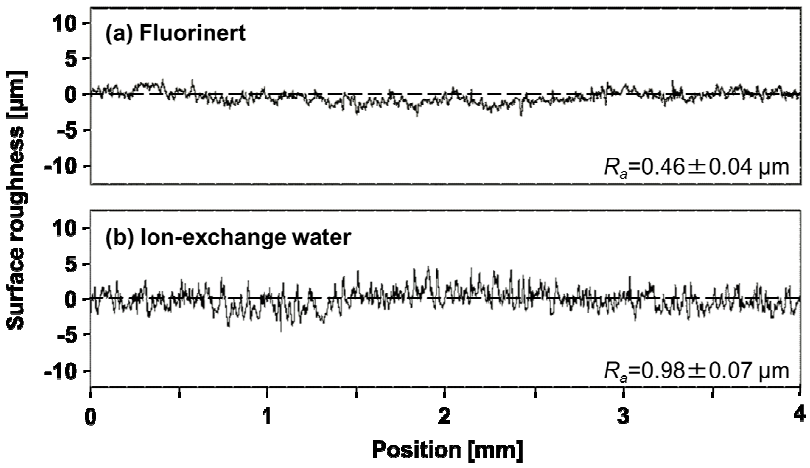

Figure 4. Surface roughness of the cutted SiC for the case of Fluorinert (a) and ion-exchange water (b).

Summary

In this paper, characteristic features of cutting in fluorine-based fluid were investigated and were compared with these in ion-exchange water. Voltage and current dependences of the cutting volume per discharge pulse in Fluorinert were different with that in ion-exchange water. Improvement of cutting speed by the effect of the etching in fluorine-based fluid is found for the case of discharge of large discharge currents. The kerf loss in Fluorinert was 20 μm narrower than that in ion-exchange water. Surface roughness (R_a) in Fluorinert was as low as, which is almost half of that in the conventional water.

Acknowledgements

This work is supported by Novel Semiconductor Power Electronics Project Realizing Low Carbon Emission Society under Ministry of Economy, Trade and Industry (METI) and New Energy and Industrial Technology Development Organization (NEDO). The authors thank to Mr. K. Uchimura and Mr. Y. Furuhashi for help to perform the experiment.

References

[1] H. Yamada, S. Yamaguchi, N. Yamamoto, T. Kato, Mater. Sci. Forum **717-720**, 861 (2013).

[2] N. Yamamoto, T. Kato, S. Yamaguchi, Mater. Sci. Forum **740-742**, 843 (2013).

[3] Y. Horie, M. Fuchiyama, Y. Tawa, N. Yoshikawa, T. Kato, abstract book of SiC and Related Materials Researches 20nd Conference, P-64 (2011).

[4] A. Itokazu et al., Mater. Sci. Forum **740-742**, 841 (2013).

[5] T. Sugimoto, T. Noro, S. Yamaguchi, H. Majima, Mater. Sci. Forum **645-648**, 869 (2010).

[6] S. Yamaguchi, T. Noro, H. Takahashi, H. Majima, Y. Nagao, K. Ishikawa, Y. Zhou, T. Kato, Mater. Sci. Forum **600-603**, 851 (2009).

En&Mat 6

Cooling experiments of the 200 m-class superconducting direct current transmission and distribution system of CASER-2

Toshio Kawahara [a,c], Masahiko Emoto [b], Hirofumi Watanabe [a], Makoto Hamabe [a], Mohamed Tallouli [c], Satarou Yamaguchi [a,c]

[a] Center of Applied Superconductivity and Sustainable Energy Research, Chubu University, Aichi 487-8501, Japan
[b] Department of Large Helical Device Project, National Institute for Fusion Science, Gifu 509-5292, Japan
[c] Department of Electrical and Electronic Engineering, Chubu University, Aichi 487-8501, Japan
E-mail: toshi@isc.chubu.ac.jp

Abstract

Superconducting transmission and distribution (T&D) system is one of the key technologies for effective use of natural energy and saving energy. The realization of superconducting T&D systems requires the low heat leak cryogenics for the high performance operation. In Chubu University, we have developed 200 m-class superconducting direct current (DC) transmission test device of CAER-2, following to 20 m-class superconducting DC transmission device (CASER-1), for the experiments of actual evidence of the low heat leak superconducting systems with several advanced cryogenics. The performance of such applied systems is determined by two large heat leaks, which are in the cryogenic pipes keeping the superconducting cable inside and at the terminals where the superconducting cable is connected to the outside systems at room temperature. We discuss about the thermal performance of the system during cooling experiments. The current of 2.0 kA was successfully fed into the CASER-2 system and we also obtained heat leak measurements at the terminals. In addition, we will discuss about the initial cooling from the operational point of view.

Keywords: superconducting transmission line, sustainable energy, applied superconductivity, cryogenics

1. Introduction

The energy problems should be solved urgently for the future world. Superconducting applications are highly demanded for energy saving in order to solve global environmental issues. Among these applications, long-distance superconducting transmission systems seem to be one of the most promising for energy saving by energy sharing. On the other hand, such large systems can be built up from smaller network systems, which can be enhanced by scaling up to the superconducting grid. For the development of superconducting transmission systems, there are several projects in Japan, the U.S., Korea and China, such as those pertaining to long-distance, high-voltage and/or grid cooperation systems [1-3]. For example, Albany projects successfully transmitted electric power to 70,000 homes in New York State [2]. Yokohama projects in Japan will represent a field test of superconducting transmission lines [3]. Direct current projects are also planned at an aluminum factory by the Chinese Academy of Science. Chubu University has already developed a 20-m class superconducting direct current (DC) superconducting transmission device (CASER-1) [4] and has proposed several technologies to improve system performance of superconducting applications. Discussions have been made concerning the current balance of superconducting tapes as stable transmission systems, low-heat leak systems using special cryogenic double pipes, etc. [5,6].

For actual applications, reducing heat leak to the low temperature part is the most important aspect of technology for high-performance superconducting applications. For long-distance transmission lines, the main heat leaks can

be reduced by high-performance cryogenic pipes [5]. On the other hand, heat leak reduction at the terminal for small-length applications is a key goal for actual uses such as those involving the high-performance current lead [7-10]. At Chubu University, we are developing a 200 m-class superconducting DC transmission and distribution system (CASER-2) following our development of the 20 m-class CASER-1 system.

In this paper, we discuss about the thermal performance of the system during cooling experiments. The current of 2.0 kA was successfully fed into the CASER-2 system and we also obtained heat leak measurements at the terminals until 1.5 kA. In addition, we will discuss about the initial cooling from the operational point of view.

2. Cooling experiments in CASER-2

We constructed CASER-2 between August 2009 and January 2010. From January to March of 2010, we first conducted cooling experiments and estimated the system performance of CASER-2. We show the temperature along the cryogenic pipe and the electric field induced in the cable in the first few days in the first cooling experiment in January (Fig. 1). Within a week, the whole system was cooled down to the liquid nitrogen temperature and superconducting cables went into the superconducting state, where the electric field on the cable was zero. In March, we successfully conducted a 1.2 kA current feeding test in a superconducting state in the system. Following the first cooling experiment, we performed 2nd and 3rd experiments. The heat leaks are summarized in Fig. 2, which shows the dependence of the heat leak on outside environmental temperature. The 3rd experiment indicated that improved multi-layer insulators and reducing spacers for inner pipes could reduce the heat leak. In the 5th cooling experiment, LN2 was transferred from the center of the cryostat during initial cooling for the usability. The system was also cooled down successfully as shown in Fig. 3.

The current of 2.0 kA was successfully fed into the CASER-2 system. Figure 4 shows the result of the current feeding test of the cable. The current was applied to the outer HTS layer in the cable at the temperature of the liquid nitrogen between 76.8 and 79.0 K. The labels of S1-1 to S1-16 are to identify the HTS tapes in the outer HTS layer. The left axis shows the voltage induced along the HTS tapes, which was measured between both the ends of the cable. As seen in the figure, the voltage was not induced, which means that the cable was in the superconducting state. The current was safely applied to the specification of the cable (2 kA).

We also obtained heat leak measurements at the terminals until 1.5 kA. Firstly, we will show the temperature distribution on the current lead without feeding a current in Fig. 5. The large temperature difference on the BiTe modules is observed both for n- and p-type. The mild slope of the temperature distribution on the copper pert in the PCL means the small heat leak on the current lead. Contrary, the Cu lead has a large slope of the temperature distribution, which was caused by the large heat leak.

Next we show the feeding current dependence of the heat leak on the terminals in Fig. 6. Above 800 A, the steep increase of the heat leak was observed. Therefore, the optimum condition for the current lead seems to be around 800 A. There is a small difference of the heat leak between the terminals A and B, because of the difference of the shape factor of the current lead for the optimum current. Since the over current condition caused the large heat leak, the further optimum design of the current lead such as thermoelectric parameters, thermal configurations and so forth will be required. On the other hand, below its optimum current, we reduced the heat leak effectively on the terminals, which lead to enhance the performance of the superconducting T&D systems.

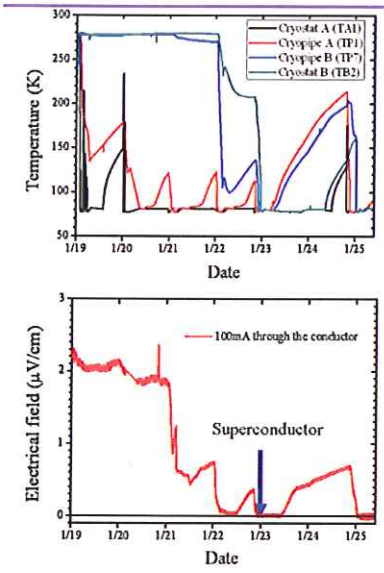

Fig. 1: First cooling experiment.

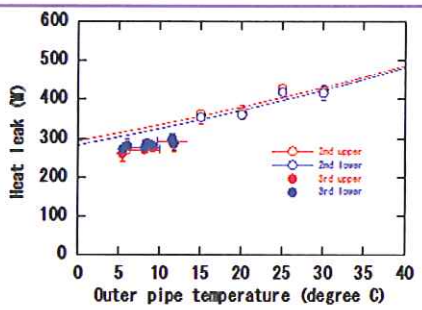

Fig. 2: Heat leak at cryogenic pipes. Upper and lower thermometers were attached to the top and bottom of the pipes, respectively

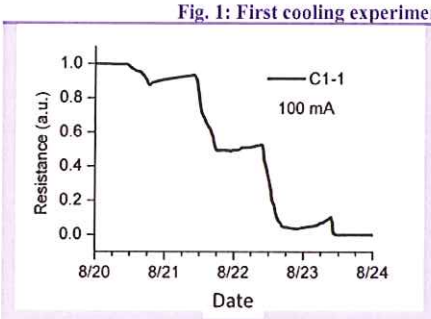

Fig. 3: 5th cooling experiment.

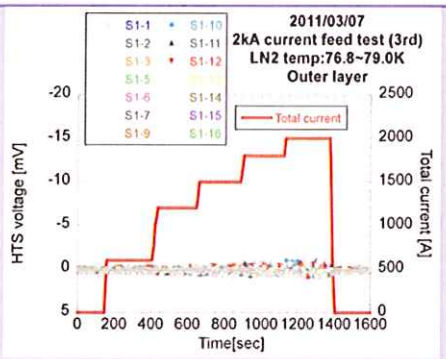

Fig. 4: The current applied to the cable and the voltage induced along the HTS tapes in the outer layer of the cable.

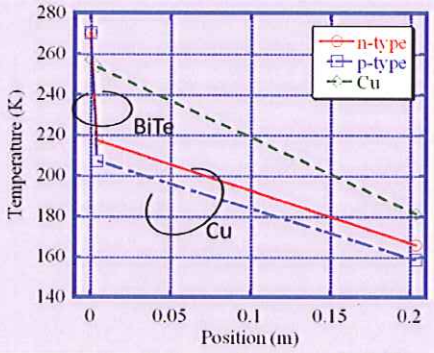

Fig. 5: Temperature distribution on the current lead. Those for PCL with n- and p-types, and also copper lead are plotted.

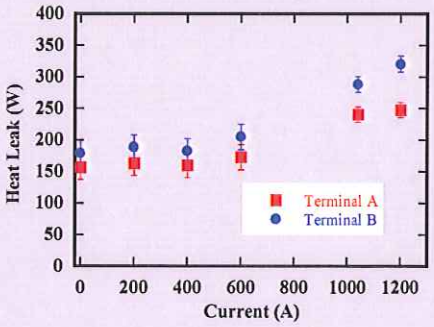

Fig. 6: Current dependence of the heat leak on the terminals. Squares and circles are for Terminals A and B, respectively.

3. Summary

CASER building was constructed at March 3, 2009, and we have developed the 200 m-class superconducting T&D system from 2010. We already had 5th cooling experiments after the first cooling experiment at 2010 (January ~ March). We have obtained many basic cooling data for the actual cooling in CASER-2 with several re-construction of the system, and the system performance was fully estimated including the cooling procedure and so forth. They seem to be useful for the future superconducting system to archive the sustainable world.

Acknowledgements

The authors thank Prof. A. Iiyoshi of Chubu University for his continuous encouragement throughout this work. We acknowledge Dr. Hiroshi Fujiwara for his support on the construction of the 200-m superconducting facilities of CASER-2. Parts of this work were supported by a grant from the Strategic Research Foundation Grant-aided Project for Private Universities, Ministry of Education, Culture, Sports, Science and Technology (MEXT), and a Grant-in-Aid for challenging Exploratory Research (MEXT). Portions of the work were also supported by the Nippon Sheet Glass Foundation for Materials Science and Engineering, and the Future Energy Research Association.

References

[1] Mukoyama, S., Yagi, M., Ichikawa, M., Torii, S., Takahashi, T., Suzuki, H. and Yasuda, K. (2007) Experimental results of a 500mHTS power cable field test. *IEEE Trans. Appl. Supercond.* **17**, 1680-1683.

[2] Masuda, T., Yumura, H., Watanabe, M., Takigawa, H., Ashibe, Y., Suzawa, C., Ito, H., Hirose, M., Sato, K., Isojima, S., Weber, C., Lee, R. and Moscovic, J. (2007) Fabrication and installation results for Albany HTS cable *IEEE Trans. Appl. Supercond.* **17**, 1648-1651.

[3] Honjo, S., Mimura, T., Kitoh, Y., Noguchi, Y., Masuda, T., Yumura, H., Watanabe, M., Ikeuchi, M. and Yaguchi, H. (2010) Status of Superconducting Cable Demonstration Project in Japan *IEEE/CSC & ESAS Eur. Supercond. News Forum (ESNF)* **14**, ST201.

[4] Yamaguchi, S., Hamabe, M., Yamamoto, I., Famakinwa, T., Sasaki, A., Iiyoshi, A., Shultz, J., Minervini, J., Hoshino, T., Ishiguro, Y. and Kawamura, K. (2008) Research activities of DC superconducting power transmission line in Chubu University *J. Phys.: Conf. Ser.* **97**, 012290.

[5] Hamabe, M., Nasu, Y., Ninomiya, A., Ishiguro, Y., Kusaka, S. and Yamaguchi, S. (2008) Radiation heat measurement on thermally-isolated double-pipe for DC superconducting power transmission *Adv. in Cryo. Eng.* **53A**, 168-173.

[6] Hamabe, M., Fujii, T., Yamamoto, I., Sasaki, A., Nasu, Y., Yamaguchi, S., Ninomiya, A., Hoshino, T., Ishiguro, Y. and Kawamura K. (2009) Recent Progress of Experiment on DC Superconducting Power Transmission Line in Chubu University *IEEE Trans. Appl. Supercond.* **19**, 1778-1781.

[7] Yamaguchi, S., Yamaguchi, T., Nakamura, K., Hasegawa, Y., Okumura, H. and Sato, K. (2004) Peltier current lead experiments and their applications for superconducting magnets *Rev. Sci. Instrum.* **75**, 207-212.

[8] Xuan, X. C., Ng, K. C., Yap, C. and Chua, H. T. (2002) On minimizing the heat leak of current leads in cryogenic vacuum systems *Cryogenics* **42**, 779-785.

[9] Kawahara, T., Fujii, T., Emoto, M., Hamabe, M., Watanabe, H., Sun, J., Ivanov, Y. and Yamaguchi, S. (2011) Double Peltier Current Lead for Heat Leak Reduction at the Terminals for Superconducting Direct Current Applications *IEEE Trans. Appl. Supercond.* **21**, 1070-1073.

[10] Kawahara, T., Emoto, M., Watanabe, H., Hamabe, M., Yamaguchi, S., Hikichi, Y. and Minowa, M. (2013) Developments of Peltier current lead for 200 m-class superconducting direct current transmission and distribution system *J. Electron. Mater.* **42**, 2337-2342.

Physica C 494 (2013) 297–301

Contents lists available at SciVerse ScienceDirect

Physica C

journal homepage: www.elsevier.com/locate/physc

Critical current behavior of a BSCCO tape in the stacked conductors under different current feeding mode

J. Sun [a,*], H. Watanabe [a], M. Hamabe [a], N. Yamamoto [a], T. Kawahara [a], S. Yamaguchi [a,b]

[a] Center of Applied Superconductivity and Sustainable Energy Research, Chubu University, 1200, Matsumoto-cho, Kasugai, Aichi 487-8501, Japan
[b] Department of Electrical Engineering, Chubu University, 1200, Matsumoto-cho, Kasugai, Aichi 487-8501, Japan

ARTICLE INFO

Article history:
Accepted 9 April 2013
Available online 25 April 2013

Keywords:
BSCCO
Critical current
DC power transmission
HTS cable
Stacked conductor

ABSTRACT

In the 200 m high temperature superconducting cable test facility, BSCCO tapes with the critical current of 160 A in self field are used for the two superconducting conductors corresponding to each polarity of DC power transmission. In order to improve the cable property by tape configuration, we have investigated the critical current of a BSCCO tape with different structures. Previous study shows that the critical current of BSCCO tape decreases by 15% for the 3-layer stack structure. However, the stack structures are needed to obtain high current capacity of a cable. Therefore we study the performance of BSCCO tape in the stacked tapes conductor. The insulated tapes are arranged in a tape-above-tape structure and different currents are applied to each tape. The critical current of the target sample is measured by the four probe method by immersing the samples into liquid nitrogen bath. The experiments show that the improvement and degradation of the critical current of BSCCO tape in the stacked conductor are observed under different current feeding mode due to the magnetic field interactions between the tapes. The critical current of BSCCO in the stacked conductor is enhanced by 50% to more than 230 A under the opposite-direction current feeding mode.

1. Introduction

A first DC high temperature superconducting (HTS) power cable was built at Chubu University [1], which is called as CASER-1. In 2009, a 200 m DC HTS cable system, called as CASER-2, was successfully constructed for the performance evaluation [2]. Fig. 1 presents a photo of a DC coaxial power cable for CASER-2 and Table 1 shows the specifications of the cable made by Sumitomo Electric Industries (SEI). In the DC HTS cable system, the coaxial cable is used and BSCCO (Bi-2223) tapes are spirally and closely wound around a former as two superconducting conductors for each polarity of the DC electric power [3]. The number of the tapes in each conductor is different because of their different radii. In order to design a HTS power cable especially for DC electric power transmission, we started to investigate the critical current of the HTS tapes [4].

The magnetic field effect is not isotropic especially for the Bi-2223 tape conductor [5], which consequently affects the characteristics of the tape conductor in the cable due to the magnetic field from the other tape conductors. To enhance the performance of the cable, the diameter of the cable must be small and the effect of the magnetic field becomes stronger [6]. In order to improve the cable property by the tape arrangements, the performance of the HTS tapes for the DC power cable was investigated through the critical current measurements [4].

Previously, we investigated the critical current of BSCCO tape in the parallel arrangements of three straight BSCCO tapes with a mono-layer and multi-layer structure to optimize the layout of the HTS tapes in the cable [7]. The performance of BSCCO tapes with a stacked structure degrades compared to that with a mono-layer and a two-layer structure. The critical current of BSCCO tape decreases by 15% when the transport current is applied to each tape in series mode. However, the HTS tapes with the stacked structures in the cable have high current capacity which is needed for large power transmission. Over a decade ago Fleshler et al. observed enhancement of the critical current of a BSCCO tape from 134 A to 210 A when the tape was sandwiched between other tapes with current flowing in the opposite direction [8]. Target of this technical paper is to study the effect of the current feeding mode on the performance of BSCCO tape with higher critical current in a stacked conductor. The insulated tapes are arranged in a tape-on-tape structure and different currents are applied to each tape. The critical current of the target sample is measured by the four probe method by immersing the samples into liquid nitrogen bath. The improvement and degradation of both the critical current and the *n*-value of BSCCO tape are observed by varing the transport current applied to the other tapes in the stacked conductor. By

* Corresponding author. Tel.: +81 568 51 9286; fax: +81 568 51 9413.
E-mail address: j_sun@isc.chubu.ac.jp (J. Sun).

0921-4534/$ - see front matter © 2013 Elsevier B.V. All rights reserved.
http://dx.doi.org/10.1016/j.physc.2013.04.031

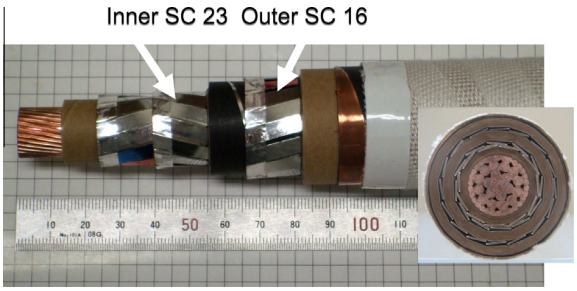

Fig. 1. A photo of a co-axial power cable for the CASER-2. The inset shows the cross sectional image of the cable. There are 23 BSCCO tapes for the inner superconducting (SC) layer and 16 BSCCO tapes for the outer SC layer by Sumitomo Electric Industries (SEI).

Table 1
Specifications of the CASER-2 power cable.

CASER-2 HTS cable	
Rated current	DC 2 kA 78 K
Rated voltage	DC ±10 kV
Length	200 m
Cable structure	Coaxial 3-layer cable
HTS tape	DI-BSCCO tapes Inner: 11/12; Outer 16

using the magnetic field calculation and the experimental results of the magnetic field effect, we can analysis the characteristics of BSSCO tape in the stacked conductor to improve the superconductivity for DC power cable applications. We will present the experimental results and analyze the magnetic field interactions between the tapes.

2. Samples and experiments

In the experiment, the samples are BSCCO tapes from those of the 200 m cable for the CASER-2. Bi-2223 tapes (Type HT-CA) are made by the method of the powder in tube (PIT) with the controlled over pressure sintering technique by SEI [9]. The cross section of BSCCO tape is 4.5 mm × 0.35 mm. The critical current of BSCCO tape is 160 A in self-field at 77 K. The HTS tape used is a reinforced tape in which two copper layers with 0.05 mm thick are laminated on both sides of the silver-sheathed multi-filamentary Bi-2223 matrix area to improve the mechanical strength of the tape.

Fig. 2 shows a scheme of the experimental setup for the critical current measurement, which is similar with that in the previous report [4]. Three tapes with a length of ~27 mm are prepared and surrounded with a single layer of the insulation tape. The tapes are arranged as a stacked structure as shown in the inset of Fig. 2.

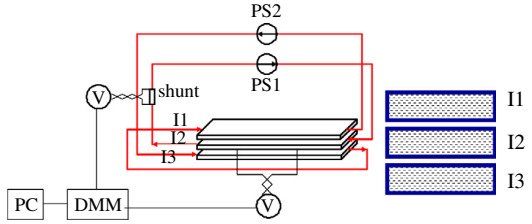

Fig. 2. A scheme of the experimental setup for the critical current measurement in the three-layer stacked conductor. The transport current applied to tape I_1 and tape I_3 are controlled by power supply (PS2) and the transport current for tape I_2 is controlled by PS1. The critical current is measured by four probe method.

Three voltage taps are soldered on each tape with the distance of 8 cm and 10 cm. Two power supplies (PS) are used to control the current feeding mode in the three-layer stacked conductor. The PS1 is used for the current feeding to middle BSCCO tape (I_2) and the PS2 for upper and down BSCCO tapes in series ($I_1 = I_3$). The transport current is measured by a current shunt resistor. The voltage signals are measured by a KEITHLEY 2700 digital multi-meter (DMM). The *V–I* curves are measured with the standard four-probe method by immersing the samples into a bath filled with the liquid nitrogen.

3. Results and discussion

3.1. Experimental results

By normalizing to the distance between the voltage taps, we obtain *E–I* characteristics of BSCCO tape. Fig. 3 shows comparisons of *E–I* curves of BSCCO tape for single and three-layer stacked tape conductor with different neighboring current of 140 A and −140 A. The significant difference of the critical current of BSCCO tape between the three-layer stacked conductors and single one is shown when the currents in the adjacent tapes are changed. The solid lines are the fitted curves by an equation of

$$E = E_0 \left(\frac{I}{I_c}\right)^n \quad (1)$$

Here, E is electric field, E_0 = 1 μV/cm, I transport current, I_c the critical current. When the neighboring current is 140 A, similar behavior can been seen compared to previous study [7]. The critical current of BSCCO tape in the three-stacked tapes conductor becomes less than that of single one. However, in the case of neighboring current of −140 A, the critical current of the central tape in the three-stacked tape conductor becomes larger than that of single one.

The critical current is determined at the electric field criterion of 1 μV/cm. Fig. 4a summarizes the critical currents of BSCCO tape with respect to the currents applied to the neighboring tapes in three-layer stacked conductor. The neighboring current is the current I_1 and I_3 applied to upper and down tapes as shown in Fig. 2. Fig. 4b shows the increase of the critical current as a function of the neighboring current. The critical current of single BSCCO tape is measured to be 161 A. As shown in Fig. 4a, the critical current of middle BSCCO tape in the three-layer stacked conductor shows strong dependence on the neighboring current. When the same-direction currents are applied to each tape in the three-layer stacked conductor, the critical current declines to less than 140 A, which shows a similar behavior compared to that in the previous report [7]. However, when the current of the opposite direction is applied, the critical current of middle tape in three-layer

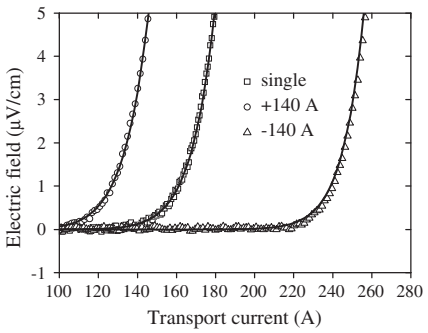

Fig. 3. *E–I* curves of BSCCO tape for single and stacked tape conductors with different currents (−140 A and 140 A) applied to the adjacent BSCCO tapes.

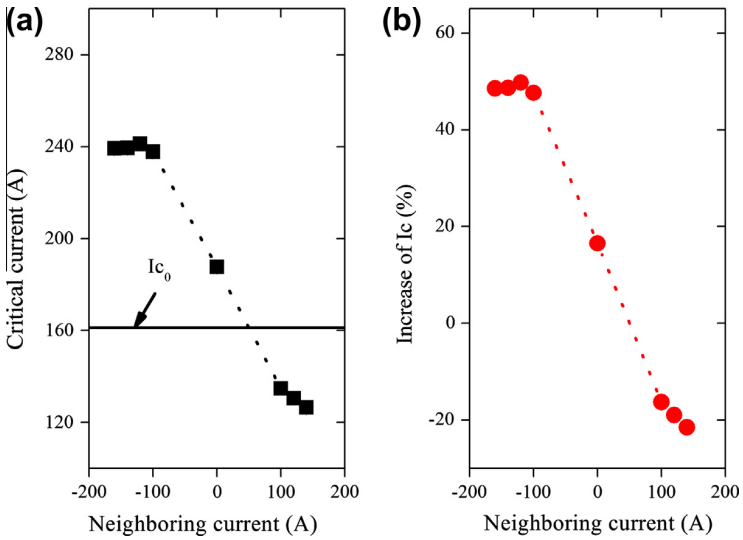

Fig. 4. (a) The critical current of BSCCO tape with respect to the neighboring current in the other tapes for three-layer stacked conductor. (b) The increase of the critical current with respect to the neighboring current.

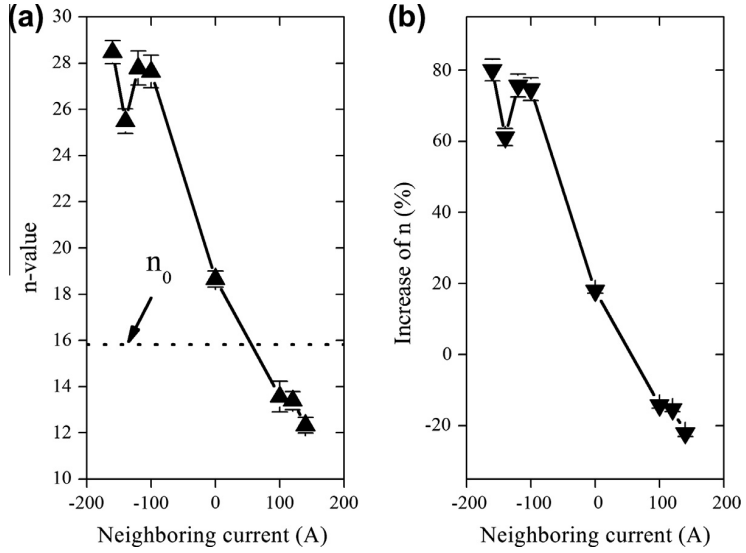

Fig. 5. (a) The *n*-value of BSCCO tape in three-layer stacked conductor as a function of the neighboring current. (b) The increase of the *n*-value with respect to the neighboring current for three-layer stacked conductor.

stacked conductor increases sharply to larger than 220 A compared to that of single one. When no current is applied to the upper and down tapes, the critical current of BSCCO tape becomes 17% larger than that of single one because of the magnetic shielding effect from the upper and down BSCCO tapes [10]. The critical current can be sharply improved by about 50% when the opposite-direction current feeding mode is applied to the three-layer stacked tape conductor in contrast to decrease by 20% for the same-direction current feeding mode as shown in Fig. 4b.

Fig. 5a shows the *n*-value of middle BSCCO tape in the three-layer stacked conductor with respect to the neighboring current. The *n*-value of single BSCCO tape is measured to be 15.8. Fig. 5b shows the increase of the *n*-value of middle BSCCO tape in the three-layer stacked conductor compared to that of single one. When the opposite-direction currents are applied to three-layer stacked conductor, the *n*-value increases sharply by 60% to larger than 25. On the other hand, the same-direction current feeding mode leads to decrease of the *n*-value. Fig. 5b shows a reduction of more than 14% in the *n*-value of middle BSCCO tape for three-layer stacked conductor.

Neighboring current dependence of the critical current and the *n*-value of middle BSCCO tape in the three-layer stacked conductor shows similar behavior as in Figs. 4 and 5. As comparing with a single tape, the three-layer stacked conductor presents the different characteristics of the critical current and the *n*-value for middle BSCCO tape because of the magnetic field effect from the currents in the neighboring tapes [11]. It is well known the fact that a magnetic field applied to a HTS tape surface causes the reduction of the critical current especially for perpendicular component of the magnetic field [12].

3.2. Calculation of magnetic field interaction

In order to analyze the improvement of the critical current in the three-layer stacked conductor due to the opposite-direction current feeding mode, the magnetic field distribution is calculated

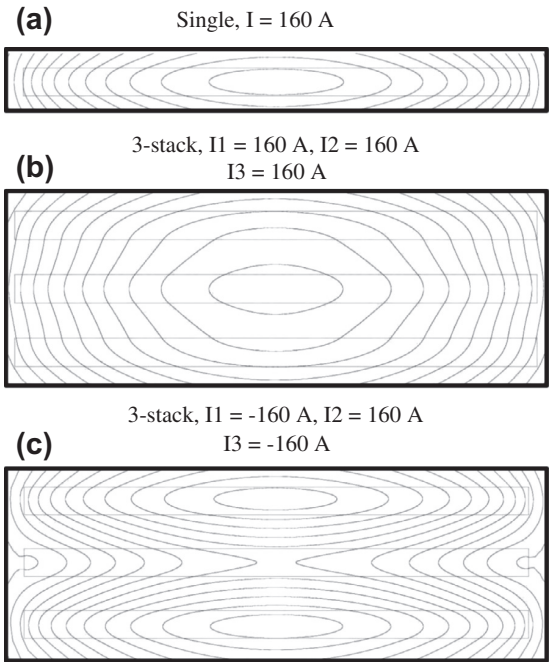

Fig. 6. Calculated magnetic flux lines by finite element method ANSYS code [13] for (a) single tape, (b) three-layer stacked tape conductors with the same direction current feeding, and (c) three-layer stacked tape conductor with the opposite direction current feeding. The transport current of each tape in (a) $I_2 = 160$ A, (b) $I_1 = I_2 = I_3 = 160$ A, and (c) $I_1 = -I_2 = I_3 = 160$ A.

Table 2
The sum (B_{sum}) and perpendicular component (B_{per}) of the magnetic flux density at the tape edge are calculated for a single tape and three-layer stacked tape conductor. Significant decrease of the perpendicular component is shown for the opposite-direction current feeding mode.

Conductor	Current feeding mode	B_{sum} (T)	B_{per} (T)
Single tape	–	0.025	0.022
Stacked tape	Same-direction	0.056	0.054
condutor	Opposite-direction	0.013	0.007

for a stacked conductor and a single tape under different current feeding mode. To study the magnetic field interaction between the tapes in the three-layer stacked conductor, the magnetic field distributions are calculated by the finite element method ANSYS code [13,14]. The transport current is simply assumed to be uniformly distributed in the silver sheathed BSCCO filaments area. The current is set to be 160 A for each tape, which transports through a cross section of 4.5 mm width and 0.25 mm thickness without the reinforcing copper layer [9]. Therefore the current density is 1.422×10^8 A/m^2. The mesh size in the area for transport current is chosen to be 10 μm due to the limit of memory size of the computer.

To illustrate the effect on self-field from the current in the neighboring tapes, Fig. 6a–c present the magnetic flux lines for single and three-layer stacked tapes conductor with different current feeding modes. Compared with the magnetic field for a single tape, the magnetic fields of the middle tape are enhanced as seen in Fig. 6b for same-direction current feeding to the three-layer stacked conductor. However, as shown in Fig. 6c, the magnetic fields around the middle tape become neutral due to the effects of the neighboring current, which results in the great improvement of the critical current as shown in Fig. 4. Hence, the opposite-direction current feeding through the three-layer stacked tapes conductor could enhance the superconductivity of BSCCO tape. In the calculations, the magnetic flux density at the tape edge presents significant difference for the three-layer stacked conductor in comparison with that for a single tape. Table 2 presents the sum (B_{sum}) and perpendicular component (B_{per}) of the magnetic flux density at the tape wide surface edge for a single tape and three-layer stacked conductor. Significant decrease of the perpendicular component is shown for the opposite-direction current feeding mode. Since the critical current of BSCCO tape is affected by the magnetic field especially for the perpendicular component to the tape wide surface [12], the opposite-direction current feeding mode leads a sharp increase of the critical current as in Figs. 4 and 5.

In the case of the HTS cable for DC power transmissions and distributions, the bipolar transmission is used, which is also a kind of opposite-direction current feeding mode. As shown above, we could apply the current to a multi-layer cable with opposite current feeding between neighboring layers, which will lead to a flexible design of a DC power cable with fewer tapes.

4. Conclusions

We studied the critical current of BSSCO tape in the three-layer stacked conductors under different current feeding mode. With the opposite-direction current applied to each tape in the three-layer stacked tape conductors, the critical current of middle tape increases sharply by 50% up to more than 230 A due to the effects on self-field from the currents in the neighboring tapes compared to that of single one. In conjunction with the magnetic field distribution calculated by the finite element method, the effects on self-field from the adjacent tapes lead to the improvement and decline of the critical current of BSCCO tape in the stacked conductor compared to that of single one. The critical current is enhanced in the opposite-direction current feeding between the neighboring tapes in the stacked tape conductors and we could make a multi-layer cable with bipolar current transporting between neighboring layer for DC power transmissions and distributions.

Acknowledgements

The authors thank Dr. A. Iiyoshi, Chancellor of Chubu University for his continuous encouragement through this work. The authors acknowledge Dr. Hiroshi Fujiwara, a professor of Keio University and the president of Nano-Opt Energy Corporation, for his financial support on the construction of 200 m superconducting facilities of CASER-2. Parts of this work were supported by a grant of Strategic Research Foundation Grant-aided Project for Private Universities Ministry of Education, Culture, Sports, Science and Technology (MEXT), and Chubu University Grant (A).

References

[1] S. Yamaguchi, M. Hamabe, I. Yamamoto, T. Famakinwa, A. Sasaki, A. Iiyoshi, et al., Research activities of DC superconducting power transmission line in Chubu University, J. Phys.: Conf. Series 97 (2008) 012290.
[2] S. Yamaguchi, T. Kawahara, M. Hamabe, H. Watanabe, Y. Ivanov, J. Sun, et al., Design and construction of 200-meter high temperature superconducting DC power cable test facility in Chubu University, in: Proc. ICEC 23 – ICMC 2010, 2011, pp. 1041–1047.
[3] J. Sun, M. Emoto, K. Yoshimura, Y. Ivanov, H. Watanabe, M. Hamabe, et al., Development and operation of the measurement system for a 200 m HTS cable, in: Proc. ICEC 23 – ICMC 2010, 2011, pp. 1035–1040.
[4] J. Sun, S. Yamauchi, M. Sugino, H. Watanabe, M. Hamabe, T. Kawahara, et al., Critical current measurements for desing of superconducting DC transmission power cable, Physica C 471 (2011) 1313–1316.
[5] M. Kang, M. Koo, H. Lee, G. Cha, Current estimation of an HTS BSCCO magnet having multiple power sources based on the field dependent E–J relation, IEEE Trans. Appl. Supercond. 19 (2009) 1257–1261.

[6] M. Hamabe, A. Sasaki, T. Famakinwa, A. Ninomiya, Y. Ishiguro, S. Yamaguchi, Cryogenic system for DC superconducting power transmission line, IEEE Trans. Appl. Supercond. 17 (2007) 1722–1725.
[7] J. Sun, H. Watanabe, M. Hamabe, T. Kawahara, A. Iiyoshi, S. Yamaguchi, A new layout of HTS tapes and their critical currents for DC power cables, Phys. Proc. 27 (2012) 372–375.
[8] S. Fleshler, M. Fee, S. Spreafico, A.P. Malozemoff, Self-field effects in high critical current density BSCCO tapes, Adv. Supercond. 12 (2000) 625–630.
[9] N. Ayai, K. Yamazaki, M. Kikuchi, G. Osabe, H. Takaaze, H. Takayama, et al., Electrical and mechanical properties of DI-BSCCO type HT reinforce with metallic sheathes, IEEE Trans. Appl. Supercond. 19 (2009) 3014–3017.
[10] J.-H. Joo, S.-W. Kim, K.J. Song, C. Park, R.-K. Ko, H.-S. Kim, J.-P. Hong, S.B. Kim, Characteristics measurements of HTS tape with parallel HTS tapes, IEEE Trans. Appl. Supercond. 16 (2006) 119–122.
[11] J.-K. Lee, S.-W. Lee, M.-J. Park, G. Cha, Magnetization loss in HTS stacked tapes by various directional external magnetic fields, IEEE Trans. Appl. Supercond. 14 (2004) 630–633.
[12] N. Ayai, S. Kobayashi, M. Kikuchi, T. Ishida, J. Fujikami, K. Yamazaki, S. Yamade, K. Tatamidani, K. Hayashi, K. Sato, H. Kitaguchi, H. Kumakura, K. Osamura, J. Shimoyama, H. Kamijyo, Y. Fukumoto, Progress in performance of DI-BSCCO family, Physica C 468 (2008) 1742–1752.
[13] ANSYS® Academic Teaching Advanced, Release 12.1 ANSYS Inc. <www.ansys.com>.
[14] S. Farinon, P. Fabbricatore, F. Gömöry, Critical state and magnetization loss in multifilamentary superconductring wire solved through the commercial finite element code ANSYS, Supercond. Sci. Technol. 23 (2010) 115004.

Physica C 494 (2013) 292–296

Contents lists available at SciVerse ScienceDirect

Physica C

journal homepage: www.elsevier.com/locate/physc

Evacuation time of cryogenic pipes for superconducting power transmission

Hirofumi Watanabe *, Jian Sun, Norimasa Yamamoto, Makoto Hamabe, Toshio Kawahara, Satarou Yamaguchi

Center of Applied Superconductivity and Sustainable Energy Research, Chubu University, Kasugai, Aichi 487-8501, Japan

ARTICLE INFO

Article history:
Accepted 9 April 2013
Available online 13 May 2013

Keywords:
Cryogenic pipe
Vacuum insulation
Evacuation time
Vacuum system
Outgassing rate

ABSTRACT

The vacuum insulation has been used for the thermal insulation of cryogenic pipes for the superconducting power transmission to reduce the heat leak from the environment at the room temperature to the low temperature parts. Since the cryogenic pipes, in particular, those for long distance power transmission, are considered to be thin long pipes, it might take a long time for evacuation. To estimate the evacuation time of the long cryogenic pipes, model calculations have been performed. According to the calculations, it is found that there is an optimum condition between the pumping speed, the diameter of the outer pipe and the length of the cryogenic pipe for efficient evacuation. It is also found that, if the outgassing is suppressed enough, the evacuation can be possible within 1 week even for the long cryogenic pipe with the length of 10 km. The reduction of outgassing is particularly important for the efficient evacuation.

1. Introduction

In the superconducting power transmission, cryogenic pipes have been used for the transmission lines for thermal insulation. The cryogenic pipes are usually double pipes. The space between the double pipes is evacuated for vacuum insulation. In the viscous flow region of the vacuum, heat transfer takes place mainly through the conductive heat transfer of the gases and, thus, the heat transfer from the room temperature parts to the low temperature parts is nearly constant with respect to the vacuum degree. In the molecular flow region, since the motion of molecules or atoms conveys heat directly from the room temperature parts to the low temperature parts, the heat transfer is proportional to the density of the molecules or the atoms, that is, vacuum degree. Even if the vacuum degree is lowered further, the heat transfer cannot be zero and takes place some amount due to the domination of the radiative heat transfer. Therefore, the evacuation down to this region is needed to obtain sufficient vacuum insulation. It is said that the vacuum below 0.05 Pa should be required for the vacuum insulation [1,2].

For the long distance transmission, the cryogenic pipes are considered to be thin long pipes and it might take a long time for evacuation. We have studied the evacuation of long cryogenic pipes for the superconducting power transmission, because the evacuation should affect the design of the cryogenic pipe and the vacuum system. It is obvious that the reduction of the outgassing and the increase of the conductance of the pipe are important for efficient evacuation [3]. In this study we calculated the time needed for evacuation of long cryogenic pipes under different conditions, such as the pumping speed, the length and the diameter of the pipes. The outgassing rate used in the calculations was based on the experimental result obtained during cooling tests with a 200 m class superconducting DC power transmission system at Chubu University (CASER2) [4,5]. We discuss the details required for the efficient evacuation of cryogenic pipes.

2. CASER2 and its evacuation system

Fig. 1 shows the layout of CASER2. The details of the system and its vacuum system have been explained elsewhere [3–5]. However, the parts of the systems which are connected with this study will be introduced briefly. The cryogenic pipe of CASER2 is about 200 m, which is mainly installed in the outdoors as shown in Fig. 1. The cryogenic pipe is concentric double pipes. The space between the double pipes is evacuated for the vacuum insulation. We adopted smooth straight pipes for the double pipes, which is contrasted with the corrugated pipes commonly used for the cryogenic pipes for the superconducting power transmission [6,7]. The outer pipe is carbon steel with the inner diameter of 204.7 mm and the inner pipe is stainless steel with the outer diameter of 60.5 mm. The inner pipe is wrapped with the layers of multi-layer insulation with the total thickness of about 10 mm. Therefore the outer diameter of the inner pipe is about 80 mm effectively. The inner pipe is supported by baffles and rods installed every few meters, which might hinder the flow of gases during evacuation.

* Corresponding author. Tel.: +81 568 51 9373; fax: +81 568 51 9413.
E-mail address: h_watanabe@isc.chubu.ac.jp (H. Watanabe).

0921-4534/$ - see front matter © 2013 Elsevier B.V. All rights reserved.
http://dx.doi.org/10.1016/j.physc.2013.04.042

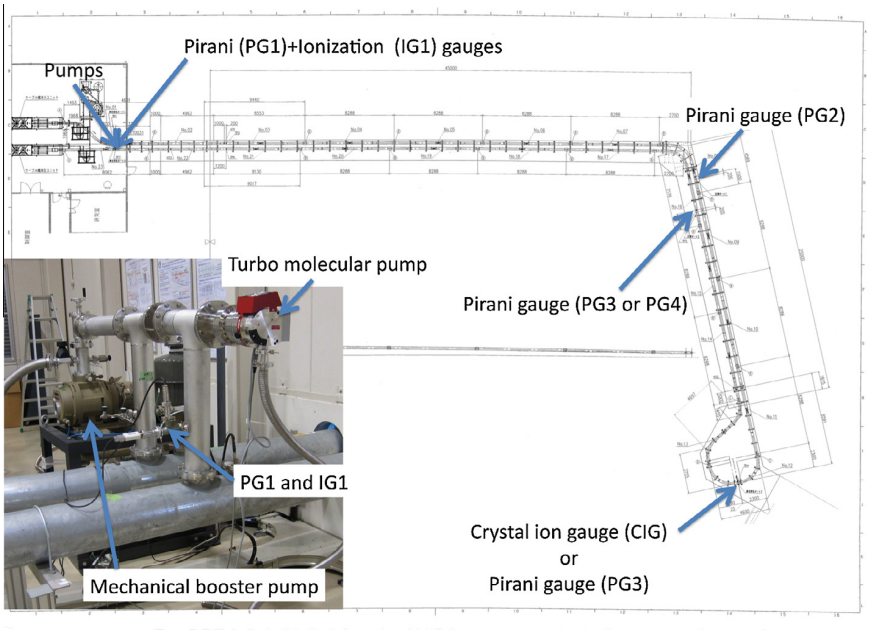

Fig. 1. The layout of CASER2 and the vacuum system.

About 8 m of the cryogenic pipes were manufactured at the factory and connected by welding at the installation site. Therefore, more or less, the inside of the cryogenic pipe was exposed to the air during the installation, though the cryogenic pipe was transported from the factory with filling nitrogen gas inside.

The space between the double pipes is connected with a pipe near the ends of the cryogenic pipe and pumps are installed on the pipe as shown in the inset of Fig. 1. This configuration corresponds to the situation that the vacuum pumping stations are installed at every 200 m along longer cryogenic pipe for the symmetry. One mechanical booster pump with the nominal pumping speed of 11,000 l/min above a few Pa and one turbo-molecular pump with the nominal pumping speed of 260 l/s below a few Pa are used for the evacuation. These pumps are backed with rotary pumps.

One ionization gauge, one crystal ion gauge and three Pirani gauges are installed along the cryogenic pipe to monitor the vacuum. The crystal ion gauge is a combination gauge using a crystal gauge in the low vacuum region and an ion gauge in the high vacuum region. We have performed cooling tests five times. During the second and third cooling tests, the crystal ion gauge had a trouble and was replaced by a Pirani gauge. Therefore we usually call the gauges IG1, PG1, PG2 CIG, PG3 in order, but IG1, PG1, PG2, PG3, PG4 only for the second and third cooling tests. IG1 and PG1 are installed at the pipe connecting the ends of the cryogenic pipe and close to the pumps as shown in the inset of Fig. 1. CIG or PG3 are installed at the furthest position of the cryogenic pipe from the pumps. The other Pirani gauges are installed at the middle of these gauges.

3. The model of calculations

We have performed calculations to estimate the evacuation times of long cryogenic pipes. If there is no inflow from the other vessels, the time evolution of the vacuum degree of a vessel can be written as

$$V\frac{dP(t)}{dt} = Q(t) - SP(t), \tag{1}$$

where V is the volume of the vessel, $P(t)$ is the vacuum degree, $Q(t)$ is the outgassing rate, S is the pumping speed. If this vessel is connected to another vessel, this equation might be changed to

$$V\frac{dP(t)}{dt} = Q(t) - SP(t) + C(P'(t) - P(t)), \tag{2}$$

where C is the conductance of the pipe connecting the vessels, $P'(t)$ is the vacuum degree of another vessel. If connected vessels are increased, the third term of right side of Eq. (2) should be added according to the number of the vessels added.

The cryogenic pipe is a flow channel of gases and at the same time a vessel to be evacuated. The cryogenic pipe with the inner pipe diameter of d_i, the outer pipe diameter of d_o and the length of l is modeled as vessels with the volume of V and the area of the surface facing to the vacuum of S connected with concentric double pipes with the inner pipe diameter of d_i, the outer pipe diameter of d_o and the length of dl, as shown in Fig. 2. In this figure, q is the outgassing rate of the vessels and c is the conductance of the concentric double pipes. The modeled pipe is supposed to be pumped from both the ends with the pumping speed of $s/2$. This configuration corresponds to the long cryogenic pipe which is evacuated by the pumps with the pumping speed of s installed by the intervals of l. Under these assumptions, the pressure variation can be written by the simultaneous differential equations as

$$\begin{aligned} V\frac{dP_1}{dt} &= q + c(P_2 - P_1) - \frac{s}{2}P_1, \\ &\vdots \\ V\frac{dP_i}{dt} &= q + c(P_{i+1} - 2P_i + P_{i-1}), \\ &\vdots \\ V\frac{dP_n}{dt} &= q + c(P_{n-1} - P_n) - \frac{s}{2}P_n. \end{aligned} \tag{3}$$

By solving these equations the time variation of the vacuum degree can be obtained.

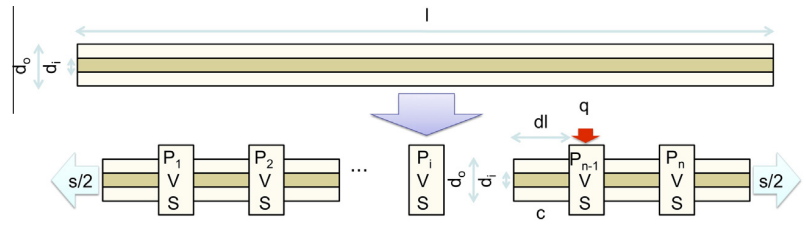

Fig. 2. The model of calculations. A cryogenic pipe is modeled as vessels connected with concentric double pipes.

4. Experiments

As one can see from Eqs. (1) and (3), since the vacuum degrees at the steady state, i.e. $dP/dt \approx 0$, are proportional to the outgassing rate, calculated results vary largely by the outgassing rate. Therefore a plausible outgassing rate is required for calculations. We measured time evolution of the vacuum degree of the 200 m class cryogenic pipe of CASER2 and estimated the time evolution of the outgassing rate. Fig. 3 shows the result of the time evolution of the vacuum degree measured with the ionization gauge near the turbo molecular pump called IG1. In this case the liquid nitrogen was filled in the cryogenic pipe. After turning on the turbo molecular pump, the vacuum degree decreased to the order of 10^{-5} Pa only 2 and a half hours. This can be contrasted with the previous result, in which the liquid nitrogen was not filled in the cryogenic pipe and even nearly 3 days after the start of evacuation all the system was not reached below 0.05 Pa [3]. To examine the reason, mass spectra of gases in the cryogenic pipe were measured with a quadrupole mass spectrometer before and after filling the liquid nitrogen to the cryogenic pipe. Before filling liquid nitrogen, a large peak of H_2O has been observed and dominated over the other peaks, while it disappeared after filling and the peak of N_2 dominated. We consider that the reason of the shorter evacuation time is that the outgassing of H_2O was strongly suppressed by the low temperature of the liquid nitrogen.

After we closed the gate valve above the turbo molecular pump and stopped the evacuation, the increase of the vacuum degree of the cryogenic pipe was measured to estimate the outgassing rate per 1 m^2 of the pipe surface facing to the vacuum. The outgassing rate was estimated with the data indicated with red symbols in Fig. 3. Before closing the gate valve, the cryogenic pipe was evacuated and a pressure gradient existed along the cryogenic pipe. Therefore we use the data from about 3 h after closing the gate valve to eliminate the effect of the pressure gradient. The vacuum degree varied as $P = 0.00016 + 2.6 \times 10^{-7} t^{0.81}$ Pa as a function of the time t in second. The volume and area of the inside of the cryogenic pipe facing to the vacuum are calculated to be 5.2 m^3 and 170 m^2. Therefore the outgassing rate per 1 m^2 of the pipe surface is obtained to be $6.5 \times 10^{-9} t^{-0.19}$ Pa $m^3/(s\ m^2)$ from Eq. (1). It should be noted that only the pipe surface was considered for the conversion of the outgassing rate to the value for an unit area, since the area of the multi-layer insulation surface was difficult to estimate. Therefore, the area used for the normalization might be underestimated and the outgassing rate per 1 m^2 of the pipe surface might be overestimated. We consider this approximation will not cause a serious problem to the calculated results, because we only want to know upper limits of the evacuation time.

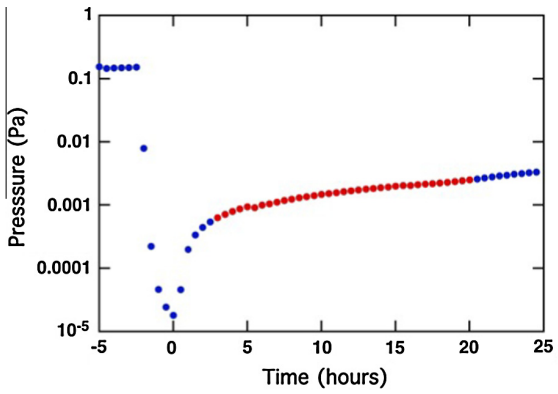

Fig. 3. An evolution of the vacuum degree measured during the third cooling test [5]. This was measured with an ionization gauge near the turbo molecular pump (IG1). The outgassing rate was estimated with the data indicated with the red symbols. (For interpretation of the references to color in this figure legend, the reader is referred to the web version of this article.)

5. Results and discussions

We calculated the time required for the evacuation from 1 to 0.05 Pa based on the simultaneous differential equation of Eq. (3). The diameter of the inner pipe is supposed 139.8 mm (125A). The outgassing rate is approximated as

$$q = 6.5 \times 10^{-9} t^{-0.19} A \ (\mathrm{Pa\ m^3/s}) \tag{4}$$

and the conductance as

$$c = 121K \frac{(d_o - d_i)^2 (d_o + d_i)}{dl} \ (\mathrm{m^3/s})\ [8]. \tag{5}$$

Here A is the area of the inner surface of the cryogenic pipe in m^2 and K takes a value between 1 and 1.7 depending on the ratio d_i/d_o [8] and shown in Table 1. The unit of d_o and d_i is meter. The outgassing rate at 60 s was used from 0 to 60 s to avoid divergence of the calculations for the divergence of the outgassing rate in Eq. (4). Initial values of the vacuum degree were set 1 Pa. We calculated the evacuation time by changing the pumping speed, the diameter of the outer pipe and the length of the cryogenic pipe.

Fig. 4 shows the results for the different pumping speeds for the 100 and 500 m cryogenic pipes. The use of turbo molecular pumps of $s = 100$ l/s (0.1 m^3/s) or $s = 200$ l/s (0.2 m^3/s) is considered. For smaller diameter of the outer pipe, the results of 100 and 200 l/s are almost the same and the evacuation time becomes shorter as increasing the diameter. Since the conductance limits the evacuation time in this region, the pumping speed of the pump does not affect the evacuation time strongly and the evacuation time becomes shorter as increasing the diameter due to the increase of the conductance. As further increasing the diameter, the evacuation time becomes longer for the increase of the volume that has to be evacuated, provided the pumping speed is the same. In this region the conductance is large enough for the pumping speed

Table 1
The K value in Eq. (5) taken from a Ref. [8].

d_i/d_o	0	0.259	0.500	0.707	0.866	0.966
K	1	1.072	1.154	1.254	1.430	1.675

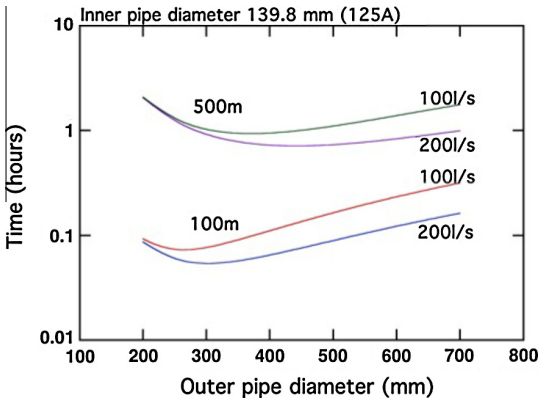

Fig. 4. The time required for the evacuation from 1 to 0.05 Pa for the different pumping speeds.

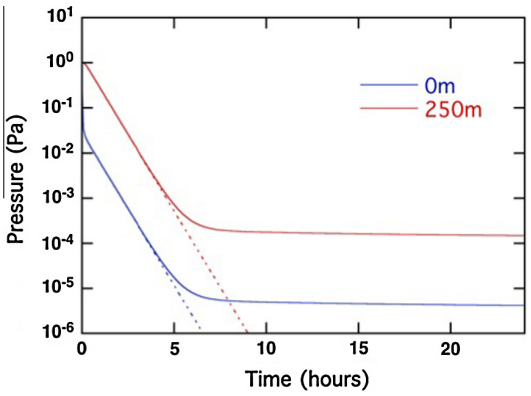

Fig. 6. The calculated time variations of the vacuum degrees at the end (0 m) and the middle (250 m) of a pipe for l = 500 m, d_i = 139.8 mm (125A), d_o = 200.0 mm and s = 100 l/s. The outgassing terms q are including in the calculations for the solid lines, while they are excluded in those for the dotted lines.

and the evacuation time becomes shorter, if a larger pump is used. As seen in the figure the evacuation time takes a minimum value as increasing the diameter of the outer pipe. From the result it can be said that there is an optimum condition between the pumping speed, the diameter of the outer pipe and the length of the cryogenic pipe. It should be noted that too large outer pipe diameter should be avoided for the efficient evacuation, which is sometimes adopted to get larger conductance.

Fig. 5 shows the results for different pipe lengths from 100 to 20,000 m. The use of a turbo molecular pump of s = 100 l/s (0.1 m^3/s) is supposed. As seen in the figure, the evacuation time is not too long to wait the end of the evacuation for all the cases. The evacuation can be finished within a few hours, if the pipe length is less than 1 km. If we can wait 1 week, even 10 km is possible. This means that vacuum pumping stations can be separated by the intervals of 10 km. It should be noted that the outgassing rate which was measured with filling the liquid nitrogen in the cryogenic pipe is used in this calculation. Otherwise, much longer time will be required for evacuation like the previous result [3].

Fig. 6 shows a calculated time variation of the vacuum degrees at the end (0 m) and the middle (250 m) of the pipe for l = 500 m, d_i = 139.8 mm (125A), d_o = 200.0 mm and s = 100 l/s, which is the same setting at d_o = 200.0 mm of the purple line in Fig. 5. The solid lines are the full calculation including the outgassing terms q, while they were ignored in the calculation for the dotted lines meaning that only the gases in the pipe are evacuated. In the case of the solid lines, the steady state is reached after smooth decrease of the vacuum degree for about 5 h. Before about 5 h, both the solid and dotted lines coincide each other. Therefore the smooth decrease of the solid lines corresponds to the evacuation of the gases in the space between the double pipes. At the steady state, the vacuum degrees decrease very slowly. As one can see from Eqs. (1) and (3), the vacuum degrees at the steady state, $dP/dt \approx 0$, are proportional to the outgassing rates. The slow variation of the vacuum degrees at the steady state comes from the time variation of the outgassing rate. At the middle (250 m), 0.05 Pa is reached only about 2 h and around 2×10^{-4} Pa is reached at the steady state. If the outgassing rate is 2.5×10^2 times higher than that used in the calculation, extraordinary long time will be required to reach 0.05 Pa, because the vacuum degree at the steady state will be higher than 0.05 Pa and the evacuation time will be determined by the time variation of the outgassing rate. Therefore, needless to say, the suppression of outgassing is important for the efficient evacuation of cryogenic pipes. To realize the condition, care should be taken during construction of the cryogenic pipe, in particular to make long transmission line, since it would be required to connect the cryogenic pipe at the construction site and the inside of the cryogenic pipe would be exposed to the humid air. The start of filling of the liquid nitrogen before reaching good vacuum for vacuum insulation might be a way. This might increase the loss of the liquid nitrogen and increase the time needed for cooling down, but will reduce the evacuation time significantly.

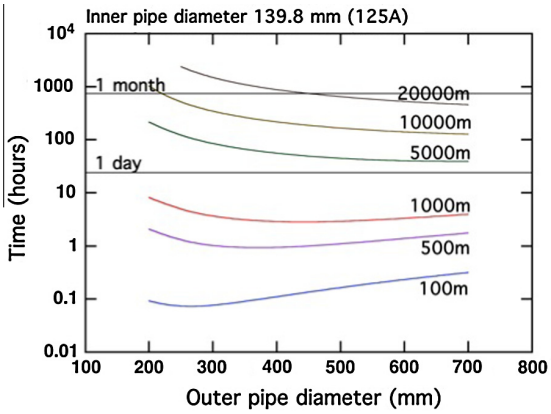

Fig. 5. The time required for the evacuation from 1 to 0.05 Pa for different pipe lengths from 100 to 20,000 m.

6. Conclusions

To estimate the evacuation time of long cryogenic pipes, model calculations have been performed with the outgassing rate which was obtained experimentally using the 200 m class superconducting DC power transmission system at Chubu University. According to the calculations, it is found that there is an optimum condition between the pumping speed, the diameter of the outer pipe and the length of the cryogenic pipe for the efficient evacuation. If the outgassing is suppressed enough, the evacuation can be possible within 1 week even for the long cryogenic pipes with the length of 10 km, which means that vacuum pumping stations can be separated by the intervals of 10 km. Reduction of outgassing is particularly important for the efficient evacuation of long cryogenic pipes for superconducting power transmission.

Acknowledgements

The authors thank Dr. Atsuo Iiyoshi, Chancellor of Chubu University, for his continuous encouragement throughout this

work. The authors acknowledge Dr. Hiroshi Fujiwara for his financial support for the construction of CASER2. Parts of this work were supported by a grant from the Strategic Research Foundation Grant-aided Project for Private Universities Ministry of Education, Culture, Sports, Science and Technology, Japan.

References

[1] A. Hofmann, Cryogenics 46 (2006) 815–824.
[2] P.J. Sun, J.Y. Wu, P. Zhang, L. Xu, M.L. Jiang, Cryogenics 49 (2009) 719–726.
[3] H. Watanabe, M. Hamabe, T. Kawahara, S. Yamaguchi, Proc. ICEC23-ICMC2010 (2011) 649–652.
[4] S. Yamaguchi, T. Kawahara, M. Hamabe, H. Watanabe, Yu. Ivanov, J. Sun, A. Iiyoshi, Physica C (2011) 1300–1303.
[5] H. Watanabe, Yu. Ivanov, J. Sun, M. Hamabe, T. Kawahara, S. Yamaguchi, Phys. Procedia 36 (2012) 1366–1371.
[6] T. Masuda, H. Yumura, M. Watanabe, H. Takigawa, Y. Ashibe, C. Suzawa, T. Kato, Y. Yamada, K. Sato, S. Isojima, C. Weber, A. Dada, J.R. Spadafore, IEEE Trans. Appl. Supercond. 15 (2005) 1806–1809.
[7] H. Yumura, M. Ohya, Y. Ashibe, M. Watanabe, T. Minamino, T. Masuda, S. Honjo, T. Mimura, Y. Kitoh, Y. Noguchi, J. Phys.: Conf. Ser. 234 (2010) 032069.
[8] R. Loevinger, in: A. Guthrie, R.K. Wakerling (Eds.), Vacuum Equipment and Techniques, McGraw-Hill, New York, 1949, pp. 37–38.

2013-h-25p

Developments of Functional Graded Thermoelectric Materials using SiGe under a strong gravitational field

By Toshio Kawahara[1)], Makoto Hamabe[1)], Hirofumi Watanabe[1)], Satarou Yamaguchi[1)], Yoichi Okamoto[2)], Yudai Ogata[3)], Tsutomu Mashimo[3)]

[1)]*Center of Applied Superconductivity and Sustainable Energy Research, Chubu University, Aichi, Japan*
[2)]*Department of Materials Science and Engineering, National Defense Academy, Kanagawa, Japan*
[3)]*Shock Wave and Condensed Matter Research Centers, Kumamoto University, Kumamoto, Japan*

Superconducting applications are highly attractive for energy saving to address environmental issues for the sustainable earth. Chubu University has already developed and tested a 20-m class superconducting DC superconducting transmission device (CASER-1) and proposed several technologies to improve the performance of superconducting applications to the grid. Now we have 200 m-class superconducting DC transmission system of CASER-2. For practical applications, reducing the heat leak to low temperature components is one of the most important technologies, and the heat leak reduction at terminations is key technology especially for short distance systems. We are using Peltier current lead (PCL) for heat insulation at the terminals. PCL consists of thermoelectric elements in series with a resistive element (usually copper or brass). Therefore, high performance thermoelectric materials near room temperature can enhance the ability of superconducting applications during operation. However, in superconducting applications, thermoelectric materials should be used in the wide temperature distribution. Therefore, functional graded materials seem to be useful. We are considering the application of a strong gravitational field to the sintering process of the thermoelectric elements. In this process, the controlled distribution of atomic concentration is possible. We can observe the distribution changes by energy distributed X-ray spectroscopy analysis. Such gradation of materials could be important for the future material design.

Key Words: strong gravity process, functional graded materials, FGM, thermoelectric materials, applied superconductivity

1. Introduction

Superconducting transmission and distribution (T&D) system is one of the key technologies for effective use of natural energy and saving energy[1-5)]. The realization of superconducting T&D systems requires the low heat leak cryogenics for the high performance operation[5)]. In Chubu University, we have developed 200 m-class superconducting direct current (DC) transmission test device of CAER-2[6)], following to 20 m-class superconducting DC transmission device (CASER-1)[5,7)], for the experiments of actual evidence of the low heat leak superconducting systems with several advanced cryogenics.

Figure 1 shows the pictures of CASER-2 and its specifications. The transmission power of CASER-2 is 40 MW and the length is approximately 200 m. There is an undulation of 2.7 m and a turn with the minimum radius of 2 m, which can emulate actual conditions of transmission lines in the field. We have already finished the 5th cooling experiment for cryogenics and a superconducting state. The first cooling experiment was done from January 2010 to March 2010 and showed the zero resistance of superconducting cables successfully. Until 5th cooling experiment that was started at August 2012, we have several experiments to obtain the cryogenic data of CAESR-2[8,9)].

The performance of such applied systems is determined by two large heat leaks, which are in the cryogenic pipes keeping the superconducting cable inside and at the terminals where the superconducting cable is connected to the outside systems at room temperature.

For the latter, we have explored the use of thermoelectric materials placed in series with the superconductor and sharing the same current in order to minimize the cryogenic load at the terminals in T&D systems. The approach consists of using a p-type material at one end of the line and an n-type material at the other end (the current in the DC system is only flowing in one direction). Since the cryogenic load in short-length superconducting cables is dominated by the terminations, the decrease in cryogenic load by the use of Peltier current lead (PCL) elements results in substantial total load reduction. As a consequence, a PCL can be integrated in the high-performance current leads for superconducting applications to reduce the heat leak at the terminals[10,11)].

The PCL, as shown in Fig. 2, consists of thermoelectric elements and a resistive element (usually copper or brass). It has been shown that the cryogenic load due to the current leads is reduced by the low thermal conductivity and large Seebeck coefficient of the thermoelectric elements. Heat leak on the PCL depends on the properties of the thermoelectric material[12)]. Many researchers are developing high performance thermoelectric materials, where large figure of merits ZT is required. Z is defined by $\sigma S^2/\kappa$, where σ is the

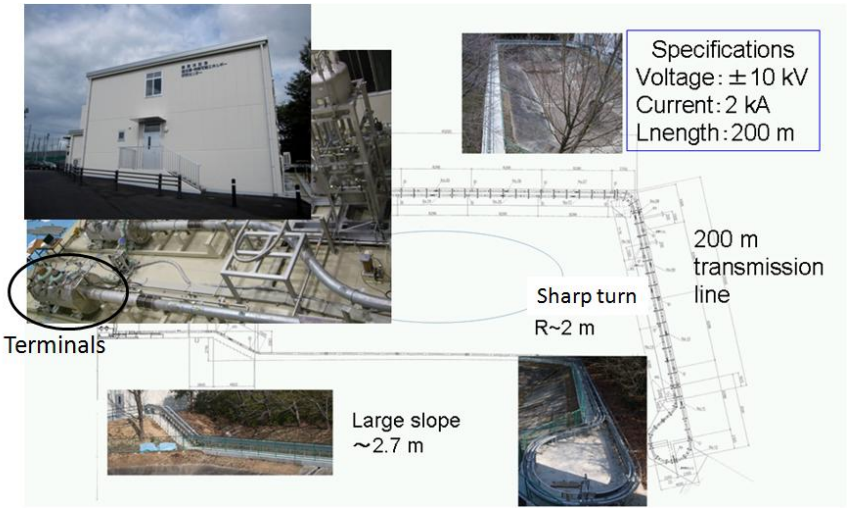

Fig. 1. Specification of CASER-2.

electric conductivity, S is the Seebeck coefficient, and κ is the

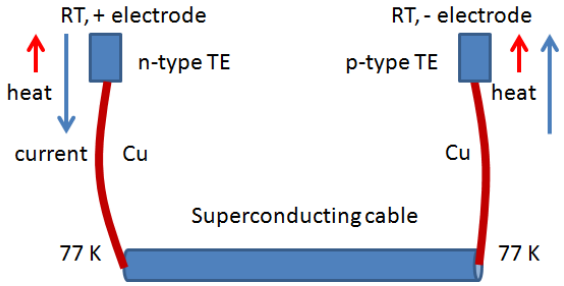

Fig. 2. PCL concepts. Thermoelectric elements are set on the higher temperature side. With DC feeding, heat can be pumped out to the higher-temperature end. Shape factors for the thermoelectric and Cu leads are optimized for minimum heat for given current such as I = 100A.

thermal conductivity. One of the candidates for the low temperature application is the SiGe systems[13,14]. They have very huge Seebeck coefficient near room temperature. To obtain such properties, quantum confinements caused by the nano clusters is important. Therefore, we should keep such nano structure for the material developments.

In this paper, we will discuss about the strong gravitational field process[15,16] for the fabrication of the high performance thermoelectric materials, which can be used for the enhancement of the performance of applied superconducting systems. Functional graded materials seem to be useful for such applications and gravitational process could be highly controllable processing technology. The SiGe samples sintered in the strong gravitational field were studied by the X-ray diffraction (XRD) and energy distributed X-ray spectroscopy (EDX) analysis to check the nano structure of the materials.

2. Experiments

SiGe sample was made by hydrostatic press process, and bulk materials with nano-sized particles could be fabricated. Si and Ge chunks (Kojundo Chemical Lab. Co., Ltd.; purity 99.999%) were ground in a planetary boll mill (FRITSCH; TYPE-P5) for 13 hours. Each powder was put in the container with the small ball for the breaking. The rotation both of the stage and the container can generate strong centrifugal force with variation, and fabricate the small size particles. To avoid the heat up of the materials, the grinding process was done by the intermittent ones in every 1 hour. After the fine particle process, the Si (60 mas %) and Ge (40 mass %) powders were mixed by a roller mill. The particle size estimated by the XRD was about 100 nm. The powders were put in the pipe of 5 mmϕ and 10 mm length, and pressed by the cold isostatic press (CIP; Nikkiso Co., Ltd.; CL3-22-60) with 3500 kg/cm^2

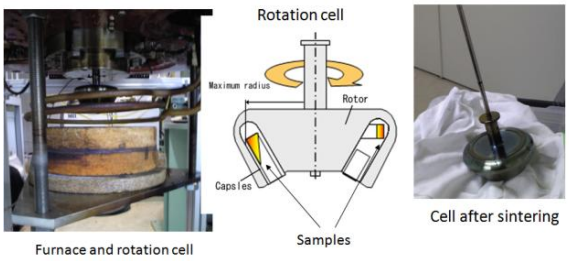

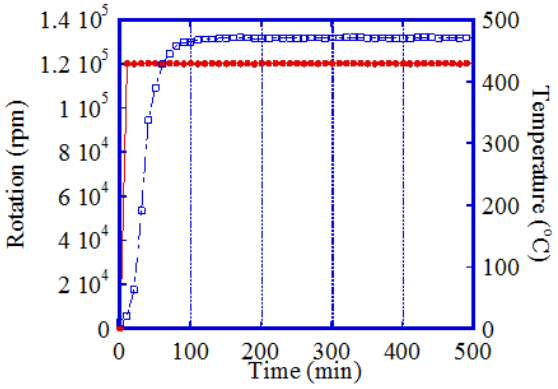

Fig. 4. Representative process parameters of rotation speed and sintering temperature.

of hydrostatic pressure.

The prepared samples were processed by the strong gravitational field using the home-made equipments in Kumamoto University (Fig. 3). The samples were set in the rotation cell and the temperature was kept at 470°C during the rotation. Total process time was 43 hours. The representative time dependence of the rotation speed and temperature are shown in Fig. 4. After reaching to the process rotation speed (process gravity), the cell temperature was heated up. For our process, the rotation speed of 12000 rpm was used which corresponds to 48000 G.

XRD for the analysis of the crystal structure of SiGe was taken by the Philip X'per MRD with Cu target, where acceleration voltage was 45 kV with 40 mA. Scanning electron microscopy image was taken by the SU-6600 (Hitachi CO. Ltd.) and EDX measurements were also used to estimate the concentration of Si and Ge in the samples.

3. Results and Discussion

At first, we will discuss about the temperature distribution on the actual current lead during the cooling operation. Fig. 5 shows the temperature distribution with I = 0 A for the PCL (n- and p- types) and conventional copper current lead (CCL).

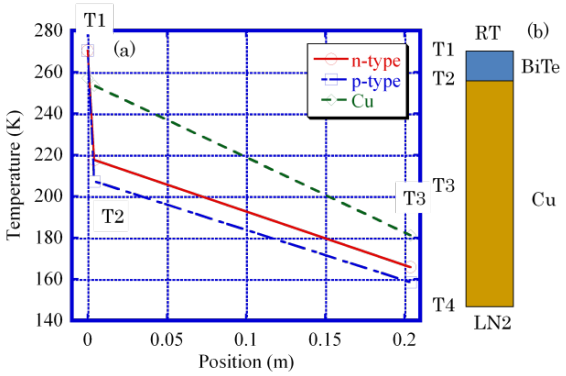

Fig. 5. Temperature distribution on the current leads. (a) is for the actual distribution during cooling experiments. (b) is for the schematics for the definition of the temperature.

T1 is temperature on the top of a current lead and T4 is the middle of a current lead, where the current leads are connected to the inner chamber in the cryostat. Thermoelectric elements are connected at T2 to the lower parts of current leads made by copper. Total temperature difference is almost the same between the CCL and PCL, but the main temperature difference exists on the thermoelectric elements in PCL. Thus, the large temperature difference on the BiTe elements can be observed both for n- and p-type PCLs. Then the mild slope of the temperature distribution on the copper part in the PCL can be observed, which means the small heat leak to the low temperature ends of the superconducting system.

The better thermoelectric materials can enhance the performance of applied superconducting systems, and then such developments are required for the future sustainable world. However, thermoelectric materials usually have the

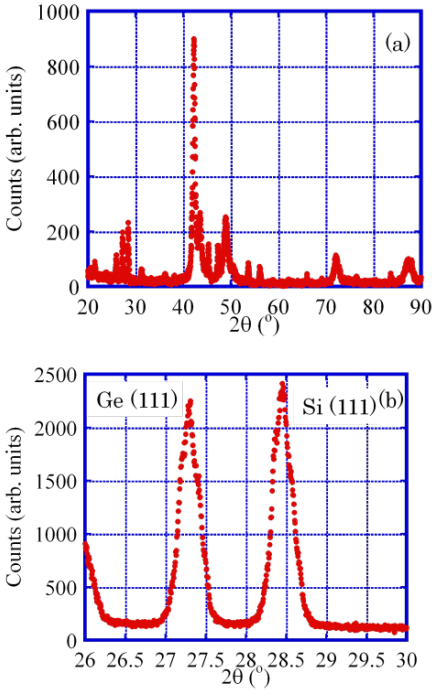

Fig. 6. XRD patterns for the processed SiGe sample.

maximum performance at the limited temperature range. Therefore the functional graded materials are sometimes discussed as thermoelectric applications. For example, we already discussed about the double Peltier current lead for the heat leak reduction using two type of commercial thermoelectric elements[17]. One is sintered materials with large resistivity and low thermal conductivity. Another is the solid solution materials grown by the Bridgeman methods with small resistivity and high thermal conductivity. When the two elements combined as single current lead (double PCL), the performance as heat leak reduction can be enhanced comparing with the single element PCLs[17]. In this case the low resistive thermoelectric elements were used at the lower temperature part of thermoelectric elements as functional graded materials.

For the optimum design of the thermoelectric elements to fit to the current leads, which are used in the large temperature distribution, the detailed optimization of the shape and thermoelectric properties should be required. Now we try to develop new functional graded materials using SiGe by the strong gravitational field process for the controllability of the gradation.

Figure 6 shows the XRD patterns for the SiGe samples processed by the strong gravitational field with sintering. Fig. 6 (a) is for the wide scan and Fig. 6 (b) is for the (111) peaks of Si and Ge. Only the XRD peaks of Si and Ge can be observed. Therefore, the Si and Ge are independently sintered by the gravitational process. There is no growth of SiGe phase. Each cluster of Si and Ge could exist in the sample, and nano cluster might safely keep its shape in the matrix of the samples.

On the other hand, we show the distribution of Si and Ge in Fig. 7. Fig. 7 (a) is the measuring points and the right hand

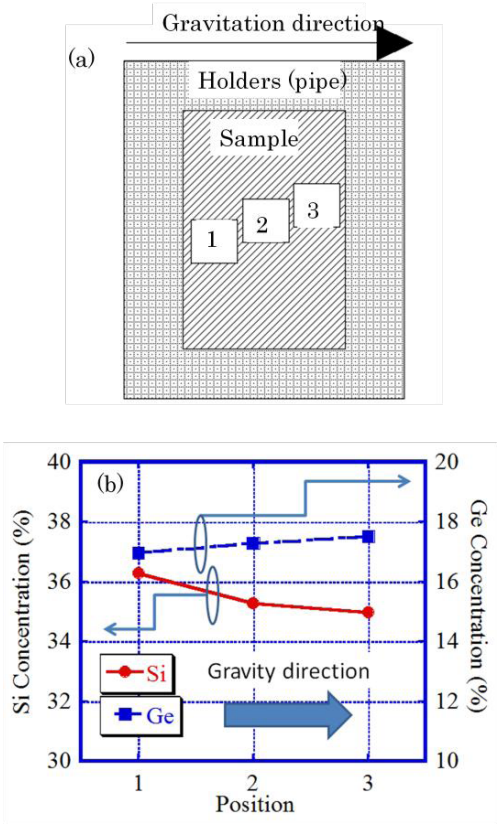

Fig. 7. Si and Ge concentration in SiGe at the different position. (a): the measurements position. (b): Si and Ge distribution measured by EDX.

side in the picture corresponds to the strong gravitational field side in the process chamber. As shown in Fig. 7 (b), heavy elements of Ge have higher concentration at the gravitational direction. On the contrary, light elements of Si have higher concentration at the opposite side of gravity direction (left hand side in the figure). Thus we succeeded in the fabrication of the functional graded materials of SiGe. And also we could keep the stating nano cluster after the strong gravitational process at 470 $^{\circ}$C. Nano cluster structure is the key for the high performance of SiGe thermoelectric systems, and then the strong gravitational process seems to be the promising process for the gradation control. Detailed study of the thermoelectric properties of the materials and the performance as applied superconducting systems is now in progress.

4. Conclusion

We have developed superconducting DC T&D systems of CASER-1 and CASER-2. To reduce the thermal loads of the applied superconducting systems, we have discussed about the special current leads of PCL. In PCL, the thermoelectric elements are suffered by the large temperature distribution. It might be hard for a single uniform thermoelectric material. Therefore, we try to develop the functional graded materials using SiGe that showed high performance in thermoelectric properties near room temperature. Using the strong gravitational field process, the SiGe sample is modified to the functional graded materials, where Si and Ge distributions have been changed depending on the mass of the elements. And the nano clusters structure might be kept. Thus we could fabricate the promising new thermoelectric materials and the sintering with a strong gravitational field could be used as controllable fabrication process for the functional graded materials.

Acknowledgments

The authors thank Dr. A. Iiyoshi, Chancellor of Chubu University, for his continuous encouragement throughout this work. We acknowledge Dr. Hiroshi Fujiwara for his support on the construction of 200-m superconducting facilities of CASER-2. This work was partly supported by the Strategic Research Foundation Grant-aided Project for Private Universities from the Ministry of Education, Culture, Sports, Science and Technology (MEXT), and a Grant-in-Aid for Challenging Exploratory Research (MEXT). This work was supported in part by the Kumamoto University Global COE Program “Global Initiative Center for Pulsed Power Engineering”.

References

1) Mukoyama, S., Yagi, M., Ichikawa, M., Torii, S., Takahashi, T., Suzuki, H., and Yasuda, K.: Experimental results of a 500 m HTS power cable field test, *IEEE Trans. Appl. Supercond.*, **17** (2007), pp.1680–1683.
2) Masuda, T., Yumura, H., Watanabe, M., Takigawa, H., Ashibe, Y., Suzawa, C., Ito, H., Hirose, M., Sato, K., Isojima, S., Weber, C., Lee, R., and Moscovic, J.: Fabrication and installation results for Albany HTS cable, *IEEE Trans. Appl. Supercond.*, **17** (2007), pp.1648–1651.
3) Yoon, J. Y., Lee, S. R., and Kim, J. Y.: Application methodology for 22.9 kV HTS cable in metropolitan city of South Korea, *IEEE Trans. Appl. Supercond.*, **17** (2007), pp.1656–1659.
4) Xi, H. X., Gong, W. Z., Zang, Y., Bi, Y. F., Ding, H. K., Wen, H., Hou, B., and Xin, Y.: China’s 33.5 m 35 kV/2 kA HTS ac power cable’s operation in power grid, *Physica C: Supercond.*, **448** (2006), pp.1054–1057.
5) Yamaguchi, S., Hamabe, M., Yamamoto, I., Famakinwa, T., Sasaki, A., Iiyoshi, A., Shultz, J., Minervini, J., Hoshino, T., Ishiguro, Y., and Kawamura, K.: Research activities of DC superconducting power transmission line in Chubu University, *J. Phys.: Conf. Ser.*, **97** (2008), 012290.
6) Yamaguchi, S., Kawahara, T., Hamabe, M., Watanabe, H., Ivanov, Y., Sun, J., and Iiyoshi, A., Experiment of 200-meter superconducting DC cable system in Chubu University, *Physica C: Supercond.*, **471** (2011), pp.1300-1303.
7) Hamabe, M., Fujii, T., Sugino, M., Sasaki, A., Sugimoto, T., Watanabe, H., Kawahara, T., Yamaguchi, S., Ishiguro, Y., and Kawamura, K.: Cooling cycle test of DC superconducting power transmission cable, *J. Phys.: Conf. Ser.*, **234** (2010), 032019.
8) Watanabe, H., Sugino, M., Sun, J., Ivanov, Y., Hamabe, M., Kawahara, T., and Yamaguchi, S.: Cooling test of the 200 m superconducting DC transmission power cable system at Chubu University, *Physica C: Supercond.*, **471** (2011), pp.1304–1307.
9) Ivanov, Y., Watanabe, H., Hamabe, M., Sun, J., Kawahara, T., and Yamaguchi, S.: Circulation pump power for 200 m cable experiment, *Physica C: Supercond.*, **471** (2011), pp.1308–1312.
10) Yamaguchi, S., Yamaguchi, T., Nakamura, K., Hasegawa, H.,

Okumura, H., and Sato, K.: Peltier current lead experiment and their applications for superconducting magnets, *Rev. Sci. Instrum.*, **75** (2004), pp.207-212.

11) Kawahara T., Fujii T., Emoto M., Hamabe M., Sun J., Watanabe H. and Yamaguchi S.: Estimation for the performance of superconducting DC transmission lines with cryogenics improvements, *Physica C: Supercond.* **470** (2010) pp.S1011-S1012.
12) Fujii, T., Fukuda, S., Emoto, M., Osada, K., Kawahara, T., Hamabe, M., Watanabe, H., Ivanov, Y., Sun, J., and Yamaguchi, S.: Thermoelectric Property Dependence and Geometry Optimization of Peltier Current Leads Using Highly Electrically Conductive Thermoelectric Materials, *J. Elec. Mater.*, **40** (2011), pp.691-695.
13) Okamoto, Y., Uchino, H., Kawahara, T., Morimoto, J.: Anomalous Large Thermoelectric Power of the Si and Au Doped Ge Superlattice Thin Film, *Jpn. J. Appl. Phys.*, **38** (1999), pp.L945–L947.
14) Kawahara, T., Lee, S. M., Okamoto, Y., Morimoto, J., Sasaki, K., Hata, T.: Anomalous Large Thermoelectric Power on Heavily B-Doped SiGe Thin Films with Thermal Annealing, *Jpn. J. Appl. Phys.*, 41 (2002) pp.L949–L951.
15) Mashimo, T., Huang, X., Osakabe, T., Ono, M., Nishihara, M., Ihara, H., Sueyoshi, M., Shibasaki, K., Shibasaki, S., Mori, N.: Advanced high-temperature ultracentrifuge apparatus for mega-gravity materials science, *Rev. Sci. Instrum.*, **74** (2003), pp.160-163.
16) Huang, X., Ono, M., Ueno, H., Iguchi, Y., Tomita, T., Okayasu, S., Mashimo, T.: Formation of atomic-scale graded structure in Se-Te semiconductor under strong gravitational field, *J. Appl. Phys.*, **101** (2007), 113502.
17) Kawahara, T., Fujii, T., Emoto, M., Hamabe, M., Watanabe, H., Sun, J., and Yamaguchi, S.: Double Peltier Current Lead for Heat Leak Reduction at the Terminals Superconducting Direct Current Applications, *IEEE Trans. Appl. Supercond.*, **21** (2011), pp.1070-1073.

Journal of ELECTRONIC MATERIALS, Vol. 42, No. 7, 2013
DOI: 10.1007/s11664-012-2419-5

Development of a Peltier Current Lead for the 200-m-Class Superconducting Direct Current Transmission and Distribution System

TOSHIO KAWAHARA,[1,4] MASAHIKO EMOTO,[2] HIROFUMI WATANABE,[1] MAKOTO HAMABE,[1] SATARO YAMAGUCHI,[1] YASUO HIKICHI,[3] and MASAHIRO MINOWA[3]

1.—Center of Applied Superconductivity and Sustainable Energy Research, Chubu University, 1200 Matsumoto, Kasugai, Aichi 487-8501, Japan. 2.—Department of Large Helical Device Project, National Institute for Fusion Science, 322-6 Oroshi, Toki, Gifu 509-5292, Japan. 3.—SWCC Showa Cable Systems Co. Ltd., 4-1-1 Minami-Hashimoto, Chuo, Sagamihara, Kanagawa 252-0253, Japan. 4.—e-mail: toshi@isc.chubu.ac.jp

Reducing cryogenic heat leaks is critical for superconducting applications. Reduction of heat leak at the terminals is essential for uses with short-length applications, where cryogenic losses at the terminals dominate. We are developing a 200-m-class superconducting direct current (DC) transmission and distribution system (CASER-2), and have used a Peltier current lead (PCL) for heat insulation at the terminals. The PCL consists of thermoelectric elements and copper leads, which enhance the performance of superconducting systems. As DC flows through the current lead, thermoelectric elements on opposite terminations of a superconducting line can be used to decrease the heat ingress to the cryogenic environment (*n*-type on one end, *p*-type on the opposite end). During the current feeding and cooling test, a large temperature difference was observed across thermoelectric elements in the PCL. This demonstrates that we have successfully insulated the heat leak at the current lead. During the fourth cooling test, we established a new PCL design with *p*-type elements at terminal B, and then compared the performance of the terminals. Several improvements were implemented, including balancing the resistances of the PCL to enhance the stability of the superconducting systems.

Key words: Peltier current lead (PCL), superconducting applications, DC transmission and distribution system, BiTe alloy

INTRODUCTION

Thermoelectric systems have been proposed as key technologies to solve environmental problems. Meanwhile, superconducting applications are also highly attractive for energy saving to address environmental issues for a sustainable Earth. Among these applications, a long-distance superconducting transmission system is one of the most promising and can be utilized to save energy through energy sharing. Such large systems can be built by incorporating smaller network systems to form a highly integrated "superconducting grid." Projects focused on the development of superconducting transmission systems are currently underway in Japan, the USA, Korea, China, and other countries, and involve long-distance, high-voltage, and/or grid-integration systems;[1–6] For example, the Albany project successfully transmitted electric power to 70,000 houses in New York State.[2] Yokohama projects will be the first field test in Japan connecting a superconducting transmission line to the electric grid.[6] A direct current (DC) system is

(Received July 6, 2012; accepted December 27, 2012; published online February 15, 2013)

also being constructed at an aluminum factory by the Chinese Academy of Science. Chubu University has already developed and tested a 20-m-class superconducting DC transmission device (CASER-1)[7] and proposed several technologies to improve the performance of superconducting applications for the grid. The current balance of superconducting tapes for stable transmission, low heat-leak systems using special cryogenic double pipes, and so forth have been discussed previously.[8,9]

For practical applications, reducing heat leakage to low-temperature components is one of the most important technologies for high-performance superconducting applications. For long-distance transmission lines, the heat leaks of the long cryostats can be reduced by high-performance cryogenic pipes,[8] but these losses still dominate over the terminations. On the other hand, for short-distance applications, heat-leak reduction at terminations is a necessary technology for practical uses, and can be addressed by the use of high-performance current leads.[10–13] At Chubu University, we are developing a 200-m-class superconducting DC transmission and distribution system (CASER-2),[14] following the 20-m-class system of CASER-1. In CASER-2, we are using a Peltier current lead (PCL) for heat insulation at the terminals.[15] A PCL consists of thermoelectric elements in series with a resistive element (usually copper or brass). It has been shown that the cryogenic load due to the current leads is reduced by the low thermal conductivity and large Seebeck coefficient of the thermoelectric elements. Several modifications of the PCL have also been proposed and discussed such as modification for use in alternating current (AC) applications,[16] multistage modules,[17] and gas-cooled systems.[12] Since CASER-2 is a DC application, in this study we adopted a conventional PCL configuration with single or multiple elements of thermoelectric materials.

In this paper, we discuss the thermal performance of current leads, where the thermoelectric elements are used for cryogenic heat-load reduction. In the next section, we summarize the fabrication processes of PCLs for CASER-2, and the test procedures for current leads during the cooling experiments. The temperature distribution and current dependence of the performance of the PCL are then discussed. We also compare the performance of a new PCL design[18] used during the fourth cool-down experiment with the performance of previous tests.

SPECIFICATION OF CASER-2 AND EXPERIMENTS

Figure 1 shows the cryogenic pipe and terminals. The cryogenic pipe with high-performance thermal insulation contains the superconducting cable. At the terminals, the superconducting cable is connected at room temperature to outside facilities such as the power supply. The power transmission capability of CASER-2 is 40 MW, and its length is approximately 200 m. There is an altitude difference of 2.7 m along the cable, and a turn with radius of 2 m, which emulate actual conditions of transmission lines in the field. We have already finished the fourth cool-down experiment. The first cool-down was done from January 2010 to March 2010 and showed zero resistance of the superconducting cable. Prior to the fourth cool-down (started August 2011), we performed several experiments to characterize the CASER-2 cryostat.

Figure 2a shows representative fabrication processes of the PCL used for thermal insulation at the terminals. The thermoelectric elements were cut to size and then soldered in a furnace to Cu blocks using silver plating. We have used several designs for PCLs, and Fig. 2b shows one of the typical designs of a PCL used in CASER-2. The dark regions are BiTe alloys. The Cu blocks are connected to the Cu current lead and superconducting tapes in the cable. In the fourth cool-down, we used a new design for the Peltier elements. To reduce thermal stress and improve the stability of the electric connection, we used multisegmented modules,[18] where nine thermoelectric elements in parallel were connected to a Cu block as shown in Fig. 2c. Improved stability and lower contact resistance were obtained with the present arrangement.

We used 46 thermometers attached in the cryostat of CASER-2 for calorimetric measurements of the system for heat-leak determination. We measured the temperature rise of liquid nitrogen before and after an experiment at the terminal cryostats for estimation of the heat leak at the terminals for several feeding currents. The current was fed into the superconducting cable from the current leads at

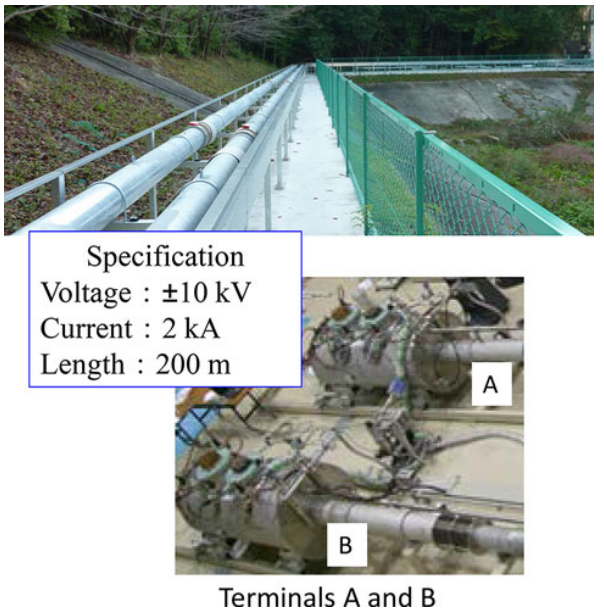

Fig. 1. Specification of CASER-2, and terminals A and B.

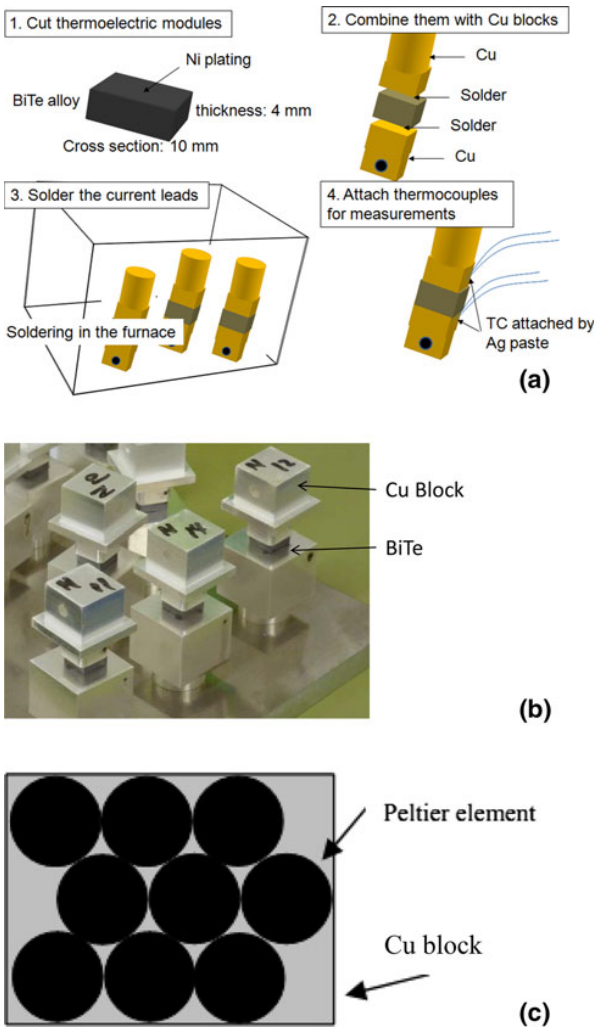

Fig. 2. Fabrication process for the PCL (a) and representative PCLs (b). (c) Schematic view of the multi segmented module.

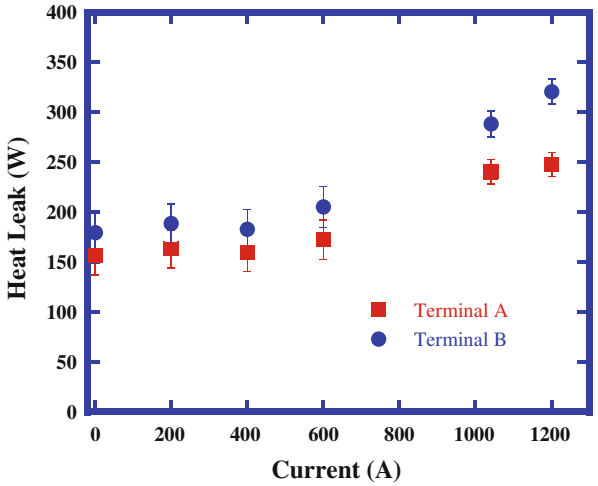

Fig. 3. Current dependence of the heat leak at the terminals.

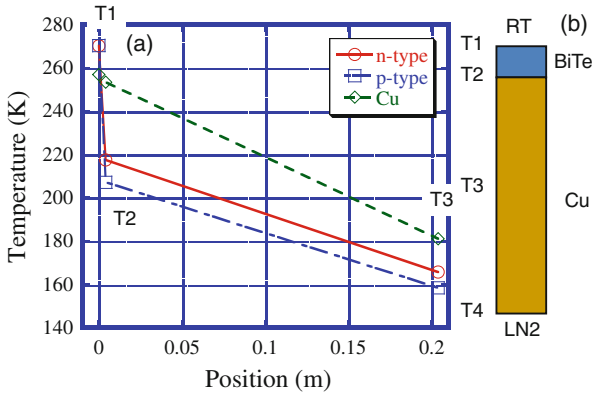

Fig. 4. (a) Temperature distribution along the current lead. Values for a PCL with *n*- and *p*-types, and also a copper current lead, are plotted. (b) Measurement positions; the position of the top of the current lead is set as zero.

one terminal and also came out from the current leads at the same end. We used a coaxial cable, and a power supply was set at terminal A. The two transmission layers of the cable were shorted at terminal B, at the opposite end of the cable. From the temperature rise and flow rate of liquid nitrogen, we estimated the heat leak at the terminals as shown in Fig. 3. The typical flow rate of liquid nitrogen was 13 L/min.

We measured the temperature along the current lead to determine the performance of the current lead. The temperature gradient on the Cu current lead (e.g., T2 and T3) corresponds to the heat leak at the low-temperature end. A representative temperature distribution with $I = 0$ is shown in Fig. 4 for both *n*- and *p*-type elements. The large temperature difference between T1 and T2 demonstrates the high performance of the PCL. We also measured the voltage along each current lead using one of the leads of the thermocouple (Cu lead). Furthermore, we estimated the resistance of the thermoelectric elements in the current lead by the two-probe method.

RESULTS AND DISCUSSION

During the operation, a large temperature difference between the ends of both thermoelectric elements in the PCL was observed as shown in Figs. 4 and 5. Figure 5a is for *n*-type elements set in terminal A, and Fig. 5b is for *p*-type elements set in terminal B. For the case of no current ($I = 0$ A), the average temperature difference is 55 K; however, the data in Fig. 5a show a large scatter. When current is applied to the system, the temperature difference increases because of the Peltier effect, and a large temperature difference at $I = 1.2$ kA was obtained, corresponding to a small heat leak, where the temperature difference on the Cu current lead was relatively small. The situation was similar

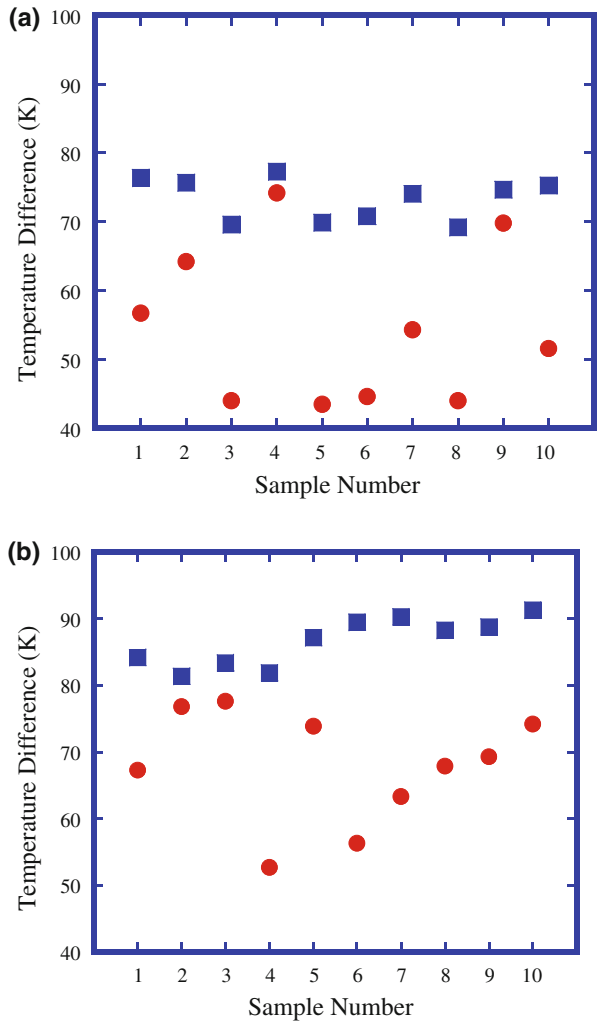

Fig. 5. Temperature difference across thermoelectric elements on the PCL. Filled circles are for a temperature difference without a current, and filled squares for that with a total current of 1.2 kA: (a) *n*-type and (b) *p*-type PCL.

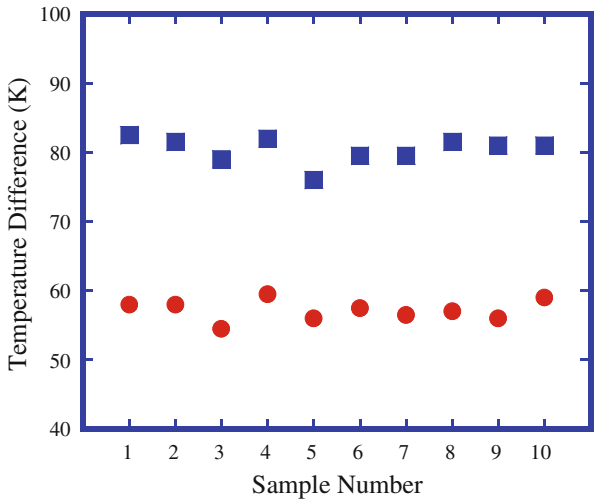

Fig. 6. Temperature difference across thermoelectric elements on the new PCL. Filled circles are for a temperature difference without a current, and filled squares for that with a total current of 720 A.

for *p*-type elements, as shown in Fig. 5b. A large temperature difference was observed during the experiment, which increased with increasing current. Figure 5b shows the temperature differential across the thermoelectric elements for a total current of I = 1.2 kA and for I = 0 A. The typical scattering width (standard deviation) of the temperature difference (ΔT) is about 8.5 K.

A large temperature difference was also observed in the fourth cool-down. Figure 6 shows the temperature difference at *p*-type elements set in terminal B, which is the improved version of the PCL. The average temperature difference is 58 K, and the scatter of the temperature difference was greatly reduced (standard deviation of temperature differences is 1.9 K). When energized, the temperature difference increased with current, improving thermal insulation. The stability during the operation was also greatly improved with the improved PCL. On the other hand, the temperature difference increases with increasing current in the measured range from 0 A to 720 A. The standard deviations of the temperature difference are also small. Of course, the temperature difference should decrease for a larger feeding current, as the current leads have optimum shape factors at the defined operating current.[19–24] However, the scatter of the temperature difference may be small.

We then investigated the resistance of the thermoelectric elements on the current leads measured by the two-probe method. Table I presents the variation of resistance (ΔR) of the thermoelectric elements, calculated by comparing the resistance under initial conditions at room temperature with that under operational conditions during the cool-down. As the PCL works under a large temperature range as shown in Fig. 4, we only consider the difference of the total resistances. The standard deviations of resistance variations decreased remarkably for the improved version used in the fourth cool-down. The variation of resistances before and after the cool-down at room temperature also showed a similar tendency. These results indicate an improved stability of the resistance of thermoelectric elements in the current lead, and also an improved stability of the temperature difference on the current leads. Stability of parameters such as the temperature difference is needed for an optimum design of the shape of current leads, and we can therefore now design higher-performance current leads as determined by the operational current.

The improved PCL also has improved performance regarding thermal insulation. Both the old (*n*-type) and improved (*p*-type) PCL coexist in ter-

Table I. Variation of the resistance ΔR of thermoelectric elements for the third and fourth cooling experiment

	RT (before)–cooling		RT (before)–RT (after)	
	ΔR (mΩ)	Δ	ΔR (mΩ)	Δ
3rd	0.73	0.92	0.073	1.48
4th	0.14	0.017	0.069	0.009

"RT–cooling" indicates the change in resistance recorded before and during the cooling experiment, whereas "RT–RT" is for that recorded before and after the cooling experiment.

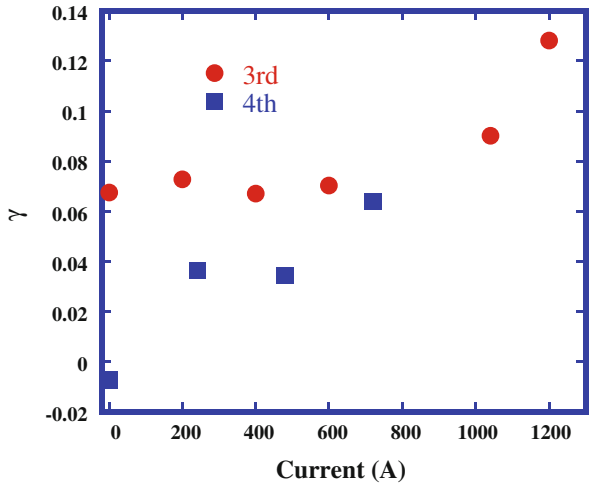

Fig. 7. Current dependence of the ratio γ of the heat leak of terminal B to terminal A.

minal B, and we cannot separately measure the heat leak for each current lead, but can only measure the total heat leak for both terminals A and B. We can calculate the ratio γ of the heat leak of terminal B to terminal A as follows: $\gamma = (Q_b - Q_a)/(Q_a + Q_b)$, where Q_a is the heat leak of terminal A and Q_b is that of terminal B. The environmental temperature differs between the third and fourth cool-downs because the third cool-down was performed during the winter and the fourth during the summer. Therefore, we normalized the heat leak difference using the total heat leak of the terminals. Figure 7 shows the dependence of γ on the current, and reveals that the heat-leak performance of the improved PCL in the fourth cool-down is better. Thus, the stability of the thermoelectric properties of each element and the better fabrication process are very important for ensuring the enhanced performance of PCLs in large superconducting systems such as CASER-2.

CONCLUSIONS

Four cool-downs were carried out on CASER-2. During the cool-down tests with current energization, large temperature differences were observed across both thermoelectric elements of the PCL. Therefore, we successfully insulated and reduced the heat leak at the current terminals. In the fourth cool-down, we improved PCL elements with a *p*-type at terminal B and compared the performance of terminals. Several improvements such as the balance of resistance of the PCLs can enhance the stability and performance of superconducting systems such as CASER-2. This approach contributes to the realization of applied superconducting systems ranging from small- to large-scale applications.

ACKNOWLEDGEMENTS

The authors thank Dr. A. Iiyoshi, Chancellor of Chubu University, for his continuous encouragement throughout this work. We acknowledge Dr. Hiroshi Fujiwara for his support of the construction of the 200-m superconducting facilities of CASER-2. We also thank Dr. Leslie Bromberg of the Massachusetts Institute of Technology, who read our manuscript and gave us many valuable comments. This work was partly supported by the Strategic Research Foundation Grant-Aided Project for Private Universities from the Ministry of Education, Culture, Sports, Science, and Technology (MEXT), and a Grant-in-Aid for Challenging Exploratory Research (MEXT).

REFERENCES

1. S. Mukoyama, M. Yagi, M. Ichikawa, S. Torii, T. Takahashi, H. Suzuki, and K. Yasuda, *IEEE Trans. Appl. Supercond.* 17, 1680 (2007).
2. T. Masuda, H. Yumura, M. Watanabe, H. Takigawa, Y. Ashibe, C. Suzawa, H. Ito, M. Hirose, K. Sato, S. Isojima, C. Weber, R. Lee, and J. Moscovic, *IEEE Trans. Appl. Supercond.* 17, 1648 (2007).
3. J.Y. Yoon, S.R. Lee, and J.Y. Kim, *IEEE Trans. Appl. Supercond.* 17, 1656 (2007).
4. H.X. Xi, W.Z. Gong, Y. Zang, Y.F. Bi, H.K. Ding, H. Wen, B. Hou, and Y. Xin, *Physica C* 448, 1054 (2006).
5. A. Geschiere, D. Willen, E. Piga, and P. Barendregt, *J. Phys. Conf. Ser.* 97, 012183 (2008).
6. S. Honjo, T. Mimura, Y. Kitoh, Y. Noguchi, T. Masuda, H. Yumura, M. Watanabe, M. Ikeuchi, and H. Yaguchi, *IEEE/CSC & ESAS European Superconductivity News Forum (ESNF)*. 14, ST198 (2010).
7. S. Yamaguchi, M. Hamabe, I. Yamamoto, T. Famakinwa, A. Sasaki, A. Iiyoshi, J. Shultz, J. Minervini, T. Hoshino, Y. Ishiguro, and K. Kawamura, *J. Phys. Conf. Ser.* 97, 012290 (2008).
8. M. Hamabe, Y. Nasu, A. Ninomiya, Y. Ishiguro, S. Kusaka, and S. Yamaguchi, *Adv. Cryog. Eng.* 53A, 168 (2008).
9. M. Hamabe, T. Fujii, I. Yamamoto, A. Sasaki, Y. Nasu, S. Yamaguchi, A. Ninomiya, T. Hoshino, Y. Ishiguro, and K. Kawamura, *IEEE Trans. Appl. Supercond.* 19, 1778 (2009).
10. S. Yamaguchi, T. Yamaguchi, K. Nakamura, Y. Hasegawa, H. Okumura, and K. Sato, *Rev. Sci. Instrum.* 75, 207 (2004).
11. Y. Hasegawa, K. Sato, H. Okumura, K. Nakamura, S. Yamaguchi, and K. Miyake, *Cryogenics* 42, 495 (2002).
12. T. Kawahara, T. Fujii, M. Emoto, M. Hamabe, J. Sun, H. Watanabe, and S. Yamaguchi, *Physica C* 470, S1011 (2010).

13. X.C. Xuan, K.C. Ng, C. Yap, and H.T. Chua, *Cryogenics* 42, 779 (2002).
14. S. Yamaguchi, T. Kawahara, M. Hamabe, H. Watanabe, Y. Ivanov, J. Sun, and A. Iiyoshi, *Physica C* 471, 1300 (2011).
15. T. Kawahara, M. Emoto, M. Hamabe, H. Watanabe, Y. Ivanov, J. Sun, and S. Yamaguchi, *J. Electron. Mater.* 41, 1205 (2012).
16. T. Yamaguchi, H. Okumura, K. Nakamura, and S. Yamaguchi, *IEEE Trans. Appl. Supercond.* 13, 1910 (2003).
17. T. Yamaguchi, H. Okumura, K. Nakamura, and S. Yamaguchi, *IEEE Trans. Appl. Supercond.* 13, 1914 (2003).
18. H. Sugane, Y. Hikichi, M. Minowa, T. Kawahara, H. Watanabe, M. Hamabe, and S. Yamaguchi, *Phys. Procedia* 27, 384 (2012).
19. M.N. Wilson, *Superconducting Magnets* (New York: Oxford University Press, 1983), p. 256.
20. H. Okumura and S. Yamaguchi, *IEEE Trans. Appl. Supercond.* 7, 715 (1997).
21. K. Sato, H. Okumura, and S. Yamaguchi, *Cryogenics* 41, 497 (2001).
22. T. Yamaguchi, S. Mizutani, M. Moriguchi, H. Okumura, K. Nakamura, and S. Yamaguchi, *IEEE Trans. Appl. Supercond.* 14, 1719 (2004).
23. T. Fujii, S. Fukuda, M. Emoto, K. Osada, T. Kawahara, M. Hamabe, H. Watanabe, Y. Ivanov, J. Sun, and S. Yamaguchi, *J. Electron. Mater.* 40, 691 (2011).
24. T. Kawahara, T. Fujii, M. Emoto, M. Hamabe, H. Watanabe, J. Sun, and S. Yamaguchi, *IEEE Trans. Appl. Supercond.* 21, 1070 (2011).

IEEE TRANSACTIONS ON APPLIED SUPERCONDUCTIVITY, VOL. 23, NO. 3, JUNE 2013 5401104

Effects of HTS Tape Arrangements to Increase Critical Current for the DC Power Cable

Jian Sun, Hirofumi Watanabe, Makoto Hamabe, Toshio Kawahara, and Satarou Yamaguchi

***Abstract*—Critical current of the high-temperature superconducting (HTS) tape is one of the important parameters for the application of power cables. After combination of the tapes in the cable, the self-field of the tape will be affected by the field from the other tapes, which will result in the degradation of the tape performance. Recently, a 200-m HTS cable test facility for dc power transmission and distribution has been constructed at Chubu University by using BSCCO tapes. In order to optimize the configuration of the HTS tapes in the cable, the effects on the critical current of the tape arrangements are investigated. In order to achieve high current capacity and efficiency of the cable, a multilayer configuration of the tapes is employed. This technical paper will present the measurements of the critical currents of the tape against the layer structures and the gaps between the HTS tapes. The critical current of the tape is measured by the four-probe method at liquid nitrogen temperature. We will present the effects on the critical current of the tape of the magnetic field from the currents applied to the neighboring tapes in the cable. An improvement of the critical current is observed, which suggests the design of DC HTS power cables regarding the tape arrangements may influence the cable property.**

***Index Terms*—Critical current, DC power transmission, DC superconducting cable, high-temperature superconductor.**

I. Introduction

SUPERCONDUCTING Power transmission (SC-PT) applications by using high temperature superconducting (HTS) tapes have attracted much interest in the world [1]–[4]. In contrast to an AC SC-PT system, a DC SC-PT system is more efficient since it is free from AC losses. Since a 200 m DC SC-PT test facility has been constructed at Chubu University [5], studies on the critical current measurements are investigated relating to the tape arrangements by using the BSCCO tapes [6]. In order to lower the heat leak through the cryogenic pipe, the compact cable should be designed to reduce the radiation effect between the low temperature and room temperature [7]. In the DC SC-PT system, the coaxial bipolar cable is used as shown in Fig. 1(a) and the inset presents a sketch of the gap between the tapes due to the shape of the former [8]. 23 and 16 tapes

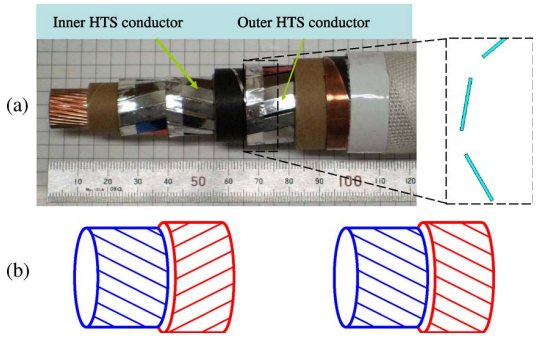

Fig. 1. (a) Photo of a dc coaxial power cable composed of DI-BSCCO tapes as two HTS conductors for bipolar DC power transmission power and a sketch of the gap. (b) Schemes of cross (left) and parallel (right) twist winding cable.

are used as the inner and outer HTS conductor, respectively. To make the magnetic flux line circular around the cable, the HTS tapes are spirally and closely wound, which leads to a different number of tapes in each conductor due to their different radii. If the same tapes are used for each HTS conductor, a space gap between the tapes will be produced. The problem is that the gap will affect the critical current of the tapes in the cable and finally reduces the current capacity of the cable thus limiting the efficiency for SC-PT system [9].

To design a HTS power cable, it is important to investigate the effects of the tape arrangement on the property of the HTS tapes in the HTS cable such as gaps between tapes in each layer and winding method [10], [11]. The effect of the tape arrangement on the AC losses is studied for an AC PT cable. Small gaps will reduce ac losses [11]. As for DC cable, the situation is different. Previously, we investigated the gap effects on the critical current of BSCCO tape in the parallel arrangements of three straight BSCCO tapes with a mono-layer and multi-layer structure to optimize the layout of the HTS tapes in the cable [12]. The critical current increases sharply by arranging the relative position of the tapes in the two-layer structure comparing with the mono-layer and stacked structure. This technical paper will present the measurements of the critical currents of the tape for a two-layer structure by using more tapes and different tape arrangements to study the behavior of a tape in the DC power cable. Fig. 1(b) shows schemes of cross and parallel twist winding for a two-layer structure. The critical currents of the five straight and twist tape arrangements in consideration of gaps and winding direction are measured. The improvement of the critical current is observed which suggests that DC HTS power cables can be improved through the careful tape arrangements.

Manuscript received October 6, 2012; accepted December 28, 2012. Date of publication January 1, 2013; date of current version January 30, 2013. This work was supported in part by the Ministry of Education, Culture, Sports, Science and Technology as "Collaboration with Local Communities" Project for Private Universities, and Chubu Grant A (II). The 200 m cable system construction was supported in part by Dr. H. Fujiwara, a Professor of Keio University and President of Nano-Opt Energy Corporation.

The authors are with Chubu University, Kasugai, Aichi 487-8501 Japan (e-mail: j_sun@isc.chubu.ac.jp).

Color versions of one or more of the figures in this paper are available online at http://ieeexplore.ieee.org.

Digital Object Identifier 10.1109/TASC.2012.2237495

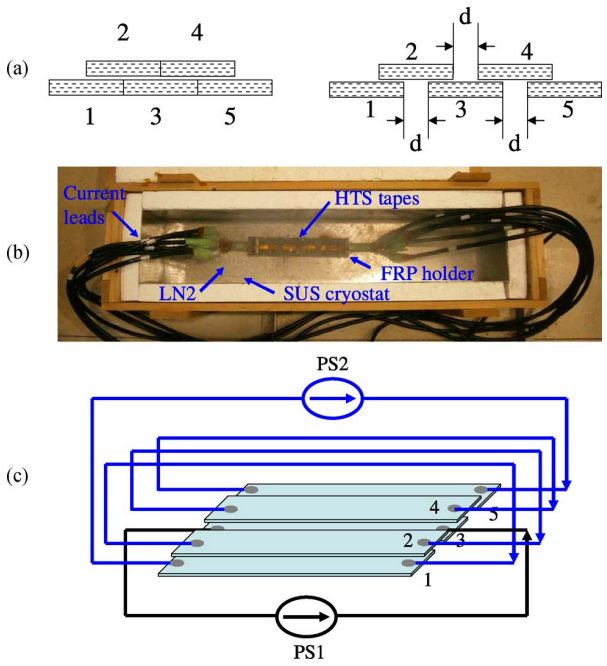

Fig. 2. (a) Arrangements of five BSCCO tapes in a two-layer structure with different gap d between the tapes and (b) an image of the experimental device. (c) Schematic diagram of current loop by two separate power supplies.

II. Samples and Experimental Procedures

In the experiment, the HTS tapes are DI-BSCCO tapes (Type HT-CA) from those in the 200 m cable manufactured by Sumitomo Electric Industries [13]. The cross section of the tape is 4.5 mm $\times$ 0.35 mm with 0.05 mm copper laminates on both sides of the tape with enhanced mechanical properties. The critical current of the BSCCO tape is 150–170 A in self field at 77 K.

Fig. 2(a) shows the layout of five BSCCO tapes arrangement in a two-layer structure with different gap between the tapes in each layer. d is the distance (gap) between the edges of the tapes. Five straight BSCCO tape wires with 27 cm length are assembled in parallel and insulated from each other. Critical current measurements are performed at 77 K by immersing the tapes into liquid nitrogen as shown in Fig. 2(b). The critical current of the tape is measured by the four probe method. Three voltage taps are soldered on each tape with space of 8 cm and 10 cm. The voltage signals are measured by a KEITHLEY 2700 multimeter with sensitivity of 0.1 μV/cm. The transport currents are measured by a 0.125 mΩ current shunt resistor. The transport current feed mode is controlled by using two power supplies as shown in Fig. 2(c). The critical current of tape #3 in the five parallel straight tapes conductor is measured by varying the current applied to the other tapes in series mode.

III. Results and Discussion

A. Critical Current for Parallel Straight Tapes Arrangements

E–I curves of the BSCCO tape are obtained by normalizing the voltages to the distance between the voltage taps. Fig. 3 shows comparisons of E–I curves of tape #3 for single and five parallel straight tapes arrangements with different gaps. The

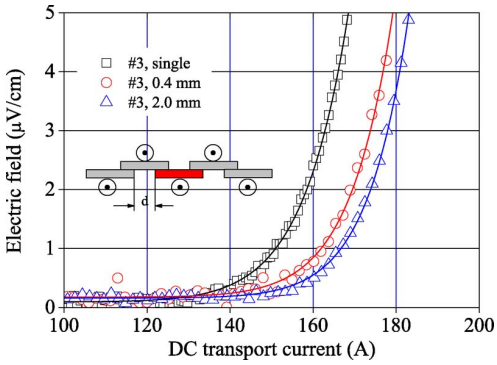

Fig. 3. E–I curves of BSCCO tape #3 for single and five straight tape arrangements with 0.4 and 2.0 mm gaps. The solid lines represent the fitting curves to determine the critical current. The inset presents the current (120 A) applied to each tape in the same direction.

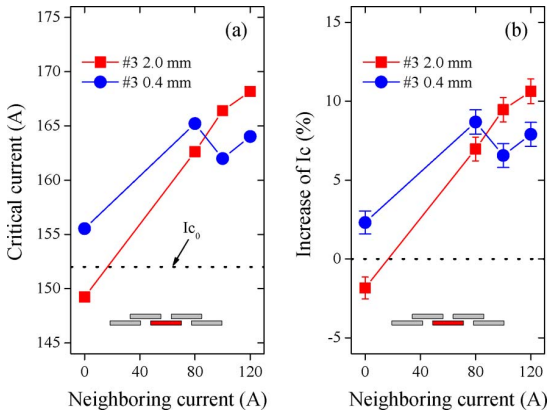

Fig. 4. (a) Critical current of the BSCCO tape with respect to the neighboring current in the other tapes for five parallel straight tape arrangements with small 0.4 mm and large 2.0 mm gaps. (b) Increase of the critical current with respect to the neighboring current.

current are applied to each tape in the same direction as the inset of Fig. 3. The neighboring current applied to tapes #1, #2, #4, and #5 is 120 A. E–I curves are quite different between small 0.4 mm and large 2.0 mm gap.

Fig. 4(a) summarizes the critical currents of the BSCCO tape with respect to neighboring current in the other tapes for different gaps between the tapes. The critical current is determined at the electric field criterion of 1 μV/cm. The critical currents of single tape is measured to be 152.0 A for the tape #3. Fig. 4(b) shows the increase of the critical current with respect to neighboring current. In the case of a two-layer structure with 2.0 mm gap, the critical currents of the tape #3 become larger than that of the single one when the neighboring current is larger than 80 A. When $d = 2.0$ mm, the critical current of the tape #3 increases by 11% from 152 A to 168 A. The critical current of a tape #3 in five parallel straight tape arrangement with large gap 2.0 mm become larger than that for small gap 0.4 mm. The critical current of BSCCO tapes are improved when there are gaps between the tapes in the same layer due to magnetic field interaction between the tapes.

To understand the magnetic field interaction on the self field due to the transport neighboring current from the other tapes, the magnetic field distributions are calculated by the commercial finite element code (ANSYS) [14], [15]. To illustrate the

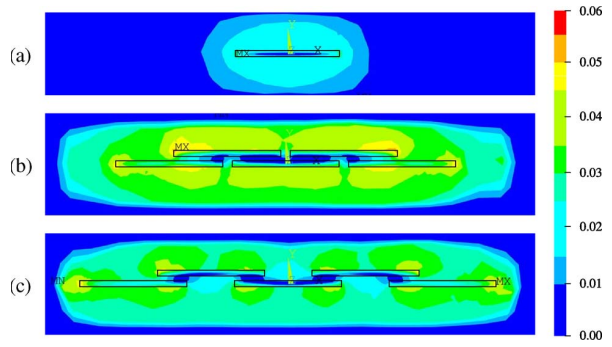

Fig. 5. (a) Calculated magnetic field distributions for single tape, (b) five tapes with 0.4 mm gap, and (c) five tapes with 2.0 mm gap.

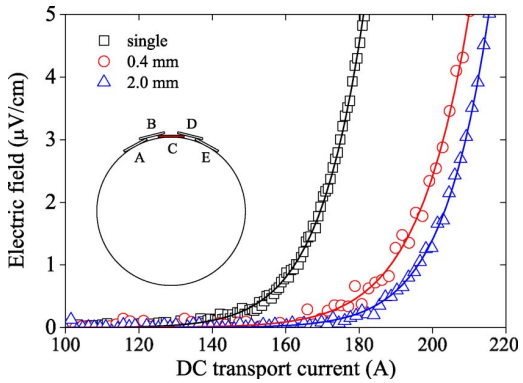

Fig. 6. *E–I* curves of BSCCO tape #C for single and five parallel twist tape arrangement with 0.4 and 2.0 mm gap. The inset shows the cross-section image of the twist conductor.

magnetic field interaction on the tape #3 by the neighboring current, Fig. 5 presents the magnetic field distributions for single tape and five tape arrangements. The transport current of 160 A in each tape is assumed to be uniformly distributed in the cross section of the Ag-sheathed BSCCO filaments area, i.e., the cross section of the transport current area is 4.5 mm × 0.25 mm without the laminated copper tape [13]. As seen in Fig. 5(c) the magnetic field in the area of sample #3 in five tape conductor with 2.0 mm gap is reduced compared to that with a 0.4 mm gap in Fig. 5(b) and also the single tape in Fig. 5(a). The reduction of self field by the neighboring current in the other tapes improves the critical current of the tape #3 for five parallel straight tapes arrangement as shown in Fig. 4.

B. Critical Current for Parallel Twist Tape Arrangement

As shown in Fig. 1, the HTS tapes are spirally wounded around a former, which will lead to twist strain on the tape together with the local magnetic field distortion due to the twisted tapes [16]. To observe the critical current for a parallel twist tape arrangement, five insulated tapes with length of 54 cm are used to make a helically wound cable as shown in the inset of Fig. 6 with 0.4 mm and 2.0 mm gaps. The tapes are wound around a former with a diameter of 2.6 cm and the twist pitch is 25 cm.

Fig. 6 shows *E–I* curves of the tape #C in the five parallel twist tape conductor with gap of 0.4 mm and 2.0 mm in

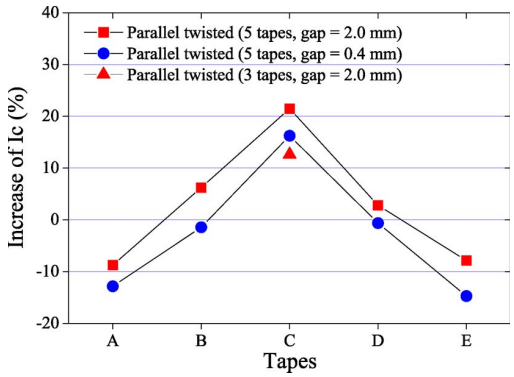

Fig. 7. Symmetrical profile of increase of the critical current for five parallel twist tapes conductor with 0.4 and 2.0 mm gap together with the three parallel twist tape conductor in previous work [12].

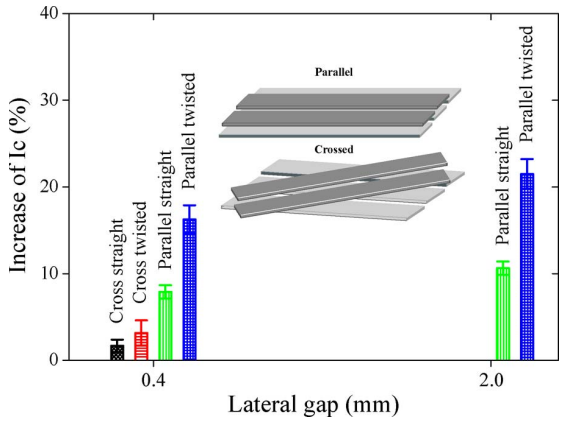

Fig. 8. Winding direction effect on the critical current of BSCCO tape for the different arrangements.

comparison with the single tape, which are similar with those in parallel straight tape conductor as shown in Fig. 3. The measured critical currents of single tape #A, #B, #C, #D and #E are 155.1 A, 162.6 A, 162.0 A, 166.8 A, and 167.2 A, respectively. Since the transport current is applied to each tape in series mode, we obtain the critical current of each tape in the five parallel twist tapes arrangement. Fig. 7 shows a symmetrical profile of the critical current distributions for five parallel twist tape conductor. The critical currents of each tape for large 2.0 mm gap are larger than those for small 0.4 mm gap. The critical current of the tape #C increases sharply by 20% to 196 A for five parallel twist tapes with gap of 2.0 mm, which shows a similar behavior as three parallel twist tape arrangements [12]. Therefore, the five tape arrangement could be a similar reasonable representation of the real cable.

C. Comparison of Parallel and Cross Arrangement

In the case of 200 m cable, the tapes for the inner HTS conductor are cross wound between each layer as shown in Fig. 1. In order to observe the winding effects on the critical current, the critical currents are measured for the cross arrangement in comparison with the parallel arrangement as shown in the inset of Fig. 8. As for the cross arrangement, the tapes are only arranged with a small gap. The measured critical currents

of the middle tape #3 and #C are 154.6 A and 167.1 A for straight and twist tapes with a little improvement of less than 3%. Fig. 8 presents the winding direction effects on the critical current of BSCCO tape for the different arrangements. The parallel arrangement is better than the cross arrangement for both straight and twist BSCCO tapes.

Through the critical current measurements and analysis on the magnetic field interactions for different tape arrangement, the tape arrangements of the inner HTS conductor could be optimized to improve the property of the HTS cable for DC power transmissions and distributions in consideration of the effects of twist and winding direction. As for the old cable in Fig. 1, 23 tapes are closely wound around a copper former with small gaps (< 0.5 mm). For a new design of a DC cable, less tapes can be used, i.e., 18 tapes are used to make the inner HTS conductor in the 2-layer structure with the gap of 2 mm without degradation of the critical current of the tape in the cable.

IV. Conclusion

We have measured the critical current of BSCCO tapes for different gaps between the tapes in the five parallel straight tape conductors with a two-layer structure. Dependence of the critical current of BSCCO tapes on the lateral space gap between the tapes in the five parallel straight tapes with the two-layer structure shows that the critical current of a BSCCO tape is improved when there exist gaps for both parallel straight tape conductor and parallel twist tape conductor. Additionally, strong improvement of critical current for the parallel arrangement is observed in contrast to that for the cross arrangement. Even if there is a gap for appropriate tape arrangements, the performance of the tape in the cable does not degraded. Thereafter, in the case of two-layer structure, the tapes can be wound in parallel with gaps between the tapes in a DC power cable with improved superconductivity of the tape, which will reduce the number of tapes and lead to reduction of the cable cost. It is concluded with that attention on the tape arrangements for DC cable fabrication may be different from AC cable.

Acknowledgment

The authors thank Dr. A. Iiyoshi, Chairman of the Board of Trustees and Chancellor of Chubu University, for his continuous encouragement throughout this work.

References

[1] M. Ichikawa, M. Kanegami, T. Okamoto, S. Akita, M. Yagi, and A. Kimura, "Thermomechanical characteristics of 500-m HTS power cable," *IEEE Trans. Appl. Supercond.*, vol. 15, no. 2, pp. 1771–1774, 2005.

[2] S. Dai, L. Lin, Y. Lin, Z. Gao, Y. Fang, L. Gong, Y. Teng, F. Zhang, X. Xu, G. Li, L. Li, and L. Xiao, "The three-phase 75 m long HTS power cable," *Cryogenics*, vol. 27, no. 7/8, pp. 402–405, 2007.

[3] J. Lim, S. Sohn, H. Ryoo, H. Choi, H. Yang, D. Kim, Y. Ma, K. Ryu, and S. Hwang, "Performance test of 100 m HTS power cable system," *IEEE Trans. Appl. Supercond.*, vol. 19, no. 3, pp. 1710–1713, 2009.

[4] R. Soika, X. Garcia, and S. Nogales, "ENDESA supercable, a 3.2 kA, 138 MVA, medium voltage superconducting power cable," *IEEE Trans. Appl. Supercond.*, vol. 21, no. 3, pp. 972–975, 2011.

[5] S. Yamaguchi, T. Kawahara, M. Hamabe, H. Watanabe, Y. Ivanov, J. Sun, and A. Iiyoshi, "Experiment of 200-meter superconducting DC cable system in Chubu University," *Phys. C, Supercond.*, vol. 471, no. 21/22, pp. 1300–1303, 2011.

[6] J. Sun, S. Yamauchi, M. Sugino, H. Watanabe, M. Hamabe, T. Kawahara, and S. Yamaguchi, "Critical current measurements for design of superconducting DC transmission power cable," *Phys. C, Supercond.*, vol. 471, no. 21/22, pp. 1313–1316, 2011.

[7] M. Hamabe, A. Sasaki, T. Famakinwa, A. Ninomiya, Y. Ishiguro, and S. Yamaguchi, "Cryogenic system for DC superconducting power transmission line," *IEEE Trans. Appl. Supercond.*, vol. 17, no. 2, pp. 1722–1725, 2007.

[8] N. Amemiya, Q. Li, K. Ito, K. Tekeuchi, T. Nakamura, and T. Okuma, "AC loss reduction of multilayer superconducting power transmission cables by using narrow coated conductors," *Supercond. Sci. Technol.*, vol. 24, no. 6, p. 065013, 2011.

[9] O. Tsukamoto, "Roads for HTS power applications to go into the real world cost issues and technical issues," *Cryogenics*, vol. 45, no. 1, pp. 3–10, 2005.

[10] O. Tsukamoto, Y. Yamato, S. Nakamura, and J. Ogawa, "Measurements of AC transport current losses in HTS tapes in an assembled conductor," *IEEE Trans. Appl. Supercond.*, vol. 16, no. 2, pp. 2895–2898, 2005.

[11] S. Fukui, R. Kojima, J. Ogawa, M. Yamaguchi, T. Sato, and O. Tsukamoto, "Numerical analysis of AC loss characteristics of cable conductor assembled by HTS tapes in polygonal arrangement," *IEEE Trans. Appl. Supercond.*, vol. 16, no. 2, pp. 143–146, 2006.

[12] J. Sun, H. Watanabe, M. Hamabe, T. Kawahara, A. Iiyoshi, and S. Yamaguchi, "A new layout of HTS tapes and their critical currents for DC power cables," *Phys. Proc.*, vol. 36, pp. 372–375, 2012.

[13] N. Ayai, K. Yamazaki, M. Kikuchi, G. Osabe, H. Takaaze, H. Takayama, S. Kobayashi, J. Fujikami, K. Hayashi, K. Sato, K. Osamura, H. Kitaguchi, S. Matsumoto, T. Kiyoshi, and J. Shimoyama, "Electrical and mechanical properties of DI-BSCCO type HT reinforce with metallic sheathes," *IEEE Trans. Appl. Supercond.*, vol. 19, no. 3, pp. 3014–3017, 2009.

[14] ANSYS, Academic Teaching Advanced, Release 12.1 ANSYS Inc. [Online]. Available: www.ansys.com

[15] S. Farinon, P. Fabbricatore, and F. Gömöry, "Critical state and magnetization loss in multifilamentary superconducting wire solved through the commercial finite element code ANSYS," *Supercond. Sci. Technol.*, vol. 23, no. 11, p. 115004, 2010.

[16] H. S. Shin and K. Katagiri, "Critical current degradation behaviour in Bi-2223 superconducting tapes under bending and torsion strains," *Supercond. Sci. Technol.*, vol. 16, no. 9, pp. 1012–1018, 2003.

IEEE TRANSACTIONS ON APPLIED SUPERCONDUCTIVITY, VOL. 23, NO. 3, JUNE 2013 5400204

Status of a 200-Meter DC Superconducting Power Transmission Cable After Cooling Cycles

Makoto Hamabe, Hirofumi Watanabe, Jian Sun, Norimasa Yamamoto, Toshio Kawahara, and Satarou Yamaguchi

***Abstract*—We constructed a facility of a 200-m HTS power transmission test cable (CASER-II) in 2010. Generally, an HTS cable contracts about 0.3% when it is cooled from room temperature to liquid nitrogen (LN2) temperature. The contraction of the 200-m HTS cable corresponds to 0.6 m. In order to realize the HTS power transmission system, it is an essential issue to absorb the mechanical stress of the HTS cable during the cycles of cooling-down and heating-up. The CASER-II uses smooth pipes as the cryogenic pipe for the cable line to reduce the pressure drop of the liquid nitrogen flow, whereas the other HTS cables use corrugated pipes to absorb the mechanical stress. The CASER-II employed (1) the movable terminals at the cable end, and (2) the extendable bellows inserted in the cryogenic pipe, to absorb the contraction of 0.6 m in cooling cycles. Even at the 4th cooling-down test, no damage was observed in the CASER-II. Use of the smooth cryogenic pipe enabled low pressure drop with low LN2 flow rate, and negative pressure drop appeared at less than 5 L/sec of the LN2 flow rate. This negative pressure drop was caused by the LN2 flow assisted by siphon effect due to the difference of LN2 density along the cryogenic pipe line with elevation of 2.6 m.**

***Index Terms*—Cryogenic system, DC power transmission, DC superconducting cables, siphon effect.**

I. Introduction

RECENTLY, SEVERAL projects of DC superconducting power transmission (SC-PT) were proposed and started [1]–[4]. They target the long power transmission [1], the link of three electrical AC grids [2], and the power transmission in a factory [3] and in a railways [4]. Previous to these projects, we started research program on the DC SC-PT system and constructed a 20-m DC HTS cable test facility (CASER-I) in Chubu University in 2006 [5]. Depending on the results achieved in the CASER-I [6], we constructed a 200-m DC SC-PT cable test facility (CASER-II) in 2010 also in Chubu University [7].

One of the important issues to realize the DC SC-PT system is the tolerance against the cooling cycles, since the thermal contraction of the LN2-cooled superconducting cable reaches about 0.3%. Employment of corrugate pipe as the cable pipe is the common method for AC [8]–[10] and DC SC-PT cable [1]–[4]. Meanwhile, the CASER-I inserted bellows in the cryopipe to absorb the contraction by 6 cm of the cable. In addition, the cable ends were not fixed to the terminals, in order for the cable to be free from the mechanical stress due to the cycles of cooling-down and warming-up processes. Cooling cycle tests by 6 times in the CASER-I proved no damage in critical current measurement of the cable [6]. The CASER-II also employed extendable bellows and movable terminals to absorb the contraction of 60 cm [7] and repeated cooling cycles to the test facility [11].

In this paper, we will describe the results of "the forth cooling down test" of the CASER-II which was carried out from Aug. to Nov. 2011. Here, we will show the procedure of the cooling-down process to the LN2 temperature and the warming-up process to the room temperature. The results of the LN2 circulation test and estimation of the heat leakage of the test facility will be also described.

Manuscript received October 9, 2012; accepted December 15, 2012. Date of publication December 20, 2012; date of current version January 13, 2013. This work was supported in part by a grant of Strategic Research Foundation Grant-aided Project for Private Universities Ministry of Education, Culture, Sports, Science and Technology (MEXT).

The authors are with Chubu University, Kasugai, Aichi 487-8501, Japan (e-mail: hamabe@isc.chubu.ac.jp; h_watanabe@isc.chubu.ac.jp; j_sun@isc.chubu.ac.jp; Norimasayamamoto-no@isc.chubu.ac.jp; toshi@isc.chubu.ac.jp; yamax@isc.chubu.ac.jp).

Color versions of one or more of the figures in this paper are available online at http://ieeexplore.ieee.org.

Digital Object Identifier 10.1109/TASC.2012.2235510

II. 200-Meter DC Superconducting Power Transmission Cable Test Facility

A. DC HTS Power Cable

Specification of the DC HTS power cable was described in [7] in detail. A DC HTS power cable core was fabricated by Sumitomo Electric Industries, Ltd. The cable consisted of co-axial three layers of DI-BSCCO HTS tapes; there were the one outside layer of 16 tapes and the two inside layers of 23 tapes for bipolar current feed with an insulation voltage of $\pm$10 kV. Designed total current of the cable was 2 kA at 78 K.

B. Cryogenic System

Fig. 1 shows a cryogenic system of the CASER-II. This cryogenic system was fabricated by AISIN SEIKI Co., Ltd, and consists of a Stirling type cryocooler, a LN2 pump unit, a mass flow meter and, two LN2 reservoir (return/send) as the LN2 line, and of a water chiller unit for the Stirling cryocooler. Specifications of the cryogenic system are shown in Table I [11].

C. Terminals and Cable Line

Fig. 2 shows the terminals and cable line of the CASER-II. Both cable ends were installed in the terminals, and HTS tapes in the cable core were connected to the current leads

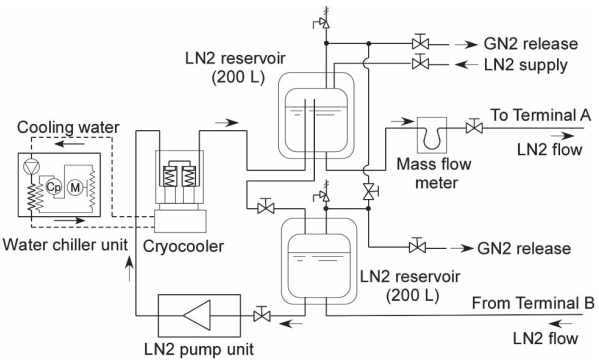

Fig. 1. Schematic diagram of cryogenic system of 200-m DC SC-PT cable test facility (CASER-II). Solid lines show the LN2 flow and dotted lines show the cooling water flow from the water chiller unit to the cryocooler.

TABLE I
SPECIFICATION OF CRYOGENIC SYSTEM OF 200-m DC SC-PT CABLE TEST FACILITY (CASER-II)

Cryocooler	Stirling type
Cooling Power	1 kW @ 77 K
COP of cryocooler	0.083 @ 77 K
LN2 Pump	> 1800 rpm
Typical LN2 flow rate	10 L/min
Volume of LN2 reservoir	200 L x 2 tanks

in the terminals. One of the features of the CASER-II is that the two terminals can move to the cable line direction, following the contraction or expansion of the cable core [7]. Moreover, cable ends were not fixed to the terminals and were able to slide against the terminals; these cable ends allowed the cable core free from the mechanical stress due to the contraction or expansion of the cable core itself. Positions of cable ends in the terminals were monitored by cameras and the slide motion of the cable ends was observed in the cooling-down/warming-up processes. Peltier current leads were installed in the terminals to reduce the heat leakage through the current lead [12].

Another feature of the CASER-II is that the cable core was placed in the smooth pipes with vacuum insulation ("smooth cryopipe"), which consisted of a zinc-coated carbon-steel pipe (216 mm in outside diameter and 5.8 mm in thickness) as the outside pipe, and a stainless-steel pipe (60.5 mm in outside diameter and 1.65 mm in thickness) as the inside pipe. Compared with the corrugated pipes, which are widely used for the cryopipe of superconducting cables, the smooth cryopipe has the advantage to reduce the pressure drop of LN2 flow [13]. Expandable bellows were inserted in the outside smooth cryopipe to absorb the movements of the terminals (Fig. 2). Several bellows were inserted also in the inside cryopipe to adjust the shape of the inside cryopipe to that of the outside cryopipe.

Fig. 3 shows the layout of the cable line of the CASER-II. The cable line was L-shaped. The two terminals A and B were placed on the left end of the L-shape in Fig. 3, and the cable line turned on the right end in Fig. 3. Elevation of the turn of the cable line was lower than that of the terminals.

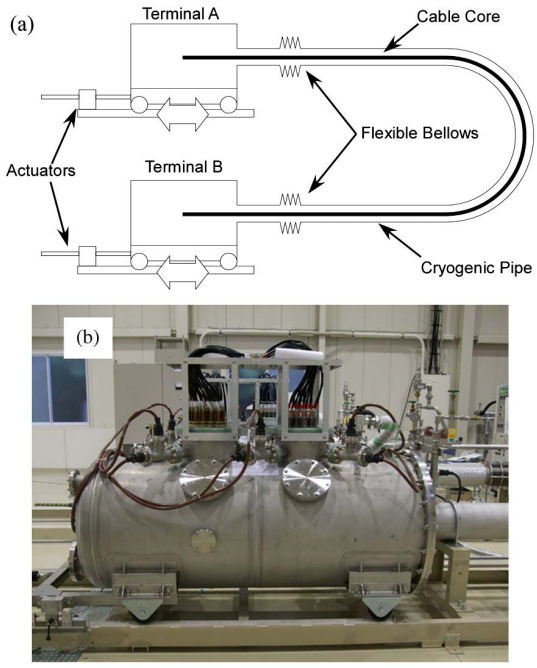

Fig. 2. (a) Structure to absorb the shrinkage/expansion of the cable core due to the cooling cycles. (b) Terminal B with wheels.

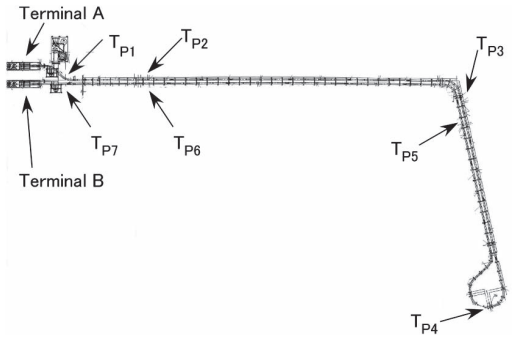

Fig. 3. Layout of the cable line. Positions of the thermosensors of the inside pipe along the cable are indicated ($T_{\mathrm{P1}} \sim T_{\mathrm{P7}}$).

III. PROCEDURE OF COOLING-DOWN AND WARMING-UP

The tolerance for the cooling cycles is the essential issue for the design of the DC SC-PT system. The movable terminals at the cable ends and the extendable bellows in the outside cryopipe were installed in the CASER-II to prevent the cable core from suffering the mechanical stress due to the cooling cycle, as shown in Section II-C; the movements of the terminals were manually controlled through the processes toward the cooling-down to the LN2 temperature and the warming-up to the room temperature.

A Procedure during the cooling-down/warming-up processes is as follows:

1) Measure the temperature profile of the inside cryopipe, with the thermosensors, shown in Fig. 3,
2) Calculate the contraction/expansion of the inside cryopipe from its temperature profile, and
3) Move the position of the terminals A and B.

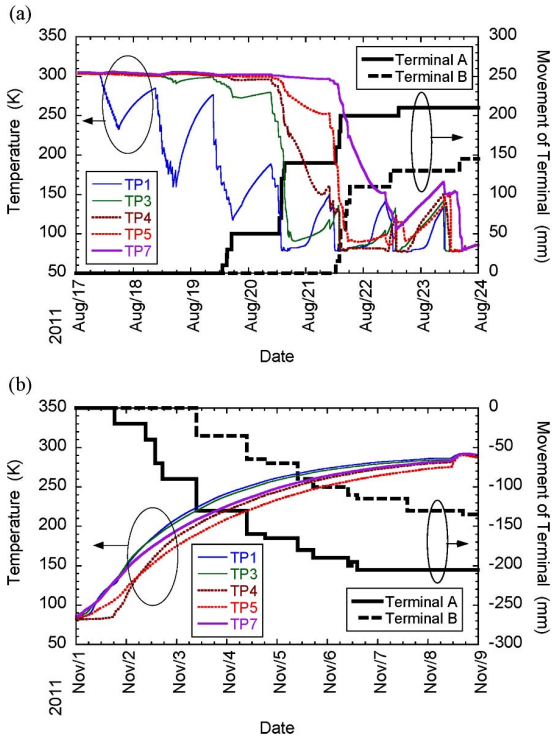

Fig. 4. Time variation of the temperature profile of the inner pipe and the movements of terminals during (a) cooling-down and (b) warming-up processes.

Fig. 4 shows the time variation of the temperature profile of the inside cryopipe and the movements of the terminals during the cooling-down/warming-up processes in the fourth cooling down test. Note that the cooling-down process was carried out only in the daytime. In the cooling-down process, the cold nitrogen gas, and then LN2 were introduced from the terminal A to the terminal B in Aug. 17, and first of all, temperature T_{P1} started to decreased. The terminal A started to be moved after T_{P3} started to decrease in Aug. 19; the terminal B started to be moved after T_{P5} started decreased in Aug. 21. Consequently, the movement of the terminal A was larger than the that of the terminal B since the cable core near the terminal A finished to contract (T_{P1} reached at the LN2 temperature), before the one near the terminal B started to contract (T_{P7} was at the room temperature).

In the warming-up process, the cryogenic system was stopped and the LN2 in the cryopipe was released in Nov. 1. The cryopipe and the cable core were left to increase their temperature naturally; temperatures $T_{\mathrm{P1}} \sim T_{\mathrm{P7}}$ increased with the similar rate. In this process, we tried to bring back the positions of the terminal A and B to their positions before the cooling down.

IV. Results of LN2 Circulation Test

After the cooling-down process, the LN2 circulation test started. At the fourth cooling-down test, LN2 circulation with the wide range of the LN2 flow rate was tested. Fig. 5 shows the pressure drop between the terminal A and the terminal B for

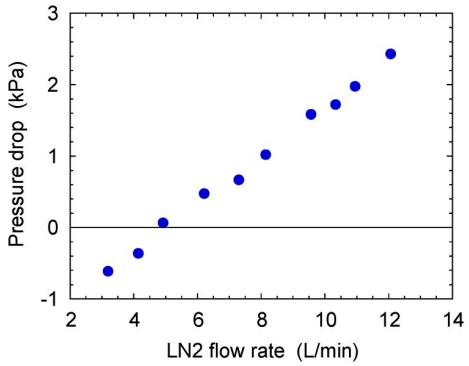

Fig. 5. Pressure drop from the terminal A to the terminal B as a parameter of LN2 flow rate. Here, temperature of LN2 was 71 $\sim$ 74 K at the output of the cryogenic system.

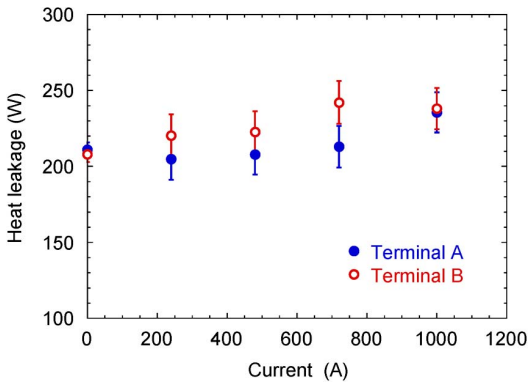

Fig. 6. Heat leakage at the terminals as the parameter of the feeding current.

the various LN2 flow rate. The lowest LN2 flow rate reached 3 L/min; this low flow rate was achieved by the reduction of the pressure loss of the LN2 flow along the cable due to the smooth cryopipe. Moreover, the pressure drop turned to be negative at low flow rate < 5 L/min; this negative pressure drop was caused by the assistance of the "thermal siphon effect", which means that the LN2 naturally circulates due to its density difference along the cable line with the elevation difference of 2.6 m [14].

V. Heat Leakage Measurement

In the DC SC-PT system, there are two main heat leakage along the SC cable; the one is the conduction heat and Joule heat through the current leads, and the other is the radiation heat at the cryopipe. The first one is the serious in particular for the short length power transmission of several hundreds meters. The second one is the main heat leakage for the long distance power transmission more than several kilometers. For the CASER-II, these two heat leakages were comparative; estimation and reduction of both heat leakages are the important issues for the discussion of the efficiency of the system. Therefore, heat leakages at the two terminals and at the cryopipe along the cable were estimated from the temperature rise of the LN2 flow at each part.

Fig. 6 shows the heat leakage at the terminals A and B. Installation of the Peltier current leads suppressed the increase

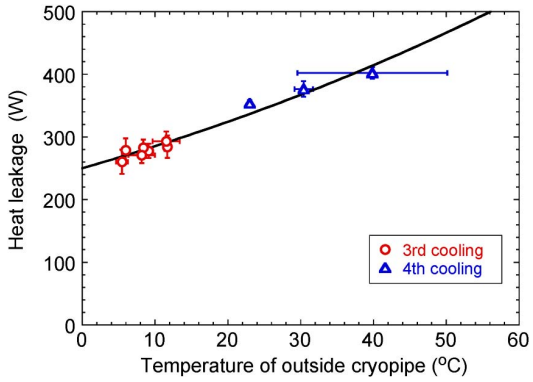

Fig. 7. Heat leakage at the cryogenic pipe line at the third cooling down to the fourth cooling down. The curve fits the third and fourth data by sum of the radiation heat and the conduction heat.

of the heat leakage by Joule heat, despite of the increase of the current feed [12].

Fig. 7 shows the heat leakage at the cryopipe at the third cooling-down (Jan. $\sim$ Mar. 2011) and the fourth cooling-down tests. The measured heat leakage was on the similar curve approximated by the sum of the radiation heat $a[(T + 273)4 - 77.34]$ and the thermal conductance $b[(T + 273) - 77.3)]$, where T (°C) is the temperature of the outside cryopipe, in Fig. 7. After the third cooling-down test, the insulation vacuum at the cryopipe was opened for the maintenance, and was re-evacuated without baking the cryopipe. Consequently, the open and the re-evacuation of the cryopipe was not affected for the heat leakage (= the thermal insulation) of the cryopipe.

VI. Conclusion

We showed the experimental results of 4th cooling down in 200-m DC superconducting power transmission cable test facility(CASER-II) in Chubu University, Japan. Employment of the movable terminals and the extendable bellows in the outside cryopipe absorbed effectively the contraction of the cable core and the inside cryopipe due to the cooling-down process. By the use of the smooth pipes as the cryogenic pipe, a low pressure drop of LN2 flow was achieved. In particular, at the lower flow rate < 5 L/min, the negative pressure drop appeared because of the assistant of "thermal siphon effect". The heat leakages at the terminals and at the cryopipe were individually measured.

Acknowledgment

The authors thank Dr. A. Iiyoshi, Chancellor of Chubu University, for his continuous encouragement through this work. The authors appreciate Dr. H. Fujiwara for his support on the construction of 200 m superconducting facilities of CASER-2.

References

[1] W. Hassenzahl, B. Gregory, S. Eckroad, S. Nilsson, A. Daneshpooy, and P. Grant, "Program on technology innovation: A superconducting DC cable," EPRI Rep. 1020458, Dec. 2009.

[2] M. Young, "Superconducting power cables," EPRI Tech. Update Rep. 1017792, Dec. 2009.

[3] X. M. Liang, S. T. Dai, Z. Y. Gao, N. H. Song, Y. S. Wang, D. Zhang, Z. F. Zhang, F. Y. Zhang, Z. Q. Zhu, X. Xu, T. B. Huang, X. C. Li, Z. C. Cao, Y. B. Lin, L. Z. Lin, and L. Y. Xiao, "Design of a 380 m DC HTS power cable," *IEEE Trans. Appl. Supercond.*, vol. 20, no. 3, pp. 1259–1262, Jun. 2010.

[4] M. Tomita, K. Suzuki, Y. Fukumoto, A. Ishihara, and M. Muralidhar, "Next generation of prototype direct current superconducting cable for railway system," *J. Appl. Phys.*, vol. 109, p. 063909, Mar. 2011.

[5] S. Yamaguchi, M. Hamabe, I. Yamamoto, T. Famakinwa, A. Sasaki, A. Iiyoshi, J. Shultz, J. Minervini, T. Hoshino, Y. Ishiguro, and K. Kawamura, "Research activities of DC superconducting power transmission line in Chubu University," *J. Phys., Conf. Ser.*, vol. 97, p. 012290, Mar. 2008.

[6] M. Hamabe, T. Fujii, M. Sugino, A. Sasaki, T. Sugimoto, H. Watanabe, T. Kawahara, S. Yamaguchi, Y. Ishiguro, and K. Kawamura, "Cooling cycle test of DC superconducting power transmission cable," *J. Phys., Conf. Ser.*, vol. 234, p. 032019, Jul. 2010.

[7] S. Yamaguchi, T. Kawahara, M. Hamabe, H. Watanabe, Y. Ivanov, J. Sun, and A. Iiyoshi, "Design and construction of 200-meter high temperature superconducting DC power cable test facility in Chubu University," in *Proc. 23rd Int. Cryogen. Eng. Conf. Int. Cryogen. Matter Conf.*, Wroclaw, Poland, 2011, pp. 1041–1047.

[8] T. Masuda, H. Yumura, M. Watanabe, H. Takigawa, Y. Ashibe, C. Suzawa, T. Kato, Y. Yamada, K. Sato, S. Isojima, C. Weber, A. Dada, and J. R. Spadafore, "Design and experimental results for Albany HTS cable," *IEEE Trans. Appl. Supercond.*, vol. 15, no. 2, pp. 1806–1809, 2005.

[9] J. F. Maguire, F. Schmidt, S. Bratt, T. E. Welsh, and J. Yuan, "Installation and testing results of Long Island transmission level HTS cable," *IEEE Trans. Appl. Supercond.*, vol. 19, no. 3, pp. 1692–1697, Jun. 2009.

[10] Y. S. Choi, D. L. Kim, H. S. Yang, S. H. Sohn, J. H. Lim, and S. D. Hwang, "Progress on the performance test of KEPCO HTS power cable," *IEEE Trans. Appl. Supercond.*, vol. 21, no. 3, pp. 1034–1037, Jun. 2011.

[11] H. Watanabe, Y. Ivanov, J. Sun, M. Hamabe, T. Kawahara, and S. Yamaguchi, "Heat leak measurement of the 200 m superconducting power transmission system at Chubu University," *Phys. Proc.*, vol. 36, pp. 1366–1371, 2012.

[12] T. Kawahara, T. Fujii, M. Emoto, M. Hamabe, J. Sun, H. Watanabe, and S. Yamaguchi, "Estimation for the performance of superconducting DC transmission lines with cryogenics improvements," *Phys. C*, vol. 470, pp. S1011–S1012, Dec. 2010.

[13] J. C. Weisend, II and S. W. Van Sciver, "Pressure drop from flow of cryogens in corrugated bellows," *Cryogenics*, vol. 30, pp. 935–941, Nov. 1990.

[14] Y. Ivanov, H. Watanabe, M. Hamabe, T. Kawahara, J. Sun, and S. Yamaguchi, "Design study of LN2 circulation in a long SC power transmission lines," *Phys. Proc.*, vol. 36, pp. 1372–1377, 2012.

IEEE TRANSACTIONS ON APPLIED SUPERCONDUCTIVITY, VOL. 23, NO. 3, JUNE 2013 4802304

Refrigeration Process to Realize a Multistage and Gas-Cooled Current Lead

Satarou Yamaguchi, *Member, IEEE*, Masahiko Emoto, Norimasa Yamamoto, Jian Sun, Hirofumi Watanabe, Makoto Hamabe, and Toshio Kawahara

***Abstract*—Heat leak from the current lead is the major source of power loss for superconducting (SC) magnets, motors and generators, and short distance SC power transmission lines. Therefore, reducing the heat leak from the current lead can improve the economy of the SC system and allow the use of SC systems commercially. The Peltier current lead was proposed and developed at Chubu University to reduce the electrical power consumption of the refrigerator. The heat leakage of the Peltier current lead saves almost 40%, but the power requirement of the refrigerator is still high. In order to realize greater power savings, the multistage current lead (MCL) and the gas-cooled MCL are proposed. The heat leakage reduction of the gas-cooled MCL depends on the characteristics of the cryogen and its pressure and the realization of high cost of performance and a high-temperature refrigerator. Here, we show the calculation results of the high-pressure effect of cryogen and discuss the performance of nitrogen trifluoride as cryogen.**

***Index Terms*—Cryogenic system, current lead, gas-cooled current lead, low heat leakage, multistage current lead.**

I. Introduction

CURRENT leads to connect the low temperature superconducting (SC) instruments to the power supplies are necessary for the operation of SC power systems. For example, for the cryogen-free SC magnet, 90% of the heat load on the refrigerator is caused by the current lead [1]. This situation is the same for the SC motors, the generators and the transformers. DC superconducting power transmission lines are under development and, if the length of the cable is short, the major heat load on the refrigerator will be the heat leakage of the current lead because the heat leakage of the cryogenic pipe is low [2]–[4]. For example, the heat leak of the cryogenic pipe is $\sim$1 W/m and the heat leak of the current lead is $\sim$50 W/kA [5], [6] for a conduction-cooled current lead. Therefore, if the cable length is 1 km, and the current is 5 kA, the heat leak of the cryogenic pipe is 1 kW, and the heat leak of the current lead is also 1 kW. Therefore, reducing the heat leakage from the current lead can significantly improve the performance and the economy of the SC system.

However, the heat leakage is not easy to reduce. If the heat leak reduction is realized through the material characteristics, the material requires high electrical conductivity and low thermal conductivity at the same time. This is a contradiction from a physical point of view. The Peltier current lead (PCL) presents one answer to the problem because of the heat pump effect of the Peltier materials, and we have successfully developed a PCL at Chubu University experimentally [1], [2], [7]–[11]. The PCL has also been studied in South Korea [12], and the other countries.

We have also proposed other ways to reduce the heat leakage from the current lead [13] based on two principles. One is called the multi-stage current lead (MCL) and the other the gas-cooled current lead. Two ideas can also be combined. The MCL was recently discussed in [14], and the design of the current lead is optimized for its length and cross-section [5], [6]. The gas-cooled MCL is based on the temperature dependence of the electrical resistivity and the thermal conductivity of the copper (pure metal), and the characteristics of the COP of the refrigerator. The electrical resistivity of the high purity copper decreases with the decreasing temperature, and therefore the Ohmic heat generation is low at low temperature. The thermal conductivity of the copper increases with decreasing temperature. The cost of performance (COP) of a high-temperature refrigerator is higher than that of a low-temperature refrigerator. Therefore, multiple refrigerators are used. A high-temperature refrigerator maintains the temperature of part of the current lead, and a low-temperature refrigerator maintains the temperature of the low temperature end of the current lead. Total heat load is the same for a single refrigerator but the electrical power consumption of the refrigerator system is reduced.

The gas-cooled current lead also can reduce the heat leakage, leading to savings in electrical power. The principle of the gas-cooled current lead is the heat transfer from the current lead conductor to the evaporated low temperature gas. Since the gas flows out from the room temperature side of the current lead, the heat leakage of the current lead can be reduced. The efficiency of the heat transfer to the gas depends on its specific heat, which is a function of gas temperature and pressure. Therefore, a closed cycle for gas circulation in the current lead and the refrigerator system should have an optimum gas pressure. The high temperature superconductor (HTS) current leads have been studied to reduce the heat leakage for larger and low temperature SC magnets [15], [16], but the paper discusses the reduction of the heat leakage in 77 K systems.

Manuscript received October 9, 2012; accepted January 25, 2013. Date of publication January 29, 2013; date of current version March 13, 2013. This work was supported in part by a grant from the Strategic Research Foundation Grant-aided Project for Private Universities Ministry of Education, Culture, Sports, Science, and Technology (MEXT).

S. Yamaguchi, N. Yamamoto, J. Sun, H. Watanabe, M. Hamabe, and T. Kawahara are with Chubu University, Kasugai, Aichi 487-8501, Japan (e-mail: yamax@isc.chubu.ac.jp).

M. Emoto is with the National Institute of Fusion Science, Toki, Gifu 509-5292, Japan.

Color versions of one or more of the figures in this paper are available online at http://ieeexplore.ieee.org.

Digital Object Identifier 10.1109/TASC.2013.2243896

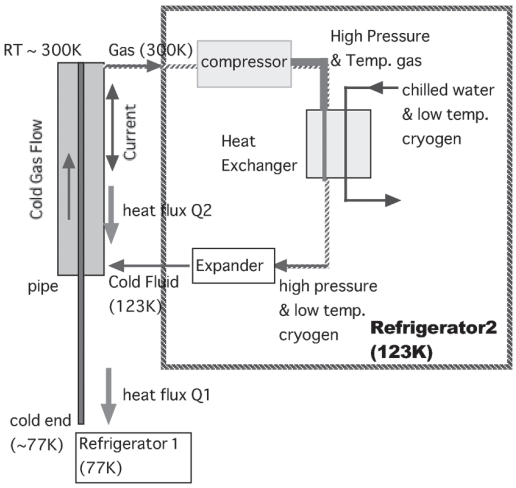

Fig. 1. Two refrigerators are used in the gas-cooled mutlistage current lead (MCL). The high-temperature refrigerator (Refrigerator 2) consists of a compressor, heat exchanger, and expander.

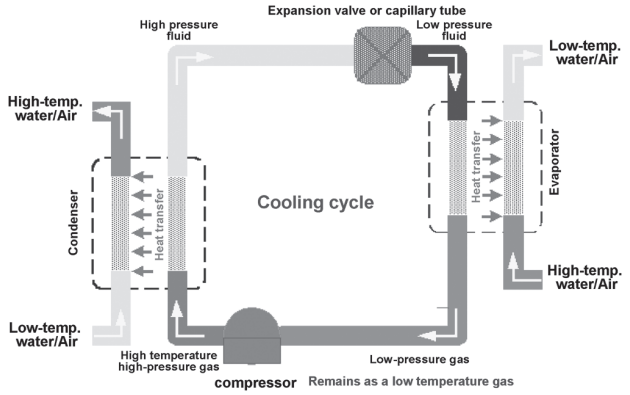

Fig. 2. Thermal cycle of the vapor compression refrigerator.

II. Model of Gas-Cooled Multi-Stage Current Lead and Refrigerator System

A. Model of the Current Lead and Cryogen Parameters

The gas-cooled MCL is shown in Fig. 1. The lower end of the current lead is cooled by the refrigerator 1 (Rfr. 1) to 77 K. The high temperature refrigerator 2 (Rfr. 2) maintains the middle of the current lead at temperature of 123 K. The gas is circulated from the cold to the warm end of the current lead, making the system is a partially gas-cooled current lead, and the heat flux to the Rfr. 1 is reduced.

However, the total heat load of the Rfr. 2 is not reduced because the warm gas returns to the Rfr. 2. Therefore, we should consider the cooling circuit of this refrigerator. Fig. 2 shows the vaporative compression refrigeration cycle. Low temperature gas flows out the low temperature heat exchanger into the compressor. The temperature of the compressor is higher than the room temperature. The cold gas flowing into the compressor in Fig. 2 represents a loss of exergy [17]. However, the warm gas returns to the compressor in Fig. 1 with no loss of exergy. Thus, the heat leak is effectively reduced by the gas-cooled current lead in Fig. 1.

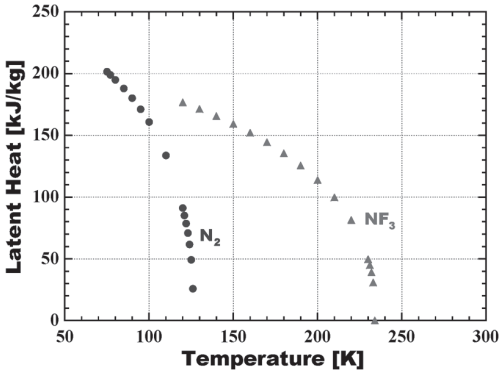

Fig. 3. Temperature dependence of the latent heats of nitrogen and nitrogen trifluoride (NF_3).

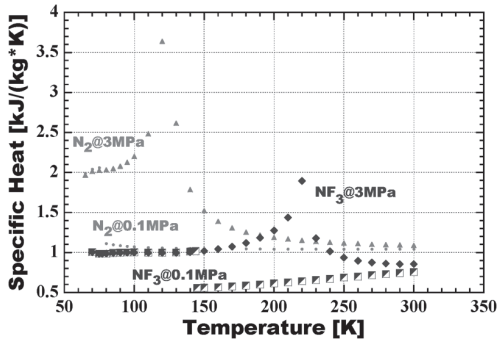

Fig. 4. Constant pressure specific heat of nitrogen and nitrogen trifluoride (NF_3) at 0.1 MPa and 3 MPa as a function of temperature.

In order to keep the intermediate temperature in the middle of the current lead, it is the best to use the latent heat of cryogen. The mass flow rate of the cryogen in Fig. 1 can be obtained by

$$Q\Big|_{T=123\ \mathrm{K}} = m \times cl\Big|_{T=123\ \mathrm{K}} \tag{1}$$

where Q is heat flux at the intermediate temperature of the current lead, m is the mass flow rate of the cryogen, and cl is the latent heat.

Fig. 3 shows the latent heat of nitrogen (N_2) and nitrogen trifluoride (NF_3).

The latent heat of nitrogen is almost zero around 123 K, and therefore it cannot be used as the cryogen for the refrigerator 2. However, NF_3 has high latent heat to 200 K, and would therefore, be a good cryogen. There are several other possible cryogens for the refrigerator 2, but we first discuss NF_3.

Fig. 4 shows the specific heats of N_2 and NF_3 at constant pressure of 0.1 MPa and 3 MPa. The boiling point of nitrogen is 77 K at 0.1 MPa, and the specific heat drops down at 77 K because the phase changes from liquid to gas. But at 3 MPa the behavior of specific heat is completely different in low temperature region. The value of the specific heat is higher than at 0.1 MPa, and therefore we can expect to reduce the heat leak of the gas-cooled current lead because the latent heat is constant for pressure.

B. One-Dimensional Equation of Heat Balance

The one-dimensional equation of the heat balance of the current lead [5], [6] in steady state is given by

$$\frac{dQ}{dx} - fmC_p\frac{dT}{dx} + \eta\frac{I^2}{S} = 0$$
$$Q = -\kappa S\frac{dT}{dx} \tag{2}$$

where x is the normalized coordinate along the current lead, f is the efficiency of heat transfer from the gas to the current lead conductor, m is the mass flow rate given by (1), Cp is the specific heat and T is the temperature of current lead, η is the electrical resistivity of current lead conductor, κ is the thermal conductivity, I the current and S its cross-section.

The purity of copper is 99.9999% (six nines) for the current lead. The gas is circulated from its temperature to the warm end of the current lead, and therefore the system is a partially gas-cooled current lead, and the heat flux to the Rfr. 2 is reduced.

The initial (boundary) condition of (2) must be

$$T(0) = 77\ \text{K}$$
$$T(1) = 300\ \text{K}. \tag{3}$$

Since (2) is the second order differential equation, it needs two initial conditions. These are given by

$$T(0) = 77\ \text{K}$$
$$\left.\frac{dT}{dx}\right|_{x=0} = -\frac{m \times cl}{\kappa}. \tag{4}$$

The second equation in (4) is obtained from (1). We must select dT/dx in such a way that equations 3 are satisfied, and we can obtain the heat flux and the temperature profiles as a function of temperature, and the heat flux at the low temperature end of the current lead.

III. Calculation Results

Fig. 5 shows the heat flux profiles of the current lead as a function of temperature for nitrogen gas. For an ordinary current lead made of copper, without gas cooling, the heat flux is 42.5 W/kA at 77 K, and 40.6 W/kA at 123 K. The heat fluxes of the gas-cooled current lead are 23.3 W/kA and 18.2 W/kA at 77 K at the pressures of 0.1 MPa and 3 MPa, respectively. The heat leak of 3 MPa is lower than that of 0.1 MPa because the specific heat of 3 MPa is higher than that of 0.1 MPa. However, the nitrogen cannot be used as the cryogen of Rfr. 2 as shown in Fig. 1.

Fig. 6 shows the heat flux profiles of the current lead as a function of temperature for NF_3 gas. The temperature of the low-end is 123 K, and the heat leaks are 27.5 W/kA and 23.3 W/kA for the pressures of 0.1 MPa and 3 MPa, respectively.

IV. Discussion and Perspectives

The COP of a 77 K refrigerator is ∼0.067 at the present time, and the Carnot efficiency is 0.345 for 77 K from 300 K. It should be improved to be 0.1 in the near future. The electrical power consumption of the refrigerator for a conduction-cooled current lead is calculated in Fig. 5 as

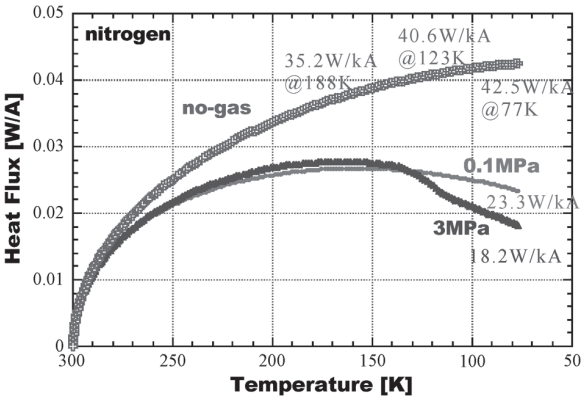

Fig. 5. Heat flux profiles of the conduction-cooled and the gas-cooled current leads at pressures of 0.1 and 3 MPa for nitrogen gas. Temperature of the low end is 77 K.

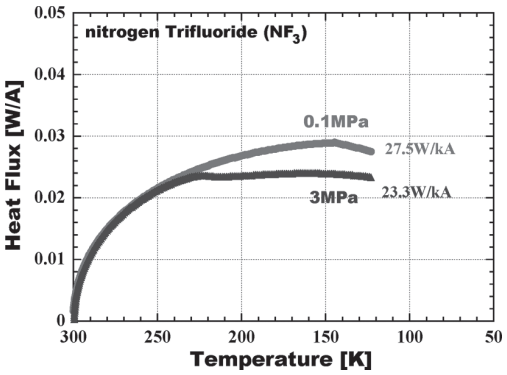

Fig. 6. Heat flux profiles of the conduction-cooled current lead and the gas-cooled current lead for nitrogen trifluoride (NF_3) at pressures of 0.1 and 3 MPa. Temperature of the low end is 123 K.

$$42.5/0.067 \sim 42.5/0.1 = 425 \sim 634\ \text{W/kA}. \tag{5}$$

If we use the MCL and the present COP of a 123 K refrigerator (∼0.22) for a Carnot efficiency of 0.695 in Fig. 1, the total electric power consumption of Rfr. 1 and Rfr. 2 is estimated to be

$$40.6/0.22 + (42.5 - 40.6)/(0.1 \sim 0.067) \approx 201 \sim 213\ \text{W/kA}. \tag{6}$$

The electric power consumption in (6) is almost one-third of that in (5) for the present refrigerator and conduction-cooled current lead. If we use the gas-cooled MCL as in Figs. 1, 5, and 6, the total electrical power consumption can be evaluated from Figs. 5 and 6 to be

$$23.3/0.22 + (42.5 - 40.6)/(0.1 \sim 0.067) \approx 122 \sim 134\ \text{W/kA}. \tag{7}$$

This estimation assumes that 123 K to 77 K is conduction-cooled and 300 K to 123 K is a gas-cooled. These estimates suggest that electrical power savings is quite large for both in the MCL and gas-cooled MCL. Their realization will depend

on the development of high COP and a high temperature refrigerator. The 123 K refrigerator should use two-stage vapor compressed cycle. The cryogen of the 123 K refrigerator flows into the middle of the current lead and out from the warm end, and finally goes into the compressor of the refrigerator. The combined system of the current lead and refrigerator yields significant saving in the electrical power consumption of the refrigerators and this is the main concept of the proposal in the paper because the cryogen flows into the current lead, it should be an electrical insulator. The COP of the 123 K refrigerator is almost one-third of the Carnot efficiency and for a small commercial refrigerator, the cooling power is about 100 W at 123 K. The COP can be improved because the COP of a high temperature refrigerator is usually higher in a larger refrigerator. Since the performance of refrigerator depends on the choice of cryogen and its operational circuit, we must design the refrigerator carefully to combine with the current lead. Here, we have only discussed the use of NF_3 for the cryogen, we continue to seek better alternatives.

ACKNOWLEDGMENT

The authors thank Dr. A. Iiyoshi, Chancellor of Chubu University, for his continuous encouragement throughout this work. The authors appreciate A. Machida and K. Yamamoto of Mayekawa R&D Center for their information about refrigerators. They also thank Prof. B. Coppi, Dr. J. Minervini, Dr. L. Bromberg, Dr. M. Takayasu, and Dr. L. Sugiyama at MIT for their helpful discussions and support.

REFERENCES

[1] M. Hamabe, A. Sasaki, T. Kasukabe, M. Oue, K. Nakamura, S. Yamaguchi, A. Ninomiya, H. Okumura, K. Kawamura, and I. Aoki, "Test of Peltier current lead for cryogen-free superconducting magnet," *IEEE Trans. Appl. Supercond.*, vol. 16, no. 2, pp. 465–468, Jun. 2006.

[2] S. Yamaguchi, Y. Ivanov, J. Sun, H. Watanabe, M. Hamabe, T. Kawahara, and A. Iiyoshi, "The experiment of 200-meter superconducting DC power cable in Chubu University and the estimation for longer cable cooling," in *Proc. Adv. Cryogenic Eng.*, 2012, vol. 57, pp. 1959–1965.

[3] M. Sugino, M. Hamabe, H. Watanabe, T. Kawahara, and S. Yamaguchi, "High accuracy measurement of heat leak of cryogenic pipes for DC superconducting power cable," in *Proc. 23rd ICEC/ICMC*, Wroclaw, Poland, 2010, pp. 639–643.

[4] X. Liang, S. Dai, Z. Gao, N. Song, Y. Wang, D. Zhang, Z. Zhang, F. Zhang, Z. Zhu, X. Xu, T. Huang, X. Li, Z. Cao, Y. Lin, L. Lin, and L. Xiao, "Design of a 380 m DC HTS power cable," *IEEE Trans. Appl. Supercond.*, vol. 20, no. 3, pp. 1259–1262, Jun. 2010.

[5] R. McFee, "Optimum input leads for cryogenic apparatus," *Rev. Sci. Instrum.*, vol. 30, no. 2, pp. 98–102, Feb. 1959.

[6] M. N. Wilson, *Superconducting Magnets Oxford*. Oxford, U.K.: Oxford Univ. Press, 1983, p. 257.

[7] H. Okumura and S. Yamaguchi, "One dimensional simulation for Peltier current leads," *IEEE Trans. Appl. Supercond.*, vol. 7, no. 2, pp. 715–718, Jun. 1997.

[8] K. Sato, H. Okumura, and S. Yamaguchi, "Numerical calculations for Peltier current lead design," *Cryogenics*, vol. 41, no. 7, pp. 497–503, Jul. 2001.

[9] S. Yamaguchi, T. Yamaguchi, K. Nakamura, Y. Hasegawa, H. Okumura, and K. Sato, "Peltier current lead experiment and their applications of superconducting magnet," *Rev. Sci. Instrum.*, vol. 75, no. 1, pp. 207–212, Jan. 2001.

[10] T. Kawahara, T. Fujii, M. Emoto, H. Hamabe, J. Sun, H. Watanabe, and S. Yamaguchi, "Estimation for the performance of superconducting DC transmission lines with cryogenic improvement," *Phys. C, Supercond.*, vol. 470, no. 1, pp. S1011–S1012, Dec. 2010.

[11] S. Yamaguchi, M. Hamabe, I. Yamamoto, T. Famakinwa, A. Sasaki, A. Iiyoshi, J. Schultz, J. Minervini, Y. Ishiguro, and K. Kawamura, "Research activities of DC superconducting power transmission line in Chubu University," *J. Phys. Conf. Ser.*, vol. 97, no. 1, p. 012290, 2008.

[12] E. S. Jeong, "Optimization of conduction-cooled Peltier current leads," *Cryogenics*, vol. 45, no. 7, pp. 516–522, Jul. 2005.

[13] S. Yamaguchi, M. Emoto, T. Kawahara, M. Hamabe, H. Watanabe, J. Sun, N. Yamamoto, and A. Iiyoshi, "A proposal of multi-stage current lead for reduction of heat leak," *Phys. Proc.*, vol. 27, pp. 448–451, 2012.

[14] L. Bromberg, P. C. Michael, J. Minervini, and C. Miles, "Current lead optimization for cryogenic operation at intermediate temperature," in *Proc. AIP Conf.*, 2010, vol. 1218, pp. 577–584.

[15] R. Wesche, R. Heller, P. Bruzzone, W. H. Fietz, R. Lietzow, and A. Vostner, "Design of high-temperature superconductor current leads for ITER," *Fusion Eng. Des.*, vol. 82, no. 5–14, pp. 1385–1390, Oct. 2007.

[16] A. Ballarino, "Large capacity current leads," *Phys. C, Supercond.*, vol. 468, no. 15–20, pp. 2143–2148, Sep. 2008.

[17] A. Razani, C. Dodson, and T. Roberts, "A model for exergy analysis and thermodynamic bounds of Stirling refrigerators," *Cryogenics*, vol. 50, no. 4, pp. 231–238, Apr. 2010.

Proceedings of ICEC 24-ICMC 2012, edited by K. Funaki, A. Nishimura, Y. Kamioka, T. Haruyama and H. Kumakura

Time dependence of terminals temperature with current feeding in the superconducting direct current transmission test device of CASER-2

Kawahara T., Emoto M.*, Watanabe H., Hamabe M., Ivanov Y., Sun J., Yamaguchi S.

CASER, Chubu University, Aichi 487-8501 Japan
*National Institute for Fusion Science, Gifu 509-5292 Japan

We are developing cryogenic systems for effective cooling of superconducting transmission and distribution (T&D) systems, and were succeeded in four times cooling experiments on 200 m-class superconducting direct current T&D system (CASER-2). We have estimated the heat leak at the terminals by a calorimetry. As the heat transfer from the current leads to cryogen requires sufficient time as stabilization, we discuss about the time dependence of the terminal temperature during the current feeding test. After obtaining the stable temperature distribution, we have estimated heat leak at the terminals with Peltier current lead as the enhancement of the performance of applied superconducting systems.

INTRODUCTION

Superconducting transmission and distribution (T&D) system is one of the key technologies for effective use of natural energy and saving energy [1-5]. The realization of superconducting T&D systems requires the low heat leak cryogenics for the high performance operation [5]. In Chubu University, we have developed 200 m-class superconducting direct current (DC) transmission test device of CAER-2 [6], following to 20 m-class superconducting DC transmission device (CASER-1) [5,7], for the experiments of actual evidence of the low heat leak superconducting systems with several advanced cryogenics.

Figure 1 shows the pictures of CASER-2 and its specifications. The transmission power of CASER-2 is 40 MW and the length is approximately 200 m. There is an undulation of 2.7 m and a turn with the minimum radius of 2 m, which can emulate actual conditions of transmission lines in the field. We have already finished the 4th cooling experiment for cryogenics and a superconducting state. The first cooling experiment was done from January 2010 to March 2010 and showed the zero resistance of superconducting cables successfully. Until 4th cooling experiment that was started at August 2011, we have several experiments to obtain the cryogenic data of CAESR-2 [8,9].

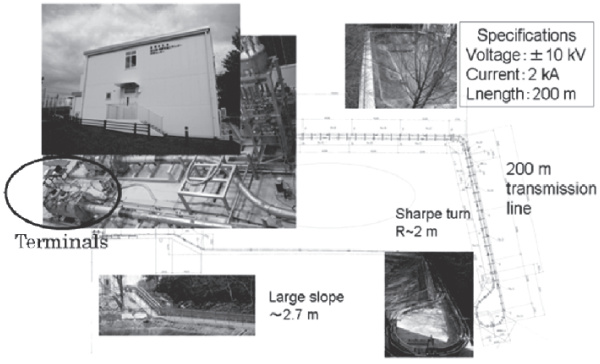

Figure 1 Specification of CASER-2.

The performance of such applied systems is determined by two large heat leaks, which are in the cryogenic pipes keeping the superconducting cable inside and at the terminals where the superconducting cable is

connected to the outside systems at room temperature. In this paper, we discuss about the thermal performance of terminals. At first, we consider the time dependence of temperature change in the terminals and then estimate the heat leak at the terminals with several feeding currents.

EXPERIMENTS

Figure 2 (a) shows terminals, and the heat leak at the terminals was effectively insulated by special current leads of Peltier current lead (PCL) [10-12]. Terminal A has 23 n-type and 16 p-type PCLs, and terminal B has 16 n-type and 23 p-type ones, as our superconducting cable has 23 tapes for the inner layer and 16 tapes for the outer. Such thermal insulation can be seen as the current leads without ices during cooling experiments, where 6 PCLs were replaced by copper current leads (CCLs) with the same shape factor for comparison and only CCLs have ices with large heat leaks (Fig. 2 (b)). For example, the calculated value of heat leak for a single n-type PCL with I = 0 A is 2.6 W and that for p-type one is 3.6 W depending on the performance of thermoelectric elements, and then those of corresponding copper current leads for n- and p-type current leads are 3.7 W and 4.3 W, respectively. The larger resistance of p-type thermoelectric elements requires the larger optimum cross-section for the connected copper lead [11].

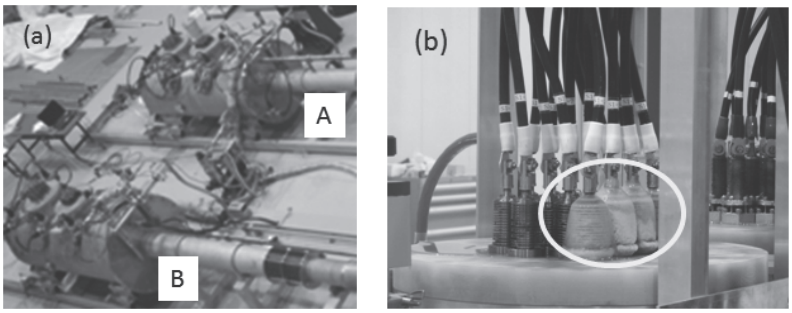

Figure 2 Terminals A and B, and Peltier current lead.

We used 46 thermometers attached in the cryostat of CASER-2 for the calorimetry for the heat leak estimation of the system. We measured the temperature rise of the liquid nitrogen in the terminals for the estimation of the heat leak at the terminals with several feeding current. The current was fed into the superconducting cable from the current lead at the terminals and also come out from the current lead. We used a co-axial cable and a power supply was set at terminal A (the two transmission lines are shorted at terminal B). From the temperature rise and the flowed volume of the liquid nitrogen, we can estimate the heat leak at the terminals. Typical flow rate of the liquid nitrogen was 13 l/min.

RESULTS AND DISCUSSION

Figure 3 shows time dependence of temperature rise of liquid nitrogen in the terminals with several feeding currents. Initial time dependence just after the current feeding varies for all conditions and it with I = 200 A seems to be stable. But it with I = 1500 A is not stable, and it with I = 400 A has the effects of the previous large feeding current of 1500 A. Therefore, we need to measure for long time depending on the feeding current to obtain the heat leak at the terminals by a calorimetry. Next, we show the time dependence of temperature rise of liquid nitrogen with I = 600 A in Fig. 3 (b). In this case, the temperature gradually increased and, after about 7 hours, it could be stable. Using these data, we can calculate the effective heat leak at the terminals in CASER-2.

To check how long time is required to obtain stable temperature rise caused by the current feeding, we plot the time dependence of the estimated heat leaks with several feeding currents in Fig. 4. The time dependences at terminals A and B are plotted in Figs. 4 (a) and (b), respectively. As we used the time dependence over 24 hours, the data were normalized by the heat leak at 20 hours after current feeding. The initial normalized heat leak rapidly increases below about 4 hours depending on the feeding current, and the normalized heat leak above 10 hours might almost the same. The latter region has the circadian vibration. It means that the heat leaks are governs by the atmosphere temperature and our data are statistically precious for the heat leak

estimation. Transient region between 4 and 10 hours has slow heat transfer from the terminals to the liquid nitrogen because the liquid nitrogen was not filled up in the terminals.

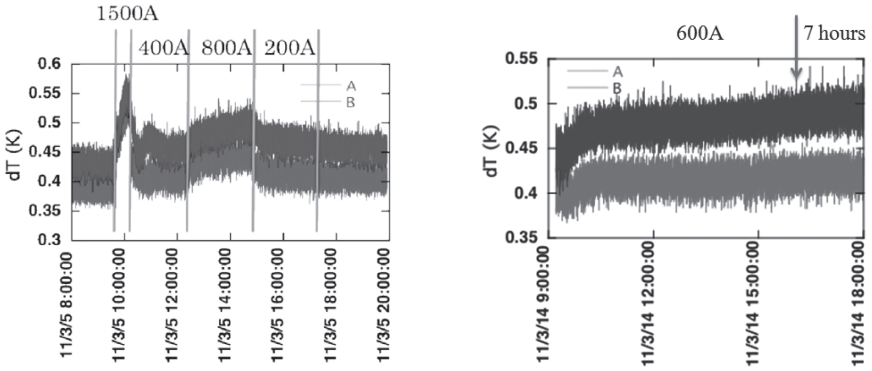

Figure 3 Temperature change with several feeding currents. (a) is for 200 A~1500 A. (b) for 600 A. An arrow shows 7 hours after current feeding.

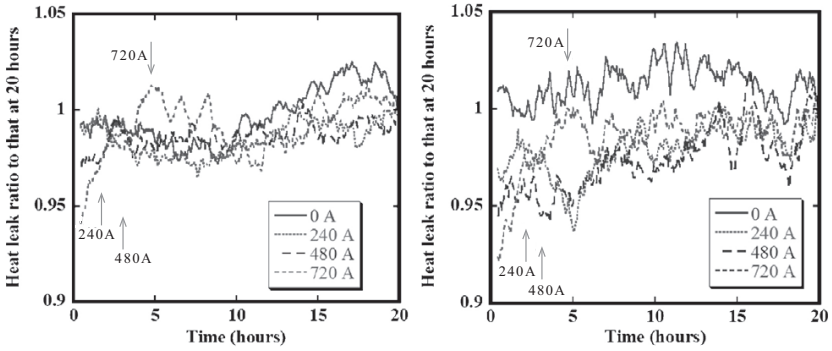

Figure 4 Time dependence of the heat leak with several feeding current. (a) is for terminal A and (b) for terminal B. Arrows point out the end of the initial large temperature rise.

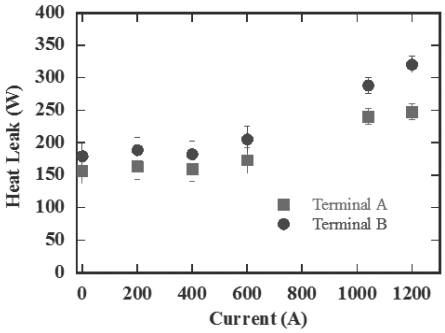

Figure 5 Current dependence of the heat leak at the terminals. Squares and circles are for terminals A and B, respectively.

The transient from the fast heat transfer to the slow ones, pointed by arrows, shifts to longer time when the feeding current increases for both terminals, as the heat income is larger for the larger feeding current. On the other hand, we conclude the estimated heat leak at the longer time after the current feeding represent the performance of the terminals in CASER-2.

Finally, we plot the feeding current dependence of the heat leak at the terminals in Fig. 5. The heat leak was estimated at the heat leak at the last measuring points of the time dependence. The heat leak rapidly increases above I = 1000 A, but the heat leak at the terminals can be reduced at the mid range feeding current with the PCL. The heat leak at terminal B was slightly larger than that at terminal A, because of the larger number of p-type PCLs. This fact supports capability of the superconducting transmission lines with the high performance terminals as actual applications.

CONCLUSION

We had cooling experiments on CASER-2, and estimated the performance of the system. The slow circulation speed of liquid nitrogen requires the long time measurements for the calorimetry of the total systems. Moreover, the heat leak estimation at the terminals requires longer time to obtain stable temperature rise during the current feeding test. We estimated the time dependence of the heat leak at the terminals with the several feeding current. The initial rapid rise of the temperature of liquid nitrogen depends on the feeding current, and large feeding current requires longer time for the stabilization. And also we can obtain the time dependence with the same periodicity of the circadian rhythm at the longer time measurements. Therefore, we can estimate the heat leak at the terminals during current feeding test. The heat leak rapidly increases above I = 1000 A, but the heat leak at the terminals can be reduced at the mid range feeding current with the PCL, which shows capability of the superconducting transmission lines with the high performance terminals.

ACKNOWLEDGMENT

The authors thank Dr. A. Iiyoshi, Chancellor of Chubu University for his continuous encouragement through this work. We acknowledge Dr. Hiroshi Fujiwara for his support on the construction of 200 m superconducting facilities of CASER-2. Parts of this work were supported by a grant of Strategic Research Foundation Grant-aided Project for Private Universities Ministry of Education, Culture, Sports, Science and Technology (MEXT), and Grant-in-Aid for challenging Exploratory Research (MEXT).

REFERENCES

1. Mukoyama, S., Yagi, M., Ichikawa, M., Torii, S., Takahashi, T., Suzuki, H., and Yasuda, K., Experimental results of a 500 m HTS power cable field test, IEEE Trans. Appl. Supercond. (2007) 17 1680–1683
2. Masuda, T., Yumura, H., Watanabe, M., Takigawa, H., Ashibe, Y., Suzawa, C., Ito, H., Hirose, M., Sato, K., Isojima, S., Weber, C., Lee, R., and Moscovic, J., Fabrication and installation results for Albany HTS cable, IEEE Trans. Appl. Supercond. (2007) 17 1648–1651
3. Yoon, J. Y., Lee, S. R., and Kim, J. Y., Application methodology for 22.9 kV HTS cable in metropolitan city of South Korea, IEEE Trans. Appl. Supercond. (2007) 17 1656–1659
4. Xi, H. X., Gong, W. Z., Zang, Y., Bi, Y. F., Ding, H. K., Wen, H., Hou, B., and Xin, Y., China's 33.5 m 35 kV/2 kA HTS ac power cable's operation in power grid, Physica C (206) 448 1054–1057
5. Yamaguchi, S., Hamabe, M., Yamamoto, I., Famakinwa, T., Sasaki, A., Iiyoshi, A., Shultz, J., Minervini, J., Hoshino, T., Ishiguro, Y., and Kawamura, K., Research activities of DC superconducting power transmission line in Chubu University, J. Phys.: Conf. Ser. (2008) 97 012290
6. Yamaguchi, S., Kawahara, T., Hamabe, M., Watanabe, H., Ivanov, Y., Sun, J., and Iiyoshi, A., Experiment of 200-meter superconducting DC cable system in Chubu University, Physica C (2011) 471 1300-1303
7. Hamabe, M., Fujii, T., Sugino, M., Sasaki, A., Sugimoto, T., Watanabe, H., Kawahara, T., Yamaguchi, S., Ishiguro, Y., and Kawamura, K., Cooling cycle test of DC superconducting power transmission cable, J. Phys.: Conf. Ser. (2010) 234 032019
8. Watanabe, H., Sugino, M., Sun, J., Ivanov, Y., Hamabe, M., Kawahara, T., and Yamaguchi, S., Cooling test of the 200 m superconducting DC transmission power cable system at Chubu University, Physica C (2011) 471 1304–1307
9. Ivanov, Y., Watanabe, H., Hamabe, M., Sun, J., Kawahara, T., and Yamaguchi, S., Circulation pump power for 200 m cable experiment, Physica C (2011) 471 1308–1312
10. Yamaguchi, S., Yamaguchi, T., Nakamura, K., Hasegawa, H., Okumura, H., and K. Sato, Peltier current lead experiment and their applications for superconducting magnets, Rev. Sci. Instrum. (2004) 75 207-212
11. Fujii, T., Fukuda, S., Emoto, M., Osada, K., Kawahara, T., Hamabe, M., Watanabe, H., Ivanov, Y., Sun, J., and Yamaguchi, S., Thermoelectric Property Dependence and Geometry Optimization of Peltier Current Leads Using Highly Electrically Conductive Thermoelectric Materials, J. Elec. Mater. (2011) 40 691-695
12. Kawahara, T., Fujii, T., Emoto, M., Hamabe, M., Watanabe, H., Sun, J., and Yamaguchi, S., Double Peltier Current Lead for Heat Leak Reduction at the Terminals Superconducting Direct Current Applications, IEEE Trans. Appl. Supercond. (2011) 21 1070-1073

Proceedings of ICEC 24-ICMC 2012, edited by K. Funaki, A. Nishimura, Y. Kamioka, T. Haruyama and H. Kumakura

Heat leak measurement of cryogenic pipe with vacuum insulation for DC superconducting power transmission

Toki Y.*, Hamabe M.**, Ivanov Y.**, Watanabe H.**, Kawahara T.*, Yamaguchi S.*·**

*Department of Electric Engineering, Chubu University, Aichi 487-8501 Japan
**Center of Applied Superconductivity and Sustainable Energy Research, Chubu University, Aichi 487-8501 Japan

We have studied a DC superconducting power transmission (DC SC-PT) system using cryogenic pipe. Considering a long DC SC-PT system of several kilometers, the heat leak on the liquid-nitrogen-cooled cryogenic pipe of the power transmission line is the main heat load, and the reduction of the radiation heat is one of the key issues to realize such a long DC SC-PT system. Multilayer insulation (MLI) is effective to reduce the radiation heat and is widely used in cryogenic systems. However, the surface area of the MLI for DC SC-PT line is huge, and the evacuation time for vacuum insulation can be extremely long; therefore, it is necessary to reseach the influence of the vacuum on the heat leak of the cryogenic pipe. Consequently, the thermal insulation of the cryogenic pipe with MLI was effective at less than 0.01 Pa, whereas that without MLI was affected by the conduction heat due to the residual gas at the same vacuum.

INTRODUCTION

Development of the high temperature superconductors (HTS) leads to the availability of the superconducting power transmission (SC-PT) cooled by liquid nitrogen (LN_2). Recently, several groups started to discuss about the commercial use of the DC superconducting power transmission [1, 2]. Yamaguchi et al., have proposed previously the DC SC-PT and continued to research for the practical application of the DC SC-PT [3-5]. One of the key issues to apply the DC SC-PT practically is the cost and the efficiency of the cryogenic system to cool the SC cable. In particular for a long distance DC SC-PT over several kilometers, heat leak on the cryogenic pipes of the SC cable can be the main part of the energy loss.

Vacuum insulation is generally used for the thermal insulation of cryogenic pipes of SC-PT and multilayer insulator (MLI) is also employed as a radiation shield [6, 7]. However, use of the MLI can cause to extend evacuation time for vacuum insulation due to its large surface area and its outgassing. Watanabe et al. reported that the heat leak reduced due to the improvement of vacuum in cryogenic pipe of 200m DC SC-PT cable system [8]. In this paper, we will describe the test bench to examine the heat leak of the cryogenic pipe cooled by LN_2 for DC SC-PT and the influence of the vacuum for the heat leak with or without MLI.

EXPERIMENTAL DEVICE

One of the features in the DC SC-PT cable in Chubu University is that we employ smooth pipes as the cryogenic pipe [3-5], since the general corrugated pipe for SC-PT cable causes a pressure drop in flowing LN_2 cryogen [9]. Hence, the smooth pipes have been tested in our test benches to measure the heat leak of the cryogenic pipes [10, 11]. Here, we used the second test bench (Fig. 1), where the test pipe was fixed horizontally. We employed the boil-off method to measure the heat leak; the time variation of the LN_2 level at the narrow "measurement part" (Fig. 1) of 19 mm in inner diameter was measured by the cylindrical-capacitor-type LN_2 level sensor, and the heat leak into the inner pipe was estimated from the evaporation heat of the consumed LN_2. Initial data of this test bench was described in [11]. Diameter of the inner test pipe and that of the outer test pipe were 60.5 mm and 216.5 mm in O.D., respectively, as the same as those of the 200-

m DC SC-PT cable system in Chubu University. In this paper, we tested the aluminum pipe of 2820 mm in length, wounded with an aluminum foil of 12 μm in thickness or with 10 sheets of MLI, for the inner test pipe. The aluminum foil was used to obtain a clear surface of the aluminum pipe. The outer pipe was zinc-coated steel pipe of 2960 mm in length, as the same as that in [11]. We added a heater on the surface of the inner pipe for the calibration, since the accuracy of the measured heat leak is not clear in [11]. Vacuum pressure between the inner test pipe and the outer test pipe was measured by the ionization gauge at the position in Fig. 1 and controlled by the injection of the N_2 gas and kept constant during the measurement.

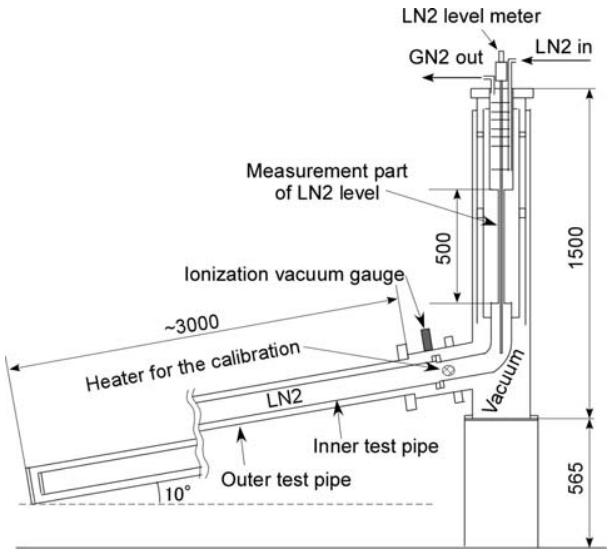

Figure 1 A schematic diagram of a test bench for heat leak measurement of cryogenic pipe.

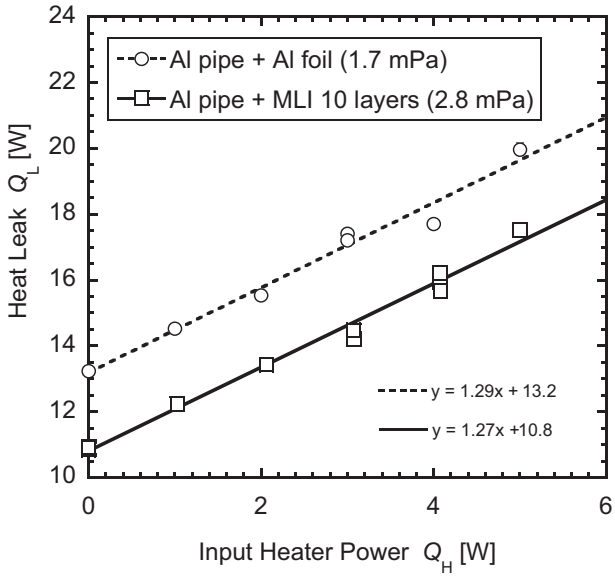

Figure 2 Example of calibration of heat leak at 1.7 mPa of vacuum pressure for Al pipe with an Al foil and at 2.8 mPa for Al pipe with10 layers of MLI.

RESULTS AND DISCUSSION

Calibration of the measured heat leak

Heat leak Q_L was measured with varying the input power Q_H to the heater for the calibration of the measured heat leak. Figure 2 shows the example of heat leak calibration when the highest vacuum was achieved without N_2 gas injection. Calibrated heat leak Q_{L0} was obtained by extrapolating the input power Q_H at the measured heat leak Q_L = 0 W. Consequently, Q_{L0} in Fig. 2 was (1) 3.27 W without the inner test pipe, (2) 11.48 W when the inner test pipe was wounded with an aluminum foil, and (3) 9.22 W when the inner test pipe was wounded with 10 sheets of MLI, for example. The heat leak was estimated from the difference of Q_{L0} with the test pipe from Q_{L0} without the test pipe; i.e. 8.21 W for the pipe with aluminum foil, and 5.25 W for that with 10 sheets of MLI.

Influence of the vacuum pressure in test pipes

Since the cryogenic pipe for the DC SC-PT cable is long and its conductance to evacuate for vacuum insulation was low, it can be hard to reach a good vacuum. In previous test bench [10], use of the MLI clearly increased the evacuation time. Therefore, we measured the influence of the vacuum pressure on the heat leak to obtain the sufficient vacuum pressure for the thermal insulation with or without MLI.

Figure 3 shows the heat leak per unit pipe length as a parameter of the vacuum pressure in the test pipe. Here, vacuum pressure was controlled by the injection of N_2 gas. At vacuum pressure, the heat leak in the cryogenic pipe consists of the radiation heat and of the conduction heat through the residual N_2 gas. The saturated heat leak corresponds to the radiation heat and the increase of the heat leak to the gas injection corresponds to the conduction heat. For the cryogenic pipe with the MLI, conduction heat was smaller than that with aluminum foil and the heat leak saturated at the vacuum pressure less than 0.01 Pa. This is natural since the MLI includes the plastic sheets to reduce the conduction heat. Although the aluminum pipe without

the MLI can reduce the radiation heat due to its high reflectance, the influence of the vacuum pressure was remarkable due to its high thermal conductivity. Consequently, the thermal insulation of the MLI was effective at vacuum of 0.01 Pa.

Figure 4 shows the comparison of the heat leak per unit surface with the previous results [10, 12]. In our results, the saturated heat leak (this means radiation heat) for the MLI was remarkably higher than the other results; ratio of the increase of the heat leak due to the injection of the gas is similar. Our test stand used here had the difference which was fixed horizontally and a set of FRP rods supported this horizontal pipe, and the designed conduction heat through the set of FRP rods was estimated as 0.16 W from the finite element method analysis using ANSYS [13] simulation software. Though the designed conduction heat through the FRP rods was relatively low, the heat leak due to the use of the FRP rods is necessary to measure experimentally to consider this high heat leak with the MLI. Moreover, mechanical pressure on the MLI increase the heat leak through the MLI when the MLI was wound around the cryogenic pipe [14]. In our results, it is possible that the MLI was tightly wound around the aluminum pipe and then the total heat leak was increased. It is also necessary for the cross-check to test the stainless steel pipe wound with MLI as the same as the previous test bench, in order to consider the influence of the cryogenic pipe material of aluminum.

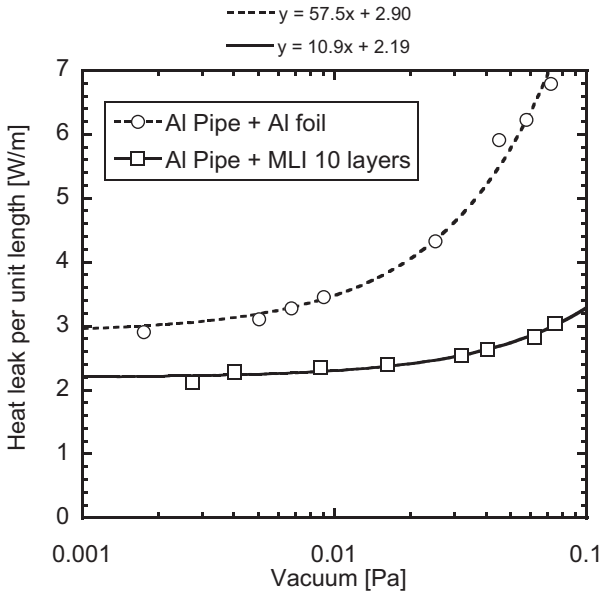

Figure 3 Measured heat leak per unit pipe length as a parameter of vacuum pressure.

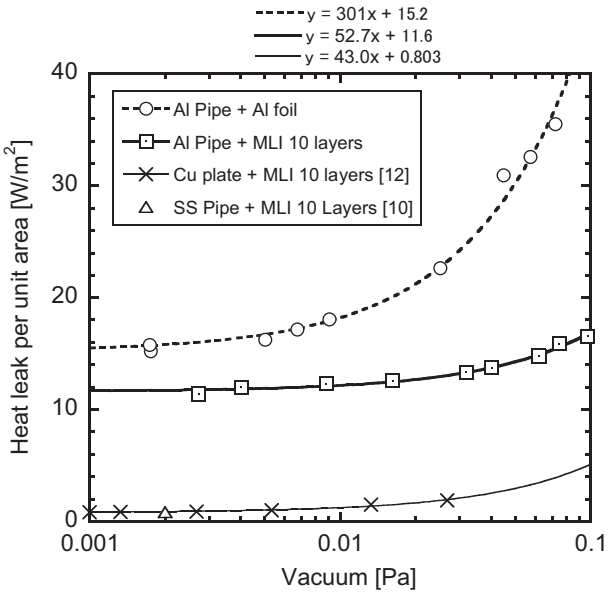

Figure 4 Comparison of the heat leak per unit surface area as a parameter of vacuum pressure [10, 12].

CONCLUSION

We measured the influence of the vacuum pressure in the thermal insulation of the cryogenic pipe for DC SC-PT cable. Consequently, the heat leak of the cryogenic pipe wound with 10 sheets of MLI was saturated at less than 0.01 Pa, whereas that without MLI was not saturated at the same vacuum. However, saturated heat leak was remarkably higher than the previous results with MLI; some cross-checks are necessary to find the cause of this high heat leak.

ACKNOWLEDGMENT

The authors thank Dr. A. Iiyoshi, Chancellor of Chubu University for his continuous encouragement through this work. We also thank JFE Steel Corp. for supplying zinc-coated steel pipe and Nippon Light Metal Company, LTD. for supplying aluminum test pipe. Parts of this work were supported by a grant of Strategic Research Foundation Grant-aided Project for Private Universities Ministry of Education, Culture, Sports, Science and Technology (MEXT).

REFERENCES

1. Liang X.M., Dai S.T., Gao Z.Y., Song N.H., and Wang Y.S., et al., Design of a 380 m DC HTS power cable, IEEE Transactions on Applied Superconductivity (2010) 20 1259–62.
2. Hassenzahl W., Daneshpooy A., Eckroad S., Grant P., Gregory B., Nilsson S., Program on Technology Innovation: A Superconducting DC Cable, EPRI Report (2009) 1020458.
3. Yamaguchi S., Hamabe M., Yamamoto I., Famakinwa T., and Sasaki A., et al., Research activities of DC superconducting power transmission line in Chubu University, Journal of Physics: Conference Series (2008) 97 012290.
4. Hamabe M., Fujii T., Sugino M., Sasaki A., and Sugimoto T., et al., Cooling cycle test of DC superconducting power transmission cable. Journal of Physics: Conference Series (2010) 234 032019.
5. Yamaguchi S., Kawahara T., Hamabe M., Watanabe H., Ivanov Yu., Sun J., et al., Design and construction of 200-meter high temperature superconducting DC power cable test facility in Chubu University, International Cryogenic Engineering Conference – 23 and International Cryogenic Material Conference 2010 (2011) Wroclaw, Poland, 1041-47.
6. Maguire. J.F., Schmidt F., Hamber F., and Welsh T.E., Development and Demonstration of a long length HTS cable to operate in the Long Island power authority transmission grid, IEEE Transactions on Applied Superconductivity, (2005) 15 1787-1792
7. Choi Y.S., Kim D.L., Yang H.S., Sohn S.H., Lim J.K., and Hwang S.D., Progress of the performance test of KEPCO HTS power cable, IEEE Transactions on Applied Superconductivity, (2011) 21 1034-1037
8. Watanabe H., Sugino M., Sun J., Ivanov Yu., and Hamabe M., et al., Cooling test of the 200 m superconducting DC transmission power cable system at Chubu University, Physica C: Superconductivity, (2011), 471 1308–1312
9. Weisend II J.G., Van Sciver S.W., Pressure drop from flow of cryogens in corrugated bellows. Cryogenics (1990) 30 935-941.
10. Nasu Y., Hamabe M., Yamaguchi S., Kusaka S., and Ishiguro Y., Heat leak measurement on zinc-coated cryogenic pipe for superconducting power transmission line, International Cryogenic Engineering Conference 22 and International Cryogenic Material Conference 2008, KIASC, Seoul, Korea (2009) 489-494
11. Sugino M., Hamabe M., Watanabe H., Kawahara T., S. Yamaguchi, Ishiguro Y., and Shinshi O., High accuracy measurement of heat leak of cryogenic pipes for DC superconducting power cable, International Cryogenic Engineering Conference – 23 and International Cryogenic Material Conference 2010 (2011) Wroclaw, Poland, 639-643
12. Shu O.S., Fast R.W., and Hart H.L., Heat flux from 277 to 77 K through a few layers of multilayer insulation, Cryogenics (1986) 26 671-677
13. http://www.ansys.com/
14. Ohmori. T, et al., Lightweight multilayer insulation to reduce the self-compression of insulation films, Advances in Cryogenic Engineering (2002) 47 1565-1572

Proceedings of ICEC 24-ICMC 2012, edited by K. Funaki, A. Nishimura, Y. Kamioka, T. Haruyama and H. Kumakura

THERMOMECHANICAL BEHAVIOR OF THE SUPERCONDUCTING CABLE OF CASER2 AT CHUBU UNIVERSITY

Watanabe H., Ivanov Y., Sun J., Hamabe M., Kawahara T., and Yamaguchi S.

Center of Applied Superconductivity and Sustainable Energy Research, Chubu University, Aichi 487-8501 Japan

In the case of superconducting power transmission using high tempreature superconductivity, the cable contracts almost 0.3% by cooling process from room temperature, which might cause strong tensile force and degrade the cable. Smooth movement of the cable in the cryogenic pipe, which temper tensile force, was confirmed by images of the cable taken with X-rays in the superconducting DC power transmission system of Chubu University.

INTRODUCTION

In the power transmission using high temperature superconductivity, a cable at room temperature has to be cooled down to liquid nitrogen temperature, during which the cable suffers temperature variation over 200 K during the cooling process. By the temperature variation the cable can contract about 0.3 % by thermal shrinkage, which might cause strong tensile force and degrade the cable. To avoid these, three cables are stranded loosely in a cryogenic pipe in the three in one cable configuration [1] or offset of a cryogenic pipe is installed along a transmission line in the one in one cable configuration [2], for example. It has been shown that these treatments absorb the contraction and expansion of cables efficiently, by images taken with X-rays [1,2].

We have developed a superconducting DC power transmission system at Chubu University (CASER2) [3]. The length of our cable is about 200 m, which could contract about 60 cm by the change from 300 K to 77 K. To manage the thermal contraction and expansion, the cable ends are not fixed at the terminals and can move with respect to the terminals. In addition, the terminals can be moved according to the contraction and expansion of the cable [3]. We have measured images of the cable with X-rays at several positions along the cryogenic pipe to know the status of the cable. From the observation we can know that thermal contraction and expansion is partly compensated by the movement of the cable inside the cryogenic pipe. Up to the present, we have not observed the damage of the cable, confirmed by feeding the rated current of the cable.

CASER2

Figure 1 shows a layout of the cryogenic pipe of CASER2 and the insets are a model of the cryogenic pipe and the cable. The cryogenic pipe has an L shaped configuration with a length of approximately 200 m, which is mainly installed in the outdoors. It has two gradients with a height of 2.6 m and a gradient ratio of 52%, two curves with 135 degrees, two curves with 100 degrees forming the L shaped configuration, and two curves with 120 degrees and a curve with 180 degrees forming a turn with a radius of about 2.3 m. The cryogenic pipe is composed of straight pipes and, in part, bellows pipes, which is quite different from corrugated pipes used commonly. The outer pipe is made of carbon steel coated with zinc with an outer diameter of 216.3 mm and the inner pipe is stainless steel with an outer diameter of 60.5 mm. The cable was pulled into the pipe. The tension caused along the cable was controlled by the measurement of pulling force. The cable is a 2kA 20kV DC cable, the composition of which is also shown in Fig.1. The diameter of the cable is 34 mm. The center is former made of copper with a diameter of 14 mm. There are two layers of HTS tapes of Bi2223 with diameters of 20 mm and 26 mm, respectively. Each layer has insulation of 10 kV to the earth and 20 kV to each other.

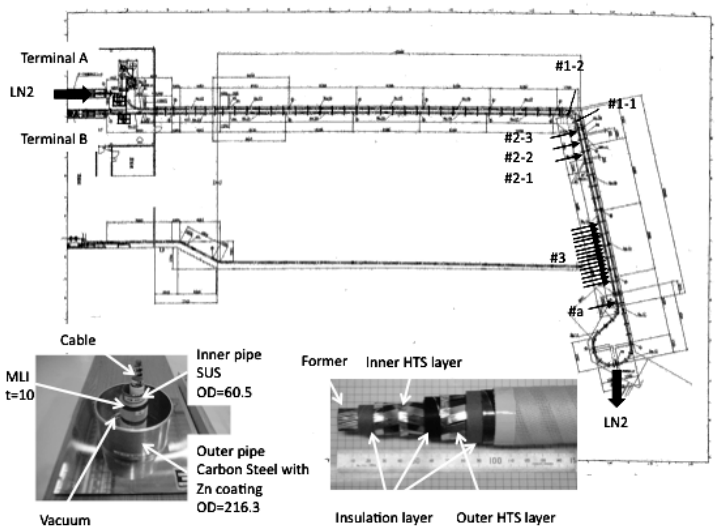

Figure 1 The layout of the cryogenic pipe of CASER2. The positions indicated by arrows #1 to #3 are those at which the images shown in this paper were taken. The position indicated by an arrow #a is the origin of the position in Fig.4. The insets are the model of the cryogenic pipe and the cable.

CASER2 has been experienced cooling tests four times. Liquid nitrogen is usually filled from the terminal A side in Fig. 1 and the cable is cooled gradually toward the lower reaches of the cryogenic pipe. Therefore contraction of the cable is started from the terminal A side and ended at the terminal B side. At the end of the cooling test, liquid nitrogen is released from the turned part shown with an arrow in Fig.1. Because the level of the turned part is the lowest, warming up of this part is slower than the other part of the cryogenic pipe. As the result, expansion of the cable is started from both the cable ends. The contraction and expansion of the cable is not uniform along the cryogenic pipe. During the first cooling test, the cable ends were well moved, corresponding to the cooling down and warming up of the cable. At the end of the first cooling test, the cable did not return to its initial position and some additional portion of the cable left in the cryogenic pipe [3]. However, during the second, third, and fourth cooling tests, the cable ends did not moved so much like the first cooling test.

OBSERVATION OF CABLE IMAGES

Figure 2 shows the images of the cable at room temperature and liquid nitrogen temperature along the curved part shown by #1-1 and #1-2 in Fig. 1. Figure 3 also shows the images of the cable along the straight part shown by #2-1 to #2-3 in Fig. 1. These images were taken after the first cooling test and during the second cooling test. Liquid nitrogen flows from the right of #1-1 to the left of #1-2 in Fig.2 and from the right of #2-1 to the left of #2-3 in Fig.3. It is clearly seen that, along the curved part, the cable at liquid nitrogen temperature moved inward, while at room temperature outward. Along the straight part, the cable at liquid nitrogen temperature was rather straight, while the cable at room temperature meandered gently. The cable moved so as to take a shortest distance at liquid nitrogen temperature and a longest distance at room temperature to compensate contraction and expansion of the cable. Similar movements of cables were observed in previous studies [1,2]. It should be noted that, in our case, the cable was pulled into the cryogenic pipe at the construction site on its installation and the cable at room temperature should take a shortest distance before the first cooling test, similar to the cable at liquid nitrogen temperature. Therefore, the cable was pulled into the cryogenic pipe by the cooling down and moved so as to take a longest distance in the cryogenic pipe by the warming up in the end of the first cooling test. This might be the reason why the cable ends well moved only in the first cooling test and did not return to its initial position.

To investigate the straight part closely, images were taken from vertical and horizontal directions to obtain 3D images of the cable in the cryogenic pipe at room temperature. The images were taken in the region shown by #3 in Fig.1 and the result is shown in Fig. 4, in which the abscissa of the figure is position measured from #a in Fig. 1 and the ordinate is displacement of the cable from the axis of the cryogenic pipe.

Solid symbols are displacement in the horizontal plane and open symbols are that in the vertical plane. Plus of the displacement is the movement to the left of the axis toward lower reaches of the cryogenic pipe in the horizontal plane and that above the axis in the vertical plane. The position of the pipe surface is shown with lines. If data is on the lines, it means that the cable is touching the pipe surface. In the horizontal plane the data oscillate in the span of the pipe diameter. On the other hand, in the vertical plane, the cable does not touch the upper inner surface, which is considered due to the weight of the cable. Sine curves are fitted to the data. These show that the cable is meandered with pitch of about 2 m in the horizontal and vertical planes, which means that the cable is nearly spiralling in the cryogenic pipe.

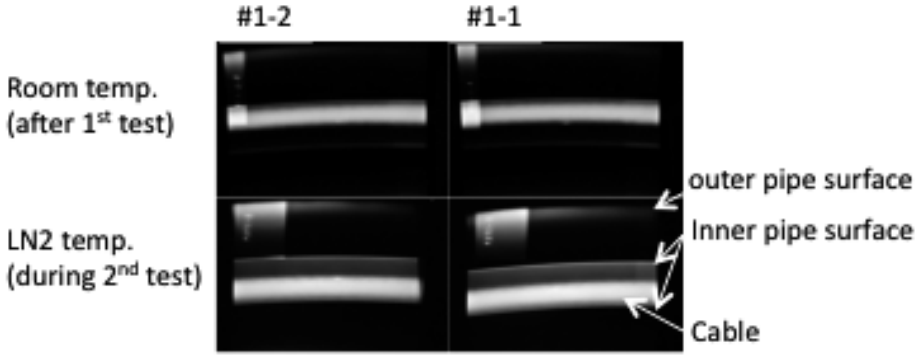

Figure 2 These images show the cable at room temperature and at LN2 temperature, which were taken with Xrays along a curved part of the cryogenic pipe. The images were taken at #1-1 and #1-2 in Fig. 1.

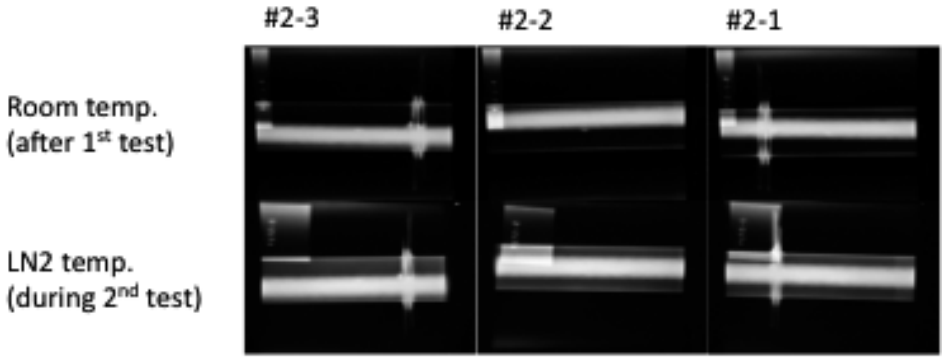

Figure 3 These images show the cable at room temperature and at LN2 temperature, which were taken with Xrays along a straight part of the cryogenic pipe. The images were taken at #2-1, #2-2 and #2-3 in Fig. 1.

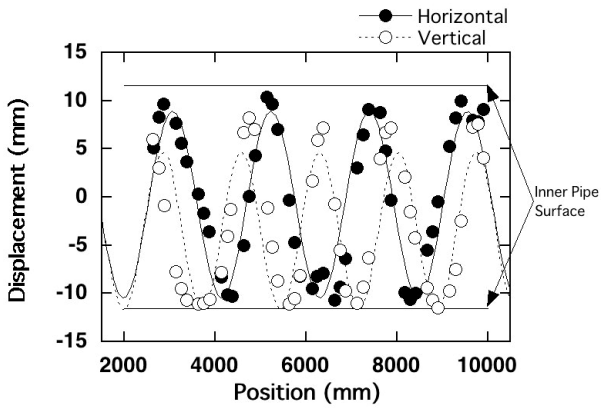

Figure 4 This figure shows the displacement of the cable at room temperature from the axis of the cryogenic pipe in the horizontal and vertical planes. + of the horizontal is displacement to the left toward the lower reaches of the cryogenic pipe. Abscissa is a position from #a shown in Fig. 1.

DISCUSSIONS

Though we have performed cooling tests four times, which means that the cable has experienced the process of cooling down and warming up four times, degradation of the cable has not been observed. This means that the issues originating from thermal contraction and expansion are well managed in our system. It is considered that thermal contraction and expansion could be partly absorbed by the cable movement in the cryogenic pipe. In curved parts along the cryogenic pipe, the absorption is estimated to be 26 cm at the maximum by the movement of the cable between inward and outward of curves. On the other hand, in straight parts, it is estimated to be 13 cm by the change between straight and spiral. Therefore 39 cm of the cable, which is 65% of the contraction, could be absorbed by the movement of the cable in the cryogenic pipe at the maximum. It should be noted that, in addition to this, the terminals are moved according to the contraction and expansion of the cable in our system, which compensates thermal contraction and expansion considerably.

The spiral of a cable is affected by several factors including the diameter of a cryogenic pipe, bending rigidity of the cable and axial force caused along the cable. By controlling these, the degree of spiral could be controlled and the spiralled cable could absorb thermal contraction and expansion. It should be noted that, in our case, the axial force is caused by thermal stress, the maximum of which is limited by the friction force between the cable and pipe surfaces. The cable was pulled into a cryogenic pipe composed of straight pipes in its installation and the force caused along the cable, i.e. the friction force, was carefully controlled during the installation. In addition, the cable ends are not fixed to the terminals. Therefore it is considered that too strong force, to the extent that it degrades the cable, did not caused along the cable.

SUMMARY

The behavior of the superconducting DC power transmission cable in a cryogenic pipe has been observed with X-rays. It was found that the cable was moved smoothly in the cryogenic pipe and tempered the tensile force. Along the curved part, the cable at liquid nitrogen temperature moved inward, while at room temperature outward. Along the straight part, the cable at liquid nitrogen temperature was rather straight, while the cable at room temperature was spiralling. By the movement of the cable 65% of thermal contraction, at the maximum, could be compensated. The thermal contraction and expansion have been absorbed well by the cable movement in the cryogenic pipe together with the use of movable terminals.

ACKNOWLEDGMENT

The authors thank Prof. Atsuo Iiyoshi, Chairman of the Board of Trustees and Chancellor of Chubu University, for his continuous encouragement throughout this work. The authors acknowledge Prof. Hiroshi Fujiwara, a professor of Keio University and President of the Nano-Opt Energy Corporation, for his financial support of this work. We also thank JFE Steel Corporation for supplying steel pipes for the construction of the test facilities. Parts of this work were supported by a grant from the Strategic Research Foundation Grant-aided Project for Private Universities Ministry of Education, Culture, Sports, Science and Technology, Japan.

REFERENCES

1. Watanabe, M., Masuda, T., Hirose, M., Isojima, S., Honjo, S., Uchiyama, T., Shimodate, M., Takahashi, Y., and Suzuki, H., Thermo-Mechanical Properties of a 66 kV Superconducting Power Cable System, IEEE Transactions on Applied Superconductivity (2003), 13 1956-1959
2. Ichikawa, M., Kanegami, M., Okamoto, T., Akita, S., Yagi, M., and Kimura, A., Thermomechanical Characteristics of 500-m HTS Power Cable, IEEE Transactions on Applied Superconductivity (2005), 15 1771-1774
3. Yamaguchi, S., Kawahara, T., Hamabe, M., Watanabe, H., Ivanov, Yu., Sun, J., and Iiyoshi, A., Experiment of 200-meter superconducting DC cable system in Chubu University, Physica C (2011), 471 1300-1303

Materials Science Forum Vols. 740-742 (2013) pp 843-846

doi:10.4028/www.scientific.net/MSF.740-742.843

Slicing of rotating SiC ingot by electric discharge machining

Norimasa Yamamoto[1,a,], Satarou Yamaguchi[2,a], Tomohisa Kato[3,c,d]

[1]Center of Applied Superconductivity & Sustainable Energy Research, Chubu University, 1200 Matsumoto-cho, Kasugai, Aichi 487-8501 Japan

[2] R&D Partnership for Future Power Electronics Technology, Central2, 1-1-1 Umezono, Tsukuba, Ibaraki 305-8568 Japan

[3]National Institute of Advanced Industrial and Technology, Central2, 1-1-1 Umezono, Tsukuba, Ibaraki 305-8568 Japan

[a]yamamoto-no@isc.chubu.ac.jp, [b]yamax@isc.chubu.ac.jp, [c]t-kato@aist.go.jp,

Keywords: electric discharge machining, ingot slicing, rotating slicing

Abstract. A new method of electric discharge machining (EDM) is proposed for slicing a large silicon carbide (SiC) ingot in order to realize low kerf loss and fast cut. This principle is based on the rotating ingot, and it is called the rotating slicing method (RSM). It would be defecate the cutting chip effectively and one-point discharge. In this paper, we reported results of examinations of the RSM experimentally. Unstable discharge was not observed. Discharge damages on the wire surface were fewer than those of the conventional method. Net cutting speed was almost the same as the present method for the 2-inches ingot. The rotation axis of the ingot should be perpendicular to the feed direction of the wire, and it is important to fix the performance of the EDM such as the kerf loss. Roughness of the cutting surface was 3.4 μm of R_a

Introduction

Since pure SiC material is expensive and high hardness, researchs for low loss and high speed machining are important. In order to slice a large SiC ingot effectively, EDM as an alternative to the diamond wire saw is studied [1-4]. Schematic image of the conventional EDM is shown in figure 1(a).

As losses in the machining, three causes of warpage, kerf loss and chippage are considered. The EDM has an advantage that warpage doesn't occur. Kerf loss is formed by gap of discharge between the wire surface and material. Kerf loss by the EDM depends strongly on wire diameter, and therefore the reduction by using fine wire is easy. For a SiC slab of thickness of 6 mm, kerf loss of 95-100 μm by using 50 μm diameter wire were obtained [5]. Of course, it is that difficult to slice thick material with fine wire. When SiC ingot is sliced, it can be damaged deeply by the breaking of the wire and/or the short. The breaking of the wire is occured by unstable discharge stemmed from the formed chips by slicing. Therefore the avoidance of the breaking of the wire is difficult. An avoidance of the short is easy, because of it is cause that migration speed of ingot is too fast than the cutting speed by discharge.

In fact, the EDM was applied to slicing the Si ingot several years ago, and when we applied the EDM for 4-inches Si ingot, the cutting speed was low qualitatively as compared with the slicing of the 2-inches Si ingot. The reasons of the slow cutting for a large ingot would depend on the defecation of the chip and the multi-discharge for the cut chip because the chips cannot be defecated between the wire and the ingot.

In order to solve problems of the breaking of the wire, and kerf loss, we propose a new method that rotates ingot as shown in Fig.1(b). The rotated ingot with turn table is discharged by one point on the wire, and even in the mechanical wire saw, one-point cutting is adopted. The formed chips by cutting are ejected without affecting to discharges. In addition, this method avoids overlap of discharge damage points on the wire. Therefore, the cutting by this point-like discharge is equivalent to cut thick material as thin material. The avoidance of the breaking of the wire, and keeping of high discharge rate are expected. In particular, we report characteristics of RSM, and stability of discharge by ejection of chips.

Experimental

We produced an equipment of the turn table. The turn table is connected on the work stage of wire electric discharge machining DWC90G (MITSUBISHI co). SiC ingot is provided by National Institute of Advanced Industrial and Technology and the diameter is 52 mm. The ingot is bonded by silver paste on a turn table, and is rotated. Rotation velocity of the ingot is 60 rpm. The wire is copper alloyed wire with diameter of 200 μm, and the feed velocity is 2.0 – 6.0 m/min. Voltage of 130-200V between the wire and ingot is applied with a period of 5 kHz.

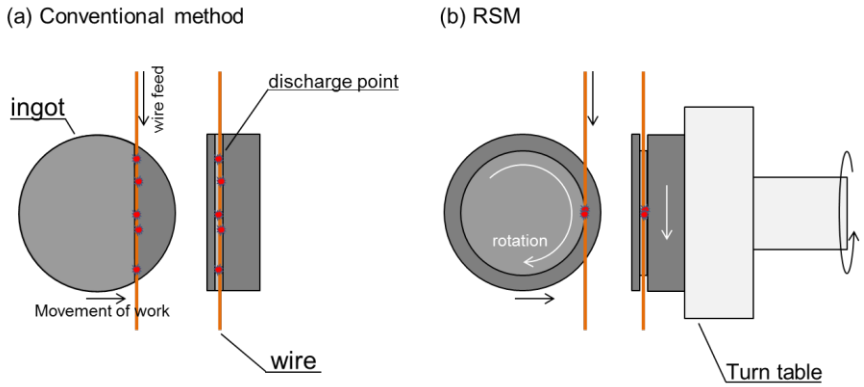

Figure 1. The schematics of the EDM on (a) conventional method and (b) RSM (clockwise rotation).

Results and discussion

In general, the cutting speed is inversely proportional to the cutting length. Figure 2(a) shows geometry in cutting. In the conventional method, the cutting length, $L_c(x) = 2\,[26^2 - x^2]^{1/2}$, where x is distance from center of ingot. $L_c(x)$ is the shortest at the start of cutting, and the longest at the center of ingot. In RSM, the length, $L_r(x)$ is $2\pi x$, equal to circumferential length. The cutting speed as function of x is shown in figure 2(b). Both cutting speed are clear to be inversely proportional to cutting length. Difference from curves is derived from uniformity of material quality. Net cutting speed is the cutting volume per unit minute on each x. It is expressed as product of the cutting speed, the cutting length, and kerf loss. Both net cutting speed were the same as 0.25-0.30 mm^3/min, and almost constant on each x.

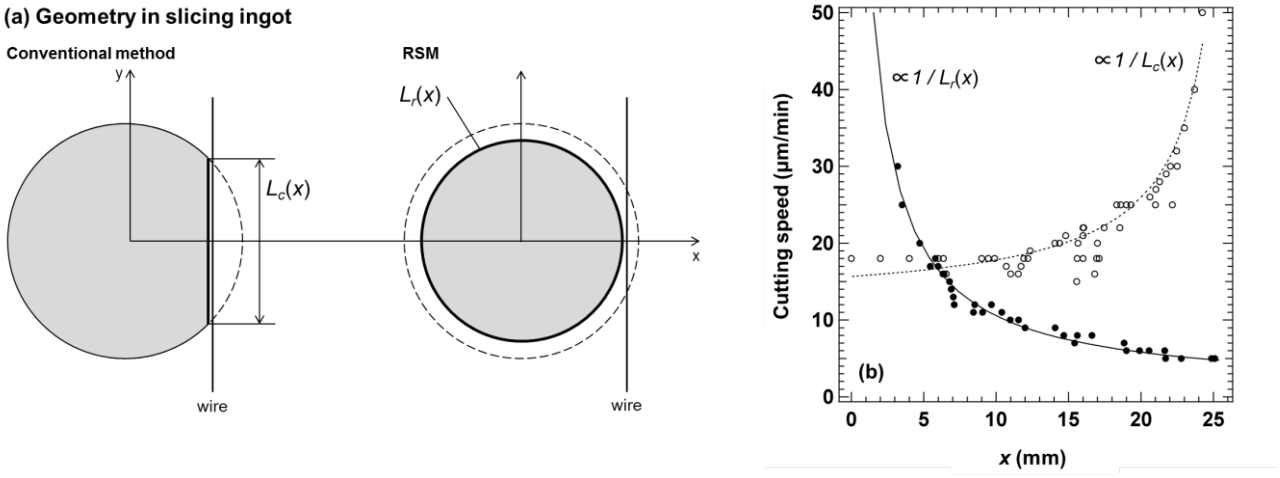

Figure 2(a) Geometry in slicing ingot and (b) cutting speed as function of x. Solid and dashed lines are $L_r(x)$ and $L_c(x)$, respectively. Closed and open circle are actual cutting speed in experiments for RSM and conventional slicing method, respectively.

Discharge rate of both method was 60-70%, and almost same. Average cutting volume per unit discharge was 1.4-1.7 mm^3. Then, 60-70% of chip was less than 1 μm. This indicate that fine chips of several hundred to a few thousands were generated by thermal stress in a single discharge. Then, the unexpected unstable discharge in the conventional method during slicing ingot was observed several times. However, electric discharge in RSM was always stable.

Wire damages

Figure 3(a) and (b) show the wire damages by the conventional method and RSM. Feed velocity of the wire was 6.0 m/min. There are spot-like signatures by discharge on both wire. Diameter of spot size was about 30 mm. The burn marks on the wire by the conventional method were distributed throughout. However, the burn marks on the wire by RSM were distributed to only in the vicinity of the spot. Moreover, gross of the original remained. The burned damages on the wire are considered to be formed by the heated chips by discharge plasma. In RSM, damages derived from chips were not occured. Therefore, the unexpected unstable discharge is considered to been avoided. The avoidance of the burned damages is expected to be important for slicing with more fine wire.

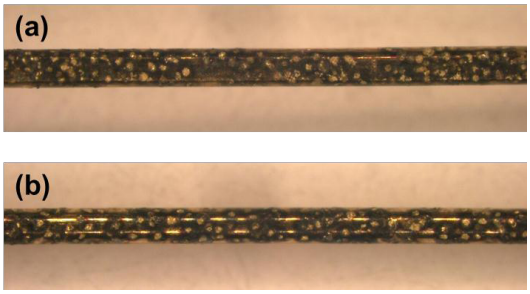

Figure 3. Damages on the wire by EDM. (a) Conventional method and (b) RSM.

Surface roughness

Figure 4 shows a photograph of the cutting surface by the conventional method and RSM. In the cutting surface by RSM, pattern of concentric circles can be seen. Although the inside was pearskin-like surface, outside was not pearskin-like surface. Surface roughness (R_a) of the conventional method and RSM were 1.6 ± 0.4 μm and 3.4 ± 0.8 μm, respectively.

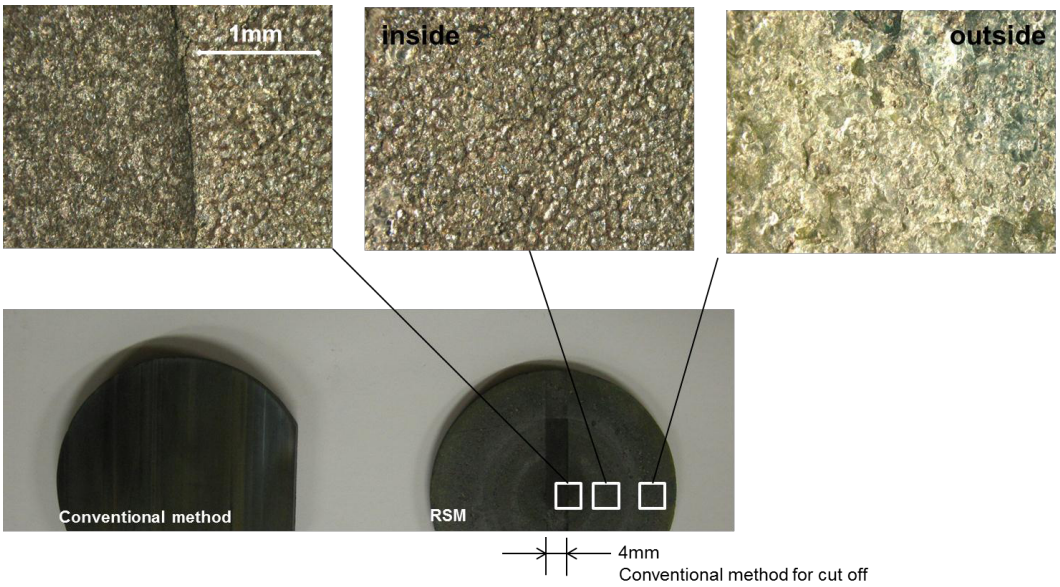

Figure 4. Surface of sliced SiC ingot.

Kerf loss

Figure 5 shows photograph of the surface to the cutting direction. Each kerf loss were estimated from photographs to be 346.0 ± 1.3 μm (conventional method), 395.5 ± 4.3 μm (clockwise rotation), and 398.1 ± 6.4 μm (counterclockwise rotation). There was no difference of kerf loss between clockwise rotation and counterclockwise rotation in the RSM. Kerf loss by RSM was about 50 μm larger than that by the conventional method. It is considered for the rotation axis of the ingot was not completely perpendicular to the feeding direction of the wire. The difference from perpendicular was 0.055 degrees.

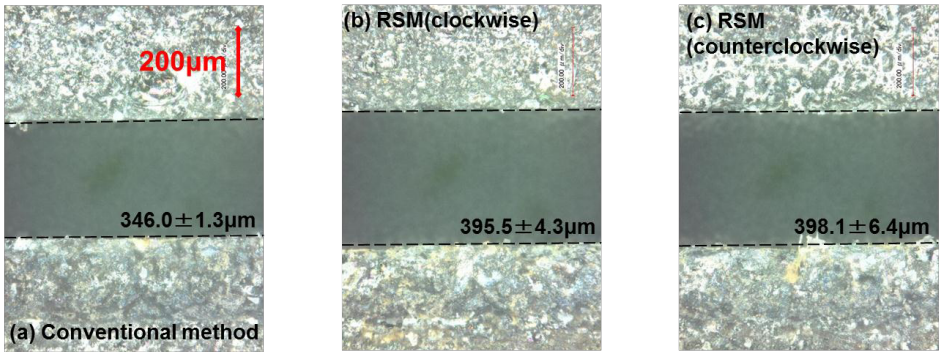

Figure 5. Kerf loss of sliced SiC ingot.

Summary

For efficiency and fast cutting of EDM, we proposed a new slicing method of the rotating ingot and examined. The stable discharge in RSM, and reduction of the burn marks on the wire was observed. In 2-inches ingot, net cutting speed of the RSM and the conventional method was almost same. Surface roughness of the sliced ingot by RSM was sufficient accuracy. In future, we will apply to larger ingot than 2-inches and consider a new method for high-speed cutting.

Acknowledgements

This work is supported by Novel Semiconductor Power Electronics Project Realizing Low Carbon Emission Society under Ministry of Economy, Trade and Industry (METI) and New Energy and Industrial Technology Development Organization (NEDO). Authors thank to Mr. H. Yamada and Mr. K. Uchimura for help in the experiments.

References

[1] S. Yamaguchi, T. Noro, H. Takahashi, H. Majima, Y. Nagao, K. Ishikawa, Y. Zhou, T. Kato, Mater. Sci. Forum 600-603, 851 (2009).

[2] T. Kato, T. Noro, H. Takahashi, S. Yamaguchi and K. Arai, Mater. Sci. Forum 600-603, 855 (2009).

[3] T. Sugimoto, T. Noro, S. Yamaguchi, H. Majima and T. Kato, Mater. Sci. Forum 615-617, 609 (2009).

[4] T. Sugimoto, T. Noro, S. Yamaguchi, H. Majima, Mater. Sci. Forum 645-648, 869 (2010).

[5] H. Yamada, S. Yamaguchi, N. Yamamoto, T. Kato, Mater. Sci. Forum 717-720, 861 (2012).

26th International Conference on Low Temperature Physics (LT26) IOP Publishing
Journal of Physics: Conference Series **400** (2012) 022114 doi:10.1088/1742-6596/400/2/022114

Critical current measurements of a tape in the hybrid multi-stacking high T_c superconducting tapes

J Sun[1], H Watanabe[1], M Hamabe[1], T Kawahara[1], A Iiyoshi[1] and S Yamaguchi[1,2]

[1]Center of Applied Superconductivity and Sustainable Energy Research, Chubu University, 1200, Matsumoto-cho, Kasugai, Aichi 4878501, Japan
[2]Department of Electrical Engineering, Chubu University, 1200, Matsumoto-cho, Kasugai, Aichi 4878501, Japan

E-mail: j_sun@isc.chubu.ac.jp

Abstract.

A new 200 m high T_c superconducting DC cable test facility was successfully constructed in 2010. This cable is composed of two superconducting layers of the DI-BSCCO® tapes spirally and closely surrounding a copper former. The number of the tapes in each layer is different due to their different radii. We have investigated the effect of the way of the tape winding on the critical current (I_c) of the tapes in order to optimize the cable configuration for the DC transmission.

This paper presents the measurements of I_c of DI-BSCCO® in a hybrid multi-stacking configuration composed of YBCO and BSCCO tapes by controlling the transport current in each tape independently. The I_c measurements were performed with the standard four-probe method at the liquid nitrogen temperature. The magnetic field distribution around the tapes was calculated by the finite element method to demonstrate the effects of the self field from the adjacent tapes. The enhancement and degradation of I_cs in the hybrid multi-stacking tapes were observed in contrast to that of single tape. Through the experiments, we started to investigate optimized tape configuration of the DC power cable to enhance the superconducting characteristics.

1. Introduction

Since the enhancement of the performance of the high T_c superconducting (HTS) tapes with high engineering critical current density ~ 10 kA/cm^2 the HTS power cables for power transmissions are extensively studied around the world [1, 2]. The performance of the DC transmission through HTS cable has been studied and tested at Chubu University since 2006 [3] and a new 200 m HTS DC cable test facility, named as CASER-2 [4], was successfully constructed in the spring of 2010. The HTS cable is installed into a vacuum insulated cryogenic pipe and operated at about 77K. This HTS cable, which was made by Sumitomo Electric Industries Ltd (SEI), is composed of two superconducting (SC) layers of the DI-BSCCO® tapes spirally and closely surrounding a copper former. There are 23 tapes for the inner SC layer and 16 tapes for the outer SC layer due to their different radii, respectively.

In order to optimize the structure of HTS cables, we started to study the effects of tape arrangements on the critical current I_c to enhance the SC characteristics of the HTS tape in the cable. Lim *et al.* studied the magnetization loss of hybrid multi-stacked wire using YBCO and

26th International Conference on Low Temperature Physics (LT26) IOP Publishing
Journal of Physics: Conference Series **400** (2012) 022114 doi:10.1088/1742-6596/400/2/022114

BSCCO wire [5]. This paper presents the measurements of I_cs of DI-BSCCO® in the multi-stacked tapes composed of YBCO and BSCCO tapes by controlling the transport current in each tape independently.

2. Experiments

The YBCO (Y-123) tapes were prepared by the method of Trifluoroacetates-Metal Organic Deposition (TFA-MOD) [6] by SWCC and the DI-BSCCO® (Bi-2223) tapes (Type HT-CA) were prepared by the powder in tube (PIT) with the controlled over pressure sintering technique by SEI [7, 8]. Table 1 shows the specifications of the YBCO tape and the BSCCO tape. The cross sections of the YBCO tape and the BSCCO tape are 4.9 mm × 0.13 mm and 4.5 mm × 0.36 mm, respectively. The thickness of the BSCCO tape includes the thickness of the reinforcing copper layer, which is 0.05 mm on both sides of the silver-sheathed multi-filamentary Bi-2223 matrix area to improve the mechanical strength of the tape [8]. The I_cs of YBCO tape and BSCCO tape are 141 A and 160 A in the self field at 77 K, respectively.

Table 1: Specifications of the YBCO tape and the BSCCO tape.

YBCO tape		BSCCO tape	
Thickness	129.7 µm	Thickness	0.36 mm
Width	4.9 mm	Width	4.5 mm
Hastelloy	100 µm	I_c (77 K)	160 A
IBAD/GZO	1.2 µm	Type	HT-CA
CeO_2	1 µm		
YBCO	1.5 µm		
Ag	26 µm		
I_c (77 K)	141 A		

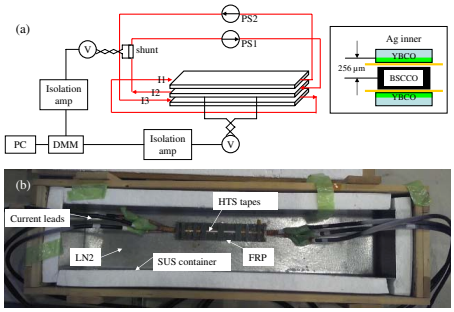

Figure 1: (a) a schematic diagram of the experimental setup and (b) a photo of the experimental device. The insert of (a) shows the arrangement of the HTS tapes.

Figs. 1a and 1b show a schematic layout of the experimental setup [9] and a photo of the experiment device. One straight BSSCO tape is sandwiched between two straight YBCO tapes with the Ag surface of the YBCO tapes inside. As the insert of Fig. 1a, each tape is insulated with each other by using one Kapton tape layer with the thickness of $\sim$ 0.05 mm and thus the vertical distance between the YBCO coated layer in the YBCO tape and the center of the BSCCO tape is 256 µm. To control the current in the BSCCO and YBCO tapes independently, two DC power supplies (PS) are used. The PS1 (300 A, 10 V) is used for the current feeding to the middle BSCCO tape ($I2$) and the PS2 (1200 A, 10 V) is for both the YBCO tapes in series ($I1 = I3$). Both the YBCO tape and the BSCCO tape are prepared with the length of $\sim$ 27 cm in consideration as a infinitely long wires. Three voltage taps are attached on the edge of the BSCCO tape with distance of 8 cm and 10 cm. The samples are immersed in the liquid nitrogen. The transport current is measured by a current shunt resistor. The voltage signals are measured by a KEITHLEY 2700 digital multimeter. The V - I characteristics of the HTS tapes are obtained by the four-probe method.

3. Results and discussion

By normalizing to the distance between the voltage taps, we obtain the E - I characteristic curves of the BSCCO tape. Figs. 2a - 2c show the comparisons of the E - I characteristic curves of the BSCCO tape for single and triply stacked HTS tapes with the different currents of -100 A, 0 A, and 100 A applied for the adjacent YBCO tapes, respectively. The significant difference

of I_c of the BSCCO tape between the triply stacked tapes and single one is shown when the currents in the adjacent YBCO tapes are changed. Even if no current in the adjacent YBCO tapes, the I_c of the BSCCO tape becomes larger than that of the single one due to the magnetic shielding on the self-field of the middle BSCCO tape by the YBCO tapes.

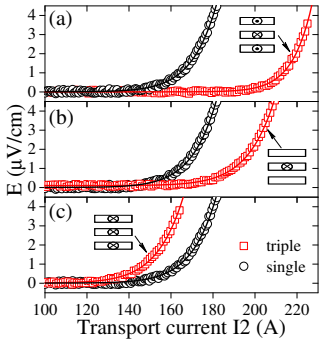

Figure 2: The E - I characteristic curves of the BSCCO tape for single and hybrid triply stacked configurations with the different currents (a) −100 A, (b) 0 A, (c) 100 A applied to the adjacent YBCO tapes.

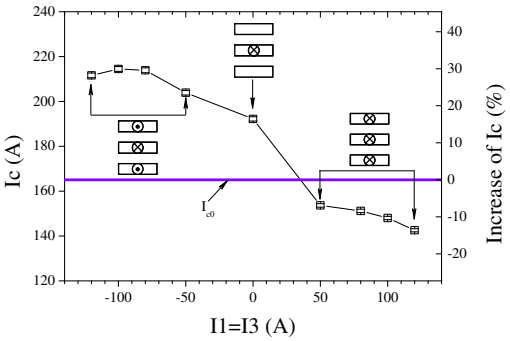

Figure 3: The dependence of I_c of the DI-BSCCO tape on the current applied to the adjacent YBCO tapes with 1 kapton layer between them.

I_c is determined according to the criterion of 1 μV/cm. Fig. 3 presents the dependence of I_c of the BSCCO tape on the currents in the adjacent YBCO tapes for triply hybrid multi-stacked tapes. The I_c of the BSCCO tape is measured to be 165 A, which is a little larger than that in the specification from SEI. When no current is applied to the adjacent YBCO tapes, the I_c of the BSCCO tape becomes 15% larger than that of the single one. In the case of antiparallel current feeding to the YBCO tapes against the BSCCO tape, the sharp increase of I_cs of the BSCCO tape is seen and is about 30% in contrast with that of the single one. However, the parallel current feeding leads to the decrease of the I_c of the BSCCO tape when the current in the adjacent YBCO tapes becomes larger than 50 A.

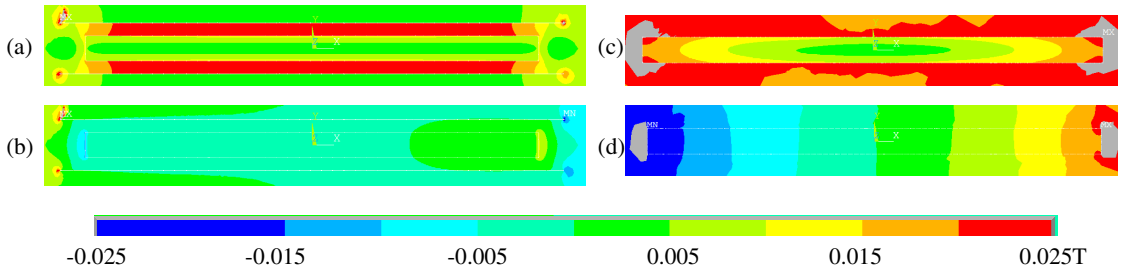

Figure 4: The sum (upper), and perpendicular component (lower) of the magnetic field distribution calculated by ANSYS [10]. Left: hybrid triply stacked tapes with the current of $I1 = I3 = -100$ A applied to the YBCO tapes and $I2 = 160$ A to the BSCCO tape; Right: single BSCCO tape with 160 A. The uniform current distributions in the cross section of the HTS tapes are assumed.

We calculate the magnetic field distribution by the commercial finite element method code (ANSYS) [10, 11, 12]. To illustrate the effect of the self-field by the adjacent YBCO tapes, we

present the magnetic field distribution for triply stacked tapes in Figs. 4a and 4b and single one in Figs. 4c and 4d. The transport current is assumed to be uniformly distributed in the BSCCO matrix area and the YBCO coated film. Hence the cross section of the transport current area is assumed to be 4.5 mm × .0.25 mm for the BSCCO tape without the reinforcing copper layer [8] and 1.5 µm × 4.9 mm for the YBCO tapes. The current is set 160 A for the BSCCO tape and −100 A for the YBCO tapes. The magnetic flux density in the BSCCO filament area is reduced comparing with that of the single one as shown in Figs. 4a and 4c. Since the I_c of the BSCCO tape is affected by the magnetic field especially for the perpendicular component to the tape wide surface [7], Figs. 4b and 4d present the perpendicular component of the magnetic flux density distribution. As seen in the figures, the perpendicular component of the magnetic flux density is reduced, which would result in the enhanced I_c in Figs 2 and 3.

4. Conclusion

We investigated the dependence of I_c of the BSCCO tapes on the current in the adjacent YBCO tapes in the triply hybrid multi-stacked tapes experimentally. Enhancement of I_c of the BSCCO tape in the triply stacked tapes composed by the BSCCO and the YBCO tapes is observed experimentally. In conjunction with the magnetic field distribution calculated by the finite element method, the effects of the self field from the adjacent tapes lead to the reduction of the magnetic flux density in the antiparallel current feeding to the triply stacked tapes. Therefore, the enhancement and degradation of I_cs of the BSCCO tape are observed in contrast with that of the single one.

Acknowledgments

The authors acknowledge Prof. Hiroshi Fujiwara for his financial support. We also acknowledge the support by NEDO, Ministry of Education, Culture, Sports, Science and Technology (MEXT), and Chubu University Grant (A).

References

[1] Lim J H, Sohn S H, Ryoo H S, Choi H O, Yang H S, Kim D L, Ma Y H, Ryu K and Hwang S D 2009 *IEEE Trans. Appl. Super.* **19** 1710–3
[2] Ichikawa M, Kanegami M, Okamoto T, Akita S, Yagi M and Kimura A 2005 *IEEE Trans. Appl. Super.* **15** 1771–4
[3] Yamaguchi S, Hamabe M, Yamamoto I, Famakinwa T, Sasaki A, Iiyoshi A, Schultz J, Minervini J, Hoshino T, Ishiguro Y and Kawamura K 2008 *J. Phys.: Conf. Series* **97** 012290
[4] Yamaguchi S, Kawahara T, Hamabe M, Watanabe H, Ivanov Y, Sun J and Iiyoshi A 2011 *Phyica C: Superconductivity* In press
[5] Lim H, Cha G and Lee H 2007 *IEEE Trans. Appl. Super.* **17** 1947–50
[6] Izumi T, Yoshizumi M, Miura M, Nakaoka K, Sutoh Y, Ichikawa Y, Miyata S, Ibi A, Fukushima H, Itoh T, Takahashi T, Aoki Y, Koizumi T, Kaneko A, Hasegawa T, Yamada Y and Shiohara Y 2009 *IEEE Trans. Appl. Super.* **19** 3119–22
[7] Kikuchi M, Ayai N, Fujikami J, Kobayashi S, Yamazaki K, Yamada S, Ishida T, Kato T, Hayashi K, Sato K, Hata R, Iihara J and Yamaguchi K, Kumakura H, Kitaguchi H, Osamura K and Shimoyama J 2008 *AIP Conf. Proc.* **986** 407–15
[8] Ayai N, Yamazaki K, Kikuchi M, Osabe G, Takaaze H, Takayama H, Kobayashi S, Fujikami J, Hayashi, Sato K, Osamura K, Kitaguchi H, Matsumoto S, Kiyoshi T and Shimoyama J 2009 *IEEE Trans. Appl. Supercond.* **19** 3014–7
[9] Sun J, Yamauchi S, Sugino M, Watanabe H, Hamabe M, Kawahara T and Yamaguchi S 2011 *Physica C: Superconductivity* In Press
[10] ANSYS® Academic Teaching Advanced, Release 12.1 ANSYS Inc. www.ansys.com
[11] Farinon S, Fabbricatore P and Gömöry 2010 *Supercond. Sci. Technol.* **23** 115004
[12] Fabbricatore P, Farinon S, Innocenti S and Gömöry 2000 *Phys. Rev. B* **61** 6413

26th International Conference on Low Temperature Physics (LT26) IOP Publishing
Journal of Physics: Conference Series **400** (2012) 052009 doi:10.1088/1742-6596/400/5/052009

Current dependence of heat leak on the terminals in the superconducting DC transmission and distribution system of CASER-2

Toshio Kawahara[1], Hirofumi Watanabe[1], Masahiko Emoto[2], Makoto Hamabe[1], Sataro Yamaguchi[1], Yasuo Hikichi[3], Masahiro Minowa[3]

[1]Center of Applied Superconductivity and Sustainable Energy Research, Chubu University, 1200 Matsumoto, Kasugai, Aichi 487-8501 Japan
[2]Department of Large Helical Device Project, National Institute for Fusion Science, Gifu 509-5292 Japan
[3] SWCC Showa Cable Systems Co. Ltd., 4-1-1 Minami-hashimoto, Chuo, Sagamihara, Kanagawa 252-0253 Japan

E-mail: toshi@isc.chubu.ac.jp

Abstract. Superconductivity can solve the energy problems in the world as energy saving technologies. In particular, superconducting direct current (DC) transmission and distribution (T&D) systems is promising, as it can be easily extended to large scale energy transmission systems for energy sharing. We are developing criogenic systems for effective cooling of superconducting T&D systems. In the cooling experiments with the 200 m-class superconducting DC T&D system at Chubu University (CASER-2), we have estimated the performance of the system. For example, our superconducting cable is connected to the outside at the terminals using Peltier current leads (PCLs). The PCL is composed of a thermoelectric material and a copper lead. Small thermal conductivity and large thermopower of the thermoelectric modules can effectively insulate the heat leak to the low temperature end. We measured the temperature along the current leads and the heat leak at the terminals. As current leads have an optimal shape factor, the optimum operation current exists. The current dependence of the system performance is discussed.

1. Introduction

The energy problems should be solved urgently for the future world. Superconductivity has a high potential as an energy saving technology, which comes from its zero direct current (DC) resistance. Therefore, superconducting transmission and distribution (T&D) systems are promising and such large scale T&D systems help the smart use of unstable natural energies by the energy sharing. The actual use of applied superconducting systems requires high performance cryogenics, because superconductivity can be archived only at the low temperature.

Chubu University has developed 20 m-class superconducting DC transmission device (CASER-1) [1] and 200 m-class superconducting DC T&D system (CASER-2). Using these facilities, we have studied several cooling technologies such as low heat leak cryogenic pipes, high performance terminal systems and so forth to obtain the pragmatic performance of actual superconducting systems [2][3].

26th International Conference on Low Temperature Physics (LT26) IOP Publishing
Journal of Physics: Conference Series **400** (2012) 052009 doi:10.1088/1742-6596/400/5/052009

High performance current leads are required for the applied superconductivity [4][5]. For examples, the gas cooled current leads opened the commercial use of superconducting magnet systems [6]. We have developed the Peltier current lead (PCL) as a low heat leak current lead [7][8][9], which is used in the terminals of CASER-2. In this paper, we discuss about the performance of PCL in CASER-2. In the actual use of superconducting T&D systems, the current feeding is changed by the power demanded. Therefore we measured the heat leak under the different currents feeded and discuss the current dependence of the heat leak.

2. Experiments in CASER-2

2.1. CASER-2 specifications

Figure 1 shows the pictures of CASER-2 and its specifications. The transmission power of CASER-2 is 40 MW and the length is approximately 200 m. There is an undulation of 2.7 m and a turn with the minimum radius of 2 m, which can emulate actual conditions of transmission lines in the field. We have already finished the 3rd cooling experiment for cryogenics and a superconducting state. As an example, we show the temperature along the cryogenic pipe and the electric field induced in the cable in the first few days in the first cooling experiment (figure 2). Within a week, the whole system was cooled down to the liquid nitrogen temperature and superconducting cables went into the superconducting state, where the electric field on the cable was zero.

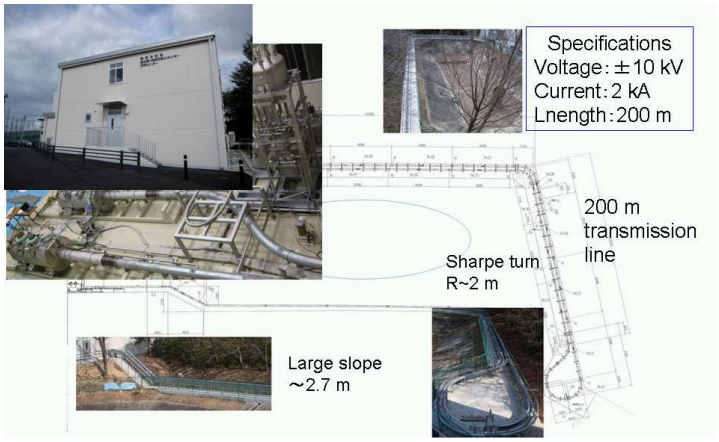

Figure 1. Specification of CASER-2.

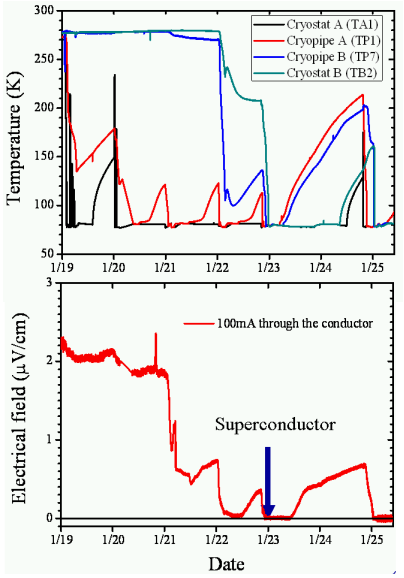

Figure 2. First cooling experiment in CASER-2.

2.2. Experiments for current lead

We also estimated the performance of the terminals. The terminals in applied superconducting systems connect between the superconductors and outer systems set in the room temperature. Since there is large conduction heat, the reduction of the heat leak on the terminals is one of the key technologies for high performance superconducting systems. Therefore we use the PCL for the thermal insulation on the current lead. In particular, as the T&D systems should carry large current for power transmission, the effect of the improvements of the current lead will be large. During the cooling experiments, we can easily observe the difference in the performance between the PCL and the copper current lead (CCL). The large heat leak of the CCL generates ice on the outside of the flange of the cryostat as shown in figure 3 (a), where two kinds of PCLs were used. One is the home made PCL including CCL (figure 3 (a)), and another is a commercial one made by SWCC (figure 3 (b)).

26th International Conference on Low Temperature Physics (LT26) IOP Publishing
Journal of Physics: Conference Series **400** (2012) 052009 doi:10.1088/1742-6596/400/5/052009

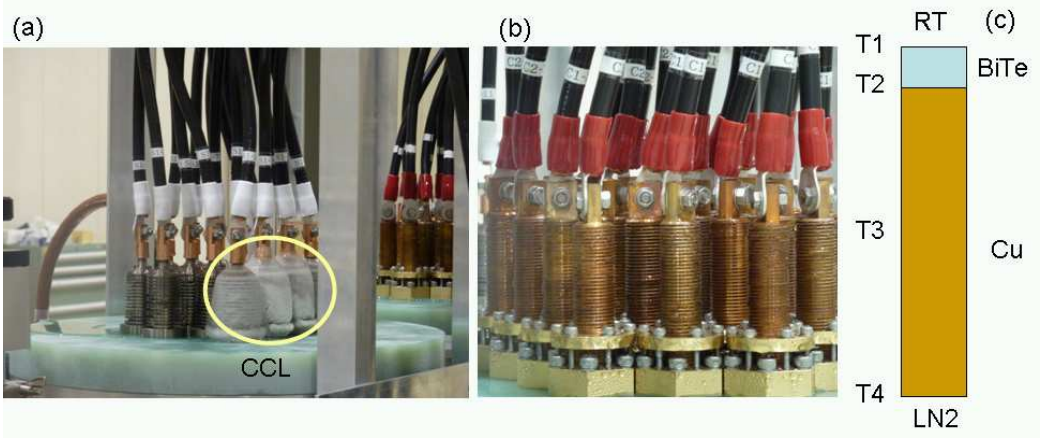

Figure 3. Pictures of PCL. (a) and (b) are the picture during the cooling experiment, and (c) is a schematic of PCL.

The schematic structure of the PCL is shown in figure 3 (c). The PCL is composed of a thermoelectric material and a copper lead. Small thermal conductivity and large thermopower of thermoelectric modules can effectively insulate the heat leak to the low temperature end [7][10][11].

We measured the temperature at the three different positions on the current lead as T1, T2 and T3. The slope of the temperature distribution can roughly tell us the amount of the conduction heat on the current lead. The temperature of the liquid nitrogen (T4) is also measured for the heat leak to the superconducting system. The feeding current for the superconducting cable is in the range between 0 to 1.2 kA. As the stabilization of the system required long time, we selected this current range for the heat leak measurements.

3. Resulets and discussion

Firstly, we will show the temperature distribution on the current lead without feeding a current in figure 4. The large temperature difference on the BiTe modules is observed both for n- and p-type. The mild slope of the temperature distribution on the copper pert in the PCL means the small heat leak on the current lead. Contrary, the CCL has a large slope of the temperature distribution, which was caused by the large heat leak and the iced lead on the flange was observed as figure 3 (a). Therefore,

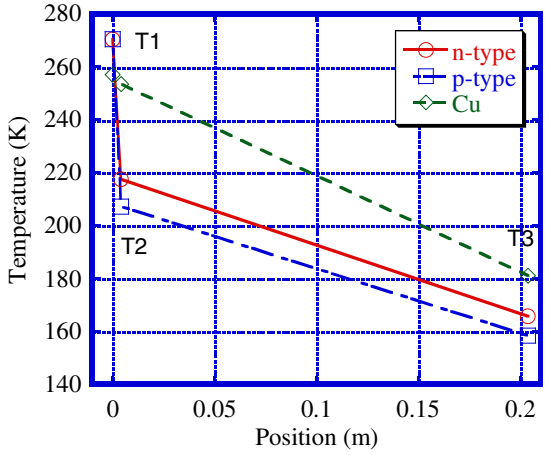

Figure 4. Temperature distribution on the current lead. Those for PCL with n- and p-types, and also copper lead are plotted.

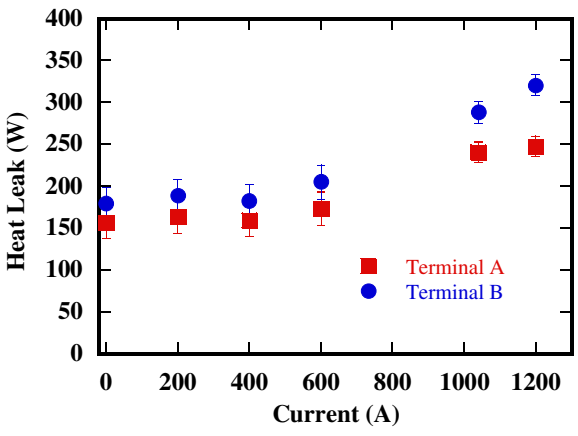

Figure 5. Current dependence of the heat leak on the terminals. Squares and circles are for Terminals A and B, respectively.

26th International Conference on Low Temperature Physics (LT26) IOP Publishing
Journal of Physics: Conference Series **400** (2012) 052009 doi:10.1088/1742-6596/400/5/052009

the temperature difference between T1 and T2 is one of the parameters for the performance of the terminals. This temperature difference increases as the feeding current increases at the lower current and have some maximum at the optimum current around 800 A. This is the optimum condition for the actual shape of the current lead.

Next we show the feeding current dependence of the heat leak on the terminals in figure 5. Above 800 A, the steep increase of the heat leak was observed. Therefore, the optimum condition for the current lead seems to be around 800 A. There is a small difference of the heat leak between the terminals A and B, because of the difference of the shape factor of the current lead for the optimum current. Since the over current condition caused the large heat leak, the further optimum design of the current lead such as thermoelectric parameters, thermal configurations and so forth will be required. On the other hand, below its optimum current, we reduced the heat leak effectively on the terminals, which lead to enhance the performance of the superconducting T&D systems.

4. Summery

The 200 m-class superconducting DC T&D system of CASER-2 was successfully constructed and we have performed several cooling experiments to show the capability of the superconducting power transmission systems. Such large power applications, we should consider the current dependence of the system performance. We measured the temperature distribution on the current lead to estimate the performance of the terminals and also measured the temperature variation of the liquid nitrogen in the terminals. We observed the optimum current for the systems and successfully insulate the heat which comes from the outside of the system.

Acknowledgements

The authors thank Dr. A. Iiyoshi, Chancellor of Chubu University for his continuous encouragement through this work. We acknowledge Dr. Hiroshi Fujiwara for his support on the construction of 200 m superconducting facilities of CASER-2. Parts of this work were supported by a grant of Strategic Research Foundation Grant-aided Project for Private Universities Ministry of Education, Culture, Sports, Science and Technology (MEXT), and Grant-in-Aid for challenging Exploratory Research (MEXT). Parts of the work were also supported by Nippon Sheet Glass Foundation for Materials Science and Engineering, and Future Energy Research Association.

References

[1] Yamaguchi S, Hamabe M, Yamamoto I, Famakinwa T, Sasaki A, Iiyoshi A, Shultz J, Minervini J, Hoshino T, Ishiguro Y and Kawamura K 2008 J. Phys.: Conf. Ser. **97** 012290
[2] Hamabe M, Nasu Y, Ninomiya A, Ishiguro Y, Kusaka S and Yamaguchi S 2008 Adv. in Cryo. Eng. **53A** 168
[3] Hamabe M, Fujii T, Yamamoto I, Sasaki A, Nasu Y, Yamaguchi S, Ninomiya A, Hoshino T, Ishiguro Y and Kawamura K 2009 IEEE Trans. Appl. Supercond. **19** 1778
[4] Wilson M N 1983 “Superconducting Magnets” (Clarendon Press, Oxford) pp.256-272
[5] Xuan X C, Ng K C, Yap C and Chua H T 2002 Cryogenics **42** 779
[6] Efferson K 1967 Rev. Sci. Instrum. **38** 1776
[7] Yamaguchi S, Yamaguchi T, Nakamura K, Hasegawa Y, Okumura H and Sato K 2004 Rev. Sci. Instrum. **75** 207
[8] Hasegawa Y, Sato K, Okumura H, Nakamura K, Yamaguchi S and Miyake K 2002 Cryogenics **42** 495
[9] Kawahara T, Fujii T, Emoto M, Hamabe M, Sun J, Watanabe H and Yamaguchi S 2010 Physica C: Supercond. **470** S1011
[10] Kawahara T, FujiiT, Emoto M, Hamabe M, Watanabe H, Sun J, Ivanov Y and Yamaguchi S 2011 IEEE Trans. Appl. Supercond. **21** 1070
[11] Fujii T, Fukuda S, Emoto M, Osada K, Kawahara T, Hamabe M, Watanabe H, Ivanov Y, Sun J and Yamaguchi S 2011 J. Electro. Mater. **50** 691

Available online at www.sciencedirect.com

SciVerse ScienceDirect

Physics Procedia 36 (2012) 1372 – 1377

Physics Procedia

Superconductivity Centennial Conference

Design study of LN_2 circulation in a long SC power transmission lines

Yury Ivanov[a*], Hirofumi Watanabe[a], Makoto Hamabe[a], Toshio Kawahara[a], Jian Sun[a], Satarou Yamaguchi[a,b]

[a]*Center of Applied Superconductivity and Sustainable Energy Research, Chubu University, Kasugai, Aichi 487-8501, Japan*
[b]*Department of Electric Engineering, Chubu University, Kasugai, Aich, 487-8501, Japan*

Abstract

In accordance with the conventional design of superconducting power transmission (SC PT) line, HTS cable should be placed into a carefully heat-insulated cryopipe filled with cryogen (usually liquid nitrogen, LN_2) in order to maintain its temperature low. Circulating LN_2 removes heat penetrating through the insulation layers. The circulation rate depends on the heat load and the length of the line. Since LN_2 working temperature range is restricted, it is easy to show that pressure drop, Δp, increases dramatically being almost cubic function of the cable length, L, and quadratic function of the specific heat load, q: $\Delta p \propto L^{n+1} q^n$, where n = 1.75...2.0. Great efforts should be made to reduce heat load on the system and hydraulic friction inside the channels. Last requirement is contrary to common practice since the entire existing test SC PT lines are constructed using corrugated cryopipes which exhibit very high Δp. Smooth cryopipes separated by short bellows inserts should be used instead. A small increase in diameter of the cryopipe also produces a large decrease in the pressure drop. The experimental results obtained at the new 200 m facility at the Chubu University confirm our approaches to the design of the long SC PT lines.

PACS: 84.71.-b 88.80.H-

Keywords: power transmission; high-temperature superconducting cables; cooling system; pressure drop

1. Introduction

The development of modern society objectively leads to an increase in energy consumption, but the amount of the fossil fuels in the Earth are limited, therefore it raises the vexed question how to reduce the

1875-3892
doi:10.1016/j.phpro.2012.06.307

energy losses and change over to renewable sources. Optimization of the energy distribution is also important to reduce the impact of natural and technological disasters. According to most researchers, the energy transfer systems based on superconductors meet these requirements. Great efforts were made to develop SC PT lines have led to the construction of a significant number of hundred meter class experimental facilities (see Table 1). The technology is already developed sufficiently well and short distance SC PT lines can be used in the industry at present. Notwithstanding the significant design feature differences, different types of HTS cables used and a wide range of operating voltages and currents, all operating projects are characterized by the use of flexible corrugated cryopipes and transfer AC current. Several research groups are already working on the construction of SC PT lines of a few kilometers class. The most interesting among the others is the project of the development of a 6 km 250 MVA HTS cable for installation in the Alliander's HV grid in Amsterdam [1]. A number of issues which were underrated in the past assume great importance now. The necessity of overcoming significant hydraulic friction in the long cryopipe is one of the problems. Because of the hydraulic friction losses are relatively small in the existing short distance lines and power of the pumps used are much more than sufficient, the pressure losses were usually neglected. Corresponding data had been published in summary form without analysis. Papers considering the pressure loss in the cryopipes began to appear in recent years, but they do not contain specific recommendations and suggestions for its reduction [2, 3]. From an economic point of view, the maximum distance between the intermediate pumping stations should be achieved in order to significantly reduce cost of equipment and maintenance expenses. In some cases, such as the laying of submarine cables (for example, North Africa - Europe, Russia - Japan), the distance between the intermediate stations are strictly determined by the location of islands and shallows, and can reach tens of kilometers.

Table 1. Representative HTS cable projects.

Project title	Length, m	Power, MVA	Phases	AC loss, W/m/phase	Heat leak, W/m	ΔT, K	Δp, bar (Pa, Pa/m)	Refs.
Albany	320+30	48	3-in-1	0.7 at 0.8 kA	2.9	1.5 (work. mode)	0.7 bar at 50 L/min	[4]
KEPCO	100	50	3-in-1	2.27 at 1.25 kA	2.2	0.73 at 40 L/min		[5, 6]
LIPA	600	574	3	4.28/3 at 2.4 kA	1.3x3		1.37 bar at 0.375 kg/s	[7]
Super-ACE	500	77	1	1.34 at 1 kA	1.21		100/380 Pa/m at 50 L/min (out./in. channel)	[8]

The heat capacity of LN_2 is high enough and under the existing thermal insulation and conventional circulation rate the temperature difference between the outlet and the inlet of the cryopipe does not exceed 1-2 K (Table 1). If necessary, ΔT can be easily increased by reducing the mass flow rate and consequently pressure drop will significantly reduce.

The situation is essentially different in the case of long SC PT lines. On the one hand, the total heat inflow is so high that ΔT should be as large as possible in order to keep the circulation rate low. On the other hand, the working range of LN_2 is limited below by the freezing point and above by the boiling point been only 77.4 K - 63.2 K = 14.2 K at 1 atm. Although it can be expanded by increasing the pressure in the system (comprising, for example, 20.6 K at 2 atm.), but the lower temperature limit (the freezing temperature) remains almost unchanged. Consequently, the expansion of the working range leads to an increase in temperature at the outlet and hence to reduce the critical current. Therefore, there is a

strong physical constraint on ΔT in this case, which can be not taken into account for the short lines. For definiteness, ΔT_{max} can be prescribed to be 10 K.

Nomenclature

A	cross sectional area, m^2	q	specific heat load, W/m
C_p	specific heat, J/kg K	q_f	specific frictional heating, W/m
D	diameter, m	Re	Reynolds number, dimensionless
D_h	hydraulic diameter, m	ΔT	temperature difference, K
f	friction factor, dimensionless	ΔT_{max}	maximum permissible ΔT, K
L	cryopipe length, m	ε	mean height roughness, m
$\dot{m}$	mass flow, kg/s	μ	dynamic viscosity, Pa s
n	index of power, dimensionless	v	flow velocity, m/s
Δp	pressure drop, Pa	ρ	density, kg/m^3

It is considered the pressure drop is proportional to the length of the pipeline. However, it is true only if the mass flow rate is constant. However as we have seen, maintaining a constant mass flow ΔT can be increased only to a certain limit. Let's estimate the effect of restriction of ΔT on the relationship between the length and the pressure drop. If we neglect the concentrated heat loads at the terminals, the mass flow of LN_2 required to remove the incoming heat and the heat released due to the friction is

$$\dot{m} = \frac{L\left(q + q_f\right)}{C_p \Delta T} \tag{1}$$

The mass flow is related with the flow velocity by following expression

$$\dot{m} = \rho v A \tag{2}$$

The pressure drop can be calculated using Darcy-Weisbach formula

$$\Delta p = f \frac{L}{D_h} \frac{\rho v^2}{2} \tag{3}$$

If we ignore the frictional heat generation q_f which is usually much smaller than q, then a new expression for the pressure drop can be immediately obtained from Eqs. (1-3)

$$\Delta p = f \frac{L^3}{2 D_h \rho} \left(\frac{q}{C_p \Delta T A} \right)^2 \tag{4}$$

The behavior of the friction coefficient f for the fluid flows in circular pipe is well-studied experimentally. For the turbulent flow regime (Re>4000) which is always realized in actual HTS cable cooling channels, f weakly depends on the flow velocity and in the extreme case of hydraulically smooth pipes is described by a semi-empirical Blasius formula, being dependent only on Re

$$f = 0.3164\,\mathrm{Re}^{-0.25} \tag{5}$$

where the Reynolds number Re is proportional to the flow velocity

$$\mathrm{Re} = \frac{\rho v D_h}{\mu} \tag{6}$$

This dependence weakens and the contribution of the relative roughness, ε/D_h, appears while Re increases. It can be approximated by the implicit Colebrook-White correlation

$$\frac{1}{\sqrt{f}} = -2\log_{10}\left(\frac{\varepsilon}{3.7D_h} + \frac{2.51}{\mathrm{Re}\sqrt{f}}\right) \tag{7}$$

At the high flow velocity f is independent of the Reynolds number and the other extreme case namely quadratic law of resistance is realized. Consequently, taking into account the important fact that ΔT=const, from Eqs. (4-7) it follows immediately that

$$\Delta p \propto L^{n+1} q^n, \quad n = 1.75...2 \tag{8}$$

Reduction of Δp to the lowest practicable level is critical to construct the long SC PT line of high efficiency. As already stated, this requirement is contrary to common practice since the entire existing test SC PT lines are constructed using flexible corrugated cryopipes which exhibit very high hydraulic resistance. Corrugated cryopipes are reasonably used to simplify cable laying process, but this approach has a number of shortcomings in other cases. On the basis of these considerations, smooth cryopipes were used in the experimental facility at the Chubu University.

Eq. 8 well illustrates one important advantage of DC over AC, namely that at the same conditions only due to the lack of AC loss the cryopipe segment between the cooling substations may be much longer. A merit can be easily estimated by

$$\frac{L_{DC}}{L_{AC}} = \left(\frac{q + q_{AC\,loss}}{q}\right)^{\frac{n}{n+1}} \tag{9}$$

2. Experimental

The experimental facility at the Chubu University is a 200-meter DC HTS cable system built in 2009-2010. DC SC PT has many advantages with respect to AC one [9] which determined the theme of our research: design and development of SC PT line having record length of the cable and the highest economic efficiency of the system. It should be noted that DC transmission attracts more and more

attention and several facilities are under developing now, but 20 m and 200 m experimental lines at the Chubu University are still unique up to the present moment. The last one is equipped with several important improvements fundamentally distinguish it from all others. As mentioned above, the smooth cryopipe is used instead of the conventional corrugated one to reduce pressure loss. A so called Peltier current leads are used to decrease heat leak at the terminals; the terminals are made movable to compensate for the shrinkage during cooldown; outer pipe of the double-pipe vacuum thermal insulation is made of large diameter in order to improve the condition of evacuation of air from the system [10, 11]. The cable route has a height difference of 2.6 m for the purpose of exploration of a natural circulation of LN_2. An automated measurement system allows to interrogate more than 500 sensors with a period of 3 s.

A series of experiments to determine the dependence of the pressure drop on the mass flow was carried out to check the effectiveness of the proposed design. LN_2 flows through a fairly narrow space between the rough surface of the cable sheath of the diameter of 35 mm and the inner smooth surface of the cryopipe with the diameter of 57.2 mm. The circulation pump capacity is up to 30 L/min and head pressure is up to 0.16 MPa. During experiments the mass flow was in the range of 4-17 L/min that corresponds to the flow rate of 0.04-0.18 m/s and Reynolds numbers of 4500-19200. Averaged over 10 min data are shown in Fig. 1. The design curve is also given.

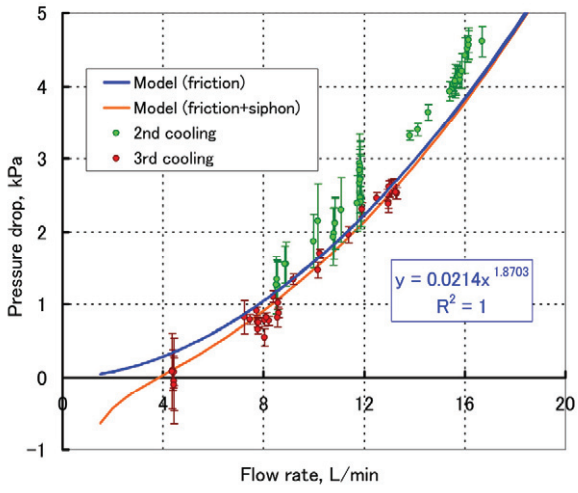

Fig. 1. (left) Experimental pressure drop as a function of LN_2 flow rate. Blue curve shows estimated behavior of Δp. Orange one is the same design curve corrected for the thermal siphon effect which obviously manifests itself at high ΔT (low flow rates).

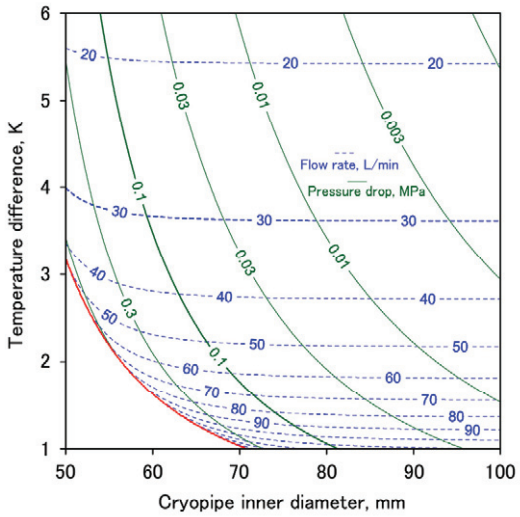

Fig. 2. (right) Dependence of the pressure drop and LN_2 flow rate on the inner diameter of the cryopipe and temperature difference for future 2 km experimental facility. Geometric parameters of the cables and the cryopipe are the same as those of 200 m facility.

The friction factor was calculated by Eqs. 5, 7 as a weighted sum of contributions of the smooth cryopipe wall and the rough cable sheath proportional to their wetted perimeters.

$$f = \frac{f_1 D_1 + f_2 D_2}{D_1 + D_2} \qquad (10)$$

Despite the fact that Eqs. 5, 7 were developed for circular pipes, we have obtained a good agreement between calculated and measured values in the case of channel of complex cross section. Therefore we arrive at the important conclusion that our physical model can be used to estimate with sufficient accuracy the pressure losses in smooth cryopipes.

After successful tests, it was decided to begin to realize a new project, namely 2 km DC SC PT line. Fig. 2 shows a behavior of two parameters, the pressure drop and LN_2 flow rate, as a function of the fixed temperature difference and the cryopipe inner diameter. This graph is convenient to select an appropriate pump. It can be seen that it is enough to expand temperature range to 5 K to be possible to extend cable up to 2 km using the same pump to circulate LN_2 through the cryopipe of the same diameter as in 200 m facility.

3. Conclusions

The importance of minimizing the pressure loss in the cooling channels of the SC PT line was examined from the hydrodynamics point of view. The advantage of application of the smooth cryogenic pipes instead of commonly used corrugated pipes was shown. The experimental data allowed to choose a physical model which provides a good accuracy of the calculated overall hydraulic friction coefficient of the channel of complex cross-section. The dependences obtained were used in the design of a new 2 km SC PT line is planned to be constructed in the Chubu University in 2013-2014. Recommendations were made to reduce the pressure drop, which may allow an increase in the cable length of several tens of percent without increasing the cost of the refrigerant circulation.

Acknowledgements

The authors thank Dr. Atsuo Iiyoshi, the Chairman of the Board of Trustees and the Chancellor of Chubu University, for his encouragement during the course of this work. The authors acknowledge financial support from Dr. Hiroshi Fujiwara, a professor of Keio University and the president of Nano-Opt Energy Corporation.

References

[1] Melnik I, Geschiere A, Willén D, Lentge H. *J Phys Conf Ser* 2010;**234**:032037.

[2] Koh D, Yeom H, Hong Y, Lee K. *IEEE Trans Appl Supercond* 2004;**14**:1746-9.

[3] Zajaczkowski B, Giesbers AJM, Holtrust M, Haenen E, den Heijer R. *Cryogenics* 2011;**51**:180-6.

[4] Weber CS, Lee R, Ringo S, Masuda T, Yumura H, Moscovic J. *IEEE Trans Appl Supercond* 2007;**17**:2038-42.

[5] Sohn SH, Hwang SD, Lim JH, Yim SW, Hyun OB, Kim HR et al. *Physica C* 2007;**463-465**:1146-9.

[6] Watanabe M, Masuda T, Yumura H, Takigawa H, Ashibe Y, Ito H et al. *Physica C* 2007;**463-465**:1132-8.

[7] Maguire JF, Yuan J. *Physica C* 2009;**469**:874-80.

[8] Mukoyama S, Yagi M, Ichikawa M, Torii S, Takahashi T, Suzuki H et al. *IEEE Trans Appl Supercond* 2007;**17**:1680-3.

[9] Hirose M, Masuda T, Sato K, Hata R. *SEI Tech Rev* 2006;**61**:29-35.

[10] Yamaguchi S, Hamabe M, Yamamoto I, Famakinwa T, Sasaki A, Iiyoshi A et al. *J Phys Conf Ser* 2008;**97**:012290.

[11] Yamaguchi S, Kawahara T, Hamabe M, Watanabe H, Ivanov Yu, Sun J et al. *Proc 23 Int Cryog Eng Conf Int Cryog Mater Conf 2010* 2011;1041-7.

Available online at www.sciencedirect.com

SciVerse ScienceDirect

Physics Procedia 36 (2012) 1366 – 1371

Physics Procedia

Superconductivity Centennial Conference

Heat leak measurement of the 200 m superconducting DC power transmission system at Chubu University

Hirofumi Watanabe, Yury Ivanov, Jian Sun, Makoto Hamabe, Toshio Kawahara, Satarou Yamaguchi

Center of Applied Superconductivity and Sustainable Energy Research, Chubu University, Kasugai, Aichi, 487-8501, Japan

Abstract

The third cooling test of the 200 m superconducting DC power transmission system at Chubu University (CASER2) has been conducted from January to March 2011. During this term, the cooling of the system and the test of the liquid nitrogen circulation were performed. The temperature variation of the liquid nitrogen along the cryogenic pipe was measured and the heat leak from the surroundings at room temperature to the liquid nitrogen was estimated. The heat leak was about 275 W for 175 m of the cryogenic pipe, which was 55 % of the value obtained during the first cooling test. Further improvement will be continued to reduce the heat leak of CASER2.

Keywords: Large scale application;Superconducting direct current transmission;Cryogenics

1. Introduction

The construction of a test facility of a 200 m superconducting DC power transmission system at Chubu University, which was named CASER2, was completed in 2010 [1], based on the results obtained with the former 20 m system constructed in 2006 [2, 3]. Cooling tests have been performed three times by the spring of 2011 with CASER2. Several kinds of tests including the liquid nitrogen circulation, the current feeding, the thermal insulation and the evacuation to make the vacuum insulation have been performed in these cooling tests [1, 4, 5, 6].

The superconducting cable is cooled by the flow of the liquid nitrogen. In the case of the superconducting DC power transmission, the heat leak from the surroundings is nearly only the origin of the temperature rise of the liquid nitrogen. The reduction of the heat leak is particularly important to rise the efficiency of the superconducting power transmission systems, because to remove the heat from the liquid nitrogen the electrical power is required for the cryocoolers, which, in turn, becomes the loss of the superconducting power transmission systems. In Chubu University every effort has been taken to reduce the heat leak. To reduce the heat leak the new cryogenic pipe [7] and the Peltier current lead [8] have been introduced.

In the third cooling test, the test of the liquid nitrogen circulation was performed. Before the third cooling test several revisions of the cryogenic system of CASER2 have been done to reduce the heat leak of the system and to obtain the stable circulation of the liquid nitrogen [4]. By measuring the liquid nitrogen temperature along the cryogenic pipe for the cable, the flow rate of the liquid nitrogen and the temperature of the surroundings the effect of the revisions was evaluated. From the evaluation, the guide to reduce the

1875-3892
doi:10.1016/j.phpro.2012.06.306

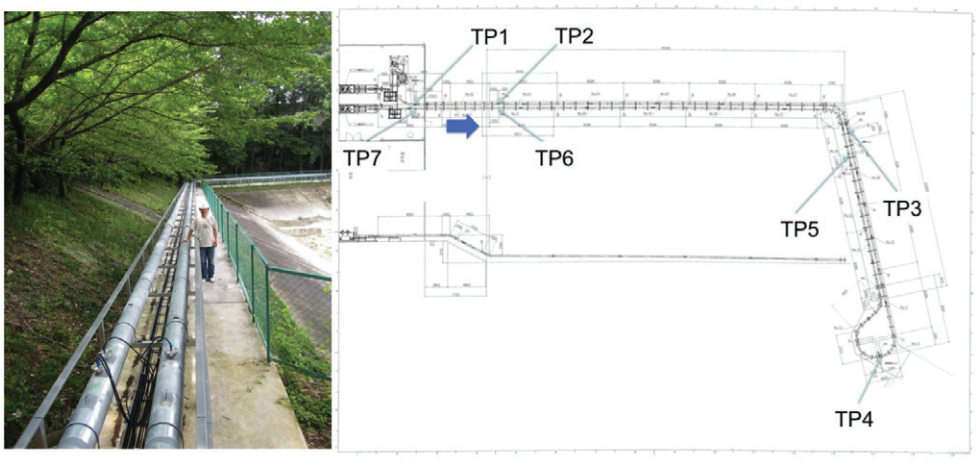

Fig. 1. The drawing of the cryogenic pipe of CASER2. The positions of the platinum resistance thermometers are indicated by TP1 to TP7. The picture on the left is taken from the blue arrow shown in the drawing.

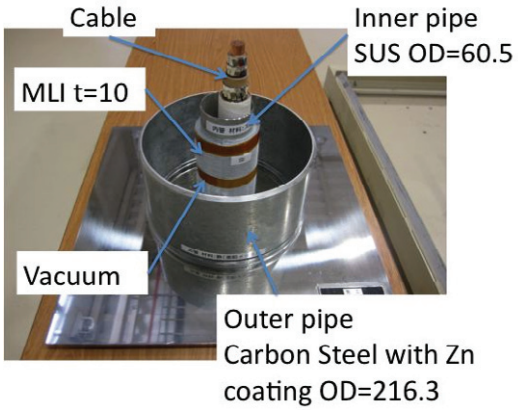

Fig. 2. The cross sectional model of the cryogenic pipe.

heat leak and to circulate the liquid nitrogen stably has been obtained for actual transmission systems. In this paper the present status of the cryogenic system of CASER2 is introduced.

2. The cryogenic system of CASER2

Figure 1 shows the drawing of the transmission line of CASER2. The cryogenic pipe for the cable of CASER2 is approximately 200 m and constructed as the L-shaped configuration, large part of which is placed in the outdoors. The left of Fig. 1 is a picture of a part of the cryogenic pipe, which was taken from the blue arrow in the drawing. The liquid nitrogen temperature is monitored at 7 positions along the cryogenic pipe. At each of the positions, platinum resistance thermometers are set on the upper and lower surfaces of the inner pipe of the cryogenic pipe. Therefore 14 platinum resistance thermometers are used. A cross sectional model of the cryogenic pipe is shown in Fig. 2. The inner pipe is made of stainless steel with the outer diameter of 60.5 mm. The inner pipe is wrapped by the multi-layer insulation, total thickness of which is about 10 mm. The outer pipe is made of carbon steel with the outer diameter of 216.3 mm, which is coated with zinc to reduce the emissivity of the outer pipe surface [7]. The space between the inner pipe

Fig. 3. The picture of the cryocooler and circulation system of CASER2.

and the outer pipe is evacuated below 0.05 Pa to achieve the vacuum insulation [6, 9]. The cryogenic pipe is continuously pumped at the moment. The inner pipe is supported with bars and plates at the several places along the cryogenic pipe. The supports are made of fiber reinforced plastics, the shape of which is designed so as to reduce the heat leak through the supports.

Table 1. Cryocooler and circulation system. The heat leak and COP of the system were measured between the second and the third cooling test. These value will be subject to change by further improvement of the cryocooler and circulation system.

Cryocooler	Stirling type
Cooling power	1 kW@77 K
COP	0.083@77 K
Circulation	Single pump
Volume of the tanks	200 l each
Overall heat leak	262 W
COP of the system	0.060@76.2 K

Figure 3 shows the cryocooler and circulation system. The system is composed of a cryocooler, a pump, a mass flowmeter, two tanks and cryogenic pipes connecting the elements. The summary of the system is listed in Table 1 . The cryocooler is a Stirling type, whose cooling power is 1 kW and its COP is 0.083 at 77K. The liquid nitrogen is circulated with a single pump. The flow rate of the liquid nitrogen is measured with a Coriolis mass flowmeter. There are two tanks to reserve liquid nitrogen. These tanks are placed vertically each other. The volume of them is 200 l. The heat leak of the cryocooler and circulation system has been measured separately from the cryogenic pipe for the cable by short-circuiting the outlet and the inlet of the system by a pipe with a heater. The heating powers which balanced the cooling power of the cryocooler were measured at several liquid nitrogen temperatures. The heat leak was obtained by subtracting the heating power of the heater from the cooling power of the cryocooler and estimated typically to be 262 W. During the heat leak measurement the power consumption of the cryocooler was measured. The heating power of the heater is the cooling power which can be used for the cooling of the cable. The ratio of the heating power to the power consumption of the cryocooler, which is a kind of COP of the system,

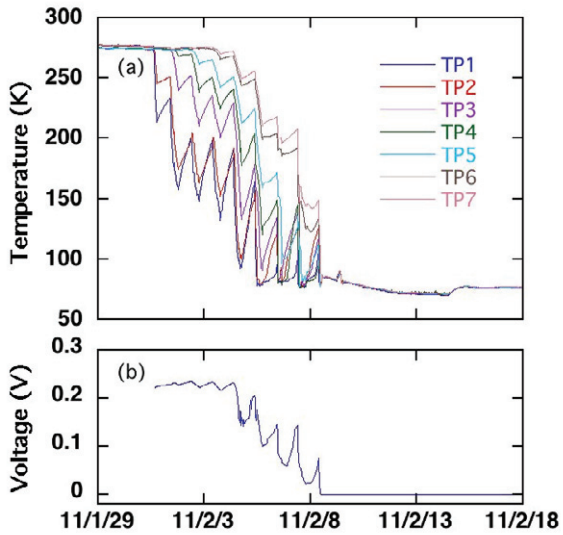

Fig. 4. The variation of the temperature along the cryogenic pipe (a) and the voltage induced between the ends of a HTS tape (b) during the cooling process of CASER2. TP1 to TP7 mean that the temperature measured at the positions of TP1 to TP7. The current of 0.1 A was applied to measure the voltage.

was obtained to be 0.060 at 76.2K. These measurements were performed between the second and the third cooling test. Because the revision of the cryocooler and circulation system is planned, these values could be changed. In our system the liquid nitrogen has been stably circulated by the cryocooler with the 1 kW cooling power and the single pump.

Figure 4(a) shows the variations of the temperatures along the cryogenic pipe measured at TP1 to TP7 in Fig. 1 after starting of the cooling. The cooling was started on January 31st. Since the liquid nitrogen was filled from the end of the TP1 side, the temperature drop was started firstly from the TP1 side and moved from TP1 to TP7 in order. Since the filling of the liquid nitrogen was performed usually only in the daytime, the temperatures dropped in the daytime and rose in the nighttime. Overall the temperatures became lower gradually. The whole system was cooled to the liquid nitrogen temperature on February 8th. In Fig. 4(b) the voltage induced along a HTS tape in the cable by the 0.1 A current is shown. This voltage was measured between both the ends of the cable. With the drop of the temperature, the voltage dropped. At the same time when the whole system was cooled down to the liquid nitrogen temperature, the voltage became zero, which meant that the cable became the superconducting state.

3. Heat leak measurement

After the inner pipe was filled with the liquid nitrogen, the circulation with the pump was started. The temperatures of the circulating liquid nitrogen along the cryogenic pipe were measured. By using the temperatures, the measured flow rate and the published specific heat capacity of the liquid nitrogen, the heat leak of the system was estimated.

Figure 5 shows the temperature difference between TP1 and TP7 with respect to the flow rate of the liquid nitrogen. The distance between TP1 and TP7 is 175 m. Though the platinum resistance thermometers have been calibrated before they set at their positions, the calibration was checked in situ with the procedure used previously [4] and the measured values were corrected. The flow rate used was from 7 to 13 l/min. In this range the temperature rose from 0.7 to 1.2 K. The lines in the figure are $y = \alpha/x$ type fitting functions. If the heat leak is constant, the temperature difference should be inversely proportional to the flow rate.

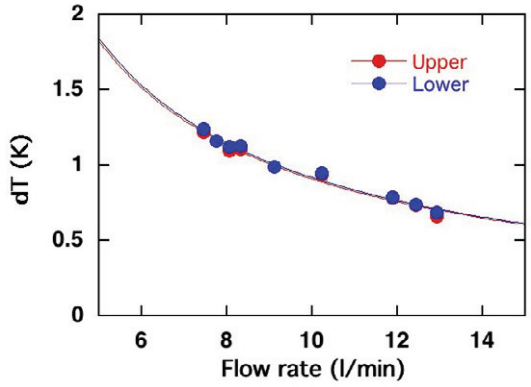

Fig. 5. The temperature difference between TP1 and TP7 measured against the flow rate of the liquid nitrogen. "Upper" means that the platinum resistance thermometers attached on the upper surface of the inner pipe were used, while "Lower" means that those on the lower surface were used.

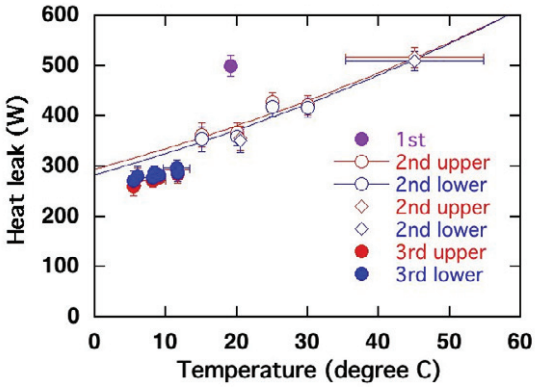

Fig. 6. The heat leak measured during the first to the third cooling test. These values are shown against the average outer pipe temperatures during the measurements. "1st", "2nd" and "3rd" mean that the data were measured during the first to the third cooling test, respectively. "upper" and "lower" mean that the platinum resistance thermometers set on the upper and lower surfaces of the inner pipe were used, respectively.

Figure 6 shows the heat leak measured during the first to third cooling tests, which are arranged against the average outer pipe temperatures. These data are based on the temperature difference between TP1 and TP7 for 175 m of the cryogenic pipe. The half of the outer pipe surface of the cryogenic pipe is exposed by the sun in the daytime, while the other half is in a shade of trees. The temperature of the former gives the maximum of the outer pipe temperature and that of the latter the minimum. The temperatures were measured at each one point in the former and the latter as representatives of the temperature along the outer pipe surface. The average outer pipe temperature is the average and the error bar of the temperature is the range of these values. The curves in the figure are $y = \alpha((x + 273)^4 - 77.3^4) + \beta((x + 273) - 77.3)$ type fitting functions. These functions were fitted to some of the data measured during the second cooling test indicated by the open circles. The other data measured during the second cooling test and indicated by the open diamond are well on the curves.

The first cooling test has been performed from January to March 2010 and the second cooling test from August to October 2010. In the first cooling test, the heat leak of about 500 W has been measured, which was significantly larger than our expectation. Between the first and the second cooling test, the vacuum system to make the vacuum insulation was improved. This improvement led to the reduced heat leak in the

second cooling test [4]. In the second cooling test, the data has been obtained rather in the wider range of the outer pipe temperature. It should be noted that by decreasing the outer pipe temperature form 45 to 15 degree centigrade the heat leak was reduced by 200 W, which is significantly large. The reduction of the outer pipe temperature is a way to reduce the heat leak.

Between the second and the third cooling test, the supports of the inner pipe and the use of the multi-layer insulation have been reexamined. A conservative design was taken for the supports, since it was considered that the supports suffered the strong force by the thermal shrinkage of the cable and the inner pipe in addition to the weight of them, which was difficult to estimate. However, the heat leak through the supports can not be ignored according to our calculations. After checking the mechanical strength of the supports, some of them were removed. The whole cryogenic pipe was constructed by connecting cryogenic pipes with approximately 8 m long. The joints of the inner pipe have not been wrapped with the multi-layer insulation properly for the construction reason. This was also revised between the second and the third cooling test. By these efforts the heat leak during the third cooling test was reduced to about 275 W on average. This value is 55 % of the value obtained during the first cooling test.

From the first to the third cooling test, the heat leak of the cryogenic pipe has been largely reduced. We are continuing revision of our system to get a further reduction of the heat leak, since the heat leak of the cryogenic pipe determines the efficiency of the system. It should be noted that the heat leak of the cryocooler and circulation system is 262 W, which is nearly the same as the value of the heat leak between TP1 and TP7. It is obvious that the reduction of the heat leak in the cryocooler and circulation system is needed. We are also continuing the revision of the thermal insulation of this part. The result will be presented near future.

4. Summary

The measured heat leak of the cryogenic pipe of CASER2 during the third cooling test was about 275 W for 175 m of the cryogenic pipe, which was 55 % of the value obtained during the first cooling test. This improvement has been achieved by reexamining the supports and the multi-layer insulation for the inner pipe of the cryogenic pipe in addition the improvement of the vacuum system done before the second cooling test. Further improvement is being continued to reduce the heat leak of CASER2.

Acknowledgements

The authors thank Dr. Atsuo Iiyoshi, the Chairman of the Board of Trustees and the Chancellor of Chubu University, for his continuous encouragement through this work. The authors acknowledge Dr. Hiroshi Fujiwara, a professor of Keio University and the president of Nano-Opt Energy Corporation, for his financial support for this work. We also thank JFE Steel Corporation for supplying steel pipes for the construction of the test facilities.

References

[1] Yamaguchi S, Kawahara T, Hamabe M, Watanabe H, Ivanov Y, Sun J, Iiyoshi A, *Physica C* 471 (2011) 1300.
[2] Yamaguchi S, Hamabe M, Yamamoto I, Famakinwa T, Sasaki A, Iiyoshi A, Schultz J, Minervini J, Hoshino T, Ishiguro Y, Kawamura K, *J. Phys.: Conf. Ser.* 97 (2008) 012290.
[3] Hamabe M, Fujii T, Yamamoto I, Sasaki A, Nasu Y, Yamaguchi S, Ninomiya A, Hoshino T, Ishiguro Y, Kawamura K, *IEEE trans. Appl. Supercond.* 19 (2009) 1778.
[4] Watanabe H, Sugino M, Sun J, Ivanov Y, Hamabe M, Kawahara T, Yamaguchi S, *Physica C* 471 (2011) 1304.
[5] Ivanov YV, Watanabe H, Hamabe M, Sun J, Kawahara T, Yamaguchi S, *Physica C* 471 (2011) 1308.
[6] Watanabe H, Hamabe M, Kawahara T, Yamaguchi S, *Proc. ICEC23/ICMC2010* (2011) 649.
[7] Nasu Y, Hamabe M, Yamaguchi S, Kusaka S, Ishiguro Y, *Proc. ICEC22/ICMC2008* (2008) 489.
[8] Yamaguchi S, Yamaguchi T, Nakamura K, Hasegawa Y, Okumura H, Sato K, *Rev. Sci. Instrum.* 75 (2004) 207.
[9] Hofmann A, *Cryogenics* 46 (2006) 815.

Available online at www.sciencedirect.com

SciVerse ScienceDirect

Physics Procedia 36 (2012) 1131 – 1136

Physics Procedia

Superconductivity Centennial Conference

Experiment of the 200-meter superconducting DC transmission power cable in Chubu University

Satarou Yamaguchi[a,b,*] , Yury Ivanov[a], Jian Sun[a], Hirofumi Watanabe[a], Makoto Hamabe[a],Toshio Kawahara[a,b], Atsuo Iiyoshi[a], Makoto Sugino[b], Hideki Yamada[b]

[a]*Center of Applied Superconductivity and Sustainable Energy Research (CASER), Chubu University, 1200 Matsumoto, Kasugai, Aichi 487-8501 Japan*

[b]*Department of Electric Engineering, Chubu University, 1200 Matsumoto, Kasugai, Aichi 487-8501 Japan*

Abstract

After we constructed the 200-meter superconducting DC power cable in spring of 2010, three experiments have been done until March, 2011. We changed and improved the experimental devices, especially to reduce the heat leak. We describe the experimental results and the data analysis for the pressure drop of liquid nitrogen circulation. We summarized the experimental results briefly, and estimate the pressure drop of the circulation for a longer cable system (~2km) depending on the experimental conditions. We also mentioned the performance of the system as compared with the copper cable.

Keywords: DC power cable; superconducting system; scale law of coolant circulation; performance comparison

1. Introduction

We started the DC superconducting power transmission experiment from the beginning of 2000 in Chubu University (CU), and the major subject was to develop a low heat leak terminal at that time. We developed the Peltier current lead [1, 2, 3]. We completed the first experimental device (CASER-1) in 2006. This is a 20-meter DC cable test facility, and the material of the HTS is Bi-2223. Several ideas were tested, the reduction of the heat leaks at the terminal, the cryogenic pipe, the pressure drop of the circulation and so on [4, 5, 6, 7]. The system was cooled down and warmed up six times until 2011, and no degradation of the DC cable was appeared in the system. We started to design and construct the 200-

* Corresponding author.
E-mail address: yamax@isc.chubu.ac.jp

1875-3892
doi:10.1016/j.phpro.2012.06.189

meter cable experiment from 2008, and it is called CASER-2. The construction was started in the 2009, and completed in January 2010, and we performed the experiment four times until now. The major subjects of the experiments are as below,

1) Safety cable system for thermal contraction and expansion,
2) Low heat leak at the terminal and the cryogenic pipe (achieve high vacuum degree without baking),
3) Low pressure drop of the coolant circulation,
4) Energy storage function using ferromagnetic materials,
5) No limitation of natural resources such as nickel and low cost of the system,
6) Data obtainment for scale law of longer cable system.

Our goal is to complete a longer cable until 20 km, therefore we focus to study the scale law of the longer cable system. We also mention the comparison between CV cable is described in the paper.

2. System Parameters of the Experiment

The parameters of the experimental device are summarized in Table 1. We performed three experiments until now (September 2011). We improved and change the system to achieve high performance continuously, such as vacuum system, the coolant circulation system, measurement system and the technique of the operation.

We cannot use the baking for the cryogenic pipe, but we need high vacuum pressure of 10^{-4} Pa to achieve high thermal insulation. The pumping time is also an important issue for the long cable system, therefore the vacuum technique is one of the first priority. We pay attention about the strain of the HTS tapes of the cable because of avoiding the reduction of the critical current of the HTS tape [8, 9, 10]. The thermal contraction of the cable is estimated to be 60 cm for the 200-meter cable. In order to reduce the strain of the cable, we adopt the movable cryostats [11]. TV camera is set to monitor the cable end. The operation temperature was varied by from 72K to 82K, depending on the experimental conditions.

The PCL is used to reduce the heat leak from the terminal. The reduction of the heat leak is crucial for a short distance application. In order to reduce the pressure drop of the coolant circulation, we mainly use the straight pipe for the cryogenic pipe. It is also effective to reduce the cost and heat leak, too.

Table 1. The Parameters of the 200-meter cable test facility

	Parameters	Comments
Cable	±10kV, 2kA@78K, Bi-2223 HTS tape, crticial current ~ 160 A, lenght ~200 meter	Bipolar co-axial cable, 23 tapes for inner (2 layers) and 16 HTS tapes for outer. Movable cryostats for reduction of the thermal stress of the HTS tape.
Cryogenic pipe	Diameters of outer pipe and the inner pipe are 204 mm and 60 mm, respectively	Bellows pipe inserted into inner straight pipe for compensation of the thermal contraction. Iron pipe for outer pipe and SS pipe for inner pipe.
Refrigerator	1kW@77K	Stirling cycle refrigerator (power consumption ~15kW), Operation temperature ~ 72K to 82K
Pump system	Flow rate ~ 10 L/min, Pressure drop ~ 1.5kPa	Upper and lower tanks are equipped to control low pressure and flow rate.

3. Scale Law of Coolant Circulation

Figure 1 shows the experimental data of the flow rate and the temperature rise between the inlet and the outlet temperatures of the liquid nitrogen. The design value of the flow rate is ~10 L/min, and the

heat load of the cryogenic pipe is less than 2 W/m. We can change the flow rate completely by the pump and the valve controls. We also may control the heat leak of the cryogenic pipe by the vacuum pressure and the heater attached inside the cryogenic pipe. When the vacuum pressure is low, the heat leak is low. Since the temperature rise varied inversely with the flow rate, the inverse functions are plotted by the least-square fitting method in Fig. 1.

We improved the thermal insulation of the cryogenic pipe after completion of the facility. The experiments were done in summer and winter, and we can conclude that the heat leaks depend on the air temperatures since the cryogenic pipe is located outside of the laboratory.

Figure 2 shows the experimental data of the flow rate and the pressure drop. The experimental data are plotted with the error bars, and a fitting curve and the design curve are shown. Error bars are calculated by the time average of 10 min. The design curve is based on the calculation of a semi-empirical formula

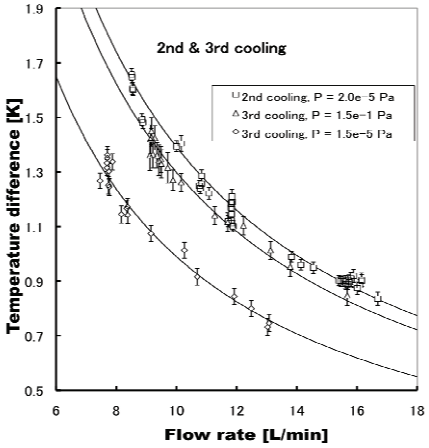

Fig. 1. The experimental data of the flow rates and temperature differences of liquid nitrogen in the second and third experiments.

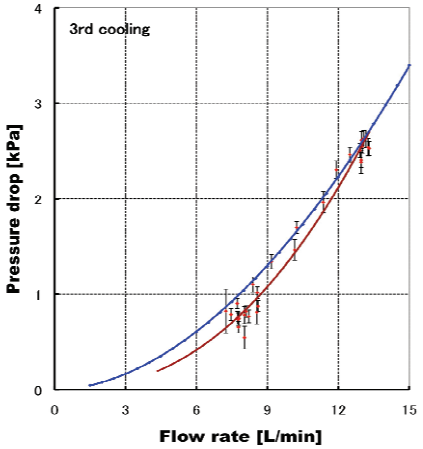

Fig. 2. The experimental data of the flow rate and temperature difference between inlet and outlet temperatures of liquid nitrogen.

of fluid dynamics. Since the elevation along the pipeline is about 3 meter, we should consider the siphon effect of the circulation [12, 13]. This effect is positive for the reduction of the circulation power. Therefore, the design calculation values are higher than the experimental data, which is apparently at low rate. The fitting curve is shown in the figure, and the power factor of the curve is about 2.34. On the other hand, the power factor of the model calculation is 1.87 if the siphon effect is not included.

The semi-empirical formula of fluid dynamics is important to estimate the pressure drop for a longer system, and we try to establish a scale law of the circulation. The pressure drop ΔP is proportional to the length, the friction factor and the square of the flow rate, and given by

$$\Delta P \propto (FrictionFactor) \times (FlowRate)^{2.0} \times (Length) \tag{1}$$

and finally we obtain the pressure drop for the fixed temperature difference as

$$\Delta P = L^{\alpha+1},\ \alpha = 1.75\sim2.0 \tag{2}$$

where L is the length of the pipeline, and the power factor α depends on the surface conditions of the pipe and the cable, and the Reynolds number [14]. Therefore, all the coefficient of the scale law should be fixed by the experiment .

The pressure drop depends on the heat leak, and it is given by

$$\Delta P = q^{\alpha} \tag{3}$$

where q is heat leak for unit length along the pipeline.

The experimental data of the pressure drop and the heat leak is shown in Figure 3. The heat leaks of the cryogenic pipe were changed by the vacuum pressure of the cryogenic pipe and the heaters on the cryogenic pipe. The fitting curve is also shown in Fig. 3, and the power factor of the curve is ~1.8. The result of the fitting is almost consistent with Eq. (3).

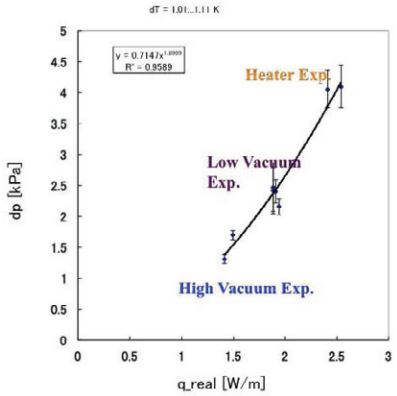

Fig. 3. The experimental data of the flow rate and the pressure drop, and the fitting curve.

Table 2. Estimation of the pressure drops of the circulation for the 2 km cable system.

Distance	0.2 km	2.0 km	2.0 km
Temperature Rise	1.5 K	1.5 K	6 K
Flow Rate	10 L/min	100 L/min	25 L/min
Pressure Drop	1.5 kPa	~ 1.5 MPa	93.8 kPa

Table 2 shows the results of the scale law for 2 km cable system from the experimental data for $\alpha = 2$. Since the output pressure of the present liquid nitrogen (LN2) pump is around 0.1 MPa, we must develop a new pump for the case of the temperature rise of 1.5K and 2 km system. But if we allow the temperature rise of 6K, the pressure drop is 93.8 kPa, and the flow rate is 25 L/min. These parameters can be realized by the present LN2 pump. If the heat leak is half, the flow rate can be half and the pressure drop is 23.4 kPa.

4. Present Performance and Radiation Shield for Heat Leak Reduction

The present heat leak of the cryogenic pipe is 1 W/m to 1.5 W/m depending on the experimental conditions. If the COP of the refrigerator is 0.1, the loss is 10 W/m to 15 W/m for 2 kA at 78 K. On the other hand, the copper cable loss is 6.5 W/m for the cable cross-section of 325 mm^2, where the current density of 1 A/mm^2 and the resistivity of 2.0×10^{-8} Ωm. It is correspond to the temperature of the cable conductor is about 80 degree Celsius. We need 12.3 cables for the same current density, and the loss of the copper cable is 6.5x12.3 = 80 W/m. Finally, the loss ratio of the copper cable and the superconducting cable is 80/15~80/10 = 5.3~8.0 times in the present time.

If we can reduce the heat leak much more, the cost performance will be improved. One of ways to reduce the effective heat leak is to use the radiation shield [15]. A large accelerator transmission line uses the radiation shield, and it is a good way to reduce the effective heat leak. The simple structure of the cross-section is shown in Fig. 4. The heat leak to the radiation shield is calculated to be 1.5 W/m to 2.1 W/m, and it to the inner pipe is also 0.098 W/m by using the experimental data. And if the COPs of the refrigerators at 180K and 77K are 0.45 and 0.1 respectively, the power consumption is 4.2 W/m to 5.6 W/m. Finally, the loss of the copper cable is 10 to 16 times higher than that of superconducting cable.

5. Discussion and Future Perspective

The final goal of the study must overcome the copper cable, and in order to realize a long transmission line, the heat leak of the cryogenic pipe is the most important issue. If we can reduce the heat leak, we can achieve the reduction of the pressure drop and the easy operation of the system.

High vacuum degree is necessary to reduce the heat leak, but we cannot use the baking. The vacuum degree of the order of 10^{-4} Pa is enough to reach the low heat leak. Fortunately, we can achieve its vacuum degree now. We should also pay attention to keep high vacuum without the pump. And the getter material is necessary to absorb the residual gases in the cryogenic pipe.

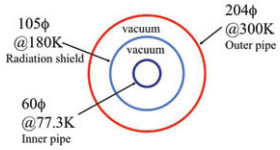

Fig. 3. Schematic structure of cryogenic pipe including the radiation shield (cross-sectional view).

From the start of the experiment in 2005, Chubu University, the cable (HTS tape) cost is dropped to be almost 1/20 until now. Therefore, I believe that we should pay attention to reduce the system cost to overcome the copper cable now.

The analysis of the fluid dynamics shows that we can construct the 2 km cable system by using the present cryogenic instruments. However, we cannot apply the present instrument for a 20 km cable system because of the pressure drop. We change the design, and use a larger diameter pipe. But the heat leak will be increased for a larger pipe, thereby increasing pressure drop. Because of these considerations, we should continue to reduce the heat leak of the cryogenic pipe and the friction factor of the pipe and cable surfaces. The 20 km cable system is our final goal to realize the global grid for us.

Another approach to realize the DC superconducting power transmission and distribution line is to apply a short cable system. We must consider to reduce the heat leak at the terminal, and we developed the Peltier Current Lead (PCL) as a low heat leak current lead. We tried various kinds of PCL‘s [16]. If the heat leak of the terminal is low, we can apply various kinds of the superconducting systems such as magnets, transformers, motors and so on.

Acknowledgements

The authors acknowledge Dr. Hiroshi Fujiwara, a professor in Keio University and the president of Nano-Opt Energy Corporation, for his financial support on the construction of 200 m superconducting facilities called CASER-2. The authors also thank to Profs. T. Matsushita and Otabe E. Soji in Kyushu Institute of Technology, and Prof. K. Osamura in Kyoto Univ. for their valuable discussions. The authors thank to Prof. B. Coppi and Drs. J. Minervini, L. Bromberg, M. Takayasu and L. Sugiyama in Massachusetts Institute of Technology (MIT) for long and kind collaboration.

References

[1] Yamaguchi S, Takita K, Motojima O. *Proc. 16th ICEC/ICMC1996*, 1996, p. 1159-1162.

[2] Okumura H, and Yamaguchi S. *IEEE Trans. Appl. Supercond*. 1997; **7**; 715-8 .

[3] Sato K, Okumura H, Yamaguchi S. *Cryogenics* 2001; **41**; 497-503.

[4] Yamaguchi S, Hamabe M, Yamamoto I, Famakinwa T, Sasaki A, Iiyoshi A, et al. *J. Phys.: Conf. Ser*. 2008; **97**; 012290.

[5] Hamabe M, Nasu Y, Ninomiya A, Ishiguro Y, Kusaka S, Yamaguchi S, *Advances in Cryo. Eng.* 2008; **53A**; 168-172.

[6] Ivanov Yu, Radovinsky A, Zhukovsky A, Sasaki A, Watanabe H, Kawahara T, et al. *Advances in Cryo. Eng.* 2010; **55**; 865-70.

[7] Hamabe M, Fujii T, Sugino M, Sasaki A, Watanabe H, Kawahara T, et al. *Journal of Physics: Conference Series* 2010; **234**; 032019.

[8] Sugano M, Shikimachi K, Hirano N, Nagaya S. *Supercond. Sci. Technol.* 2010; **23**; 085013.

[9] van der Laan DC, Ekin JW, Douglas JF, Clickner CC, Stauffer TC, Goodrich LF, *Supercond. Sci. Technol.* 2010; **23**; 072001.

[10] Ochiai S, Okuda H. *J. Cryo. Soc. Jpn*. 2011; **46**; 212-19 (in Japanese).

[11] Yamaguchi S, Kawahara T, Hamabe M, Watanabe H, Ivanov Yu, Sun J, et al. *Physica C* (in press).

[12] Ivanov Yu, Radovinsky A, Zhukovsky A, Sasaki A, Watanabe H, Kawahara T, et al. *Physica C* 2010; **470**; 1895-98.

[13] Ivanov Yu., Watanabe H, Hamabe M, Sun J, Kawahara T, Yamaguchi S, *Physica C* (in press).

[14] Yamaguchi S, Ivanov Yu, Sun J, Watanabe H, Hamabe M, Kawahara T, Iiyoshi A, accepted for publication in *Proc. Of CEC/ICMC2011*.

[15] Rubbia C. private communication.

[16] Kawahara T, Fujii T, Emoto M, Hamabe M, Sun J, Watanabe H. et al. *Physica C* 2010; **470**; S1011-12.

Available online at www.sciencedirect.com

SciVerse ScienceDirect

Physics Procedia 36 (2012) 1290 – 1295

Physics Procedia

Superconductivity Centennial Conference

Critical current distributions of BSCCO tapes in the multi-layer HTS conductors

Jian Sun[a], Shun Yamauchi[b], Hirofumi Watanabe[a], Makoto Hamabe[a], Toshio Kawahara[a], Satarou Yamaguchi[a,b]

[a]*Center of Applied Superconductivity and Sustainable Energy Research, Chubu University, Kasugai, Aichi 487-8501, Japan*
[b]*Department of Electrical Engineering, Chubu University, Kasugai, Aichi 487-8501, Japan*

Abstract

We have successfully constructed a 200 m high temperature superconducting (HTS) cable test facility for DC transmission in 2010. This coaxial power cable is composed of two superconducting (SC) conductors of DI-BSCCO tapes spirally surrounding a copper former. The tapes are arranged closely to make the magnetic field lines surrounding the cable uniformly. The number of tapes in each conductor is different because of their different radii. Previously, we have investigated the dependence of critical current (I_c) on the gap between the tapes in order to optimize the cable configuration for DC transmission.

This paper report the investigation of I_c distributions in the multi-layer conductors which consist of 2, 3 and 4 tapes with a tape-on-tape structure by setting currents in each tape separately. The I_c measurement is performed with four-probe method at 77 K. The I_cs of the tapes in the different structures are measured and compared with that of the single one. The enhancement and degradation of I_c are observed due to magnetic field interaction and magnetic shielding between the tapes in the multi-layer conductors. We will present the experimental results and show the dependence of the Ic distribution in the multi-layer conductors on the structures and transport currents in the neighboring tapes.

Keywords: HTS cable, Critical current, BSCCO, Magnetic field effect, DC transmission
PACS: 74.25.Sv, 84.71.Mn, 88.80.hr

1. Introduction

Due to the improvements of high temperature superconducting tapes (HTS) with high critical current (100 A) [1], power applications such as HTS power cables have been being studied in many countries [2, 3, 4]. Since 2006, we started to study the HTS cable for DC transmission since there is no AC loss in comparison with that for AC transmission [5]. Based on the experiments of the 20 m HTS cable, we continued to study the performance of the HTS cable for DC power transmission and successfully constructed a 200 m HTS cable test facility for DC transmission in 2010 [6]. The HTS cable is installed into a vacuum insulated cryogenic pipe and operated at about 77K by the circulation of the liquid nitrogen. A measurement system composed of 600 channels was developed to monitor the system [7].

The 200 m cable was made by Sumitomo Electric Industries, Ltd (SEI). The cable has a coaxial structure composed of two superconducting (SC) conductors for each polarity of the DC power as shown in Fig. 1.

1875-3892
doi:10.1016/j.phpro.2012.06.292

The DI-BSCCO® tapes were used as SC conductors and spirally surrounding a copper former in the center of the cable. The tapes were arranged closely to make the magnetic field lines surrounding the cable uniformly. The number of the tapes in each conductor is different because of their different radii. There are 23 tapes for the inner conductor and 16 tapes for the outer conductor, respectively.

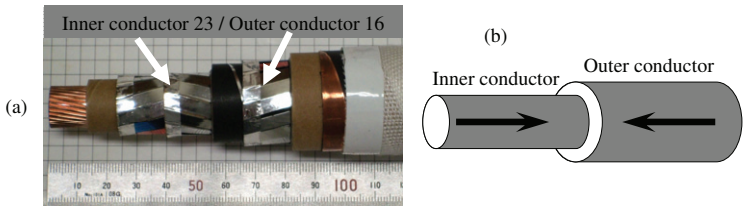

Fig. 1: A photo of a coaxial HTS cable composed of two superconducting conductors (a) and a scheme of bipolar power transmission for DC power (b).

Previously, we reported the effects of the gap on the critical current (I_c) in order to optimize the cable configuration for DC transmission [8]. In the monolayer composed of three paralleled straight tapes, the I_c of the middle tape increased with decreasing the gaps between the tapes and approached to that of a single one with increasing the gaps. The HTS tapes for applications such power cable should have high current capacity ($\sim$ 10 kA) [9]. Since the current of one HTS tape is limited, numerous tapes should be utilized and arranged in the multi-layer structure, which motivates us to study the performance of the multi-layer conductors.

The effects of the multi-layer conductors were studied by many researchers [10, 11, 12]. This paper will present the investigation of I_c distributions in the multi-layer HTS conductors which consist of 2, 3 and 4 tapes with a tape-on-tape structure by setting transport currents in each tape independently. The I_c measurement is performed with four-probe method at liquid nitrogen temperature. The I_cs of the tapes in the different structures are measured and compared with that of the single one. The enhancement and degradation of I_c are observed. We will present the experimental results and show the dependence of the I_c distribution in the multi-layer conductors on the structures and transport currents in the neighboring tapes.

2. Experiments

The DI-BSCCO® tapes (Type HT-CA) are used in the experiment [13, 14]. Table 1 shows the specifications of the BSCCO tape. The cross section of the BSCCO tape is 4.5 mm $\times$ 0.35 mm. The thickness of the BSCCO tape includes the thickness of the reinforcing copper laminated layer, which is 0.05 mm on both sides of the silver-sheathed multi-filamentary Bi-2223 matrix area to improve the mechanical strength of the tape [14]. The I_cs of BSCCO tape is 160 A in the self field at 77 K. The tapes were prepared by the powder in tube (PIT) with the controlled over pressure sintering technique by SEI [13].

DI-BSCCO tape	
Width	4.5 mm
Thickness	0.35 mm
I_c (77 K, s. f.)	160 A
Type	HT-CA

Table 1: Specifications of the BSCCO tape.

The measurement of I_c is similar with that of the previous report [8]. The samples with the length of $\sim$ 27 cm are used in consideration as an infinitely long wire. Three voltage taps are attached on the tapes with the distance of 8 and 10 cm. The tapes in the multi-layer tape conductors are insulated with each other by surrounding each tape with one Kapton tape layer. Fig 2 shows the arrangements of the multi-layer conductors composed of 2, 3 and 4 tapes with a tape-on-tape structure and a photo of the setup for a

3-layer tape conductor. Two power supplies with the rated currents of 1200 A and 300 A are used to set the transport current in the tapes separately. As shown in Figs. 2 (a)-(h), the currents are fed into the multi-layer conductors with the different current configurations. The transport current is measured by a current shunt resistor. The voltage signals are measured by a KEITHLEY 2700 multimeter. The *I* - *V* curves are measured by the standard four-probe method at the temperature of 77 K by immersing the samples into the liquid nitrogen in the air. In the 2-layer conductor, the target sample is one of them. The target samples are the middle tape and the middle two tapes for the 3-layer and 4-layer tape conductors, respectively.

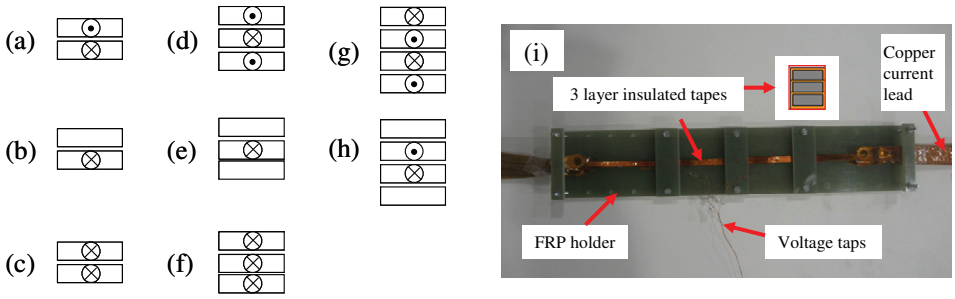

Fig. 2: (a) - (h) The configuration of the current feeding mode for 2-layer, 3-layer and 4-layer conductors. (i) a photo of the experimental setup for the 3-layer conductor.

3. Results and discussion

The *E* - *I* characteristic curves of the BSCCO tape are obtained by normalizing the voltages to the distance between the voltage taps. Figs.3 (a) - (c) show the comparisons of the *E-I* characteristic curves of the BSCCO tape for single and multi-layer tape conductors with the different current feeding mode. The significant difference of the *E-I* characteristic curves is shown between the multi-layer tape conductors and the single one. Comparing with the single tape, the I_c of the BSCCO tape is enhanced even if no current applied to the neighboring tapes in the multi-layer tape conductors, which results from the magnetic shielding effects of the neighboring tapes [10, 12].

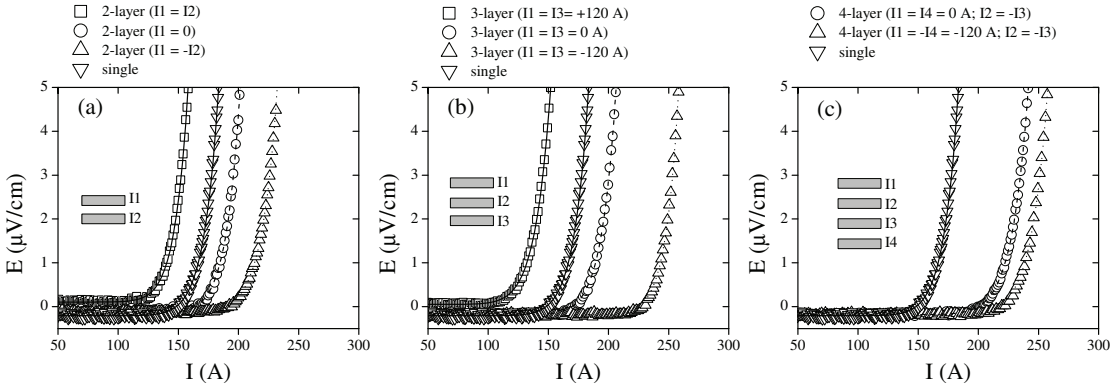

Fig. 3: The *E-I* characteristic curves of the BSCCO tape for single and 2-layer (a), 3-layer (b) and 4-layer (c) tape conductors with the different currents feeding mode.

Figs. 4(a)-(c) summarize the I_c of the BSCCO tape in the multi-layer tape conductors with respect to the applied current to the neighboring tapes. The measured I_c is determined with the electric field criterion of 1 μV/cm. The I_c of single BSCCO tape is measured to be 164 A (sample A), 161 A (sample B), 164 A

(sample D) and 161 A (sample E), respectively, which are a little larger than that in the specifications. In the case of 2-layer and 3-layer tape conductors, the I_cs decrease with increase of the current in the neighboring tapes. When there is no current applied to the other tapes, the I_cs of sample A and B become 183 A and 177 A, respectively. It is obvious that the current with the same direction fed into the tapes for the 2-layer and 3-layer conductors leads to decrease of the I_c. However, the anti-direction current feeding between each tape enhance the I_c of the tape in the 2-layer conductor and the middle tape in the 3-layer conductor. Hence, in the case of the 4-layer conductor, the currents with anti-direction between the neighboring tapes are transported through the 4-layer conductor as shown in Fig. 2(g) and (h). The I_c of second and third tape in the 4-layer conductor become larger than 210 A as shown in Fig. 4(c).

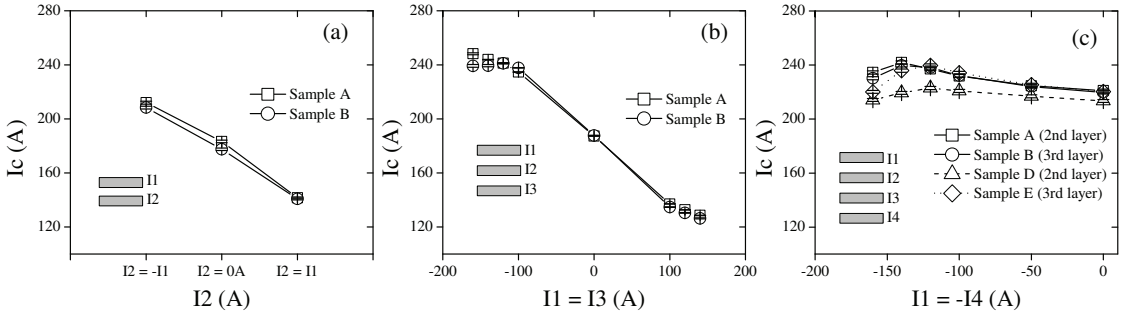

Fig. 4: The I_c of a BSCCO tape (I1) in 2-layer (a), the middle tape (I2) in 3-layer (b) and the middle two tapes (I2 and I3) in 4-layer (c) tape conductors with respect to the current in the neighboring tapes.

Figure 5 shows the increase of I_c for the multi-layer tape conductors with respect to the current applied to the neighboring tapes in comparison with that for the single one. With the anti-direction current feeding of -160 A, the I_cs are improved by 38%, 50% and 29% for 4-layer, 3-layer and 2-layer tape conductors, respectively.

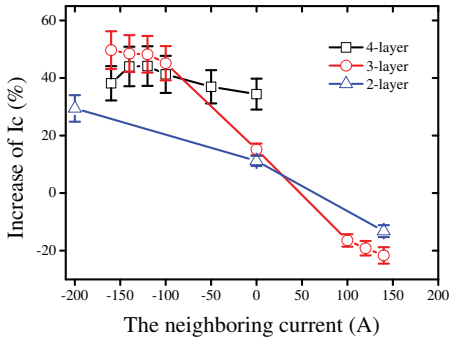

Fig. 5: The ratio of the increase of I_c in the multi-layer conductors with respect to the neighboring current.

We calculate the magnetic field distribution by the commercial finite element method code (ANSYS) [15, 16, 17]. To illustrate the effect of the self-field by the neighboring tapes, Figs. 6(a)-(g) present the magnetic field distribution for single tape, 2-layer, 3-layer and 4-layer tape conductors, respectively. The transport current is 160 A and assumed to be uniformly distributed in the cross section of the Ag-sheathed BSCCO filaments zone. Hence the cross section of the transport current area is assumed to be 4.5 mm $\times$ 0.25 mm without the laminated copper layer [14]. Figs. 6(b)-(d) show the magnetic field distributions for the multi-layer tape conductor with the anti-direction current feeding between the neighboring tape in comparison with those with the same current feeding in Figs. 5(e)-(g). The magnetic flux density in the BSCCO filament area is strengthened for the multi-layer tape conductors with the same current feeding comparing with that of the single one as shown in Figs. 6(e)-(g) and 6(b). For the anti-current feeding, the

magnetic flux density in the tape area is reduced compared with that in the single one.

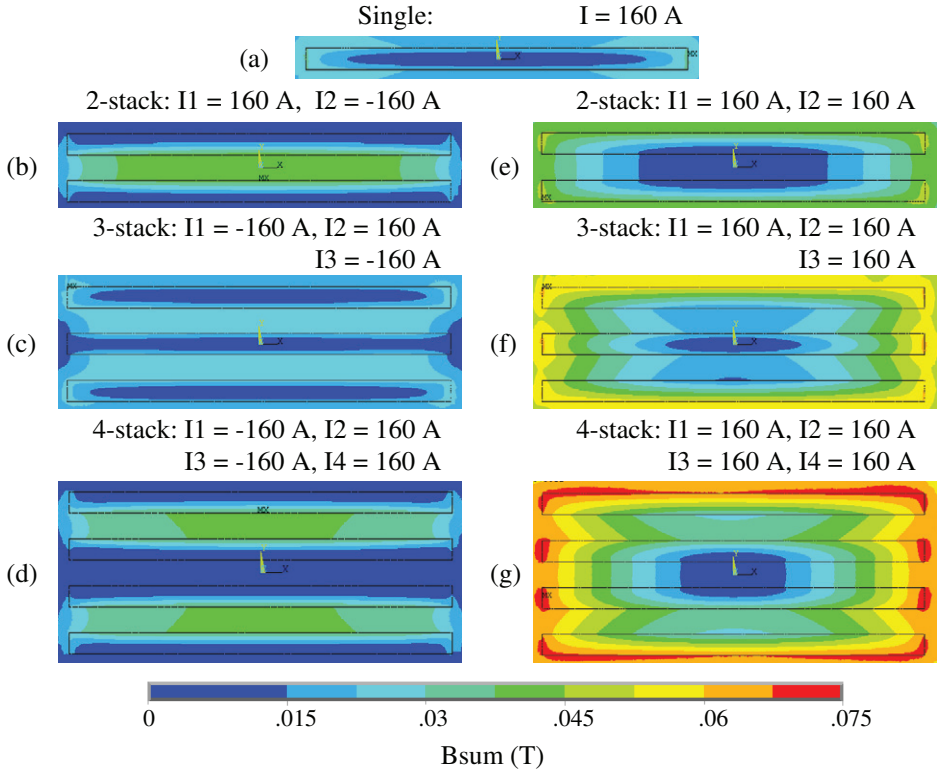

Fig. 6: The calculated contour images of the magnetic flux density distributions for the multi-layer conductors by the finite element code (ANSYS) [15].

Table 2 shows the maximum magnetic flux density B_{max} of the magnetic field distributions for the multi-layer tape conductors. When the same current are fed into each tape, the B_{max} increases with increasing the number of the layers. However, the B_{max} for anti-direction current feeding is similar with each other in spite of the number of the layers.

Number of layers	1	2	3	4	8
++	0.03319	0.04869	0.06765	0.07328	0.10675
+−	0.03319	0.04119	0.03076	0.03848	0.03575

Table 2: The maximum magnetic flux density of the magnetic field distributions for the multi-layer conductors calculated by ANSYS code [15]. ++ : same current and +−: anti-current feeding.

Both the calculation of the magnetic field distributions and the measurements of the I_cs in the multi-layer BSCCO conductors suggest that the anti-direction current feeding through the multi-layer tape conductors could enhance the superconductivity of the BSCCO tape in the HTS cable. In the case of the HTS cable for DC power transmissions and distributions, we could apply the current to a multi-layer cable with bipolar current feeding between each neighboring layer as shown in Fig. 7.

4. Conclusion

We investigated the effect on the critical current of the BSCCO HTS tapes of the multi-layer tape conductors consist of 2, 3 and 4 tapes. The current feeding mode affects the performance of the tape in the

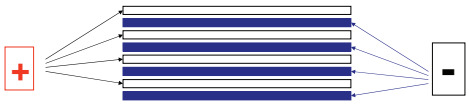

Fig. 7: A scheme of a multi-layer tape conductor with anti-current feeding mode for DC power transmission.

multi-layer tape conductors. With anti-direction current applied to each tape in the multi-layer HTS conductors, the critical currents of BSCCO tape increase sharply up to 210 A, 235 A and 220 A for 2-layer, 3-layer and 4-layer conductors, respectively. The I_cs are enhanced with the anti-direction current feeding between the neighboring tapes in spite of the number of the layers. It is in agreement with the calculation of the magnetic field calculations by the finite element method. Thereafter, the critical current is enhanced in the anti-current feeding between the neighboring tapes in the multi-layer conductors and we could make a multi-layer cable with bipolar current feeding between each adjacent layer especially for DC power transmissions and distributions.

Acknowledgement

The authors thank Prof. A. Iiyoshi for his continuous encouragement through this work. The authors acknowledge Prof. Hiroshi Fujiwara for his financial support. We also acknowledge the support by NEDO, Ministry of Education, Culture, Sports, Science and Technology (MEXT), and Chubu University Grant (A).

References

[1] Larbalestier D, Gurevich A, Feledmann DM, Polyanskii A. High-T_c superconducting materials for electric power applications. *Nature* 2001;**414**:368–77.
[2] Lim JH, Sohn SH, Ryoo HS, Choi HO, Yang HS, Kim DL et al. Performance test of 100 m HTS power cable system. *IEEE Trans Appl Super* 2009;**19**:1710–3.
[3] Ichikawa M, Kanegami M, Okamoto T, Akita S, Yagi M, Kimura A. Thermomechanical characteristics of 500-m HTS power cable. *IEEE Trans Appl Super* 2005;**15**:1771–4.
[4] Wang Y, Zheng Y, Liu H, Dai S, Zhang H, Guan X et al. A novel approach for design of DC HTS cable. *IEEE Trans Appl Super* 2011;**21**:1042–5.
[5] Yamaguchi S, Hamabe M, Yamamoto I, Famakinwa T, Sasaki A, Iiyoshi A et al. Research activities of DC superconducting power transmission line in Chubu University. *J Phys Conf Series* 2008;**97**:012290.
[6] Yamaguchi S, Kawahara T, Hamabe M, Watanabe H, Ivanov Y, Sun J et al. Design and construction of 200-meter high temperature superconducting DC power cable test facility in Chubu University. *Proc ICEC 23 - ICMC 2010*; p. 1041–7.
[7] Sun J, Emoto M, Yoshimura K, Ivanov Y, Watanabe H, Hamabe M et al. Development and operation of the measurement system for a 200 m HTS cable. *Proc ICEC 23 - ICMC 2010*;p.1035–40.
[8] Sun J, Yamauchi S, Sugino M, Watanabe H, Hamabe M, Kawahara T et al. Critical current measurements for desing of superconducting DC transmission power cable. *Physica C* 2011;**471**:1313–6.
[9] Furuse M, Fuchino S, Higuchi N, Ishi I. Feasibility study of low-voltage DC superconducting distribution system. *IEEE Trans Appl Super* 2005;**15**: 1759–62.
[10] Lee J, Park M, Lim H, Lee H, Cha G, Lee S. Magnetization loss and shield effect in multi-stacked tapes with various stacking configurations. *IEEE Trans Appl Super* 2006;**16**:131–4.
[11] Lee S, Lee HJ, Cha G, Lee J. Comparison of AC losses of HTS pancke winding with single tape and multi-stacked tape. *IEEE Trans Appl Super* 2005;**15**:1603–6.
[12] Park M, Choi M, Hahn S, Cha G, Lee J. Effect of the stack in HTS tapes exposed to external magnetic field. *IEEE Trans Appl Super* 2004;**14**:1106–9.
[13] Kikuchi M, Ayai N, Fujikami J, Kobayashi S, Yamazaki K, Yamada S et al. Progrss in high performance DI-BSCCO wire. *AIP Conf Proc* 2008;**986**:407–15.
[14] Ayai N, Yamazaki K, Kikuchi M, Osabe G, Takaaze H, Takayama H et al. Electrical and mechanical properties of DI-BSCCO type HT reinforce with metallic sheathes. *IEEE Trans Appl Supercond* 2009;**19**:3014–7.
[15] ANSYS® Academic Teaching Advanced, Release 12.1 ANSYS Inc. www.ansys.com.
[16] Farinon S, Fabbricatore P, Gömöry F. Critical state and magnetization loss in multifilamentary superconducting wire solved through the commercial finite element code ANSYS.*Supercond Sci Technol* 2010;**23**:115004.
[17] Fabbricatore P, Farinon S, Innocenti S, Gömöry F. Magnetic flux shielding in superconducting strip arrays. *Phys Rev B* 2000;**61**:6413–21.

Available online at www.sciencedirect.com

SciVerse ScienceDirect

Physics Procedia 27 (2012) 448 – 451

Physics Procedia

ISS2011

A Proposal of Multi-stage current lead for reduction of heat leak

Satarou Yamaguchi[a*], Masahiko Emoto[b], Toshio Kawahara[a], Makoto Hamabe[a], Hirofumi Watanabe[a], Yury Ivanov[a], Jian Sun[a], Norimasa Yamamoto[a], Atsuo Iiyoshi[a]

[a]*Center of Applied Superconductivity and Sustainable Energy Research (CASER), Chubu Univ., Matsumoto-cho 1200, Kasugai Aichi 487-8501 Japan*

[b]*National Insitute of Fusion Science (NIFS), Oroshi-cho 322-6, Toki, Gifu 509-5292, Japan*

Abstract

The reduction of the heat leak from the terminal is one of important issues to realize the applications of superconductivity, and the Peltier current lead (PCL) has been developed until now. The reduction of the PCL as compared with the usual copper lead is almost 40%, however the reduction of heat leak is still required to improve the total efficiency of the superconducting system. Therefore, we estimate the performance of the multi-stage current lead (MCL) and propose a gas-cooled MCL in this paper. The principle of the MCL depends on that the COP of the refrigerator is higher in a high temperature, and the resistivity of the copper is lower at lower temperature. But MCL was not tested experimentally until now. Fortunately, the COP of the various kinds of the refrigerators has been improved recently. The preliminary estimation of the MCL and the gas-cooled MCL shows that the saving power is high as 50% to 70%, depending of the assumption of the refrigerator COP. Therefore, it is a good time to examine the concept of MCL experimentally.

Keywords: Current lead; Heat leak reduction; COP of refrigerator; Multi-stage current lead; Gas-cooled current lead

1. Introduction

The heat leak from the terminal is one of major losses in many superconducting systems. For example, we assume the specifications of the DC power transmission as below,

1) Heat leak of the copper lead is ~ 50W/kA at one terminal,
2) Length of the DC superconducting power transmission line is 500 meter,
3) Heat leak of the cryogenic pipe is 1W/m,
4) Current is 10 kA,
5) Other heat leak and heat load can be neglected because of no AC losses.

The heat leak of the cryogenic pipe is 500m × 1W/m = 500W, and the heat leak at the terminal is 10kA × 50W/kA × 4 = 2000W. Since we will be not able to construct a long transmission line at the first stage because of many reasons [1, 2], and if we cannot reduce the heat leak at the terminal, the competitiveness of the DC superconducting power transmission line is weak for the copper cable. Therefore, if we can reduce the heat leak at the terminal, it is effective that DC superconducting power transmission will become common infrastructure in the world.

Moreover, if we consider the system of the superconducting magnets, the heat leak at the terminal is 90% or higher, especially high for the cryogen-free superconducting magnet. Therefore, if we can reduce the heat leak at the terminal,

* Corresponding author. Tel.: +81-568-51-9419; fax: +81-568-51-9413.
E-mail address: yamax@isc.chubu.ac.jp.

1875-3892 © 2012 Published by Elsevier B.V. Selection and/or peer-review under responsibility of ISS Program Committee
doi:10.1016/j.phpro.2012.03.508

we can use a small refrigerator system to cool down the superconducting system including the superconducting motors. However, the reduction of the heat leak at the terminal is limited and not easy because we must find the materials that can pass through the electric current but should prevent to pass the heat flux, and/or we must find a new mechanism to save the electric power of the refrigerators. The Peltier current lead (PCL) [3, 4, 5] has been proposed to reduce the heat leak at the terminal in National Institute for Fusion Science (NIFS). After one of authors SY moved to Chubu University, the experiment of the PCL was started and we demonstrated the effectiveness of the PCL [6, 7]. The principle of the PCL depends on the thermoelectric effect. The performance of the PCL depends on the figure of merit and the parameters of Peltier material [8], and the heat leak of the PCL is ~26W/kA in the present materials.

In order to reduce the heat leak much more, we propose a new scheme of the current lead system in this paper. This is called the multi-stage current leads (MCL) [9]. The heat leaks of the MCLs are calculated by the one-dimensional numerical software [4, 5], and estimate the electric power consumption of the refrigerators by assuming the COPs of the refrigerators. And we also propose the gas-cooled MCL in the paper, and estimate the performance of the gas-cooled MCL.

2. Multi-stage current lead

The current lead is optimized to minimize the heat leak at terminal for the copper lead [10, 11]. The heat leak flux and temperature profile are calculated to solve the equation given as below,

$$dQ/dx - fmC_P dT/dx + \eta I^2/S = 0 \qquad (1)$$

where Q is heat flux as $Q = =\kappa dT/dx$, T is temperature, x is the coordinate along the current lead, κ is thermal conductivity, I is current, η is electrical resistivity, S is cross-section of current lead, f is efficiency of heat transfer between gas and current lead, m is mass flow rate of gas, C_P is specific heat of constant pressure, and the boundary conditions of the Equations are set as

$$T|_{x=0} = 77K, T|_{x=1} = 300K \qquad (2)$$

The heat leak of the current lead depends on the cross-section and length of the current lead, and in order to minimize the heat leak, we must find the shape of the current lead to solve the Equation (1) to find the optimum cross-section and length ratio. The heat flux per unit current (kA) profile for the temperature is shown in Fig. 1 (a). The heat leak at 77K is 42.5W/kA. The heat flux is zero at 300K, and it increase quickly around the room temperature (RT) side because the electrical resistivity of copper is high in high temperature. The heat flux is 42.5W/kA at 77K, and it is 40.7W/kA at 123K and 35.2W/kA at 188K, respectively.

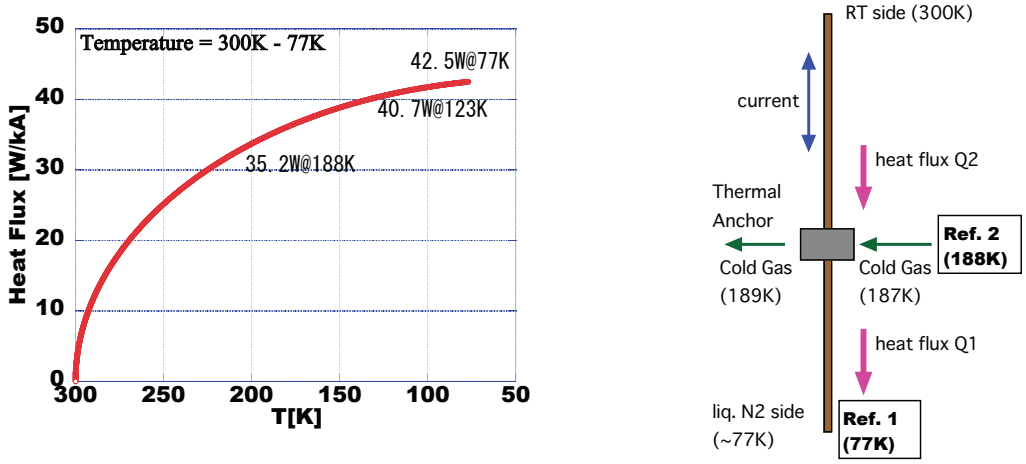

Fig. 1. (a) Profile of heat flux per current (kilo-ampere) for temperature of current lead for the ratio of length and cross-section = 35960m^{-1}; (b) Schematic structure of the multi-stage current lead (MCL). Two refrigerators are used to keep the temperatures of 77K and 188K.

The ratio of the length and cross-section of the current lead is optimized to be 35960m^{-1} for the current of 100A and the copper lead. Therefore, it was proposed that the thermal anchor was installed into the current lead, and the different refrigerator was also installed to keep the temperature of the thermal anchor [9]. The configuration of the proposed current lead is shown in Fig. 1 (b), and it is called MCL.

The temperature of the thermal anchor is 188K in Fig. 2, and we must prepare two different refrigerators, one is a 77K refrigerator (Ref. 1) and the other is the 188K-refrigerator (Ref. 2). The total amount of the heat load to two refrigerators is the same as that of one refrigerator system at 77K, and it is 35.2 W/kA for Ref. 2 and 7.3W/kA for Ref. 1, those are obtained from Fig. 1(a). However, the COP of refrigerator is higher in high temperature, and we can assume that the COP of Ref. 1 is 0.067 and it is ~ 0.5 for Ref. 2's. Therefore, the total electric power consumption of two refrigerators is 7.3/0.067 + 35.2/0.5 = 179.4W/kA. On the other hands, the original one refrigerator system consumes 42.5/0.067 = 634.3W/kA. Therefore, we can save the electric power of 454.9W/kA, and it corresponds to 71.7% basically. The saving power depends on the COP of refrigerator and its anchor temperature fundamentally. Because of the engineering points of view, we should find the correct refrigerators for the multi-stage current lead actually, and we will realize the experimental device along the estimation of the saving power.

3. Multi-stage and gas-cooled current lead

We use the coolant gas to reduce the heat leak of the current lead [10], and this system is called the gas-cooled current lead. It is one of the great inventions in applied superconductivity, and we can apply this idea to the MCL. Figure 3 shows a proposal of the gas-cooled MCL. The gas is circulated inside the parts of the current lead and the refrigerator. The temperature of the thermal anchor is 123K in Fig. 2 (a), and the cold gas is supplied to keep the temperature at the 123K from the Ref. 2. The gas goes up to the RT side of the current lead, and goes out from the current lead, and finally goes back to the Ref. 2 in Fig. 2 (a). Therefore, the current lead is the heat exchanger, but a part of the current lead below 123K is not cooled by the gas.

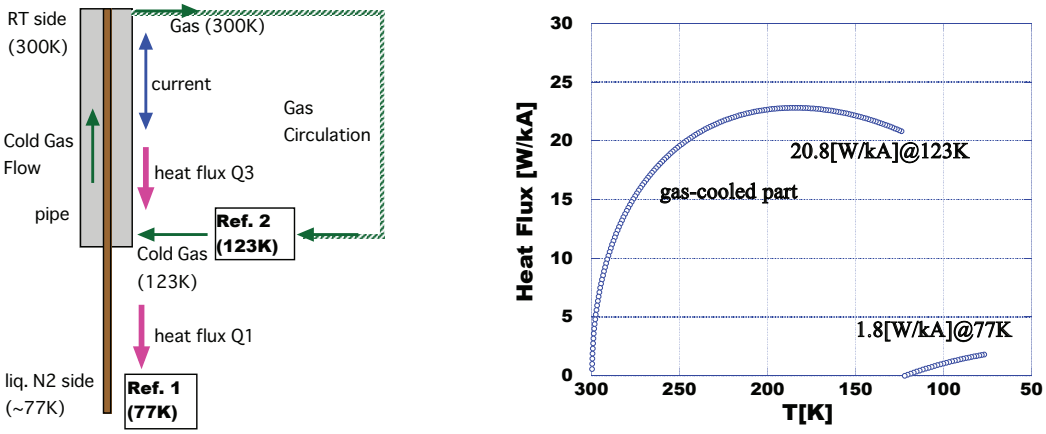

Fig. 2. (a) Schematic structure of the gas-cooled and multi-stage current lead (gas-cooled MCL). Two refrigerators are used to keep the temperatures of 77K and 123K; (b) Heat flux profile of gas-cooled MCL for temperature. The temperature of thermal anchor is 123K, and the heat load is 20.8W/kA at 123K and 1.8W/kA at 77K

Since the cold gas can cool the current lead by the heat exchange process, the heat flux from the RT side to the thermal anchor is reduced. Therefore, the heat load of the Ref. 2 is reduced, and finally the electric power consumption of the Ref. 2 can be low. The heat flux profile is obtained to solve Eq. (1), but the boundary condition is difference from Eq. (2), and shown in Fig. 2 (b). Since we use the thermal anchor, the heat flux is zero at the cold side of the thermal anchor in the current lead, on the other hand, the heat flux at the warm side of the thermal anchor is 20.8W/kA. Therefore, the heat flux is not continuous profile. The heat leak to the 77K system is 1.8W/kA, and this value is integrated heat flux from 123K to 77K, that is estimated from Fig. 1 (a).

The material of the current lead is copper, and the calculation conditions are that the coolant gas is nitrogen, and the term *fm* in Eq. (1) is 10.0g/min at the gas pressure of 0.1MPa [12]. The term *fm* in Eq. (1) is not free parameter in an usual gas-cooled current lead because the mass flow rate is determined by the vaporization of the coolant by the heat leak at the cold end of the current lead, and/or the heat load of the cryostat of the current lead. Moreover, we should pay attention to keep the quantity of the coolant if the coolant gas goes out from the cryostat because the coolant gas goes out from the cryostat through the current lead. However, the term *fm* is a free parameter in a proposed

scheme because it is circulated. Therefore, we can set the value of *fm* by the additional condition of the system, such as the refrigerator operation, the magnitude of current and so on. If the COP of the 123K-refrigerator is 0.228, and we use the same refrigerator of 77K, the total electric power consumption of the system is 20.8W/kA / 0.228 + 1.8W/kA / 0.067 = 118.1W/kA. This is only 18.6% of the one refrigerator system.

4. Discussion and future perspectives

The assumptions of the refrigerator's COP and its performance depend on the discussion with several persons who work for refrigerator manufacturing company, and therefore it is a realistic estimation. Since the calculation results of the MCL and the gas-cooled MCL are attractive, it is important that its concept works well to realize high performance superconducting system because the saving power is high. Usually the maximum COP is given by the constant operation of the refrigerator, but we should consider the actual operation of the superconducting system that is not always operated constantly. Therefore, we should test the concepts experimentally.

PCL can save electric power, but it is effective to apply the DC system because when the direction of current is reversed, the direction of Peltier heat flux is reversed, and the heat leak is enhanced in this case. However, the MCL and the gas-cooled MCL can be applied to not only DC system but also AC system because the physical process of the MCL does not depend on the direction of the current. The multi-stage PCL was also evaluated [13] because the multi-stage Peltier element is already used for several purposes in commercially. But the meaning of "multi-stage" in PCL is different from the MCL's in the paper. Since the principle of the heat leak reduction in MCL is different process of the PCL, we can use both of two processes to reduce the heat leak. It means that we can propose the multi-refrigerator Pelteir current lead, and this is the next subject for our studies.

Acknowledgements

The authors also acknowledge Mrs. A. Machida and K. Yamamoto of Mayekawa Mfg. Corp. and Mrs. Y. Yamada and Y. Okubo of AISIN SEIKI Co., Ltd for their useful discussions on performance of refrigerators. We also thank to Drs. J. Minervini, L. Bromber, M. Takayasu, Prof. B. Coppi and Dr. L. Sugiyama in Massachusetts Institute of Technology (MIT) for their useful and kind discussion about the multi-stage current leads.

References

[1] Yamaguchi S, Hamabe M, Yamamoto I, Famakinwa T, Sasaki A, Iiyoshi A, Schultz J, Minervini J, Hoshino T, Ishiguro Y, Kawamura K. Research acitivies of DC superconducting power transmission line in Chubu Univesity. *J. Physics Conf. Series* 2008;**97**:012290.

[2] Yamaguchi S, Kawahara T, Hamabe M, Watanabe H, Ivanov Yu, Sun J, Iiyoshi A. Experiment of 200-meter superconducting DC cable system in Chubu University. *Physica C* 2010;**471**:1300-1303.

[3] Yamaguchi S, Takita K, Motojima O, A proposal for Peltier current lead. *Proc. 16th Int. Cryogenic Eng. Conf./Int. Cryogenic Mat. Conf.*, May, 1996, pp. 1159-1162.

[4] Okumura H, Yamaguchi S. One dimensional simulation for Peltier current leads. *IEEE Trans. Appl. Supercond.* 1997; **7**:715-718.

[5] Sato K, Okumura H, Yamaguchi S. Numerical calculations for Peltier current lead design. *Cryogenics* 2001;**41**:497-503.

[6] Hamabe M, Sasaki A, Kasukabe T, Oue M, Nakamura K, Yamaguchi S, Ninomiya A, Okumura H, Kawamura Km Aoki I. Test of Peltier current lead for cryogenin-free superconducting magnet. *IEEE Trans. Appl. Supercond.* 2006;**16**:465-468.

[7] Yamaguchi S, Yamaguchi T, Nakamura K, Hasegawa Y, Okumura H, Sato K. Peltier current lead experiment and their applications for superconducting magnets. *Rev. Sci. Instruments* 2004;**75**:207-212.

[8] Hasegawa Y, Sato K, Okumura H, Nakamura K, Yamaguchi S, Miyake K. Reduction of heat leak in cryogenic system using Peltier current leads. *Cryogenics* 2002;**42**;495-500.

[9] Bromberg, L., Michael, P.C., Minervini, J.V. and Miles, C. Current Lead Optimization for Cryogenic Operation at Intermediate Temperatures. *AIP Conference Proceedings* 2010;**1218**:577-584.

[10] Wilson M. N. *Superconducting Magnets* Oxford, Oxford University Press, 1983.

[11] McFee, R., Optimum Input Leads for Cryogenic Apparatus, *Rev. Sci. Instruments* 1959;**30**:98–102.

[12] Kawahara T, Fujii T, Emoto M, Hamabe M, Sun J, Watanabe H, Yamaguchi S, Estimation for the performance of superconducting DC transmission lines with cryogenic improvements. *Physica C* 2010;**470**:S1011-S1012.

[13] Yamaguchi T, Okumura H, Nakamura K, Yamaguchi S. Multi-stage Peltier current lead system for liquid helium free magnets. *IEEE Trans. Appl. Supercond.* 2003;**13**:1914-1917.

Available online at www.sciencedirect.com

SciVerse ScienceDirect

Physics Procedia 27 (2012) 380 – 383

Physics Procedia

ISS2011

Possibility of a gas-cooled Peltier current lead in the 200 m-class superconducting direct current transmission and distribution system of CASER-2

Toshio Kawahara[a*], Masahiko Emoto[b], Hirofumi Watanabe[a], Makoto Hamabe[a], Sataro Yamaguchi[a], Yasuo Hikichi[c], Masahiro Minowa[c]

[a]*Center of Applied Superconductivity and Sustainable Energy Research, Chubu University, 1200 Matsumoto, Kasugai, Aichi 487-8501 Japan*
[b]*Department of Large Helical Device Project, National Institute for Fusion Science,Gifu 509-5292 Japan*
[c]*SWCC Showa Cable Systems Co. Ltd, 4-1-1 Minami-hashimoto, Chuo, Sagamihara, Kanagawa 252-0253 Japan*

Abstract

Global energy problems should be solved quickly, and superconducting applications are highly demanded as energy saving technologies. Among them, long-distance superconducting transmission seems to be one of the most promising for energy saving by energy sharing. On the other hand, such large systems can be constructed from smaller network systems that can be enhanced by scaling up to the superconducting grid. Reducing heat leak to the low temperature end is the most important aspect of technology for practical superconducting applications, and heat leak reduction at the terminal is a key goal especially for small-length applications. At Chubu University, we have developed a 200 m-class superconducting direct current transmission and distribution system (CASER-2), in which we also used a Peltier current lead (PCL) as heat insulation at the terminal. PCL is composed of a thermoelectric material and a copper lead. In actual transmission and distribution applications, the cables are also cooled by the coolant. After the circulation, the coolant could also be used to cool the current lead. We will discuss the performance of such gas-cooled systems as the total performance of applied superconducting systems using the experimental parameters obtained in CASER-2.

Keywords: Direct current transmission; Cryogenics; Peltier current lead; high temperature superconductors

1. Introduction

Superconducting applications are highly demanded for energy saving in order to solve global environmental issues. Among these applications, long-distance superconducting transmission systems seem to be one of the most promising for energy saving by energy sharing. On the other hand, such large systems can be built up from smaller network systems, which can be enhanced by scaling up to the superconducting grid. For the development of superconducting transmission systems, there are several projects in Japan, the U.S., Korea and China, such as those pertaining to long-distance, high-voltage and/or grid cooperation systems [1-3]. For example, Albany projects successfully transmitted electric power to 70,000 homes in New York State [2]. Yokohama projects in Japan will represent a field test of superconducting transmission lines [3]. Direct current projects are also planned at an aluminum factory by the Chinese

* Corresponding author. Tel.: +81-568-51-9314; fax: +81-568-51-9413.
E-mail address: toshi@isc.chubu.ac.jp.

1875-3892 © 2012 Published by Elsevier B.V. Selection and/or peer-review under responsibility of ISS Program Committee
doi:10.1016/j.phpro.2012.03.490

Academy of Science. Chubu University has already developed a 20-m class superconducting direct current (DC) superconducting transmission device (CASER-1) [4] and has proposed several technologies to improve system performance of superconducting applications. Discussions have been made concerning the current balance of superconducting tapes as stable transmission systems, low-heat leak systems using special cryogenic double pipes, etc. [5,6].

For actual applications, reducing heat leak to the low temperature part is the most important aspect of technology for high-performance superconducting applications. For long-distance transmission lines, the main heat leaks can be reduced by high-performance cryogenic pipes [5]. On the other hand, heat leak reduction at the terminal for small-length applications is a key goal for actual uses such as those involving the high-performance current lead [7-10]. At Chubu University, we are developing a 200 m-class superconducting DC transmission and distribution system (CASER-2) following our development of the 20 m-class CASER-1 system. In CASER-2, we also used a Peltier current lead (PCL) as heat insulation at the terminals. PCL is composed of a thermoelectric material and a copper (Cu) lead. The small thermal conductivity and large Seebeck coefficient of thermoelectric materials can effectively insulate the heat leak to the low temperature end. Several modifications of the PCL have also been proposed and discussed such as an alternating current mode, multi-stage modules, and gas-cooled systems [7]. Here, as CASER-2 was associated with DC-mode applications, we used normal PCLs of a single thermoelectric segment.

In actual transmission and distribution applications, the cables are also cooled by the coolant. After the circulation, the coolant could also be used to cool the current lead. Such gas-cooled current leads under over-gas conditions seem to be candidates for use in high-performance terminal systems [9]. In this paper, we will discuss the performance of such gas-cooled systems as the total performance of applied superconducting systems using the actual parameters obtained in the cooling experiments of CASER-2.

2. Experiments in CASER-2

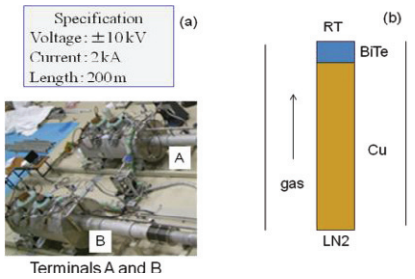

Fig. 1. Specification of CASER-2 (a) and PCL (b).

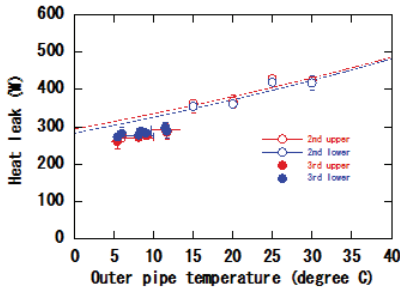

Fig. 2. Heat leak at cryogenic pipes. Upper and lower thermometers were attached to the top and bottom of the pipes, respectively.

We constructed CASER-2 between August 2009 and January 2010. Specifications of CASER-2 and a picture of the terminals are shown in Fig. 1 (a). The transmission power of CASER-2 is 40 MW and the length is approximately 200 m. There is an undulation of 2.7 m and a turn with a minimum radius of 2 m, which can emulate actual conditions of transmission lines in the field. From January to March of 2010, we first conducted cooling experiments and estimated the system performance of CASER-2. In January, the whole system was cooled down to liquid nitrogen temperature within one week and we set up the circulation systems using 1 kW-class cryo-cooler and circulation pump systems. In March, we successfully conducted a 1.2 kA current feeding test in a superconducting state in the system. Following the first cooling experiment, we performed 2nd and 3rd experiments. The heat leaks are summarized in Fig. 2, which shows the dependence of the heat leak on outside environmental temperature. The 3rd experiment indicated that improved multi-layer insulators and reducing spacers for inner pipes could reduce the heat leak. The current of 2.0 kA was successfully fed into the CASER-2 system and we also obtained heat leak measurements at the terminals until 1.5 kA. The currents used for the heat leak measurements on the terminals are summarized in Table 1. We are now able to conduct a 4th cooling experiment with the improved cryogenic setups.

3. Simulation methods

We used the thermal balance equation (1) for heat leak estimation [11] with the Seebeck effect [12,13].

$$\frac{d}{dx}\left(k(\theta)A\frac{d\theta}{dx}\right)-\dot{m}C_p\frac{d\theta}{dx}+\frac{I^2\rho(\theta)}{A}=0 \quad , \tag{1}$$

where k is the thermal conductivity, θ is the temperature, Cp is the specific heat, A is the cross-section of the current lead, I is the current, and ρ is the resistivity. The Seebeck effect ($\alpha I\theta$) is added in the first term for the PCL. Gas cooling is expressed by the heat exchange ratio f between cold gas and the current lead with a mass flow $\dot{m}$ of liquid nitrogen. $f = 0$ indicates no heat exchange, which represents conduction cooling. $f = 1$ indicates that the cold gas can exchange the heat with the current lead in the equilibrium condition, which is self cooling. A schematic of the PCL is also shown in Fig. 1 (b).

We used thermoelectric materials (BiTe) of 10-mm squares with a thickness of 4 mm. Under this constraint, we optimized the shape of the current lead for the operational current of 160 A. As we used high-Tc superconductors cooled by liquid nitrogen; the cold temperature was set as 77 K and the higher temperature at the other end was set as 300 K. The optimized shape factor L/A for minimum Q was obtained by these boundary conditions, where L is the length of the current lead and Q is the heat load at the lower end of the current lead.

Table 1. Feeding current conditions for heat leak measurements at the terminals.

2nd cooling experiment	200 A, 400 A, 500 A, 600 A, 800 A, 1000 A, 1200 A, 1500 A
3rd cooling experiment	200 A, 400 A, 600 A, 800 A, 1000 A, 1040 A, 1200 A, 1500 A

4. Discussion

Figure 3 shows the heat leak at the terminals. When this heat is used for the gas-cooling systems, f equals 1, which represents a self-cooling condition. If we use the gas from the cryogenic pipe, we can use additional gas to cool the current leads. Now we suppose that the gas-cooling systems keep the ambient pressure at equilibrium conditions and

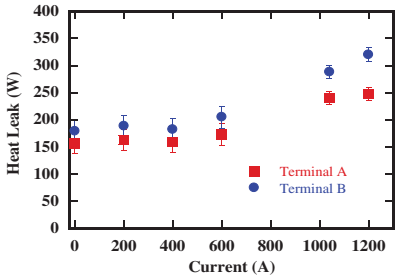

Fig. 3. Current dependence of the heat leak on the terminals. Squares and circles are for Terminals A and B, respectively.

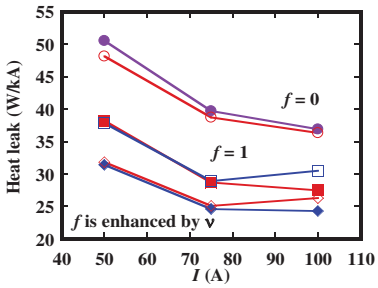

Fig. 4. Current dependence of heat leak. Open and closed symbols denote n-type and p-type PCLs, respectively. Circles are for $f = 0$, squares for $f = 1$, and diamonds represent gas cooling with extra gas coming from the cryogenic pipe system.

the remaining liquid nitrogen will circulate to cool the transmission systems with the cryo-cooler. Under this condition, the enhanced factor ν for the heat exchange ratio, where νf is used as the exchange ratio instead of f, can be estimated from the ratio between the heat leak at the terminals (Fig. 3) and the transmission system as stated in section 2 (Fig. 2). In CASER-2, as liquid nitrogen flows from terminal A to terminal B, ν is calculated using the heat leak of terminal B and data at the 3rd cooling are used. On the other hand, if we used data at the 2nd cooling, a ν value enhanced by over 10% can be obtained with a higher environmental temperature.

Figure 4 shows the current dependence of heat leak at the current leads. The heat leak of conduction cooling, which is the actual situation in CASER-2 ($f = 0$), and the self-cooling condition ($f = 1$) are also plotted. The gas-cooled conditions can reduce the heat leak, and a gas cooling system using extra gas from the cryogenic pipe could have a higher potential for use in low-heat leak terminal systems. For example, reduction of the heat leak for $I = 75$ A between circular and diamond symbols in Fig. 4 is 39%. The performance increases under smaller current conditions because of the greater amount of extra gas. Therefore, stability of the dependence on current seems to be improved. 25 W/kA is one of the requirements needed to reduce heat leak at the terminals with the optimal shape factors [14], and when using extra gas, it can also be achieved under smaller current conditions.

Finally, we consider the transmission length dependence of the extra gas effect. The enhanced factors for the heat exchange ratio are plotted in Fig. 5

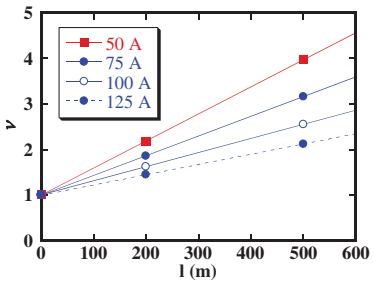

Fig. 5. Transmission length dependence of the enhanced factor for the heat exchange ratio.

with several feeding current conditions. Gas-cooling systems using extra gas coming from the transmission lines could have a higher performance for longer lines. Therefore, the heat leak of terminals becomes relatively small for the total transmission system, and total performance can be enhanced. Of course, part of the liquid nitrogen circulated could be used as the extra gas. Such flow-type systems are now being considered when estimating the cooling power of the circulation.

5. Conclusion

Using the experimental parameters in CASER-2, we estimated the heat leak of current leads with the gas-cooling effect. The gas-cooled conditions can reduce the heat leak, and a gas-cooling system using extra gas coming from the cryogenic pipe could have higher potential as a low-heat leak terminal system. For example, a heat leak reduction of 39% is obtained at I = 75 A. Such gas-cooling systems using extra gas coming from the transmission lines could have a higher performance for longer lines. Therefore, the heat leak of terminals becomes relatively small considering the total transmission system, and then the total performance can be enhanced. This concept could be improved using the flow-type cryostat for small-length power applications. We discussed the performance of these gas-cooled systems as the total performance of applied superconducting systems.

Acknowledgements

The authors thank Prof. A. Iiyoshi of Chubu University for his continuous encouragement throughout this work. We acknowledge Dr. Hiroshi Fujiwara for his support on the construction of the 200-m superconducting facilities of CASER-2. Parts of this work were supported by a grant from the Strategic Research Foundation Grant-aided Project for Private Universities, Ministry of Education, Culture, Sports, Science and Technology (MEXT), and a Grant-in-Aid for challenging Exploratory Research (MEXT). Portions of the work were also supported by the Nippon Sheet Glass Foundation for Materials Science and Engineering, and the Future Energy Research Association.

References

[1] Mukoyama S., Yagi M., Ichikawa M., Torii S., Takahashi T., Suzuki H., Yasuda K., "Experimental results of a 500mHTS power cable field test," *IEEE Trans. Appl. Supercond.* 2007; **17**: 1680-1683.

[2] Masuda T., Yumura H., Watanabe M., Takigawa H., Ashibe Y., Suzawa C., Ito H., Hirose M., Sato K., Isojima S., Weber C., Lee R., Moscovic J., "Fabrication and installation results for Albany HTS cable," *IEEE Trans. Appl. Supercond.* 2007; **17**: 1648-1651.

[3] Honjo S., Mimura T., Kitoh Y., Noguchi Y., Masuda T., Yumura H., Watanabe M., Ikeuchi M., Yaguchi H.,"Status of Superconducting Cable Demonstration Project in Japan," *IEEE/CSC & ESAS Eur. Supercond. News Forum (ESNF)* 2010; **14**: ST201.

[4] Yamaguchi S., Hamabe M., Yamamoto I., Famakinwa T., Sasaki A., Iiyoshi A., Shultz J., Minervini J., Hoshino T., Ishiguro Y., Kawamura K., "Research activities of DC superconducting power transmission line in Chubu University," *J. Phys.: Conf. Ser.* 2008; **97**: 012290.

[5] Hamabe M., Nasu Y., Ninomiya A., Ishiguro Y., Kusaka S., Yamaguchi S., "Radiation heat measurement on thermally-isolated double-pipe for DC superconducting power transmission," *Adv. in Cryo. Eng.* 2008; **53A**: 168-173.

[6] Hamabe M., Fujii T., Yamamoto I., Sasaki A., Nasu Y., Yamaguchi S., Ninomiya A., Hoshino T., Ishiguro Y., Kawamura K., "Recent Progress of Experiment on DC Superconducting Power Transmission Line in Chubu University," *IEEE Trans. Appl. Supercond.* 2009; **19**: 1778-1781.

[7] Yamaguchi S., Yamaguchi T., Nakamura K., Hasegawa Y., Okumura H., Sato K., "Peltier current lead experiments and their applications for superconducting magnets," *Rev. Sci. Instrum.* 2004; **75**: 207-212.

[8] Xuan X. C., Ng K. C., Yap C., Chua H. T., "On minimizing the heat leak of current leads in cryogenic vacuum systems," Cryogenics 2002; **42**: 779-785.

[9] Kawahara T., Fujii T., Emoto M., Hamabe M., Sun J., Watanabe H., Yamaguchi S., "Estimation for the performance of superconducting DC transmission lines with cryogenics improvements," *Physica C* 2010; **470**: S1011-S1012.

[10] Kawahara T., Fujii T., Emoto M., Hamabe M., Watanabe H., Sun J., Ivanov Y. and Yamaguchi S. "Double Peltier Current Lead for Heat Leak Reduction at the Terminals for Superconducting Direct Current Applications," *IEEE Trans. Appl. Supercond*. 2011; **21**: 1070-1073.

[11] Wilson M. N., *Superconducting Magnets* Oxford: Clarendon Press; 1983 pp.256-272.

[12] Okumura H., Yamaguchi S., "A simulation for Peltier current lead," *IEEE Trans. Appl. Supercond.* 1997; **7**: 715-718.

[13] Sato K., Okumura H., Yamaguchi S., "Numerical calculations for Peltier current lead designing," *Cryogenics* 2001; **41**: 497-503.

[14] Minervini J. V., Bromberg L., Michael P., Miles C., LaBounty N. R., "Superconducting DC Power Transmission and Distribution," PSFC/RR-09-2 2009.

Available online at www.sciencedirect.com

SciVerse ScienceDirect

Physics Procedia 27 (2012) 376 – 379

Physics Procedia

ISS 2011

Cooling of the 200 m superconducting DC power transmission system at Chubu University

Hirofumi Watanabe*, Jian Sun, Yury Ivanov, Makoto Hamabe, Toshio Kawahara, Satarou Yamaguchi

Center of Applied Superconductivity and Sustainable Energy Research, Chubu University, Kasugai, Aichi, 487-8501, Japan

Abstract

The fourth cooling test of the superconducting DC power transmission system of Chubu University was conducted in August of 2011. The heat leak from the cryogenic pipe and the effect of reducing the outer pipe temperature were tested. The heat leak from the cryogenic pipe was improved relative to that recorded during the second cooling test performed in the previous summer, a season similar to that in which the fourth cooling test was conducted. A significant reduction of the outer pipe temperature was achieved by an infrared reflective coating, and a reduction of the heat leak was observed.

Keywords: Large scale application;Superconducting direct current transmission;Cryogenics

1. Introduction

We completed the construction of a 200 m class superconducting DC power transmission system at Chubu University, named CASER2, at the beginning of 2010 [1, 2, 3] and performed four cooling tests by the end of autumn in 2011. During the cooling tests, the temperature of the liquid nitrogen was measured under several experimental conditions and the amounts of heat leak were estimated [1, 2]. In the case of superconducting DC power transmission, heat leak to low temperature parts determines the efficiency of the system. Therefore, reduction of the heat leak is important for application of the superconducting DC power transmission system to actual power grids. In particular for long distance power transmission, the heat leak from the cryogenic pipe accounts for the majority of the losses of the system and reduction of this heat leak is essential. We have therefore been making efforts to reduce the heat leak of the superconducting DC power transmission system [4, 5].

The cryogenic pipe of CASER2 is a coaxial double straight pipe [1, 2]. The space between the outer pipe and inner pipe is evacuated for the vacuum insulation. The cable is installed and liquid nitrogen flows in the inner pipe. Reducing the outer pipe temperature of the cryogenic pipe is obviously effective in reducing the heat leak, because the radiative heat transfer and conductive heat transfer strongly depend on its temperature. Since the transmission line of CASER2 is installed mainly in the outdoors, strong sunlight during the summer heats the outer pipe of the cryogenic pipe. Thus, experiments in the summer

*Tel:+81-568-51-9373;Fax:+81-568-51-9413;E-mail:h_watanabe@isc.chubu.ac.jp

1875-3892 © 2012 Published by Elsevier B.V. Selection and/or peer-review under responsibility of ISS Program Committee
doi:10.1016/j.phpro.2012.03.489

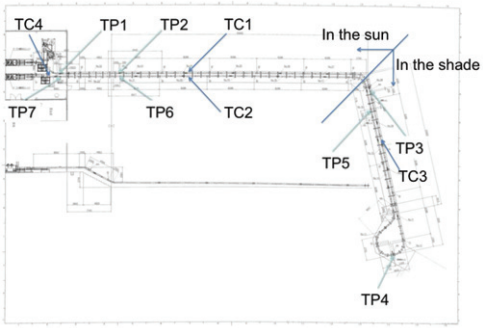

Fig. 1. Layout of the cryogenic pipe of CASER2. Positions of the platinum resistance thermometers, which measure the liquid nitrogen temperature, are indicated by TP1 to TP7. Positions of outer pipe temperature measurements are indicated by TC1 to TC4.

provide stringent tests for liquid nitrogen circulation and the heat leak. In the experiment during the fourth cooling test, the effect of reducing the outer pipe temperature was tested. An infrared reflective coating was applied to the outer pipe surface to reduce the heat caused by direct sunlight. The temperatures of the outer pipe surface along the cryogenic pipe and the temperature increase of the circulating liquid nitrogen were measured. Based on the temperature measurements, the heat leak of the cryogenic pipe was estimated and compared with results obtained during the first to third cooling tests [1, 2].

2. Experiment and results

Figure 1 shows the layout of CASER2. Details of the system are explained elsewhere [1, 2, 3]. The length of the cryogenic pipe of CASER2 is approximately 200 m and nearly 85% is laid in the outdoors with an L-shaped configuration. The temperature of the liquid nitrogen circulating in the cryogenic pipe is measured with platinum resistance thermometers, which are set at 7 positions along the cryogenic pipe, TP1 to TP7. Each position has two thermometers on the upper and lower surfaces of the inner pipe of the cryogenic pipe. About 60% of the cryogenic pipe in the outdoors receives direct sunlight during the daytime, while the remaining portion is under trees and therefore lies in the shade. As a consequence, temperatures at different positions along the cryogenic pipe and at different times of the day are quite different.

It is clearly necessary to reduce the outer pipe temperature of the cryogenic pipe in order to reduce the heat leak. The portion of the cryogenic pipe receiving direct sunlight is heated. An infrared reflective coating was applied to part of the cryogenic pipe surface to test the effect on reduction of the outer pipe temperature. The coating was a ZEFFLE infrared reflective coating construction of Daikin Industries, Ltd. It is fluoropolymer based coating in which tetrafluoroethylene is used as the ingredient of the resin backbone structure of the varnish and titanium dioxide is used as the white pigment. It is a painted coating, which allows the pipe to be coated easily in the outdoors. Only part of the pipe between TP5 and TP6 was coated, which was about 23% of the length between TP1 and TP7 and which received direct sunlight during the daytime. As seen in Fig. 1, since portions of the cryogenic pipe between TP2 and TP3 and between TP5 and TP6 run parallel to each other, sunlight conditions are nearly the same. By comparing the temperature increases of the liquid nitrogen between TP2 and TP3 and between TP5 and TP6, the effect of the coating on the heat leak can be determined.

Figure 2 shows the outer pipe temperature along the cryogenic pipe. The temperatures were measured on the outer pipe surface of the cryogenic pipe and on the opposite side of the illuminated surface in order to avoid heating the thermocouples by direct sunlight. The approximate positions at which the temperatures were measured are also shown in Fig. 1. Overall, the temperature rises in the daytime and falls in the nighttime. The temperature of a non-shaded position is nearly 20 degrees centigrade higher, at maximum, than that in the shade during the daytime, while temperatures become almost the same during the nighttime. The

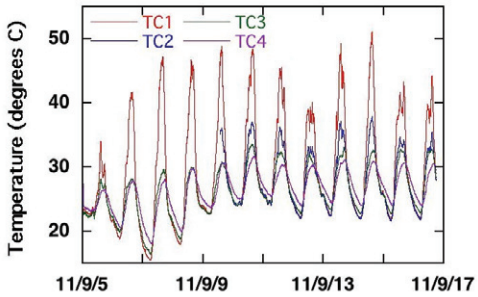

Fig. 2. Typical outer pipe temperatures along the cryogenic pipe. TC1, TC3 and TC4 are the temperatures of the cryogenic pipe surface in the sun, in the shade and in the laboratory, respectively. TC2 is the temperature of the cryogenic pipe surface on which the infrared reflective coating was applied.

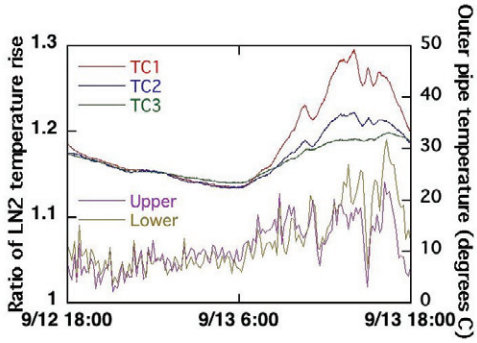

Fig. 3. Left axis represents the ratio of the liquid nitrogen temperature rise between TP2 and TP3 to that between TP5 and TP6. The terms “Upper” and ”Lower” denote temperatures measured using platinum resistance thermometers on the upper and lower surfaces of the inner pipe, respectively. Right axis represents the typical temperature on the cryogenic pipe surface. TC1 and TC3 are the temperatures of the cryogenic pipe surface in non-shaded and shaded conditions, respectively. TC2 is the temperature of the cryogenic pipe surface on which the infrared reflective coating was applied.

strong effect of direct sunlight can be seen in this figure. The temperature variation in the shade is very similar to that recorded in the laboratory, although the variation in the shade was slightly greater probably due to movement of the air. If the weather is cloudy and not warm, the difference between shaded and non-shaded temperatures becomes small, such as that recorded on September 5. On September 9, the construction of the coating was finished. Although sunlight conditions were nearly the same, the temperatures of surfaces with and without the coating were quite different. The temperature was reduced by over 10 degrees centigrade due to the coating. On the basis of the reduction of the outer pipe temperature, a reduction of the heat leak is expected.

The effect of the reduction of the outer pipe temperature on the heat leak is shown in Fig. 3. The left axis is the ratio of the liquid nitrogen temperature increase between TP2 and TP3 to that between TP5 and TP6. The terms “Upper” and “Lower” denote thermometers used on the upper and lower surfaces of the inner pipe, respectively. Outer pipe temperatures are shown for comparison. Data of the ratio are rather jagged and undermine the accuracy of the measurement system, but there is an obvious rise in accordance with the rise in the outer pipe temperature for positions exposed to the sun during the daytime between 6:00 and 18:00. It should be noted that the ratio during the nighttime, in which the three outer pipe temperature curves almost coincide with each other, is not unity. This is probably due to the structure of the cryogenic pipe and the heat leak therefore is not completely the same for the two regions. The ratio increases by around 10% from the nighttime to the daytime, which means that the heat leak is reduced by approximately 10%. By reducing the outer pipe temperature, a non-negligible heat leak reduction is obtained.

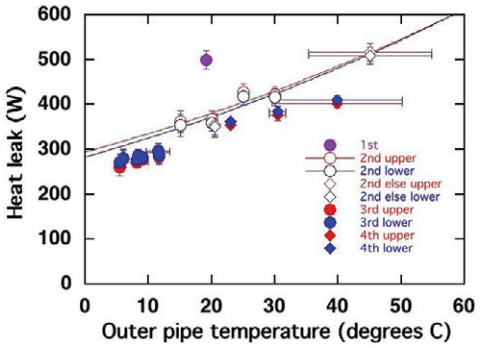

Fig. 4. The heat leak measured during the first to fourth cooling tests. These values are arranged according to average outer pipe temperatures. "1st", "2nd", "3rd" and "4th" denote data measured during the first to fourth cooling tests, respectively. "Upper" and "lower" indicate that the temperatures were measured using platinum resistance thermometers on the upper and lower surfaces of the inner pipe, respectively.

The results of the heat leak measured during the first to fourth cooling tests are shown in Fig. 4. The heat leak was estimated using the temperature rise between positions TP1 and TP7, a distance of about 175 m, the measured flow rate, and the published specific heat capacity of liquid nitrogen. Although the platinum resistance thermometers were calibrated before they were set at their positions, the calibration was checked in situ using the procedure described elsewhere [1] and the measured values were corrected by the result. Data are arranged with respect to the average outer pipe temperature. The outer pipe temperatures were measured at the points shown in Fig. 1 and the average outer pipe temperature is the weighted average of these temperatures by the length of the pipe in the sun, in the shade and coated. The error bar of the outer pipe temperature is the range of the measured outer pipe temperatures.

The heat leak was reduced during the cooling tests [1, 2]. It might be difficult to see the effect of the coating applied between the third and fourth cooling tests on values of the heat leak because only 23% of the cryogenic pipe between TP1 and TP7 was coated at that time, and variation of the heat leak following application of the coating was smaller than the estimated uncertainty of the measurement. The reduction of the heat leak during the fourth cooling test relative to the second is mainly derived from the improvement achieved between the second and third cooling tests. During this time, the number of supports for the inner pipe was reduced and parts of the inner pipe that had not been wrapped properly by the multilayer insulation were also amended [2]. Application of the coating to the whole cryogenic pipe would lead to a reduction of the heat leak during the daytime. Our research group is planning to further reduce the heat leak of CASER2.

Acknowledgements

The authors thank Dr. Atsuo Iiyoshi, Chairman of the Board of Trustees and Chancellor of Chubu University, for his continuous encouragement throughout this work. The authors acknowledge Dr. Hiroshi Fujiwara, a professor of Keio University and President of the Nano-Opt Energy Corporation, for his financial support of this work. We also thank JFE Steel Corporation for supplying steel pipes for the construction of the test facilities. Parts of this work were supported by a grant from the Strategic Research Foundation Grant-aided Project for Private Universities Ministry of Education, Culture, Sports, Science and Technology, Japan.

References

[1] Watanabe H, Sugino M, Sun J, Ivanov Y, Hamabe M, Kawahara T, Yamaguchi S, *Physica C* 471 (2011) 1304.
[2] Watanabe H, Ivanov Y, Sun J, Hamabe M, Kawahara T, Yamaguchi S, in preparation.
[3] Yamaguchi S, Kawahara T, Hamabe M, Watanabe H, Ivanov Y, Sun J, Iiyoshi A, *Physica C* 471 (2011) 1300.
[4] Nasu Y, Hamabe M, Yamaguchi S, Kusaka S, Ishiguro Y, *Proc. ICEC22/ICMC2008* (2008) 489.
[5] Yamaguchi S, Yamaguchi T, Nakamura K, Hasegawa Y, Okumura H, Sato K, *Rev. Sci. Instrum.* 75 (2004) 207.

Available online at www.sciencedirect.com

SciVerse ScienceDirect

Physics Procedia 27 (2012) 372 – 375

Physics Procedia

ISS2011

A new layout of HTS tapes and their critical currents for DC power cables

Jian Sun[a,*], Hirofumi Watanabe[a], Makoto Hamabe[a], Toshio Kawahara[a], Atsuo Iiyoshi[b], Satarou Yamaguchi[a]

[a] *Center of Applied Superconductivity and Sustainable Energy Research, Chubu University, 1200, Matsumoto-cho, Kasugai, Aichi 487-8501, Japan*

[b] *Chubu University, 1200, Matsumoto-cho, Kasugai, Aichi 487-8501, Japan*

Abstract

We investigated the gap effects on the critical current of the middle tape in the paralleled arrangements of three straight BSCCO tapes with monolayer, 2-layer and 3-layer structures to improve the cable superconducting performance by the tape arrangement. The critical current of the BSCCO tape increases with the decreasing of the gap for the monolayer structure, increases by 11% for the 2-layer and decreases by 15% for the 3-layer structure. A new layout of HTS tapes for the DC power cable is presented. The critical current of the BSCCO tape in a cable with a new layout may increase by 10%.

Keywords: HTS cable; Critical current; BSCCO; DC transmission; Gap effect

1. Introduction

The DC superconducting power transmission (SC-PT) system has been studied at Chubu University for being free from of AC losses [1]. In the DC SC-PT system, the coaxial cable is used and the high temperature superconducting (HTS) tapes are spirally and closely wounded along a former as two conductors for each polarity of the DC electric power [2]. The number of the tapes in each conductor is different because of their different radii. In order to make the magnetic flux line circular around the cable, the HTS tapes are wounded as close as possible. However, the gap can not be avoided by using the tape conductors for their polygonal shape [3]. If the same number of the same tapes are used for each conductor, additional space between the tapes will be produced because of the different circumference of each layer.

The property of the HTS tapes in the HTS cable is affected by their configurations such as gaps and layer-structures [4]. In the AC HTS cable, the gap effect are studied to reduce the AC losses [5]. The critical current of a tape in the cable is affected by the external field from the other tapes recently reported by Hamabe et al. [6]. Previously, we investigated the gap effects on the critical current of the tape in the triple paralleled arrangements of three straight BSCCO tapes with a mono-layer structure to optimize the

*Corresponding author. Tel.: +81 568 51 9286; Fax: +81 568 51 9413
Email address: j_sun@isc.chubu.ac.jp (Jian Sun)

1875-3892 © 2012 Published by Elsevier B.V. Selection and/or peer-review under responsibility of ISS Program Committee
doi:10.1016/j.phpro.2012.03.488

layout of the HTS tapes in the cable. In the case of mono-layer structure, the critical current increases with the decreasing of the gap and would be enhanced for close winding [7]. On the other hand, the multi-layer structure is necessary for high current capacity transmission. The gap for each layer and the relative position are important parameters for the tape winding in the cable with the multi-layer structures.

In this technical report, the measurement of the critical current against the gap is continued by varying the lateral position for the multi-layer structures. We consider a new layout of HTS tapes for the DC power cable through the experiment. The critical current of a tape in the cable with new layout is tested. Through the experiments, we investigate the design of DC HTS power cables to improve the cable property by the tape arrangements.

2. Experiments

The DI-BSCCO® tapes (Type HT-CA) are used in the experiment [8, 9]. The cross section of the tape is 4.5 mm × 0.35 mm with 0.05 mm copper laminated layer on both sides of the tape [9]. The critical current of the BSCCO tape is 160 A in the self field at 77 K.

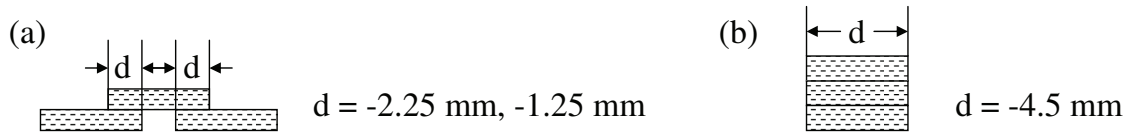

Fig. 1: A diagram of the arrangements of three HTS tapes for (a) 2-layer and (b) 3-layer with different gaps.

The setup of the critical current measurement is similar with that in the previous report [7]. The samples with the length of ~ 27 mm are prepared in consideration as an infinitely long wire and surrounded with one Kapton tape layer for insulation with each other. Three voltage taps are soldered on each tape with space of 8 and 10 cm. The voltage signals are measured by a KEITHLEY 2700 multimeter. The I - V curves are measured by the standard four-probe method at the temperature of 77.3 K. The current is fed into three tapes in series mode. Figs. 1a and b show the arrangements of three HTS tapes for 2-layer and 3-layer structure with different lateral space gaps. d is the distance between the edges of the tapes. There is a gap of 2 mm between the tapes in the second layer for $d = -1.25$ mm and no gap for $d = -2.25$ mm as in Fig.1a.

3. Results and discussion

The E - I characteristic curves of the BSCCO tape are obtained by normalizing the voltages to the distance between the voltage taps. Fig. 2a shows comparisons of E-I curves of a BSCCO tape for single and triple arrangements with different gaps. The critical current is determined at the electric field criterion of 1 μV/cm. Fig. 2b summarizes the critical currents of the BSCCO tape with respect to the gap between the tapes in the 2-layer and 3-layer structures together with the mono-layer structures as in the previous report [7]. The critical current of single tape is measured to be 166 A. In the case of 2-layer structure, the critical current of the middle tape becomes larger than that of the single one. When $d = -1.25$ mm, the critical current increases by 11% to 184 A compared with the single one. The critical current of a tape in the 2-layer structure becomes maximum even if there is a gap between the tapes in the second layer. However, the critical current of the BSCCO tape decreases sharply by 17% to 137 A for the 3-layer structure.

The magnetic field distributions are calculated by the commercial finite element method code (ANSYS) [10, 11, 12]. To illustrate the effect of the self-field from the current by the neighboring tapes, Figs. 3 a - d present the magnetic flux lines for single and triple tape arrangement in the 2-layer and 3-layer structure with different gaps, respectively. The transport current of 160 A in each tape is assumed to be uniformly distributed in the cross section of the Ag-sheathed BSCCO filaments zone. Hence the cross section of the transport current area is assumed to be 4.5 mm × 0.25 mm without the laminated copper layer [9]. For 2-layer structure, the flux lines become flat and loose. When the gap is −1.25 mm, the magnetic flux lines

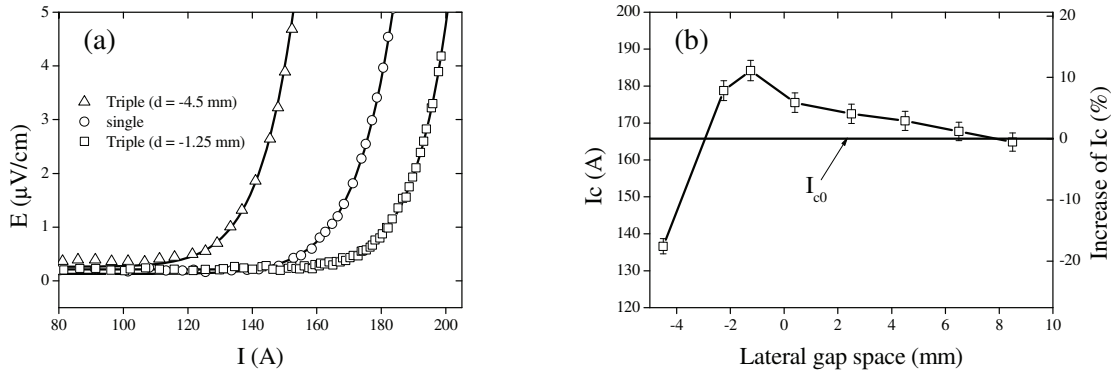

Fig. 2: (a) The E - I curves of the BSCCO tape for single and triple arrangements with d of −4.5 mm and −1.25 mm. (b) The dependence of I_c of the DI-BSCCO tape on the gap between the tapes.

are almost parallel to the tape wide surface of the middle tape as Fig. 3b, which results in the reduction of the perpendicular component of the magnetic field. Therefore, the critical current becomes maximum.

Through the measurements and calculations, we could optimize the tapes arrangement in the cable. Figure 4 shows a new layout of the cross section configuration of the tapes for a 2 kA DC HTS cable together with the present one. The inner diameter of the inner and outer conductor for both configurations are same, i.e., 18 mm and 26 mm, respectively. In the case of present cable, 16 and 23 tapes are spirally wounded as close as possible around a supporter with small gaps (< 0.5 mm) between the tapes for the outer and inner conductor. In the optimized cable, 16 tapes for the outer conductor is wounded as present one. 18 tapes are used for the inner conductor and arranged in the 2-layer structure. The gaps between the tapes for the inner and outer layer of the inner conductor is 1.9 and 2.2 mm because of the different diameter of each layer.

Figure 5a shows a diagram of three insulated tapes spirally winding around a supporter with a diameter of 2.6 cm and the twist pitch is around 25 cm. The same current flows through the three 54-cm-long BSCCO tapes. As shown in the cross-sectional view, there is a gap of 2 mm between two tapes in the inner layer close to the supporter. The measured $E - I$ curves of the tape in the cable is shown in Fig. 5b. Compared with single one, the critical current increases by 10% to 182 A and hence could be improved by optimizing the tape arrangements in the DC HTS power cable.

4. Conclusion

We have investigated the dependence of critical current of the BSCCO tapes on the lateral space gap between the tapes in the three straight paralleled tapes with the 2-layer and 3-layer structures. Critical current of a BSCCO tape is improved by arranging relative position in the 2-layer structures. However,

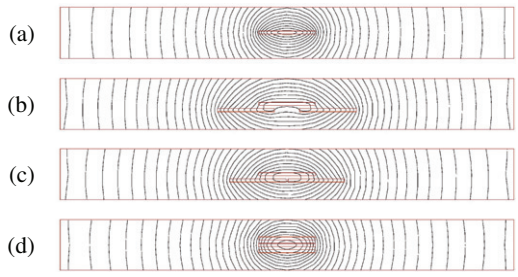

Fig. 3: The calculated magnetic flux lines for single (a) and triple arrangements (b-d) with 160 A in each tape.

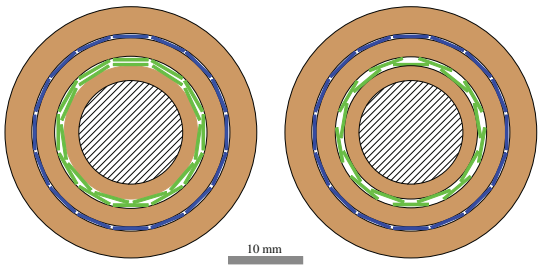

Fig. 4: A scheme of the cross section configuration of the tapes for 2 kA DC HTS cable.

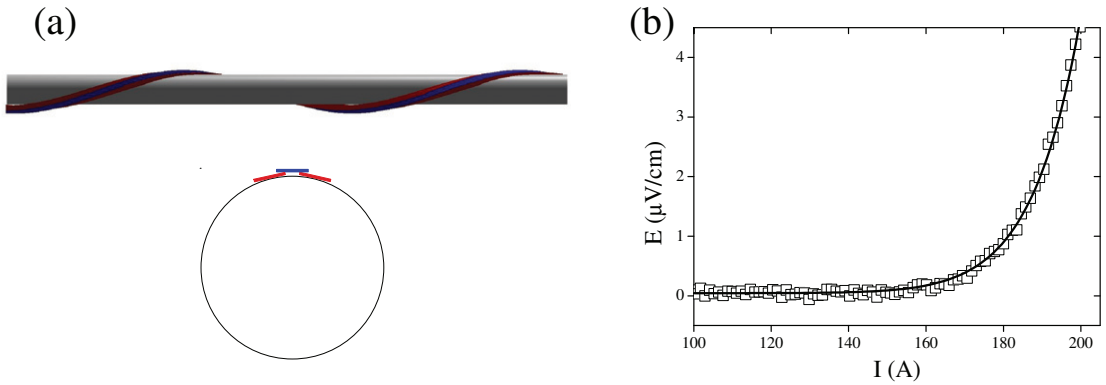

Fig. 5: (a) Three DI-BSCCO tapes helically surrounding a supporter with 2-layer structure with the gap 2 mm in the second layer as the cross section image in the insert. (b) $E - I$ characteristics of a tape in the cable winding.

critical current is degraded in the 3-layer structure with a tape-on-tape stack arrangement. Through the experiments and calculations, a new layout of the cable configuration is given, which may improve the superconductivity of the BSCCO tapes in the DC HTS power cable.

Acknowledgement

The authors acknowledge Dr. Hiroshi Fujiwara, a professor of Keio University and the president of Nano-Opt Energy Corporation, for his financial support. We also acknowledge the support by NEDO, Ministry of Education, Culture, Sports, Science and Technology (MEXT), and Chubu University Grant (A).

References

[1] Hamabe M, Sasaki A, Famakinwa T, Ninomiya A, Ishiguro Y, Yamaguchi S.Cryogenic system for DC superconducting power transmission line. *IEEE Trans Appl Super* 2007;**17**:1722–5.
[2] Yamaguchi S, Kawahara T, Hamabe M, Watanabe H, Ivanov Y, Sun J et al. Design and construction of 200-meter high temperature superconducting DC power cable test facility in Chubu University. *Proc ICEC 23 - ICMC 2010*; p.1041–7.
[3] Amemiya N, Li Q, Ito K, Tekeuchi K, Nakamura T, Okuma T. Ac loss reduction of multilayer superconducting power transmission cables by using narrow coated conductors. *Supercond Sci Technol* 2011;**24**:065013.
[4] Sato S, Amemiya N. Electromagnetic field analysis of YBCO coated conductors in multi-layer HTS cables. *IEEE Trans Appl Super* 2006;**16**:127–30.
[5] Jiang Z, Amemiya N, Nakhata M. Numerical calculation of AC losses in multi-layer superconducting cables composed of coated conductors. *Supercond Sci Technol* 2008;**21**:025013.
[6] Hamabe M, Sugino M, Watanabe H, Kawahara T, Yamaguchi S, Ishiguro Y et al. Critical current and its magnetic field effect measurement of HTS tapes forming DC superconducting cable. *IEEE Trans Appl Super* 2011;**21**:1038–41.
[7] Sun J, Yamauchi S, Sugino M, Watanabe H, Hamabe M, Kawahara T et al. Critical current measurements for desing of superconducting DC transmission power cable. *Physica C* 2011;**471**:1313–6.
[8] Kikuchi M, Ayai N, Fujikami J, Kobayashi S, Yamazaki K, Yamada S et al. Progrss in high performance DI-BSCCO wire. *AIP Conf Proc* 2008;**986**:407–15.
[9] Ayai N, Yamazaki K, Kikuchi M, Osabe G, Takaaze H, Takayama H et al. Electrical and mechanical properties of DI-BSCCO type HT reinforce with metallic sheathes. *IEEE Trans Appl Super* 2009;**19**:3014–7.
[10] ANSYS® Academic Teaching Advanced, Release 12.1 ANSYS Inc. www.ansys.com.
[11] Farinon S, Fabbricatore P, Gömöry F. Critical state and magnetization loss in multifilamentary superconducting wire solved through the commercial finite element code ANSYS.*Supercond Sci Technol* 2010;**23**:115004.
[12] Fabbricatore P, Farinon S, Innocenti S, Gömöry F. Magnetic flux shielding in superconducting strip arrays. *Phys Rev B* 2000;**61**:6413–21.

Available online at www.sciencedirect.com

SciVerse ScienceDirect

Physics Procedia 27 (2012) 368 – 371

Physics Procedia

ISS2011

Observation of the thermosiphon effect in the circulation of liquid nitrogen in HTS cable cooling system

Yury Ivanov[a*], Hirofumi Watanabe[a], Makoto Hamabe[a], Toshio Kawahara[a], Jian Sun[a], Satarou Yamaguchi[a,b]

[a]*Center of Applied Superconductivity and Sustainable Energy Research, Chubu University, Kasugai, Aichi 487-8501, Japan*
[b]*Department of Electric Engineering, Chubu University, Kasugai, Aich, 487-8501, Japan*

Abstract

It is traditionally considered that superconducting technology is just the way that will help to overcome the energy crisis and improve the environmental safety of the electricity production. However, real achievements in this field still insufficient to build commercial long power transmission lines. In particular, cooling systems constructed using expensive coolant circulation pumps have to be improved. Our previous calculations show that the use of a thermosiphon effect may reduce both the heat load and the required coolant circulation pump power and, ideally, would completely abandon the forced circulation. Direct experimental verification of this approach has been carried out at the new 200-meter HTS DC experimental facility of the Chubu University. The thermosiphon effect was clearly observed in satisfactory agreement with theory, although the change in elevation of the cryopipe was small. Our results will be used to design an effective HTS cable cooling system based on natural circulation of the coolant.

Keywords: power transmission; high-temperature superconducting cables; liquid nitrogen; cooling system; thermosiphon effect

1. Introduction

According to current concepts, future power delivery and distribution systems will be based on superconducting technology. Widely discussed "Smart Grids" are very important to reduce energy losses and improve resistance against natural and technological disasters. Despite the fact that superconductivity was discovered a century ago and superconducting power transmission (SC PT) lines are being developed for a long time, but their industrial application has not yet begun. Recently, DC SC PT lines have begun to attract more and more attention due to their significant advantages over traditional AC ones [1, 2]. Although energy dissipation is negligible in the real DC HTS cables, the power is required to remove heat incoming through thermal insulation in order to keep temperature below critical value. The creation of the high-performance heat insulation can be attributed as main technological problem now. Moreover, SC PT lines are very expensive apparatuses that slow down their development and implementation.

A new scheme that allows to address both issues was proposed several years ago. Namely, it was suggested to use natural circulation of coolant which may arise due to its density difference along the circulation loop if the system has elevation change. Therefore, it is possible to reduce the capacity of the coolant circulation pump or even completely abandon the forced circulation of the coolant and consequently reduce the heat load and save cost. The feasibility of

* Corresponding author. Tel.: +81-568-51-9286 ; fax: +81-568-51-9413 .
E-mail address: ivanov@isc.chubu.ac.jp .

1875-3892 © 2012 Published by Elsevier B.V. Selection and/or peer-review under responsibility of ISS Program Committee
doi:10.1016/j.phpro.2012.03.487

this approach was shown by theoretical calculations for different configurations of the system [3, 4]. Since all existing experimental facilities are characterized by use of corrugated cryopipes with high coefficient of hydraulic resistance and the difference of elevation of circulation circuit is usually small, the thermosiphon effect could not be seen against the background of a large pressure drop and did not attract attention of researchers.

Nomenclature

g	gravitational acceleration, 9.81 m/s^2
H	difference in elevation between highest and lowest points of cryopipe, m
h_{HT1}	difference in elevation between heater HT1 and lowest point of cryopipe, m
J	volume flow rate, l/min
Δp	pressure drop, Pa
$TP_1 ... TP_7$	average temperatures measured by pairs of thermometers TP11/TP12...TP71/TP72, K
ΔT_{eff}	effective temperature difference, K
$\alpha_{HT1} = h_{HT1}/H$	relative difference in elevation between heater HT1 and lowest point of cryopipe
γ	thermal expansion coefficient of liquid nitrogen, 4.4 kg/m^3 K

2. Experimental

An experimental study was undertaken using 200 meter test facility at the Chubu University. This is DC SC PT line built in 2009-2010, having a number of significant differences from other similar devices designed to achieve a record length of the cable and the minimum cost of the apparatus. In particular, straight cryopipes are applied to reduce to a minimum hydraulic resistance instead of commonly used corrugated ones [5, 6]. The elevation difference of the cable route is about 2.6 m which allows to appear thermosiphon effect. Liquid nitrogen (LN_2) flows through a fairly narrow space between the cable of the diameter of 35 mm and the inner surface of the cryopipe with the diameter of 57.2 mm. The actual temperature distribution can be estimated by 7 pairs of platinum resistance thermometers located at different positions. In order to simulate heat load and vary LN_2 density the cryopipe was equipped with three compact heaters with capacity of up to 350 W, two of which are located at the downstream and upstream sections of the cryopipe. The pressure drop was measured between termination cryostats by means of two pressure gages (see Fig. 1). Automated measurement system reads data from more than 500 sensors with a period of 3 s [7].

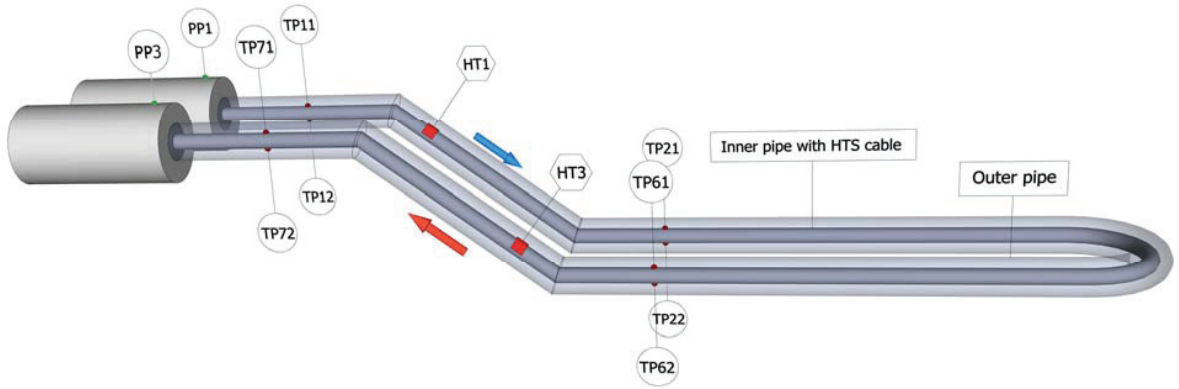

Fig. 1. Sketch of the HTS cable experimental facility at the Chubu University. Only terminal units, cryopipes, several thermometers (TP), pressure gages (PP), and heaters (HT) are shown in the picture. Level difference is 2.6 m.

The single-phase thermosiphon effect is very weak accounting for 44 Pa per 1 m elevation difference per 1 K temperature difference of LN_2. Therefore, a minimum circulation rate should be used to achieve a large temperature difference in order to reveal the effect.

3. Results

The experiments described were carried out during the third cooldown of the system (February-March 2011). The dependence of the pressure drop on the circulation rate of LN_2 was determined at first. The results are shown in Fig. 2. The measurements were made under the ambient heat load of about 240 W distributed between the inclined segments of the cryopipe. Data were collected by varying the LN_2 flow rate within 4.4-13.3 l/min that corresponds to the flow velocities within 0.045-0.14 m/s and Reynolds numbers within 4700-14200 (turbulent flow). The temperature difference was from 2.0 to 0.7 K. Points represent data averaged over 10 min (200 samples). The upper (blue) curve shows the design pressure drop obtained by the method described in [7]. The bottom (orange) curve shows the same curve corrected for the thermosiphon effect. It can be seen that the experimental points at lowest flow rates correspond to the second curve well.

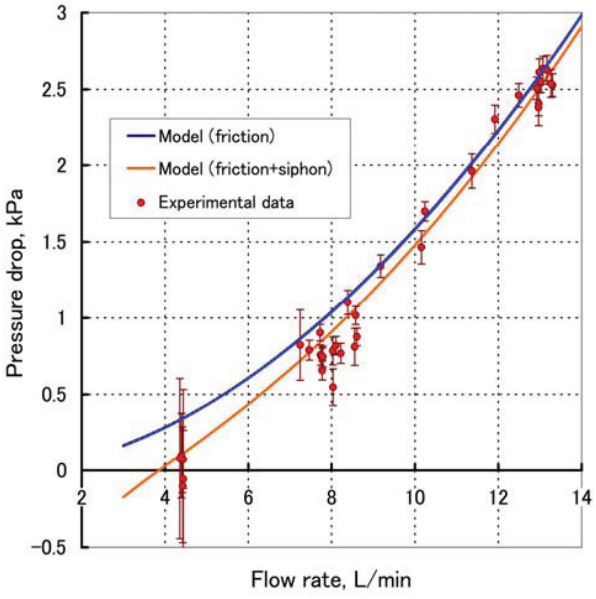

Fig. 2. Pressure drop as a function of LN_2 flow rate at constant heat load. Design curve is shown in blue. Orange curve is the design curve corrected for the natural thermosiphon effect. Experimental points represent averaged over 10 min data.

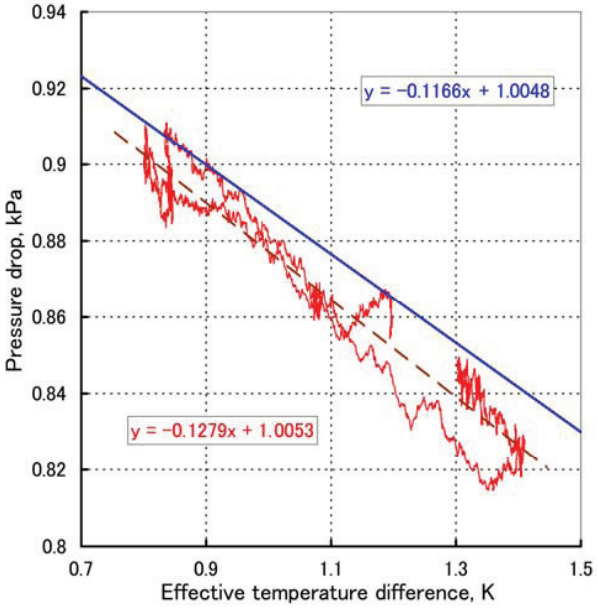

Fig. 3. Pressure drop as a function of the effective temperature difference between the inclined segments of the cryopipe varied by the heater HT1. Flow rate is fixed at 7.85±0.05 l/min. The data are smoothed over 4 min.

The second series of the experiments was carried out to study the behavior of the pressure drop as a function of the temperature difference between the inclined sections of the cryopipe at the constant LN_2 flow rate. The presence of the heater HT1 at the downstream section allows rapid heating of LN_2 to create up to a negative temperature difference that expands the range of the measurements. The actual temperature distributions inside the inclined sections of the cryopipe were estimated from the readings of pairs of the thermometers TP11/TP12, TP21/TP22, TP61/TP62, and TP71/TP72 with consideration for the flow velocity. Fig. 3 shows the results obtained by using the heater HT1 at J = 7.85±0.05 l/min. If HT1 temperature changes slowly, the pressure difference due to the thermosiphon effect can be described by a linear expression

$$\Delta p = A\Delta T_{eff} + B \qquad (1)$$

where

$$\Delta T_{eff} = (TP_7 - TP_1) - \alpha_{HT1}(TP_2 - TP_1)$$
$$A = gH\gamma \qquad (2)$$
$$B = A(1.77\alpha_{HT1} - 1.1)/J$$

Complex form of the effective temperature difference, ΔT_{eff}, is due to the heater HT1 is in an intermediate position. Numerical coefficients in Eq. 2 give the experimentally determined correction for the additional heating of the LN_2 that occurs at sites between inclined segments of cryopipe and thermometers. Heater power was varied trapezoidally from 0 to 250 W at the rate of 2 W/min. The total duration of the experiment was 5 hours. The data are smoothed over 4 min in order to reduce noise. The solid line exhibits the calculated pressure drop. The dashed line fits unsmoothed full set of the experimental points. Fig. 3 can be easily interpreted. The efficiency of the thermosiphon is characterized by the slope of the line. A point of intersection with the vertical axis ($\Delta T_{eff} = 0$) gives the net pressure drop without the influence of the thermosiphon effect. A point of intersection with the horizontal axis ($\Delta p = 0$) defines effective temperature difference at the given total heat load when the pump can be switched off and the natural circulation of LN_2 will occur. The observed behavior of the pressure drop is in satisfactory agreement with the calculated one. Deviations are caused by the inability to take into account accurately the temperature distribution in the inclined sections of the cryopipe, as well as some unreported slope of the horizontal part of the cryopipe.

4. Conclusions

We investigated experimentally the thermosiphon effect arising in the real HTS cable cooling system in the presence of elevation difference which can be used to save coolant circulation pump power. The study was carried out using 200 m DC SC PT line at the Chubu University. Experimental facility was not adapted to utilize natural circulation, but because we have achieved record low values of the pressure drop, it was allowed direct observation both the natural effect (caused by the heat penetrating through the insulation) and effect due to intentional local heating of LN_2. The obtained results show that by using bypass between termination cryostats the natural circulation can occur at the flow rate of about 4 l/min.

Acknowledgements

The authors thank Dr. Atsuo Iiyoshi, the Chairman of the Board of Trustees and the Chancellor of Chubu University, for his encouragement during the course of this work. The authors acknowledge financial support from Dr. Hiroshi Fujiwara, the professor of Keio University and the president of Nano-Opt Energy Corporation.

References

[1] Hirose M, Masuda T, Sato K, Hata R. High-Temperature Superconducting (HTS) DC Cable. *SEI Tech Rev* 2006;61:29-35.

[2] Hassenzahl W, Gregory B, Eckroad S, Nilsson S, Daneshpooy A, Grant P. *A superconducting DC cable. EPRI Report 1020458.* CA: Palo Alto: EPRI; 2009.

[3] Ivanov Yu, Watanabe H, Kawahara T, Hamabe M, Sun J, Yamaguchi S. Superconducting power transmission line cooled with naturally circulating LN_2. *Proc 23 Int Cryog Eng Conf Int Cryog Mater Conf 2010* 2011;1017-22.

[4] Ivanov Yu, Radovinsky A, Zhukovsky A, Sasaki A, Watanabe H, Kawahara T, et al. Compact counter-flow cooling system with subcooled gravity-fed circulating liquid nitrogen. *Physica C* 2010;470:1895-8.

[5] Yamaguchi S, Hamabe M, Yamamoto I, Famakinwa T, Sasaki A, Iiyoshi A, et al. Research activities of DC superconducting power transmission line in Chubu University. *J Phys Conf Ser* 2008;97:012290.

[6] Yamaguchi S, Kawahara T, Hamabe M, Watanabe H, Ivanov Yu, Sun J, et al. Design and construction of 200-meter high temperature superconducting DC power cable test facility in Chubu University. *Proc 23 Int Cryog Eng Conf Int Cryog Mater Conf 2010* 2011;1041-7.

[7] Ivanov YV, Watanabe H, Hamabe M, Sun J, Kawahara T, Yamaguchi S. Circulation pump power for 200 m cable experiment. *Physica C* 2011;471:1308-12.

OPTIMIZATION OF PELTIER CURRENT LEAD FOR APPLIED SUPERCONDUCTING SYSTEMS WITH OPTIMUM COMBINATION OF CRYO-STAGES

Toshio Kawahara[1], Masahiko Emoto[2], Hirofumi Watanabe[1], Makoto Hamabe[1], Jian Sun[1], Yury Ivanov[1], and Satarou Yamaguchi[1,3]

[1]Center of Applied Superconductivity and Sustainable Energy Research, Chubu University, 1200 Matsumoto, Kasugai, Aichi 487-8501 Japan

[2]Department of Large Helical Device Project, National Institute for Fusion Science, Gifu 509-5292 Japan

[3]Department of Electric Engineering, Chubu University, 1200 Matsumoto, Kasugai, Aichi 487-8501 Japan

ABSTRACT

The reduction of electric power consumption of the cryo-cooler during the working conditions of applied superconducting systems is important, as superconductivity can only be stored at low temperature and the power required for the cooling determines the efficiency of the systems employed. Use of Peltier current leads (PCLs) represents one key solution to effect heat load reduction on the terminals in systems. On the other hand, the performance of cryo-coolers generally increases as the temperature increases given the higher Carnot efficiency. Therefore, combination with suitable mid-stage temperatures represents one possible approach since the thermal anchor can enhance the performance of the system by reducing the electric power consumption of the cryo-coolers. In this paper, we discuss this possibility utilizing an advanced configuration of PCL with a commercially available high temperature cooler. Over 50% enhancement of the performance is estimated.

KEYWORDS: Peltier current lead, PCL, DC transmission and distribution system, cryo-cooler performance, heat leak on the current lead

Advances in Cryogenic Engineering
AIP Conf. Proc. 1434, 1017-1024 (2012); doi: 10.1063/1.4707020

INTRODUCTION

One key technology available to help mitigate the energy problems in the world involves the use of superconducting (SC) systems given the energy-saving zero direct current (DC) resistance associated with such systems. Many applications have been proposed, and among these applications SC transmission lines have been intensively examined in several countries. SC transmission and distribution systems have the capability to make unstable natural energy available worldwide, and it is one of the reasons why SC transmission lines have been intensively investigated.

We have developed SC DC transmission lines of 20 m [1] and 200 m for use in working trial systems [2], and investigated high performance cryogenics for the purpose of reducing the heat leak, a requirement for the development of effective competitive applications. For example, high performance terminal systems are key technologies employed for small applications such as internet data centers, and the conduction heat leak on the current leads has a large effect on system performance. Thus, many researchers have been interested in high performance current leads [3]. We have studied the Peltier current lead (PCL) as a high performance current lead for use in SC applications, including gas-cooled systems [4-11].

On the other hand, we should consider the performance of cryo-coolers for system optimization, where the coefficient of performance (COP) of cryo-coolers generally becomes large at higher working temperatures. In this context, effective cooling of the coolant and current leads allows for a new optimization scheme which could enhance system performance. We are considering multi-stage configurations for PCLs and discuss the use of such advanced current lead designs in applied SC systems.

MODELS

Simulation Methods

We used thermal balance equation (1) for the heat leak estimation [12] and the Seebeck effect [4,13],

$$\frac{d}{dx}\left(k(\theta)A\frac{d\theta}{dx} + \alpha I\theta \right) - f\dot{m}C_p\frac{d\theta}{dx} + \frac{I^2\rho(\theta)}{A} = 0 \qquad (1)$$

where k represents the thermal conductivity, θ is the temperature, Cp is the specific heat, A is the cross section of a current lead, I is the current, and ρ is the resistivity. The Seebeck effect ($\alpha I\theta$) is added in the first term for considering the PCL. Gas cooling is expressed by the heat exchange ratio f between the cold gas and the current lead with the mass flow $\dot{m}$ of liquid nitrogen. $f = 0$ signifies no heat exchange, and represents conduction cooling. $f = 1$ signifies that the cold gas can exchange heat with the current lead under equilibrium conditions, and represents self-cooling. In this paper, we assume that there is no gas cooling, and hence f is set to 0.

We optimized the shape of the current lead to calculate the minimum heat load Q per 1 kA. As we have been using high Tc superconductors cooled by liquid nitrogen, the cold side temperature was set at 77 K and the higher side temperature at another end was 300 K. The optimized shape factor L/A for minimum Q was obtained using these boundary conditions, where L represents the length of the current lead and Q the heat load at the lower end of the current lead.

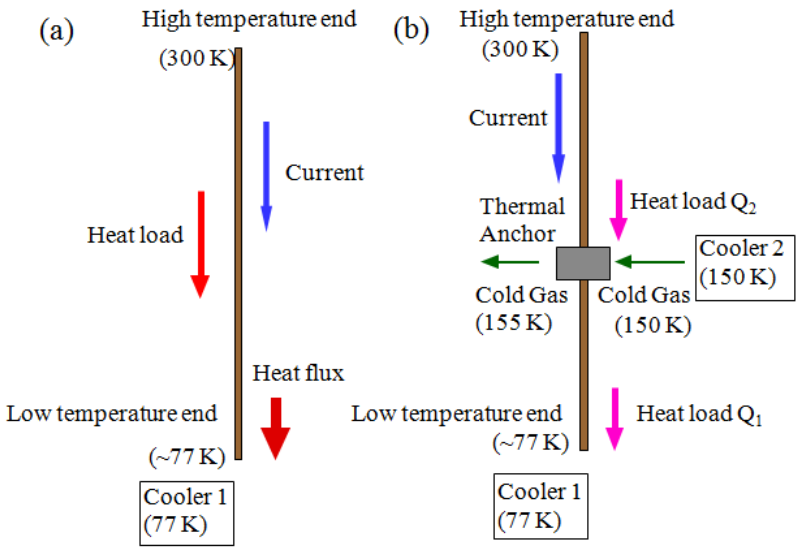

FIGURE 1. Schematics of the multi-stage current lead. (a) conventional and (b) multi-stage configurations.

Current Lead Design

A comparison of a conventional current lead and multi-stage current lead is shown in FIGURE 1. In the conceptual design, the conventional single stage current lead (FIGURE 1 (a)) possesses a single copper lead. The higher temperature end is set at room temperature (300 K) while the other end is set at, for example, 77 K. Then, the lower temperature end is cooled by a single cryo-cooler worked at low temperature. The multi-stage current lead has a mid-temperature stage as shown in FIGURE 1 (b), and this stage is cooled by another cryo-cooler (cooler 2) working at higher temperature, for example around 150 K.

During current feeding, the entire heat load goes into the lower temperature end for the single stage configuration. With the multi-stage configuration, the heat load (Q_2) emanating from the higher temperature end is removed by cooler 2 and only Q_1 generated at the lower side on the current lead is removed by cooler 1. Although the total heat load is the same, part of the heat load is removed by the higher performance of cooler 2.

Next, we show how this heat load is split on the current lead. FIGURE 2 (a) shows the temperature distribution on the current lead. The positions are normalized by the length of the current lead. The top and bottom temperatures are set to 300 K and 77 K, respectively. In this case, we can see the flat position-dependence at 300 K, which reflects the balance between the heat coming from the outer side and heat load, and then the entire heat load generated on the current lead goes into the lower temperature end. The temperature-dependence of this heat load is plotted in FIGURE 2 (b). The heat load at each temperature should be removed by the corresponding cryo-cooler. As an example of the multi-stage configuration operating at a mid-temperature stage of 188 K, the heat load of 35.2 W/kA should be removed by cryo-cooler 2. For the single stage configuration, the heat load of 42.5 W/kA must be removed by the single cryo-cooler working at 77 K. For the multi-stage configuration, only the difference in heat load generated between the stages has to be removed, and the cryo-cooler working at 188 K should have a higher COP.

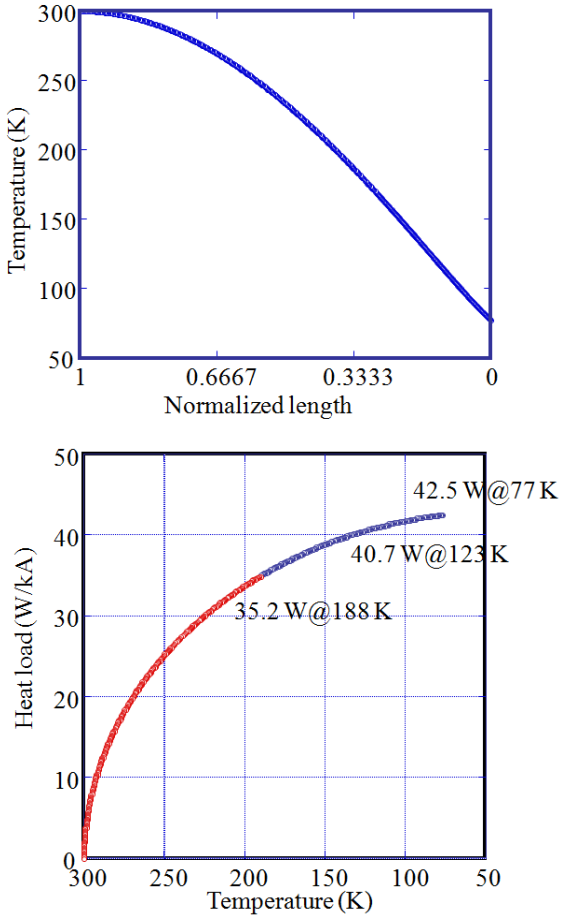

FIGURE 2. Temperature distribution on the current lead (a), and heat load distribution (b) as a function of temperature.

Peltier Current Lead

For effective thermal insulation on the current lead, use of the PCL has been extensively discussed [11]. The PCL is a current lead which consists of thermoelectric elements and copper leads for HTS applications. Two fundamental processes contribute to the reduction in heat leak on the PCL. Firstly, low thermal conductivity can insulate the conduction heat. Secondly, the Peltier effect of the thermoelectric elements removes the heat on the PCL.

Therefore, the properties of the thermoelectric elements will determine the performance of the PCL. In an effort to estimate these properties, we employed representative thermoelectric parameters measured at actual elements. FIGURE 3 shows the properties determined in the present study. The temperature-dependence of the Seebeck coefficient is plotted in FIGURE 3 (a) and that of the resistivity in FIGURE 3(b). The resistivity is larger than that of the copper lead and the Seebeck coefficient is only large near room temperature. Therefore, the combination of the thermoelectric elements at the higher temperature side and the copper lead set on the other side represents the usual configuration in the PCL.

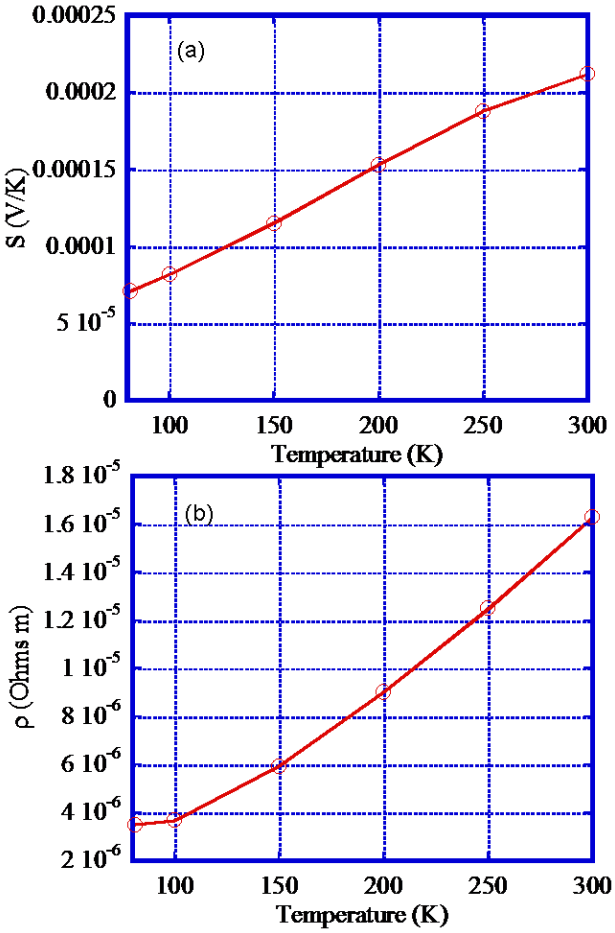

FIGURE 3. Temperature-dependence of thermoelectric properties. (a) Seebeck coefficient, and (b) resistivity.

Using these parameters, the temperature distribution was calculated using thermal balance equation (1) as shown in FIGURE 4. In this figure, the temperature distribution is plotted as a function of the form factor L/A multiplied by the current I. Given the small thermal conductivity, a large temperature difference is observed on the thermoelectric elements and then a relative small temperature difference is observed on the copper current lead, where the short copper lead can be used in the PCL compared to a whole copper current lead. With this configuration, the heat leak of the PCL is 31.6 W/kA. Thus, we can achieve an approximate 40% reduction in heat load in comparison with the copper current lead.

DISCUSSION

TABLE 1 shows examples of the COP of a commercially available cryo-cooler at 77 K. The Stirling cycle cryo-cooler has higher performance (COP 0.067) compared with other coolers [14], and about 20% of the Carnot efficiency at 77 K. In this case, when we remove heat of 1 W, the electric power for the operation is 15 W. Thus, in the case of the PCL with a single stage, the electric power for the cryo-cooler is 458 W.

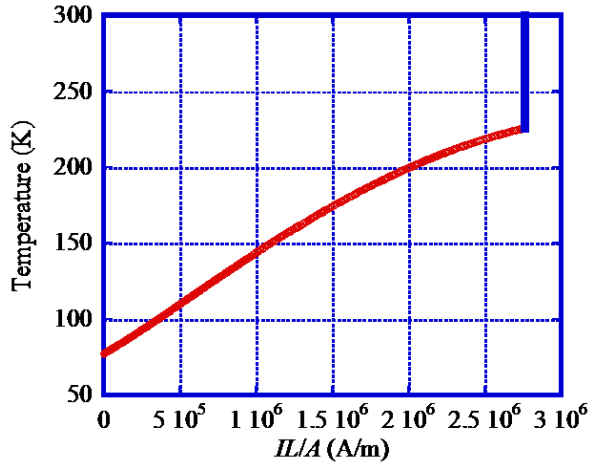

FIGURE 4. Temperature distribution on the current lead. Positions are normalized by current, length and cross-section of the current lead, where *L*/*A* is a form factor.

Now we combine the multi-stage configuration on the copper part in the PCL. FIGURE 5 shows the heat load split to on the current lead at the higher and lower temperatures. The heat load at the higher temperature part of the current lead decreases as the mid-stage temperature increases, and the heat load at the lower temperature part of the current lead also increases. Although the total heat load is the same, the COP of the cryo-cooler changes with temperature, and the total electric power required for the cooling is dependent on the mid-stage temperature.

We have several commercial cryo-coolers which operate at 188 K, and these have been widely used for bio materials [15]. This cryo-cooler can now be used for cooling on the mid-stage. Therefore, we set the mid-stage temperature to 188 K and estimated the electric power consumption to cool down the current lead. We supposed that the COP of the cryo-coolers is 20% of the Carnot efficiency. As the heat load is split to 20.8 W/kA at 188 K and 10.9 W/kA at 77 K, the electric power consumption at the cryo-cooler is 221 W/kA. In this case, the electric power for a single stage with COP of 20% (equivalent to a Stirling cooler) is 458 W/kA. Thus, the energy saving is about 52 %, which corresponds to a current lead with performance of 15.2 W/kA.

Now we do not modify the thermoelectric elements in the simulation, and this results in a 52% saving of energy for the applied superconducting systems. Further optimization including the shape factor of the thermoelectric elements might be effective, and this approach is currently in progress. The next generation cryo-cooler should have a COP of 0.1 at 77 K, which corresponds to about 30% of the Carnot efficiency. For a high

TABLE 1. COP and energy consumption of representative cryo-coolers [14,16]

	Pulse tube	GM	Stirling
COP (77 K)	0.018	0.045	0.067
Electric power for the heat load of 1W	55 W	22 W	15 W

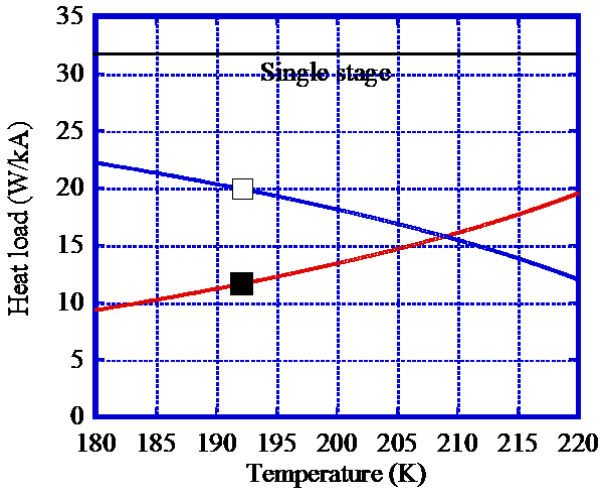

FIGURE 5. Mid-stage temperature-dependence of heat loads. Filled squares denote heat load on the current lead at the lower temperature part, and open squares denote heat load on the current lead at the higher side. The single stage case is also plotted.

temperature cryo-cooler working at for example 188 K, such a high performance cooler can easily be developed. Moreover, a triple stage configuration can be employed for the optimization. We are now considering the mid-stage temperature with the view to optimizing the current lead as the total performance of the systems.

SUMMARY

With respect to thermoelectric materials, use of a PCL shows significant heat leak reduction compared with a copper current lead. In this case, a multi-stage configuration is also useful when employing a copper current lead in the PCL. As the heat load at the higher and lower temperature sides of the current lead can be removed by the use of a different cryo-cooler, the total electric power consumption for the cryo-cooler can be reduced by over 50% with the use of a 188 K (-85^{o}C) cryo-cooler. This type of cooler is commercially available and should have a higher performance.

Therefore, employment of a multi-stage configuration is very useful in reducing the working heat load on the current lead. Future optimizations are important, such as determination of the optimal configuration of shape factors and thermoelectric materials. Investigations concerning these issues are now in progress.

ACKNOWLEDGEMENTS

We acknowledge Dr. Hiroshi Fujiwara for his support with construction of the 200 m superconducting facilities of CASER-2 and also the Ministry of Education, Culture, Sports, Science and Technology (MEXT) as “Collaboration with Local Communities” Project for Private Universities for support with the 20 m facilities (CASER-1). Part of this work was supported by a grant from the Strategic Research Foundation Grant-aided Project for Private Universities (MEXT) and a Grant-in-Aid for challenging Exploratory Research (MEXT). Additional support for part of this work was provided by the Nippon

Sheet Glass Foundation for Materials Science and Engineering, and the Future Energy Research Association.

REFERENCES

1. Yamaguchi, S., Hamabe, M., Yamamoto, I., Famakinwa, T., Sasaki, A., Iiyoshi, A., Shultz, J., Minervini, J., Hoshino, T., Ishiguro, Y. and Kawamura, K., *J. Phys.: Conf. Ser.* **97**, 012290 (2008).
2. Yamaguchi, S., Ivanov, Y., Sun, J., Hamabe, M., Watanabe, H. and Kawahara, T., *Advances in Cryogenics Engineering* **57** (this publication) (2011).
3. Xuan, X. C., Ng, K. C., Yap, C. and Chua, H. T., *Cryogenics* **42**, pp. 779-785 (2002).
4. Yamaguchi, S., Yamaguchi, T., Nakamura, K., Hasegawa, Y., Okumura, H. and Sato, K., *Rev. Sci. Instrum.* **75**, pp. 207-212 (2004).
5. Hasegawa, Y., Sato, K., Okumura, H., Nakamura, K., Yamaguchi, S. and Miyake, K., Cryogenics, **42**, pp. 495-500 (2002).
6. Yamaguchi, T., Okumura, H., Nakamura, K. and Yamaguchi, S., *IEEE Trans. Appl. Supercond.* **13**, pp. 1910-1913 (2003).
7. Yamaguchi, T., Okumura, H., Nakamura, K. and Yamaguchi, S., *IEEE Trans. Appl. Supercond.* **13**, pp. 1914-1917 (2003).
8. Sato, K., Okumura, H. and Yamaguchi, S., *Cryogenics* **41**, pp. 497-503 (2001).
9. Yamaguchi, T., Mizutani, S., Moriguchi, M., Okumura, H., Nakamura, K. and Yamaguchi, S., *IEEE Trans. Appl. Supercond.* **14**, pp. 1719-1722 (2004).
10. Kawahara, T., Fujii, T., Emoto, M., Hamabe, M., Sun, J., Watanabe, H. and Yamaguchi, S., *Physica C: Supercond.* **470**, pp. S1011-S1012 (2010).
11. Fujii, T., Fukuda, S., Kawahara, T., Emoto, M., Sugino, M., Sun, J., Hamabe, M., Watanabe, H. and Yamaguchi, S., *Advances in Cryogenic Engineering*, **55**, pp. 561-568 (2010).
12. Wilson, M. N., "*Superconducting Magnets*" Clarendon Press, Oxford, 1983, pp.256-272.
13. Okumura, H. and Yamaguchi, S., *IEEE Trans. Appl. Supercond.* **7**, pp. 715-718 (1997).
14. http://www.aisin.com/
15. Takemasa, K. and Yoshida, F., *Sanyo Technical Review* **23**, pp. 42-53 (1991) in Japanese.
16. http://www.cryomech.com/

THE EXPERIMENTS OF 200-METER SUPERCONDUCTING DC POWER CABLE IN CHUBU UNIVERSITY AND THE ESTIMATION FOR LONGER CABLE COOLING

Satarou Yamaguchi[1,2], Yury Ivanov[1], Jian Sun[1], Hirofumi Watanabe[1], Makoto Hamabe[1],Toshio Kawahara[1,2] and Atsuo Iiyoshi[1]

[1]Center of Applied Superconductivity and Sustainable Energy Research (CASER), Chubu University, 1200 Matsumoto, Kasugai, Aichi 487-8501 Japan

[2]Department of Electric Engineering, Chubu University, 1200 Matsumoto, Kasugai, Aichi 487-8501 Japan

ABSTRACT

After the 200-meter superconducting DC power cable experimental facility had been completed in spring of 2010, three experiments have been done until March, 2011. We adapt the straight pipe for the inner cryogenic pipe to reduce the heat leak and the pressure drop of liquid nitrogen circulation because the surface area is minimized for the straight pipe, and the terminal cryostats of the cable ends are movable to absorb the shrinkage of the cable in the cooling-down phase and the expansion in warming-up phase to reduce the tensile strain of the high temperature superconductor tape. We also continue the Peltier current lead experiment to reduce the heat leak at the terminal. We performed several kinds of the experiments to obtain the basic data for a long cable system. We changed and improved the experimental devices during the experiments. The pressure drop of the liquid nitrogen circulation was around 1 kPa for the flow rate of 10 L/min in the experiment. We summarized the experimental results briefly, and estimate the pressure drop of the circulation for a longer cable system (~2 km) depending on the experimental conditions.

KEYWORDS: DC transmission and distribution system, superconducting system, coolant circulation, cryogenic pipe, vacuum pumping.

INTRODUCTION

Advances in Cryogenic Engineering
AIP Conf. Proc. 1434, 1959-1965 (2012); doi: 10.1063/1.4707135

We began a DC superconducting power transmission experiment from the beginning of 2000 in Chubu University (CU), and the major subject was to develop a low heat leak terminal, and we developed the Peltier current lead [1, 2, 3]. We completed the first experimental device (CASER-1) in 2006 by the aid of Japanese government (MEXT). This is a 20-meter DC cable test facility, and the high temperature superconductor (HTS) tapes were used to make the superconducting (SC) cable bought from Sumitomo Electric Industries, Ltd (SEI). The material of the HTS is Bi-2223. Several ideas were tested to realize an actual system, such as the reduction of the heat leaks at the terminal and the cryogenic pipe, and the pressure drop of the circulation [4, 5, 6]. The system was cooled down and warmed up six times until 2010, and no degradation of the DC cable was found in the system. After the experiment of CASER-1, we started to construct the 200-meter cable experiment in 2008, and it is called CASER-2. The construction was started in the middle of 2009, and completed in January 2010. The major subjects of the experiments are as below,

1) Safety cable system for thermal contraction and expansion,
2) Low heat leak at the terminal,
3) Low heat leak in the cryogenic pipe (achieve high vacuum degree without baking),
4) Low pressure drop of the coolant circulation,
5) Energy storage function using ferromagnetic materials,
6) No limitation of natural resources such as nickel and low cost of the system,
7) Data obtainment for longer cable system.

Until June 2011, we performed the experiments three times, and try to get the data for a longer cable system. In this paper, we describe the experimental results, and discuss the coolant circulation of a longer cable system mainly based on the experimental data.

SYSTEM PARAMETERS AND MODIFICATION OF EXPERIMENT

The parameters of the experimental device are summarized in TABLE 1. The first experiment had been done from January 2010 to March 2010. The second experiment had been done from August 2010 to October 2010, and the third experiment has been performed from January 2011 to March 2011.

After the first experiment, we modified the experimental device to improve its performance. The vacuum pressure of the cryogenic pipe is the order of the 10^{-1} Pa in the first experiment because we used the mechanical booster pump, but a turbo-molecular pump was used in the second and third experiments to achieve high vacuum degree. It is quite effective even if we did not use the baking of the cryogenic pipe, and the vacuum pressure of 10^{-5} Pa was achieved. The pumping time is also important issue for the long cable system, and we did several experiments for this subject.

TABLE 1. The Parameters of the 200-meter cable test facility

	Parameters	Comments
Cable	±10kV, 2kA@78K, Bi-2223 HTS tape, ~200 meter	Bipolar co-axial cable, 23 tapes for inner (2 layers) and 16 HTS tapes for outer
Cryo-pipe	Iron pipe for outer pipe, SS pipe for inner pipe.	Bellows pipe inserted into inner straight pipe for compensation of the thermal contraction.
Refrigerator	1kW@77K	Stirling cycle refrigerator (15kW), Operation temperature ~ 72K to 82K
Pump system	flow rate ~ 10 L/min, pressure drop ~ 1.5kPa	Upper and lower tanks are equipped to control low pressure and flow rate.

We pay attention about the strain of the HTS tapes in the cable because if the tensile strain of the HTS tape is high, the critical current of the HTS tape was reduced [7, 8, 9]. The thermal contraction of the cable is about 0.3 % and is 60 cm in the 200-meter cable. In order to avoid the strain of the cable, the cable ends were not fixed to the terminal cryostats in the direction of the thermal contraction, but the other two directions are fixed to the cryostats [10]. We added thermometers to more precisely measure the temperature, and made several changes and additions of other instruments for the second and third experiments. The liquid nitrogen temperature of the refrigerator was controlled from 72 K to 82 K by the experimental conditions. Finally, we achieved a current of 2 kA at 78 K.

COOLANT CIRCULATION

FIGURE 1 shows the relation of the flow rate and the temperature difference between the inlet and the outlet temperatures of the liquid nitrogen in the second and the third experiments. The design value of the circulation flow rate is around 10 L/min because we can neglect the ac losses of the cable and the heat load should be low. We could control the flow rate in the experiment completely for the different vacuum pressure. Since the temperature difference varied inversely with the flow rate, the inverse functions are plotted as the least-square fitting curves in FIGURE 1. When the temperature difference is low for the same flow rate, it means that the heat leak is low. Therefore, when the vacuum pressure is low, the heat leak is low in the third experiment. In order to estimate the effect of the vacuum degree of the thermal insulation of the cryogenic pipe, we performed the experiment for vacuum pressures of about 0.1 Pa and 10^{-5} Pa in the third experiment.

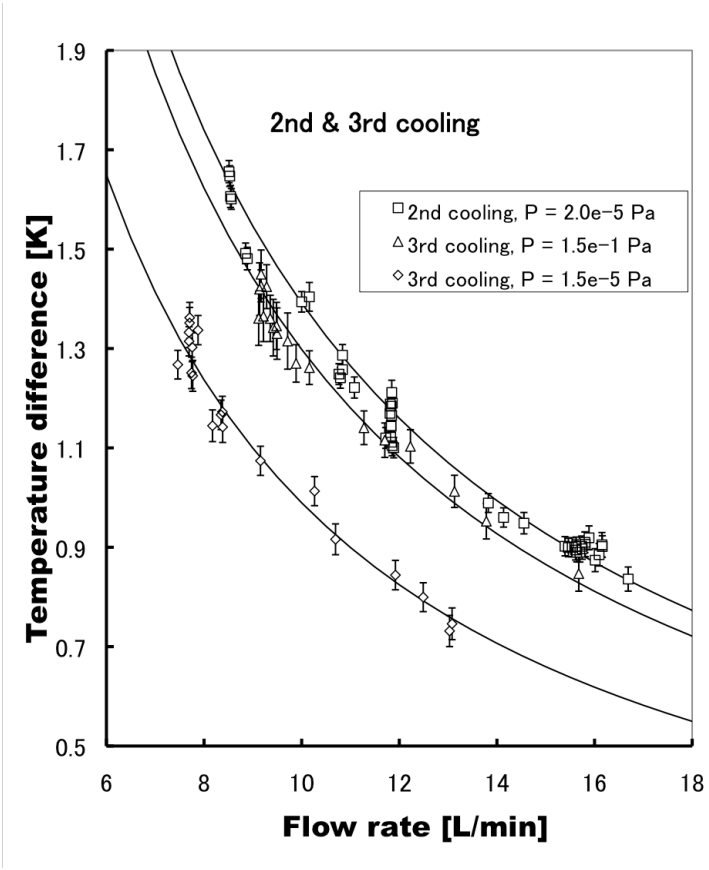

FIGURE 1. The experimental data of the flow rates and temperature differences of liquid nitrogen in the second and third experiments.

The heat leak is almost 25% lower in high vacuum degree. We changed the thermal insulation design of the cryogenic pipe in the third experiment from the second experiment, and this design is effective to reduce the heat leak. The heat leak also was affected by the temperature of the ambient conditions since the cryogenic pipe is located outside of the laboratory. The second experiment was done in the summer, and the third experiment in the winter, therefore the difference of the heat leak between the second and the third experiments also depends upon the difference of the ambient temperatures.

FIGURE 2 shows the experimental data of the flow rate and pressure drop in the third the present liquid nitrogen pump, we use an upper and lower tank system. The liquid nitrogen flows into the cryogenic piping from the upper tank, and flows back into the lower tank from the piping. The pump forces flow of the liquid nitrogen from the lower tank to the upper tank through the refrigerator. The elevation difference between two tanks is 2 meters. The experimental data are plotted with the error bars, and a fitting curve is shown. Error bars are calculated by the time average of the pressure drop. The model calculation results, based on semi-empirical formula of fluid dynamics, are also plotted in the figure. This is the design curve of the experimental device. Two cryostats of the terminals are located in the same laboratory, and the pipeline is out-door, and their elevation levels are different (see FIGURE 3). Therefore, thermal siphon effect should be considered for the circulation [11, 12] that reduces the circulation power because the density in low temperature nitrogen is high and the inlet of the cryogenic pipe is located at a higher place within the pipeline.

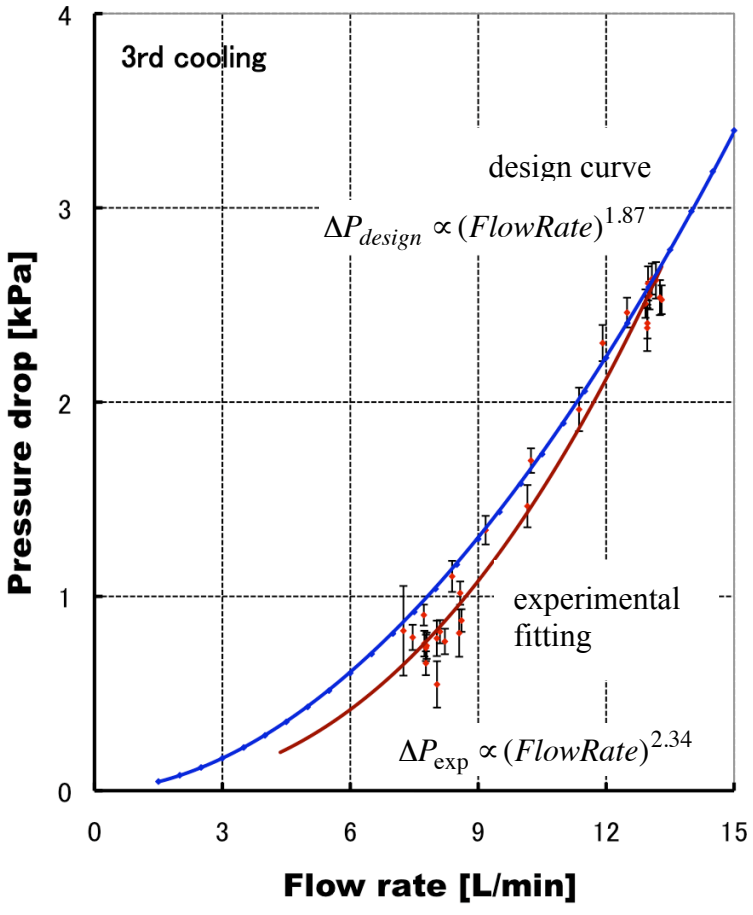

FIGURE 2. The experimental data of the flow rate and pressure drop between inlet and outlet temperatures of liquid nitrogen.

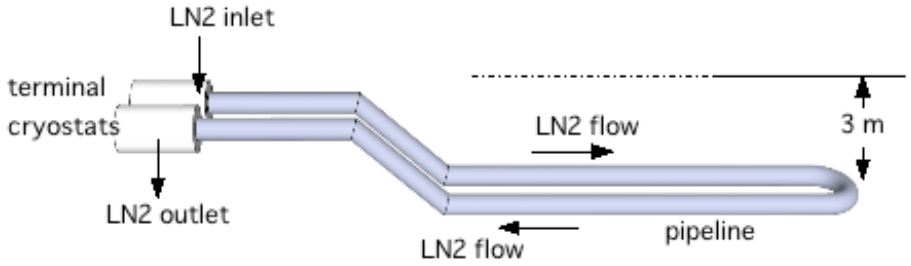

FIGURE 3. Layout of the terminal cryostats and the pipeline.

Therefore, the model calculation pressure drops are higher than the experimental data due to the siphon effect. The curve fitting to the experimental data is shown in the FIGURE 2, and the power factor of the flow rate for the pressure drop is about 2.34. On the other hand, the power factor of the model is 1.87 because the model calculation does not include the siphon effect.

When the heat leak is low, the pressure drop is lower for the same temperature difference between the inlet and the outlet temperature by theoretical consideration, this is confirmed by the experimental data as compared with the second and the third experiments. The quantitative data is still being analyzed.

ESTIMATION FOR LONGER CABLE SYSTEM

The final goal of the research is to make a long power transmission line; therefore, we should obtain the experimental data that can be applied to a longer cable system. Depending on the semi-empirical formula of fluid dynamics, the pressure drop ΔP is proportional to the length, the friction factor and the square of the flow rate, and given by

$$\Delta P \propto (FrictionFactor) \times (FlowRate)^{2.0} \times (Length) \tag{1}$$

If the temperature difference of the inlet and the outlet temperatures is fixed, the flow rate should be proportional to the length; therefore the pressure drop is given by

$$\Delta P \propto (FrictionFactor) \times L^3 \tag{2}$$

where L is the length of the pipeline. But the friction factor for the straight smooth pipe is lower for higher flow rate slightly, as given by

$$FrictionFactor \propto (\mathrm{Re})^{-0.25} \tag{3}$$

where Re is the Reynolds number. Finally the pressure drop is presented by

$$\Delta p \propto L^{\alpha+1} \qquad \alpha = 1.75 \sim 2.00 \tag{4}$$

where the power factor α depends on the surface conditions of the pipe and the cable. If we use α of 2, it gives the highest-pressure drop of the circulation. Therefore, we can estimate the pressure drop of a longer cable system. TABLE 2 shows one of the examples to estimate the pressure drop for 2 km cable system from the experimental data of 200-meter cable's. Since the output pressure of the present liquid nitrogen pump is around 0.1 MPa,

TABLE 2. Estimation of the pressure drop of the circulation for the 2 km cable system.

Distance	0.2 km	2.0 km
Temperature Rise	1.5 K	1.5 K
Flow Rate	10 L/min	100 L/min
Pressure Drop	1.5 kPa	~ 1.5 MPa

we must develop a new pump for the temperature difference of 1.5 K for 2 km system. The centrifugal pump is used in the present time, and it is good for large flow rate and low output pressure. Therefore, we should start the selection of the pump type if we develop a high output pressure pump.

On the other hand, the temperature difference is inversely proportional to the flow rate and the pressure drop is almost proportional to the square of the flow rate indicated as below,

$$\Delta T \propto \dot{m}^{-1}$$
$$\Delta p \propto \dot{m}^{\alpha} \tag{5}$$

where ΔT is the temperature difference, and $\dot{m}$ is the mass flow rate.
Therefore, if we allow the temperature difference of 6 K (for example, 70 K to 76 K), the flow rate is 25 L/min, and the pressure drop is 93.8 kPa approximately. The heat leak of the cryogenic pipe has been studied in Chubu Univ., and the value of 0.5 W/m has been achieved in the test stand [13], it is less than half of cryogenic pipe's in the 200-meter cable experiment in the present time. And if the heat leak is half, the flow rate can be half. Therefore, the pressure drop is 23.4 kPa for the flow rate of 12.5 L/min. These estimated parameters will able to be achieved by the present pump, and it is not necessary to develop a new pump.

DISCUSSIONS AND SUMMARY

The estimated result mentioned above shows that we will be able to go to the next stage of the 2 km cable system. The estimate used a power factor α of 2.0 in Eqs. (4) and (5) in the previous section; therefore, the estimated value of the pressure drop will be highest and it should be possible to perform the experiment. However, if we construct the cable length of 20 km, the pressure drop will be exceeded the value of 10 MPa for the present diameter of the cryogenic inner pipe. Therefore, we must use a larger diameter pipe to reduce the pressure drop of the circulation for a long cable system, but the heat leak will be increased for a larger pipe, thereby increasing pressure drop. Because of these considerations, we should continue to emphasize the effort to reduce the heat leak of the cryogenic pipe and the friction factor of the pipe and cable surfaces.

Another way is to use liquid helium as the coolant because it is already used in the large accelerator systems [14] as the several kilometer transmission line. However, the pressure drop and the pump power are higher than those of the liquid nitrogen system to remove the same heat leak. But if we use the liquid helium system, the cost of the superconducting wire is every cheap because we can use NbTi as the superconductor. Therefore, if we use the liquid helium system, the cost of the superconducting wire is

cheap, but the refrigeration system is expensive. This consideration also reveals the different temperature and material system such as MgB2 and liquid hydrogen system.

The outline approach might be a good way to develop from a short cable system to a long cable system. But if the length is shorter than several kilo-meter, we must consider the heat leak at the terminal, but the fundamental request is to overcome the copper cable's performance. In order to realize the high performance of the short distance superconducting power cable, we should develop the low heat leak current lead. We continue to develop Peltier Current Lead (PCL) in the past 10 years, and we tried various kinds of PCL's [15, 16]. If the heat leak of the terminal is low, we can apply various kinds of the superconducting systems such as magnets, transformers, motors and so on; therefore, it is important to develop the low heat leak current lead.

ACKNOWLEDGEMENTS

The authors acknowledge Dr. Hiroshi Fujiwara, a professor in Keio University and president of Nano-Opt Energy Corporation, for his financial support on the construction of 200 m superconducting facilities called CASER-2. The authors also thank Profs. T. Matsushita and Otabe E. Soji in Kyushu Institute of Technology, and Prof. K. Osamura in Kyoto Univ. and Prof. Ryo. Fukuda in Chubu Univ. for their valuable discussions. The authors thank Prof. B. Coppi, Drs. J. Minervini, L. Bromberg, M. Takayasu and L. Sugiyama in Massachusetts Institute of Technology (MIT) for long and kind collaboration. We also acknowledge JFE Steel Corporation for supplying the iron pipe to construct the 20-meter and the 200-meter test facilities.

REFERENCES

1. Yamaguchi, S., Takita, K. and Motojima, O., *Proc. 16th ICEC/ICMC1996*, 1996, pp. 1159-1162.
2. Okumura, H. and Yamaguchi, S., *IEEE Trans. Appl. Supercond.* **7**, pp. 715-718 (1997).
3. Sato, K., Okumura, H. and Yamaguchi, S., *Cryogenics* **41**, pp. 497-503 (2001).
4. Yamaguchi, S., Hamabe, M., Yamamoto, I., Famakinwa, T., Sasaki, A., Iiyoshi, A., Shultz, J., Minervini, J., Hoshino, T., Ishiguro, Y. and Kawamura, K., *J. Phys.: Conf. Ser.* **97**, 012290 (2008).
5. Hamabe, M., Nasu, Y., Ninomiya, A., Ishiguro, Y., Kusaka, S. and Yamaguchi, S., *Advances in Cryogenic Engineering* **53A**, 2008, pp. 168-172.
6. Ivanov, Yu., Radovinsky, A., Zhukovsky, A., Sasaki, A., Watanabe, H., Kawahara, T. and Yamaguchi, S., *Advances in Cryogenic Engineering* **55**, pp. 865-870 (2010).
7. Sugano, M., Shikimachi, K. Hirano, N. and Nagaya, S., *Supercond. Sci. Technol*. **23** 085013 (2010).
8. van der Laan, D. C., Ekin, J. W., Douglas, J. F., Clickner, C. C., Stauffer, T. C. and Goodrich, L. F., *Supercond. Sci. Technol*. **23** 072001 (2010).
9. Ochiai, S. and Okuda, H., *J. Cryo. Soc. Jpn.* **46**, pp. 212-219 (2011) (in Japanese).
10. Yamaguchi, S., Kawahara, T., Hamabe, M., Watanabe, H., Ivanov, Yu., Sun, J. and Iiyoshi, A., *Physica C* (2011) (in press).
11. Ivanov, Yu., Radovinsky, A., Zhukovsky, A., Sasaki, A., Watanabe, H., Kawahara, T., Hamabe, M. and Yamaguchi, S., *Physica C* **470**, pp. 1895-1898 (2010).
12. Ivanov, Yu. V., Watanabe, H., Hamabe, M., Sun, J., Kawahara, T. and Yamaguchi, S., *Physica C* (2011) (in press).
13. Nasu, Y., Hamabe, M., Yamaguchi, S., Kusaka, S. and Ishiguro, Y., *Proc. ICEC23-ICMC2008*, 2009, pp. 489-494.
14. Rubbia, C., Institute of Advanced Sustainability Studies (IASS), private communication.
15. Kawahara, T., Fujii, T., Emoto, M., Hamabe, M., Sun, J., Watanabe, H. and Yamaguchi, S., *Physica C* **470**, pp. S1011-S1012 (2010).
16. Kawahara, T., Emoto, M., Watanabe, H., Hamabe, M., Sun, J., Ivanov, Yu. and Yamaguchi, S., "Optimization of Peltier current lead for applied superconducting systems with the optimum combination of cryo-stages", CEC/ICMC2011, C2PoC-07, Spokane, USA (2011).

Journal of ELECTRONIC MATERIALS, Vol. 41, No. 6, 2012
DOI: 10.1007/s11664-011-1877-5

Thermoelectric Property Dependence on Performance of Peltier Current Leads Under Overcurrent Conditions

TOSHIO KAWAHARA,[1,3] MASAHIKO EMOTO,[2] MAKOTO HAMABE,[1] HIROFUMI WATANABE,[1] YURY IVANOV,[1] JIAN SUN,[1] and SATAROU YAMAGUCHI[1]

1.—Center of Applied Superconductivity and Sustainable Energy Research, Chubu University, Aichi 487-8501, Japan. 2.—National Institute for Fusion Science, Gifu 509-5292, Japan. 3.—e-mail: toshi@isc.chubu.ac.jp

Superconductivity can potentially provide a solution to the world's energy needs because superconducting transmission and distribution (T&D) systems can decrease losses and are also capable of integrating renewables into the power grid. At Chubu University we have built a 200-m-class superconducting direct-current T&D system (CASER-2). To minimize heat leakage from the current leads, we investigated thermoelectric materials. The Peltier current lead (PCL) is one of the key technologies that will enhance the performance of superconducting systems: as direct current (DC) flows through the current lead, thermoelectric elements on opposite terminations of the superconducting line can be used to decrease the heat ingress to the cryogenic environment (*n*-type on one end, *p*-type on the opposite end). The heat leakage to the cryogenic environment depends on the properties of the thermoelectric materials. In this paper, we estimate the performance of PCLs in cryogenic operations, including the potential for overcurrent operation, through both modeling and experiments at CASER-2.

Key words: Peltier current lead (PCL), superconducting applications, DC transmission and distribution system, BiTe alloy

INTRODUCTION

Thermoelectrics can help address the urgent need for energy. Superconducting systems can, on the other hand, improve the efficiency of generation and power delivery because the direct-current (DC) resistance (and power loss) of superconductors is zero. However, the total system performance of superconducting transmission and distribution (T&D) needs to be considered because superconductivity can only be achieved at low temperatures and refrigeration losses need to be considered. The overall efficiency of superconducting T&D is determined, in part, by the characteristics of the thermal insulation of the cryogenic environment. Superconducting T&D systems can also be useful for integration of intermittent renewables (wind, solar) by providing large power sharing coupled with large-scale transmission.

Several superconducting power delivery technologies have been studied at Chubu University[1] using 20-m-class and 200-m-class superconducting (T&D) test devices called CASER-1 and CASER-2, respectively. We have been investigating methods of improving the cryogenic performance of the superconducting system, including surface treatment of cryogenic pipes and low-power circulation systems to enhance system performance.[2,3] In addition, we have explored the use of thermoelectric materials placed in series with the superconductor and sharing the same current in order to minimize the cryogenic load in T&D systems. The approach consists of using a *p*-type material at one end of the line and an *n*-type material at the other end (the current in the DC system only flows in one direction). Since the cryogenic load in short-length superconducting cables is dominated by the terminations, the

(Received July 14, 2011; accepted December 17, 2011; published online January 26, 2012)

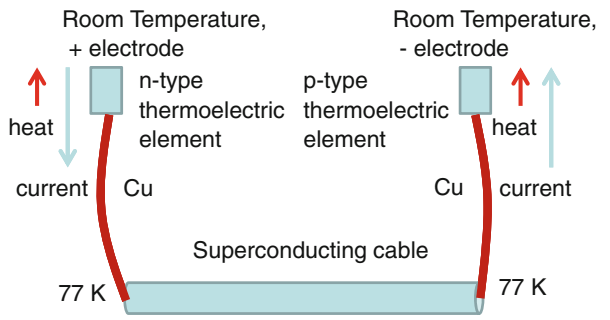

Fig. 1. PCL concepts. Thermoelectric elements are set on the higher temperature side. With DC feeding, heat can be pumped out to the higher-temperature end. Shape factors for the thermoelectric and Cu leads are optimized for minimum heat for given current such as I = 100 A.

Table I. Specifications of CASER-2 (200-m-class superconducting DC T&D system)

	Specification
Voltage	10 kV (bipolar)
Current	2 kA (inner 23 tapes, outer 16 tapes)
Length	~200 m
Undulation	2.7 m
Turn radius	2 m (minimum)

decrease in cryogenic load by use of Peltier current lead (PCL) elements results in substantial total load reduction. As a consequence, PCLs can be integrated into high-performance current leads for superconducting applications to reduce heat leakage at the terminals.[4,5]

A PCL, as shown in Fig. 1, consists of thermoelectric elements and a resistive element (usually copper or brass). It has been shown that the cryogenic load due to the current leads reduces the thermal conductivity and large Seebeck coefficient of the thermoelectric elements. Heat leakage from the PCL depends on the properties of the thermoelectric material.[6] We have investigated the performance of thermoelectric materials using the parameters of CASER-2. The specifications of CASER-2 are summarized in Table I. We have calculated the heat leakage from the PCL using a thermal balance equation with measured model parameters.[7]

It is known that there is an optimum shape factor (L/A, ratio of length L to cross-sectional area A of the current lead) for a given current.[8] Electric power applications have a wide range of operating currents; however, current leads are usually optimized for the maximum current. As a consequence, current leads are sometimes used with under- or overcurrent. In this paper, we discuss the dependence of the heat leakage from the PCL on the current and material parameters and compare these findings with the performance of the current lead measured during cooling experiments with CASER-2.

EXPERIMENTAL PROCEDURES AND SIMULATION METHODS

Thermoelectric parameters for modeling were measured for four commercial BiTe alloy samples, designated 1, 2, 3, and 4. Samples 1 and 2 were n-type materials, and samples 3 and 4 were p-type. Samples 1 and 3 were sintered materials, and samples 2 and 4 were solid-solution samples grown by the Bridgman method; therefore, the former samples should have higher electrical resistivity than the latter samples.

The resistivity ρ was measured by the four-terminal method at constant current. The Seebeck coefficient α was measured under small temperature differences that varied between 0 K and 6 K, controlled by a small heater attached to the electrode. The thermal conductivity κ was measured by the steady-state method through the same temperature variation. These values were used to calculate the figure of merit Z of the thermoelectric materials ($Z = \alpha^2/\rho\kappa$).

We estimated the heat leakage from the PCL by using a thermal balance equation described elsewhere[9–11] with model parameters measured in different experiments using test elements of samples 1–4 mentioned above. Here, the heat leakage is the cryogenic load at the lower-temperature end, including conductive heat by thermal conductivity and heat pumped by the Seebeck effect, where we used n-type material for the positive terminal and p-type material for the negative terminal (Fig. 1). The optimum L/A ratio and minimum heat leakage can be determined with the model.[4,6,12] The optimum length could be defined by the balance of the heat pump effect (for thermoelectric materials), conduction heat, and Joule heat generation in the current lead. We assumed current of 160 A for the initial optimization, as CASER-2 uses 160-A-class $Bi_2Sr_2Ca_2Cu_3O_{10}$ (BSCCO) tapes (DI-BSCCO; Sumitomo Electric Industries).

To determine the performance of the PCL in CASER-2, we measured the temperature of each component of the current leads, such as the thermoelectric elements and the copper leads. When the current I was zero, the heat leakage allows us to determine the effective thermal conductivity of the leads. We estimated the performance of the current lead for a finite current between 0 kA and 1.5 kA. The heat pump effects can be estimated by the temperature difference between the two ends of the thermoelectric materials, which increases with increasing current.

RESULTS AND DISCUSSION

Figure 2 shows the model thermoelectric parameters of the elements used with CASER-2. We used two different thermoelectric materials with higher

or lower resistivity as described in the previous section, with different temperature dependence of Z. The resistivity, which seems to be the most important factor in defining the shape factors, is plotted in Fig. 2. Samples 1 and 3 had higher resistivity (Fig. 2) and lower thermal conductivity than samples 2 and 4. On the other hand, the Seebeck coefficient was comparable for all samples. Samples 2 and 4 exhibited maximums of Z below room temperature and are therefore promising for use as PCLs.

Using these thermoelectric parameters, we calculated the heat leakage from the PCL with the optimum shape factor at I = 160 A. The optimized shape factors L/A are summarized in Table II and are indicated as PCL1, PCL2, PCL3, and PCL4. The optimum L/A ratios for the samples with low-resistivity thermoelectric elements are smaller compared with those with high resistivity. With shape factor L/A values optimized for 160 A, the current dependence of the heat leakage is shown in Fig. 3. The cryogenic load has a minimum at I = 160 A under these conditions for PCL1, PCL2, PCL3, and PCL4. For PCL1, the increase of the heat leakage is small for undercurrents below 160 A and steep for overcurrent above 160 A when compared with PCL2 of n-type material (Fig. 3a). A similar tendency can be seen for the p-type material (PCL3 and PCL4) in Fig. 3b.

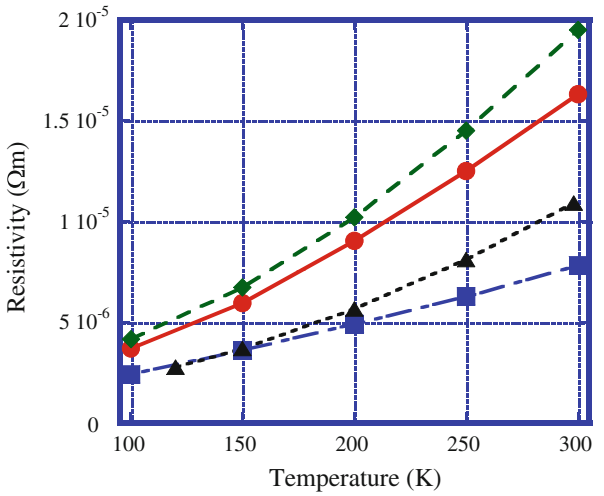

Fig. 2. Temperature dependence of resistivity for samples 1 (circles), 2 (squares), 3 (diamonds), and 4 (triangles).

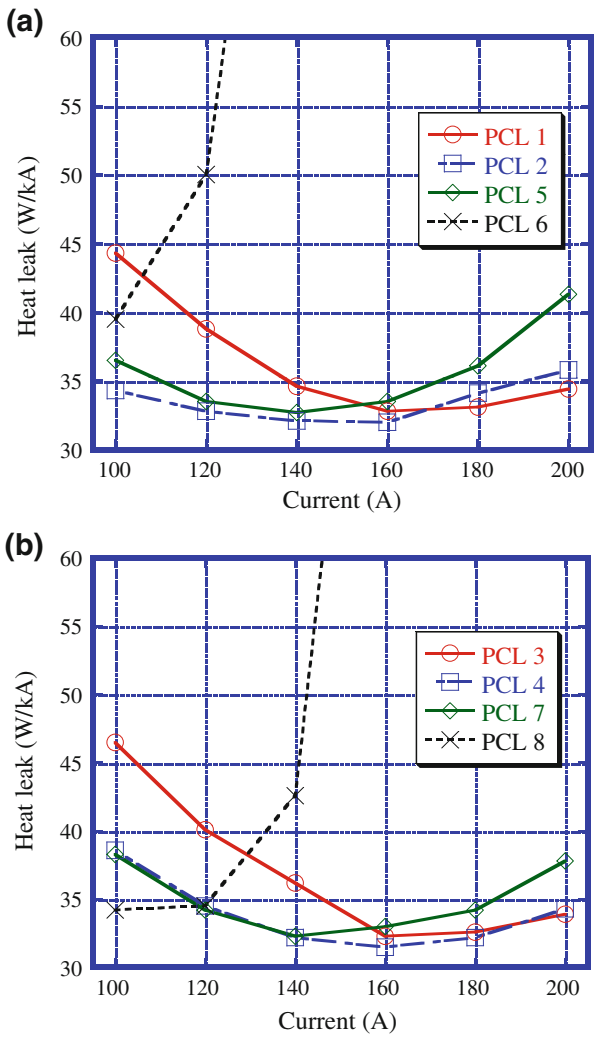

Fig. 3. Current dependence of heat leakage for: (a) n-type and (b) p-type materials. Open circles denote PCL1 and PCL3; open squares denote PCL2/PCL4. Open diamonds and crosses are simulated values on doubling the length of the elements of PCL4/PCL6 and PCL5/PCL7, respectively.

Table II. Optimized PCL shape factors (L/A)

	PCL				PCL (Double Length)				CCL	
	1	**2**	**3**	**4**	**5**	**6**	**7**	**8**	**9**	**10 (double length)**
L/A (BiTe) (1/m)	25	50	24	40	50	100	48	80	0	0
L/A (cooper) (1/m)	17,250	13,875	15,625	17,062	17,250	13,875	15,625	17,062	22,500	45,000

PCL1, PCL2, PCL3, and PCL4 are optimum. PCL5, PCL6, PCL7, and PCL8 are double length, as discussed in the text. L/A values of CCLs used in the simulation are also summarized.

We then estimated the heat leakage from the PCLs on doubling the length of the thermoelectric elements while keeping the shape factors of the copper lead constant. These results are referred to as PCL5, PCL6, PCL7, and PCL8, whose *L*/*A* values are summarized in Table II. One of the reasons why the current leads experience overcurrent conditions is the deviation of the optimum *L*/*A* caused by variation of the thermoelectric properties. Therefore, we only change the *L*/*A* of thermoelectric elements to compare the actual devices in CASER-2.

Due to these parameters and the shift of the optimum current giving the minimum heat leakage to a lower value, the initial optimum current of 160 A corresponds to an overcurrent condition. The current dependence of the heat leakage for the double-length PCL is shown in Fig. 3. In the calculation, the optimum current for the actual current leads with the minimum heat leakage is actually shifted. As shown for the current dependence, PCL6 and PCL8 are in a condition of severe overcurrent. The heat leakage rapidly increases as the current increases above 100 A, and it is very large at 160 A. On the other hand, the heat leakage increase is small for PCL5 and PCL7. Thus, the highly resistive samples such as PCL5 and PCL7 are better in overcurrent conditions.

For comparison, we also calculated the dependence of the cryogenic load on current for conventional current leads (CCL, without the thermoelectric element). For the case where the length of the optimized current lead is doubled, the cryogenic load at 100 A is approximately 5 W (about 50 W/kA) and increases very quickly for current above 140 A.

If the current lead is expected to experience overcurrent conditions, the PCL shape factor should be chosen for the high-resistivity samples. In CASER-2, we optimized the PCL shape factors using the parameters of samples 1 and 3. Unfortunately, the thermoelectric parameters of the materials used have different values, resulting from variation of the thermoelectric properties across samples. However, in this case we could achieve a suitable PCL current dependence for actual operation.

Figure 4 shows the measured current dependence of the temperature difference in the thermoelectric elements on the terminals of CASER-2. Large temperature difference (large heat pump effects) in the thermoelectric elements corresponds to low heat leakage from the low-temperature ends of the current lead. The initial optimum current is I = 160 A using the parameters of samples 1 and 3, and the shift of the maximum temperature difference is observed around I (total) = 1000 A, which corresponds to an average current of 63 A for the single PCL. The tendency in the current dependence resembles the condition of overcurrent operation with samples 5 and 7. The *L*/*A* ratio of the PCL thermoelectric elements in CASER-2 could be two times larger than the optimum value. There are additional deviations in the heat leakage as the actual variations of the thermoelectric parameters also cause current imbalance across the current leads. Another factor is that the actual temperature distribution could be affected by the liquid nitrogen level during the cooling experiments. On the other hand, the heat leakage at overcurrent conditions is suppressed, and we can operate at larger current. Thus, we actually succeeded in performing heat leakage measurements at 1.2 kA and a current feeding test at over 1.5 kA.

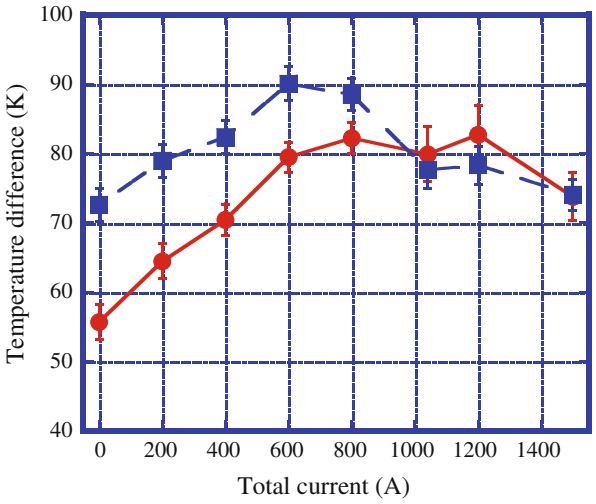

Fig. 4. Current dependence of the temperature difference between PCL thermoelectric elements. Current is the total current for the superconducting cable in CASER-2. Circles are for *n*-type PCLs, and squares for *p*-type PCLs.

Finally, we discuss the energy saving resulting from the different optimizations of the shape factors for the different thermoelectric elements. The difference of the heat leakage between samples 5 and 6 at I = 120 A is approximately 16.5 W/kA. This corresponds to consumed cryocooler power of 891 kWh/kA under a typical coefficient of performance (COP) of 0.15 at 77 K.[13] Additionally, the heat leakage difference of samples 2 and 6 at 140 A and the consumed power are 10.3 W/kA and 556 kWh/kA, respectively. Therefore, suitable optimization of the shape factors can affect the total performance of the transmission lines as the saving energy during the operation.

CONCLUSIONS

We estimated the heat leakage from PCLs using a thermal balance equation, and investigated the dependence of the heat leakage from current leads optimized for 160 A and operating at higher currents. These conditions could roughly explain the current dependence of the temperature difference in CASER-2. We observed a large temperature difference on the thermoelectric elements in the PCLs, which relates to a large heat pump effect on the current leads. The optimum performance (lowest value of heat leakage divided by current) was shifted away from the designed optimum current, and

the actual operating current corresponded to overcurrent conditions.

In general, electric power applications have a wide range of feeding currents, and current leads are therefore sometimes used under overcurrent conditions. Based on the current dependence of the heat leakage and analysis of the overcurrent conditions, higher-resistivity elements seem to be better for the lowest increase in heat leakage at overcurrent conditions. For PCL, Z and resistivity seem to be important factors for optimization.

ACKNOWLEDGEMENTS

The authors thank Dr. A. Iiyoshi of Chubu University for his continuous encouragement throughout this work. We acknowledge Dr. Hiroshi Fujiwara for his support in construction of the 200-m superconducting facilities CASER-2. We also thank Dr. Leslie Bromberg of the Massachusetts Institute of Technology, who read our manuscript and gave us many valuable comments. We acknowledge the support of the Ministry of Education, Culture, Sports, Science, and Technology (MEXT) for this work as a Strategic Research Foundation Grant-aided Project for Private Universities, and a Grant-in-Aid for Challenging Exploratory Research. Parts of the work were also supported by Nippon Sheet Glass Foundation for Materials Science and Engineering, and the Future Energy Research Association (T.K.).

REFERENCES

1. S. Yamaguchi, M. Hamabe, I. Yamamoto, T. Famakinwa, A. Sasaki, A. Iiyoshi, J. Schultz, J. Minervini, T. Hoshino, Y. Ishiguro, and K. Kawamura, *J. Phys.: Conf. Ser.* 97, 012290 (2008).
2. M. Hamabe, Y. Nasu, A. Ninomiya, Y. Ishiguro, S. Kusaka, and S. Yamaguchi, *Adv. Cryog. Eng.* 53A, 168 (2008).
3. M. Hamabe, T. Fujii, I. Yamamoto, A. Sasaki, Y. Nasu, S. Yamaguchi, A. Ninomiya, T. Hoshino, Y. Ishiguro, and K. Kawamura, *IEEE Trans. Appl. Supercond.* 19, 1778 (2009).
4. S. Yamaguchi, T. Yamaguchi, K. Nakamura, Y. Hasegawa, H. Okumura, and K. Sato, *Rev. Sci. Instrum.* 75, 207 (2004).
5. T. Kawahara, T. Fujii, M. Emoto, M. Hamabe, Jian. Sun, H. Watanabe, and S. Yamaguchi, *Physica C: Supercond.* 470, S1011 (2010).
6. T. Fujii, S. Fukuda, M. Emoto, K. Osada, T. Kawahara, M. Hamabe, H. Watanabe, Y. Ivanov, J. Sun, and S. Yamaguchi, *J. Electron. Mater.* 40, 691 (2011).
7. K. Sato, H. Okumura, and S. Yamaguchi, *Cryogenics* 41, 497 (2001).
8. R. McFee, *Rev. Sci. Instrum.* 30, 98 (1959).
9. T. Yamaguchi, H. Okumura, K. Nakamura, and S. Yamaguchi, *IEEE Trans. Appl. Supercond.* 13, 1914 (2003).
10. M.N. Wilson, *Superconducting Magnets* (New York: Oxford University Press, 1983) 257.
11. H. Okumura and S. Yamaguchi, *IEEE Trans. Appl. Supercond.* 7, 715 (1997).
12. T. Kawahara, T. Fujii, M. Emoto, M. Hamabe, H. Watanabe, J. Sun, Y. Ivanov, and S. Yamaguchi, *IEEE Trans. Appl. Supercond.* 21, 1070 (2011).
13. http://www.aisin.com/product/energy/index.html. Accessed 19 October 2011..

Design and construction of 200-meter high temperature superconducting DC power cable test facility in Chubu University

Yamaguchi S., Kawahara T., Hamabe M., Watanabe H., Ivanov Yu., Sun, J., Iiyoshi A.

Center of Applied Superconductivity and Sustainable Energy Research (CASER), Chubu University, 1200 Matsumoto-cho, Kasugai, Aichi, 487-8501, Japan

The 200-meter DC cable project was started in Chubu University from 2008. This is the second experimental device to demonstrate the performance of the DC high temperature superconductor (HTS) cable system. The main subjects are related with the cryogenic engineering to realize low heat leak system. The heat leak from the cryogenic pipe and the terminal end must be low, and the pump power of the liquid nitrogen (LN2) circulation should be minimized, and therefore the straight pipe system is adopted. The iron steel pipe is also used for the outer pipe of the cryogenic pipe because of low cost. We describe the cable and cryogenic design for the circulation of LN2, and the cable support to absorb the thermal shrinkage of the cable. The preliminary results of the experiment are also mentioned.

INTRODUCTION

We started a DC superconducting power transmission line experiment from the aid of Japanese government (MEXT) in 2005, and the experimental device was completed in 2006. This is a 20-meter DC cable experiment, and the high temperature superconductor (HTS) tapes were used to make the cable by Sumitomo Electric Industry according to our design parameters. The material of the HTS is Bi-2223. The system had been cooled down and warmed up six times until 2010. No degraduation of the HTS cable was found. We performed several experiments [1, 2], such as the Peltier current lead experiments [3], the current imbalance experiments [4], the critical current experiment [2], the heat leakage experiment in the different test bench [5, 6]. The results of these experiments almost satisfied our original objectives. Because of the achievement, we started to construct a 200-meter cable system in 2009 as the next step.

In this paper, we describe the fundamental idea and the design of the system, the design and the construction of the expérimental system, especially about the cryogenic engineering aspects, such as the HTS cable, cryogenic pipe, the circulation for liquid nitrogen (LN2). We also mention the preliminary results of the experiments.

CABLE AND CRYOGENIC INNER PIPE

In order to minimize heat leak from cryogenic pipe, the best way is to make small for the inner pipe of the cryogenic pipe. Therefore, we made an effort to make the cable small, and there is no hole inside the former like the 20-meter cable experiment [1]. Figure 1 shows the cable, and the diameter of the cable is 35ϕ. The cable is the co-axial structure, and two conductors are insulated 20 kV, and composed of the HTS tapes of 16 (one layer) and 23 (two layers) for each polarity. If the magnitudes of the current of two conductors are the same, no magnetic field is generated outside the cable. This structure is similar to the ac cable [7]. The insulation voltage is 20 kV for two conductors, and insulated 10 kV from earth, individually. The rated current of the cable is 2 kA at 78 K, and is determined by the number of 16 HTS tapes.

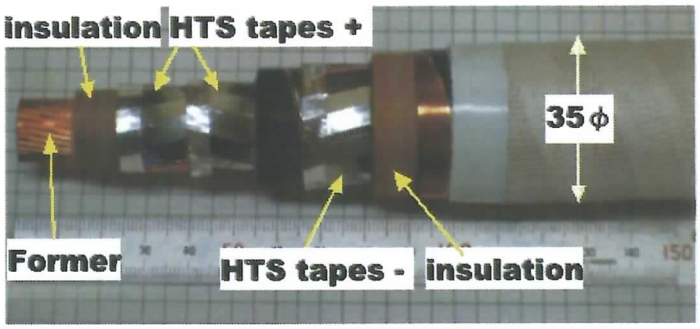

Figure 1. Photo of DC-SC cable of CASER2

Since the configuration of the inner pipe of the cryogenic pipe and the cable is also important to circulate the liquid nitrogen (LN2), we should calculate the circulation power of the system. The length of the cryogenic pipe is almost 200 m, but we should pay attention to extend the longer system, too. The inner pipe is composed of the straight and bellows pipe because he bellows pipe can absorb the thermal contraction and expansion. But the part of the bellows pipe is shorter than 5%. Many other pipe systems are used corrugate pipe [7, 8], but we estimated the pressure drop and other parameters for the circulation, we adopted a straight pipe system for longer cable system [9]. This is the main difference from the other pipe design in the present time. Therefore, we can calculate the pressure drop by the formulation of the fluid dynamics are given by

$$\Delta P = 2 f \rho v^2 L / D_h$$

$$\Delta T = q_W L / v A_h \rho C_p \qquad (1)$$

$$R_e = \rho v D_h / \mu$$

$$f = 0.0791 / R_e^{0.25}$$

ΔP: pressure drop [Pa],
L: length of the pipe [m],
v: velocity of fluid [m/s],
q_W: heat leak (load) to the inner pipe [W/m],

ρ: density [kg/m^3],
Re: Reynolds number
Dh: hydraulic diameter [m], and for circular pipe $D_h = D_2 - D_1$,
μ: viscosity [Pa s]
f: friction factor

We did many calculations to determine the size of the pipe, and finally we chose the diameter of the inner pipe shown in Fig. 2. The calculation result of the temperature rise is shown in figure 3. The vertical axis is the temperature rise and the horizontal axis is the LN2 flow rate. The calculations had been done for the heat leak of 0.5 [W/m] to 2.0 [W/m], respectively.

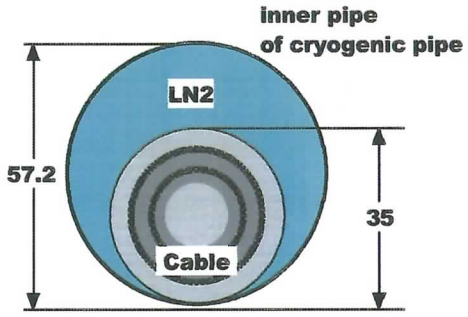

Figure 2. Cryogenic inner pipe and the SC cable

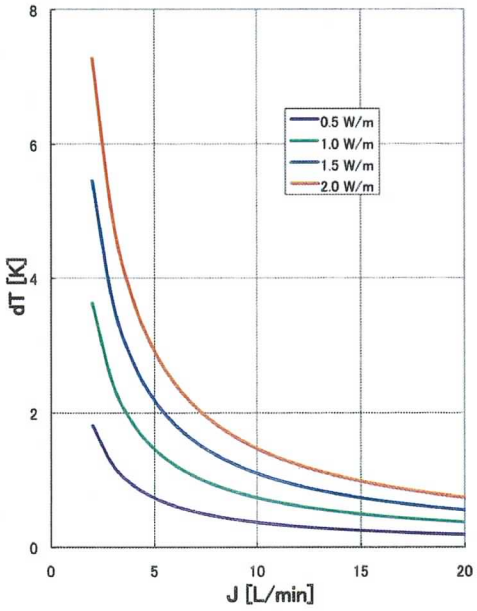

Figure 3. Temperature rise vs. Flow rate

We made the test stand to measure the heat leak preciously, and the heat leak is almost the same as 0.5 W/m for the same structure of the cryogenic pipe [5, 6]. Depending on the calculation results, we set the fluid flow rate of 5 [L/min] to 15 [L/min] in the experiment. These values are lower for the ac cable experiments. And we expect that the temperature rise will be lower than 2 K.

The pressure drop and pump power is proportional to the square of the flow rate. Figure 4 shows the results of the calculations. These almost do not depend on the heat leak from the cryogenic pipe. Since we adopt the straight pipe and the single cable, the pressure drop and the pump power is low as compared with the ac cables' [7, 9]. The magnitude of the pump power is lower than 5 W, and therefore the major heat load to the cryogenic system is the heat leak from the cryogenic pipe and the current lead. The out put pressure of the present LN2 pump is higher than this values, therefore it is not better that the present LN2 pump connected to the circulation system directly, and we found the different way to install the pump system.

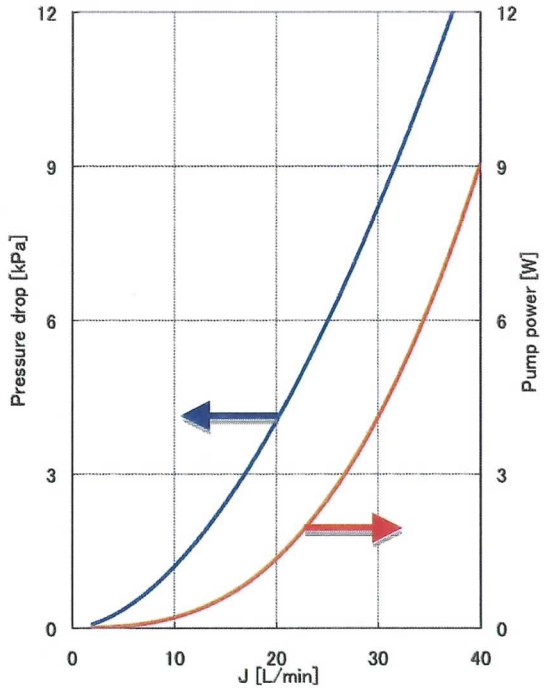

Figure 4. Pressure drop and pump power for the flow rate

CRYOGENIC OUTER PIPE

We adopted the iron-steel pipe for the cryogenic outer pipe because it is cheap, high strength and not low temperature. Figure 5 shows the pipe line of the 200-meter cable experiment, and it is the straight pipe. The arrow shows the flow direction of LN2. We constructed the pipe line to connect the short straight pipe by the welding after the inner pipe was installed into. We already used the straight outer pipe in the 20-meter cable experiment [1, 2], but we used the stainless steel pipe. Before we installed the iron-steel pipe, we tested the performance of the vacuum and thermal insulation in the test bench. If the iron pipe is coated by zinc, we can achieve high vacuum and high thermal insulation for radiation [5]. The emissivity of zinc is low as the aluminium's and the surface area of the straight pipe is not wider than the corrugated pipe's. Therefore, the vacuum pumping is not difficult. This structure looks like the water or oil pipes, and the construction way is similar to those. After we constructed the cryogenic pipe, we install the HTS cable into the cryogenic inner pipe. The construction method is different from the other cable systems [7. 8] completely. Since the cable path is not simple way in the experiment, we had tested the installation method of the HTS cable for short length in the factory. Fortunately, the installation is similar to the present method of the underground copper and aluminium cables in the present time, and Sumitomo has

many experiences to install the cable into the small diameter pipes as the usual commercial constructions. After the several exercises, the cable installation had been done within half day successfully. The structure of the straight and iron pipe system is also available even for the ac cable system if the cable structure is co-axial and the magnitude of the currents for inner and outer conductors are the same because no magnetic field is generated outside the cable. This means that the hysteresis loss of the iron pipe is zero even for the ac cables. If we apply the DC power transmission line, we do not need to pay attention to the hysteresis loss of the iron material. Moreover, the permeability of the iron is high and if the magnetic field is generated outside the cable, the electric circuit of the HTS cable has high inductance. High inductance of the circuit can reduce the current ripple of the power converter, and it should be discussed in detail because the power converter has huge inductor in the present design.

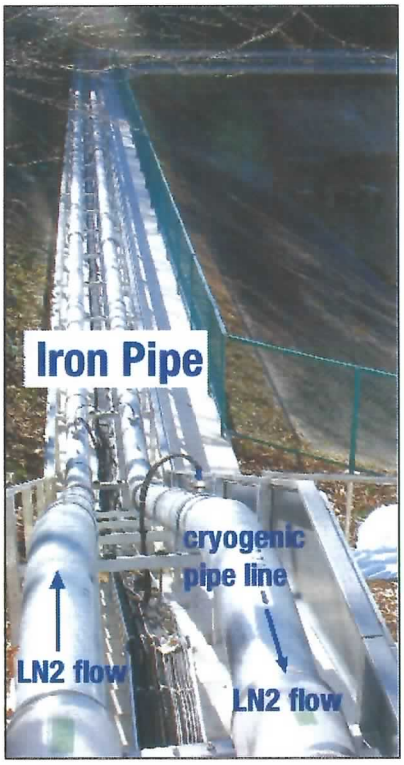

Figure 5: Picture of the outer straight pipe of the cryogenic pipe

The other important difference of the construction method is related with the cable length and its connection. The cable length is limited by the size of the cable drum, and the maximum length of the HTS cable will be ~5 km for the usual drum. But if we wind the cable with the cryogenic pipe for the same size of the drum, the cable length is around 0.5 km. Therefore, when we will construct the 5-km cable, the cable connection is zero by the proposed and tested method, but the usual method needs 10 times connections. These are disadvantages of the usual method for the cost, safety and reliability of the cable.

LN2 CIRCULATION, REGRIGRATION AND CABLE SUPPORT

The output pressure of the present commercial LN2 pump is 20 times higher than the calculation's at least, and the power of the pump is too high to circulate the LN2. Therefore, we prepare two LN2 tanks and their vertical drop is 2 m. The capacity of the tank is 200 L for each. The pressure difference between two tanks can

circulate the LN2 along the design values of the flow rate. We achieved the flow rate from 5 L/min to 15 L/min by the control of the valve experimentally. This means that the calculation should be almost correct. This system is useful to perform the thermal siphon circulation [9] and the slush N2 experiment.

After the cable is installed into the cryogenic pipe, the vacuum pumping of the cryogenic pipe is important. The pumping time and the related subjects should be discussed. After the cooling down is started, the cable will contract with the temperature decrease. Since the thermal contraction ratio is ~0.3%, the contraction length of 60 cm for 200 m cable. And if the thermal stress of the HTS tape is not small, the critical current of the HTS tape would be reduce. Therefore, we installed the extendable bellows into the connection between the terminal cryostat, and used the movable cryostat for the terminal. The schematic structure of the movable cryostat and the photo of the extendable bellows are shown in Fig. 6. The principle way to absorb the thermal contraction of the cable was already adopted in the 20-meter cable experiments since 2006, but the structure is different. We believe that this kind of the support structure is important to keep cable system safety and high reliability for long time operation.

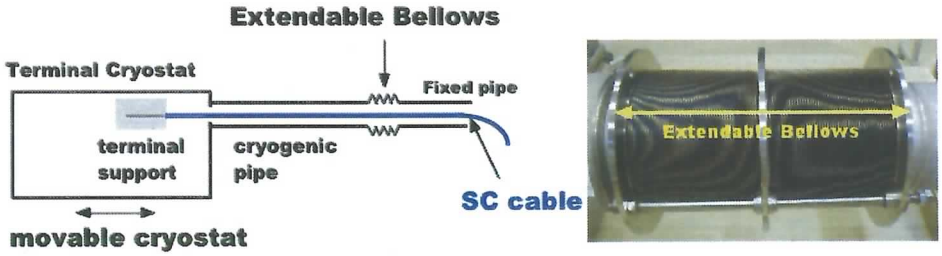

Figure 6. Schematic structure of the movable cryostat and the picture of the extendable bellows.

PRELIMINARY RESULTS AND FUTURE PLAN

We started the construction of the 200-meter cable experiment in August 2009, and completed in the end of 2009. The first cooling down hade been done in January 2010 and we kept the cable in low temperature until the middle of March. During this period, we did many tests and experiments. The

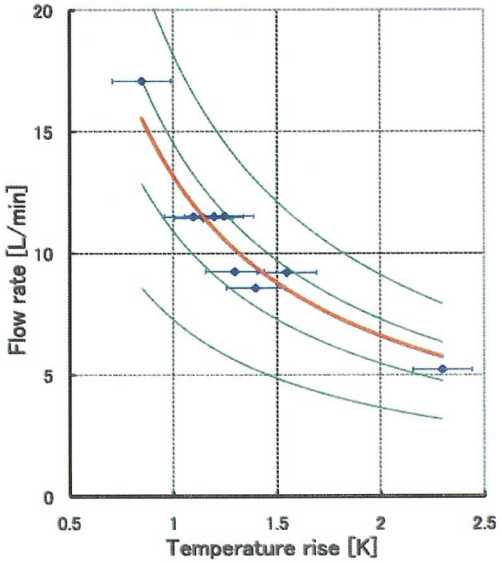

Figure 7. The comparison of the calculation and the experimental data

current of the cable was reached to 1.2 kA, and we controlled the flow rate of 5 L/min to 15 L/min. Figure 7 shows the comparisons of the design parameters of the flow rate and the temperature rise. The experimental data are shown with error bars. These data and the calculation indicate that the 2 km cable system is available along the present design.

REFERENCES

[1] S. Yamaguchi, M. Hamabe, I. Yamamoto, T. Famakinwa, A. Sasaki, A. Iiyoshi, J. Shultz, J. Minervini, T. Hoshino, Y. Ishiguro, and K. Kawamura, "Research activities of DC superconducting power transmission line in Chubu University," Jour. of Phys.: Conference Series, vol. 97, pp. 012290-012296, Mar. 2008.

[2] Hamabe, M, Fujii T., Yamamoto I., Sasaki A., Nasu Y., Yamaguchi S., Ninomiya A., Hoshino T., Ishiguro Y., Kawamura K., "Recent progress of Experimnt on DC Superonducting Power Transmission Line in Chubu University", IEEE trans. Appl. Supercond. vol. 19, pp. 1778-1781, 2009.

[3] Yamaguchi S, Yamaguchi T, Nakamura K, Hasegawa Y, Okumura H and Sato K, "Peltier current lead experiment and their applications for superconducting magnets," Rev. Sci. Instrum., vol. 75, pp. 207-212, 2004.

[4] Yamaguchi S, Seo K and Morita M, "A small-scale experiment demonstrating the current lead resistance method of preventing a current imbalance,"1998 Cryogenics vol 38 pp. 875-880, 1998.

[5] Hamabe, M et al., IEEE trans. Appl. Supercond. (2009)19 1778.

[6] M. Hamabe, Y. Nasu, A. Ninomiya, Y. Ishiguro, S. Kusaka, and S. Yamaguchi, "Radiation Heat "Measurement on Thermally-Isolated Double-Pipe for DC Superconducting Power Transmission," Adv. In Cryo. Eng., vol. 53A, pp. 168-173, Aug. 2008.

[7] Nasu, Y., Hamabe M., Yamaguchi S., Kusaka S., Ishiguro Y., "Heat leak measurement of Zinc-coated cryogenic pipe for superconducting power transmission line", Proc. ICEC 22-ICMC 2008 (2008) 489.

[8] T. Masuda, H. Yumura, M. Watanabe, H. Takigawa, Y. Ashibe, C. Suzawa, H. Ito, M. Hirose, K. Sato, S. Isojima, C. Weber, R. Lee, and J. Moscovic, "Fabrication and installation results for Albany HTS cable," IEEE trans. Appl. Supercond., vol. 17, no. 2, pp. 1648-1651, Jun. 2007.

[9] S. Mukoyama, M. Yagi, M. Ichikawa, S. Torii, T. Takahashi, H. Suzuki, K. Yasuda, "Experimental results of a 500 m HTS power cable field test," IEEE trans. Appl. Supercond., vol. 17, no. 2, pp. 1680-1683, Jun. 2007.

[10] Yu. Ivanov, A. Radovinsky, A. Zhukovsky, A. Sasaki, H. Watanabe, T. Kawahara, 265 S. Yamaguchi, Adv. Cryog. Eng. Trans.: Cryog. Eng. Conf. vol. 55, 2010, in press.

Development and operation of the measurement system for a 200 m HTS cable

Sun J.[1], Emoto M.[2], Yoshimura K.[3], Ivanov Y.[1], Watanabe H.[1],
Hamabe M.[1], Kawahara T[1], Yamaguchi S.[1,3]

[1]Center of Applied Superconductivity and Sustainable Energy Research (CASER),
Chubu University, 1200 Matsumoto-cho, Kasugai, Aichi 487-8501, Japan
[2]National Institute for Fusion Science, 322-6 Oroshi-cho, Toki, Gifu 509-5292, Japan
[3]Department of Electrical Engineering, Chubu University, 1200 Matsumoto-cho,
Kasugai, Aichi 487-8501, Japan

A new biaxial 200 m HTS cable test facility was constructed at Chubu University for testing the performance of DC power transmission. Various kinds of sensors are installed to collect the electrical and cryogenic signals. The measurement system provides up to about 600 channels. This paper presents the development and operation of this measurement system and some preliminary results are reported during the first cooling cycle test on this new cable test facility. It was confirmed that the measurement system was able to collect sufficient data with high precision and reliability for 2 month continuous operation.

INTRODUCTION

With the development and commercialization of high temperature superconducting (HTS) tapes, HTS cable for power transmissions has attracted extensive interests around the globe [1-4]. A first 20 m HTS DC cable was constructed at Chubu University in 2006 [5] and we continued to build a new above-ground 200 m HTS cable test facility with rated voltage and current of ±10 kV and 2 kA. We want to test the performance of HTS cable for DC power transmission. The construction of this new test facility was finished in December, 2009. The HTS cable is composed of two-layers of helically wound 39 DI-BSCCO HTS tapes supplied by Sumitomo Electric Industries [6]. The critical current of the DI-BSCCO used is 160 A on the criterion of 1 μV/cm. There are 23 and 16 HTS tapes in the inner and outer layer, respectively. 72 Peltier current leads (PCLs) [7] are installed into the current leads together with the 6 conventional current leads (CCLs) for comparison.

The purpose of this work is to develop a measurement system for collecting sufficient information about the operation of this large scale test facility. The performance of this HTS cable includes the performance of the cryogenic system, PCLs and CCLs, HTS tapes and the vacuum system. Therefore, a number of signals should be collected for a long term running test. The accuracy, cost effectiveness and security of the measurement system are required.

In this paper, we describe the development and operation of the measurement system for this new 200 m HTS DC cable test facility. Some preliminary results of the first cooling cycle test on the facility will be reported with this measurement system.

DEVELOPMENT OF MEASUREMENT SYSTEM

The test facility, similar to previous 20 m HTS cable [8], consists of a LN2 circulation system (CS), a HTS cable, a vacuum system, the power supplies and the measurement system. The HTS cable is installed in the thermally-insulated double-pipe called as cryopipe. In order to test the performance of the facility, the following things should be considered.

1. In order to evaluate the performance of the PCL, the temperature profile of each current lead and their electrical features should be observed [9].
2. I-V characteristic curve of each HTS tape should be observed.
3. It is vital to investigate the cryogenic characteristics of LN2 circuit.
4. The current loading and vacuum status of the cryopipe needs to be observed.

Hardware description

Figure 1 shows a configuration of total measurement system.

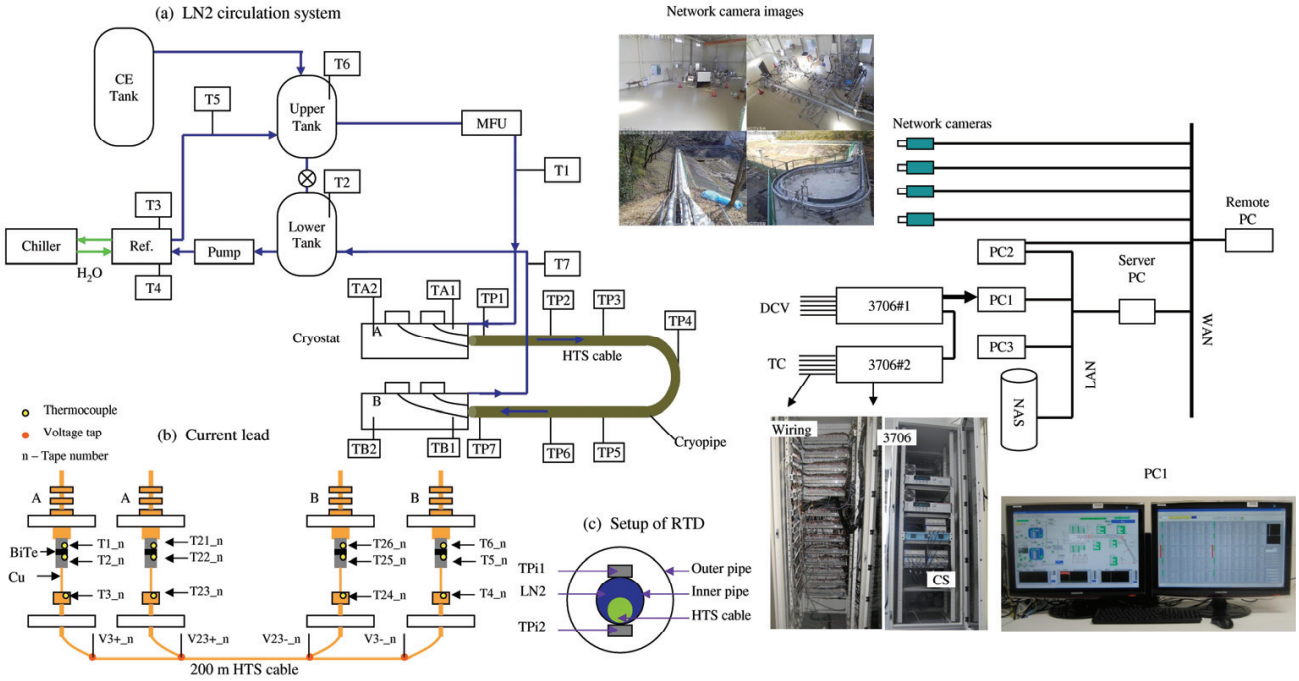

Figure 1. Configuration of total measurement system

Table 1 summarizes the measured data and sensor types. Pt resistive thermometer devices (RTDs) are installed on the wall of the cryostat, cryopipe and LN2 CS (Figure 1(a) and (c)). The main signals (429 channels) are located at the current leads (Figure 1(b)). T-type thermocouples (TCs) are chosen and manually made by ourselves because of their low cost. The copper (Cu) wires of TCs together with 78 voltage taps attached at both ends of HTS tapes are used to measure the electrical property of the conductor section (Figure 1(b)). All analog signals from sensors are fed into the KEITHLEY model 3706 multimeters. In the multimeters, the signals are amplified, converted to digital signals via the analog-digital converter (ADC) and stored into the buffer. At last these data are transferred to the personal computer (PC1) through the NI GPIB-USB-HS cable. Two KEITHLEY model 3706 multimeters are used and have 600 channels. Two BB-HCM715 and two BB-HCM735 network cameras from Panasonic were employed for the surveillance system of the whole facility. The PC2 are used to record the video images from the cameras and the PC3 and NAS HDD are used to back up the measured data simultaneously.

These PCs are assigned to the local area network (LAN). Through the server PC, the measured values are accessible online in a wide area network (WAN). For the stable operation of the DAS, these PCs are supplied by an uninterrupted power supply (UPS).

Table 1. Various measured data and sensor types for the HTS cable system

Name	Location	Sensor type	Quantity
Potential difference	Current lead A,B	Voltage tap	195
Conductor's temperature	Current lead A,B	T-type thermocouple	234
LN2 temperature	LN2 CS, Cryostat A and B, Cryopipe	Platinum resistor	38
LN2 flow rate	MFU	Coriolis	1
LN2 level	Upper and lower tank	Capacitance	2
LN2 pressure	Cryopump	Strain gauge	2
Transport current	Terminal A,B	Hall current transducer	39
Power supply		Voltage	6
Former's voltage		Voltage tap	1
Vacuum pressure	TIDP	Pirani gauge	5
		Ion gauge	4
Cryopump speed	Cryopump		2
TOTAL			529

We adopted KEITHLEY model 3706 multimeter as the data acquisition equipment because of some merits. The resolution of ADC is high, 26-bit. The data acquisition system is easily expanded by using the Test Script Processor link (TSP-link) master/slave connection when the system grows up. It supports GPIB interface and LabVIEW program language. The DMM provides several built-in measurement functions including DC voltage, thermocouple temperature, etc. At last, the 3706 multimeter is cost-effective comparing with the other data acquisition equipment.

Software description

LabVIEW is chosen as the programming environment. The software can be programmed with a minimum time of development by using the instrument I/O GPIB function in LabVIEW. Figure 2 shows a LabVIEW graphical user interface (GUI) of the LN2 CS and HTS cable with the data plots as a function of time. The software provides the functions to analyze, display and record the data. Two monitors are used to display the GUI with the display resolution of 3840 x 1200 pixels.

The data are written to a storage disk with the capacity of 1 TB. The data file's format is a LabVIEW measurement file (lvm). The scientific data with the width of 10 characters are recorded as ASCII codes

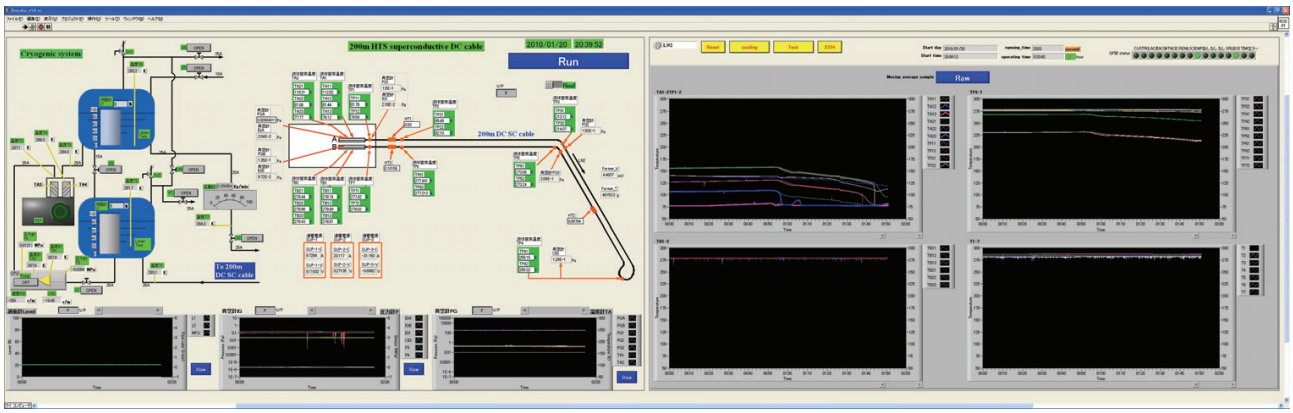

Figure 2. A picture of the LabVIEW graphical user interface for the 200 m cable when we started cooling down the HTS cable

same as the format of the original data from the 3706 multimeters. The data are divided into four files of voltage, cryogenic, vacuum and thermocouple. The new files are automatically produced and named every 3600 times of measurements to limit each file size.

OPERATION OF MEASUREMENT SYSTEM AND PRELIMARY RESULTS

Table 2 shows the accuracy of the measurement system. The accuracy of the measurement system increases with the number of power line cycle (NPLC). The time interval of one cycle of 600 channels' measurement can be as fast as 0.5 s when NPLC is 0.006. In the LabVIEW program, the NPLC is chosen to be 0.1 with the optimation between the accuracy and the speed of the measurement system. Therefore, the reading rate of the DAS is about 1.7 s per 600 channels.

Table 2. Accuracy of the measurement system

Resolution			26-bit
NPLC (number of power line cycles)			0.1
Aperture time			1.67 ms
Digits			$5^{1/2}$
Accuracy	DC voltage	0 to 0.1V	< 11 μV
		0 to 1 V	< 58 μV
	Pt thermometer	50 to 300 K	< 0.06 K

It took about 2 month for wiring all these signals with the help of several technical workers. After the construction of the cable, we performed the first cooling cycle test on this new HTS cable from Jan 19 to March 8. The measurement system has been implemented from Jan. 19 to Mar. 23 until the HTS cable warmed up to room temperature. The size of one data file is ≈ 8 kB and about 13 GB data are obtained in the first cooling cycle test.

Cooling down measurement

We cooled down the system by LN2. Because of the contraction of the cable due to huge temperature decrease, we cooled down the cable slowly. The LN2 was filled from cryostat A to cryostat B with the

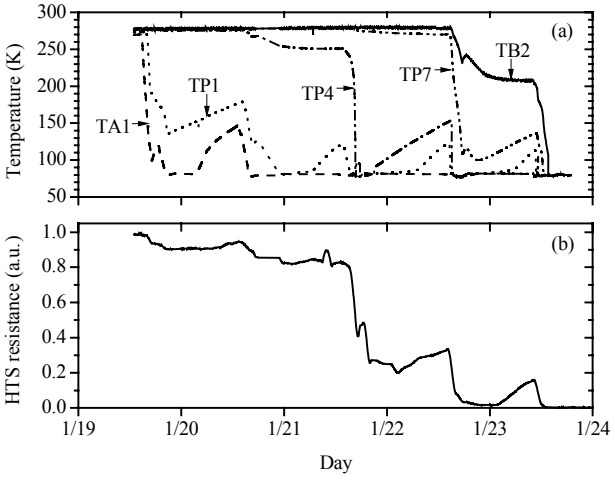

Figure 2. Time dependence of (a) cryostat and cryopipe temperatures, and (b) HTS resistance normalized at room temperature

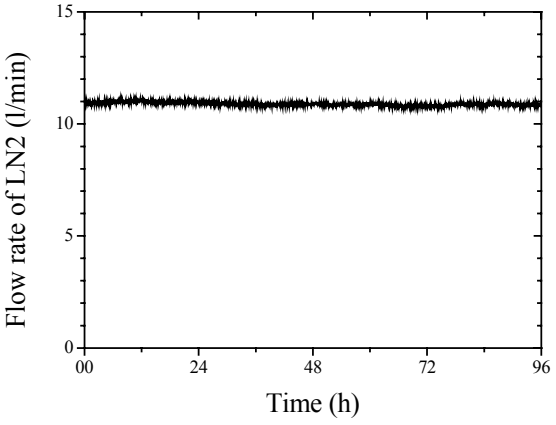

Figure 3. A record of LN2 circulation test for 4 days

filling rate of ~ 1 l/min for ~ 5 h at the daytime. The cooling down process was monitored by two kinds of methods. First one is Pt RTD seen in Figure 1. Another one is the voltage of one HTS tape at 100 mA.

Figure 3 (a) shows the time dependence of the cryopipe (TP1, TP4 and TP7 in Figure 1(a)) and cryostat temperature (TA1 and TB2 seen in Figure 1(a)). On the fifth day, the whole cable was cooled down to 77 K. In Figure 3 (b), HTS resistance was normalized by the data at room temperature before cooling down. The time dependence of HTS resistance is similar to that of TP4, because they reflect the average status of the cable. In both cases, it needs to take 5 days to achieve superconductivity of the HTS tapes and to finish the cooling-down process.

LN2 circulation test measurement

After cooling down the HTS cable, we tested the cryogenic circulation system. Figure 4 shows a record of circulation test by sub-cooled LN2 for 4 days with flow rate of 10.8 l/min. The temperature difference decreases with the increase of the flow rate. We estimated the heat loss of the cryopipe by calorimetric measurements [10]. The heat loss of the cable system was determined by the temperature of LN2 at the inlet and the outlet of the cryopipe together with the flow rate of LN2. The heat loss amounts to be about 330 W. In addition we verified the operation of other components of the test facility with this measurement system.

CONCLUSION

A compact centralized measurement system was developed to monitor the new 200 m HTS cable test facility. It measures about 529 data about the operation of the cable such as the temperature, pressure, level and flow rate of LN2 coolant, loading current, voltage and temperature of the conductors and vacuum pressure in the thermal-insulated double pipes. During our first preliminary cooling down and warm up cycle test on the test facility, the measurement system functioned satisfactorily and sufficient data were collected.

REFERENCES

[1] Masuda, T., Yumura, H., Watanabe, M., Recent progress of HTS cable project, Physica C (2008) 468 2014-2017.

[2] Shimoyama, K., Ozcivan, N., Soeda, S., Hu, N., Onoe, Y., Yagai, T., Tsuda, M., Hamajima, T., Experimental results of tri-axial HTS cable, Cryogenics (2009) 49 398-401.

[3] Wu, S., Wu, Y., Song, Y., Wu, W., Bi, Y., Xi, W., Xiao, L., Wang, Q., Ma, Y., Liu, X., Zhang, P., Xin, Y., Hou, B., Liu, R., Zhang, H., Han, Z., Zheng, J., Wang, J., Wang, S., Shi, J., Tang, Y., Qiu, M., Wei, B., Tan, Y., Recent main events in applied superconductivity in China, IEEE T. Appl. Supercon. (2009) 19 1069-1080.

[4] Malozemoff, A. P., High Tc for the power grid, Nat. Mater. (2007) 6 617-619.

[5] Yamaguchi, S., Hamabe, M., Yamamoto, I., Famakinwa, T., Sasaki, A., Iiyoshi, A., Schultz, J., Minervini, J., Hoshino, T., Ishiguro, Y., Kawamura, K., Research activities of DC superconducting power transmission line in Chubu University, J. Phys.: Conf. Ser. (2008) 97 012290(7pp).

[6] Ayai, N., Kobayashi, S., Kikuchi, M., Ishida, T., Fujikami, J., Yamazaki, K., Yamada, S., Tatamidani, K., Hayashi, K., Sato, K., Kitaguchi, H., Kumakura, H., Osamura, K., Shimoyama, J., Kamijyo, H., Fukumoto, Y., Progress in performance of DI-BSCCO family, Physica C (2008) 468 1747-1752.

[7] Yamaguchi, S., Yamaguchi, T., Nakamura, K., Hasegawa, Y., Okumura, H., Sato, K., Peltier current lead experiment and their applications for superconducting magnets, Rev. Sci. Instrum. (2004) 75 207-212.

[8] Hamabe, M., Fujii, T., Yamamoto, I., Sasaki, A., Nasu, Y., Yamaguchi, S., Ninomiya, A., Hoshino, T., Ishiguro, Y., Kawamura, K., Recent progress of experimental on DC superconducting power transmission line in Chubu University, IEEE T. Appl. Supercon. (2009) 19 1778-1781.

[9] Kawahara, T., Fujii, T., Emoto, M., Hamabe, M., Sun, J., Watanabe, H., Yamaguchi, S., Estimation for the performance of superconducting DC transmission lines with cryogenics improvements, Physica C (2010) (in press).

[10] Tønnesen, O., Däumling, M., Jensen, K. H., Kvorning, S., Olsen, S. K., Træholt, C., Veje, E., Willén, D., Østergaard, J., Operation experiences with a 30 kV/100 MVA high temperature superconducting cable system, Supercond. Sci. Technol. (2004) 17 S101-S105.

Superconducting power transmission line cooled with naturally circulating LN_2

Ivanov Yu., Watanabe H., Kawahara T., Hamabe M., Sun J., Yamaguchi S.

Center of Applied Superconductivity and Sustainable Energy Research (CASER), Chubu University, 1200, Matsumoto-cho, Kasugai, Aichi, 487-8501, Japan

Conventional design of superconducting power transmission lines presupposes application of cryogenic pumps to circulate liquid refrigerant. However, cryopumps are one more powerful source of heat load on the system and they possess a number of other disadvantages. Alternatively, natural circulation of refrigerant (thermal siphon effect) can be used to keep superconducting cable at low temperature. This approach simplifies the cooling system significantly and reduces the incoming heat. Numerical simulation of circulation process confirmed feasibility of the proposed design for power transmission lines up to 1 km long.

INTRODUCTION

Significant progress achieved in the field of development of high temperature superconducting (HTS) materials allows us to manufacture high-quality HTS cables of hundreds-meter class. Technology of superconducting power transmission (SC PT) is well developed already and commercial SC PT lines is expected to be constructed in the near future. It is essential that heat leakage through thermal insulation should be minimized in order to increase the efficiency of SC PT line. Works in that direction include the optimization of multi-layer insulation (MLI) and current leads. In particular, there are current leads equipped with Peltier elements, allowing to reduce significantly heat leakage [1]. Standard design of SC PT lines involves the application of cryogenic pumps to circulate liquid nitrogen (LN_2), which is usually used as refrigerant. Unfortunately, these equipments have a number of disadvantages. Cryopumps are one more powerful source of heat load on the system. They have a large hydraulic resistance, require power supply and maintenance. In addition, they are quite expensive. Another technical decision can be proposed. LN_2 absorbs the incoming heat load when moving through the cryopipe. This leads to increase in its temperature and decrease in density simultaneously. The effect can be used to run a natural circulation of LN_2, i.e. operation in a thermal siphon mode without using any pump power [2]. Many kinds of machines based on the principle of thermal siphon are widely used in various fields of industry due to their low cost, relative simplicity and reliability [3]. The feasibility of the proposed design was confirmed for long (up to 100 km) SC PT lines laid in a mountainous terrain with the up/down-hill elevations varying by up to 2 km [2]. The operating modes and cooling efficiency of the inclined thermal siphon with a counter-flow circulation loop composed of a cryogen flow channel and an inner cable channel were discussed in our recent works. The main feature of this scheme is the strong parasitic heat exchange between upwards (internal) and downwards (external) flows. Numerical analysis of system of

the design equations revealed that circulation occurs over all range of values of initial parameters both without [4] and with slight subcooling [5]. Consequently, thermal siphon cooling technology can significantly improve the efficiency of SC PT lines and reduce maintenance costs, which is particularly important when the line runs through the hard-to-reach places such as mountains or the sea bottom. Our study shows that in many areas of industry DC power transfer has a number of advantages over AC one. We believe that the first fully commercial lines can be short SC PT lines from the electrical substation to the powerful DC consumers, such as Internet data centers (iDC) [6]. This article discusses the operating modes of knee siphon, which is most suitable for cooling of HTS cables.

DESIGN

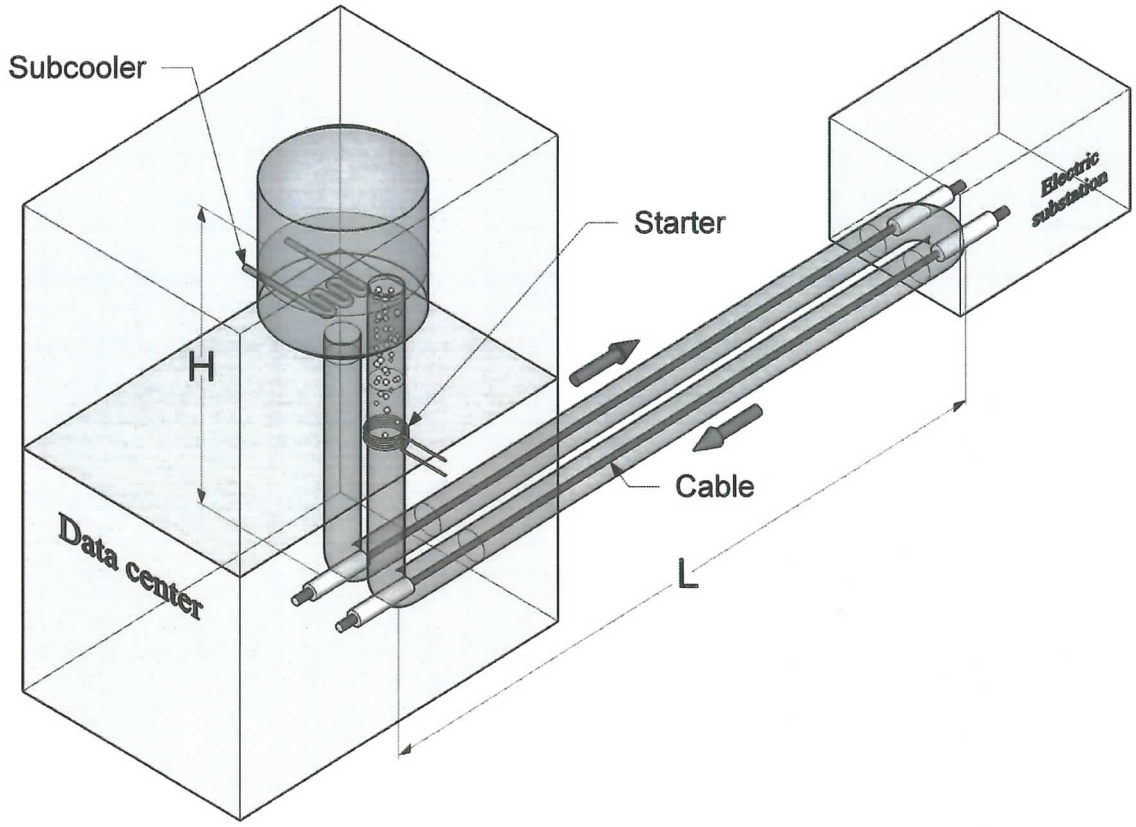

Figure 1. Conceptual design of the HTS cable cooling system based on thermal siphon

The apparatus (Figure 1) consists of a vertical pressure segment and a horizontal cooling (working) segment. A tank with LN_2 is placed at the top of the circuit. Temperature of refrigerant in the tank is maintaining below the boiling temperature by subcooler in order to remove incoming heat and to control siphon operating mode. Heavy "cold" LN_2 moves down through the first vertical cryopipe, and then flows through two long horizontal sections containing HTS cables, maintaining its temperature below T_c. Being heated by the heat passing through the thermal insulation and current leads, light "warm" LN_2 raises through the second vertical cryopipe and returns back into the tank. The driving force of the process is the difference between the gravity of "cold" and "warm" refrigerant in vertical cryopipes. A heater, which can evaporate small amount of LN_2 and thereby

significantly increase driving force, is used as a starter. At steady state a raised pressure prevents the boiling up of "warm" LN_2 in the most part of the apparatus. However, under certain conditions, temperature of LN_2 rises significantly exceeding the boiling temperature at local pressure and effervescence takes place prior to its return to the tank. Therefore, we can distinguish two operating modes of the thermal siphon cooling apparatus, namely one- and two-phase modes. It should be emphasized, that the term "two-phase mode" means only the presence of a certain amount of gaseous nitrogen at the outlet of the cryopipe (see Figure 2) [7]. In this case the actual two-phase flow exists only in a small part of the cryopipe, namely from 0 to 3 m before the outlet. Nitrogen bubbles can not affect on the quality of electrical insulation in the HTS cables because of the boiling occurs in vertical cryopipes far from the cables.

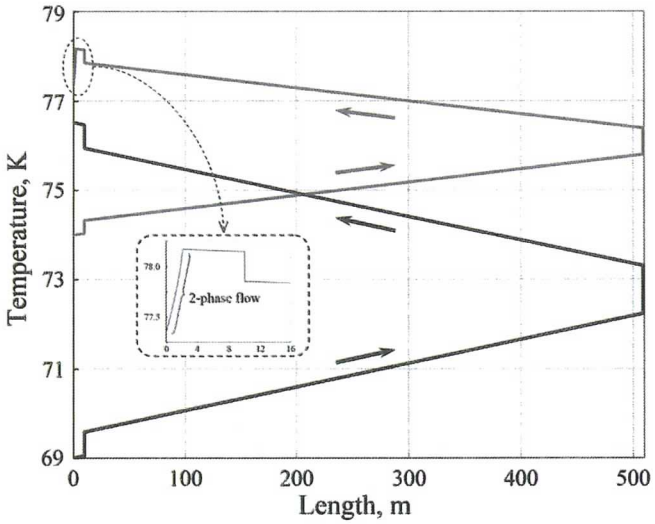

Figure 2. Typical temperature profiles of LN_2 in cryopipes [7].
Top curve is for two-phase mode, bottom curve is for one-phase mode. $P_0 = 1$ bar, $L = 500$ m, $H = 10$ m

Geometrical parameters of the cable and the cryopipe were selected in accordance with geometry of 200 m experimental facility in Chubu University in order to properly simulate the circulation process of LN_2. Namely, we prescribed that the cable of outer diameter 34.8 mm is placed in the cryopipe of inner diameter 57.2 mm. It was assumed that the distributed heat load is 1 W/m, and the loss of heat through each of the end current leads is 100 W. Length of the siphon varies from 200 to 1000 m and height varies from 2 to 20 m. Steady-state design equations were obtained from Bernoulli's formula

$$p + \rho g h + \rho \frac{v^2}{2} = \text{const}$$

and heat balance conditions. Properties of LN_2 flow from the inlet to the boiling point are described by

$$\begin{cases} \dot{m} C_{pl} \dfrac{dT}{dx} = q(x) \\ \dfrac{dp}{dx} = \rho_l g \sin\beta - \dfrac{2 f G^2}{\rho_l D_h} \end{cases}$$

and from the boiling point to the outlet are as follows

$$\begin{cases} \dot{m}\left[(1-\chi)C_{pl}+\chi C_{pg}\right]\dfrac{dT}{dx}+r\dot{m}\dfrac{d\chi}{dx}=-q(x) \\ \dfrac{dp}{dx}=\left(\dfrac{\chi}{\rho_g}+\dfrac{1-\chi}{\rho_l}\right)^{-1} g\sin\beta+\dfrac{2fG^2}{\rho_l D_h}\dfrac{1+\left(\rho_l/\rho_g-1\right)\chi}{\left[1+\left(\mu_l/\mu_g-1\right)\chi\right]^{0.25}} \\ T=T_{sat}(p) \end{cases}$$

where C_p is the specific heat, D_h is the hydraulic diameter, f is the friction factor, g is the gravitational acceleration, G is the specific mass flow, $\dot{m}$ is the mass flow, p is the pressure, q is the heat load, r is the specific heat of vaporization, $\sin\beta$ is the sine of inclination, T is the temperature, $T_{sat}(p)$ is the saturation curve, μ is the dynamic viscosity, ρ is the density, and χ is the vapor quality. Subscripts l and g denote liquid and gas, respectively. The temperature and pressure dependences of the physical properties of the nitrogen are taken into account.

ANALYSIS AND RESULTS

A numerical fourth-order Runge-Kutta method was used to solve the systems of design equations. Analysis revealed that refrigerant flow is turbulent over the entire range of lengths (200-1000 m), heights (2-20 m), tank pressures (1-3 bar), and temperatures at inlet (65-77.35 K). Typical temperature profiles of LN_2 in cryopipes are shown in Figure 2, where bottom and top curves correspond to one-phase and two-phase operating modes, respectively [7]. Modes can be characterized in detail by 2D graphs. Figure 3 shows both vapor quality at the outlet and mass flow versus cryopipe length and height. Region to the left where χ=0 (absence of gas in the outgoing refrigerant) corresponds to the one-phase mode. Circulation is supported by a small difference in the densities of refrigerant in vertical cryopipes. Therefore, the intensity of circulation and, as a consequence, the temperature difference between the inlet and the outlet can be controlled in a certain range by changing of the pressure segment height. The rest part of the graph shows the behaviour of parameters in the two-phase mode. It reveals the feature in the case of small heights and large lengths. The design equations provide formal solution with high values of χ in this area which is physically understandable, but simple two-phase flow model is not applicable there. Furthermore, loss of a few percents of the working medium in every circle is not technologically optimal. Therefore, a small area with χ > 2% can be removed from our consideration.

Since the average density of the two-phase medium is a very sensitive function with respect to vapor quality (which is determined by the amount of the incoming heat), the intensity of circulation strongly depends on the distance between the boiling point and the upper level of refrigerant (i.e. on the depth of the boiling point), and weakly depends on the height. One-phase mode can be regarded as more technologically advanced because of there is not necessary to dispose of gaseous nitrogen released. For a given length of the SC PT line, L, position of the boundary between modes is determined by the subcooling, tank pressure, and height of the pressure segment, i.e. by parameters which can be varied relatively easy to set the desired operating mode. Transition between modes can be also caused by change in heat load. These possibilities are illustrated in Figure 4. Thermal siphon demonstrates remarkable stability of mass flow: when geometry varies in wide range, namely length is from 200 to 1000 m.

(5 times) and height is from 2 to 20 m (10 times), $\dot{m}$ changes only twice. As a result, transition between modes occurs smoothly that is very important to stable operation.

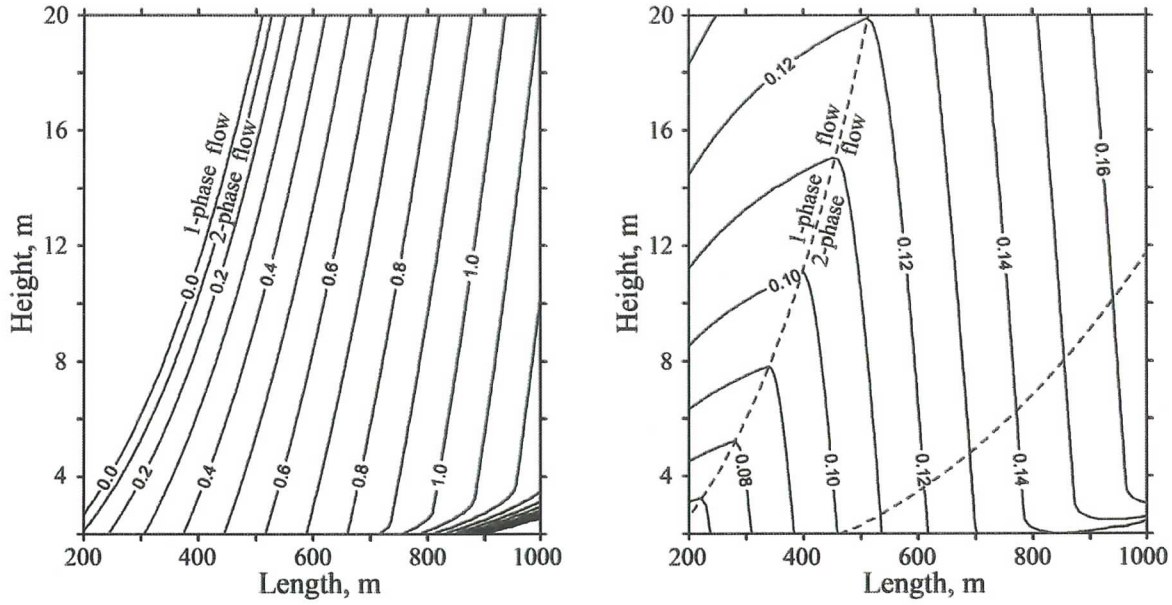

Figure 3. Vapor quality (left) and mass flow (right) as a function of siphon geometry.
Tank pressure P_0 is 1 bar. Right dashed line indicates shift of boundary between modes at $P_0 = 2$ bar

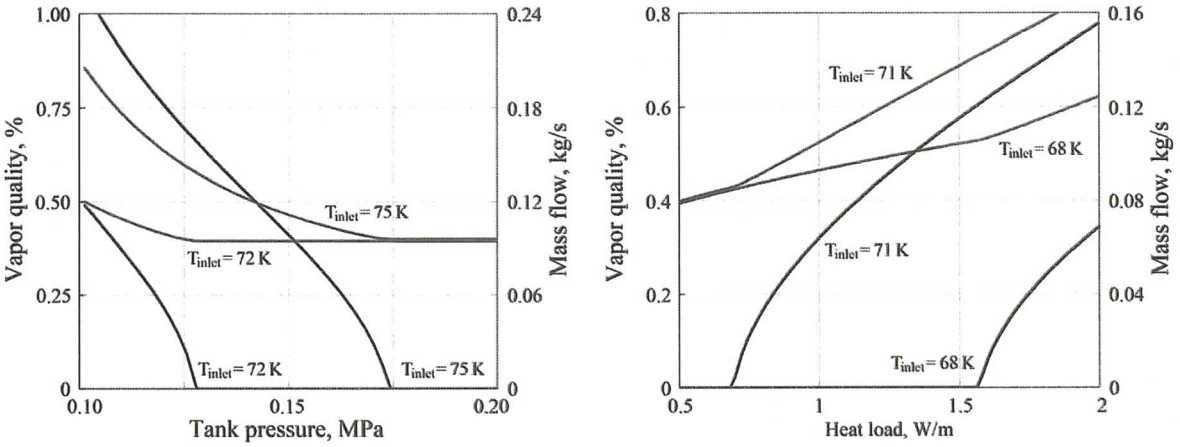

Figure 4. Mass flow and vapor quality versus tank pressure P_0 (left)
and versus distributed heat load Q (right) at different temperature at the inlet T_{inlet}. $L = 500$ m, $H = 10$ m

CONCLUSION

It was theoretically confirmed that thermal siphon effect can be used to significantly increase the efficiency of cooling system of hundreds-meter class HTS cables. Natural circulation of LN_2 inside cryopipes is characterized by remarkable stability of mass flow that corresponds to smooth and secure transition between one- and two-phase operating modes, and is very important in practice.

REFERENCES

[1] Yamaguchi, S., Hamabe, M., Yamamoto, I., Famakinwa, T., Sasaki, A., Iiyoshi, A., Schultz, J., Minervini, J., Hoshino, T., Ishiguro, Y., and Kawamura, K., Research Activities of DC Superconducting Power Transmission Line in Chubu University, J. Phys.: Conf. Ser. (2008) 97 012290.

[2] Radovinsky, A. and Zhukovsky, A., HVDC-MIT- ARadovinsky-022106-1 (2006).

[3] Pioro, L. S. and Pioro, I. L., Industrial Two-Phase Thermosyphons, Begell House Publishers, New York, USA, 1997, 288 p.

[4] Ivanov, Yu., Radovinsky, A., Zhukovsky, A., Sasaki, A., Watanabe, H., Kawahara, T., and Yamaguchi, S., A Compact Cooling System for HTS Power Cable Based on Thermal Siphon for Circulation of LN_2, Adv. Cryogenic Eng.: Trans. Cryogenic Eng. Conf. (2010) 55 865-870.

[5] Ivanov, Yu., Radovinsky, A., Zhukovsky, A., Sasaki, A., Watanabe, H., Kawahara, T., Hamabe, M., and Yamaguchi, S., Compact Counter-Flow Cooling System with Subcooled Gravity-Fed Circulating Liquid Nitrogen, Physica C. (2010) 470 1895-1898.

[6] Ton, M., Fortenbery, B., and Tschudi, W., DC Power for Improved Data Center Efficiency, Lawrence Berkeley National Laboratory Report (2008).

[7] Ivanov, Yu., Radovinsky, A., Zhukovsky, A., Watanabe, H., Kawahara, T., Hamabe, M., and Yamaguchi, S., Cooling of HTS Cable for Short Distance Power Transmission by Naturally Circulating Liquid Nitrogen, Abstr. CSJ Conf. (2009) 81 159.

Evacuation procedures of long cryogenic pipes for superconducting power transmission

Watanabe H., Hamabe M., Kawahara T., Yamaguchi S.

Center of Applied Superconductivity and Sustainable Energy Research (CASER), Chubu University, 1200 Matsumoto-cho, Kasugai, Aichi, 487-8501, Japan

The evacuation systems of cryogenic pipes for the superconducting power transmission have been studied based on the results obtained by a 200 m cryogenic pipe for a superconducting DC power transmission. Small pumps with the pumping speed much less than 100 l/s are enough for long cryogenic pipes. Since small increase of the pipe length increases the evacuation time significantly, the interval of pumps should be planned carefully depending on the conductance of the pipes. The reduction of outgassing and the increase of conductance are particularly important to get shorter evacuation time for the long cryogenic pipes for actual applications.

INTRODUCTION

Reducing emission of green house gases has been highly demanded to prevent from global warming recently. This problem could be partly solved by introducing renewable energies including photovoltaic and wind power generation connected to cities with superconducting power transmission lines, which can send the electricity for long distance with high efficiency.

High temperature superconducting power transmission cables are used in the flow of liquid nitrogen to keep a superconducting state. Heat leak from the parts at the room temperature to those at the liquid nitrogen temperature causes loss of the liquid nitrogen, which reduces the energy efficiency of the superconducting power transmission due to the requirement of the power for cooling. For vacuum insulation to prevent the heat leak along transmission lines, cryogenic pipes, which are concentric double pipes evacuated in between, are used. Since the heat leak is reduced by the vacuum between the pipes, obtaining good vacuum is important [1]. Several types of cryogenic pipes have been used for the superconducting power transmission, such as corrugate pipes and straight pipes. In any cases, since the cryogenic pipes used for the superconducting power transmission are ranged from several hundred meters to several hundred kilometers, the evacuation speed will be limited by the conductance of the pipes strongly. Moreover to reduce radiation heat transfer, the inner pipe of the cryogenic pipes is usually laminated with multi-layer insulation (MLI). The outgassing from MLI materials also limits the evacuation speed and the pressure reached. Therefore, to construct longer superconducting power transmission lines, careful consideration of the evacuation system is needed.

We have been constructing a superconducting DC power transmission line with 200 m length named CASER2 in Chubu University based on the results obtained by 20 m cable system [2,3] and started operation from the beginning of 2010. As the first step of the operation, the test of the evacuation system was performed. The evacuations were repeated several times by changing conditions. Based on the information obtained during the evacuations, we will discuss evacuation systems required for long cryogenic pipes for actual applications.

Figure 1 shows the schematic picture of CASER2. The cryogenic pipe of CASER2 is approximately 200 m and is installed mainly in the outdoors in the L shaped configuration. It is running over 100 m from the laboratory and back to the same place. Two terminals are installed at the each end of the cryogenic pipe, which are placed next to each other. The each end of the cryogenic pipe is connected with a pipe, on which pumps are installed (Figure 2). From the symmetry, the evacuation with this configuration corresponds to that pumps are installed at every 200 m, if longer cryogenic pipe are considered. CASER2 has one mechanical booster pump (MBP) backed with a rotary pump (RP) and one turbo molecular pump (TMP). The MBP is ULVAC PMB-006C and the RP is ULVAC VS1501. The maximum pumping speed of PMB-006C is 11000 l/min and that of VS1501 is 3000 l/min. The TMP is Pfeiffer HiPace300, whose pumping speed is 260 l/s. The TMP is usually used in our laboratory after reaching the pressure of around 2 Pa by the pumping with the MBP. Along the cryogenic pipe, several vacuum gauges are set to see the vacuum conditions. At the moment, there are four Pirani gauges at the pipe connecting the pumps to the cryogenic pipe and at almost every 50 m along the cryogenic pipe. One ionization gauge is set also at the pipe connecting the pumps to the cryogenic pipe.

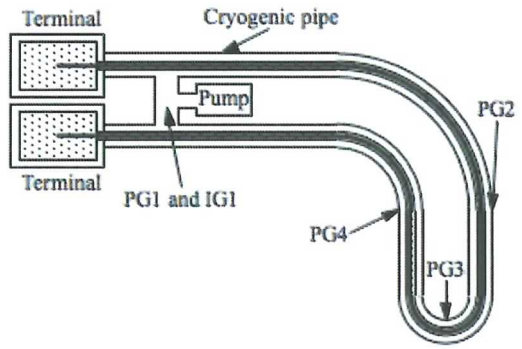

Figure 1. The schematic picture of CASER2

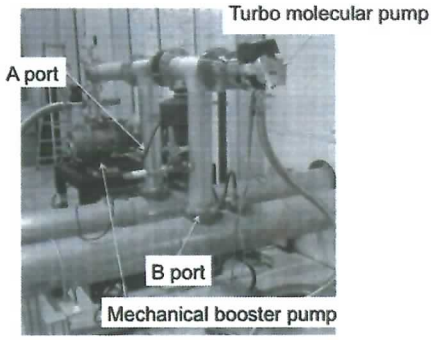

Figure 2. The pump system of CASER2

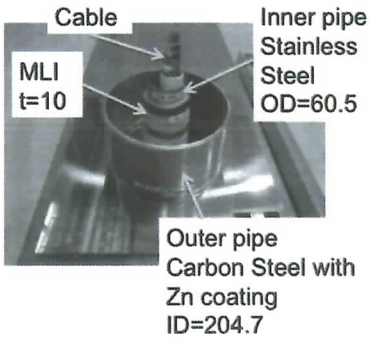

Figure 3. The model of the cryogenic pipe

Figure 3 shows a cross sectional model of the cryogenic pipe. The cryogenic pipe of CASE2 is a concentric double straight pipe. The inner pipe is stainless steel with the outer diameter of 60.5 mm and the outer pipe is carbon steel coated with zinc with the inner diameter of 204.7 mm. The inner pipe is covered with MLI with about 10 mm thickness. This configuration has been shown to be good for vacuum insulation by our previous study [4, 5]. In the actual cryogenic pipe of CASER2, there are many rods and supporting boards to support the inner pipe.

EVACUATION OF CASER2

Figure 4 shows the pressure variation after the start of roughning by the MBP and the RP. The pressures were measured with the Pirani gauges, positions of which were shown in Figure 1. At first, the cryogenic pipe was evacuated by the RP and, then, the MBP was started. The pumping by the RP was started at 300 s and the bend in the figure at around 500 s is for the start of the MBP. Down to about 50 Pa the curves are almost coincident, which is due to the large conductance in the viscous flow region. In this vacuum region the cryogenic pipe could be treated as a single vessel, not as a thin long pipe. Below 50 Pa, the curves are separated due to the change of the conductance. By 1500 s, the vacuum, at which the TMP could be used, was achieved. This rather short time is due to the high pumping speed of the MBP and high conductance in the viscous flow region.

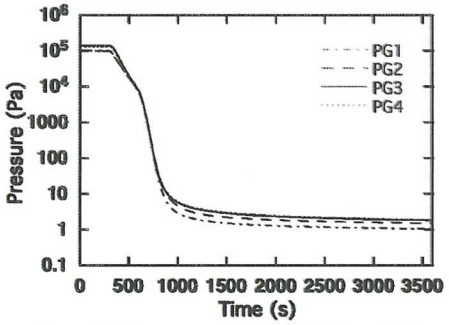

Figure 4. The evacuation by MBP and RP

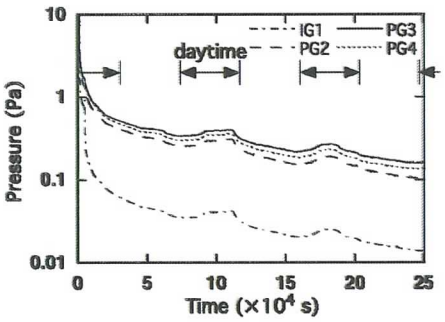

Figure 5. The evacuation by the TMP

Figure 5 shows the pressure variation after the start of the TMP. The ionization gauge was used instead of the Pirani gauge at the PG1 position. Just after the start of the TMP, the pressure measured by IG1 decreased rapidly and then decreased slowly like PG2, PG3 and PG4, while those by PG2, PG3 and PG4 decreased slowly from the beginning. As the result, the difference between the pressure measured by IG1 and those measured by the other gauges became large. This is a clear indication of the effect of the conductance in the molecular flow region. In fact, for the ideal concentric double pipe with the outer diameter of the inner pipe of 80.5 mm, with the inner diameter of the outer pipe of 204.7 mm, and with the length of 100 m, the conductance is calculated to be only 6 l/s. This means that the evacuation speed is determined mainly by the conductance, not by the pumping speed of the TMP. The reduction of the pumping speed doesn't make the evacuation speed worse too much. Therefore small pumps with the pumping speed much less than 100 l/s would be enough for long thin cryogenic pipes. A TMP with the pumping speed of 260 l/s was chosen for CASER2 just for the margin to test optimum evacuation systems.

In the slow varying region in Figure 5, pumping and outgassing is balanced. The pumping speed is almost constant in this vacuum region and also the conductance could be considered constant. Therefore, the slow decrease of the pressure reflects the slow decrease of the outgassing rate. Therefore to decrease the pressure faster, the reduction of outgassing is needed. There are bumps in the curves. The period, during which the bumps appeared, corresponds to the daytime. The cryogenic pipe of the CASER2 is placed in the outdoors, so it is affected strongly by the environmental changes, such as the temperature and the weather. The bumps are due to the increase of outgassing by the rise of the outer pipe temperature by the sunshine. The outgassing rate could be reduced by baking, though it is difficult in the case of long cryogenic pipes. Cautious treatments of the cryogenic pipes during construction might reduce the outgassing. Since the use of MLI increases the outgassing significantly, developing the way of thermal insulation with less MLI is expected [4, 5].

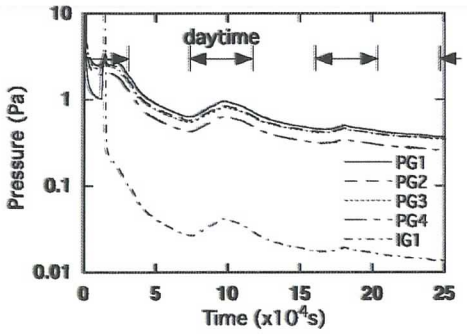

Figure 6. The evacuation by the TMP only from the B port

Though the cryogenic pipe of CASER2 can be pumped from both the ends, pumping was performed only from the B port shown in Figure 2 to see the evacuation characteristics of longer cryogenic pipes as an attempt. The result is shown in Figure 6. In this case the order of the gauges is IG1, PG4, PG3, PG2 and PG1 from the TMP. Similar tendency is seen as Figure 5, while the decrease of the pressure is much slower. The highest pressure of the one side pumping at the time of 25×10^4 s (2.9 days) was 0.37 Pa, while this pressure was achieved at 11×10^4 s (1.3 days) in the case of the both side pumping. This indicates that small increase of the pipe length could increase the evacuation time significantly. Therefore, the interval of pumps should be planned carefully. The one side pumping roughly makes the conductance to the furthest point from the TMP a quarter. Obviously, the slow decrease of the pressure comes from the smaller conductance. When the cryogenic pipe is designed, the inside structure of the pipe, such as the support of the inner pipe, should be re-examined to increase the conductance, before increasing the inner diameter of the outer pipe. The increase of the diameter increases the inner surface area, which leads to the increase of the outgassing, and also increases the cost of the cryogenic pipes.

SUMMARY

We have evacuated the 200 m cryogenic pipe of CASER2 for the superconducting DC power transmission. Based on the time evolution of the pressures along the cryogenic pipe, the evacuation systems required for cryogenic pipes were discussed. Small pumps with the pumping speed much less than 100l/s are enough for the cryogenic pipes for the superconducting power transmission and the interval of the pumps should be planned carefully. The reduction of the outgassing and the increase of the conductance are efficient to get shorter evacuation time.

REFERENCES

[1] Shu, Q. S. et al., An experimental study of heat transfer in multilayer insulation systems from room temperature to 77 K, Adv. Cryo. Eng. (1986)31 455-463.

[2] Yamaguchi, S et al., Research activities of DC Superconducting power transmission line in Chubu University, J.Phys: Conf. Ser. (2008) 97 012290-1-7.

[3] Hamabe, M et al., Recent progress of experiment on DC superconducting power transmission line in Chubu University, IEEE trans. Appl. Supercond. (2009)19 1778-1810.

[4] Hamabe, M et al., Cryogenic system for DC superconducting power transmission line, IEEE trans. Appl. Supercond. (2007)17 1722-1725.

[5] Nasu, Y et al., Heat leak measurement on zinc-coated cryogenic pipe for superconducting power transmission line, Proc. ICEC 22-ICMC 2008 (2008) 489-494.

High accuracy measurement of heat leak of cryogenic pipes for DC superconducting power cable

Sugino M., Hamabe M.*, Watanabe H.*, Kawahara T.*, Yamaguchi S.*, Ishiguro Y.**, and Shinshi O.**

Department of Electrical Engineering, Chubu University, 1200, Matsumoto-cho, Kasugai, Aichi, 487-8501, Japan
*Center of Applied Superconductivity and Sustainable Energy Research, Chubu University, 1200, Matsumoto-cho, Kasugai, Aichi, 487-8501, Japan
**Steel Research Laboratory, JFE Steel Corporation, 1-1, Kawasaki-cho, Handa, Aichi, 475-8611, Japan.

Considering a long DC superconducting power transmission (DC SC-PT) system, the radiation heat leak on the liquid-nitrogen(LN2)-cooled cryogenic pipe of the power transmission line is the main heat load, and the reduction of the radiation heat is one of the key issues to realize such a long DC SC-PT system. We have proposed to employ smooth bore cryogenic pipe to reduce the pressure drop of LN2 flow. We have also proposed to use zinc coating on cryogenic pipe surface to reduce the radiation heat. Recently, we constructed a new experimental device for a inclined smooth bore cryogenic pipe to measure more accurately the radiation heat of 0.5 W/m. Consequently, zinc coating on both the inner and the outer pipes achieved 0.59 W/m, whereas the zinc-coated outer pipe and the multilayer-insulated inner pipe achieved 0.37 W/m.

INTRODUCTION

Recently, many researches started in the world, aiming to demonstrate the large-scale AC superconducting power transmission(SC-PT)[1], [2]. In Chubu University, we carried out a series of experiments using a test bench of 20 m-class DC superconducting power cable (CASER-1) [3] and then we constructed a 200 m-class DC superconducting power cable (CASER-2) [4]. Reduction of the radiation heat leak on the power transmission line is one of the key issues to realize a long distance DC SC-PT system, since the radiation heat into the cryogenic pipe is the main heat loss on the long cryogenic line. High heat radiation on the cryogenic pipe needs to increase the flow rate of cryogen in the cryogenic pipe, in order to keep the low temperature; the increase of the cryogen flow rate leads to increase of the cryogen pump power. Furthermore, the increase of the pump power causes the heat load on the pump itself, and the more pump power is necessary to remove the heat load on the pump. Hence, the reduction of the radiation heat on the cryogenic pipe can reduce the power consumption of the DC SC-PT system. Smooth bore pipes, instead of usual corrugate pipes, were used for cryogenic line of our cables, since the use of the corrugate pipes also causes a high pressure drop of cryogen flow and increases the cryogen pump power[5].

Multilayer insulator (MLI) is a strong tool to reduce the radiation heat, and is widely employed for vacuum-insulated low temperature systems [6]-[9]. However, considering a low gas-flow conductance of

long cryogenic lines for SC-PT, outgassing from MLI leads to the long evacuation time to achieve a good vacuum insulation. Moreover, installation of MLI can increase the construction cost of the cryogenic line. We have proposed zinc (Zn) coating on the vacuum-insulated cryogenic pipe instead of MLI to reduce the emissivity of the pipe surface [10], [11]. A vertical experimental device had been used to measure the radiation heat of the cryogenic pipes of 1.65 m in length with various surfaces, and consequently Zn-coated pipe showed a very low radiation heat of 3.0W/m [11]. A report from Navigant Consulting, Inc. points out that the energy loss on the cable line needs to be less than 0.5 W/m for the practical use of the SC-PT system [12]. Since our previous device was hard to measure such a low radiation heat accurately, we constructed a new experimental device for accurate radiation-heat measurement. In this paper, we will describe the experimental results using the new experimental device and show the low radiation heat for Zn-coated cryogenic pipe.

EXPERIMENTAL SETUP

Figure 1 shows a schematic diagram of a new experimental device of vacuum-insulated cryogenic pipe. Cryogen was liquid nitrogen (LN2) since the CASER-1 cable and the CASER-2 cable use Bi2223 superconductor tapes. Similar to the previous device [11], heat leak into the inner pipe was estimated from evaporation speed of LN_2 at the "measurement part of LN_2 level" in Figure 1. This narrow part of 19 mm in diameter increased the reduction rate of LN_2 level to shorten the experiment time and to prevent conduction heat from top flange. Height of LN_2 level x at the measurement part was measured by LN_2 level meter (CryoVac Corp., 08E032).

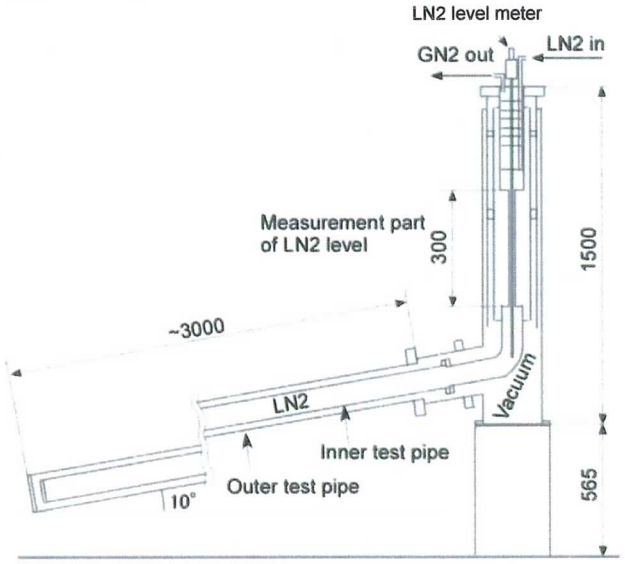

Figure 1. A schematic diagram of a new experimental device for the radiation-heat measurement on vacuum-insulated cryogenic pipe

Test pipes were transversely connected to the device, and with an angle by 10° for evaporated N2 gas not to remain in the inner test pipe. The radiation heat can reduce by using a small inner pipe. In this experiment (also in the CASER-2 cable), the diameter of the inner test pipe was 60.5 mm; whereas, the diameter of the inner pipe was 86 mm for the previous device and for the CASER-1 cable. Stainless-steel pipe and Zn-coated stainless-steel pipe were prepared for this experiment. The outer test pipe was the same one for the CASER-2 cable, which is made of the Zn-coated steel with a diameter of 216.5 mm.

The vertical inner pipes above and below the measurement part was supported by FRP tube since this vertical inner pipe line suffers the mechanical torque due to the long and inclined inner test pipe. This line and FRP tube was wound with MLI for the radiation-heat shielding.

Namely, we designed the new experiment device for the accurate radiation-heat measurement after following two points:

1) vertical connecting of the test pipes can enlarge the length of the test pipes; therefore, the heat leak due to the radiation heat can reach enough high to measure, even if the radiation heat per unit pipe length is very low, and
2) sufficient suppression of background heat leak on the experimental device (the baffle plates on the gaseous N_2 space above the measurement part, the narrow cross-section of the measurement part, FRP supporting for these vertical line with sufficient MLI shielding, etc.).

RESULTS AND DISCUSSION

Figure 2 shows time variations of LN2 level for various inner pipes. In Figure 2, we measured four types of the inner pipe configuration,

1) "No pipe" means the configuration without the test inner pipe,
2) SUS304 is the bare 304 stainless-steel inner pipe,
3) "Zn-coated SUS304" means the 304 stainless-steel inner pipe with Zn-coated by galvanizing process, and
4) "SUS304 + MLI 10 layer" means the bare 304 stainless-steel inner pipe wound with ten layers of MLI.

The lengths of all inner test pipes were 2.9 m and 1.76 times longer than that of the previous device. Total heat leak Q_{total} was estimated from

$$Q_{\text{total}} = qcA\frac{\mathrm{d}x}{\mathrm{d}t}, \tag{1}$$

where q is evaporation heat of LN_2; c is mass density of LN_2 at 77.4 K; A is cross-section of the measurement part of LN_2 level, and $\mathrm{d}x/\mathrm{d}t$ is decreasing speed of the height of LN_2 level. Background heat leak without the test inner pipe Q_0 was measured three times (as shown in Table 1) to examine the accuracy of the experimental device. Consequently, estimated Q_0 was 0.55±0.01 W and reduced by 54% compared with the previous experimental device (Q_0 = 1.2 W).

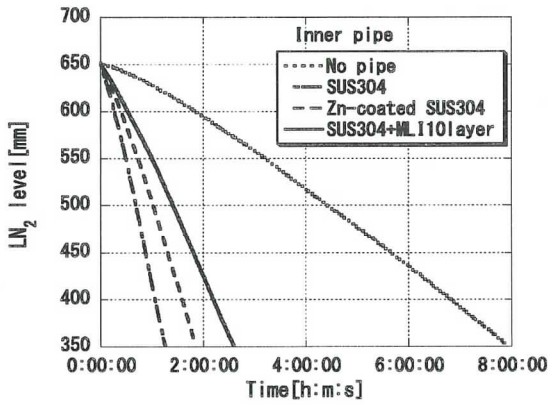

Figure 2. Time variaton of LN2 level for the various inner pipes

Table 1. Background heat leak measurement of Q_0

Experiment No.	Outer pipe temperature T_H [K]	Decreasing of LN2 level dx/dt [mm/s]	Background heat leak 00 [W]
1	302.6	0.0116	0.528
2	302.5	0.0123	0.558
3	302.6	0.0123	0.558

Table 2 shows the measured radiation heat Q_R (= Q_{total} - Q_0), the radiation heat per unit pipe length q_R. The variation of the outer pipe temperature T_H strongly affects the comparison of Q_R and q_R, since Q_R is proportional to (T_H^4 - T_L^4) from Stefan-Boltzmann's law (T_L is the inner pipe temperature); therefore, q_R in Table 2 was calibrated at T_H = 300 K and T_L = 77.4 K for the precise comparison using Stefan-Boltzmann 's law [10].

The target value of radiation-heat reduction is 0.5 W/m for the practical DC SC-PT [12]. As shown in Table 2, Zn coating on both the inner stainless steel pipe and the outer steel pipe reached 0.59 W/m, i.e. just 18 % higher than the target value with no MLI. Meanwhile, combination of the Zn-coated outer pipe and only ten layers of MLI on the stainless-steel inner pipe achieved the target value, and a long evacuation time for MLI surface is the essential problem for the practical use of this combination.

Reduction of the inner pipe diameter can reduce the radiation heat more. However, SC cable diameter is limited and was 40 mm for CASER-1 cable [3], and the small inner pipe causes the LN_2 circulation loss due to the small cross-section of the LN_2 flow. Consequently, Zn coating on the pipe surface has a potential for the cryogenic pipes to be free from MLI for the small diameter inner pipe, if we carefully consider the balance between the radiation heat and the LN_2 circulation loss for the design of the cable and the cryogenic line diameter.

Table 2. Measured radiation heat

Inner pipe material	Q_{total} [W]	Q_R[W]	q_R[W/m]
SUS304	3.30	2.75	1.01
Zn-coated SUS304	2.11	1.56	0.59
SUS304+ MLI 10 layers	1.56	1.01	0.37

outer pipe : Zn-coated steel pipe(200A)

CONCLUSION

Considering a long DC SC-PT system, the reduction of the radiation heat to less than 0.5 W/m is one of the key issues for practical use. We have proposed to employ smooth bore cryogenic pipe to reduce the pressure drop of cryogen flow, and also proposed to use zinc coating on cryogenic pipe surface to reduce the radiation heat. A new experimental device for a inclined smooth bore cryogenic pipe was constructed for the more accurate heat leak measurement of less than 0.5 W/m. Consequently, zinc coating on both the inner and the outer pipes achieved 0.59 W/m, whereas the zinc-coated outer pipe and the bare stainless-steel inner pipe wound with ten layers of MLI achieved 0.37 W/m.

ACKNOWLEDGMENT

Authors are grateful to Dr. A. Iiyoshi, chancellor of Chubu University for his continuous encouragement through this work. Authors also thank for Mr. Y. Toki in Chubu University and his continuous efforts to carry out the experiment.

REFERENCES

[1] Maguire. J.F, et al., Development and Demonstration of a long length HTS cable to operate in the Long Island power authority transmission grid, IEEE Trans. Appl. Supercond., (2005) vol.15 No.2 1787-1792.

[2] Weber. C.S, et al., Overview of the underground 34.5kV HTS power cable program in Albany, NY , IEEE Trans. Appl. Supercond., (2005) vol.15 No.2 1793-1797.

[3] Yamaguchi. S, et al., Research activities of DC superconducting power transmission line in Chubu University, Jour. of Phys.: Conference Series, (2008) 97 012290.

[4] Yamaguchi. S, et al., Construction and operation of 200-meter high temperature superconducting DC power cable test facility in Chubu University, Int. Cryogenic Eng. Conf. 23 (this conference), (2010).

[5] Sasaki. A, et al., A numerical analysis in LN2 channel for DC-SC power transmission line, Adv. in Cryogenic Eng. (2008) 53 75-82.

[6] Boroski. W.N, Gonczy. J.D, and Niemann. R.C, Thermal performance measurement of a 100 percent polyester MLI system for the superconducting super collider; part 1 : instrumentation and experimental preparation (300K-80K) , Adv. in Cryogenic Eng. (1990), 35 487-496.

[7] Gonczy .J.D, Boroski .W.N, and Niemann. R.C, Thermal performance measurement of a 100 percent polyester MLI system for the superconducting super collider ; part2 : laboratory results (300K-80K), Adv. in Cryogenic Eng. (1990), 35 497-506.

[8] Ohmori. T, et al., Lightweight multilayer insulation to reduce the self-compression of insulation films, Adv. in Cryogenic Eng. (2002) 47 1565-1572.

[9] Ohmori. T, Nakajima. M, and Yamamoto. A, Thermal performance of multilayer insulation fabricated around a horizontally supported cylinder, Adv. in Cryogenic Eng. (2004) 49 595-604.

[10] Hamabe. M, et al., Radiation heat measurement on thermally-isolated double-pipe for DC superconducting power transmission, Adv. in Cryogenic Eng. (2008) 53 168-173.

[11] Nasu. Y, et al., Heat leak measurement on zinc-coated cryogenic pipe for superconducting power transmission line, Proc. of Int. Cryogenic Eng. Conf. 22 and Cryogenic Mat. Conf.2008 , KIASC, Seoul, Korea (2009) 489-494.

[12] High Temperature superconductivity Market Readiness Review, http://www.suptech.com/pdf/articles/07 Navigant HTS Market Readiness Study.pdf (2006).

Physica C 471 (2011) 1313–1316

Contents lists available at ScienceDirect

Physica C

journal homepage: www.elsevier.com/locate/physc

Critical current measurements for design of superconducting DC transmission power cable

J. Sun [a,*], S. Yamauchi [b], M. Sugino [b], H. Watanabe [a], M. Hamabe [a], T. Kawahara [a], S. Yamaguchi [a,b]

[a] Center of Applied Superconductivity and Sustainable Energy Research, Chubu University, 1200, Matsomot-cho, Kasugai, Aichi 487-8501, Japan
[b] Department of Electrical Engineering, Chubu University, 1200, Matsumoto-cho, Kasugai, Aichi 487-8501, Japan

ARTICLE INFO

Article history:
Available online 13 May 2011

Keywords:
DC transmission
HTS cable
Critical current
Magnetic field effect

ABSTRACT

In the present experiments three straight high temperature superconducting BSCCO tapes were set parallel to each other on a board and the currents were fed to the tapes. The critical currents of the tape which was set between two tapes were measured with respect to the gap between the tapes. We observed that the critical current increases with decreasing the gap. The calculation of the magnetic flux lines around the tape by finite element method demonstrates the effect on self magnetic field by the adjacent tapes. We could provide some hints on how to arrange the tapes in the power cable for DC power transmission.

1. Introduction

A 20 m superconducting (SC) DC transmission power cable is composed of two layers of high temperature superconducting (HTS) tapes, which are wound close to each other along a copper former to make the magnetic field produced by the current in the cable uniformly [1]. However, this means that either of the layers has additional HTS tapes, since the circumferences of the layers are different for their different radius.

A 200 m coaxial HTS power cable has been installed into a test facility at Chubu University in 2009 [2]. Fig. 1 shows a cross section of this cable composed of two SC layer for each polarity of the DC power. Each layer has 23 and 16 BSCCO HTS tapes spirally surrounding the cable, respectively [3,4]. The outer SC layer is composed of monolayer HTS tapes and the inner SC layer is composed of two-layer HTS tapes. Since the rating current of the cables is determined by that of the layer which has less HTS tapes, the additional HTS tapes are wastes and cause the increase of the cable cost. If it is possible to make the number of the HTS tapes the same for the two SC layers, flexibility can be obtained for the manufacture of the cables. However, this makes either of the layers become sparse and causes disorder of the magnetic field along the cables, which might decrease the maximum current of the cables and affect the rating current of the cables.

Many works has been done to study the AC losses due to the gap effect theoretically and experimentally [5–9], since the gap cannot remove in practical cable winding by using HTS tape conductors. The situation of the DC cable becomes simple and it is unnecessary to consider the AC losses. In order to investigate the effect caused to the maximum current of the cables by the way of the tape winding, we investigate the dependence of the critical current of the HTS tape on the gaps between the tapes due to the magnetic field from the current through the adjacent tapes. The calculation of the magnetic flux lines around the tape by finite element method demonstrates the effect on self magnetic field by the adjacent tapes. We could provide some hints on how to arrange the tapes in the power cable for DC power transmission.

2. Experiments

The multifilamentary DI-BSCCO® tapes (Type HT-CA) are used provided by Sumitomo Electric Industries, Ltd. (SEI) [3,4]. The cross section of the HTS tape is 4.5 mm wide and 0.35 mm thick. The thickness of the HTS tape includes the thickness of the reinforcing layer, which is 0.05 mm on both sides of the Bi2223 filaments to hold the mechanical strength of the tape [3].

Fig. 2 shows a schematic layout of the experimental setup and a photo of the experimental scenario. Three straight HTS tapes with length 28 cm are set parallel to each other on a FRP (Fiber-reinforced plastic) plate. The transport currents are fed into three tapes in series mode. Each tape is surrounded with one Kapton-tape layer with thickness of ~69 μm to be insulated with each other. The critical currents of the tapes which were set between two tapes were measured with respect to the gap between the tapes on the criterion of 1 μV/cm. Three voltage taps were attached on each tape with distance of 8 cm and 10 cm as shown in Fig. 1. The samples are immersed in liquid nitrogen. The voltage signals were measured with KEITHLEY 2700 multimeter.

* Corresponding author. Tel.: +81 568 51 9286; fax: +81 568 51 9413.
E-mail address: j_sun@isc.chubu.ac.jp (J. Sun).

0921-4534/$ - see front matter © 2011 Elsevier B.V. All rights reserved.
doi:10.1016/j.physc.2011.05.185

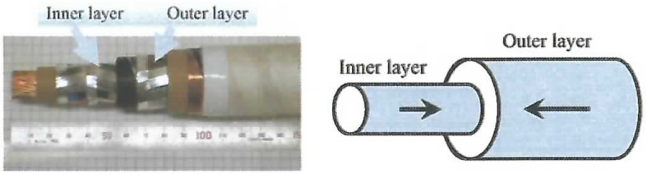

Fig. 1. A photo of DC HTS cable composed of two superconducting layers for each polarity from DC power.

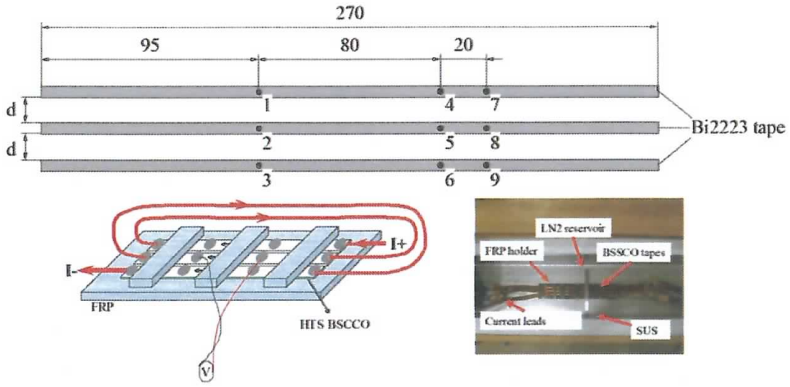

Fig. 2. A scheme of the experimental setup and a photo of the experimental scenario.

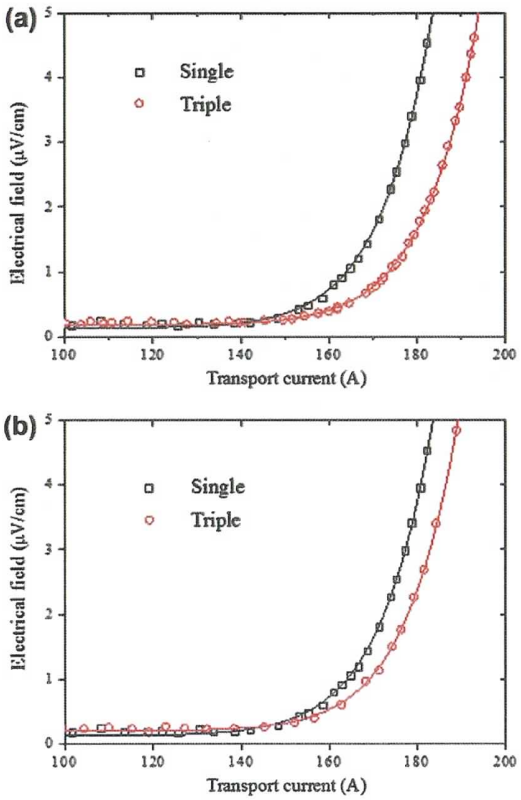

Fig. 3. A comparison of *E–I* characteristic curve of single HTS tape with that in monolayer composed of three straight tapes. (a) $d = 0.4$ mm and (b) $d = 4.5$ mm.

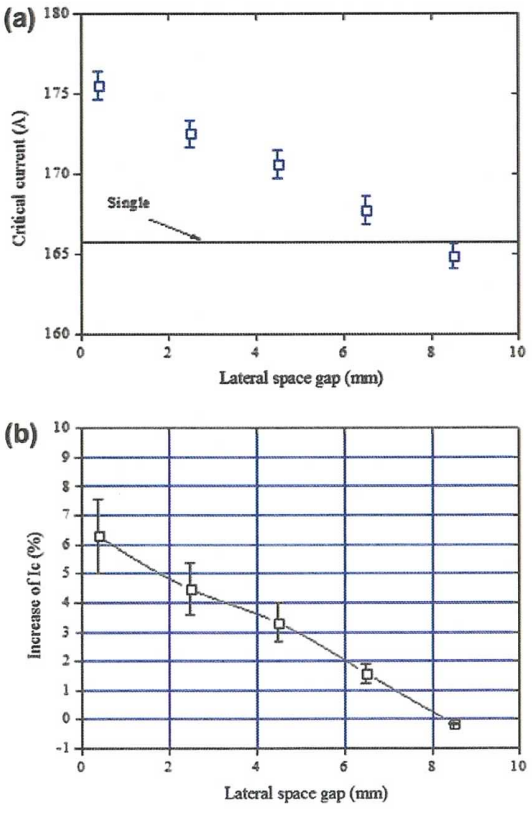

Fig. 4. (a) Dependence of the critical current of the middle HTS tape in the triple arrangement on the lateral space gap between the tapes. (b) Increase of the critical current with respect to the gap.

3. Results and discussion

Fig. 3a and b shows the comparisons of E–I characteristics curves of a HTS wire for single and triple tape arrangement with different gap of 0.4 mm and 4.5 mm, respectively. Fig. 4a presents the dependence of the critical current on the lateral space gap between the tapes and Fig. 4b shows the ratio of increase of the critical current with respect to the lateral space gap. The critical current of the middle tapes increases with decrease of the lateral space gap. With increasing the lateral space gap, the critical current of the middle tape in three straight tapes arrangement approaches to that of the single one.

We simulate the magnetic flux lines distributions by the commercial finite element code (ANSYS) [10,11]. To illustrate the effect on the self-field by the magnetic field from the current in the adjacent tapes, we show the magnetic flux lines surrounding the tapes for single tape in Fig. 5a and three paralleled tapes with d = 8.5 mm, 6.5 mm, 4.5 mm, 2.5 mm and 0.4 mm in Fig. 5b–f, respectively. The transport current is assumed to be uniformly distributed in the BSCCO filaments area in the tape. Hence the cross section of transport current area is 4.5 mm × 0.25 mm by subtracting the thickness of the reinforcing layer [4]. The current is set to be 160 A, nearly same as the critical current in the self-field at 77 K. It can be seen from Fig. 5 that the magnetic flux lines is similar to that of the single one when d = 8.5 mm. When decreasing the gap, the magnetic flux lines density becomes small at the edge of the middle tape. The magnetic flux lines become loose and flat above the wide tape surface, which results in a reduction in the magnetic field component perpendicular to the tape wide surface. Therefore, the critical current of the middle HTS tape increases as shown in Fig. 4. When increasing the gap, the magnetic flux lines surrounding the middle tape for triple HTS tapes arrangement become similar to those of the single one. Therefore, we conclude with that the critical current of the tape in triple arrangement do not become smaller than that of the single tape in spite of loose or close space for present used DI-BSCCO tapes.

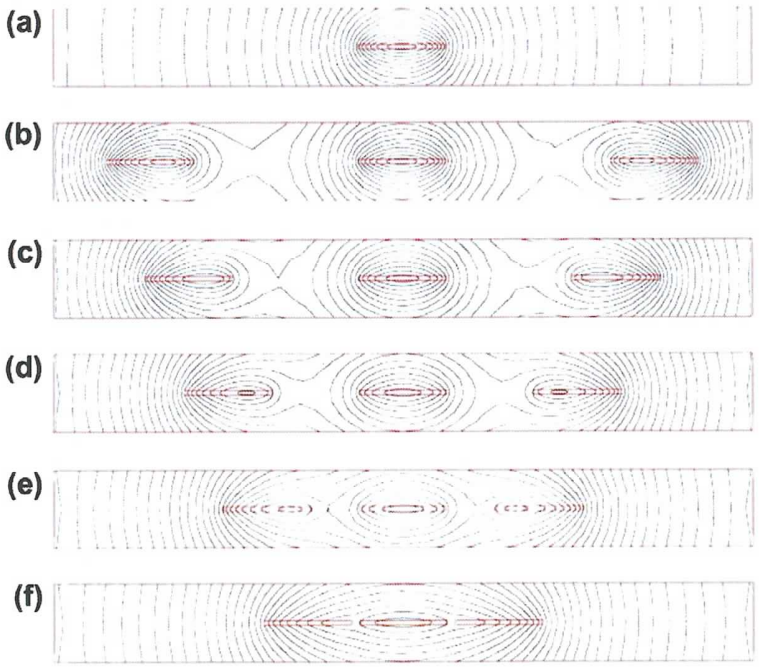

Fig. 5. Magnetic flux lines distribution of single tape (a) and triple paralleled tapes with d = 8.5 mm (b), 6.5 mm (c), 4.5 mm (d), 2.5 mm (e) and 0.4 mm (f) by finite element code (ANSYS). The current is 160 A uniformly distributed in the tape.

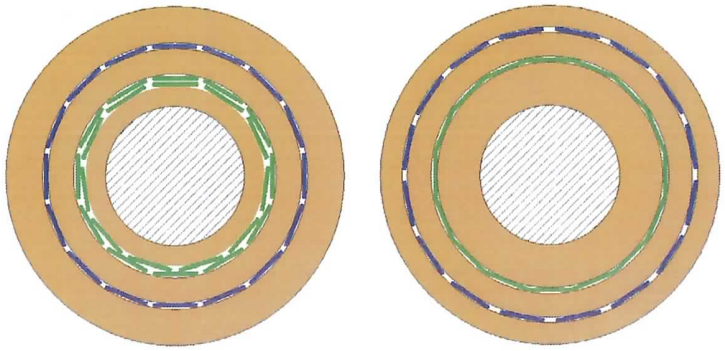

Fig. 6. A scheme of the DC cable with the same number of the HTS tapes for each polarity.

Both the measurement of the critical current of the middle tape and the calculation of the magnetic flux lines for three straight paralleled tapes arrangement give some hints to manufacture a HTS power cable for DC power transmission. Fig. 6 shows a scheme of a new power cable of two monolayer composed of same number of HTS tapes in each layer for each polarity of the DC power together with present used cable. The number of HTS tapes in each layer is 16. The inner diameter of the inner and outer SC layer in the present cable is 18 mm and 25.3 mm, respectively. The thickness of the insulation layer between them is 2 mm. With the same insulation layer thickness, the tapes in the inner layer are wound as close as possible ($d \sim 0$ mm) and the outer layer becomes sparse with the gap of $\sim$1.2 mm. The inner diameter is 22.6 mm and 28.6 mm of the inner and outer SC layer of the new power cable. Based on our experimental results, we consider that the maximum current of the outer layer is estimated to be 16×172 A = 2752 A. The ratio of the maximum current and the rating current is 72%.

4. Conclusion

We have investigated the dependence of the critical current of the BSCCO HTS tapes on the lateral space gap between the HTS tapes in the three straight paralleled tapes. We observed that the critical current of the middle tape increases with decrease of the gap between the tapes. Through the experimental data and the calculation of the magnetic flux lines in the triple tapes with the same transport current, we expect that the critical current of a tape in a single layer cable does not decrease to less than that of the single tape. We concluded with that the HTS tapes winding in the outer layer with larger perimeter could be sparse, which results in less than 7% of the maximum current comparing with the close winding layer. In near future, we must investigate the twisted effects on the critical current of the HTS tapes in the real single layer cable.

Acknowledgements

The authors thank Prof. A. Iiyoshi, Chancellor of Chubu University for his continuous encouragement through this work. The authors acknowledge Prof. Hiroshi Fujiwara for his financial support. This work is partly supported by NEDO through ISTEC as a part of Material & Power Applications of Coated Conductors Project (M-PACC). This work is also partly supported by The Hori Information Science Promotion Foundation (J.S.).

References

[1] S. Yamaguchi, M. Hamabe, I. Yamamoto, T. Famakinwa, A. Sasaki, A. Iiyoshi, J. Schultz, J. Minervini, T. Hoshino, Y. Ishiguro, K. Kawamura, J. Phys.: Conf. Ser. 97 (2008) 012290.
[2] S. Yamaguchi, T. kawahara, M. Hamabe, H. Watanabe, Y. Ivanov, J. Sun, A. Iiyoshi, Presented at ICEC 23-ICMC 2010, 20M-OR-3.
[3] N. Ayai, K. Yamazaki, M. Kikuchi, G. Osabe, H. Takaaze, H. Takayama, S. Kobayashi, J. Fujikami, K. Hayashi, K. Sato, K. Osamura, H. Kitaguchi, S. Matsumoto, T. Kiyoshi, J. Shimoyama, IEEE Trans. Appl. Supercond. 19 (2009) 3014.
[4] M. Kikuchi, T. Kato, K. Ohkura, N. Ayai, J. Fujikami, K. Fujino, S. Kobayashi, E. Ueno, K. Yamazaki, S. Yamade, K. Hayashi, K. Sato, T. Nagai, Y. Matsui, Physica C 445–448 (2006) 717.
[5] O. Tsukamoto, Y. Yamato, S. Nakamura, J. Ogawa, IEEE Trans. Appl. Supercond. 15 (2005) 2895.
[6] J.-H. Joo, S.-W. Kim, K.J. Song, C. Park, R.-K. Ko, H.-S. Kim, J.-P. Hong, S.B. Kim, IEEE Trans. Appl. Supercond. 16 (2006) 119.
[7] S. Stavrev, B. Dutoit, F. Grilli, IEEE Trans. Appl. Supercond. 13 (2003) 3807.
[8] F. Gömöry, L. Frolek, J. Šouc, G. Coletta, S. Spreafico, IEEE Trans. Appl. Supercond. 13 (2003) 1968.
[9] K. Ryu, K.B. Park, G. Cha, IEEE Trans. Appl. Supercond. 11 (2001) 2220.
[10] http://www.ansys.com/.
[11] E. Pardo, A. Sanchez, D.-X. Chen, C. Navau, Phys. Rev. B 71 (2005) 134517.

Physica C 471 (2011) 1308–1312

Contents lists available at ScienceDirect

Physica C

journal homepage: www.elsevier.com/locate/physc

Circulation pump power for 200 m cable experiment

Yu.V. Ivanov *, H. Watanabe, M. Hamabe, J. Sun, T. Kawahara, S. Yamaguchi

Chubu University, Matsumoto-cho 1200, Kasugai, Aichi 487-8501, Japan

ARTICLE INFO

Article history:
Available online 13 May 2011

Keywords:
High-temperature superconducting cables
Power transmission
Cooling system
Natural circulation
Thermal siphon
Heat transfer

ABSTRACT

Efficiency of the energy management can be significantly enhanced using the technology of superconducting (SC) power transmission. A high cost of the existing experimental SC lines is determined to a great extent by the use of expensive cryopumps. Moreover, pumping stations require maintenance, and cryopumps are a source of additional heat load for the system. It was proposed to utilize a thermal siphon effect to naturally circulate liquid nitrogen (LN2) through the cryopipes. Calculations showed the feasibility of this idea. Currently, there is an opportunity to verify of our estimations using new 200 m experimental facility at Chubu University. The level difference of circulation loop is almost 5 m, therefore noticeable driving force due to the difference in densities of "cold" LN2 near the inlet and "warm" LN2 near the outlet adds to the pump power. The cryopipe is equipped with heaters, allowing to carefully change the intensity and distribution of heat load to make it possible to analyze in details the influence of thermosiphon effect on the circulation of LN2 and pump energy saving.

1. Introduction

A steady growth of energy consumption, reducing of fossil fuel reserve and deterioration of the ecological situation on Earth act as a driving force to develop new energy-saving technologies, using renewable energy sources and to optimize methods of delivery and distribution of electric energy. Currently, most interest are high-temperature superconductors (HTS), opening the possibility for high-density energy transfer with very low loss that cannot be done using conventional conductors. The phenomenon of superconductivity is studied for a century. Actually researchers have closely approached to creation of the commercial power transmission (PT) lines based on HTS. Unfortunately, there are a number of unresolved technical problems that impede the achievement of maximum efficiency of the HTS lines; therefore the length of the existing experimental cables remains within a few hundred meters. The main difficulty is creation of an effective heat insulation, without which the cost of HTS cable cooling becomes very high. It is now widely accepted to use superinsulation. Published data shows that it allows to reduce the heat load to an acceptable level of about 1–3 W/m. Another significant source of the heat is the AC loss which is in the same order (see Table 1); therefore it is preferable to use DC. It should be noted that the short distance PT lines are very different from the long distance ones due to heat leak through current leads dominates. In our work we consider the long DC PT line. Circulating refrigerant is used to remove heat penetrating through the insulation layers. In the case of HTS it is usually liquid nitrogen (LN2). Its working temperature range is rather narrow being bounded below by the melting point (63.2 K) and above by the boiling point (77.4 K) (at 1 atm). Increase in pressure expands the range, but critical temperature of HTS at the given current will be other restriction on the range. If we consider the distributed heat load (which dominates in the case of long PT lines) only, the mass flow of LN2 required to remove heat is expressed by a well-known relation

$$\dot{m} = \frac{Lq}{C_p \Delta T} \tag{1}$$

The pressure drop can be obtained by Darcy–Weisbach equation

$$\Delta p = f \frac{L}{D_h} \frac{\rho v^2}{2} \tag{2}$$

Taking into account relation between mass flow and velocity

$$\dot{m} = \rho v A_h \tag{3}$$

and assuming ΔT = const, we can obtain the pressure drop dependence of the cable length and heat load as

$$\Delta p = f \frac{L^3}{2 D_h \rho} \left(\frac{q}{C_p \Delta T A_h} \right)^2 \tag{4}$$

where A_h is the cross sectional area, m^2; C_p is specific heat, J/kg K; D_h is hydraulic diameter, m; f is dimensionless friction factor; L is cryopipe length, m; $\dot{m}$ is mass flow, kg/s; Δp is pressure drop, Pa; q is heat load, W/m; ΔT is temperature difference, K; v is flow velocity,

* Corresponding author. Address: Center of Applied Superconductivity & Sustainable Energy Research, Chubu University, Matsumoto-cho 1200, Kasugai, Aichi 487-8501, Japan. Tel.: +81 568 51 9286; fax: +81 568 51 9413.
E-mail address: ivanov@isc.chubu.ac.jp (Yu.V. Ivanov).

0921-4534/$ - see front matter © 2011 Elsevier B.V. All rights reserved.
doi:10.1016/j.physc.2011.05.184

Table 1
Representative HTS cable projects.

Project title	Length (m)	Power (MVA)	Phases	AC loss (W/m/phase)	Heat leak (W/m)	Refs.
Albany	320 + 30	48	3-in-1	0.7 at 0.8 kA	2.9	[1]
KEPCO	100	50	3-in-1	2.27 at 1.25 kA	2.2	[2]
LIPA	600	574	3	4.28/3 at 2.4 kA	1.3 × 3	[3]
Super-ACE	500	77	1	1.34 at 1 kA	1.21	[4]

m/s; and ρ is density, kg/m^3. In the case of turbulent flow in smooth pipe the friction factor f weakly depends on flow rate. It can be expressed by the Blasius correlation

$$f = 0.3164\mathrm{Re}^{-0.25} \tag{5}$$

where Re denotes the dimensionless Reynolds number, which is directly proportional to flow velocity

$$\mathrm{Re} = \frac{\rho v D_h}{\mu} \tag{6}$$

where μ is the dynamic viscosity, Pa s.

It is easily seen that the pressure drop increases dramatically being almost cubic function of the cable length. It should also be added that at high pressure drop and high mass flow frictional heating becomes noticeable. Therefore, the pressure drop is the limiting factor on the maximum length of a cable segment between pumping stations. Great efforts should be made to reduce heat load on the system and hydraulic friction inside the circulation channels. This requirement is contrary to current practice, when all of the existing experimental HTS PT lines are constructed using corrugated pipes as flexible cryostats. Both calculations and experiments show that the hydraulic resistance of such channels is several times larger than the resistance of the smooth pipes of similar diameter [5–7]. From this point of view it is necessary to use smooth cryopipes separated by short bellows inserts to compensate for the mechanical stresses and thermal expansion/contraction. As far as we know this design was realized only at experimental facility at the Chubu University. It is also important to use a smooth outer jacket for HTS cables.

Circulation cryopumps represent powerful source of heat load. Several years ago it was suggested to use natural circulation of LN2 (thermal siphon effect) to reduce pump power [8]. Conceptual design of the HTS cable cooling system based on thermal siphon effect is shown in Fig. 1. The apparatus is comprised of a vertical pressure segment and a horizontal cooling (working) segment. A tank with LN2 and cooler are placed at the top of the circuit. Heavy "cold" LN2 moves down through the vertical cryopipe, and then flows through long horizontal sections containing HTS cables, maintaining its temperature below T_c. Being heated by the heat passing through the superinsulation and current leads, light "warm" LN2 raises through the second vertical cryopipe and returns back into the tank. The driving force of the process is the difference between the gravity of "cold" and "warm" refrigerant in vertical segments. A heater, which can vaporize small amount of LN2 and thereby significantly increase driving force, can be used as a starter. Thermal siphons are widely used in industry. Our theoretical calculations confirmed feasibility of this proposal [8].

The 200 m test facility at Chubu University, Japan, which was successfully installed and commissioned on the beginning of 2010 offers the possibility to verify this approach experimentally. The level difference of circulation loop is almost 5 m, therefore noticeable driving force due to the difference in densities of "cold" LN2 near the inlet and "warm" LN2 near the outlet adds to the pump power. The cryopipe is equipped with heaters, allowing to carefully change the intensity and distribution of heat load to make it possible to analyze in details the influence of thermosiphon effect on the circulation of LN2. We carried out preliminary experiments to study the behavior of LN2 flow under the strong local heating. The results obtained coincided with the expected ones. Boiling of LN2 was observed under high heat load. The data obtained allow plan a full-scale experiment, which will be performed probably during the next cooling cycle.

2. Experimental

Construction of a new experimental facility at the Chubu University was launched in 2009 and completed in March 2010. 200 m DC cable using Bi-2223 HTS tapes was manufactured by

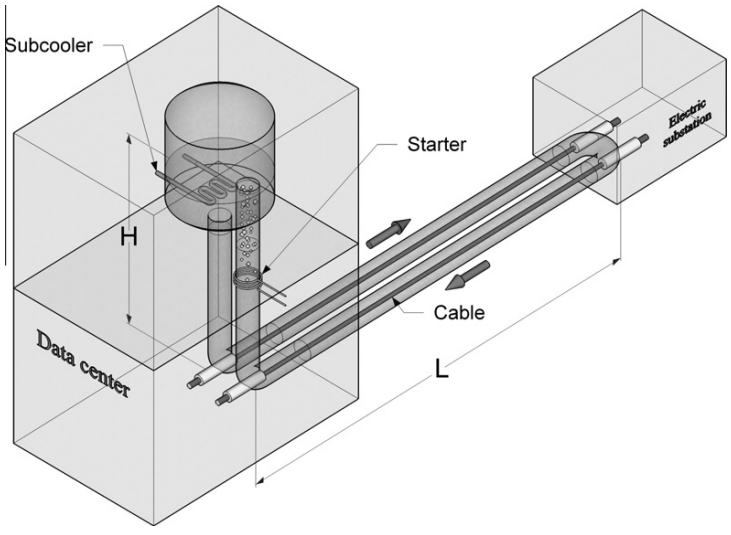

Fig. 1. Conceptual design of the HTS cable cooling system based on the thermal siphon effect.

Sumitomo Electric Industries, Ltd. in accordance with our design. The facility is equipped with several enhancements that distinguish it from all the existing ones. In particular, the current leads are equipped with a Peltier element to reduce heat leakage; smooth cryogenic pipes instead of corrugated ones are used in order to reduce hydraulic friction and pressure drop; terminal units are made movable to compensate for thermal contraction/expansion of the cable. The facility can be divided into two parts: "horizontal" (which includes cryopipe with cable and terminals) and "vertical" (which includes subcooler, circulation pump, LN2 tanks, and flow meter). A sufficiently large difference of elevation between overhead tank and cryopipe allows, under appropriate conditions, to realize the natural circulation of LN2. Automated measurement system reads data from more than 500 sensors with a period of 3 s.

For experiments we used only horizontal part of the test facility (Terminal A – cryopipe – Terminal B) which simulates single segment of the long PT line between two cooling stations. Difference of elevation between terminals and cryopipe is 2.6 m. The first set of measurements was carried out to determine the actual heat load and to evaluate the quality of superinsulation. The temperature distribution was measured by seven pairs of platinum resistance thermometers located at different distances from the inlet (see Table 2). Measurements revealed significant non-uniformity of the heat load distribution. It can be explained by the complexity of achieving high quality insulation in the vicinity of joints, bends, gates, and inner pipe holders. Experimental curve is shown in Fig. 2. Points represent data averaged over 10 min (200 samples). The average heat leak obtained by least-squares fit of Eq. (1) amounted to 2.1 W/m which should be recognized as sufficiently large value. According to our estimations it is due to the insufficient vacuum level. The scatter of points on the graph is connected, obviously, with heat leak dependence on weather conditions. This dependence will be analyzed in future.

The next series of measurements was carried out to evaluate the hydraulic resistance of the channel formed by the HTS cable with outer diameter of 34.8 mm inserted in cryopipe with inner diameter of 57.2 mm. Estimation shows that the flow in this channel is characterized by the Reynolds number 9000–20,000 (turbulent character) at working flow rate 8–17 L/min. The pressure difference Δp was measured between terminals. Averaged over 10 min data are shown in Fig. 3. Precise calculation of the pressure drop is difficult because of the commonly used correlations were obtained for the smooth and rough circular pipes, but in our case cable is placed inside pipe and shifted downwards. The design behavior of the pressure drop was estimated using Eq. (2). Friction factor f was calculated as the sum of contributions of smooth wall of the pipe and rough outer jacket of the cable proportional to the corresponding wetted perimeters. The roughness of the cable outer jacket was taken as 1 mm.

Table 2
Location of thermometers and heaters.

Unit	From A (m)	To B (m)	Elevation (m)	Comment
Terminal A	0	191	0	
TP11, TP12	7.6	183.4	0	Horizontal pipe
HT1	19.2	171.8	−2.6	Horizontal pipe
TP21, TP22	19.4	171.6	−2.6	Horizontal pipe
TP31, TP32	65.2	125.8	−2.6	Horizontal pipe
TP41, TP42	95.2	95.8	−2.6	Horizontal pipe
HT2	107	84	−2.6	Not in use
TP51, TP52	124.1	66.9	−2.6	Horizontal pipe
TP61, TP62	172.2	18.8	−2.6	Horizontal pipe
HT3	178	13	−0.46	Sloping pipe
TP71, TP72	184	7	0	Horizontal pipe
Terminal B	191	0	0	

TP denotes thermometers; HT denotes heaters.

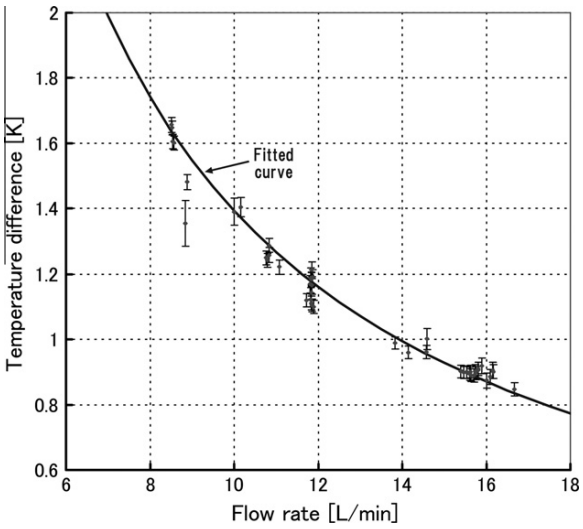

Fig. 2. Temperature difference between TP7 and TP1 as a function of the flow rate. Fitted curve represents theoretical values at 2.1 W/m of the heat load.

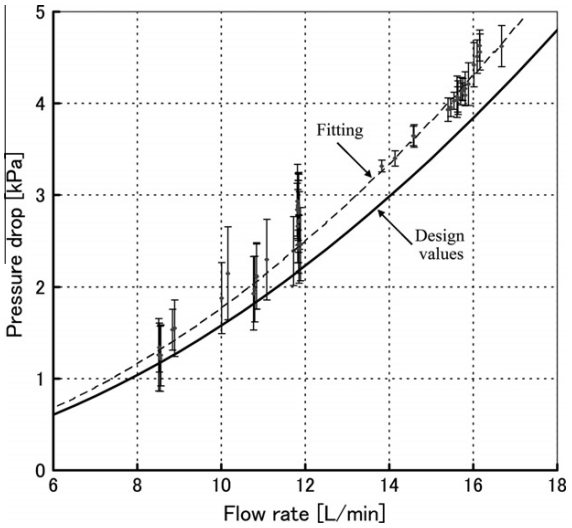

Fig. 3. Pressure drop as a function of LN2 flow rate. Smooth curve shows design values, dashed curve is the result of fitting of the experimental data.

$$f = \frac{f_1 D_1 + f_2 D_2}{D_1 + D_2} \tag{7}$$

where D_1 is the inner diameter, and f_1 is friction factor of smooth cryopipe calculated by Eq. (5); D_2 is the outer diameter, and f_2 is friction factor of rough cable defined implicitly by Colebrook–White equation

$$\frac{1}{\sqrt{f}} = -2\log_{10}\left(\frac{\varepsilon}{3.7 D_h} + \frac{2.51}{\mathrm{Re}\sqrt{f}}\right) \tag{8}$$

where ε is the pipe roughness height, m. Minor losses that occur in pipeline due to joints, bends, etc. were also evaluated. They were of the order of 0.5% due to the large radius of curvature of the cryopipe. The measured values of the pressure drop exceed the calculated ones by 12% on average (see fitted curve in Fig. 3), that can be considered as unexpected high accuracy of the design equations. This allows us to use conventional correlations to estimate pressure drop in the long HTS PT lines.

The cryopipe is equipped with three compact heaters with capacity of up to 350 W (specific heat load up to 17.5 kW/m^2), mounted at the upper surface of inner pipe. Their locations are specified in Table 2. A series of experiments on the local heating of the LN2 were done. In the first series of measurements heater power was changed step-like. Representative results for heater #3 (HT3) can be seen in left column of Fig. 4. This heater is located almost midway between the pairs of thermometers TP6 and TP7 being mounted on the sloping part of the pipe. Additional temperature rise recorded by TP7 is strictly corresponds to the power applied. A sudden drop in heater temperature caused by a sharp increase in heat transfer coefficient due to a boiling of thin layer of LN2 which is in direct contact with the pipe wall is observed at about 80 W. Temperature of LN2 before the heater is 1–2 K below the boiling point. LN2 flow passes along the heater very quickly namely within 1–2 s. If we assume that all incoming heat expended for vaporization of LN2, then at mass flow rate of 10 L/min and at heater power of 250 W vapor quality is of the order of 1%. This is a sufficiently large value corresponds to approximately 1/2 volume ratio of gas in two-phase mixture. But no visible change is observed in the pressure curve. It may be safely suggested that because of the rapid mixing most of the heat is transferred to the lower layers of LN2 raising their temperature without vaporization and creating a high temperature gradient. Being flowing in the upper part of the channel, nitrogen gas is cooling down with cold LN2 and re-liquefying. This is confirmed by the fact that two thermometers (TP71, TP72) placed upstream did not record changes in the temperature difference between the upper and lower parts of the flow after beginning of the boiling. Therefore, the lifetime of the bubbles is less than 1 min, it is the time until the flow reaches the location of TP71 and TP72 (under the assumption that the velocities of both phases are equal).

Fig. 4 (right column) corresponds to another experiment. HT1 power was varied continuously at a rate of 2 W/min from 70 W to 150 W and then from 150 W to 60 W. This allows us to accurately record the moment of beginning of the transition in the refrigerant. A pair of thermometers TP21 and TP22 is mounted in close proximity (20 cm) to the heater HT1. Strong signal from the upper thermometer and lack of signal change recorded by the lower one confirm our assumption about the local nature of the boiling. The formation of gas bubbles drastically reduces the average density of the medium, causing a sharp increase in the driving force of natural circulation. In the case of pure LN2 flow, temperature difference of 1 K produces additional pressure of about 44 Pa per 1 m of vertical pipe. In the case of two-phase flow characterizing by 1% vapor quality, average density of medium decreases by almost half producing additional pressure of 3.5 kPa per 1 m. However, fast condensation of gas limits the use of such a regime over short distances. Two-phase operating mode requires an accurate experimental study; in addition, it is necessary to take care of keeping the cable insulation quality. Fig. 5 shows the overpressure which supports the circulation due to the thermal siphon effect, as a function of the heater power. The ambient heat load on the cryopipe between two inclined segments is 340 W.

3. Conclusions

Heat load, behavior of LN2 circulation, and influence of local heating on the circulation were observed using the new 200 m HTS DC test facility in order to estimate parameters of thermal

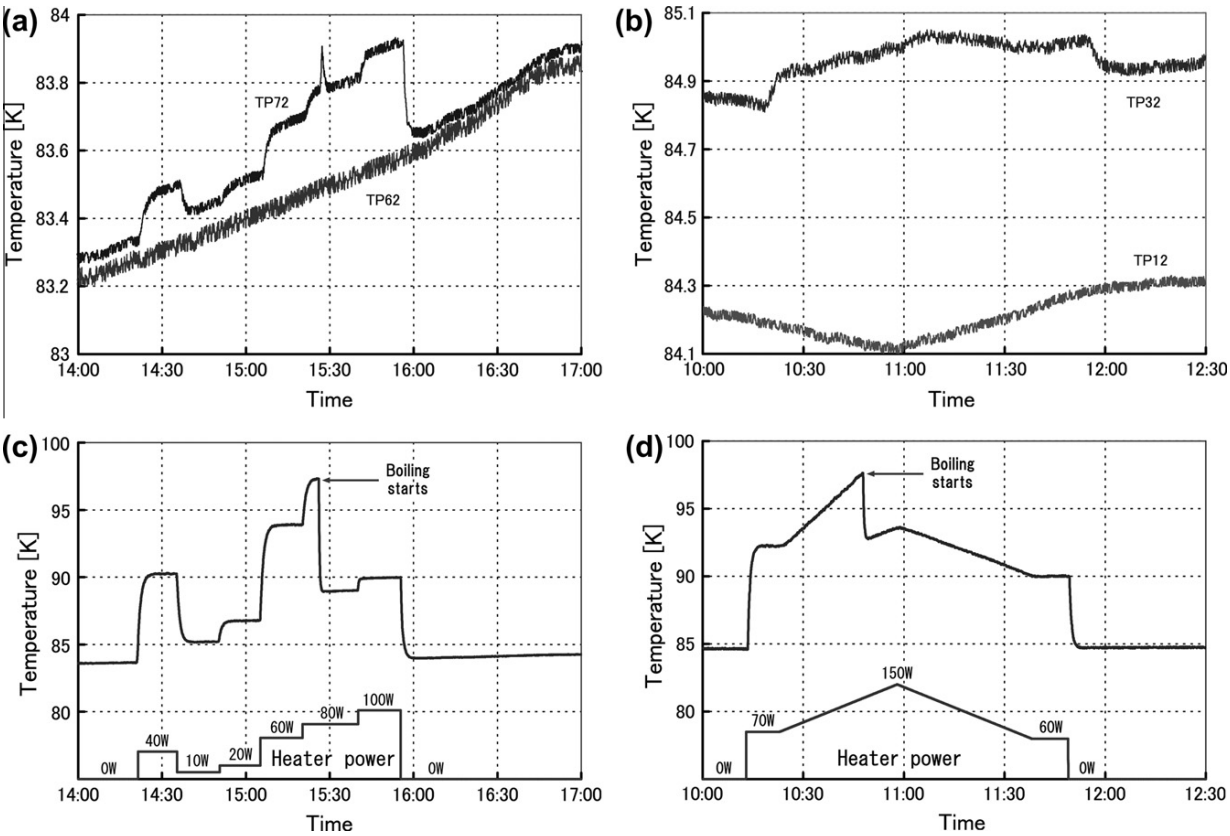

Fig. 4. Left and right graphs present data of experiments with heaters HT3 and HT1, correspondingly. Upper graphs show the temperature of LN2 before and after the heater. Lower ones show the applied power and temperature of the heater.

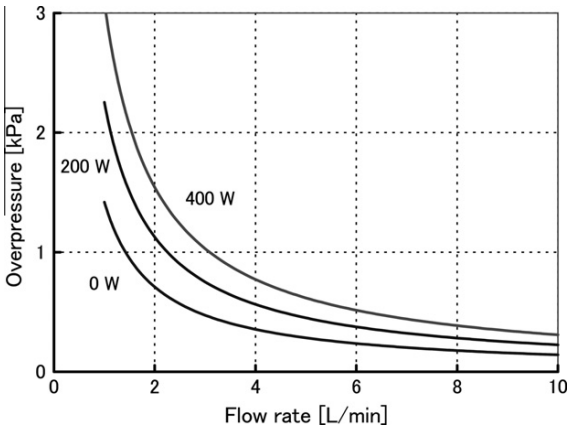

Fig. 5. Overpressure produced due to the thermal siphon effect as a function of the heater power.

siphon operating mode. No changes in LN2 flow rate were observed in these experiments. It can be explained by a small temperature difference achieved between the vertical sections of the cryopipe. The strong effect should be seen at low flow rate of the refrigerant. The second necessary condition to observe additional circulation is the presence of sufficient buffer gas in the terminals. It is necessary to smooth blocking effect of main cryopump which fixing the flow rate. The calculations by method described in [8] shows that the natural circulation may occur without using the main cryopump and heaters at 4–5 L/min of flow rate and ΔT is of the order of 3 K. In this case, the heater HT3 can be used to initiate an initial circulation. Additional driving force can significantly save power of the cryopump.

References

[1] H. Yumura, T. Masuda, M. Watanabe, H. Takigawa, Y. Ashibe, H. Ito, M. Hirose, K. Yatsuka, K. Sato, R. Hata, SEI Tech. Rev. 64 (2007) 27.
[2] S.H. Sohn, S.D. Hwang, J.H. Lim, S.W. Yim, O.B. Hyun, H.R. Kim, K. Yatsuka, T. Masuda, S. Isojima, M. Watanabe, H.S. Ryoo, H.S. Yang, D.L. Kim, Physica C 463–465 (2007) 1146.
[3] J.F. Maguire, J. Yuan, Physica C 469 (2009) 874.
[4] M. Yagi, S. Mukoyama, M. Ichikawa, T. Takahashi, H. Suzuki, A. Kimura, J. Phys.: Conf. Ser. 43 (2006) 849.
[5] S.D. Hwang, I.H. Jang, H.H. Cho, Int. J. Heat Fluid Flow 27 (2006) 21.
[6] D.M. Bernhard, C.K. Hsieh, J. Fluid Eng. 118 (1996) 409.
[7] K. Mimura, A. Isozaki, Desalination 22 (1977) 131.
[8] Yu. Ivanov, A. Radovinsky, A. Zhukovsky, A. Sasaki, H. Watanabe, T. Kawahara, M. Hamabe, S. Yamaguchi, Physica C 470 (2010) 1895.

Physica C 471 (2011) 1304–1307

Contents lists available at ScienceDirect

Physica C

journal homepage: www.elsevier.com/locate/physc

Cooling test of the 200 m superconducting DC transmission power cable system at Chubu University

H. Watanabe*, M. Sugino, J. Sun, Y. Ivanov, M. Hamabe, T. Kawahara, S. Yamaguchi

Center of Applied Superconductivity and Sustainable Energy Research, Chubu University, 1200 Matsumoto-cho, Kasugai, Aichi 487-8501, Japan

ARTICLE INFO

Article history:
Available online 13 May 2011

Keywords:
Large scale application
Superconducting direct current transmission
Cryogenics

ABSTRACT

A second cooling test of CASER2, the 200 m class superconducting direct current power transmission system at Chubu University, was performed from August to October 2010. During this time, the system was cooled down and the liquid nitrogen which cooled the superconducting power cable was circulated in the cryogenic pipe of CASER2. The heat leak of the cryogenic pipe was measured and the values of about 300 W was obtained. This result will be used further improvements of CASER2.

1. Introduction

The construction of a 200 m class superconducting direct current (DC) power transmission system (CASER2), which was constructed with using the results obtained by a 20 m class system (CASER1) [1–3], was completed at the beginning of 2010 and the first cooling and current feeding test was performed from January to March 2010 at Chubu University. After the first cooling, the second cooling test was performed from August 2010 to October 2010. High temperature superconducting power transmission systems are usually cooled by the flow of liquid nitrogen. The heat leak from the surroundings at room temperature to the power cable at the liquid nitrogen temperature raises the temperature of the circulating liquid nitrogen. Since cooling power is required to compensate the heat leak for keeping low temperature, the amount of it determines the efficiency of the superconducting power transmission systems. Therefore it is significant to know the heat leak for development of superconducting power transmission systems.

At Chubu University, every effort has been made to reduce the heat leak. The developments of a new cryogenic pipe which is composed of concentric double straight pipes [4] and Peltier current leads [5] are the examples. During the cooling and current feeding tests, the temperatures of the liquid nitrogen were measured along the cryogenic pipe and the amounts of the heat leak were estimated. In this paper we will report the results obtained during the second cooling term started from August 2010 and ended on October 2010 and show the present status of our system.

2. CASER2

Fig. 1 shows the schematic drawing of CASER2. In the laboratory there are two terminals, which are placed next to each other. At the terminals the superconducting power cable at the liquid nitrogen temperature is connected to the devices at the room temperature. Each of high temperature superconducting tapes composing the cable is separately connected to Peltier current leads [5] at the terminals. The Peltier current leads can significantly reduce the heat leak by the thermoelectric effect together with their low thermal conduction. The cryogenic pipe extended from the terminals goes out into the outdoors. The transmission line is L-shaped and running over about 100 m from the laboratory and back to the same place. Thus the total length of the transmission line is about 200 m. The cryogenic pipe of CASER2 is concentric double pipes, in which straight pipes and, in part, bellows pipes, are used. The use of straight pipes significantly reduces the loss due to the fluid friction, which improves circulation of the liquid nitrogen [6]. This is contrasted with the corrugated double pipes, which are commonly used as the cryogenic pipes for the superconducting power transmission [7–9]. Fig. 2 shows the cross sectional model of the cryogenic pipe used for CASER2. The outer pipe is carbon steel coated with zinc and the inner pipe is stainless steel. The inner pipe is wrapped by multi-layer insulation (MLI). The resent results of our laboratory on the cryogenic pipes were reflected to the design of the cryogenic pipe for CASER2 [4].

Along the cryogenic pipe, as shown in Fig. 1, there are seven places at which the temperatures of the liquid nitrogen are measured. At each of the places, platinum resistance thermometers (PRT) are set upper and lower surfaces of the inner pipe of the cryogenic pipe. Therefore 14 PRTs are measuring the temperatures of the liquid nitrogen along the course of it. Three heaters with the

* Corresponding author. Tel.: +81 568 51 9373; fax: +81 568 51 9413.
E-mail address: h_watanabe@isc.chubu.ac.jp (H. Watanabe).

0921-4534/$ - see front matter © 2011 Elsevier B.V. All rights reserved.
doi:10.1016/j.physc.2011.05.183

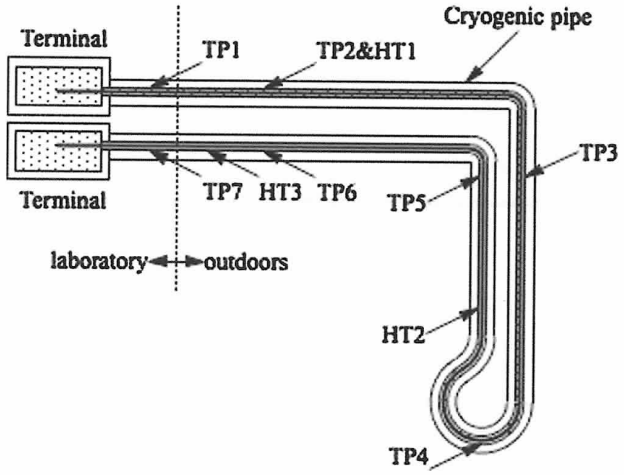

Fig. 1. The schematic drawing of CASER2. TP1–TP7 are the positions where the PRTs are set and HT1–HT3 are those where the heaters are set. At each of TP1 to TP7, two PRTs are installed.

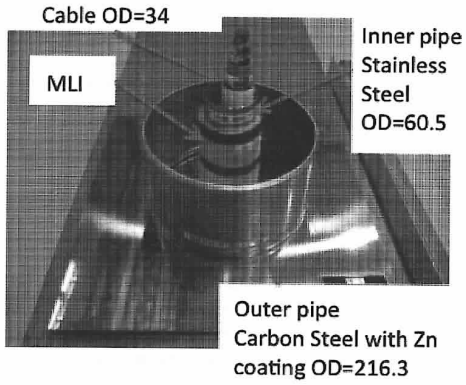

Fig. 2. This figure shows the cross sectional model of the cryogenic pipe of CASER2. The outer pipe is carbon steel coated with zinc with the outer diameter of 216.3 mm and the inner pipe is stainless steel with the outer diameter of 60.5 mm. The inner pipe is wrapped with MLI with about 10 mm thickness. The superconducting DC power cable with the outer diameter of 34 mm (the cross section of 9.08 cm^2) is seen in the inner pipe.

maximum capacity of 350 W are stuck on the inner pipe to give the heat load to the liquid nitrogen. These heaters are used for the calibration of the PRTs and the estimation of the heat leak of the cryogenic pipe, which will be explained in the next section. The temperatures and the other parameters relating to the CASER2 conditions are monitored by a computer through a digital multimeter system with a Labview based software. The liquid nitrogen circulated with one pump is cooled by one reversed Stirling cycle cryocooler, which has the cooling power of 1 kW at 77 K enough to cool the liquid nitrogen circulating around CASER2.

3. Results and discussion

Fig. 3 shows the temperature variation during the cooling process of CASER2. The temperatures shown were measured at TP1, TP4 and TP7. TP1 and TP7 are near the ends of the cryogenic pipe, and TP4 is almost at the middle of it. The liquid nitrogen was filled from the TP1 side terminal. Therefore the temperature of TP1 dropped at first, followed by the temperature drop at TP4 and finally at TP7. The caution was used for the speed of the cooling process,

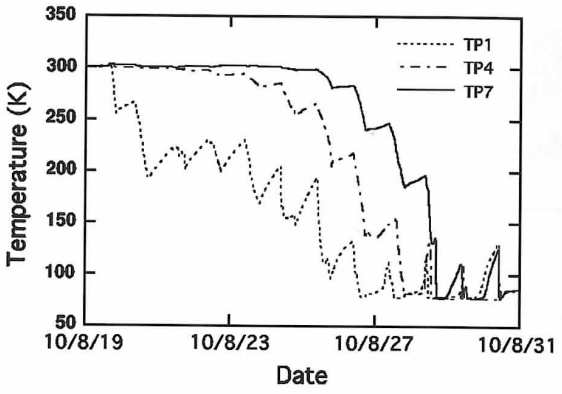

Fig. 3. The variation of temperature measured at TP1, TP4 and TP7 during the cooling process started on 19th August 2010 and ended on 30th August.

because the abrupt cooling might give damage to the superconducting power cable for the thermal shrinkage. The liquid nitrogen was introduced into the cryogenic pipe usually in the daytime and stopped in the nighttime. The temperature, thus, dropped in the daytime and rose in the nighttime. Overall the temperature of the cryogenic pipe became gradually lower. The cooling process was started on 19th August and ended on 30th August. After then the liquid nitrogen had been circulated by the pump and cooled by the cryocooler.

The heat leak of the cryogenic pipe was measured with the PRTs at TP1 and TP7 in Fig. 1. The circulation of the liquid nitrogen is usually performed with the flow rate between 5 l/min and 16 l/min. In this range of the flow rate, an 0.1 K rise in the temperature between TP1 and TP7 corresponds to the heat leak from 15 W to 50 W. This means that a small error in the temperature measurements causes a large error in the estimation of the heat leak in our system. In particular, since the target of our heat leak measurements is much less than 500 W, the error of 50 W seriously affects the evaluation of the efficiency of the system.

Though the PRTs were, of course, calibrated before they were set to the cryogenic pipe, there were obvious offsets in the temperatures measured at different PRTs, which might affect the estimation of the heat leak. The reasons why these offsets arose were not clear at the moment, but the unrecognizable tiny difference of the way to set the PRTs in the cryogenic pipe might affect the offsets. Though it is difficult to measure the offsets directly after setting the PRTs in the cryogenic pipe, the estimation of the offsets was tried firstly.

The heat leak along the cryogenic pipe can be written by

$$Q = mC\,dT \tag{1}$$

where Q is the heat leak, m is the mass flow rate, C is the specific heat capacity of the liquid nitrogen and dT is the true difference of temperatures measured at different PRTs. When there is an offset between the true and measured values, the measured difference can be written by

$$dT' = dT + \alpha, \tag{2}$$

where dT' is the measured difference and α is the offset. From Eq. (1), dT' becomes

$$dT' = (Q/C)\frac{1}{m} + \alpha. \tag{3}$$

Therefore, if the differences of two temperatures dT' are measured against the reciprocals of the mass flow rate $1/m$, the extrapolated value of dT' at $1/m = 0$ is the offset α.

The differences of the temperatures at TP1 and TP7 have been measured against different flow rates. The measurement was

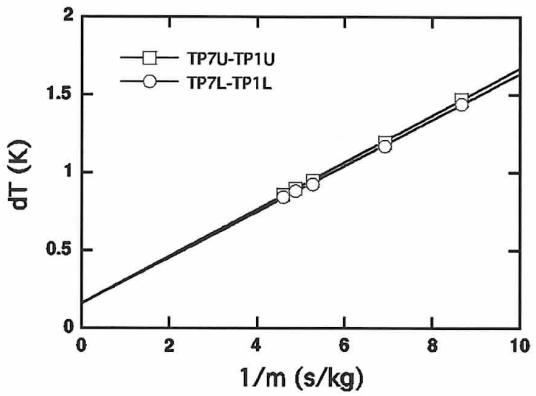

Fig. 4. The temperature difference between TP1 and TP7 with respect to the reciprocals of the mass flow rate. TP1U and TP7U mean that the temperatures were measured with the PRTs set on the upper surface of the inner pipe of the cryogenic pipe, while TP1L and TP7L mean that the temperatures were measured with those set on the lower surface.

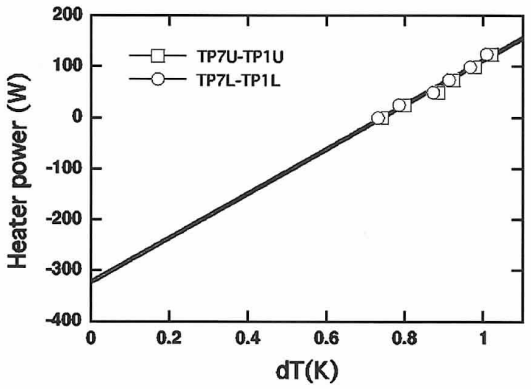

Fig. 5. The heat loaded into the liquid nitrogen by the heater, HT1, with respect to the temperature difference between TP1 and TP7. TP1U and TP7U mean that the temperatures were measured with the PRTs set on the upper surface of the inner pipe of the cryogenic pipe, while TP1L and TP7L mean that the temperatures were measured with those set on the lower surface.

performed on a cloudy day to keep the environmental variation small, since the large part of the cryogenic pipe is laid in the outdoors and the variation of the heat leak will affect the result as shown in Eq. (3). The variation of the outer temperature during the measurement was within ±2° C.

Since the distance between TP1 and TP7 is about 175 m, it takes about 30 min for the liquid nitrogen to travel from TP1 to TP7 in the case of the 10 l/min flow rate. In the analysis, this time difference was considered. For example, in the case of 10 l/min, the temperature at TP7 was compared with that at TP1 which was measured at 30 min prior to the measurement at TP7.

The results are shown in Fig. 4. TP1U and TP7U mean that the PRTs set on the upper surface of the inner pipe of the cryogenic pipe were used, while TP1L and TP7L mean that those set on the lower surface were used. Obviously the difference of the temperatures are linearly proportional to the reciprocals of the mass flow rate. Liner functions were fitted to the data and the intercepts at the abscissa were obtained. The offset of TP7U to TP1U was 0.159(8) K and that of TP7L to TP1L was 0.157(8) K. The values in the parentheses are uncertainties, in which the uncertainties due to the signal fluctuation, the determination of the mass flow rate and the accuracy of the digital multimeter were included.

Secondly, the heat leak was measured. The differences of the temperatures at TP1 and TP7 have been measured against the quantities of the heat loaded by a heater. The heater shown as HT1 in Fig. 1 was used. If q denotes the quantity of the heat loaded by the heater and Q the heat leak, Eq. (1) is written as

$$q = mC\,dT - Q. \tag{4}$$

Q can be obtained from q at $dT = 0$. Since q does not take negative values, Q is estimated by extrapolation. By considering Eq. (2), Eq. (4) is changed as

$$q = mC(dT' - \alpha) - Q. \tag{5}$$

In Fig. 5, q is plotted against dT and the lines in the figure are from Eq. (5) fitted to the data. The heat leak Q is the intercepts of the abscissa. With this procedure the heat leak can be obtained without introducing the uncertainties from the specific heat capacity of the liquid nitrogen and the mass flow rate. The heat leak measured with TP7U and TP1U was 326(14) W and that with TP7L to TP1L was 321(14) W. The values in the parentheses are also uncertainties. The uncertainties considered are the signal fluctuation and the accuracies of digital multimeters used for the heater power and temperature measurements. The measured results agree with each other within the range of uncertainties.

The heat leak measured during the first cooling term was 419 W, which was calculated with the temperature difference between TP1 and TP7 together with the specific heat capacity and the mass flow rate. The first cooling term was started on January 2010 and ended in March 2010. The typical temperature of the cryogenic pipe surface during the measurement in early March was about 20° C, while that during the present measurement measured at the same place late in September was about 24° C. From the first to second cooling term, a significant improvement of the heat leak is seen, according to the results measured under the similar environmental conditions. This improvement was obtained by improving the quality of the vacuum for the vacuum insulation. Though the significant improvement was obtained from the first to second cooling term, the heat leak is considerably larger than our expectation yet. We made every effort to seek for the reason and found that some parts of the inner pipe of the cryogenic pipe were not wrapped with MLI properly. It has been shown that the application of MLI to our type of the cryogenic pipes makes the heat leak nearly 20 times smaller [4]. We are planning to revise this point before third cooling term planned to start at early 2011. We expect this revision will reduce the heat leak as low as our design.

4. Summary

The test of the heat leak along the cryogenic pipe of CASER2, the 200 m class superconducting DC power transmission system, was performed in the second cooling term conducted from August to October 2010. The heat leak of about 300 W was measured for the cryogenic pipe, which was significantly reduced from the result obtained in the first term. This improvement was not small, but we expected a further improvement. It is found that some parts of the inner pipe of the cryogenic pipe were not wrapped by MLI properly. The revision of these parts is expected to reduce the heat leak to the level which has been obtained by our researches until now.

Acknowledgements

The authors thank Dr. Hiroshi Fujiwara, a professor of Keio University and the president of Nano-Opt Energy Corporation, for his financial support for this work. This work is partly supported by NEDO through ISTEC as a part of Material & Power Applications of Coated Conductors Project (M-PACC) project. We also thank JFE Steel Corporation for supplying steel pipes to the construction of the test facility.

References

[1] S. Yamaguchi, M. Hamabe, I. Yamamoto, T. Famakinwa, A. Sasaki, A. Iiyoshi, J. Schultz, J. Minervini, T. Hoshino, Y. Ishiguro, K. Kawamura, J. Phys.: Conf. Ser. 97 (2008) 012290.

[2] M. Hamabe, T. Fujii, I. Yamamoto, A. Sasaki, Y. Nasu, S. Yamaguchi, A. Ninomiya, T. Hoshino, Y. Ishiguro, K. Kawamura, IEEE Trans. Appl. Supercond. 19 (2009) 1778.

[3] M. Hamabe, T. Fujii, M. Sugino, A. Sasaki, T. Sugimoto, H. Watanabe, T. Kawahara, S. Yamaguchi, Y. Ishiguro, K. Kawamura, J. Phys.: Conf. Ser. 234 (2010) 032019.

[4] Y. Nasu, M. Hamabe, S. Yamaguchi, S. Kusaka, Y. Ishiguro, in: Proc. ICEC22/ICMC2008, 2008, pp. 489.

[5] S. Yamaguchi, T. Yamaguchi, K. Nakamura, Y. Hasegawa, H. Okumura, K. Sato, Rev. Sci. Instrum. 75 (2004) 207.

[6] A. Sasaki, M. Hamabe, T. Famakinwa, S. Yamaguchi, A. Radovinsky, Adv. Cryog. Eng. 53 (2008) 75.

[7] T. Masuda, H. Yumura, M. Watanabe, H. Takigawa, Y. Ashibe, C. Suzawa, H. Ito, M. Hirose, K. Sato, S. Isojima, C. Weber, R. Lee, J. Moscovic, IEEE Trans. Appl. Supercond. 17 (2007) 1648.

[8] J. Maguire, D. Folts, J. Yuan, D. Lindsay, D. Knoll, S. Bratt, Z. Wolff, S. Kurtz, IEEE Trans. Appl. Supercond. 19 (2009) 1740.

[9] H. Yumura, M. Ohya, Y. Ashibe, M. Watanabe, T. Minamino, T. Masuda, S. Honjo, T. Mimura, Y. Kitoh, Y. Noguchi, J. Phys.: Conf. Ser. 234 (2010) 032069.

1070 IEEE TRANSACTIONS ON APPLIED SUPERCONDUCTIVITY, VOL. 21, NO. 3, JUNE 2011

Double Peltier Current Lead for Heat Leak Reduction at the Terminals for Superconducting Direct Current Applications

Toshio Kawahara, Tomohiro Fujii, Masahiko Emoto, Makoto Hamabe, Hirofumi Watanabe, Jian Sun, Yury Ivanov, and Satarou Yamaguchi

***Abstract*—For superconducting direct current applications, heat leak reduction at the terminal is a key issue for high performance systems and especially for small ones such as the distribution in internet data centers. We propose a double Peltier current lead (PCL), where the suitable combination of two Peltier modules can enhance the performance of PCL. Using the model parameters of actual thermoelectric materials, we estimated the heat leak on PCL using a thermal balance equation. At the double PCL, the large temperature difference on the current lead can be split to two thermoelectric materials and then the performance of PCL can be enhanced. As each of the thermoelectric materials has better working temperature range, an optimized combination of shape factors can be used for the high performance current lead at the terminals for superconducting application systems.**

***Index Terms*—Cryogenics, DC power transmission, high-temperature superconductors, Peltier current lead.**

I. Introduction

RECENT energy problems should be solved by state of the art technologies such as superconductivity. One superconducting application utilized for energy saving is the superconducting power transmission and distribution (T&D) system. There are several projects currently in the world concerned with the development of technologies related to superconducting power transmission systems such as those pertaining to long distance, high voltage and/or grid cooperation systems [1]–[5]. Chubu University has already developed a 20 m-class superconducting direct current superconducting transmission device [6]. The current balance of superconducting tapes as stable transmission systems, low heat leak systems using special cryogenic double pipes, and so forth have been discussed [7], [8]. Recently, we have completed the construction of a 200 m-class device. For these systems, we have also used a special current lead in the form of a Peltier current lead (PCL) for heat leak reduction at the terminals [9], [10].

As the thermal optimization of terminals largely affects the performance of total superconducting systems, the improvement of current leads represents one key issue in the development of superconducting applications [9], [11], [12]. Several modifications of PCL have been proposed and discussed such as an alternating current mode [13], multi-stage modules [14], and gas-cooled systems [12]. Since the heat leak on PCL is dependent on the properties of the thermoelectric modules, a variety of materials possessing better parameters for PCL should be examined.

Given that a superconducting state can only be achieved at low temperature, where high Tc superconducting cables are used around liquid nitrogen temperature, PCL must be connected to large temperature differences. One end of the current lead is at room temperature while the other should be at about 77 K. Therefore, it is possible to use a combination of thermoelectric materials to generate better Peltier modules in PCL since thermoelectric materials are temperature-dependent and each material possesses its own optimal temperature range.

In this paper, we will discuss double PCL that employs two different thermoelectric modules connected in series. At first, we measured the thermoelectric properties of the actual materials and then calculated the heat leak with an optimum shape factor using a thermal balance equation. The temperature distribution on Peltier modules in PCL will also be addressed.

II. Experiments and Simulation Methods

Model thermoelectric parameters were measured for 4 BiTe alloy samples designated A, B, C and D. Samples A and B are n-type materials, and samples C and D are p-type. The resistivity was measured by the 4 terminal method with constant current. Seebeck effects were measured under the small temperature difference scanned between 0 and 6 K and controlled by a small heater attached on the electrode. The thermal conductivity was measured by the steady state method under the scanned temperature difference. These values were used to calculate the figure of merit Z of thermoelectric materials. The temperature dependence of Z is useful in defining the order of the thermoelectric materials in the structure of double PCL.

We used two different model parameters of thermoelectric materials for both n- and p-type PCLs. Atomic ratios measured by X-ray fluorescence (XRF) for each material are summarized in Table I. For the n-type materials, sample B has a large amount

Manuscript received August 01, 2010; accepted November 24, 2010. Date of publication January 06, 2011; date of current version May 27, 2011. This work was supported by the Ministry of Education, Culture, Sports, Science and Technology as "Collaboration with Local Communities" Project for Private Universities. Part of the work was also supported by the Nippon Sheet Glass Foundation for Materials Science and Engineering, and the Future Energy Research Association (T.K.).

T. Kawahara, T. Fujii, M. Hamabe, H. Watanabe, J. Sun, Y. Ivanov, and S. Yamaguchi are with Chubu University, Kasugai, Aichi 487-8501, Japan (e-mail: toshi@isc.chubu.ac.jp).

M. Emoto is with the National Institute for Fusion Science, Gifu 509-5292, Japan (e-mail: emo@nifs.ac.jp).

Color versions of one or more of the figures in this paper are available online at http://ieeexplore.ieee.org.

Digital Object Identifier 10.1109/TASC.2010.2096451

TABLE I
ATOMIC RATIOS FOR MODEL SAMPLES

n-type	Bi	Te	Si	Cl
Sample A	2.29	4.08	0.04	0
Sample B	2.31	4.01	0.06	0.08

p-type	Bi	Te	Sb	
Sample C	0.5	4.83	2.3	
Sample D	0.58	4.92	2.06	(arb. units)

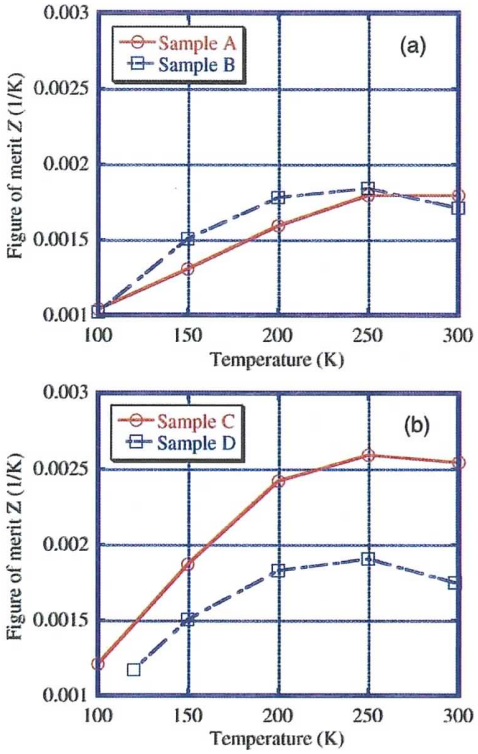

Fig. 1. Thermoelectric properties of model thermoelectric materials. (a) n-type (Samples A and B), and (b) p-type (Samples C and D) materials.

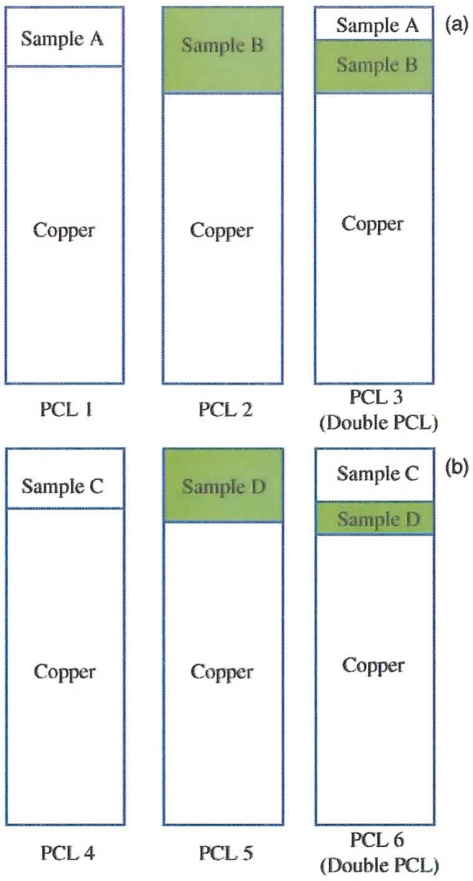

Fig. 2. Schematic model structures for PCL and double PCL. The upper temperature is set to room temperature and the bottom temperature to 77 K. (a) n-type and (b) p-type materials.

of dopants such as Si and Cl and therefore should have smaller resistivity compared with sample A. For the p-type materials, sample D has a smaller ratio of Sb and therefore smaller resistivity compared with sample C. Thus we used two modules with different resistivity and temperature dependence of Z for the n- and p-type materials.

We estimated the heat leak on PCL with a thermal balance equation [15], [16] using model parameters measured for samples A, B, C and D. From the shape factor L/A dependence of heat leak [17], the optimum L/A can be estimated and the minimum heat leak on the current lead can be determined. We used a current of 100 A for the simulation, which seems to be a typical value for a single superconducting tape.

III. Results and Discussion

Fig. 1 shows the figure of merit Z for the model thermoelectric materials. All samples have larger Z above 200 K. Therefore, Peltier modules should be incorporated on the higher temperature side. However, as there is a difference in temperature dependence, module combinations should affect the performance of PCL. Samples B and D have maximum Z at lower temperature compared with samples A and C, respectively. Thus, Samples B and D seem to be better suited for the lower temperature side in double PCL.

Fig. 2 shows schematic representations of the double PCL analysed in this paper for n- and p-type materials. Sample B has lower resistivity and seems to have better performance at lower temperature as shown in Fig. 1(a). The optimum shape factor of L/A might therefore be longer for sample B (PCL 2). For double PCL, sample A should be used at the higher temperature side. In Fig. 2(a), this double PCL is schematically shown as PCL 3.

Using a thermal balance equation, the heat leak through the current lead dependent on L/A can be calculated. For example, the L/A dependence of heat leak of double PCL (PCL 3) is plotted in Fig. 3(a), where the L/A for sample B is set as 40 m^{-1}. The optimized heat leak for single PCL of PCL 1 is also shown as a solid line in the figure, which is 31.8 W/kA as shown in Table II. The minimum heat leak can be seen at $L/A = 25$ m^{-1}, and the heat leak of PCL 3 is 30.7 W/kA. Thus we can improve the performance of PCL using double PCL. Sample B's L/A dependence of double PCL is also plotted,

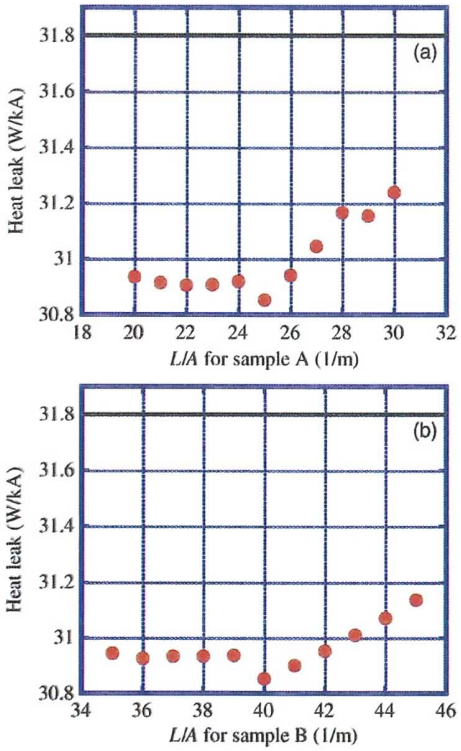

Fig. 3. Shape factor L/A dependence of heat leak. In (a), L/A for sample B is set as 40 m^{-1}, and in (b) L/A for sample A is set as 25 m^{-1}.

TABLE II
OPTIMUM SHAPE FACTOR L/A AND THE HEAT LEAK FOR PCL AND DOUBLE PCL

(a)

	L/A (1/m) (Sample A)	L/A (1/m) (Sample A)	L/A (1/m) (Copper)	Q (W/kA)
PCL 1 (A)	41	0	27600	31.8
PCL 2 (B)	0	80	22200	31.9
PCL 3 (A+B)	25	40	25850	30.8

(b)

	L/A (1/m) (Sample C)	L/A (1/m) (Sample D)	L/A (1/m) (Copper)	Q (W/kA)
PCL 4 (C)	39	0	25000	28.8
PCL 5 (D)	0	64	27300	31.6
PCL 6 (C+D)	38	0.5	26150	28.2

where L/A for sample A is 25 m^{-1}. In this case, the heat leak minimum can be seen at L/A of 40 m^{-1}. Therefore, the combination of 25 m^{-1} and 40 m^{-1} for L/A of sample A and B, respectively, can be obtained as optimum values. Additionally, we can note that the shorter thermoelectric materials have higher tolerance for the actual applications as shown in Fig. 3.

The same procedure can be used for the optimum L/A for all PCLs. These values are summarized in Table II. For the n-type PCLs, single PCLs have an optimum heat leak of 31.8 W/kA and 31.9 W/kA for PCLs 1 and 2, respectively. Comparing these values, the optimum heat leak for PCL 3 is 30.8 W/kA. Thus we can improve the heat leak by about 1 W/kA with an optimum combination of double PCL using the same materials as with single PCL. For the p-type materials, there is a large imbalance of the initial performance between PCL 4 and PCL 5, where PCL 4 using a single module of sample C has much better performance compared with PCL 5. However, use of sample D can improve performance in double PCL as with PCL 6 using samples C and D, and the minimum heat leak can be estimated as 28.2 W/kA. In this case, although the improvement is small, we can reduce the heat leak with sample D that has a lower thermoelectric performance Z than that of sample C in all temperature ranges. Employing the best combination of thermoelectric materials seems to be useful in the optimization of PCL.

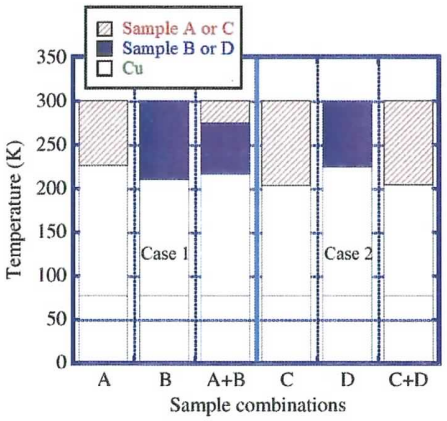

Fig. 4. Temperature distribution on PCL and double PCL. Case 1: n-type and Case 2: p-type materials.

Finally, we show the temperature distribution on each PCL as shown in Fig. 4. For the single PCL, sample A which has higher performance near room temperature should be used as a short Peltier module in PCL. On the other hand, as sample B has better performance at lower temperature and has lower resistivity, it should be used as a long Peltier module in PCL. However, low performance near room temperature prevents effective insulation of heat. Therefore, the combination of samples A and B, where the higher temperature part comprises sample A such as PCL 3, represents the better combination as double PCL. The same situation can be seen in case 2 for p-type PCLs. In this case, sample C has better performance but the low resistivity of sample D can also assist the performance as double PCL. PCL should be used under a wide temperature range. Thus, suitable combinations of two thermoelectric materials can operate as better PCL as one of the functional graded materials. The geometry should be optimized depending on the operating current. In this actual case, such a fabrication process is preferable since we can select several modules and combine these as double PCL to form a custom current lead. This custom PCL can show suitable temperature distribution to reduce heat leak on the current lead.

IV. CONCLUSION

Better combinations of thermoelectric materials could have higher performance compared with single materials. The em-

ployment of double PCL using two different materials for the Peltier modules in PCL was addressed. For example, if two materials have minimum heat leak of 31.8 W/kA and 31.9 W/kA, respectively, the double PCL using these same materials will have a heat leak of 30.8 W/kA. Therefore, using the best combination of thermoelectric materials can be marginally useful in the minimization of heat leak. This approach can also be used with high performance superconducting systems given the heat leak reduction at the terminals. We believe these fabrication processes to generate functional graded Peltier current leads could be utilized to enhance current technologies pertaining to superconducting applications.

ACKNOWLEDGMENT

The authors thank Dr. A. Iiyoshi, Chancellor of Chubu University for his continuous encouragement through this work. Profs. J. Morimoto and Y. Okamoto of National Defense Academy assisted us with the X-ray florescence data measurements.

REFERENCES

[1] S. Mukoyama, M. Yagi, M. Ichikawa, S. Torii, T. Takahashi, H. Suzuki, and K. Yasuda, "Experimental results of a 500 mHTS power cable field test," *IEEE Trans. Appl. Supercond.*, vol. 17, no. 2, pp. 1680–1683, Jun. 2007.

[2] T. Masuda, H. Yumura, M. Watanabe, H. Takigawa, Y. Ashibe, C. Suzawa, H. Ito, M. Hirose, K. Sato, S. Isojima, C. Weber, R. Lee, and J. Moscovic, "Fabrication and installation results for Albany HTS cable," *IEEE Trans. Appl. Supercond.*, vol. 17, no. 2, pp. 1648–1651, Jun. 2007.

[3] J. Y. Yoon, S. R. Lee, and J. Y. Kim, "Application methodology for 22.9 kV HTS cable in metropolitan city of South Korea," *IEEE Trans. Appl. Supercond.*, vol. 17, no. 2, pp. 1656–1659, Jun. 2007.

[4] H. X. Xi, W. Z. Gong, Y. Zang, Y. F. Bi, H. K. Ding, H. Wen, B. Hou, and Y. Xin, "China's 33.5 m 35 kV/2 kA HTS ac power cable's operation in power grid," *Physica C*, vol. 448, pp. 1054–1057, Oct. 2006.

[5] A. Gesciere, D. Willen, E. Piga, and P. Barendregt, "HTS cables open the window for large-scale renewables," *J. Phys., Conf. Ser.*, vol. 97, p. 012183, Mar. 2008.

[6] S. Yamaguchi, M. Hamabe, I. Yamamoto, T. Famakinwa, A. Sasaki, A. Iiyoshi, J. Shultz, J. Minervini, T. Hoshino, Y. Ishiguro, and K. Kawamura, "Research activities of DC superconducting power transmission line in Chubu University," *J. Phys., Conf. Ser.*, vol. 97, p. 012290, Mar. 2008.

[7] M. Hamabe, Y. Nasu, A. Ninomiya, Y. Ishiguro, S. Kusaka, and S. Yamaguchi, "Radiation heat measurement on thermally-isolated double-pipe for DC superconducting power transmission," *Adv. Cryo. Eng.*, vol. 53A, pp. 168–173, Aug. 2008.

[8] M. Hamabe, T. Fujii, I. Yamamoto, A. Sasaki, Y. Nasu, S. Yamaguchi, A. Ninomiya, T. Hoshino, Y. Ishiguro, and K. Kawamura, "Recent progress of experiment on DC superconducting power transmission line in Chubu University," *IEEE Trans. Appl. Supercond.*, vol. 19, no. 3, pp. 1778–1781, Jun. 2009.

[9] S. Yamaguchi, T. Yamaguchi, K. Nakamura, Y. Hasegawa, H. Okumura, and K. Sato, "Peltier current lead experiments and their applications for superconducting magnets," *Rev. Sci. Instrum.*, vol. 75, no. 1, pp. 207–212, Jan. 2004.

[10] Y. Hasegawa, K. Sato, H. Okumura, K. Nakamura, S. Yamaguchi, and K. Miyake, "Reduction of heat leak in cryogenic system using Peltier current leads," *Cryogenics*, vol. 42, no. 8, pp. 495–500, Aug. 2002.

[11] X. C. Xuan, K. C. Ng, C. Yap, and H. T. Chua, "On minimizing the heat leak of current leads in cryogenic vacuum systems," *Cryogenics*, vol. 42, no. 12, pp. 779–785, Dec. 2002.

[12] T. Kawahara, T. Fujii, M. Emoto, M. Hamabe, J. Sun, H. Watanabe, and S. Yamaguchi, "Estimation for the performance of superconducting DC transmission lines with cryogenics improvements," *Physica C*, Feb. 2010, DOI: 10.1016/j.physc.2010.01.054.

[13] T. Yamaguchi, H. Okumura, K. Nakamura, and S. Yamaguchi, "Characteristics of Peltier current lead system for alternating current mode," *IEEE Trans. Appl. Supercond.*, vol. 13, no. 2, pp. 1910–1913, Jun. 2003.

[14] T. Yamaguchi, H. Okumura, K. Nakamura, and S. Yamaguchi, "Multi-stage Peltier current lead system for liquid helium free magnets," *IEEE Trans. Appl. Supercond.*, vol. 13, no. 2, pp. 1914–1917, Jun. 2003.

[15] H. Okumura and S. Yamaguchi, "A simulation for Peltier current lead," *IEEE Trans. Appl. Supercond.*, vol. 7, no. 2, pp. 715–718, Jun. 1997.

[16] K. Sato, H. Okumura, and S. Yamaguchi, "Numerical calculations for Peltier current lead designing," *Cryogenics*, vol. 41, no. 7, pp. 497–503, Jul. 2001.

[17] T. Yamaguchi, S. Mizutani, M. Moriguchi, H. Okumura, K. Nakamura, and S. Yamaguchi, "Experimental and numerical characteristics of Peltier current lead for direct current mode," *IEEE Trans. Appl. Supercond.*, vol. 14, no. 2, pp. 1719–1722, Jun. 2004.

Iron-Steel Cryogenic Pipe for DC Superconducting Power Transmission Line

Satarou Yamaguchi, Tomohiro Fujii, Makoto Sugino, Makoto Hamabe, Hirofumi Watanabe, Toshio Kawahara, and Atsuo Iiyoshi

Abstract—**The 200-meter DC cable test facility was constructed in Chubu University. The cryogenic pipe is composed of two pipes, and the material of the inner pipe is stainless steel (SS304). The outer pipe is the straight pipe, and made from the iron steel because of high strength, low cost and not low temperature. If the cable structure is co-axial, the magnetic field is not generated outside the cable, and the ferromagnetism of the iron steel is not affected to the electric circuit. However, if the single core cable is used, the ferromagnetic effect of the outer pipe should be considered. Therefore, we measured the inductances of the cable after the construction of the experimental device. The measured inductance of the co-axial cable is matched with the analytical value, and it is very small. But the measured inductance of the single core cable configuration, it is 0. 4 mH. This is a large value, and therefore we can save the inductor in the power converter. Moreover, the energy storage can be available in the grid power line if large current operation is used.**

Index Terms—**Cryogenic pipe, DC power transmission, energy storage, high-temperature superconductors.**

I. Introduction

RECENTLY several projects to install AC superconducting power transmission (SC-PT) in the practical power grid have been carried out in the world [1]–[4]. These systems used magnetic shielded three high temperature superconductor (HTS) power cables because of three-phase AC transmission line to minimize the eddy current loss of the cryogenic pipe. The current density included the cryogenic pipe is still high as compared with the usual copper cables. On the other hand, DC application as the HTS technology is also attractive because of no AC losses of HTS tape and its system, and it is low cost because one cable is used enough [5], [6]. A 200-meter cable test facility had been constructed in Chubu University, Japan [7]. The cryogenic pipe is composed of the outer iron-steel pipe and the inner stainless-steel (SS) pipe. They are not corrugated pipes, but straight pipe for the outer pipe, and SS straight and bellows pipes for the inner pipe. The straight part is 97% of the inner pipe, and the bellows part is shorter than 3% for the length. The reasons of the cryogenic engineering views are as follows:

1) high strength;
2) narrow surface area to minimize the radiation heat leak;
3) low pressure drop for liquid nitrogen circulation;
4) not low temperature;
5) low cost.

It is needed to use high strength pipe for the outer pipe because it will be installed into underground. In order to minimize the heat leak of the cryogenic pipe, the surface area of the pipe must be small. The surface area of the corrugate and bellows pipes is wider than that of the straight pipe. The heat leaks of several cryogenic pipes are investigated, and we achieved the heat leak of 0.5 W/m for the straight pipes [8]. In order to circulate the liquid nitrogen (LN2) in the pipe, the pressure drop should be low to minimize the heat load to the low temperature system because the cryogenic pump power is the heat load. It is a key issue for the long system because the pressure drop is proportional to the square of the length and the flow velocity [9]. Usually, iron steel is not used in low temperature because of the cold brittleness of iron, but the temperature of the outer pipe is not low as the cryogens. Therefore, we can use the iron-steel for the outer pipe, and it is not expensive like SS pipe. The nickel is inevitable element to make SS for low temperature use, but it is strictly limited of the nickel resources in the earth. Therefore, it is natural way to use the iron for the cryogenic outer pipe.

However, we must discuss the ferromagnetism of iron. Usually the ferromagnetic material is not used for the AC power transmission line because of its high hysteresis loss. But the hysteresis loss is almost zero for DC circuit, and the transformer and some magnets or inductors use the ferromagnetic materials for their cores even in AC cirucits. Here, we propose and discuss the iron-steel pipe for the cryogenic outer pipe in this paper.

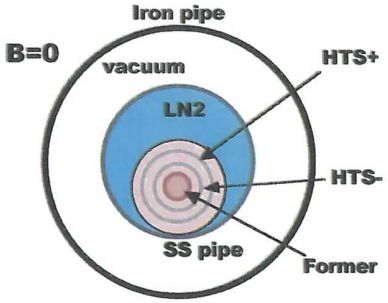

Fig. 1. The cross-section of the co-axial HTS cable, and its cryogenic pipe. The currents of the HTS+ and HTS- layers are same.

II. Configuration of HTS Cable and Cryogenic Pipe and Current Source Power Converter

Fig. 1 shows the cross section of the HTS power cable and the cryogenic pipe. The cable structure is co-axial, and this structure is used for the AC HTS cable usually [2] in order to re-

Manuscript received August 03, 2010; accepted October 24, 2010. Date of publication February 17, 2011; date of current version May 27, 2011.

The authors are with Chubu University, Aichi 487-8501, Japan (e-mail: yamax@isc.chubu.ac.jp).

Color versions of one or more of the figures in this paper are available online at http://ieeexplore.ieee.org.

Digital Object Identifier 10.1109/TASC.2011.2106472

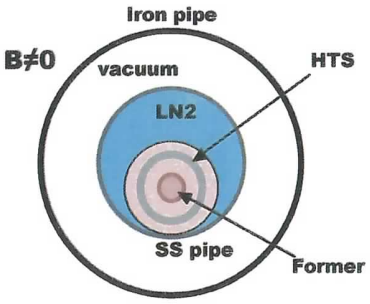

Fig. 2. The cross-section of the single core cable, and its cryogenic pipe. Magnetic field is not zero outside of the cable. The outer pipe material is ferromagnetic.

duce the eddy current loss of the cryogenic pipes. The center core of the cable is made from the copper wire and it is called the former. Usually it is connected to the earth. The cable conductors are composed of two layers, and they are composed of the HTS tapes. These layers are insulated each other. They are connected into positive and negative polarities of the DC power supply. Therefore, the same electric current flows in each HTS layer, and no magnetic field is generated outside of the outer layer of HTS tapes. This means that if we use the ferromagnetic materials for the cryogenic pipe, it is not necessary to consider the hysteresis loss of the ferromagnetic materials even for the ac power line. The inductance of the co-axial cable is very small.

On the other hand, Fig. 2 shows the cross-section of the single core cable and its cryogenic pipe. The cable has one conductor, and therefore, magnetic field is generated outside of the cable, and we should consider the characteristics of the ferromagnetism of the outer iron pipe. There are two major effects to use the ferromagnetic materials for the pipe. One is the hysteresis loss, and the second is the inductance of the circuit. Fortunately, the hysteresis loss of the outer pipe is almost zero because of DC. In order to estimate the hysteresis loss preciously, we consider the ripple current. But this depends on the design of the power converter and its operation, and it is usually small. The permeability of the iron pipe is high, and relative permeability exceeds 1000, therefore the inductance of the cable circuit is high. This kind of the characteristics is often used to make a magnet and a large inductor. Moreover, the iron pipe can shield the magnetic field outside of the outer pipe.

Large inductance in the cable circuit is not good for the AC line because high voltage is necessary to transmit the power. However, the large inductors are used in high voltage DC power transmission line (HVDC). Fig. 3 shows the typical electric circuit of the HVDC, and it is called "Back-to-Back (B-to-B)" system. The efficiency of the HVDC is high for long distance (several hundred km to 2000 km) transmission, and many HVDC are installed all over the world. Usually the cable is not used in HVDC, and the overhead wire is used. But the underground cable is used in the metropolitan area and the electrically insulated cable is applied in water. It is often used to connect the different AC power lines even for short transmission because it can transmit the power both directions. It is the interconnection of the AC power transmissions. There are two kinds of the power converters, and one is "current source converter (CSC)", and the other is "voltage source converter (VSC)". The CSC is used in the B-to-B and SMES [10], and it needs large inductor to reduce the ripple current and to suppress the short circuit current at the accidents. The circuit breaker is connected in AC sides, but DC circuit breaker is sometimes used in DC circuit, too. The AC filter is used to reduce the ripple current in the DC circuit. The inductances of the inductors are 0.1 to 1.0 H for high power transmission line (several hundreds MW), and their size is huge, and sometimes is almost the size of two floors building. Moreover, the loss of the inductor is not small because it is made from the copper. Therefore, if the HTS cable has large inductance, we can save the inductor in the circuit of the B-to-B system, and reduce the loss of the inductor. Actually the iron core inductor is also used in the B-to-B system.

III. 200-Meter Cable Experiment and Measurement Results

Fig. 4 shows the plan layout of the 200-meter cable test facility in Chubu University, the photo of the cryogenic pipe and the HTS cable, and the photo of the 200-meter pipeline of the experiments. The diameter of the HTS cable is 35 mm, the diameter of the inner SS pipe is 57.2 mm, and the diameter of the outer iron pipe is ~260 mm. The multi-layer insulation (MLI) is used to reduce the radiation heat flux to the inner pipe. Two terminals are set in the same laboratory. The pipelines are set outside of the laboratory mainly, and it return back around 100 meter. The arrow shows the directions of LN2 flow. The total length of the cable is 200 meter approximately.

LCR-meter was used to measure the inductance of the HTS cable. The current to measure the inductance is 1 A. It is larger than the ordinary LCR meter's, and if the current is around 10 mA, we could not measure the inductance. The cable design is the co-axial like Fig. 1, and it has two conductors. Therefore, we can measure the inductance of the co-axial cable if we connect two conductor layers at the ends and the other ends are connected to the LCR meter. And if we use one conductor layer and connect to the LCR, we can measure the inductance of the single core cable like Fig. 2. The measurement wire is connected to the outer layer of the cable conductor. The experimental result shows in Fig. 5. The inductance of the co-axial cable is low and ~ 20 μH for ~200-meter length around 1 Hz, and its value is almost constant for the frequency. On the other hand, the inductance of the single core cable configuration is about 0.4 mH around 1 Hz, and it changes with the frequency significantly because the magnetic field is shielded partially by the inner pipe and its shielding effect is high for higher frequency. The current direction of the cable is the same as the LN2 flow direction of the pipe line as shown in Fig. 4, the length of the single core cable should be half of the total length, and is ~100 m.

IV. Discussion and Conclusion

The inductance of the co-axial cable is small, and given by

$$L = l\frac{\mu}{2\pi}Ln\left(\frac{b}{a}\right) \tag{1}$$

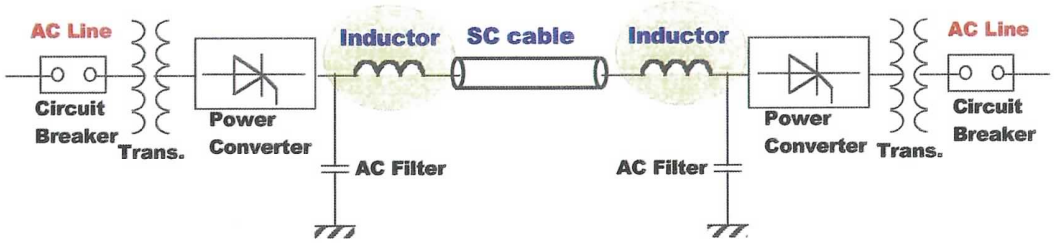

Fig. 3. High voltage DC power transmission, called "Back-to-Back". The power converters are equipped at both ends, and huge inductors are connected to the cable in series.

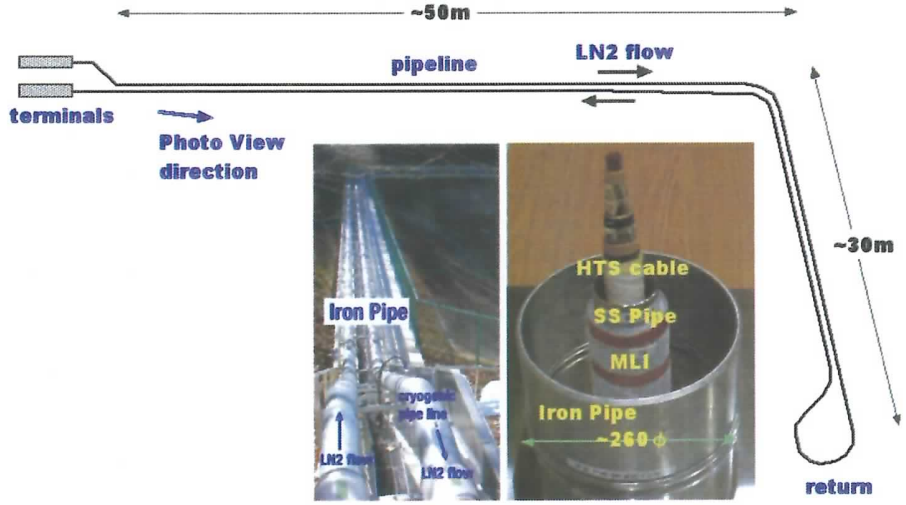

Fig. 4. Plan layout of the 200-meter cable test facility, the photos of cryogenic pipe and HTS cable, and the iron pipeline of the power transmission experiment.

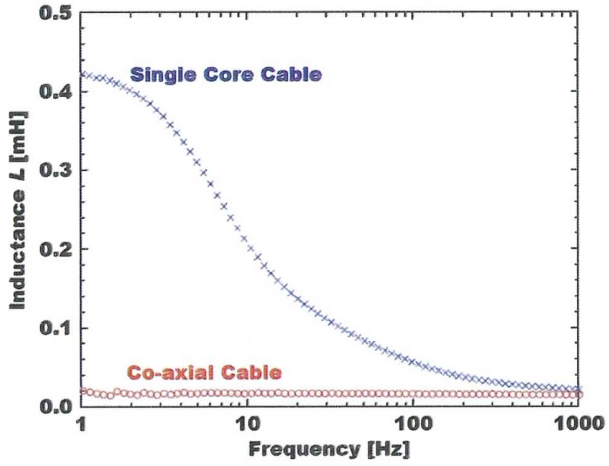

Fig. 5. Inductances of the single core cable and the co-axial cable versus the frequency.

where l is the length of the cable, μ is the permeability of the insulation material between two co-axial conduction layers, a is the radius of the inner conductor, and the b is the radius of the outer conductor as seen in Fig. 1. Thus, we can calculate the analytical value of the inductance, and it is $\sim$ 50 μH/km for the 200-meter cable experiment [7]. This is the same order of the measurement results. On the other hand, the inductance of the single core cable is larger, and it is $\sim$4 mH/km. Therefore, if the length of the cable is 100 km, the total inductance of the cable circuit will be 0.4 H, and this value is the same order of the inductor in the present HVDC. But the inductance of the single core cable should be considered and analysed its non-linear behavior and the hysteresis because the value depends on the character of the iron steel.

If we use the HTS cable for long DC transmission, we do not need to use high voltage system, but it should a large current system. The choice of the low voltage system can reduce the short circuit current, and increase the magnetic energy of the cable system. The magnetic energy of the system is given by

$$E = \frac{1}{2} L \cdot I^2 \tag{2}$$

where I is the current.

The magnetic energy is 80 MJ for the current of 20 kA and the inductance of 0.4 H. This value may be overestimated because the magnetic field of the iron will be saturated for larger current. However, if we calculate the air-core inductance of the parallely-reciprocated cable, the calculated inductance should be the minimum, and its values is $\sim$1 mH/km. This value is one fourth of the above-mentioned value. Therefore, the magnetic energy is larger than that of the present SMES [10]. Therefore, we call it is the SMES effect. The effect of large current DC transmission line can flat and smooth the unstable power from the renewable energy sources, such as the wind power and solar power. The other subject is the ripple current loss of the HTS

tape conductor. Even if it is the DC operation, we should consider the ripple current loss. Fortunately, it was reported to be not large [11].

ACKNOWLEDGMENT

The authors thank Dr. J. Sun and Dr. Y. Ivanov of Chubu University for their help performing the construction and experiment. They also thank to JFE Steel Corporation for supplying the iron pipe for this study. They also acknowledge Prof. H. Fujiwara of Keio University and the President of Nano-Opt Energy, Inc., for his support to construct the experimental device. They also thank to Dr. J. Minervini, Dr. L. Bromberg, and Dr. M. Takayasu, Plasma Science and Fusion Center at MIT, for their useful discussions.

REFERENCES

[1] S. Mukoyama, M. Yagi, M. Ichikawa, S. Torii, T. Takahashi, H. Suzuki, and K. Yasuda, "Experimental results of a 500 mHTS power cable field test," *IEEE Trans. Appl. Supercond.*, vol. 17, no. 2, pp. 1680–1683, Jun. 2007.

[2] T. Masuda, H. Yumura, M. Watanabe, H. Takigawa, Y. Ashibe, C. Suzawa, H. Ito, M. Hirose, K. Sato, S. Isojima, C. Weber, R. Lee, and J. Moscovic, "Fabrication and installation results for Albany HTS cable," *IEEE Trans. Appl. Supercond.*, vol. 17, no. 2, pp. 1648–1651, Jun. 2007.

[3] J. F. Mguire, F. Schmidt, F. Hmber, and J. Y. Kim, "Development and demonstration of a long length HTS cable to operate in the long island power authority transmission grid," *IEEE Trans. Appl. Supercond.*, vol. 15, no. 2, pp. 1787–1792, Jun. 2005.

[4] H. X. Xi, W. Z. Gong, Y. Zang, Y. F. Bi, H. K. Ding, H. Wen, B. Hou, and Y. Xin, "China's 33.5 m 35 kV/2 kA HTS ac power cable's operation in power grid," *Physica C*, vol. 448, pp. 1054–1057, Oct. 2006.

[5] S. Yamaguchi, M. Hamabe, I. Yamamoto, T. Famakinwa, A. Sasaki, A. Iiyoshi, J. Shultz, J. Minervini, T. Hoshino, Y. Ishiguro, and K. Kawamura, "Research activities of DC superconducting power transmission line in Chubu University," *J. Phys.: Conf. Series*, vol. 97, p. 012290, Mar. 2008.

[6] M. Hamabe, T. Fujii, I. Yamamoto, A. Sasaki, Y. Nasu, S. Yamaguchi, A. Ninomiya, T. Hoshino, Y. Ishiguro, and K. Kawamura, "Recent progress of experiment on DC superconducting power transmission line in Chubu University," *IEEE Trans. Appl. Supercond.*, vol. 19, no. 3, pp. 1778–1781, Jun. 2009.

[7] S. Yamaguchi, T. Kawahara, M. Hamabe, H. Watanabe, Y. Ivanov, J. Sun, and A. Iiyoshi, Design and Construction of 200-meter High Temperature Superconducting DC Power Cable Test Facility in Chubu University 20M-OR-3, ICEC 23_ICMC 2010, Jul. 2010.

[8] M. Hamabe, Y. Nasu, A. Ninomiya, Y. Ishiguro, S. Kusaka, and S. Yamaguchi, "Radiation heat measurement on thermally-isolated double-pipe for DC superconducting power transmission," *Adv. Cryo. Eng.*, vol. 53A, pp. 168–173, Aug. 2008.

[9] Y. Ivanov, A. Radovinsky, A. Zhukovsky, A. Sasaki, H. Watanabe, T. Kawahara, M. Hamabe, and S. Yamaguchi, "Compact couter-flow cooling system with subcooled graity-fed circulating liquid nitrogen," *Physica C: Superconductivity*, in press.

[10] S. Nomura, H. Tsutsui, S. Tsuji-Iio, and R. Shimada, "Flexible power interconnection with SMES," *IEEE Trans. Appl. Supercond.*, vol. 16, no. 2, pp. 616–619, Jun. 2006.

[11] D. W. Kim, J. G. Kim, A. R. Kim, M. Park, I. K. Yu, K. D. Sim, S. H. Kim, S. J. Lee, J. W. Cho, and Y. J. Won, "Ripple current loss measurement with DC bias condition for high temperature superconducting power cable using calorimetry method," *Physica C: Superconductivity*, in press.

Critical Current and Its Magnetic Field Effect Measurement of HTS Tapes Forming DC Superconducting Cable

Makoto Hamabe, Makoto Sugino, Hirofumi Watanabe, Toshio Kawahara, Satarou Yamaguchi, Yasuhide Ishiguro, and Kuniaki Kawamura

***Abstract*—We constructed a test stand of 20 m-class DC superconducting power transmission cable in Chubu University, in 2006. The cable consisted of thirty-nine Bi-2223 HTS tapes in two layers; nineteen tapes were used in the first layer and twenty tapes were used in the second layer. One of the features of the cable is that each HTS tape in the first layer is electrically isolated. Therefore, we can apply the current to the individual HTS tapes in the first layer. We measured critical current of the one HTS tape in the first layer when current was applied to the other HTS tapes, and compared the result with the magnetic field calculation due to the applied current. The critical current increased by $2 \sim 4\%$ when the current was applied to all other eighteen HTS tapes in the same layer. From the magnetic field calculation, we concluded that the self magnetic field of the measured HTS tape was eliminated at the tape edge by the applied magnetic field from the neighbor HTS tapes, and then the critical current increased.**

***Index Terms*—DC power transmission, DC superconducting cables, high-temperature superconductors.**

I. Introduction

SEVERAL projects to install AC superconducting power transmission (SC-PT) in the practical electricity networks have been carried out or started in the world, following the success in fabricating very long, high current density HTS tapes [1]–[4]. Meanwhile, DC SC-PT also attracts people's interest, since the DC SC-PT is free from AC losses and the current capacity of the DC SC-PT cable is higher than that of the AC SC-PT cable [5], [6].

In Chubu University, we constructed a 20 m-class DC SC-PT cable test stand in 2006, and started the first cooling-down in October 2006 [7]. Afterward, we carried out experiments on DC characteristics of the cable through the four periods of cooling test [8], [9]. One of the features of the test stand is that the cable consisted of two layers of HTS tapes and nineteen HTS tapes in the one layer were mechanically and electrically isolated each other; therefore, HTS characteristics of these nineteen HTS tapes could be tested individually [8]. Using this feature, we have measured the critical currents of these nineteen HTS tapes and have proved that the HTS tapes suffered no damages in their superconducting characteristics after the repetition of the cooling cycles [9]. This test stand also have the features to employ the Peltier current leads as the current leads connected to the HTS tapes in the liquid nitrogen (LN2) in order to reduce the heat leakage through the current leads [7], [8].

In case of AC SC-PT cable, self-field of HTS cable configuration affects AC loss properties [10]–[13]. A small gap between the HTS tapes in a single layer can reduce the AC loss, since the perpendicular magnetic field component of the self-field reduces at the tape edge due to the currents in the surrounding HTS tapes [10], [11]. It is also reported that the reduction of the self-field can enhance the critical current of a HTS tape [14], [15]. Therefore, in case of DC SC-PT cable, the self-field reduction at the tape edge in the cable configuration is possible to increase the critical current of HTS tapes.

In this paper, we will describe the results of the critical current measurement of the one HTS tape of the 20 m-class SC-PT cable under the magnetic field applied by the current feed to the other HTS tapes to consider the effect of the cable configuration of HTS tapes.

II. DC Superconducting Power Transmission Cable Test Stand

Fig. 1 shows (a) a layout of the 20 m-class DC SC-PT cable test stand and (b) a cut-model of the cable core used in the test stand [7]–[9]. The DC SC-PT cable was cooled by the circulation of sub-cooled liquid nitrogen (LN_2). The cryogen circulation system in Fig. 1(a) consisted of a LN_2 reservoir, a LN_2 pump, and two G-M cryocoolers. Total cooling power of the cryocoolers was 440 W at 80 K, 60 Hz. The DC SC-PT cable core was manufactured by Sumitomo Electric Industry Ltd. Designed specification of the DC SC-PT cable was 2 kA in current feed and 20 kV in insulation voltage at 78 K, and thirty-nine Bi2223 HTS tapes of 4 mm in width were used. The HTS tapes were divided to the insulated two layers, as shown in Fig. 1(b); nineteen tapes were in the inside layer and twenty tapes were in the outside layer. Since the shield HTS layer is not necessary for the DC SC-PT cable, power transmission current can feed in these two layers. Electric insulation between the HTS layers

Manuscript received August 02, 2010; accepted October 22, 2010. Date of publication December 03, 2010; date of current version May 27, 2011. This work was supported in part by "Collaboration with Local Communities" Project for Private Universities: matching fund by subsidy from MEXT, Japan, 2005–2009.

M. Hamabe, M. Sugino, H. Watanabe, T. Kawahara, and S. Yamaguchi are with Chubu University, Kasugai, Aichi 487-8501, Japan (e-mail: hamabe@isc.chubu.ac.jp).

Y. Ishiguro is with JFE Steel Co., Chita, Aichi 475-8611, Japan.

K. Kawamura is with Mayekawa Mfg. Co. Ltd., Moriya, Ibaraki 302-0118, Japan.

Color versions of one or more of the figures in this paper are available online at http://ieeexplore.ieee.org.

Digital Object Identifier 10.1109/TASC.2010.2089964

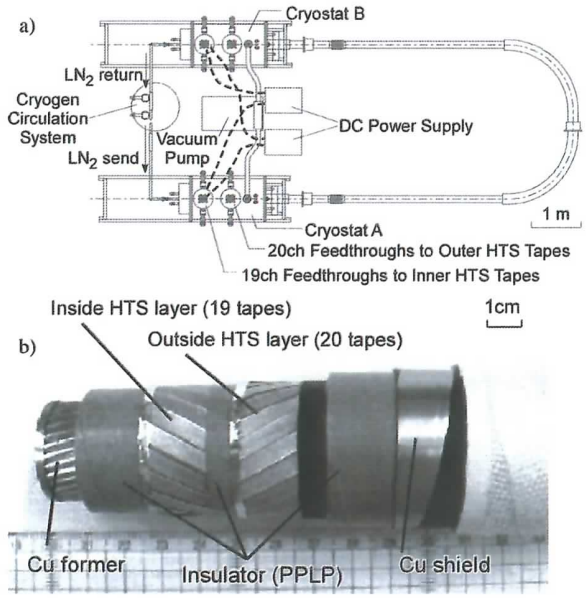

Fig. 1. (a) Layout of a test stand of 20 m-class DC superconducting power transmission (DC SC-PT) cable and (b) a cut-model of DC SC-PT cable core.

and the copper former and shield was provided by PPLP. Between the two HTS layers, a few PPLP was also inserted for insulation. Cryostats A and B of the test stand equipped also thirty-nine feedthroughs divided to 2 parts, as shown in Fig. 1(a), so that one feedthrough is connected to the one HTS tape. The nineteen HTS tapes in the inside layer were not mechanically attached, and then were electrically isolated. Therefore, we can feed current individually to any HTS tapes in the inside layer. In this experiment, the critical current of the one target HTS tape was measured, while the magnetic field was applied to the target HTS tape by a current feed to several HTS tapes using a 1.2 kA DC power supply.

III. Experimental Results and Discussion

A. Critical Current Measurement

Fig. 2 shows the arrangements of the target HTS tape and the current-feed HTS tapes tested here; i.e., type O: self-field only by the target HTS tape, type A: with the magnetic field applied by the current feed on the same HTS layer, type B: applied by the current on the same HTS layer except for the closest HTS tapes, and type C: applied by the current on the 1/3 of the same HTS layer. Current of the target HTS tape and the current feed I_{feed} to the other HTS tapes were in the same directions through this experiment.

The critical current strongly depend on the cable temperature. In order not to change LN_2 temperature through the experiment, we continuously measured I_{C0}: the critical current in Type O and I_C: that in the other arrangement type, as shown in Fig. 3, and compared I_C/I_{C0} in each arrangement. Fig. 4 shows the $I-V$ curve at the same measurement as in Fig. 3. We picked up two HTS tapes (#2-14 and #2-16) as the target HTS tapes for

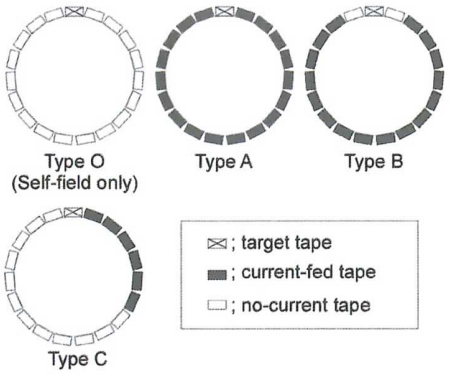

Fig. 2. Current feed arrangements tested in the experiment. Only the inside layer HTS tapes were used.

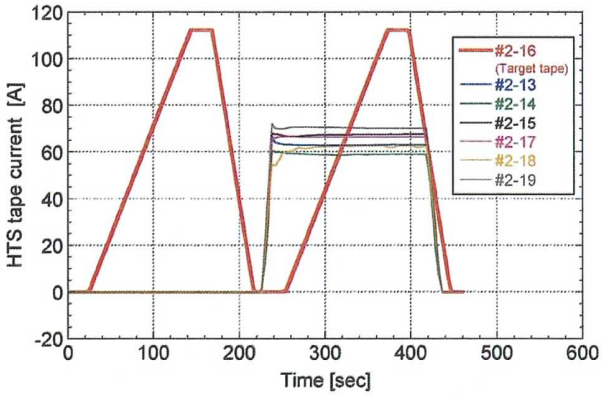

Fig. 3. An example of the time chart of the current to the target HTS tape #2-16 and the current feed to HTS tapes near to #2-16 tape at arrangement TYPE A.

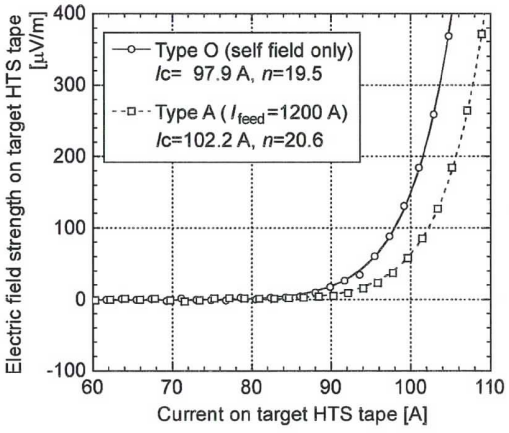

Fig. 4. Comparison of I-V characteristics of a HTS tape at 79.1 K for Type O (self-field only), Type A (1200 A/18 tapes except for the target tape). The target HTS tape number is #2-16.

comparison. Table I shows the comparison of I_C/I_{C0} in each arrangement. Consistently in both of the target tapes, I_C increased by 4% in Type A and by 2% in Type B. Fig. 5 shows the I_{feed} dependence of I_C/I_{C0}. Increase of I_C was linear to the I_{feed} up to 1.2 kA for both target tapes.

TABLE I
CHARACTERISTICS OF HTS TAPES UNDER THE MAGNETIC FIELD BY THE CURRENT FEED ON THE OTHER TAPES

Target HTS tape	Arrangement (I_{feed})	I_C [A]	I_{C0} [A]	I_C/I_{C0}
#2-14	Type A (1200 A)	102.9	98.9	1.040
	Type B (1200 A)	100.2	98.1	1.021
	Type C (480 A)	95.2	99.0	0.962
#2-16	Type A (1200 A)	102.2	97.9	1.044
	Type B (1200 A)	100.5	98.5	1.020
	Type C (480 A)	95.7	99.9	0.958

LN2 temperature: 79 1 ~ 79.3 K

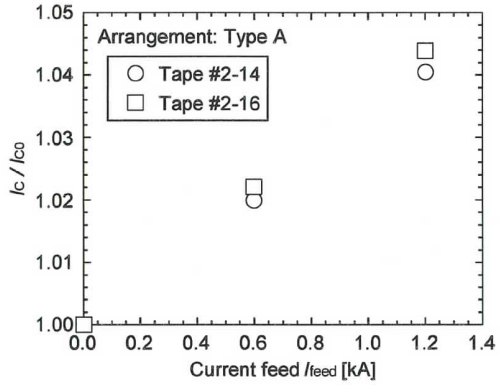

Fig. 5. Increase of critical current I_C of the target HTS tapes by the magnetic field due to the current feed I_{feed} at Type B.

B. Calculation of Magnetic Field

Generally, a magnetic field perpendicular to a HTS tape surface reduces its critical current. Considering the magnetic field applied by the current feed of Types A ~ C, the applied magnetic field was in the one-sided perpendicular direction over the target tape in Type C, and then I_C reduced. Meanwhile, in Types A and B, the applied magnetic field was supposed to be zero at the target tape center, and the direction of the applied field was opposite to the self-field at the tape edge when the current flows to the target tape and the other tapes were in the same direction. Therefore, it is necessary to compare the amplitude of the self-field and that of the applied field, in order to explain the increase of I_C in Types A and B.

We calculated the magnetic field on the target HTS tape for the DC SC-PT cable configuration by the 3D finite element method code ANSYS [16], including the winding of the HTS tapes at the resolution of 10^{-9} T. In this calculation, we assumed for simplicity that the current distributions in the HTS tapes were uniform. Table II shows the calculated magnetic field at the target tape edge, and Table III shows the magnetic field at the center of the target tape, perpendicular to the target tape. The calculated magnetic field at the tape center is not zero as shown in Table III because of the winding of the HTS tapes. The self-field at the tape edge in Table II is remarkably higher than that at the tape center in Table III. Moreover, the applied field at the tape edge of Type A is higher by one order than that of Type B, whereas the applied field at the tape center of Type B is slightly larger than that of Type A. Considering the increase of I_C in Type A is higher than that in Type B, the applied field reduces the perpendicular magnetic field at the both tape edges, and consequently I_C increases.

TABLE II
CALCULATED MAGNETIC FIELD AT HTS TAPE EDGE OF A DC SC-PT CABLE

Arrangement	Self-field [T] (100 A)	Applied field [T] (1200 A)	Total[T]
Type O	0.01199	0.00000	0.01199
Type A	0.01199	-0.00460	0.00739
Type B	0.01199	-0.00069	0.01130

TABLE III
CALCULATED MAGNETIC FIELD AT HTS TAPE CENTER OF THE DC SC-PT CABLE

Arrangement	Self-field [T] (100 A)	Applied field [T] (1200 A)	Total[T]
Type O	1.71E-07	0.00E-07	1.71E-07
Type A	1.71E-07	-1.11E-07	0.60E-07
Type B	1.71E-07	-3.67E-07	-1.97E-07

Gaps between the HTS tapes in the AC SC-PT cable cause the AC loss and no gaps are desirable. From results in Table I, the gaps for the DC SC-PT cable have also a meaning since small gaps can lead to the high I_C potential of HTS tapes. Moreover, current balance of the HTS tapes can reduce I_C in the DC SC-PT cable, if the gaps is not balanced (as shown in Type C) and the applied field is one-sided.

IV. CONCLUSION

The 20 m-class DC SC-PT cable in Chubu University has the feature that the nineteen HTS tapes wound in the same layer were electrically isolated. Using this feature, the critical current of the one target HTS tape was measured under the magnetic field applied by the current feed to the other HTS tapes in the same layer. Consequently, the critical current increased by several percents when the magnetic field was applied from both sides of the target tape. We supposed from the 3D magnetic field calculation that the critical current of the target HTS tape increased since the magnetic field by the current feed to the other HTS tapes eliminated the self-field at the tape edges.

ACKNOWLEDGMENT

The authors thank Dr. A. Iiyoshi, chancellor of Chubu University for his continuous encouragement through this work.

REFERENCES

[1] H. Yumura, T. Masuda, M. Watanabe, and H. Takigawa, "Albany HTS cable project long term in-grid operation status update," in *Adv. in Cryo. Eng.: Trans. Cryo. Eng. Conf.—CEC*, Aug. 2008, vol. 53A, pp. 1051–1058.

[2] J. F. Maguire, F. Schmidt., S. Bratt, T. E. Welsh, and J. Yuan, "Installation and testing results of long island transmission level HTS cable," *IEEE Trans. Appl. Supercond.*, vol. 19, no. 3, pp. 1692–1697, Jun. 2009.

[3] T. Masuda, H. Yumura, M. Ohya, T. Kikuta, M. Hirose, S. Honjo, T. Mimura, Y. Kito, K. Yamamoto, M. Ikeuchi, and R. Ohno, "A new HTS cable project in Japan," *IEEE Trans. Appl. Supercond.*, vol. 19, no. 3, pp. 1735–1739, Jun. 2009.

[4] A. Geschiere, D. Willén, E. Piga, and P. Barendregt, "HTS cables open the window for large-scale renewables," *Jour. of Phys.: Conference Series*, vol. 97, p. 012183, Mar. 2008.

[5] W. V. Hassenzahl, S. E. C. Eckroad, P. M. Grant, B. Gregory, and S. Nilsson, "A high-power superconducting DC cable," *IEEE Trans. Appl. Supercond.*, vol. 19, no. 3, pp. 1756–1761, Jun. 2009.

[6] X. M. Liang, S. T. Dai, Z. Y. Gao, N. H. Song, Y. S. Wang, D. Zhang, Z. F. Zhang, F. Y. Zhang, Z. Q. Zhu, X. Xu, T. B. Huang, X. C. Li, Z. C. Cao, Y. B. Lin, L. Z. Lin, and L. Y. Xiao, "Design of a 380 m DC HTS power cable," *IEEE Trans. Appl. Supercond.*, vol. 20, no. 3, pp. 1259–1262, Jun. 2010.

[7] S. Yamaguchi, M. Hamabe, I. Yamamoto, T. Famakinwa, A. Sasaki, A. Iiyoshi, J. Shultz, J. Minervini, T. Hoshino, Y. Ishiguro, and K. Kawamura, "Research activities of DC superconducting power transmission line in Chubu University," *Jour. of Phys.: Conf. Ser.*, vol. 97, p. 012290, Mar. 2008.

[8] M. Hamabe, T. Fujii, I. Yamamoto, A. Sasaki, Y. Nasu, S. Yamaguchi, A. Ninomiya, T. Hoshino, Y. Ishiguro, and K. Kawamura, "Recent progress of experiment on DC superconducting power transmission line in Chubu University," *IEEE Trans. Appl. Supercond.*, vol. 19, no. 3, pp. 1778–1781, Jun. 2009.

[9] M. Hamabe, T. Fujii, M. Sugino, A. Sasaki, T. Sugimoto, H. Watanabe, T. Kawahara, S. Yamaguchi, Y. Ishiguro, and K. Kawamura, "Cooling cycle test of DC superconducting power transmission cable," *Jour. of Phys.: Conf. Ser.*, vol. 234, p. 032019, Jul. 2010.

[10] S. Fukui, R. Kojima, J. Ogawa, M. Yamaguchi, T. Sato, and O. Tsukamoto, "Numerical analysis of AC loss characteristics of cable conductor assembled by HTS tapes in polygonal arrangement," *IEEE Trans. Appl. Supercond.*, vol. 16, no. 2, pp. 143–146, Jun. 2006.

[11] N. Amemiya, Z. Jiang, M. Nakahata, M. Yagi, S. Mukoyama, N. Kashima, S. Nagaya, and Y. Shiohara, "AC loss reduction of superconducting power transmission cables composed of coated conductors," *IEEE Trans. Appl. Supercond.*, vol. 17, no. 2, pp. 1712–1717, Jun. 2007.

[12] Y. Mawatari and K. Kajikawa, "Hysteretic ac loss of polygonally arranged superconducting strips carrying ac transport current," *Appl. Phys. Let.*, vol. 92, no. 1, p. 012504, Jan. 2008.

[13] A. P. Malozemoff, G. Snitchler, and Y. Mawatari, "Tape-width dependence of AC losses in HTS cables," *IEEE Trans. Appl. Supercond.*, vol. 19, no. 3, pp. 3115–3118, Jun. 2009.

[14] S. Spreafico, L. Gherardi, S. Fleshler, D. Tatelbaum, J. Leone, D. Yu, and G. Snitchler, "The effect of self-field on current capacity in Bi-2223 composite strands," *IEEE Trans. Appl. Supercond.*, vol. 9, no. 2, pp. 2159–2162, Jun. 1999.

[15] F. Gömöry and B. Klinčok, "Self-field critical current of a conductor with an elliptical cross-section," *Supercond. Sci. Technol.*, vol. 19, no. 8, pp. 732–737, Aug. 2006.

[16] [Online]. Available: http://www.ansys.com

Journal of ELECTRONIC MATERIALS, Vol. 40, No. 5, 2011
DOI: 10.1007/s11664-011-1513-4

Thermoelectric Property Dependence and Geometry Optimization of Peltier Current Leads Using Highly Electrically Conductive Thermoelectric Materials

TOMOHIRO FUJII,[1] SHINJI FUKUDA,[1] MASAHIKO EMOTO,[2] KOUDAI OSADA,[1] TOSHIO KAWAHARA,[3,4] MAKOTO HAMABE,[3] HIROFUMI WATANABE,[3] YURY IVANOV,[3] JIAN SUN,[3] and SATAROU YAMAGUCHI[1,3]

1.—Department of Electrical Engineering, Chubu University, Kasugai, Aichi 487-8501, Japan. 2.—National Institute for Fusion Science, Toki, Gifu 509-5292, Japan. 3.—Center of Applied Superconductivity and Sustainable Energy Research, Chubu University, Kasugai, Aichi 487-8501, Japan. 4.—e-mail: toshi@isc.chubu.ac.jp

Thermoelectric materials are promising candidates for use in energy-saving devices in many fields. They are also useful in superconducting applications such as those using Peltier current leads (PCLs) to reduce system heat loss. In the case of PCLs, consideration must be given to Joule heating. Furthermore, the performance of PCLs is intricately dependent on their thermoelectric properties. In addition to the figure of merit Z, consideration of the electrical conductivity is also important for the design of high-performance PCLs. In this paper, we discuss the resistivity dependence of the performance of PCLs using model parameters obtained from real devices.

Key words: Peltier current lead (PCL), superconducting applications, DC transmission and distribution system, BiTe alloy

INTRODUCTION

We must solve environmental problems such as global warming and energy resource exhaustion to ensure a sustainable world. Several solutions have been developed, and thermoelectric systems are one of them.

It is known that superconductors have zero resistance, and they can therefore carry electric power without resistive loss. They can also transmit electric power for a very long distance, which is useful to incorporate more renewable energy into the electric grid. One of the goals of such systems was proposed as the Genesis Project and involved a worldwide grid for energy transmission.[1] As superconducting alternating-current (AC) transmission systems have AC losses, direct-current (DC) systems therefore seem to be more suitable for low-energy-loss transmission systems. At Chubu University, we have developed 20-m DC superconducting transmission lines (CASER-1) as a working trial system for actual applications. This is the first high-temperature superconducting DC transmission system in the world.[2] Using this testing facility, the feasibility and superiority of superconducting transmission systems over copper cables were discussed.[3] On the other hand, the performance of superconducting transmission systems is governed by the heat loss from cryogenics,[4] and several CASER-1 heat reduction experiments have been discussed.[3]

When the transmission distance is small, heat loss at the terminals is dominant, where the heat can conduct through current leads connected to the outside of the system. In this case, Peltier current leads (PCL) can be used as high-performance current leads for superconducting applications to reduce the heat loss.[5,6] In general, large figures of merit Z relate to high-performance thermoelectric materials. Here, Z is equal to $\sigma\alpha^2/\kappa$, where σ is the electrical conductivity, α is the Seebeck coefficient,

(Received May 9, 2010; accepted January 5, 2011; published online February 2, 2011)

and κ is the thermal conductivity. The same applies for PCLs. However, Joule heating must be taken into account in PCLs, where a large operating current flows not only in transmission but also in the feed lines made of thermoelectric materials. Besides a large figure of merit at low temperature, thermoelectric materials for use in PCLs must have very low electrical resistivity. n- and p-type materials, which are used as input and output terminals, are also needed.

In this paper, the thermoelectric properties of Bi_2Te_3 alloy for use in PCLs have been measured. The PCL geometry was optimized as a function of the electrical conductivity varied by about 3% around the measured values. The change in the thermal conductivity was calculated by the Wiedemann–Franz law. The heat loss on the current lead was calculated using the optimized geometry.

EXPERIMENTAL PROCEDURES

Bismuth telluride (BiTe) alloy samples were commercially obtained products (solid-solution samples grown by the Bridgeman method). Figure 1 shows a BiTe sample and its holder. Samples have a rectangular shape with dimensions of 2.4 mm × 2.4 mm in cross-section and 3.5 mm in length. Copper blocks with copper current leads were soldered to both ends of the sample. Small heaters with a resistance of 1 kΩ were attached to one of the copper blocks. Copper–constantan thermocouples with a diameter of 100 μm were connected to the copper blocks using Ag paste.

The sample was installed in a vacuum chamber. The pressure was below 0.1 Pa. The temperature of the sample was scanned from 100 K to 300 K. The temperature gradient along the sample achieved using small heaters was between 0 K and 6 K. We measured the temperatures and temperature differences of the sample using the thermocouples, and recorded voltages for both the Seebeck coefficient and electrical resistivity measurements using the copper wires of the thermocouples. Thermal conductivities were measured by the steady-state method.

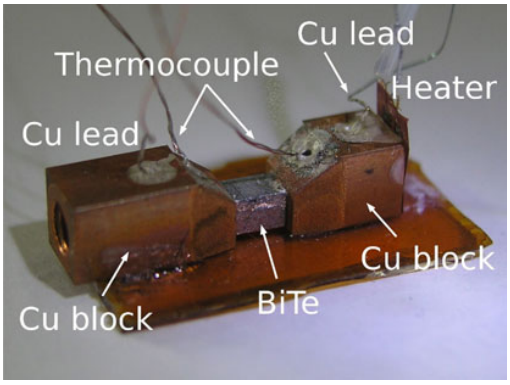

Fig. 1. Configuration used to measure the transport properties of the thermoelectric materials.

SIMULATION METHODS

We used thermal balance (Eq. 1) to estimate the heat leakage[7] and Seebeck effect.[6,8]

$$\frac{dQ_0}{dx} - f\frac{dm}{dt}C_p\frac{d\theta}{dx} + \frac{I^2\rho(\theta)}{A} = 0, \quad (1)$$

where θ is the temperature, C_p is the specific heat, A is the cross-section of the current lead, I is the current, and ρ is the resistivity. Q_0 is the conduction heat as represented by $k(\theta)A\frac{d\theta}{dx}$, where $k(\theta)$ is the thermal conductivity. The Seebeck effect ($\alpha I\theta$) is added to Q_0 for a PCL.[6–8] Gas cooling is expressed by the heat exchange ratio f between cold gas and the current lead with a mass flow dm/dt of liquid nitrogen, whose mass is m. f is the efficiency of heat transfer and is defined by the ratio between the rate of heat transfer to the coolant H and $dm/dt \times C_p\delta\theta$ with the local temperature change of the current lead $\delta\theta$. Therefore, $f = 0$ represents no heat exchange. In this case, cooling takes place by conduction. $f = 1$ means that heat is transferred from the current lead to the cold gas by convection. In this paper, we assume no gas cooling, and as such f is set to 0.

For the calculation, we used an operational current of 100 A, because the critical current for typical superconducting tapes was around 100 A. As we used high-T_c superconductors cooled by liquid nitrogen, the cold temperature of the current lead was set to 77 K, and the higher temperature at the other end was 300 K.

Using the thermal balance equations, we can calculate the temperature at the higher-temperature end of the current lead, presupposing the shape factors L/A and the heat load at 77 K at the lower-temperature end of the current lead, where L is the length of the current leads made of copper and BiTe. If the higher temperature is 300 K, those parameters are solutions for the heat loss with given shape factors in a reverse problem, and the temperature distribution on the current lead can also be obtained. For PCLs constructed by series connection of thermoelectric materials and a copper lead, the Seebeck term is only added for the thermoelectric materials.

RESULTS AND DISCUSSION

For estimation of the performance of the PCL, we optimized the shape factor of the current lead to obtain the minimum heat loss on the current lead. Using the thermal balance equations in the reverse method, we obtain the heat loss for each shape factor with boundary conduction at 77 K and 300 K at the two ends of the current lead. Then, the optimized shape factor L/A that has minimum heat loss can be obtained for both the BiTe lead and copper

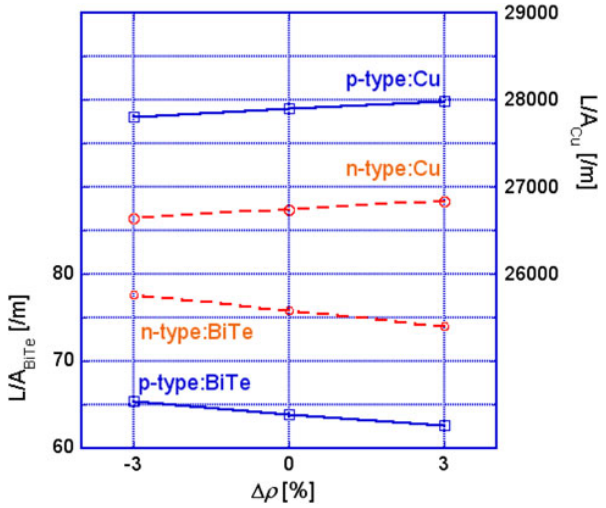

Fig. 2. Resistivity dependence of the optimum shape factor L/A. Dashed lines are for n-type material and solid lines for p-type material in the PCL.

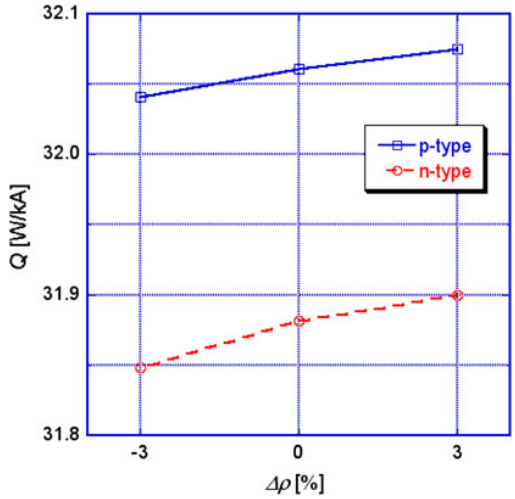

Fig. 3. Resistivity dependence of the optimized heat loss. The dashed line is for n-type material and the solid line for p-type material.

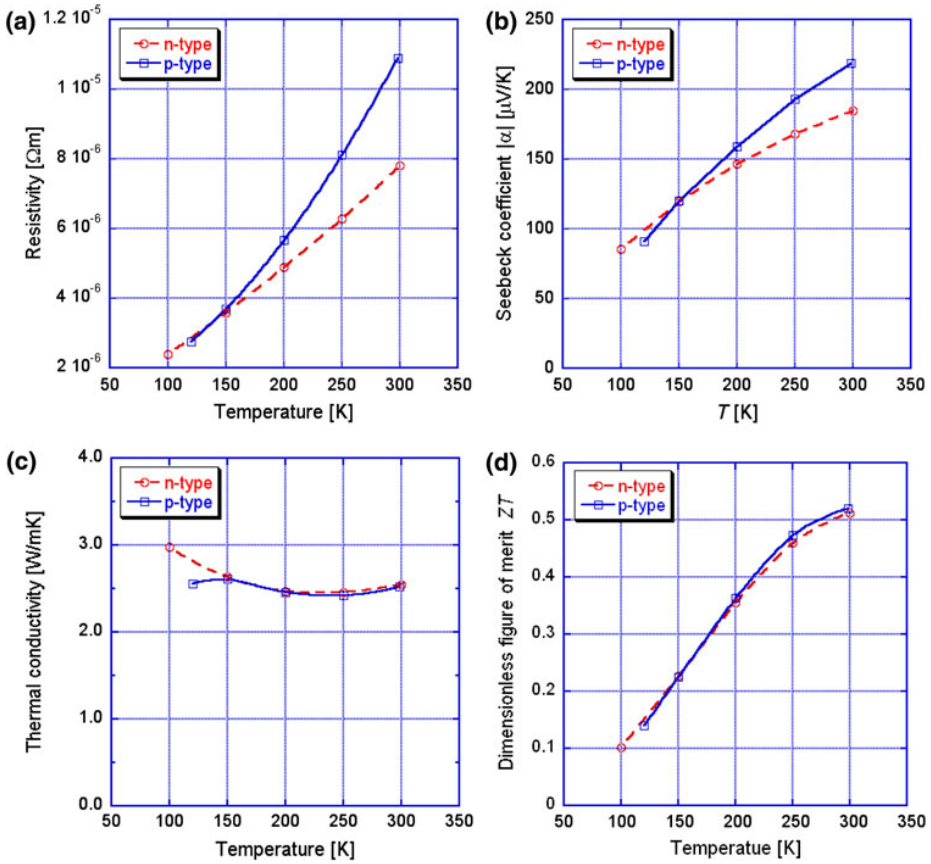

Fig. 4. Temperature dependence of the thermoelectric parameters measured for n-and p-type materials. Dashed lines are for n-type materials and solid lines for p-type material: (a) resistivity, (b) Seebeck coefficient, (c) thermal conductivity, and (d) dimensionless figure of merit ZT.

leads as L/A_{BiTe} and L/A_{Cu}, respectively. The heat loss obtained is the optimum heat loss with minimum Q; for example, such optimized L/A_{BiTe}, L/A_{Cu}, and Q are shown at $\Delta\rho$ = 0% in Figs. 2 and 3 for the actual model thermoelectric parameters explained in the next paragraph.

Table I. Model thermoelectric parameters with 3% reduced resistivity

T (K)	ρ (Ωm)	α (μV/K)	κ (W/mK)
n-Type, −3%			
100	2.33×10^{-6}	−84.6	3.01
150	3.48×10^{-6}	−118.3	2.66
200	4.74×10^{-6}	−145.3	2.50
250	6.08×10^{-6}	−166.9	2.49
300	7.59×10^{-6}	−182.9	2.58
p-Type, −3%			
120	2.68×10^{-6}	90.1	2.59
150	3.58×10^{-6}	119.1	2.64
200	5.49×10^{-6}	157.2	2.49
250	7.87×10^{-6}	190.6	2.44
298	1.06×10^{-5}	216.8	2.54

Table II. Model thermoelectric parameters with 3% enhanced resistivity

T (K)	ρ (Ωm)	α (μV/K)	κ (W/mK)
n-Type, +3%			
100	2.47×10^{-6}	−86.2	2.95
150	3.70×10^{-6}	−120.5	2.60
200	5.04×10^{-6}	−147.9	2.44
250	6.46×10^{-6}	−170.0	2.43
300	8.05×10^{-6}	−186.4	2.52
p-Type, +3%			
120	2.84×10^{-6}	91.7	2.53
150	3.80×10^{-6}	121.3	2.58
200	5.83×10^{-6}	160.3	2.43
250	8.35×10^{-6}	194.6	2.40
298	1.12×10^{-5}	221.6	2.50

Figure 4 shows the model parameters measured for actual modules, with rather higher electrical and thermal conductivity than for usual high-Z BiTe materials. The temperature dependence of the resistivity is plotted in Fig. 4a for both n- and p-type materials. The resistivity is 7.8×10^{-6} Ωm at 300 K for the n-type and 10.9×10^{-6} Ωm at 298 K for the p-type material, smaller than those of typical BiTe thermoelectric modules. The resistivity decreases at low temperature, especially for the p-type material. These properties seem to be very desirable for PCL applications. The temperature dependence of the Seebeck coefficient is also plotted in Fig. 4b. Values are around 200 μV/K at room temperature for both material types, being typical for high-performance thermoelectric materials. However, the Seebeck coefficient decreases at low temperature. Therefore, BiTe can be used for the high-temperature end of the PCL. Figure 4c shows the temperature dependence of the thermal conductivity. Our materials have rather higher thermal conductivity than usual high-Z BiTe materials, which should be improved for high-performance PCL applications. However, a maximum dimensionless figure of merit ZT seems to occur above 300 K, as shown in Fig. 4d. Therefore, new thermoelectric materials still need to be developed for PCL applications.

We then calculated modified thermoelectric parameters to evaluate the effect of a modification of the resistivity. A change of about 3% of the resistivity by doping at constant Z is achievable. Doping could be considered viable for commercial production. Since the electron contribution to thermal conductivity can be calculated using the Wiedemann–Franz law, we can then estimate the corresponding modified thermal conductivity, where the Lorenz number L is set as 2.45×10^{-8} WΩ/K^2, and we assume the phonon contribution to thermal conductivity is unmodified for each temperature in this parameter range. The estimated values are summarized in Tables I and II for the 3% reduction and enhancement of resistivity, respectively. Z was kept constant.

Using these model parameters, we estimated the performance of the PCL. The resistivity dependence of the optimum heat loss and shape factors are plotted in Figs. 2 and 3, respectively. Lower resistivity can reduce the heat loss. In this low-resistivity case, the optimum shape factor is enlarged, and then the Peltier modules can effectively work as thermal insulators with smaller heat loss because of the smaller Joule heating. Thus, lower resistivity is more favorable for the same Z for PCL applications.

CONCLUSIONS

We investigated the effect of the electrical resistivity of current leads made of thermoelectric materials (PCLs) in the case of a superconducting transmission line. The optimal PCL geometry is found to be a function of the electrical resistivity. Lower resistivity is favorable as long as the figure of merit is not decreased. Therefore, highly electrically conductive thermoelectric materials must be developed, and the PCL geometry designed accordingly.

ACKNOWLEDGEMENTS

We acknowledge the support of the Ministry of Education, Culture, Sports, Science, and Technology for this work as a “Collaboration with Local Communities” Project for Private Universities. Parts of the work were supported by Nippon Sheet Glass Foundation for Materials Science and Engineering (T.K.).

REFERENCES

1. Y. Kuwano, *4th International Photovoltaic Science and Engineering Conference.* (Sydney, Australia, 1989), p. 557.
2. S. Yamaguchi, M. Hamabe, I. Yamamoto, T. Famakinwa, A. Sasaki, A. Iiyoshi, J. Schultz, J. Minervini, T. Hoshino, Y. Ishiguro, and K. Kawamura, *J. Phys.: Conf. Ser.* 97, 012290 (2008).
3. M. Hamabe, T. Fujii, I. Yamamoto, A. Sasaki, Y. Nasu, S. Yamaguchi, A. Ninomiya, T. Hoshino, Y. Ishiguro, and K. Kawamura, *IEEE Trans. Appl. Supercond.* 19, 1778 (2009).
4. T. Kawahara, T. Fujii, M. Emoto, M. Hamabe, J. Sun, H. Watanabe, and S. Yamaguchi, Physica C, doi:10.1016/j.physc.2010.01.054 (2010).

5. T. Yamaguchi, H. Okumura, K. Nakamura, and S. Yamaguchi, *IEEE Trans. Appl. Supercond.* 13, 1914 (2003).
6. S. Yamaguchi, T. Yamaguchi, K. Nakamura, Y. Hasegawa, H. Okumura, and K. Sato, *Rev. Sci. Instrum.* 75, 207 (2004).
7. M.N. Wilson, *Superconducting Magnets* (New York: Oxford University Press, 1983), p. 257.
8. H. Okumura and S. Yamaguchi, *IEEE Trans. Appl. Supercond.* 7, 715 (1997).

日刊工業出版プロダクション発行「工業材料」誌　2016年1月号　別刷

特集　超電導は21世紀のキーテクノロジー —最新の応用展開をさぐる

TOPICS 1

高温超電導ケーブルの現状と将来

中部大学　山口 作太郎

特集
超電導は21世紀のキーテクノロジー —最新の応用展開をさぐる

TOPICS 1

高温超電導ケーブルの現状と将来

中部大学　山口 作太郎*

はじめに

1987年の高温超電導体(HTS)の発見からすぐの1989年には、大規模太陽電池からの電力を超電導直流送電によって世界各国を送る電力網の提案[1]があった。これは超長距離送電の直流高圧送電である。2000年以降になって、高温超電導線材が工業的に安定して使える状況になり、同様な提案[2)~4)]があり、検討が進んでいる。

一方、HTS発見直後からケーブルへの応用はすぐに始まった。そして、2010年くらいまでは交流ケーブル[5]の研究発表が一般的であったが、その後直流ケーブル[6),7)]の研究開発も広く行われるようになった。現在、日本では北海道・石狩で直流ケーブルの実証研究が行われている。また、横浜では交流ケーブルが系統に接続された研究[7]が行われている。そこで、この時点で超電導直流ケーブルと交流ケーブルの比較は、将来展望を考えるうえで有用であろう。

*やまぐち　さたろう：工学部 電気システム工学科 教授
〒487-8501　愛知県春日井市松本町1200
☎0568-51-9419

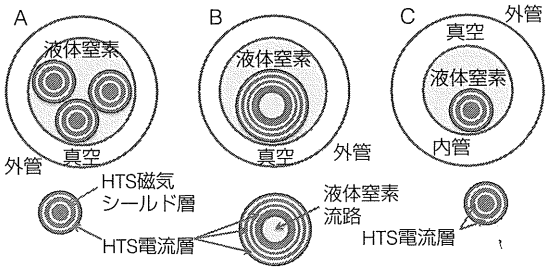

図1　2種類の交流ケーブルと直流ケーブルの断面模式図

図1に現在研究が行われている断熱二重管を含む2種類の交流ケーブル[A、B][7),8)]と直流ケーブル[C][6]の断面模式図を示す。

A構造は「三相一括ケーブル[9]」と呼ばれ、現在NEDOの横浜プロジェクトで東京電力、住友電工、前川製作所が共同で開発している。交流三相ケーブルであり、ケーブルは3本からなる。それぞれのケーブルは、交流電流を流すHTS電流層とその電流によって発生する交流磁場をシールドするためのHTS磁気シールド層が同軸状に構成される。内側のHTS電流層電流と逆位相の電流が磁気結合よって磁気シールド層に流れ、この外側には磁場はほとんど発生しない。この2つの層はケーブル定格電圧で電気絶縁され、断熱二重管の渦電流による発熱を防止し、低温系への熱負荷を低減している。

Bに示した構造は三相交流を同軸上の3つの層にそれぞれ流す。これはそれぞれの相電流が同じであれば、それらの和は時間的に常にゼロになる特徴を生かし、ケーブル外側に磁場を発生させない。このため、磁気シールド層が省くことが原理的に可能である。また、このデザインでは液体窒

素循環のために流路が往復2つ必要になるが、それがケーブルの中心部と外側の2つとし、断熱二重管の熱侵入低減につなげている。

Cは直流ケーブルである。直流電流では渦電流は発生しないが、同軸構造をとり、往復導体が一本のケーブルを形成している。また、この構造では単相交流も流すことができる。これはケーブル外部に磁場が発生しないので磁気シールド層は不要である。なお、冷媒の往復循環のためにはもう一本配管が必要である。

現在、これらのケーブルは実証実験が行われていて、送電電力やHTS線材量(導体数)について**表1**にまとめた。

I_0は実効電流であり、V_0は実効電圧である。また、cosϕは力率である。直流ケーブルでは交流のピーク電流とピーク電圧で運転をするとした。

もし、ケーブルコストの多くがHTSテープ線材とすると、導体当たりの送電電力が大きいほうが望ましい。するとBケーブルはAケーブルに比べて2倍コスト競争力が高いと言える。しかし、Bケーブルは各相の電流が等しくなるように運転をしないと、著しく交流損が増大する。また、短絡時の保護のために文献10)では、FCL(Fault Current Limiter：短絡電流制限装置)を組み込んでいるため、FCL用のHTSテープ線材が必要であり、HTSテープ線材使用量は2倍もの差はないであろう。また、ケーブル内側流路断面積が大きくできないので、ケーブルの電気特性と熱設計が独立に決められなく、設計上の制約は大きい。

一方、Cの単相交流ケーブルは現在実験が行われていないが、これは磁気シールド層に流れる電流は、電流層電流と完全に逆位相で同じ大きさになるので、A、Bの交流ケーブルに比べて交流損は低くなるであろう。つまり、Aケーブルの場合には、磁気シールド層に流れる電流が完全に電流層電流による磁場を消すことができなく、5%から10%程度の磁場が外に出てくると言われている。また、導体当たりの送電電力はAケーブルに比べてよく、Bケーブルのように交流三相のそれぞれの電流を同じにしなくても交流損を考えなくても使えるので、使い勝手はよさそうである。さらに、三相交流発電機との接続でも工夫次第と思われる。複数本を同時に使うので、冷媒循環路の確保も可能になる。

表1　交流ケーブルおよび直流ケーブルの導体数と送電電力

	導体(層)数	タイプ	送電電力	導体当たりの送電電力
A 三相一括ケーブル	6	三相交流	$\sqrt{3}I_0V_0\cos\phi$	$\sqrt{3}/6I_0V_0\cos\phi$
B 三相同軸ケーブル	3	三相交流	$\sqrt{3}I_0V_0\cos\phi$	$\sqrt{3}/3I_0V_0\cos\phi$
C 同軸ケーブル	2	単相交流	$I_0V_0\cos\phi$	$1/2I_0V_0\cos\phi$
	2	直流	$2I_0V_0$	I_0V_0

Cケーブルを直流で利用すると、導体当たりの送電電力は一番大きい。したがって、直流ケーブルの経済性が一番高い可能性と思われる。ただし、交流発電機に接続するときには、電力変換器が必要になる。一般に高電圧電力変換器は高価であるため、システム・コストを考える必要がある。また、受電側の電力変換器は、ユーザー側で個々の機器別に準備しているのが一般的であったが、これを一括でまとめることができれば、電力変換器コストはユーザー側に含まれる。また事故時の遮断は、電力変換器で遮断が数μsで可能である。このためFCLと遮断器の機能も電力変換器はもっている。したがって、FCLを使わないシステム選択もある。以上の検討から、比較的電圧の低い電力システムでは、直流超電導ケーブルの実現可能性が高いと言えよう。

当面の応用と課題

文献[1)~4)]では、長距離送電ケーブルとして超電導直流ケーブルの利用を想定している。現在、世界で利用されている長距離送電は、最も長いもので2,300kmほどであり、地球規模の送電では、これより1桁長いケーブルが必要になる。しかし、現状の技術でこのような長いケーブルシステムを作ることは無理であり、世界の現在のプロジェクトでは精々1km程度である。このため、短い距離でも超電導ケーブルの特性が生かせる応用を考える必要がある。一方、そもそも電力ケーブルは損失を低くすることが求められて開発されてきたので、短い距離では損失はそれほど大きくない。超電導ケーブルの長所は少ないと考えられてきた。このため、超電導ケーブルの初期の提案では

低損失ではなく、ケーブルの小型化を大きな特徴として提案された。電力を多く使う都市部では地下共同溝に入れるケーブルの小型化が進むと、工事費を減らしたり、新たな共同溝の建設が不要になったりするので、全体として安価に電力ケーブルを増設できることが強調された。都市の共同溝に入れるケーブル長は数km～10km程度であり、それほど長くないので、超電導ケーブルの最初の応用先としては適切と考えられた。そして、開発は交流ケーブルとされた。

しかし、2000年以降日本をはじめOECD加盟国では人口減少が始まり、一次エネルギーにおける電力エネルギーの割合は増大しているにもかかわらず、省エネルギー技術の進展などもあり、都市部の電力需要の増大は当初予想から減った。さらに、銅ケーブルでは電流通電時のみ損失が発生し、電流値の二乗に損失は比例するが、超電導ケーブルは常に一定の能力で冷却する必要があるため、設備利用率の低い送電経路への利用は超電導ケーブルが高価であることもあり、損失低減が強く求められるようになった。このため、交流損がない安価な直流ケーブルが選択肢にあがってきた。そして、設備利用率の高い応用先として、インターネット・データーセンタ(iDC)が検討された。

iDCは大電力を消費し、現代社会インフラの基礎をなし、金融取引、商品の販売、情報の保存・広報・交換・輸送が行われ、Internet of Things(IoT)やビッグデータの提案もあり、今後も利用が増大する。そして、消費電力の増大が予想されている。実際、日本では全電力需要は減少しているが、iDCの増強は続いていて、電力消費も増大している。また、iDCの電力需要は昼夜あまり変わらなく、設備利用率が高い。そして、最近iDC用に直流サーバーが開発され、設備投資と消費電力の節減[11]が同時に達成されるようになった。特に、iDCでは高電圧ではなくて、低電圧・大電流で利用するため、超電導ケーブルの特徴を生かすやすい。

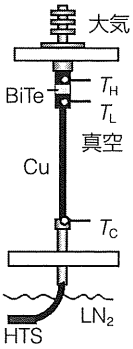

図2
ペルチェ電流リード(PCL)の構成

直流電力の大きなユーザーとしては、ほかにも金属精錬やシリコン製造などがあり、これらの業界では設備利用率が高い。さらに、低電圧・大電流利用である。ただし、現在は電力コストの増大によって、業界としてかなり厳しい状況であり、応用検討はこれからである。ほかには、再生可能エネルギーとの接続がある。これは直流との相性がよいからである。ただし、一般に再生可能エネルギーの設備利用率は高くないので、発電部の複数化などの工夫が必要になる。

一方、短い距離では断熱二重管の熱侵入より端末部常温端からの熱侵入が課題になる。従来の端末は、常温部から低温部まで銅リード接続のため、低温系への熱侵入量が大きい。銅の電流リードは最適設計が行われ、現状では単位電流当たり

$$50\mathrm{W/kA} \qquad (1)$$

である。このため、大電流では、電流に比例して熱侵入量が増大し、損失が大きくなる。また、待機時にも大きな熱侵入がある。このため、低電圧大電流の給配電では端末での熱侵入量低減が重要な課題になる。iDCで利用される直流電圧は400V程度であり、10MWの消費電力なら、電流は25kAとなる。文献12)では式(1)の半分程度(～25W/kA)の熱侵入量が経済性の確立には必要としている。電流リードの熱侵入量低減は電流を通し、熱は通さない材料を求めるので、物理的には矛盾した要求であり、材料とシステム構成に新しいアイデアが必要になる。

このため、筆者はペルチェ効果を利用する方法を考案し、今までに開発[13),14)]を行ってきた。**図2**にペルチェ電流リード(PCL)の模式図を示す。ペルチェ材料としてビスマス・テルル合金(BiTe)を用い、ペルチェ効果によって温度差が100K近くつき、大きな熱絶縁になる。また、BiTeは熱伝導率が銅の0.3%程度のため、非通電時でも熱侵入量の低減につながる。

直流ケーブルの課題としては、断熱二重管の熱侵入量の低減、冷媒循環抵抗の低減など低温工学に関連する研究課題が実際の応用では重要になろう。そして、短い距離でも超電導ケーブルの特徴

表2　石狩プロジェクトの主要パラメータ

			石狩(回線1)	石狩(回線2)
送電システム	送電距離		500m	1,000m
	送電方式		直流	直流
	送電容量	電　圧	20kV(対地10kV)	20kV(対地10kV)
		電　流	5.0kA	2.5kA
		容　量	100MW	50MW
	ケーブル	材　料	ビスマス系	ビスマス系
		ケーブル構造	同軸	同軸
		構　成	内層：12本＋12本＋13本/外層：17本＋18本	内層：12本＋12本/外層：15本
		線材臨界電流	190A	内層：180A/外層：220A
		中間接続箇所	1カ所	2カ所
	電流リード	材　料	ペルチェ材料、銅	ペルチェ材料、銅
		熱侵入量(目標値)	～35W/kA	～35W/kA
冷却システム	冷凍機		スターリング式(1台)、ターボブレイトン式(1台)	スターリング式(2台)、ターボブレイトン式(2台)
	冷却方法		サブクールLN2循環	サブクールLN2循環
	循環流量/圧力損失		～40L/min/＞100kPa	～40L/min/＞100kPa
	冷却能力		3kW(@77K)	6kW(@77K)
	総熱侵入量(kW)		1.4(速報値)	2.0～4.0
	断熱二重管	構　造	高断熱性能二重管 (内管2本、外管1本)	高断熱性能二重管 (内管2本、外管1本) うち430m分輻射シールド付き
		外管材料	亜鉛めっき鋼管 (ポリエチレンライナー付き)	亜鉛めっき鋼管 (ポリエチレンライナー付き)
		外管サイズ	250A	250A/300A(シールド付き)
		内管材料	SUS304	SUS304
		内管サイズ	60A(ケーブル配管)/ 50A(リターン管)	60A(ケーブル配管)/ 50A(リターン管)
		MLI	9層、21層	21層
		熱侵入量(W/m)	1.4(速報値)	1.3～1.5(目標値)
設置場所			敷地内(地下埋設)	試験用(地上設置)

を生かして、順次長くすることが技術的な発展になる。

石狩プロジェクトと現状

2012年の経済産業省補正予算によって、北海道石狩市に超電導直流ケーブルの実証研究として2回線作ることになった。このケーブル仕様は**表2**にまとめる。現在(2015年10月)までで、回線1については装置完成後2015年6月と9月に2回の通電試験を行った。負荷はさくらインターネットの石狩iDCであり、電源は太陽電池パネルである。また、回線2については、執筆段階で建設中であり、2015年11月から冷却試験が始まる予定である。

このプロジェクトでの大きな目的は、長距離ケーブル建設に関連する下記の課題[15]の解決である。

① ケーブルの熱収縮対策

② 低温系への熱侵入量の低減

③ 長距離の液体窒素循環

ケーブルを冷却すると熱収縮する。収縮率は0.3%ほどであり、1kmでは3mとなり、100kmケーブルでは熱収縮量は300mにもなる。このため、両端を固定し、特に対策をとらないと大きな応力がケーブルに発生し、危険である。石狩プロジェクトでは、ケーブルを常温でヘリカル変形させて断熱二重管内に設置し、低温時にはケーブルが直線状になるようにして応力緩和を図った。現時点までで、かなりうまくいっている。なお、断熱二重管はベローズ管を部分的に利用し、熱収縮を吸収させている。

熱侵入量の低減の必要性は前項でも述べたが、回線1の断熱二重管は中部大の200mケーブル実験装置に比べてほぼ半分の熱侵入量となった。また、端末での熱侵入量低減のためにPCLを利用した。**図3**に中部大学でのテストベンチでの熱

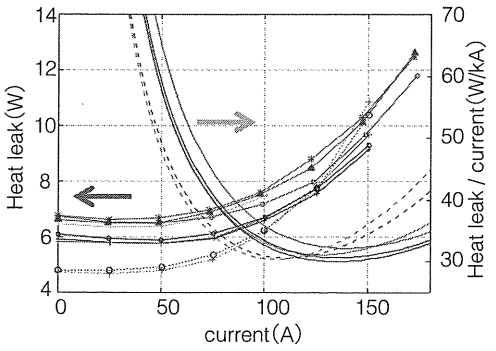

図3　ペルチェ電流リードの熱侵入量と電流の関係

侵入量測定結果[14]を示す。

単位電流当たりの最小値は、

$$30\mathrm{W/kA} \qquad (2)$$

となった。液体窒素循環については、従来の装置に比べてほぼ1/100の圧力損となり、長距離化のめどがたったと考えている。

まとめと展望

2015年8月18日付日本経済新聞朝刊1面の記事では、日本でこれから必要とする送電線のコストは10億円/kmであった。一方、石狩プロジェクトでは、2回線で合計1.5kmを建設した。研究開発は、40億円のプロジェクトである。したがって、コストは～20億円/kmとなり、2倍の差である。したがって、まとまった長さの発注があれば、架空送電線と競争ができる段階に到達しつつあると思われる。

ただし、今後も研究開発を進め、より高性能な送配給電ケーブルシステムを開発することは必須である。特に、最初に述べたように、まだケーブル構造が決まっているわけではないようなので、今後も技術開発が進む中で選択が進むのであろう。

また、日本ではFCLの研究開発があまり行われていないが、短絡事故シナリオによって決まる側面があり、規格などと絡んだ議論が必要であろう。

[謝　辞]

筆者が中部大学に移籍以降、変わらぬ援助と支援をいただいている中部大学理事長・飯吉厚夫先生に感謝する。また、中部大学・超伝導センターの研究者、学生諸君、さらに石狩超電導・直流送電システム技術研究組合のメンバーの協力と支援に深くお礼申しあげる。

参考文献

1) Y. Kuwano：“PROGRESS OF AMORPHOUS SILICON SOLAR CELLS”, 4th International Photovoltaic Science and Engineering Conference, Sydney, Australia (February, 1989), 桑野幸徳「グローバルエネルギーネットワーク - ジェネシス計画の提案 -」サンシャインジャーナル 1990、Vol.11、No.1(1990)
2) K. Kurokawa, K. Komoto：Peter van der Vleuten, David Faiman, “energy from the desert, Practical proposals for very large scale photovoltaic systems”, Earthscan UK, 2007
3) 鯉沼秀臣　https://ja.wikipedia.org/wiki/サハラソーラーブリーダー計画
4) 北澤宏一：「科学技術者からみた日本・経済の夢」、丸善アドスリー(2002)
5) 湯村、ほか：「長尺三芯一括型高温超電導ケーブルによる世界初の実線路建設と商用運転(米国 ALBANY プロジェクト)」、SEI テクニカルレビュー・第170号(2007年1月)、p.10
6) S. Yamaguchi, T. Kawahara, M. Hamabe, H. Watanabe, Yu. Ivanov, J. Sun and A. Iiyoshi：“Experiment of 200-meter superconducting DCcable system in Chubu University,” Physica C, Vol.471(2011), pp.1300-1303
7) X. Liang, S. Dai, Z. Gao, N. Song, Y. Wang, D. Zhang, Z. Zhang, F. Zhang, Z. Zhu, X. Xu, T. Huang, X. Li, Z. Cao, Y. Lin, L. Lin and L. Xiao：“Design of a 380 m DC HTS Power Cable”, *IEEE Trans. Applied Supercond.*, Vol. 20(2010), p.1259
8) C. S. Weber, R. Lee, S. Ringo, T. Masuda, H. Yumura and J. Moscovic：“Testing and Demonstration Results of the 350 m Long HTS Cable System Installed in Albany, NY”, *IEEE Trans. Applied Supercond.*, Vol.17(2007), p.2038
9) 大屋正、渡部充彦、湯村洋康、中西辰雄、広田博史、増田孝人、廣瀬正幸、大野隆介、下田将大、仲村直子、矢口広晴、市川裕士、三村智男、本庄昇一、原築志：「三心一括型超電導ケーブルによる国内初の実系統送電(高温超電導ケーブル実証プロジェクト)」SEI テクニカルレビュー・第182号(2013)、p.39
10) M. Stemmle, F. Merschel, M. Noe and A. Hobl：“Ampacity project — Worldwide first superconducting cable and fault current limiter installation in a German city center”, 22nd International Conference and Exhibition on Electricity Distribution (CIRED 2013), p.1, 2013
11) http://ishikari.sakura.ad.jp
12) Navigant Consulting, “Costing predictions of Superconducting components in 2008-2012”
13) S. Yamaguchi, Y. Hasegawa, H. Okumura and K. Sato：*Rev. Sci. Instr.*, **75**, 207(2004)
14) S. Miyata, Y. Yoshiwara, H. Watanabe, K. Yamauchi, K. Makino and S. Yamaguchi：12th European Conference of Applied Superconductivity, **2A-LS-P-07.04**, 2015
15) S. Yamaguchi, H. Koshizuka, K. Hayashi and T. Sawamura：“Concept and Design of 500 meter and 1000 meter DC Superconducting Power Cable in Ishikari, Japan”, *IEEE Applied Supercond.*, Vol.25(2015)
16) L. Bromberg, P. C. Michael, J. V. Minervini and C. Miles：*AIP Conf. Proc.*, 1218(2010), pp.577-584
17) S. Yamaguchi, M. Emoto, T. Kawahara, M. Hamabe, H. Watanabe, Y. Ivanov, J. Sun, N. Yamamoto and A. Iiyoshi：*Physics Procedia*, **27**, 448(2012)

2014 年 4 月 1 日発行

超電導 Web21

（公財）国際超電導産業技術研究センター　〒213-0012 神奈川県川崎市高津区坂戸 3-2-1 KSP　Tel: 044-850-1612

「研究室紹介」

中部大学・超伝導・持続可能エネルギーセンター
教授　筑本知子

エネルギースーパーハイウエイ（Energy Super Highway）構想を目指して

超伝導の最大の利点は、送電ロスの少ないことによる電力の長距離送電が可能なことです。従って、究極的には直流発電を特徴とする太陽光発電等の再生可能エネルギーと組み合わせることによって、昼夜等の不安定さを地域レベルから地球レベルで解消し、人類に等しく安価なエネルギーを提供することが目的になります。これはちょうど 20 世紀末に情報が光ファイバーによって伝送されたように、安定した電力を全世界に届けることが可能となるでしょう。私たちはこれを「エネルギー・スーパーハイウェイ構想」と呼んでいます。

中部大学ではこのエネルギー ・スーパーハイウェイの構築を究極の目標として（図 1)、超伝導直流送電を主テーマとして低損失システム開発を行うとともに、関連技術としてケーブルの長尺及び大容量化、パワーエレクトロニクスの基礎研究等に取り組んできています。直流送電システムに関しては、2005 年に文部科学省の補助を受け、世界初の 20 m 級高温超伝導直流送電（CASER−1）に成功した後、さらに 200 m の装置（CASER-2）（図 2）を藤原洋氏（ナノオプトエネジー社社長）の寄附により 2010 年に建設し、原理実証試験に成功しました。この成功を受けて、昨年度、経済産業省からの委託により、石狩での「高温超電導直流送電システムの実証研究」（web21,2013 年 11 月号及び 2014 年 3 月号）の中心メンバーの一員として、世界最長となる 500 m および 2 km のケーブルシステムの設計、研究開発及び建設をすすめているところです。この他に、サハラ・ソーラーブリーダー計画（http://www.jst.go.jp/global/kadai/h2202_algeria.html）にも参画して、北アフリカ（チュニジア、アリジェリア）との研究交流や、ドイツの Desertec 計画関係者との交流も含まれています。このため、センターに太陽光発電設備を設置し、太陽光発電との連携実験を行おうとしています。

2014 年 4 月 1 日現在のメンバーは、教員は山口作太郎センター長を筆頭に、高野廣久特任教授、河原敏男教授（兼任)、浜辺誠准教授、渡邉裕文准教授、ユーリ・イワノフ准教授と筆者、研究員は 5 名、事務系の女性 3 名、学生 2 名と大所帯になっています。昨年 9 月からロシアよりイワノフさん、10 月に筆者が加わったことで、山口センター長の最近の口癖は「当センターは、昨今いわれているグローバル化、男女共同参画化でも先端となった」です。

主な研究テーマ

- 超伝導直流送電システムの開発と運転研究
- 低熱侵入真空断熱配管の開発と熱侵入測定
- 低熱侵入型電流リード（ペルチェ電流リード）の開発と特性評価
- 送電大容量化に向けた最適ケーブル構造の研究
- 電力変換器の効率化、パワー素子加工技術の開発

など

2014 年 4 月 1 日発行

超電導 Web21

（公財）国際超電導産業技術研究センター　〒213-0012 神奈川県川崎市高津区坂戸 3-2-1 KSP　Tel: 044-850-1612

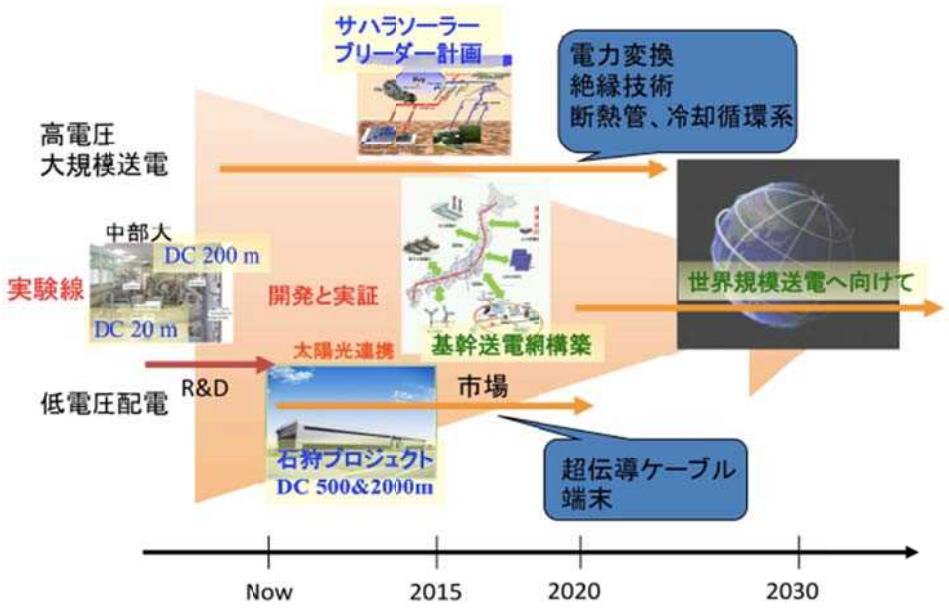

図 1　世界規模送電に向けた中部大学での超伝導直流送電システム研究開発

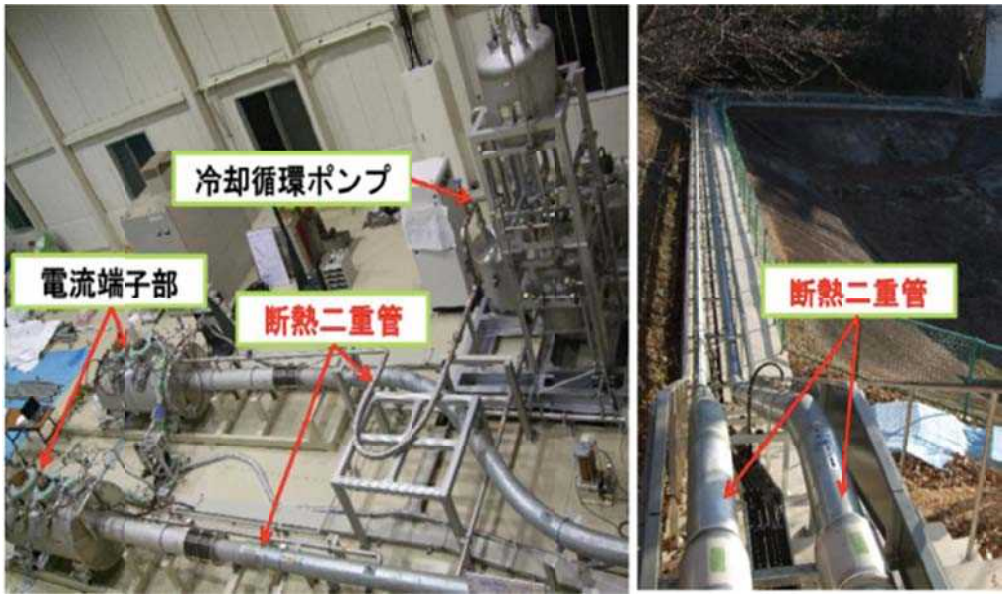

図 2　200 m 超電導直流送電実証設備（CASER-2）

超電導 Web21 トップページ

第１４３回フォーラム　セミナー2

テーマ：「世界をつなぐ超伝導直流送電」

山口　作太郎　氏
（中部大学　教授、超伝導センター長）

超伝導発見の歴史

本日は、このような機会をいただきましてありがとうございました。元々は核融合の研究者だったのですが、今から 10 年ほど前に、核融合は僕の生きている間にはものにならないと考えて、目が黒いうちに実現するであろう超伝導をやろうと考えました。ちょうど核融合の実験装置は、磁場を発生するのに超伝導マグネットを使用するということもあり、知識があったからです。

元々、僕はプラズマ屋だったのですが、三菱電機をやめて核融合科学研究所に移った時に、プラズマだけでやるよりは超伝導マグネットもやってくれと上司から言われて、40 歳を過ぎてから超伝導マグネットの勉強をすることになりました。そこから、研究の重点が超伝導に移りました。

超伝導の説明をします。発見者はオランダのオネス先生で、発見が 1911 年 4 月 8 日とのことです。昨年（2011 年）が発見 100 周年ということで、世界中でお祝いしました。19 世紀には絶対零度という概念が既にありました。つまり、温度は下限があるのです。温度を下げると金属の抵抗が下がり、そのまま絶対零度まで冷やしていくとどうなるのかが議論されていました。そこで、オネス先生が水銀の抵抗測定を低温で行ったところ、ある温度で抵抗がストンと落ちることを発見したのです。オネス先生は超伝導の発見者として有名なのですが、実は、ノーベル賞はヘリウムの液化でもらっています。それは、一見抵抗がゼロに見えても、精密測定すると抵抗が若干残っているのではないかと多くの人が疑ったからです。それはある意味では当然で、測定精度の問題であります。そのため発見がすぐに信じられなかったのですが、オネス先生の巧妙な実験によって、抵抗がゼロでよいのではないかと周囲に納得し、その後２年ほどでオネス先生は亡くなりました。

電気抵抗率というのは、普通はテスターで測りますが、その次元は時間の逆数であるため、原理的にはストップウォッチで測れることになります。オネス先生は電気抵抗率をストップウォッチで測定できることを示し、それが銅よりも桁違いに小さいことを実験的に証明します。これをもって超伝導の発見とされています。現在の機器は高精度ですが、やはり測定限界があり、ある値以下は測れません。僕らは電気抵抗率をΩ・m（オーム・メータ）という単位で測定します。銅は 10 のマイナス 8 乗Ω・m です。温度を下げると 1/100 から 1/10000 くらいほど小さくなります。それでも 10 のマイナス 12 乗Ω・m です。現状では、最も良い計測機器で測ると 10 のマイナス 20 乗以下になりますが、今後も超伝導の抵抗率の精密測定は行われて、もっと下がるでしょう。

そうした現象と材料を応用しようとするのですが、水銀の次は鉛で超電導現象が発見されました。銅を半田で接合し、温度が低くなると半田中の鉛の部分が超伝導になるため、

銅は超伝導でつながります。つまり、ヘリウム温度になると、銅は電気抵抗がゼロになりませんが、ハンダの部分は超伝導になります。ただし、磁場が低いときだけです。

1911 年という年は、直後に第一次世界大戦、そして第二次世界大戦が起こり、ヨーロッパで学術的な研究がしばらくできませんでした。その後に超伝導研究の進展は、1950 年代にロシアや米国でおこなわれ、材料及び理論の進展がありました。そして、超伝導マグネットとして実際に使用できる材料研究や応用研究が進みました。その後、1986 年ぶ高温超伝導がＩＢＭの研究者のミュラーとベドノルツによって発見されますが、そのきっかけは日本でした。

東京大学に物性研究所があります。そこの中嶋先生（所長）が超伝導は電気抵抗がゼロになる性質を何とか人間の役に立たないかと考えて、ノーベル物理学賞を超伝導と半導体で 2 回もらっているアメリカのバディーン先生に、「高温で超伝導になる材料」を探してみたいと手紙を書きました。現在の超伝導の標準理論であるＢＣＳ理論の「Ｂ」の先生です。しかし、彼は高い温度の超伝導は私の理論ではありえないので、やめておけと言いました。しかし、それでも東大の中嶋先生は 1981 年に文科省の重点領域の課題に「高温で超伝導になる物質探査」を申請され、日本で多くの大学の研究者に研究費が配られ、日本で本格的に超伝導物質探査が始まりました。当時の超伝導材料の見通しは、常温では比較的抵抗の大きい材料が低温では超伝導になると言う指針でした。電気が流れにくいものは、絶縁物なので、絶縁物に近い少し電気が流れる材料を探すことになります。例えばセラミックスとか有機物です。ここで、中嶋先生は日本の国力からすると両方は同時に出来ないと考えて、偶然にも有機物を選んだと聞いています。あの時にセラミックスを選んでいたら、2 年後には日本人の手によって狙って高温超伝導材料が発見された可能性が高いので、やはりサイコロの目というのは面白いと思っています。

当時、ＩＢＭのミュラーとベドノルツはチューリッヒ研究所の研究員だったのですが、会社からの研究だけではなくて、日本が高温超伝導材料探査をやろうとしたことを聞いて、我々もやってみることにしました。当時、IBM では研究時間と研究費の 15%程度は他に使っても良かったそうです。その際、日本が有機物を選んだので、同じ分野であれば、研究費も研究者数も負けてしますので、違う分野が良いであろうと言ってセラミックスを選んだとのことです。セラミックスは元々彼らの研究対象でした。そして、こちらに勝利の女神がほほ笑みました。

ＩＢＭ研究所の所長は、彼らは絶縁物の研究者であり、超伝導の研究者ではないので、高い温度で超伝導になる材料が見つかったと彼らが言っても、「へえー」と思った程度でした。だから、会社内の研究所公開ではポスターで紹介しているに過ぎなく、大きく取り上げられることはなかったようです。当時まだドイツ物理学会には論文は投稿されておらず、特許申請もされていませんでした。もちろん、これは後で分かったことです。その後、チューリッヒの IBM 研究所から年報が出たのですが、そこに高い温度で超伝導になったセラミック材料がＡ４一枚で紹介されていたそうです。その時に、東大の田中先生が IMB 研究所を訪れて所長に紹介されて年報を見て、興味を持たれ、7 月に帰国され、研究室の学部 4 年生の学生にやってみろと話したら、9 月ごろに本当に超伝導かもしれないとの実験結果が出たそうです。そこで、田中先生は大急ぎで超伝導であることを確認することに集中し、

11 月の終わりには確認し、すぐに論文を書いて日本物理学会に、一週間で論文を出版して欲しいとお願いされたと聞いています。しかし、ＩＢＭのミュラーとベドノルツの方は 10 月にドイツ物理学会誌に論文が通っていて、ノーベル賞が出ました。ただし、IBM は特許を取っていなかったので、ミュラーとベドノルツのノーベル受賞時に、所長は解雇されます。もし、ＩＢＭが特許出願していると、この分野は全てＩＢＭのものになっていたでしょう。

このセラミック超伝導材料はランタン、バリウムと銅の酸化物であり、構造などがすぐに判明しました。ランタンと似た性質の元素は複数知られていて、研究は加速し、より高温で超伝導になる材料が次々に見つかりました。以上は山口が三菱電機時代に聞いた話です。一度、時間があったら以上の話しの裏付け資料を入手したいと思っています。

超伝導材料とその構造

超伝導体の結晶構造について説明します。高温超伝導体は層状構造であります。従来の低温超伝導体は 3 次元ではどちらの方向でも超伝導になりますが、層状構造の高温超伝導体はある面が超伝導になり、別の軸方向では超伝導にならないとのことです。これは大やっかいな性質で、結晶面がずれた時には、電流が結晶面を渡るときに電気抵抗を発生します。この点がこれまでの超伝導材料と大きく違います。また、セラミックスであることも問題です。超伝導体で電線を作るのですから、銅の電線のように曲げたいのですが、一般的にセラミックスは曲げると割れてしまうので、超伝導状態も破れます。もしも超伝導が破れれば電気抵抗が上がるので、電流によって発熱し、いきなり燃えてしまうこともあります。それを避けるために低温超伝導体は周りを銅や銀などの良く電流が流れる材料で覆って、超伝導が破れても大丈夫なように作ってあります。つまり、金属と超伝導体は一緒にして冷やします。しかし、セラミックが金属とは同じ収縮率であることは必ずしも自明ではありません。

もう一つ、セラミックスは酸化物ですから、材料に酸素が付いた焼けた状態と考えることができます。一方、超伝導線材は周りに金属があり、超伝導は薄い層状ですが、今つくられている一つの方法は、最初にパイプの中に材料を入れてから焼きます。温度を上げて酸素を入れると普通の金属は燃えますが、金属が燃えては困ります。金属を酸素が通り抜けて、中に入れた材料だけがセラミックスになって欲しいわけです。そういう材料や手法を開発するために、20 年かかったのです。このため、高温超伝導体はとても性格の悪い材料だと思っています。

その材料が少しずつ使用できるようになり、次の段階として応用が色々検討されるようになりました。現在、高温超伝導体は主にビスマス系とイットリウム系の 2 つの材料が開発されています。しかし、日本人が発見したビスマス系材料の開発には一時国の研究費がほとんどゼロになりました。しかし、住友電工がかなり頑張り、その製品が国費を投じたイットリウム系の材料よりも現在実用に近いようです。高温超伝導体は基本的には電気応用であれば何にでも使えますが、高温超伝導は性格が悪くて使いにくいので、使い方に関しては今までの以上のノウハウが必要だと感じました。そこで、一度に難しいものへの挑戦はやめて、簡単な応用から始めようと思い、ケーブルを選びました。

ケーブルには色んな種類があります。主に三相交流ケーブルと直流ケーブルの二種類が

あります。現在、電力ケーブルはほとんどが交流であり、送電には３本のケーブルが必要です。一方、直流ケーブルでは一本のケーブルで送電できますが、交流直流変換機が必要になります。超伝導ケーブルは、低温に保つために大きさの違う２つの金属パイプを用意し、一方のパイプにもう一方のパイプを内部に入れ込み、その間を真空にした魔法瓶のような断熱容器を用意し、その中にケーブルを入れます。これをクライオスタットと言います。交流電流が流れると、交流磁場が発生します。この時間的に変化する磁場はクライオスタットの金属管に渦電流を流します。すると、クライオスタットのパイプが発熱します。つまり、冷蔵庫の中にヒーターを入れるような状態になりますので、交流ケーブルでは電流を流す層のもう一つ外側に超伝導層をつけて、交流磁場が外に出ないように磁気シールドします。これが基本的な交流超伝導ケーブルの構造です。磁場をシールドしている層はアース電位にしますので、2 つの導体層間には送電電圧がかります。一方、この構造では、ケーブル一本で直流電力を送ることができます。三本と一本で送れる電力が同じだったらどちらが安いかと言うことになります。

もう少し直流と交流の差を考えます。パイプが太くなれば値段が上がります。しかも、低温のパイプは太くなると熱がたくさん入ります。3 本の問題を除いても技術経済的に交流ケーブルは大変です。更に、少し専門的になりますが、もう一つ大きな問題がありました。超伝導は直流だと電気抵抗がゼロになりますが、交流だと電気抵抗がそれなりに残ります。侵入熱の問題よりも大きな問題なので、超伝導研究は主にこの問題を扱ってきました。一方、直流にすればこの問題が無くなります。ケーブル自身が発熱することは大きな問題です。超伝導線の電気が流れる部分は電気絶縁します。電気絶縁物は紙やプラスチックに使用しますので、一般に熱伝導率が低いです。そして、外側を液体窒素で冷やします。つまり、ヒーターをふとんにくるんで、外側からエアコン・扇風機で冷やそうとしているわけです。

しかし、10 年前に僕がやろうとしたときは世界中が三本必要な交流ケーブルを研究していました。それは、一般的には三相交流が広く利用されていたからです。一方、中部大学で独自に超伝導送電の研究をやろうとしても、世界全体でそれぞれの国が号令をかけてやっているものと競争しても敵わないし、直流の方が超伝導ケーブルとしては経済性も高いのです。このため、やはり直流ケーブルの方が良いと考えて検討を始めました。つまり、話をまとめると、直流ケーブルは安価で、高性能であり、技術的にも容易と最初に考えました。

そして、研究を始めた後になりますが、交流では事故が起こって短絡電流を流れた場合の規格が決まっています。66 キロボルト系ですと、1 キロアンペアのケーブルに 32 キロアンペアの電流が 2 秒間流れても、それに耐えられることになっています。現在の銅ケーブルはその規格に耐えられ、流す電流には十分な余裕があります。しかし、超伝導ケーブルでは元々超伝導導線材は極めて小さいので、超伝導が破れた状態で大電流が流れると直ぐに燃えます。だから、交流超伝導ケーブルでは超伝導線材を直流ケーブルに比べて数倍以上多く使うことになります。このため、コストは数倍以上違うことに気が付きました。

直流の問題は市場関連事項です。超高圧の直流送電は既に実用になっていましたが、そ

れでは研究開発費を投入すべき十分な市場とは思いませんでした。考えた時に、トヨタ自動車のプリウスが目に留まりました。プリウスは 98 年 12 月に発売されていましたが、99 年になって、バッテリーは直流でモーターや発電機は交流なので、その間にインバーターがあって直流と交流を変換していることに気がつきました。直流送電をするときは、発電機が交流なので、交流を直流に変換してから送電することになりますが、そのインバーターは極めて高価です。プリウスの最初のインバーターは 50 キロワット出力でしたが、私は三菱電機にいた時に聞いたのですが、僕の記憶では 50 キロワットで 250 万円でした。今でも（2012 年）太陽電池の電力変換機はそのくらいの価格で売っています。このため、プリウスには何か秘密があるなと考えて、値段を調べようとしましたが、なかなか教えてはもらえません。そこで、自動車屋さんに電話をして、購入したいが、新しい技術がたくさん使用されているので、もしも故障した時にどれくらいかかるかと質問しました（笑）。すると、インバーターが壊れたら 30 万円で新しいものに変えることが出来ると話してくれました。この 30 万円には整備費も入っているそうです。このため、変換機は一桁以上値段が下がったと思いました。

スマートグリッドは言い方を変えると、電力網に電力貯蔵能力のある機器をうまく入れることでもあるのですが、電力貯蔵機器の多くは電池です。その電池は直流なのに電力網が交流なので、その間の電力変換機が必要になります。そのロスやコストがどうなるかで、普及を決めます。それで、電力用と自動車用のどちらの電力変換器の信頼性が高いかを調べました。トヨタさんは「電力会社よりもうちの方が信頼性については厳しくやっています。もしも数万台のうちの１台でも故障して人が死んだら、その商品は終わってしまう。電力会社は故障しても、停電になるだけでも、ごめんなさいで済む。」と話していました。僕はそれに納得しました（笑）。

もう一つ、超伝導は電気抵抗がゼロですので、損失を下げるために電圧を上げる必要がありません。つまり、低い電圧でも大電力送電が出来ます。一方、プリウスは電圧として 600Ｖくらいを選んでいました。それは、現状の半導体シリコンの材料特性から考えると、半導体素子は 1200Ｖまでは大変安く、電力制御も容易です。むしろ、シリコン半導体素子よりも放熱板の方が高いくらいです。また、ビルや家庭で使用する建物内の配線は 600V のケーブルがほとんどです。だから、汎用製品をそのまま使用できるので、うまいところを選んでいるなと感じました。

こうして、直流超伝導送電のための電力変換器も安価に出来るという目処が立ったと思い、直流超伝導送電の研究を始めました。長距離送電の特徴を具体的に考えながら、中部大学に 20m の直流超伝導送電実験装置を 2006 年につくりました。幸い、高温超伝導を利用した実験設備としては世界最初言われています。

日本の信用力を高めるチャンス

昨年は JST から日本の国内に直流超伝導送電を導入するための調査研究でお金をいただい、報告書を書きました。本日は会社を経営されている方が多いので、お金の話もさせていただきます。ご存知かもしれませんが、2022 年までにドイツは原発を廃止して、北海・バルチック海とサハラ砂漠での風力発電や太陽熱発電、太陽光発電電力をヨーロッパにつ

なげようとしています。デザーテックプロジェクトと言います。高温超伝導の直流送電を始めたのが世界初ということで、僕はドイツのデザーテックプロジェクトで送電線を超伝導化する委員会のアドバイザーになりました。これは最終的には 100 兆円くらいを使う野心的な計画です。

僕は、明日はチュニジアに行きますが、この地域は過去 200 年くらいヨーロッパの植民地で、ヨーロッパが持ってきた上手い話を了解すると収奪されることを経験しています。今回も脱原発でエネルギー問題を解決できるという、良いアイデアが来ているが、今度だまされると 1,000 年くらい騙され続けることになるので、地元ではしっかり考えようとしています。

これは重要なポイントであります。元々サハラ砂漠での発電に興味を持った原因は東大の鯉沼先生に誘われためです。そして、サハラ砂漠で太陽光発電を行い、人口密集地に送電を行う SSB プロジェクトのメンバーとして加わりました。多くの先生は日本から離れたところでやってもダメだと言われるそうですが、僕はそうではないと思います。アフリカ地域の人たちは長くヨーロッパの植民地にされてため、西洋を基本的には信頼していないようです。このため、良い話があってもすぐに飛びつきません。本年５月にアルジェリアに行った時に、向こうの大臣は、我々は石油輸出でお金がたまっているので、3 年間全く輸出をしなくても、必要なものは全て輸入できると豪語していました。このため、良い話を持ってきても、自分たちのお金で出来ると主張します。だから、今回のヨーロッパからの話が正しいかどうかは、自分たちで判断すると言っていました。そこで私は、北アフリカの国は一番良くできる学生をヨーロッパに留学させたが、それでは帰国した学生はヨーロッパの大学の先生と同じことを言うと思う。と話しました。先方の返事は、それはそうだと言いました。そこで、本当にヨーロッパが言っていることが正しいかどうかを second opinion として判断するのであれば、一番良くできる学生を日本に送り、勉強させる必要があるのでは？と話しました。すると、なるほどと言って、一番良い学生を日本に出そうと返事が来ました。おかげさまで、中部大学にもチュニジアの有名大学から一番優秀な学生が１名来たので、3 年くらいでドクターを取らせて帰したいと思っています。もっとも、これから学生の数を増やす必要があると思っています。この様なことになった背景には、日本が彼の地で大変尊敬されていることがあります。第二次大戦後、地道に国の発展を応援してきた成果と思います。

これは歴史上始まって以来の出来事だと思います。従来は日本が新しいことを始めたら、ヨーロッパがそれを判断（Judge）していたのですが、今回はヨーロッパの提案をアフリカが依頼するような形で、日本が判断（Judge）する立場になっています。間違いなく日本が信用度を高めるチャンスになります。日本の経済はこれから小さくなって行くでしょうから、信用のブランドを高めることは重要です。

長距離送電は政治的役割も果たす

長距離送電の話ですが、2020 年にはデザーテックとしては部分的に送電を開始するとしています。中国も上海、北京から西域までの送電線を 2020 年までにつくる計画が進んでいます。ウイグルでは石炭が採れるので、そこの石炭火力発電所からの電力を送電線につな

げ、東の大都市に送っています。このため、もしかすると、超伝導でなくても、2050 年にはベルリンから上海まで送電線がつながるかもかもしれません（笑）。

今回の 3.11 震災を踏まえて、アジアでもあちこちで国をまたがる送電線を作る話が出ているのですが、実際にはだれが具体的に運転をし、投資するかが問題になります。しかも、経済的に成り立つかどうかじは極めて重要です。一方、電気代は各国が違うので、互いにつないで電気を輸送すれば輸出入になりメリットが生まれるという意見があります。つまり、ソウルと日本では電気代は倍以上違うので、ソウルから日本に送れば輸出になりますし、日本側は安く買えます。先週、韓国大使館で日韓を海底ケーブルでつなぐシンポジウムがありました。2 ギガワットの電力を、距離 250 キロくらい（釜山と福岡や下関間）を 380 ミリオン米ドルでできるということです。とても安価と思いました。これですとキロワットアワー当たり 2 円くらい乗せればペイできるので、かなり現実味はあります。したがって、技術的な問題よりも、日韓の誰がどのようにオペレーションするかのルール作りが課題です。やろうと思えば数年で出来るはずです。驚いたのは、韓国ラッキースターが交流と直流の電力変換器を、世界で一番実績のあるヨーロッパの ABB 社の半値で値付けしていたことです。

韓国も、すでに済州島までに直流ケーブルは引っ張っています。済州島で火力発電所を廃止する計画があり、再生可能エネルギーを大きく導入し、それでは足りない分は本土から直流送電する構想です。実際、一部の直流送電は既に稼働中であります。これは済州島をリゾート地で売り出しているためで、技術的には朝鮮半島から九州まで引っ張るのは容易です。

2009 年時点で 450 基くらいの発電用原子炉が世界にあります。そして、電気が不足するという論理で、2050 年までに各国政府の計画を総合すると 2000 基くらい世界中で発電用原子炉をつくることになっています。原子炉は出力が一定なので、昼は足らなくて、夜は余ることになります。そこで、ケーブルで上手に東西をつなげれば、ヨーロッパが深夜に電力を安く買って日本に送ることが出来ます。イギリスは夜間の深夜料金は昼間の 5 分の 1 程度であり、日本は 3 分の 1 くらいです。そして、日本も夜間電気を昼間のヨーロッパに売れば、送電線をつくるお金が出来てきます。もちろん、途中に砂漠がたくさんあるので、そこで太陽光発電した電力を利用することも出来ます。貧しい国は通行料を取れば、世界中でつくる原子炉の数を節約でき、事故が起きる確率も減ります。2009 年にストックホルムでこの構想を話しましたら、大変興味を持っていただいたようです。これは、デザーテックの重要ポイントになってきています。

こうやってつなぐことはとても重要です。ブラックジョークかと思いますが、冷戦時代に大陸間核弾道ミサイルをピースキーパーと呼びました。それは、核戦争が怖くて戦争ができなくなると言う理由です。おそらく、送電線がつながっていて、1 日で送電方向が変われば送電線はピースキーパーになります。世界中どこでも隣国同士は仲が悪いことが多いのですが、電力融通のために良い関係を継続せざるを得ないからです。ここで肝心なことは、双方向であることです。

例えば、ガスの輸出を考えてみます。ガスを隣国にパイプラインで送っている場合、一番寒いときにガスを止めて、ガス代を上げろと主張すれば値段は上がります。実際、2006

年の冬にロシアと西ヨーロッパ（ウクライナ）の間で起きました。これはガスを出す方向と受け取る方向が常に同じだから起こる事態であると思っています。つまり、1 日や 1 週間の単位で双方向にエネルギーが行き来していればこの様な事態にはなりません。インターネットは現在戦争中であってもつながり続けます。それによって、第二次世界大戦の頃と違って情報統制がとりにくく、戦争継続の力が削がれ、長い戦争がしにくくなってきています。エネルギーの場合、戦争に必要な兵器がつくにくくなくなりますので、戦争を止める力はもっと大きいのではないでしょうか？　つまり、超長距離送電を行うと、経済性だけではなく政治的に平和をより希求するシステムになるのではないでしょうか？

超伝導は具体的な実験段階のフェーズにある

こうしたことを考えながら、2006 年に超伝導送電実験用のケーブル製作を住友電工さんに最終的に依頼しました。しかし、最初のある会社の見積もりは 20mで 5000 万円でした。文科省にいただいたお金が 5 年間で 1 億 6000 万円だったので、もっと安くしてくださいと頼みこんだ所、いくらだったら払えるか聞かれました。そこで、0 を一つとってくださいとお願いして、安くしてもらいました（笑）。経費節約のために大学の倉庫で作ったのですが、いまでも現役で使用できます。

実験装置ができてデータが得られるようになり、順調に研究が進展するようになってからですが、インターネット総研をつくった藤原洋さまを紹介していただき、財政的な支援を受けて 200mの送電線実験装置を学内につくりました。2010 年の 3 月に完成して、既に 5 回実験したのですが、データが上手く取れているので、次は 2 キロのものにチャレンジしたいと思っています。2 キロになれば企業の設備として利用することになり、実験しながら実利用することで問題点を洗い出すフェーズに入ります。現時点での見積もりで、2 キロメートルで 40 億円くらいかかると思っています。ちなみに、200mの装置は 2 年半ほどで作りましたが、人件費込みで 4 億 2000 万円でした。東京電力が実験している交流超伝導ケーブルの施設は 250mで 23 億円かかるようなので、ケーブルと冷凍機の数が少なくなることなどが金額上に表れていて、全く違うものが出来ていると思っています。

ポイントは 2005 年には 20mで 5000 万円だったケーブルの価格が、2009 年には 200mで 1 億円になった点です。4 年間で金額が 5 分の 1 になったのですが、現在つくるとさらに半値になります。イメージとしては、80 年代、90 年代にシリコンチップの性能が上がりながら値段が安くなっていましたが、その段階に超伝導線材も来たのではないでしょうか。そういう意味ではスタートしたタイミングが良かったのかもしれません。

注意しないと行けないことに、超伝導のケーブルは温度が下がると 200mのケーブルが 60㎝ くらい縮まります。両端を固定すれば、破断の恐れがあります。その対応として端末台座をケーブル長に合わせて可動式にしているのは我々だけだと思います。

もう一つ、ポイントは安く作ることです。20 メートルのものを作った時は、まっすぐなステンレス管を断熱 2 重管に使いました。そこにベローズという伸び縮みするパイプを入れたのですが、200mはステンレス管から鉄管に変えました。これによって、この部分の価格が 5 分の 1 から 10 分の 1 になりました。鉄管を真空容器として利用し、これだけの距離を真空状態にしたのも世界初です。

先ほど話しましたが、ケーブルが縮むので端末を台座ごと動かします。ケーブル端はマイナス 200 度くらいになりますが、そこをＬＥＤ照明してカメラで監視しています。これは画像処理してケーブル端が動いたときには自動運転で台座を可動できるようにもしています。また、断熱２重管内にあるケーブルは常温時と低温時でケーブル形状を X 線写真で観測してきました。これによって最終的な調整をしています。

さらに大きなポイントは、2 重管内を真空にしなければいけないのですが、一般的には真空にするためにはベーキングといって最初に温度を上げて温めます。しかし、地中に埋設する長いケーブルを温めるわけにはいかないので、それを解決するための真空技術も開発し、既に特許も出願しています。建設前に、真空にする時間を見積もるために、どのくらいのポンプを買えばよいかを企業に問い合わせた所、日本の真空機器メーカーはわからないと言いました。その理由は、粘性流から分子流までのポンプを引く時間を見積もるには適当な計算機コードがないことでした。もしも粘性流の領域で 200m を引いた場合は 3 時間、分子流の領域では 3 か月かかるそうです。これでは見積もりをした内に入らないのですが、現在は中部大の実験室では 3 日間くらいで引いています。

ここまでは我々の今までの研究成果ですが、次の段階のチャレンジ先を考えています。直流利用で節電になる所で応用するのが本質であると考えていました。そして、データセンターを思いつきました。データセンターは北に持っていくとエアコンの電気代を節約できます。日本で初めて北海道にデータセンターを作った会社と現在相談しています。北海道のデータセンターを動かし始めて今年の 11 月で 1 年が経ったのですが、電気代が予定通りに半分程度になったそうです。データセンターでは電気代の支払いが大きく、10%の電気代を節約すると利益が倍になるそうです。もしも 50%の節約をするとどうなるかと思うのですが（笑）、この結果を見ていると、データセンター協会の会員企業さんは大挙して北に移動するのではと思っています。

さらに、実験装置をつくると、お金がどこに一番かかるかがわかります。ここがシステムを取りまとめる時の醍醐味かもしれません。実は一番高いのは超伝導ケーブルではなく、200m ケーブル実験装置では冷凍機でした。冷凍機はある意味、金属の塊ですので、簡単に値段が下がりません。一方、日本は原発事故の前からＬＮＧを大量に輸入しています。ＬＮＧの温度はマイナス 160 度くらいです。それを使用して液体窒素（マイナス 200℃）をつくれば、安価になります。

また、世界中で日本だけが超伝導送電に関する機器を全て国内で作れます。その国に、冷たい冷媒が世界で一番集まっています。北海道のＬＮＧ基地は本年 12 月に出来るのですが、そこでデータセンターと組み合わせて技術開発がうまくいけば、日本中にＬＮＧ基地に超伝導直流送電システムを置いて、幅広い展開できるようになると考えています。

ヨーロッパ各国の電力供給システム

一つの課題は、再生可能エネルギーをどう使用するかです。これを本格的に利用するには長距離送電線が重要になります。ドイツのテネット社はドイツ最大手の送電会社ですが、昨年見学に行ったら多くの洋上風力も含めて風力発電所からの電力を上手く需要家に届けていました。一か所の洋上風力で 400 メガワットの発電能力があり、隣に 800 メガワット

のものを既に建設中でした。この規模はすごく大きいと思いました。日本でメガソーラーが話題になっていますが、一か所で 2 メガとか 20 メガなので、ドイツと比較すると桁違いに違います。しかも、日本はドイツの倍の電力消費をしているのですから、如何に再生可能エネルギーの割合が大きいかが分かります。ドイツは北海に 8GW の洋上風力発電所を 3 年間程度で建設すると言っていました。そして、遅れても 1 年程度と言っていました。

風力発電からの電力が系統に多く入る時には系統の安定化が課題となります。足りないときは火力発電所から供給することになります。一方、電気が余った時にどうするかも問題です。早朝に風が強く吹くことが多いそうですが、風力発電の割合が巨大になっているので、電気が余ったら系統が不安定になるのではないかと質問しました。びっくりしたことに、現状では電気を使ってくれたらお金を払うそうです。この仕組みならば皆が電気を使いますので、余ることはありません（笑）。もちろん、これを継続するわけにはいかないので、将来どうするか尋ねたところ、スイスに揚水発電所を作ると答えていました。その原因は、スイスには原子力発電所が 4 基ありますが、福島県くらいの大きさなので、原発事故が起きたら国が成り立たなくなり、大変です。このため、心底から何とか原発を止めたいと考えているそうです。そこで、スイスに揚水発電所を作って、再生可能エネルギーからの電力を貯蔵しながら、スイスにも分けてあげるというのが、ドイツの基本方針のようです。

北海から電気をひいて、スイスで貯蔵しながら再度ヨーロッパ各地に送電して使用するので、ドイツを南北に縦断することになり、長距離送電が必要になります。その上、何度も送電線を往復することもあるので、送電ロスが見かけの距離以上に大きくなり、損失低減は重要な技術課題になります。そういう意味では、超伝導の可能性が大きいと考えています。

もう一つ驚いたのは、テネット社の制御室に入れてくれたことです。そして、オランダ、ドイツ、スイス、オーストリア、ポーランド、チェコ、スロバキア、ハンガリーが送電線で既につながっていて一つの画面でこれらの国との電力のやり取りが表示されていました。2011 年の段階で実質上一つの送電システムになっていますが、このくらいの規模になると日本よりも大きくなります。

ドイツとの他の違いは以下のようです。日本の電力卸市場は次の日の 30 分間単位で売買をおこなっていますが、風力発電で、このような仕組みで運用することは難しいです。明日のある時間からある時間までの 30 分間に風がどれくらい吹くかを予測して、どのくらい電気を売るかを約束するわけですから、天気予報を見ているとその困難さがわかると思います。これでは風力発電は普及しません。このため、ドイツでは、当日の 1 時間前や 2 時間前という市場を考え、15 分単位でコンピュータを使用して売買していました。これはスペインも同様です。

今年（2012 年）はデンマーク、ノルウェー、スウェーデン、フィンランドの電力系統がドイツ圏と統合されるそうです。一方、フランスは原子力を使用し続けたいので、まだつながらないそうです。おそらくフランス大統領が変わって 70%の原子力シェアーが、50%にするとつなぐことになるかと見ています。つまり、減ったその分を何かで埋め合わせしようとするからです。へえーと思ったのはフランスの原発はドイツなどとの国境沿いに作ら

れているので、事故で放射性物質が出てくると、風が西から吹くので多くがドイツに来るそうです。ここで重要なポイントは、ドイツはフランスから原子力の電気を買うから原子力を全廃できると思われている方が多いですが、よく調べてみると違います。2008 年ではドイツの電力輸出は国内消費電力の 11%で、輸入は 8%です。つまり、輸出分が大きいです。しかも、フランスから買うのは夜間で、昼間は出している分が多いので、お金のやり取りではプラスになっているはずです。この割合は年によって変化していますが、ドイツの輸出超は最近の一般的な傾向です。

現状で困っているのはスペインだそうで、フランスとのやり取りは 1 ギガワットしかありません。これは、四国と和歌山を結ぶ線くらいの規模ですが、スペインの電力網は日本の関西電力くらいです。スペインはフランスと接続回線容量を増すように要求しています。更に、イギリスもフランスとの接続増強を要求したのですが、拒否されているとのことです。スペインはフランスに拒否されると地理的に孤立してしまうので、風力発電の良い場所であるモロッコと太い電力線を結ぶ工事をすすめています。

スペインには RED 会社という中央送電会社があり、これが全国の送電制御を担当しています。スペインの主な発電は風力発電、原子力、揚水を含む水力、コジェネがあり、国際連携の輸出入も多いときには数%あります。これが実時間でインターネットに色分けされて公開されています。それを見ると冬季は風力だけで 60%近いシェアーになる時があります。そして、風力発電の割合が 30%以上なることが一週間以上続くことがあります。その上、更に風力発電を増強すると言っています。一方、北海道電力は系統に風力が 3% ～ 5%くらい入ると不安定になると言っています。このため、日本では風力発電に対してこの 20 年間で 2000 億円くらいの研究開発投資をして、風力発電の出力の安定化を電池でやろうとして来ました。それが僕の念頭にあったので、スペインでは風力安定化のために多くの電池を使用しているのかと思い尋ねたところ、彼らは電池を入れたら電力料金が高くなるから使用していませんと話していました。実際に調べてみると、日本の 90%の風力発電業者も電池を使用していないようです。ですから、電池が無くても風力発電は結構使えるのではないかと思うようになりました。北海道管内でも電力規模も含めて色々検討することが多いように思います。

スペインでの電池なしで風力発電からの電力を安定供給するかの方法ですが、まずは需要予測を行います。日本の全ての電力会社でもそれぞれ本店で電力予想をする部署があり、毎日需要予測を行っています。それに伴って火力発電などの稼動・停止・出力の微調整を行います。基本的に交流系統なので、消費側よりも多く発電することが必要になり、新聞報道でも何%の余裕があるかが毎日出ていたことがありました。これが全て直流系統になると、足りなかったら電圧が下がるだけで、システム全体がズドンと落ちることはありません。

次に、風力発電の発電予測を衛星データや気象データを用いて行います。そして、それらの再生可能エネルギーからの発電予測と需要予測の引き算をして、その差を水力（揚水発電を含む）で埋めていきます。尚、原子力は出力が一定だから、需要予測からこの分をはやり先に引き算しておきます。最後の残りは火力発電から供給で調整します。この部分は日本と同じです。このようにして風力発電のシェアーが 60%近くになっても、安定に電力

供給ができると話していました。そして、スペインは今後も風力発電の出力量を増強すると言っていました。また、電力貯蔵能力を高めるために揚水発電所の計画もあります。

スペイン RED 社の中央制御所は全土を制御しますが、地方には小型制御所が４つあります。400 キロボルト系と 200 キロボルト系の送電線は中央制御所が管理して全ての指令を出しますが、それ以下の電圧は４つの制御所はでの送電線の制御を行っています。また、実際の指令が出る前に安全のため本当にその指令が実行可能かをコンピュータで検証しから、スイッチが投入されるそうです。驚くことに、地方のある小型制御所ではオペレーター人で 2000 台の風力発電と複数の小型水力発電所の制御をしていました。風力発電所と制御所はインターネットでつながり、早い制御は水力で行っていると言っていました。水力は火力よりもかなり早い出力制御ができるので、急な需要の変化に対応できるため、系統安定化には重要と話していました。

ご存知のように、ドイツは 2050 年までに再生可能エネルギーを 40%、60%、80%、100%普及させるというシナリオを長く検討してきました。一方で、日本が原発事故以降に急に再生可能エネルギーを極大化するシナリオを考えても、うまくいかないのは当然だと複数のドイツ人から聞きました。それは、このシナリオ作りにドイツは 20 年間かけて議論しているからです。日本でも同様な時間が掛かるのでしょうか？ 50%シナリオでは 47 ギガワットを北アフリカ等から調達するようです。ヨーロッパのグリッドはスイスがハブになっていて、スイスに電気を送ればヨーロッパの各地に電力が届くようになります。このため、スイスに揚水発電所を作り、ここで電力貯蔵を行うのは、技術的合理性が高いと思います。

結局、ある意味では原発は出力が一定なので使いにくい電源なのかもしれません。昼間は多く、夜間は少なく発電するのが使い勝手の良い電源です。つまり、需要に応じて簡単に出力を変える事ができる電源です。こんな電源はできるのでしょうか？スペインはシェスタがあるのでラッシュアワーが二回あります。これに応じて電力需要ピークも 2 回あり、日本とはピークが異なります。

再生可能エネルギー導入に向けて

日本全体では年間 1100 テラワットアワーの電力消費をします。ピークは 180 ギガワット程度で８月第１週の午後２時ころです。現在、太陽電池をたくさん入れると、昼間のピーク電力を下げるので効果的です。ですから、ある程度までの太陽電池の導入は経済性がありますが、稼働率の低さが大きな問題です。ドイツやスペインの例から考えると、グリッドがどのように構成されているかが再生可能エネルギーを使いこなすための重要な課題であります。それで、グリッドが理想的にできているとして、どの位の太陽電池が導入可能かを簡単に見てみましょう。日本の一戸建て住宅は 2000 万戸あって、一戸に 4 キロワットを入れることにします。但し、50%に導入されたとします。他に、休耕田が 145 万ｈａあるそうなので、10%程度にいれてみることとします。すると、一戸建てには 40 ギガワット入ります。日本の太陽電池の稼働率が 0.12 なので、年間 42 テラワットアワーの電気が作られます。休耕田の 10%に入れると、145 ギガワットになり、年間の発電量は 152 テラワットアワーとなります。さて、日本のピーク電力は 18０ギガワットで、消費電力が 1100 テラワットアワーです。太陽電池からのピーク電力は 40＋145＝185 ギガワットとなり、ピーク電

力は太陽電池のみでカバーできます。一方、年間消費電力の 18%程度しか供給できません。

したがって、もしも日本中が全て晴れると夏の電力ピークを越えて太陽電池が発電するので、他の発電所を全て止めて、その上揚水発電所などで電力貯蔵する事が必要になります。ちなみに、日本の揚水発電所は 25 ギガワットと言われていますが、春や秋に 185 ギガワット発電すると、電力がかなり余ることになるので、太陽電池をここまでは入れることができません。すると、太陽電池のシェアーは最大 18%以下と言う事になります。

すると、もっと多くの揚水発電所や二次電池を作り電気を貯蔵するか、海外に輸出しないと太陽電池は導入できません。このような事情は他の国でもそれほど変わりませんので、送受電は電力貯蔵と機能的には同じと考えることが出来ます。もちろん、国内的にもどうような機能を送電線は持ちます。

日本の太陽電池導入量はドイツの４分の１～５分の 1 ですが、2011 年現在で 3.6 ギガワットくらいです。しかし、今年（2012 年）はフィードインタリフが実施されるので一年間で 10 ギガワット程度入るでしょう。２年程度で 20 ギガワットくらい入るかも知れません。ドイツが 2008 年で 17 ギガワットですので、同程度になるでしょう。ドイツの年間消費電力は日本の半分程度なので、グリッドがドイツ並みになれば、現状の技術で 34 ギガワット程度は日本国内に導入することは可能ではないでしょうか。

揚水発電所は電力貯蔵設備の中で一番強力です。そのコストはリチウムイオン電池のコストと 20 倍くらい違うので、電池は安くならないと揚水発電所のように大規模な電力貯蔵設備を作ることはできないでしょう。それでは、日本国内で電池に投資することは良いのでしょうか。電池に貯めても、ロスがあるので、本当はスペインのようにあまり電力貯蔵を行わないで、そのまま使用した方がエネルギー的には節電になります。もちろん、スペインも揚水発電所を持って、電力貯蔵を行っています。そして、これを増強しようとしています。しかし、最小限にすることが必要かと思います。このため、電池への投資は発電設備、グリッド、消費動向などを勘案し、具体的な計画を総合的に判断する必要があると思います。

ドイツに行ってＴＳＯ（送電制御を行う会社）を見学時に伺ったのですが、ＴＳＯの収入（＝送電サービス価格）は最終的には国の委員会が決定するそうで、基本的には日本の総括原価方式と同じです。つまり、ＴＳＯが会社として持続可能であるように送電料が決められるのです。つまり、発電業者間には競争がありますが、送電線事業は競争的ではありません。このような性格を持つ理由は、工場や住居は個人に属しますが、道路には私道が極めて少なく、国や地方自体がつくり、公共性が高いように、送電線は公共性が高いからではないかと考えました。そして、送電線をどう引くかによって、再生可能エネルギーの導入量が決定すると思います。競争原理が働く分野と公共性の高い部分を明確にすることがドイツなどの取っている社会システムと考えます。

風力発電は再生可能エネルギーの中では一番安価です。平成 22 年の原発事故の前になりますが、経済産業省の報告書には太陽光発電が一番高価で、風力はずいぶん安く、10 円/kWh から 14 円/kWh とありました。更に、この調査報告書では風力発電からの電力価格は将来この 3 分の 2 になるとしています。もし、この報告書が正しければ、風力発電からの電力は原発と同等になります。日本国内には風力を入れる所はたくさんありますが、北海道の北

や東北には十分な容量の送電線が無いので、風力発電を増やせません。そして、スペインの例のように電池なしで導入できる可能性があるかもしれません？　一方、世界で日本だけが太陽光発電設備が風力発電設備の 2 倍も入っています。他の国は全て風力発電設備が太陽光発電設備より多いのです。なぜそうなったのでしょうか？　来年度の経産省の予算では、北海道や東北の風力適地に送電線を配備するお金が補助金としてつくことになりそうだと聞いて言います。この補助金が本当に使われるのでしょうか？　また、本州と北海道の間の送電線容量はおおきくないので、北海道でつくったものを東京に送電するより、北海道で電気を大量に消費する産業を配置するのが技術・経済的に正しい選択かもしれません。

長距離送電のメリットですが、原子力は一定なので、供給電力は火力発電所のストップ&ゴーで制御します。しかし、火力発電は、発電してないときもボイラーを少したいています。それはボイラーの火を完全に落としてしまうと寿命が短くなってしまうからです。日本の場合では、天気がいいと電力をたくさん使うので、明日の天気が良くなりそうだと、午前 3 時位からボイラーに火を入れて発電準備をします。しかし、天気予報は外れて雨になると、その燃料費が無駄になってしまいます。この時に、広い領域に電力が供給できるようにグリッドが整備されていると、このような見積もりミスによる燃料のムダが減ります。火力発電所は最高出力の時に効率が最も良くなるように設計されているので、出力が落ちると効率も落ちます。天気予報をよく見るとわかりますが、雲の大きさは電力会社 1, 2 社分位の領域にまたがって、常に動いています。つまり、送電線で全国を結び、全て平均してしまえば、日本全体の火力発電所の効率がよくなるのではないかと思います。つまり、送電網を大きくすると日本全体で最適化が進むと思います。長距離送電には直流は適していますし、50Hz, 60Hz の周波数の違いも乗り越えることができます。広域にわたり「直流」送電をすると、同様な理由で風力や原子力も上手く回ります。そして、究極的には地球全体をつないでしまうことが理想的な送電網という話になると思っています。

ちなみに、日本、ドイツ、スペインの電気代を比べると、ドイツは上がっていますが、スペインの電気代はそれほど高くなっていません。やはり、風力は安いのではと思います。

超伝導でアジアを結ぶ

最後になりますが、超伝導送電では地中線を考えています。日本では架空線では鉄塔が一機基数億円で、300ｍか 400ｍごとにありますので、1 キロメートルで十数億円になり、結構高価です。先ほど紹介した中部大の実験装置の送電管は大きめに作ったので、1 本のケーブルで 2 ギガワット程度まで送電が可能です。人の歩く幅があれば原子力発電所２基分の電力を運べます。これのため、超伝導は高価ですが、超伝導ケーブルによる送電と架空線とのコストの違いは桁違いではありません。ファクター２程度の話になっていると思っています。現在、架空線を利用して、例えばカナダのネルソン川からニューヨークやボストンまで電力を送っていますが、架空線下の木を全て切ってしまうため、大きな自然破壊になっています。アメリカは 2003 年に大停電が起きましたが、ある送電線に規格以上の電流が短時間ですが流れ、架空線の温度が上がり、伸びて大きく垂れ下がりまた。そこに、下の木が伸びてきて垂れた送電線に木が触ってしまいショートし、大停電になりました。

これが直流だったら、電圧が下がり、大電流がながれにくくなり、大停電には発展せず、照明器具が少し暗くなったくらい済んだかもしれません。

中国の例ですが、北京五輪の時に空気をきれいにしようとしました。このため、北京での石炭火力発電所を止めて、ウイグルの石炭火力発電所で発電した電力北京に送りました。すると、公害はウイグルの地元が引き受けて、空気を汚さないで必要な電気だけを北京が受け取るという構図になります。長距離送電になるため、中国は直流送電を主にして増強しました。しかし、冬になると強い風が吹いたり、雪が降ったりして、送電線が切れたり鉄塔が倒れたりしました。すると、北京市のかなりの部分がブラックアウトしてしまい、一週間もその状態が続いたこともあったそうです。このため、長い送電線は安全性を考えると、地中線にしなければいけないでしょう。さらに、架空線はテロリストにも弱いです。アメリカではライフルの練習とか言って送電線をライフルで撃つことがあるそうですが、いきなり都市のある地区がブラックアウトします（笑）。こんなことを考えると、中東を通せばどうなるかは想像に難くないので、デザーテックは基本的に地中に埋めることになると思っています。もっとも、現時点では架空線を考えているようですが・・・。

架空線のメリットは「送電線」が安いことです。裸線なので絶縁を施す必要が無いからです。また、電気が流れて熱くなると空気が冷やしてくれます。地中線は電気（熱）絶縁物で覆うので、熱伝導率が低く地中のために冷却効果も少ないので、流せる電流が小さくなります。すると、値段が架空線に比べて 20 倍くらい上がることになります。すると超伝導の出番があるというのが私の主張です。

中国では、西側で発電した電気を北京へ送っているのですが、北京オリンピックを機会に超高圧送電が普及しました。中国には国家電網という民間会社がありますが、これが国家資本主義と言われる所以です（笑）。送電線への投資の 3 分の 2 が直流になっていて、送電容量の 3 分の 2 が直流ということです。そうなると、長距離送電のデザーテックをアジア版でやってみたいと考えて見ることは自然です。

先日、韓国大使館で何か話せと言われたので、僕が生きている間に核融合は出来ないであろうが、超伝導は出来ると話してきました。ただし、ユーロのようなアジア共通通貨が早いか、アジア諸国を結ぶ共通の送電線が早いかは気になるところです。アジア各国の状況はＥＵ内よりも経済格差が大きいので、調整が難しいのかもしれません。しかし、それが大きければ大きいほど、ピースキーパーとしての役割も大きくなるでしょうし、電力の輸出入による価値創造も大きくなるのでしょう。電力価格や売買ルール作りにはいろんな分野が関係しますが、僕は韓国大使館では国際（超伝導）送電研究所をつくってみたらどうですかと提案してきました。日本創生会議がアジアの電力網をつくる提案をしていたのですが、僕は折角なので、それを超伝導してはどうか考えています。

もう時間をオーバーしたのでこれで終わりにします。本日はご清聴ありがとうございました。

ディスカッション

Q.（池上徹彦氏　元文部科学省宇宙開発委員会　委員長）

原発事故の後に、事故調査委員会が出来て、大体が責任追及のプロセスばかりで面白くなかったです。しかし、原子力発電所は広い土地でないと駄目という話は興味深かったです。例えばシベリアやサハリンに原発を作って、海底ケーブルで日本に電気を送るのが現実的かと思うのですが、技術的には問題はないのでしょうか。

A.（山口氏）

海底ケーブルに関しては、技術的にはマレーシアとボルネオ島の間が 700 キロで一番長いです。架空線はロシアで一番長いもので 3000 キロくらいですが、現状では動いていません。現時点では日本で事故の起こった原発を新たに作るのは嫌がると思うので、ロシアは水力があるので、それをもらってもよいと思います。

<トピックス 1>

石狩市でのデータセンターへの電力輸送 — 超電導直流ケーブルプロジェクト —

Electric Power Transmission for Internet Data Center in Ishikari, DC Superconducting Power Cable Project

中部大学 超伝導センター
山口 作太郎、浜辺 誠、渡邉 裕文、ユーリ イワノフ
Center of Applied Superconductivity & Sustainable Energy Research (CASER), Chubu University
S. Yamaguchi, M. Hamabe, H. Watanabe and Y. Ivanov

1. はじめに

中部大学では2000年から高温超伝導(HTS)システムの研究を開始し、2005年から文部科学省の援助を得て、HTSテープ線材を利用した直流ケーブル実験装置(CASER-1)を建設した。これはHTSを利用した世界最初の直流ケーブル実験装置となった。そして、2010年3月にはナノオプト・エナジー社の藤原洋社長から中部大学への資金提供によって200 mケーブル実験装置(CASER-2)を建設し、研究開発を進めてきた。これらの研究開発については未踏科学技術協会からFSST News No. 134に「直流超伝導送配電システムの研究開発とその役割」と題した解説を参照されたい。

以上の技術開発が基礎の一つになって、平成24年度の補正予算で石狩市に500 mと2 kmのHTS直流ケーブルを建設することになった。この2本のケーブルの送電端はさくらインターネットの石狩データセンターに接続されている。これは経済産業省の委託事業として「高温超電導直流送電システムの実証研究」と題され、平成25年度及び26年度の2ヶ年での建設を予定している。実施主体は千代田化工、住友電工、さくらインターネット(株)及び中部大学の共同事業であり、住友電設、みずほ総研、東芝などの複数の企業や大学からの支援・協力を得て、設計作業を現在進めている。この稿では、現時点でのこの実証研究が目指す方向や設計での基本的な考え方などを紹介する。

2. データセンター(iDC)の現状

iDCは現代社会では最も重要な社会情報インフラであり、社会生活に無くてはならない存在であり、同時に多くの企業が参入し、成長が著しい産業分野でもある。

iDCには多くのユーザからインターネット(光ファイバー)を通じて接続される数多くのサーバが設置してあり、膨大なデータを保管し、各種サービスを行っている。このため、24時間稼働が要請され、膨大な電力を消費している。そして、電力消費はほぼ昼夜を問わず一定であり、iDC運用コストのかなりの部分が電気料金となり、iDCの節電は経営上も地球保全の観点からも極めて重要である。

今回チームを組んださくらインターネットは石狩市にiDCを設置し、節電については日本で最も進んだ取り組みを行っている[1]。北海道という冷涼な気候を利用してサーバを冷却しエアコンの消費電力を節約し、更に直流給電を行い、機器の消費電力を抑え、最も消費電力の少ないiDCと言われている。特に、直流給電によって電力機器の設備コストも節約できるため、今後のiDCでは直流給配電は必須と考えられている。

以上のような状況でさくらインターネットの田中邦裕社長が、次のステップとして「超電導直流給配電」と「再生可能エネルギー」の導入に興味を持たれ、検討を行っていたことが、今回のプロジェクトがスタートできたもう一つのきっかけとなった。

3. 開発を進める上での基本的考え方

超電導直流ケーブルが一般民生で広く利用されるためには、銅ケーブルより経済的に優位に立つことが必要である。これには低電力損失であることが第一条件となる。しかし、銅ケーブルとの損失比較はそれほど簡単ではない。つまり、銅ケーブルでは通電時のみに損失が発生するが、超電導ケーブルでは冷凍機で常時低温に保持するために非通電時でも損失が発生することがまず挙げられる。このため、負荷変動が少なく常時利用されるiDC等のシステムでの利用が最初の用途になることは合理性が高く、その意味で今回プロジェクトは良い例となろう。但し、一般にケーブル利用率が高い場合には銅ケーブルはより多く並列に布設され、電流密度を下げることによって損失を下げる。このため、銅ケーブルとの損失比較は基準の決め方でかなり変わる。

以上を考慮すると、超電導ケーブル損失低減はこれからも長い研究課題となろう。エディソンが最初に銅ケーブルを使ってから、長い時間をかけて銅純度が上がっていった過程とよく似るのであろう。同時に、超電導ケーブルを構成する機器コスト及び運転コストの低減も今後の長い研究課題である。つまり、超電導ケーブルの実現には、高温超伝導(HTS)線材の安価で高性能化だけでは不十分で、これを低温に保持するための機器システム全ての最適設計を通じた高性能化(低損失及び低熱侵入)が求められる。

一方、超電導ケーブルの特長は小型(高い電流密度)で、電気抵抗が実効的に極めて低いため(工学的

には色々な理由で完全なゼロにはならない)、高電圧を用いる必要性は低い。これは銅ケーブルと比較して比較的低電圧・大電流で使うことができることを意味し、従来とは違った利用方法が出てくる。例えば、電圧を変える変電所を少なくできる。これは変電所コストを削減できるため、大きなメリットではあり、比較的高価なケーブルでも利用可能性がある。更に、低電圧の布設路はケーブルを収納する共同溝コストをより安価にすることも可能になろう。また、直流の場合には電力変換器(交流への変換と直流での電圧変換など色々なタイプがある)が必要になる。超高圧電力変換器は極めて高価であるが、比較的低電圧の電力変換器は安価で損失が低い。したがって、超電導ケーブルを利用する長所はシステム全体で考える必要がある。

4. 超電導ケーブルについて

超電導ケーブルの熱収縮率は0.3%と言われ、2 kmの超電導ケーブルでは6 mほど縮む。0.3%に対応する引っ張り応力を印加しても利用可能なケーブル開発も一つの方向であろうが、ケーブルが長くなれば熱収縮は一様ではないと考える方が安全サイドになるため、できる限りケーブルに熱収縮などによる応力発生を避ける技術開発を行うことにした。このため、CASER-2では端末真空断熱容器をケーブルの熱収縮に応じて移動できるようにし、ケーブルに熱応力が発生しない構造を取った[2]。しかし、CASER-2では熱収縮長さは0.6 mほどであったが、石狩プロジェクトでは6 mを吸収する必要があり、別の方法が求められる。幸い平成24年度に科学技術振興機構(JST)のA-STEPで熱収縮対策の研究開発を住友電工と中部大学が共同で行うことが認められ、昨年10月からその開発を進めていた。このため、石狩プロジェクトではその成果を生かす形で現在研究開発と設計作業を進めている。

基本的な考え方は、超電導ケーブルが常温では断熱2重管内にヘリカル状になり、低温でケーブルが縮むと直線状になることによって熱収縮を吸収する方式である。このアイデアはCASER-2の実験結果から得た。CASER-2のケーブルをX 線撮影したところ、常温でヘリカル、低温で直線状に変形し、このため端末真空断熱容器の移動距離は当初の予定より短くなっていたことが直接のきっかけである[3]。図1にCASER-2の常温時のケーブルの水平方向と垂直方向からX 線撮影からヘリカル変形している様子を示す。2つの線は内管を示していて、上部方向には少し余裕があり、左右方向は内管一杯にケーブルがヘリカル変形していることが分かる。

このため、端末真空断熱容器の移動距離は0.3%に対応する長さよりも短くなった。但し、新しいアイデア

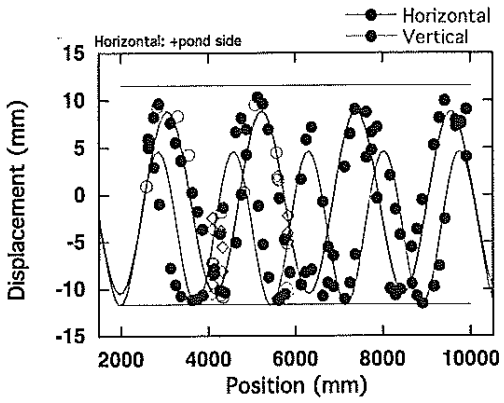

図1 CASER- 2のケーブルX線撮影結果

(技術)を利用することになるため、最初に500 mケーブルを布設し、その経験を生かす形で2 kmケーブルの布設に臨む予定である。このため、500 mケーブルと2 kmケーブルの仕様は全く同じであり、以下のようである。

電流:5 kA (テープ線材数 ≦ 37本)

電圧 ±10 kV

同時にできるだけ細いケーブルを作ることを目標としている。上記のパラメータを選択した理由は下記のようである。

両極性の電源を利用すると、電圧を低く設定しても送電電力は大きくなるため、ケーブルの線材コストが下がる。つまり、HTSテープ線材の節約につながる。また、多くの大電力用銅ケーブルの電流は2 kA程度であるが、超伝導ケーブルの特長を生かすためにはそれを超した電流にした方が良いと考えた。また、電圧の設定には電力変換器コストを考える必要がある。一般に電圧が高くなると変換器コストは急激に高くなる傾向がある。そして、コロナが発生しない電圧(20 kV~30 kV)では短絡電流もそれほど大きくならないため、超電導ケーブルの大電力輸送として検討すべきパラメータとして選んだ。

尚、ケーブル長が1 kmを超すため、HTSテープ線材をケーブル中で半田接続することにした。これは今後テープ線材コストを考えると必ず必要になる技術となろう。また、ケーブルは1 km長で中間接続部を設け、ケーブル接続をする。

5. 断熱2重管について

断熱2重管の熱侵入量測定とその低減は中部大学ではCASER-1を建設すると同時にテストベンチを建設し、長年検討を行ってきた[4, 5, 6]。これは2 kmを超すような長さになると、断熱2重管からの熱侵入が大部分

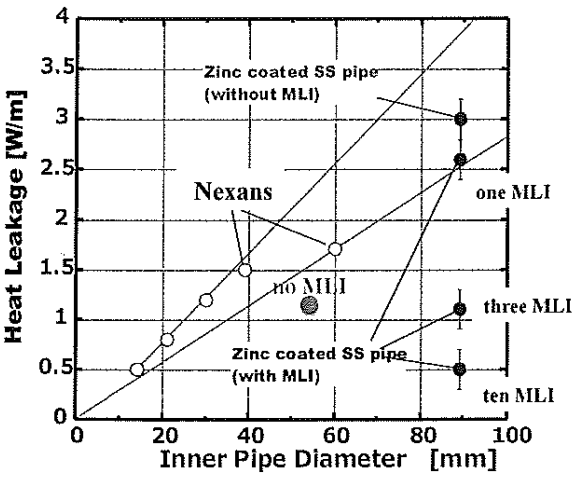

図2　Test Benchでの熱侵入量測定結果

になると予測されたからである。図2にテストベンチでの熱侵入量測定の実験データを示す[4]。ここでは80 Aと50 Aの配管の測定結果を示している。これは縦型クライオスタットでの実験であり、横軸は内管径である。

この図には同時にNexans社の断熱2重管の熱侵入量データをプロット(白抜きのプロット)した。此に見られるように、同じ内管径では中部大学の測定結果はNexans社の製品より熱侵入量が少ない。これはNexans社の製品が2重コルゲート管を利用し、表面積が直管に比べて大きくなることに加えて内管の力学的支持がナイロンやテフロン線を内管に巻き付けて行っていて、十分に熱絶縁距離が取れていないためではないかと考えている。この構造はケーブルを曲げた場合には内管が外管により近づくため、更に厳しくなる。また、一般に多層断熱膜(MLI)はその自重だけでも熱侵入量が大きくなると言われていているが、内管とケーブル自重は最終的にはMLIに全て印加されるため、将来的にもこの構造では熱侵入量低減が困難ではないかと考えている。更に、コルゲート管は直管に比べて冷媒循環のための流体損が大きくなるため、より長いケーブルを考えるとCASER-1, CASER-2と同様に直管を用いることにした。そして、コストを下げるために、外管は亜鉛メッキ鋼管を用い、内管のみにステンレス管を用いることとした。

従来までの断熱2重管との大きな違いは、冷媒循環のためにリターン管が必要になることである。このリターン管への熱侵入も考慮すると、外管を太めにして、ケーブルを内蔵している内管と同じ外管に入れ構造がベターである。このため、この構造で全熱侵入量の測定を行うテストベンチの準備を進めている。

但し、直管を用いると現地で溶接などの工事が必要になる。そして、真空度を高くするためのベーキングができない。このため、現地工事については、今までの経験[2, 7]を生かすと同時に法規制なども含めて幅広い検討を進めている。

6. 電流リードについて

電流リードも大きな熱侵入源である。したがって、ここからの熱侵入はできる限り小さくしたい。例えば、東京電力他のYokohama Projectでは1.75 kAに対して1100 Wの熱侵入量[8]となっている。これは端末クライオスタット全体での値ではあるが、電流リード当たり105 W/kAの熱侵入量となる。また、構造的には、太めの一本の銅リードを用いている。一方、中部大学では熱電半導体材料を電流リードに用いていて、熱侵入量を低減してきた[9, 10]。このため、CASER-2では上記の半分程度の熱侵入量[11]である。

また、電流リードの電気回路はHTSテープ線材にそれぞれリード部の素線が独立して接続される方式である。図3に回路図を示す。

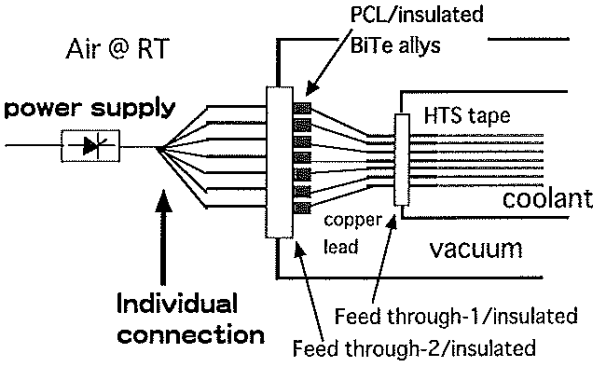

図3　電流リード端末の電気回路

この回路ではHTSテープ線材にそれぞれ電流リードの素線(銅リード及び熱電半導体)が直列に接続されている。これによって、それぞれのHTSテープ線材に流れる電流比はほぼ電流リード部の抵抗比になる。電流リード部の抵抗は電流によって最適値が変化するが、電圧は銅や熱電半導体の物性値で決まり、ほぼ50 mVから100 mVが最適値になる。したがって、この部分の抵抗(今回の設計では350 $\mu\Omega$ – 700 $\mu\Omega$程度)によって偏流を防止することができる[12, 13]。実際、超電導マグネットでは偏流によってクエンチが観測[14]され、偏流防止の研究開発が長く行われた。

この技術はケーブルが長くなるときには極めて重要になる。石狩プロジェクトではケーブル長が2 kmとなるため、中間でケーブル接続を行う。更に、HTSテープ線材のコスト低減のために、一本のケーブルの中でも線材の半田接合部が予定されている。この抵抗は90 nΩ以下とされるが、図3のような対策を取らないと、この部分の抵抗比でテープ線材の電流比が決まる恐れがあり、ケー

ブルの臨界電流低下が懸念されるからである。

まとめると電流リードには2つの役割が有り、一つは熱侵入低減であり、もう一つは偏流防止である。そして、石狩プロジェクトでは、以上に付加して電気絶縁性能の向上や輻射による熱侵入量低減対策を取ることを予定している。

7. その他の機器等について

以上で述べてきた機器以外に必要な個別機器としては、冷凍循環機器(冷凍機、循環ポンプ、冷媒タンク)がある。現在、冷凍機についてはスターリング冷凍機(ST)とターボ・ブレイトン冷凍機(TB)の2つを混在して利用することを想定している。特に、TBをケーブル実験で利用するのは初めてのケースであるため、ケーブルとは切り離して別途に実験ができるように設計を進めている。特に、小型TBでは成績係数(COP)がSTに比べて低くなるが、寿命は大幅に向上するということなので、この辺に着目して試験を進める予定である。更に、今後のより長いケーブルを想定すると、冷媒循環のためのポンプの検討は、温度、圧力、熱侵入量など色々なパラメータが関連するため、CASER-2の実験データを元に今までの経験[15, 16]を慎重に検討を進めている。

他には、計測制御系の設計を同時に進めている。CASER-2ではインターネットに接続し、世界中どこからでも実験室の制御画面を見ることができるようにしてある。今回も同様なシステム構築の検討している。また、事故時対応は基本的には計測制御系からの信号で判断することになるため、多重化やハードワイヤーの導入なども検討項目に入っている。

また、今回の予算では含まれていないが、直流ケーブルであるため、通電実験を行うためには電源(電力変換器)が必要になる。つまり、交流受電を行い、送電後それを直流に変換する変換器が必要になる。そして、このような直流機器向けの安全機器が必要になる。例えば、直流遮断器(DCCB)や直流限流器などが挙げられよう。特に、DCCBは複数箇所への電力供給を行うには必ず必要になるため、今後の重要な開発項目になると考えている。

電力変換器の仕様や性能は最終ユーザの意向を取り入れることは当然であるが、今回は最初に述べたように再生可能エネルギーを十分に取り込めように研究開発を進めることになる。但し、現時点での予算では変換器製作は含まれていなく、現在は仕様の机上検討や一部試作・試験などを進めている。

以上述べてきた機器以外に石狩プロジェクトでは現地工事も重要な検討項目で有る。断熱2重管の項で述べたように、現地で溶接作業やケーブルを配管内に引き入れる工事などがあるからである。布設ルートは道路に沿って行うので、長い期間工事のために占有することはできない。順次、埋め戻しが要請されている。したがって、工事手順はシステム性能確保に極めて重要な検討項目である。更に、工事は法規制などと強く関連するため、関連省庁及び北海道庁、石狩市の了解を取りつつ進めている。このため、大学での研究開発とはかなり異なった感触を受けているが、超電導送電の実用に近づいていることも実感している。

8. まとめ

現時点(2013年9月)では、以上述べて機器類や工事などについての検討が急ピッチで進められている。同時に中部大学ではテストベンチを利用して仕様の確定作業を進めている段階である。実際、これだけの規模のケーブルシステムを2年ほどの短期間で製作・布設することはかなりの作業量となっている。

法規制関連については、今回は電気事業法の適用を想定し、高圧ガス保安法については準拠することで進めている。但し、今回のプロジェクトを通じて、電気事業法に直接高圧ガス保安法の条文などを一部変更して書き込むことも検討されている。

今後の予定であるが、本年度と来年度(平成26年度)で500 mケーブルについては、設備を完成し、通電試験を予定している。そして、平成27年度以降は太陽電池パネルとの接続を行うことを予定している。また、2 kmケーブルについては、装置完成までとして、実際の運転・稼動は平成27年度以降を予定している。これは、2 kmケーブル用の電源整備が平成27年度以降になることも理由の一つである。

以上、石狩プロジェクトの概略を紹介した。最初に述べたように、これは千代田化工、住友電工、さくらインターネット(株)と中部大の共同事業で有り、更に多くの企業や大学からの支援を頂いて進めている。本来ならこの稿の著者になってもらうのが適切とも考えられるが、この稿は山口がまとめたこともあり、著者は全て中部大関係者のみとさせて頂いた。

最後に、千代田化工の腰塚博美、田中昌司、大石前次さま、住友電工の林和彦、増田孝人、湯村洋康さま、住友電設の阿部洋一さま、さくらインターネット(株)の田中邦裕、澤村徹さまには大変お世話になっています。ここに記して感謝を表します。更に、プロジェクトの発足に当たり新金属協会専務理事・織山純さま、石狩市長・田岡克介さまにも多大なご援助を頂きました。記して感謝を表します。また、中部大学理事長／総長・飯吉厚夫先

生には変わらない支援を頂いています。そして、本年になり中部大学特任教授・高野廣久さまにはマネジメント含め色々とご支援して頂いています。共に記して感謝を表します。

参考文献

[1] http://ishikari.sakura.ad.jp/
[2] S. Yamaguchi *et al.*, Prof. ICEC23/ICMC2010, (2011) 1041-1047.
[3] H. Watanabe *et al.*, ICEC24/ICMC2012, (2012) 15P-P07-04.
[4] M. Hamabe *et al.*, Advances in Cryogenic Engineering **53A** (2008) 168-173.
[5] Y. Nasu *et al.*, Proc. ICEC22/ICMC2009, Seoul, Korea, (2009) 489-494.
[6] M. Sugino *et al.*, Proc. ICEC23/ICMC2010, (2011) 639-643.
[7] H. Watanabe *et al.*, Physics Procedia **27** (2012) 376-379.
[8] H. Yumura *et al.*, IEEE Trans. Appl. Supercond. **19**, (2013) 5402306.
[9] S. Yamaguchi *et al.*, RSI **75** (2004) 207-212.
[10] T. Fujii *et al.*, J. Elec. Mater **40** (2011) 691-695.
[11] T. Kahawara *et al.*, J. Physics: Conference Series **400** (2012) 052009.
[12] S. Yamaguchi *et al.*, Cryogenics **38**. (1998) 875-880.
[13] S. Yamaguchi *et al.*, J. Physics: Conference Series, **97** (2008) 012290
[14] N. Koizumi *et al.*, Cryogenics **34** (1994) 155-162.
[15] Yu. Ivanov *et al.*, Physics Procedia **27** (2012) 368-371.
[16] Yu. Ivanov *et al.*, Physics Procedia **36** (2012) 1372-1377.

<トピックス 2>

ハイブリッド型人工ピン導入による Y系超伝導線材の J_c 特性への影響

Effect of introduction of hybrid-APCs on J_c properties in YBCO coated conductors

九州工業大学
松本 要、堀出朋哉
Kyushu Institute of Technology
K. Matsumoto, T. Horide

1. はじめに

$YBa_2Cu_3O_{7-x}$ (YBCO) 超伝導体を用いたY系線材は、65-77 Kの磁場中において高い臨界電流密度J_cを有しているため、液体窒素近傍における種々の応用において有望な材料である。しかし、粒界問題のため、その線材化にはIBAD法やRABiTS法などを用いてYBCO結晶の2軸配向化を行う必要がある[1]。さらには長尺化、交流損失低減、および機械的特性向上などが応用上重要な課題となっており、その課題克服に向けて盛んに研究開発が進められている。中でも磁場中J_cの向上は優れたY系線材実現のためには大変重要な課題となっている。

YBCO線材においては結晶粒界および磁束ピン止めがそのJ_cを決めていると考えられるが、高度に結晶配向したYBCO薄膜の場合には、一般に転位や酸素欠損等の自然に導入された結晶欠陥がピン止め点として作用する。しかし最近では$BaZrO_3$ (BZO)、$BaSnO_3$ (BSO)、$BaHfO_3$ (BHO)などのナノロッド、あるいはY_2O_3やBZOなどのナノ粒子を人工的に薄膜中に導入する人工ピン導入法で、大幅なJ_c向上が達成されるようになっている[2]。特に、薄膜のc軸方向に成長したナノロッド状のc軸相関ピンを用いることで磁場中での高J_cと高い不可逆磁場B_{irr}が実現している。

65-77 Kにおける磁場中J_cのさらなる進展においてはJ_cの磁場印加角度依存性の制御が欠かせない。YBCOの結晶異方性に依存して、YBCOのJ_cにもイントリンシックな異方性が生まれ、ab軸方向に平行に磁場を印加した場合、c軸方向に磁場を印加した場合に比べて一般にJ_cが大きくなる。ここでナノロッドのようなc軸相関ピンを導入するとJ_cの角度依存性においてc軸方向にJ_cの大きなピークが現れる。こうしてこの温度領域におけるYBCOのJ_cの角度依存性にはab軸方向とc軸方向の2方向にJ_cのピークが現れることになる。しかしながらab軸方向とc軸方向の間の角度領域では、J_cは期待に反してそれほど向上することはなく異方性が残ったままと

2013年6月3日発行

超電導 Web21

（公財）国際超電導産業技術研究センター　〒135-0062 東京都江東区東雲 1-10-13　Tel: 03-3536-7283

特集：冷凍・冷熱技術

「超伝導ケーブル用の断熱2重管及び低温系について」

中部大学大学院工学研究科
超伝導・持続可能エネルギー研究センター
教授　山口作太郎
准教授　渡邊裕文

中部大学は 千代田化工建設、住友電工、さくらインターネットと協力して北海道石狩市で稼働中のデータセンター向けに直流給配電を行う超電導直流ケーブル設備を経済産業省予算で建設することになった。長さは 500 m と 2000 m であり、2 本のケーブル・システムを作り、石狩プロジェクトと呼んでいる。建設の基本的な考え方は、将来に向けてより長いケーブルを安価に作ることが目標であり、このために設計標準化や LNG 冷熱利用などの検討を行っている。以下では断熱 2 重管の基本構造と LNG 冷熱利用について考え方を簡単に紹介する。

リターン・パイプの組み込み

超伝導ケーブルは同軸構造を取るため、一本で往復導体がある。一方、今回の装置は実際に利用するため送電端と受電端が離れている。このため、リターン・パイプが必要になる。冷凍機への熱負荷はケーブルを収納している低温パイプとリターン・パイプの熱負荷の和となる。これをできるだけ低くすることが求められる。図 1 に断面構造例を 2 つ示した。一番外側のパイプは真空を保持するための常温パイプであり、内管には液体窒素冷媒が流れている。そして、一方の内管には HTS ケーブルが入っている。左図は 2 本の常温パイプにそれぞれ低温配管が 1 本ずつ入っている。右図は一つの常温配管に 2 本の低温配管が入っている。輻射熱の検討では、右図構造の熱侵入量が少ない。低温配管が互いに常温壁に対して影になるからである。また、この方が将来的には安価に製造できると考えている。一方、狭い配管内で現地溶接の必要性が出てくるので、溶接信頼性を高める工夫も必要と考え、現地で溶接ロボットを使うことを検討中である。

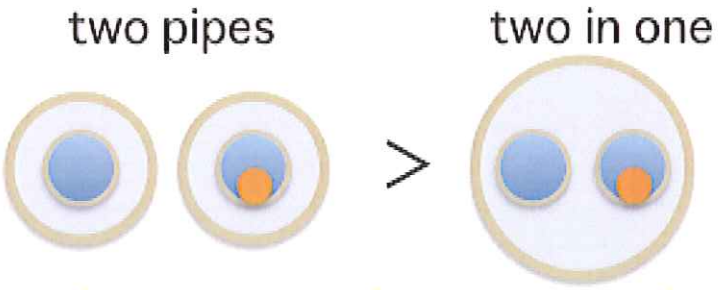

図 1　断熱 2 重管の基本構造：
2 本の低温配管を一本の真空配管に入れると熱侵入量が低い

2013年6月3日発行

超電導 Web21

（公財）国際超電導産業技術研究センター　〒135-0062 東京都江東区東雲 1-10-13　Tel: 03-3536-7283

尚、流量は2つの配管は同じであり、一方にはケーブルが入っているので、リターン・パイプ径は少し小さくすることになる。また、安価に作るために、外管は亜鉛メッキ鉄管を利用し、低温配管はステンレス管を使う予定である。長距離冷媒循環の圧力損を最小にするために、直管を配管に多用し、2000 m であっても流量～40 L/min, 圧力損～0.1 MPa 程度を想定している。このため、現状のポンプで循環が可能と考えている。

真空排気系にはケーブルの両端で真空ポンプを用いる予定である。排気速度は～500 L/s であり、ターボ分子ポンプの利用を想定している。但し、排気時間がコンダクタンスや多層膜断熱材（MLI）からの outgas 量によって大きく変わるので、ケーブル中間部にも真空ポンプを設置することを予定し、実質的な排気時間は長くても1週間程度になることを目標としている。

LNG 冷熱利用

LNG は主にメタンから成り、LNG 温度は 113 K 程度とされる。液体窒素温度より 40 K ほど高いだけなので、この冷熱を利用して超伝導ケーブルを低コストで低温保持する検討を行っている。簡単な検討では、冷凍機 COP は 300 K-77 K の熱サイクルで 0.2 – 0.3 程度まで上がるようである。現状のスターリング冷凍機が 0.067 程度なので、5 倍程度の改善となり、実現すると大きなシステム経済性の向上につながる。

現在、日本には 25 箇所の LNG 基地があり、世界最大の輸入国である。一方、LNG 冷熱は 90 % 以上が捨てられている。LNG の多くは発電所の燃料になっていることやその多くが東京湾や大阪、名古屋などの大電力消費地にあるため、LNG 冷熱利用を利用し、超電導送電することは技術的な合理性が高い。このため、LNG 冷熱利用は超電導利用の標準モデルになると思われる。このため、冷凍機の COP 改善の机上検討を行う予定である。そして、次のステップとして、LNG 冷熱利用の冷凍機開発が行われることを期待している。

超電導 Web21 トップページ

SUPERCOM
SUPERCONDUCTIVITY COMMUNICATIONS
超電導コミュニケーションズ
Vol.22 No.2 April 2013 通巻121号

石狩市で始まる超伝導直流送配電プロジェクト

__千代田化工建設、住友電工、さくらインターネット、中部大学__

2013 年 3 月 26 日に経済産業省から平成 24 年度「高温超電導直流送電システムの実証研究」に関して、千代田化工建設、住友電工、さくらインターネット、中部大学が採択業者となったとの発表があった。これは 1 月 18 日に経済産業省から発表されたプロジェクト(「民間投資の喚起による成長力強化」p.12、http://www.meti.go.jp/main/yosan2012/index.html)の公募結果である。 (5 ページに続く)

DI-BSCCO 最新情報 ー強度向上に進展ー __住友電工__

住友電気工業株式会社が製造する DI-BSCCO 線材はケーブル応用において近年数多くの実証プロジェクトに採用されており、国内では本誌でも採り上げられている NEDO 委託の実証プロジェクト(Vol. 21, No. 2, No. 6 など)や社内実証試験(Vol. 22, No. 1)、国外ではドイツの AmpaCity プロジェクトやロシア・サンクトペテルブルグ市での直流送電プロジェクトが進められている。 (7 ページに続く)

SQUID を用いた鉱物探査実用機最新情報

__超電導工学研究所、三井金属資源開発、JOGMEC__

(公財)国際超電導産業技術研究センター超電導工学研究所は三井金属資源開発(株)と共同で、JOGMEC((独)石油天然ガス・金属鉱物資源機構)からの委託研究「次世代 SQUITEM 機器開発・SQUID 磁力計開発」により開発してきた、地下資源探査システム、SQUITEM 3 号機が完成したことを 2013 年春季電子情報通信学会総合大会で発表した。 (9 ページに続く)

鉄系超伝導体線材、実用レベルに迫る！ __(独)物質・材料研究機構__

2008 年に発見された鉄系超伝導体は、銅系酸化物に次ぐ高い臨界温度 T_c と高い臨界上部臨界磁界(H_{c2})を有するために、物性研究のみならず応用面からも注目されている。そのため、パウダー・イン・チューブ(PIT)法による線材の試作が発見直後から行われてきたが、粒間弱結合のために測定される輸送臨界電流密度(J_c)が実用レベルには程遠く低い問題があった。しかし、図 1 に示すように、この数年の間に PIT 線材の輸送 J_c は急速に上昇して実用レベルに接近しつつある。 (11 ページに続く)

低温超電導デバイス開発用､新クリーンルーム稼働開始 __(独)産業技術総合研究所__

平成 24 年 11 月、産業技術総合研究所において低温超電導デバイス作製を主目的とする新たなクリーンルームが稼働を開始した。

このクリーンルームは、その名称を超電導アナログ–デジタル計測デバイス開発拠点 (Clean Room for Analog & Digital Superconductivity：CRAVITY)といい、その名の通り、超電導アナログ応用とデジタル応用の融合を目指しているそうである。 (13 ページに続く)

応する。つまり、上記両超伝導材料特性が回転特性として明確に現れていると考えられる。以上の結果から、リラクタンストルク発現形 HTS-ISM の実現可能性が示されたものと考えられている。同グループでは、上記成果を 2013 年度春季低温工学・超電導学会(東京)で報告[2]するとともに、第 23 回国際磁石技術会議(23rd International Conference on Magnet Technology, Boston, MA, USA)にて発表[3]する予定である。

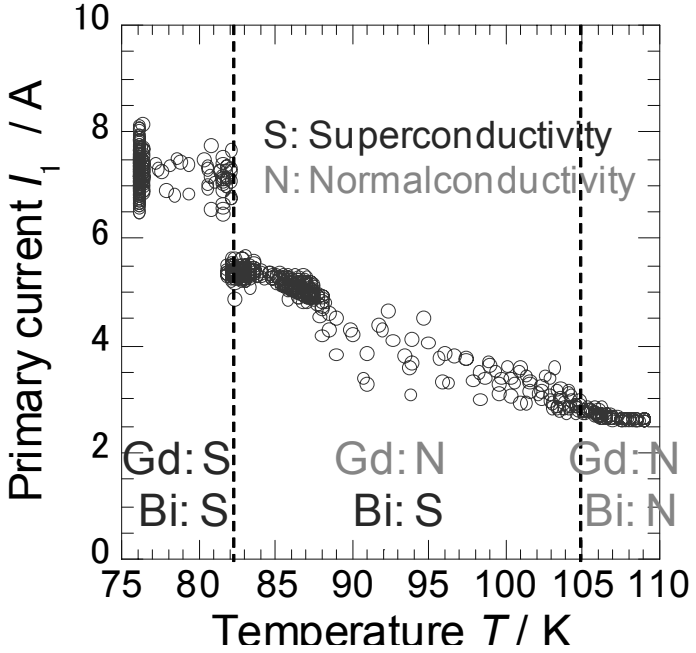

図3　昇温過程における無負荷回転特性(一次電流)の試験結果

研究責任者の中村准教授は、「超伝導リラクタンス回転機の研究については、これまでロシアなどで精力的に実施されてきたが、駆動原理上低力率や低効率であることが課題であった。それに対して本提案では、高トルクが必要な駆動モードでのみリラクタンストルクが発現し、通常走行時は自動的に消失する設計が可能であることから、広い速度範囲に亘る高効率化と高トルク密度化の両立が可能になると期待される。今後は、HTS 磁気遮蔽体の構造や配置を最適化する検討を推進し、輸送機器応用への具体的展開を目指したい。」と話している。

本成果は、科学研究費補助金(挑戦的萌芽研究、No. 23656199)の助成によって得られた。(京大 TN)

参考文献
[1] T. Nakamura et al., Electronic Materials and Applications 2013(January, 23-25, 2013, Orlando, USA)
[2] 西村立男 他, 2013 年度春季低温工学・超電導学会研究発表会(2013 年 5 月 14 日, 江戸川区)
[3] T. Nishimura *et al.*, 23rd International Conference on Magnet Technology (July 14-19, 2013, Boston, MA, USA)

石狩市で始まる超伝導直流送配電プロジェクト

__千代田化工建設、住友電工、さくらインターネット、中部大学__

(1 ページより続く)

これによると平成 24 年度補正予算で 25 億円をかけて、図 1 に示すように変電所等から直流送配電システムを構築し、大口需要家に直流電力供給を行うことを予定している。システム長として 2 km 以上

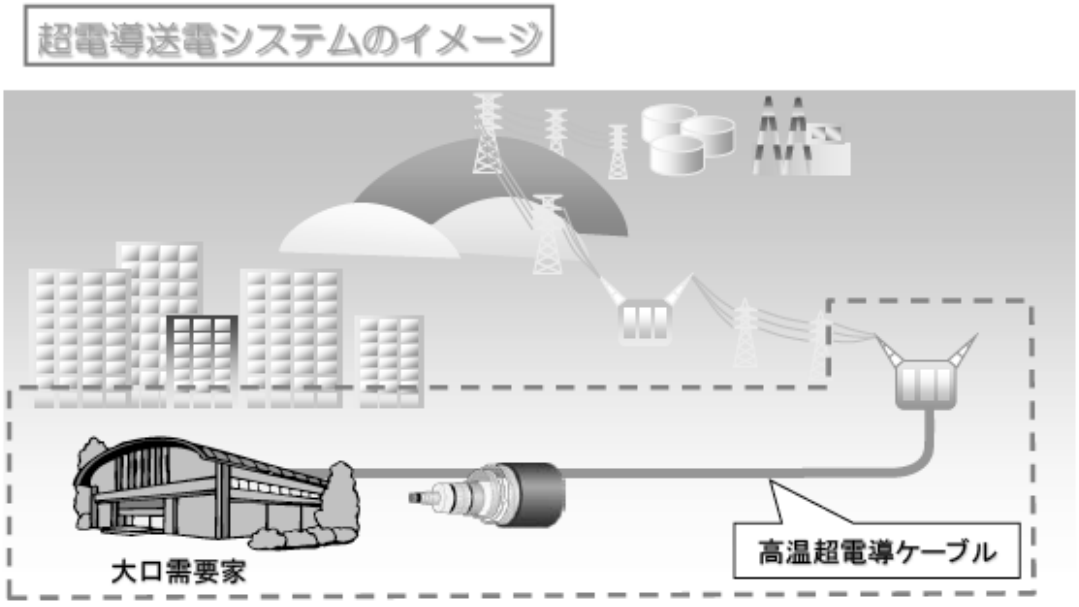

図 1 データセンタ等大口需要家への直流超伝導送電のイメージ

であり、ケーブルの送電電力は 50 MW 以上を目標としているプロジェクトである。同時に、このプロジェクトには太陽光などの再生可能エネルギーからの直流低圧電源からの給配電ケーブルを 500 m 程度建設することも含まれている。

これについて問い合わせを行い、担当者である中部大学・超伝導センターの山口作太郎氏より下記のような返答を得た。

問 1：導入する場所とデータセンタへの導入の意義は？

場所は北海道・石狩市を想定している。地元との調整も進んでいる。ここには最新の技術を導入したデータセンタがある。その特徴は寒冷地に設置することによってエアコンなどの消費電力を節約していることであり、さらに直流給電によってデータセンタでの消費電力を節約している。図 2 はさくらインターネットの HP からの引用である。

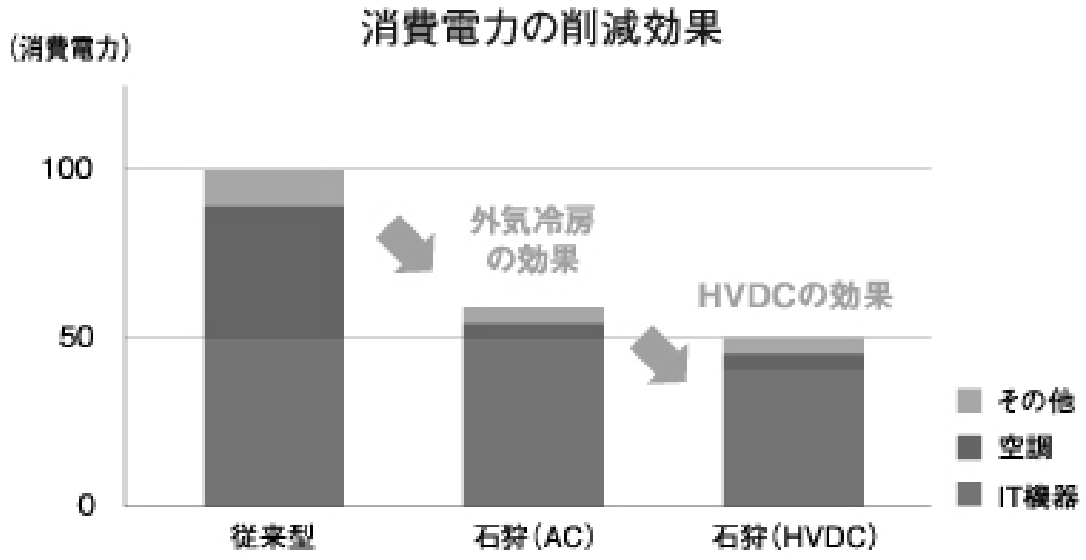

図 2　データセンタの消費電力の節約

これに見られるように､東京や大阪などに設置するデータセンタに比べて消費電力が半分程度になる。このため、日本で最も競争力のあるデータセンタである。日本国内のデータセンタを海外から利用すると、これは利用料金が輸出に対応するので、日本の競争力強化と貿易外収支の黒字に貢献する。

さらに、石狩市を中心にした「北海道グリーンエナジーデータセンター推進フォーラム」(http://www.hokkaido-gedc.com/)があり、新しい技術を導入することについての地元の受け入れや支援体制などの環境が整っていた。

加えて、北海道の石狩から稚内までの日本海沿岸側は風力発電の適地であり、昨年度から政府部内で送電線網の整備や再生可能エネルギーの導入が検討されている。また、石狩市には北海道で最初の LNG 基地が建設され、運用に入っている。LNG の温度は－160°C 程度であり、この冷熱を利用することは高温超伝導応用にとって損失及びコスト低減に極めて重要と思われる。特に、日本は LNG 輸入が世界で一番であり、今後 LNG 輸入は増えると考えられるので、LNG の冷熱利用は益々求められる。

以上から、高温超伝導直流送配電システムを石狩市で導入することは極めて適切と考えられる。

問 2：ケーブル電流や電圧などのパラメータやケーブル長は？

ケーブルの送電能力として 50 MW を満たす。一方、直流システムでは電力変換器コストが大きな割合を占めるので、ケーブル、変換器及びユーザー要求仕様を考慮して最適設計を行う必要がある。さらに、将来的には再生可能エネルギーからの電力輸送のためのパラメータ検討を行う必要がある。現時点では、電圧電流は 5 kA, 10 kV を中心にして設計検討を進めている。また、太陽電池からの仕様は 5 kA, 400 V である。

ケーブル長は 2 km を超すことが目標であり、世界最長ケーブルとなろう。このため、今までに開発された技術だけでなく、長尺ケーブルの建設には新しいアイデアを持ち込むことは、必要不可欠になろう。超電導ケーブルは損失が少ないが、それは長いケーブルになって始めて発現するため、長尺ケーブルの開発はケーブル研究の基本である。このために、本格的な普及を見据えてコスト低減や設計標準化なども目指す。

問 3：補正予算として単年度予算であるが、今後のプロジェクト展開はどうなりますか？

平成 24 年度の補正予算なので、平成 25 年度までは利用することができる。一方、2 km ケーブルの建設を考えると 1 年間では短いので、最終的にはもっと長い期間のプロジェクトになるのではと思っている。

実際、北海道でこのような開発を進める大きな目標には、超電導送電の他に直流給配電、再生可能エネルギーの利用がある。これらはお互いに関連し合い、今後複数のプロジェクトが立ち上がることが期待されている。

また、期間が短いこともあり今回は 4 者が採択機関となったが、将来的にはより多くの機関が加わっていく必要があると思われる。幸い、石狩市に「石狩超電導直流送電プロジェクト推進協議会」が 2 月 15 日に設立され、これに布設する研究会を中心にして多くの企業に加わってもらう仕組みができた。

(取材者：福山一夫)

DI-BSCCO 最新情報　－強度向上に進展－　　__住友電工__

(1 ページより続く)

一方、コイル応用では超電導マグネットの高磁場化や大型化が進んでおり、それに伴い超電導線材にはより大きなフープ応力に耐えられるだけの機械強度が求められている。DI-BSCCO 線材の場合、素

SUPERCONDUCTIVITY COMMUNICATIONS, Vol.21, No.5 October, 2012

＜解説＞ 第二部　日本の電力網の現状と超伝導直流送電導入

みずほ情報総研・サイエンスソリューソン部 石原範之

中部大学・人文学部 桃井治郎

中部大学・超伝導センター 山口作太郎

この記事は SUPERCOM8 月号に掲載された「第一部　ヨーロッパの電力網の紹介」に続く記事であり、「中部大学と科学技術振興機構（ JST ）の 2011 年度に行われた共同研究「高圧直流超伝導送電の社会実装に関する調査研究」の報告書要約である。今回は第二部として、「日本の電力網の現状と超伝導直流送電導入」と題して、現状の問題点や最近の政府の政策及び将来の超伝導直流送電導入についての議論を述べる。

日本の電力網の現状

日本の電力供給は、基本的には地域ごとに電力会社がその地域で必要とされる電力需要に応じて発電し、電力供給を賄っている。その地域では賄いきれない一時的な状況（ 設備事故、自然災害、天候等により負荷の大幅な変動 ）でおいてのみ各事業者（ 電力会社 ）間調整を通じて電力融通を行っている。この中で直流送電は主に海底ケーブルによる送電と周波数変換所で利用されている。

海底ケーブルは北海道 – 本州、四国 – 関西の連携に利用されている。海底ケーブルによる送電を行う場合交流を使用するとケーブルの静電容量が大きくなるので、無効電力が多くなり、十分な送電容量が確保できない、そのため直流により送電が行われている。また、日本は東地区の電源周波数が 50 Hz 、西地区の電源周波数が 60 Hz になっている。異なる周波数地区間の電力融通を行うため、3 箇所の周波数変換所（ 新信濃変電所、佐久間変電所、東清水変電所 ）がある。周波数変換器には電流型変換器（ 多励式変換器 ）が用いられている。 60 Hz の交流電力は一旦直流に変換され、再び 50 Hz の交流電力に変換される。短い距離ではあるが周波数変換所で直流送電が行われている。

以下に日本の代表的な直流送電である「北海道本州直流連結設備（ 北本連携 ）」と「紀伊水道直流連携設備」の概要を示す。

「北海道本州直流連結設備（ 北本連携 ）」

北海道本州直流連結設備は函館と上北を結ぶ海底ケーブル 43 km と架空線 124 km で構成された直流連携設備である（ 図 1）。 1979 年に運転を開始し送電容量は 60 万 kW である。高電圧送電では送電損失が小さくなるため、双極 250 kV 、 1200 A の構成で送電が行われている。このため、 3 本のケーブルが敷設され、アース線は断面積が小さくなっている。 2012 年に船舶のいかりで海底ケーブルの 1 本が損傷したが、現在は修復されている。より多く海底送電が行われているヨーロッパではこのような事故が頻繁に生じると報告されている。一方、交流の場合は 1 本が破損しても送電が出来なくなるが、直流送電の場合1本の破損でも送電が可能である場合があり、メリットとなろう。

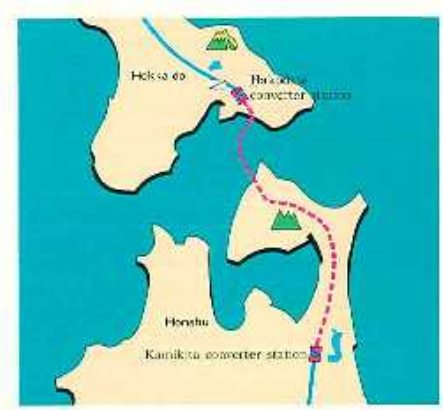

図 1　北本連系ルート図

「紀伊水道直流連携設備」

紀伊水道直流連携設備は四国の阿波と由良を結ぶ海底ケーブル 50 km と架空線 50 km で構成された直流連携設備である（図 2）。2000 年に運転を開始し送電容量は 140 万 kW で、500 kV で送電されている。ケーブル布設は海底を 3 m 堀り、地中に設置されている。これによって、船舶からのいかりや漁船の地引き網などからの損傷を避けている。紀伊水道は船舶の交通量が多く、漁業も行われているので、布設工事は専用海中布設ロボットを開発し、10 日以内という極めて短い工期で海中ケーブルの布設が行われた。

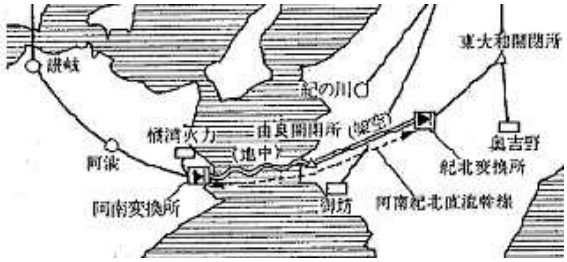

図 2　紀伊水道直流連携設備ルート図

将来の電力網を考える場合出力が不安定な再生可能エネルギーを如何に取り込むかが大きな課題である。日本の再生可能エネルギー利用の現状を簡単に述べる。

日本の風力発電の設備は中国、米国の 1/20 程度（2010 年）と少ない。北海道や東北は風況が良好で、大規模な土地の確保が容易なため風力発電の適地であるが、電力の消費地である首都圏とつなぐ系統の容量が小さく導入拡大が進んでいない。今後北海道を本州と太い幹線で接続することによって、北海道での風力発電の安定利用を促進することができる。また、太陽電池は固定価格買取制度の開始で住宅への導入や、メガソーラー計画に伴い導入量が増えてきているが、電力全体に占める割合は風力発電を含めても約 1% と少ない。

以上のように、現在日本の再生可能エネルギー利用は少ないが今後導入の増加が推進されているため、電力線の幹線を整備し、電力の広域連係による電力調整により電力系統安定化が期待される。また、欧米では不安定な再生可能エネルギーを取り込むための広域的な電力融通が電力市場を介して利用されている。日本では電力を取引する場として日本卸電力取引所があるが、国内の消費電力量に対する取引所取引の比率は約 1% にとどまっており、取引量はヨーロッパ等に比べて極めて少なく、卸電力市場のルール整備も今度の課題である。

最近の日本政府の施策について

日本の電力網の再整備については、2011 年 3 月の東日本大震災と福島原発事故を受けて議論が活発化している。

政府レベルでも、経済産業省・資源エネルギー庁の総合資源エネルギー調査会が 2012 年 2 月から電力システム改革専門委員会を開き、50/60 Hz の連系線の増強を含めた将来の電力網のあり方について検討した。同委員会において、連系線増強については、電力中央研究所が報告を提出し、電力予備率 3% の確保のため、東西連系の FC 容量の現状（120 万 kW）から 90 万 kW 程度の上積みを前提とした既設 FC サイトの増強や日本海方面新規連系など 5 つの案に関する技術的な検討が行われた [1] 。また、送電工事費用については、監査法人トーマツが上記の 5 つの案に関して工事費用の試算をしている（ 表 1)[2] 。なお、同報告においてトーマツは送電網 敷設 コストも試算している（ 図 3) 。

なお、連系線増強で大きなコストを占める変換所導入費用については、中部大学・ JST 共同研究の報告書内で、従来の国内価格に比べて格段に安価な見積もりを ABB 社が提供しており、その工期の短さとともに、今後検討すべき内容である。

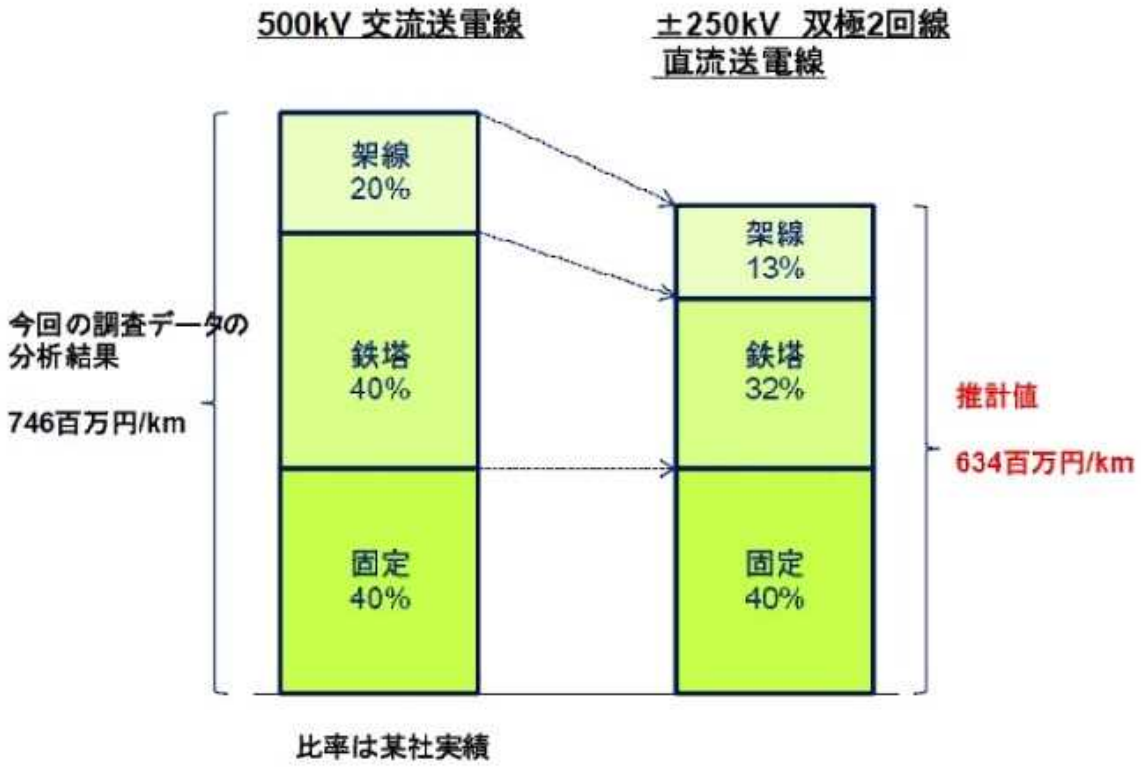

図 3 交流送電線および直流送電線の敷設費用試算

	増強地点	電力会社見積 単位:億円	参考価格 単位:億円	電 見
案A	既設地点 FC増強:90万kW	1,980 (102)	1,936 (100)	
案B	既設地点 直流送電連系新設:90万kW (双極2回線設計)	1,320～1,410 (93～100)	1,417 (100)	
案C	既設地点 FC増強:30万kW 新規連系または既設地点 FC新設:60万kW	1320～1,380 (107～110)	1,202～1,295 (100)	
案D-1	日本海方面連系(東京/中部) 直流送電連系新設:90万kW (双極2回線設計)	1,950～2,500 (83～106)	2,351 (100)	
案D-2	日本海方面連系(東京/関西) 直流送電連系新設:90万kW (双極2回線設計)	2,550～3,550 (78～108)	3,282 (100)	

表 1 連系線増強費用についての費用および工期試算

なお、経済産業省・資源エネルギー庁の同委員会は、2012 年 7 月に最終とりまとめを発表し、送配電分野の改革として、公平性と中立性の徹底を基本原則とし、発送電の機能分離または法的分離を提言している [3] 。今後、発送電分離および電力網整備に関する議論は具体的な検討の段階に入り、来年の通常国会において、発送電分離や中立機関の設置などを含めた電気事業法改正案が提出される見通しである。ただし、電力各社は基本的に民間企業であり、国が電力会社の経営にどこまで直接的な介入を及ぼし得るのか、課題も多い。

さらに、これまでは電力会社の独占的事業であったと言える送電網の整備に関して、新たな動きも始まっている。2012 年 8 月、政府は官民で 3000 億円基金をもとに特別目的会社を設立し、送電線の新設を進める計画を発表した [4] 。同基金は、特に北海道や東北など風力発電の適地への送電網の整備を目指したものである。電力会社による地域独占体制が整備されて以来、国が送電網の整備を支援するのは初めてのことだという。

いずれにせよ、電力会社の地域独占という戦後の電力システムは大きな変革を求められているのは確かである。数年前であれば、直流 (超伝導) 送電の社会実装という論点は議論の対象にさえならなかったであろうが、現在は国民生活にとって喫緊の課題となっている。技術的・経済的・社会的観点から開かれた議論を継続することが求められる。

超伝導直流送電の導入

第一部でも書いたように、ヨーロッパでは再生可能エネルギーを最大限導入するに広域連携を行っていて、長距離送電や海を渡っての送電も必要になるため、直流送電の導入が行われている。直流送電は送電ロスを最小限にすることや電力網での事故を他の電力網に伝搬させないので、導入が広く進んでいて、今後の増強が予定されている。この特長は日本でも当然生かすことができる。

前節までで述べたように、日本の電力会社間の電力融通は大きくなく、電力網はそれぞれの電力会社でほぼ閉じるような運用がされてきた。このため、再生可能エネルギーの利用は広域連携ではなくて、二次電池を利用した安定化などの研究開発が進められてきた。電力会社間の電力融通を長距離送電によって大きくすると、再生可能エネルギーだけでなく既存の火力発電所や水力発電所の設備利用率や効率改善などにつながる。日本では今まで電力会社間をまたがる広域連携がほとんど行われてこなかったので、直流送電を本格的に導入すれば、ヨーロッパ以上にメリットが大きいと思われる。

さらに、日本では周波数が 50 Hz(東日本) と 60 Hz(西日本) で分かれていて、ヨーロッパ (50 Hz) や米国 (60 Hz) のように単一周波数で送電網が作られていない。このため、周波数が異なる地域をま

たがって送電を行うために今までは周波数変換所が建設されてきた。一方、直流送電は「交流を一度直流に変換し、送電を行い、再び直流を異なった周波数の交流に変換する設備」であるため、直流送電は基本的に周波数変換所の設備に送電線を接続したことになる。このため、日本での直流送電導入はヨーロッパや米国以上のメリットがあるはずである。

さて、限られた予算内で日本の電力網の新たな建設や整備を行うためには、設備や工事を安価に仕上げるだけでなく、各種法規制を満足する必要がある。架空送電線を建設するには、下記の 18 の法規制をクリアする必要がある。電気事業法関係＊，航空法関係，電波法関係，自然環境保全法，自然公園法，都市公園法，都市計画法，森林法，農地法，砂防法，地滑り等防止法，道路法＊，河川法，海岸法＊，文化財保護法，鳥獣保護法，環境影響評価法＊，種の保存法＊である。なお、＊印は高速道路に地中送電線を埋設する場合に係わる法規制であり、全部で 5 つと大きく減る。

このため、日本では架空送電線を新たに建設するには多くの地権者の同意を取り付けることも相まって、極めて長い時間が必要である。このような状況はヨーロッパでも同様であり、実質的に新しい送電線を短い期間で建設することは極めて困難と聞いている。

このような事態を回避するアイデアとして、高速道路や線路に沿った送電線の地中化がある。例えば、高速道路に埋設する例を図 4 に示す。図中にケーブルを埋設する場所を示した。橋桁下やケーブルトレイ、サービストンネル及び歩道や盛り土部分への直接埋設なども想定される。これ以外にも設置場所は複数あろう。また、高速道路は日本各地に延びている上に地権者が少数で明確であるため、導入交渉も行い易いであろう。この状況は鉄道路線に導入する場合もほぼ同じである。

図 4　高速道路に設置した場合（四角や濃い灰色の断面でケーブル部を示す）

送電線の地中化は大都市では広く行われているが、一般に架空線より高価と言われている。架空線では鋼芯アルミ裸線が使われることが一般的である。安価なアルミを利用し、強度を補強するために中心部に鋼芯を入れてある。そして、導体表面には電気絶縁を行わないため、裸線とも呼ばれる。通電によって発熱するが、電気絶縁物で被覆してないため空気によって直接冷却される。一方、地中に設置するには導体を電気絶縁する必要があり、導体は厚い電気絶縁物で覆われている。これは、送電線の高い電圧に耐えため、数百 km に渡ってピンホール一つもない。このため、絶縁電圧が高くなるとケーブルは急に高価になる。さらに、一般に電気絶縁物の熱伝導率は低いため、電気絶縁部表面を空

冷しても内部の導体温度はあまり下がらない。また、地中に設置するため空気が循環することによる冷却の効果も少ない。このため、通電電流は架空送電線よりかなり下がるため、導体部分も高価になる。そして、地中ケーブルでは、高電圧利用が制限される。

以上の状況で超伝導ケーブルの導入のメリットを考える。最初に、超伝導ケーブルは低温冷却の必要があるため、裸線は使えない。超伝導では直流電気抵抗が完全にゼロになるため、高電圧を利用する必然性が低い。これはケーブルだけでなくて、直流と交流を変換する電力変換器のコストに大きく関係する。一般に、電力変換器コストは電圧が低いと安価になる。また、最近開発が進んでいる電圧型電力変換器では、半導体素子に IGBT が利用され、多端子電力網の構築が可能になるが、サイリスターを利用する電流型電力変換器に比べてケーブル電圧は下がる。つまり、超伝導ケーブルを導入すれば電力変換器コストが低減され、電力変換器機能を向上させることが可能になる。距離が 200 km 以下であれば、電力変換器コストは送電システム全体コストの半分以上を占めるため、この特長は導入理由として重要である。

もう一つの特長は電力送電密度が高いため、ケーブルが小型になることである。これは交流超伝導ケーブル導入に当たっても最も重要な特長として言われてきた。しかし、交流超伝導ケーブルに比べて、直流超伝導ケーブルは数倍から一桁近く電力送電密度を高くできる。したがって、地中の送電線路がよりコンパクトになる。縦横 1 m ほどの線路があれば、数 GW の送電も可能になり、工事費の節約につながろう。さらに、交流損と言われる超伝導ケーブルシステムの発熱がほとんどないため、現状では冷凍機能力は半分以下になり、冷凍循環系コストを大きく下げる。

このような直流超伝導送電の特長は世界広く利用できるため、日本での開発と導入を進めれば、日本の重要なインフラ輸出産業になることが期待できよう。

謝辞

本調査研究には国内外の多くの関連機関の皆様から多大なご協力をいただいた。特に、ヨーロッパの調査は ABB 社に負うことが多い。以下に記して、深く感謝申し上げたい。（以下、敬称略、五十音順）

ABB 株式会社、Enel 社、J-Power（電源開発株式会社）、REE 社、Tennet 社、一般社団法人日本卸電力取引所、学校法人中部大学、学校法人明治大学、株式会社クリハラント、株式会社シーテック、株式会社東芝、株式会社前川製作所、株式会社三菱総合研究所、関西電力株式会社、住友電気工業株式会社、独立行政法人科学技術振興機構（JST）、みずほ情報総研株式会社、三菱電機株式会社

なお、中部大学と科学技術振興機構（JST）の 2011 年度に行われた共同研究「高圧直流超伝導送電の社会実装に関する調査研究」の報告書を入手したい方は中部大学・超伝導センターにお問い合わせ下さい。

【参考文献】

[1] 経済産業省・資源エネルギー庁総合資源エネルギー調査会総合部会電力システム改革専門委員会（平成 24 年 3 月 26 日）、「参考資料 1 ：送電線工事費用と期間に関する考察（有限責任監査法人トーマツ）」（http://www.meti.go.jp/committee/sougouenergy/sougou/chiikikanrenkeisen/003_s01_00.pdf）

[2] 同上（平成 24 年 3 月 26 日）、「参考資料 2 ：連系線増強の技術的実現可能性検証報告書（(財）電力中央研究所）」

(http://www.meti.go.jp/committee/sougouenergy/sougou/chiikikanrenkeisen/003_s02_00.pdf)

[3] 同上（平成 24 年 7 月）「「電力システム改革の基本方針」について」（http://www.meti.go.jp/committee/sougouenergy/sougou/denryoku_system_kaikaku/pdf/report_001_00.pdf）

[4] 日経新聞 2012 年 8 月 22 日付け記事

SUPERCOM
SUPERCONDUCTIVITY COMMUNICATIONS
超電導コミュニケーションズ
Vol.21 No.4 August 2012 通巻117号

SQUID-TEMによる鉱物探査試験始まる！

__超電導工学研究所、三井金属資源開発、JOGMEC__

(公財)国際超電導産業技術研究センター超電導工学研究所は三井金属資源開発（株）と共同で、JOGMEC((独)石油天然ガス・金属鉱物資源機構)からの委託研究「次世代 SQUITEM 機器開発・SQUID 磁力計開発」により、地下資源探査への応用を目指した高温超電導磁力計を開発している。その経過や成果が 2012 年春季応用物理学関係連合講演会、HTSHFF(High Temperature Superconductors in High Frequency Fields)2012 （本号会議報告参照)で発表された。 (2 ページに続く)

鉄系超伝導体と関連化合物に関する最近の話題

__中国科学院ほか__

鉄系超伝導体は、正方格子状に配置された Fe^{2+}イオンを基本構造としており、その上下に配置されるアニオンとブロック層の種類により様々な物質が報告されている。AFe_2Se_2(A = K, Rb, Cs)系 [1]や Ca-Pt-Fe-As 系超伝導体[2]の発見以降新物質の報告は途絶えていたが、最近新たに $Ba_2Ti_2Fe_2As_4O$（著者らは 22241 と呼称）が発見された。 (4 ページに続く)

＜解説＞ CERN-LHC 超伝導加速器による『ヒッグス粒子とみられる素粒子』の発見

山本 明、中本建志 (KEK)

欧州合同原子核研究機関(CERN、ジュネーブ)において、大型ハドロン衝突型加速器(Large Hadron Collider: LHC)が、1994 年の建設決定以来、14 年の歳月を経て 2008 年に完成した。円周 27 km におよぶ粒子加速器は、7,000 台を越える様々な超伝導磁石、加速空洞システムによって構成され、超伝導技術が本質的な役割を担っている。稼働直後に発生した超伝導ケーブルの焼損インシデントに対応した一時運転停止を乗り越え、2010 年春から、新たなエネルギーフロンティアにおける素粒子物理実験が順調に進展している。 (5 ページに続く)

＜解説＞ ヨーロッパの電力網の紹介

中部大学・超伝導センター 山口作太郎
みずほ情報総研・サイエンスソリューソン部 石原範之

この記事は、中部大学と科学技術振興機構(JST)の 2011 年度に行われた共同研究「高圧直流超伝導送電の社会実装に関する調査研究」の報告書要約であり、2 回に分けて発表することにした。第一部として「ヨーロッパの電力網の紹介」と題して、主にドイツ、スペインを中心にしてヨーロッパの電力網を紹介する。この中では再生可能エネルギーの導入を積極的に進めている両国がどのように電力網を構築しているかについて紹介を行う。また、「日本での直流幹線導入の可能性（仮)」と題した続編を本誌 10 月号に掲載予定であり、そこでは日本国内に直流送電網を導入するメリットや課題などについてまとめると同時に直流送電への超伝導技術の適用を検討する。 (12 ページに続く)

＜解説＞　ヨーロッパの電力網の紹介

中部大学・超伝導センター　山口作太郎
みずほ情報総研・サイエンスソリューソン部　石原範之

(1 ページより続く)

はじめに

本調査研究は平成 23 年 3 月 11 日の東日本大震災（以下 311 震災）及びそれによる東京電力福島第一原子力発電所の事故がきっかけになった。議論は、50 Hz-60 Hz の周波数変換所を安価に短い建設期間で作ることから始まり、日本のエネルギー供給をどのように行うかについて議論を行った。海外でも 311 震災を受けて、ドイツではメルケル首相が 2022 年までに原子力発電所を全廃し、再生可能エネルギー(RE)の大規模利用を国家目標として掲げた。そして、インターネットなどでの調査では、スペイン(全土で関西電力程度の規模)では現状で全電力の約 20%が風力発電から得ていることが分かった。そして、今後も増強する方針とあった。一方、日本では RE は出力が不安定であるため、全電力の 3%程度が安定に利用できる限界であると言われ、NEDO では 2 次電池による出力安定化研究開発が長く行われてきた。RE は火力や原子力に比べて元々高価であり、2 次電池を安定化に利用すれば、ますます電力料金は高くなる。このため、再生可能エネルギーは経済的理由で広く利用できないというのが「日本の常識」であった。しかし、ヨーロッパの状況は全く異なるようである。これは、経済合理性に反し、国の基本方針として間違っているように思われる。しかし、そのような非合理的な政治判断をドイツやスペインが何故行うかについては、調査が必要であろう。これがヨーロッパの電力網を調査し、その結果を報告する理由である。

本調査研究には国内外の多くの関連機関の皆様から多大なご協力をいただいた。特にヨーロッパの調査は ABB 社に負うところが多い。以下に記して、深く感謝申し上げたい。(以下、敬称略、五十音順)
ABB 株式会社、Enel 社、J-Power (電源開発株式会社)、REE 社、Tennet 社、一般社団法人日本卸電力取引所、学校法人中部大学、学校法人明治大学、株式会社クリハラント、株式会社シーテック、株式会社東芝、株式会社前川製作所、株式会社三菱総合研究所、関西電力株式会社、住友電気工業株式会社、独立行政法人科学技術振興機構(JST)、みずほ情報総研株式会社、三菱電機株式会社

ヨーロッパの電力広域連携

ヨーロッパでは各国の電力網が密接につながっており、一国で電力の安定供給が出来なくなった場合でも、周辺国から電力を融通することで電力の安定供給を図っている。図 1 に周辺地域を含めたヨーロッパの電力連携網の現状を示す。電力網は、主に 4 つのグループ(ドイツ・フランス・スペインなどからなる「大陸部」、スカンジナビア半島を中心とした「北欧部」、英国、アイルランド)に分かれており、最も大きな「大陸部」の発電量は、日本の電力の約 2 倍にあたる 2400 TWh である。

広域連携により、各国の電力を融通

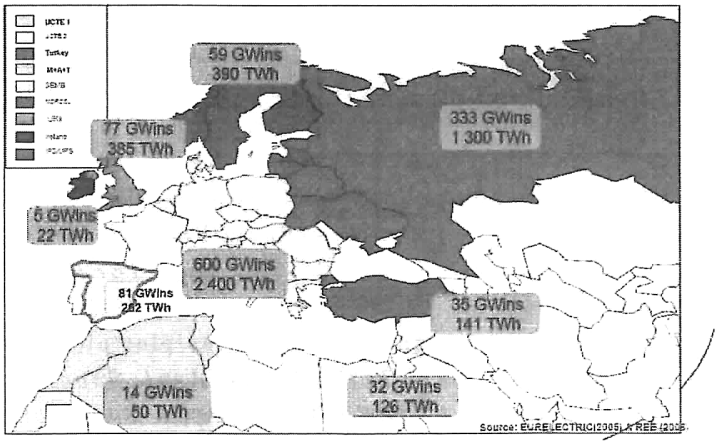

図 1.　ヨーロッパ周辺の電力広域連絡網
(出典)Integration of large scale wind in the grid
– The Spanish Experience. REE 社.2008

することで、火力、水力、原子力などの発電設備の構成のバランスを取り、電力安定化に努めている。また、ヨーロッパでは卸電力取引市場が発達しており、実時間での需給調整が可能な時間前取引が行われており、実時間系の接続による広域連携が電力の安定運用に貢献している。

直流超電導送電の導入を検討するにあたり、出力が不安定な再生可能エネルギー(RE)との接続は大きな課題である。以下で RE 導入が進んでいるドイツとスペインの導入状況を述べ、直流超伝導送電導入の市場と成りうるヨーロッパの直流送電設備の導入状況および計画を述べる。

ドイツの再生可能エネルギー利用

ドイツでは 2014 年までに北海沖に原発 8 基分(800 万 kW = 8 GW)に相当する洋上風力発電設備の導入が進められ、最終的には洋上風力は 21 GW を導入する予定である。陸上に設置する風力発電は 25 GW を建設する計画である。図 2 に導入計画の図を示す。日本に比べて 1 つの発電所で 1 桁から 2 桁以上大きな導入量である。

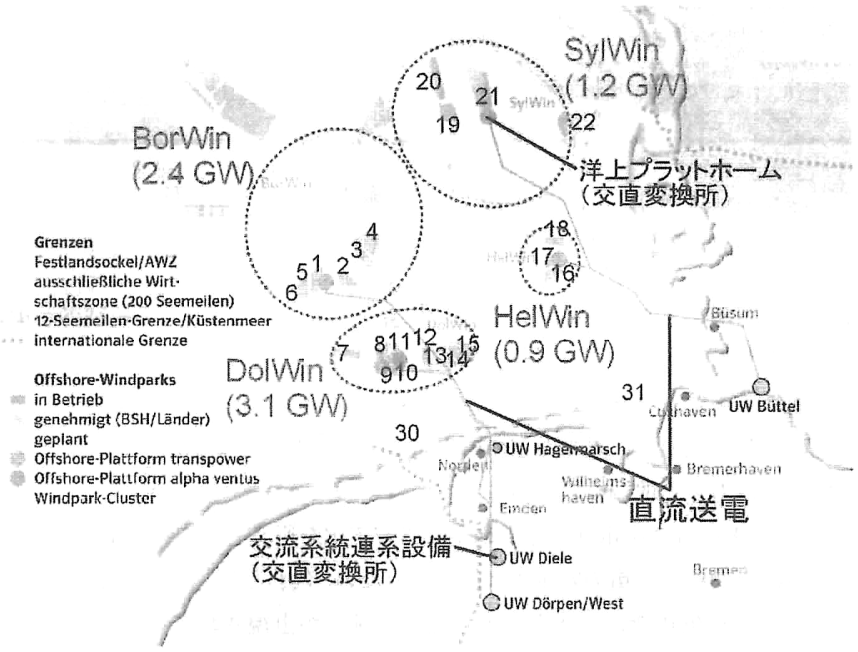

図 2.　ドイツにおける北海沖大規模洋上風力発電導入計画

(出典)ドイツの送電会社 TenneT 社からの資料

風力発電コストは太陽光発電コストより安価のため、再生可能エネルギーとしては風力発電が主であり、太陽光発電が電力網の中で占める割合はそれほど大きくはない。今後、技術開発によって、風力発電及び太陽光発電はより安価で高性能になると考えられ、研究開発が行われている。

ドイツは RE の固定価格による買い取り制度により、電力需要の少ない時間帯でも風力発電の電力を買い取る必要がある。余剰電力は揚水式水力発電(揚水発電)による電力貯蔵設備の建設が検討されている。北海沖で発電した風力による電力が長距離直流送電によりドイツ国内を南下してスイスまで送電・貯蔵され、ドイツ国内で電力を使うときは再び北上して消費されることになる。現状では、導入実績と経済性を考慮した場合、長距離直流送電と揚水発電による電力貯蔵の組み合わせが最善の策と考えられている。一方、太陽光発電はコストが高いため、全量買い取り制度について再検討が行われていて、複数の案が提案されている状況である。

スペインにおける再生可能エネルギー導入と電力系統制御

スペインは世界第 4 位の風力発電の導入国であり、2011 年 3 月には月平均で約 21%と風力が最大の動力源となった。さらに、瞬間的には電力の 6 割近くを風力発電でまかなっているような場合もある(2011 年 11 月 6 日 2:00 には需要に対する風力発電の供給量が 59.6%となっている(図 3))。

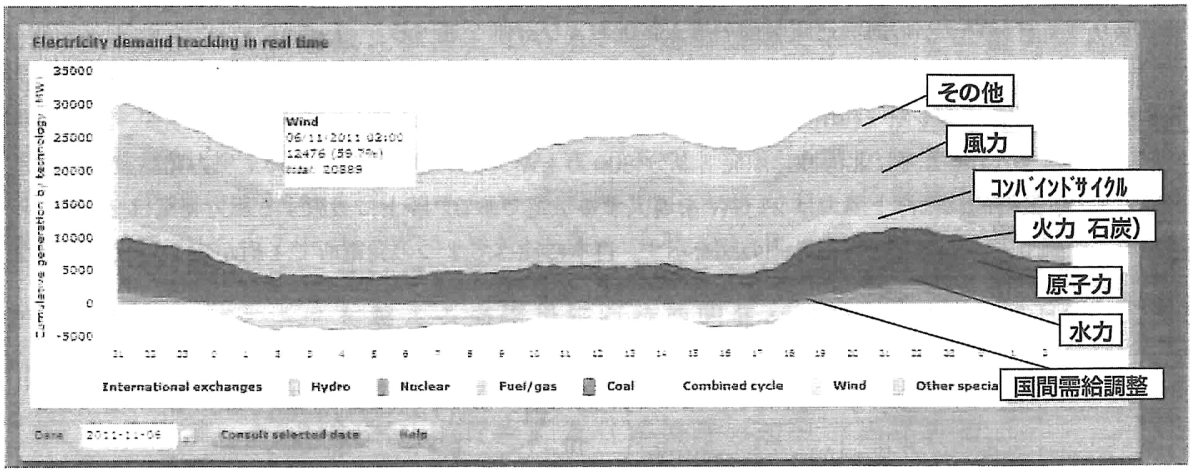

図 3.　2011 年 11 月 6 日の動力源別発電量推移
(出典)REE 社ホームページより

出力が不安定な再生可能エネルギーの導入割合が大きいスペインでは電力系統制御が重要となる。スペインでは単一の系統運用会社(REE 社)が電力系統全体の制御システムを運営し、そのシステムの配下で「CECRE(再生可能エネルギーコントロールセンター)」が再生エネルギーの制御を行っている。CECRE はマドリッド郊外にあり、風力、太陽光などの再生可能エネルギーとコジェネレーションを対象として、電力需要に応じて発電電力を管理調整している。

また、再生可能エネルギーは 2 次電池などを利用して安定化を行うとさらに電力料金が高価になるため、スペインでは 2 次電池を使用した電力安定化は行っていない。代わりに、電力の安定的な需給管理のため、「需要予想」に加えて、再生可能エネルギーの「発電予測」が重視されている。発電予想に関し、2009 年の平均予測誤差は、24 時間先で 20%以内、二乗平均誤差で 5%以内であり、現在も精度向上に努めている。電力需給バランスは、主として水力・火力発電により調整が行われているが、これに加え国際間での電力の売買や揚水発電(~4 GW)による電力貯蔵で調整し、安定供給を行っている。スペインで大規模な風力発電が可能になった理由としては以下の 5 つの点が挙げられる。

①風力発電適地が多い
②二次電池ではなく、広域連携を利用して安定供給を行っている
③電力卸市場の整備が進んでいる
④再生可能エネルギーの発電予測技術が進んでいる
⑤制御指令系統が整備されている

ヨーロッパの直流送電設備の導入状況および計画

今後、直流超伝導送電の市場と成りうるヨーロッパの直流送電設備の導入状況および計画を以下に述べる。EU は 1990 年代からエネルギー市場を自由化し、市場を統合する指令を定めた。発電、送電、配電の分離、送電系統運用者(TSO)などを設置するなど、電力市場の独立性を進めた。送電設備は公共性が高

く、系統の域内の送電系統運用者が建設し維持している。しかし従来型送電設備の建設には用地買収、環境評価、地元への対応などが必要で長期間を要すため自由競争下では投資のインセンティブが働きにくい。一方、欧州では国際間の電力取引が増え、送電容量が不足してきており、送電線の新増設が問題になっている。

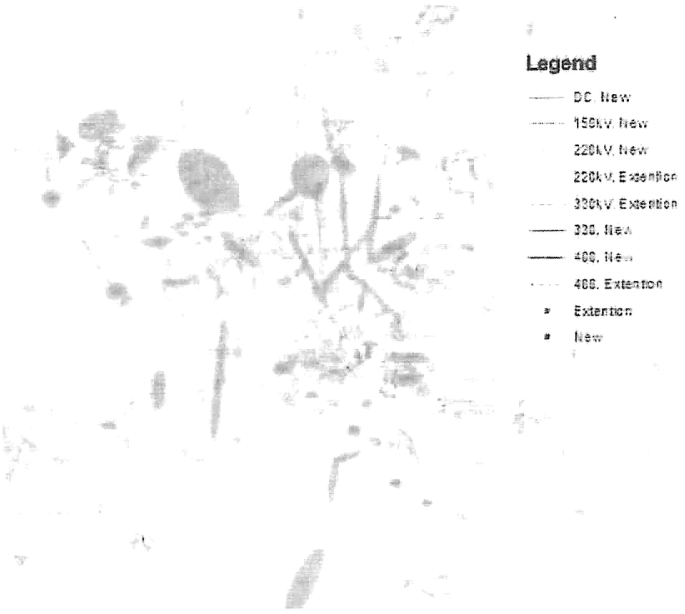

図 4. ENTSO-E の送電網計画

4 ヵ国 41 の送電系統運用者が加盟する ENTSO-E は 2 年毎に 10 年間の系統開発計画“Ten-Year Network Development Plan(TYNDP)”を発行している。2012 年 3 月に発表されたドラフト版によると、今後 10 年間で 100 を超える送電線の新設・改修案件が計画されており、送電距離長では 5 万 km にも達する(図 4)。およそ 40%が国家間の相互接続である。また、交流系統が大半の 39,000 km を占めるが、12,600 km は直流送電による連結である。直流送電案件の内訳の多くは海底接続への投資であり交流では代替できない。一方、内陸部の系統の相互接続は交流系統に平行する直流送電で計画されている。投資金額は約 1040 億ユーロ(約 11 兆円)にのぼる。うち約 301 億ユーロが原子力発電を 2022 年までに全廃すると決定したドイツからであり、190 億ユーロが大規模洋上風力発電設備を進める英国の予定投資金額である。

洋上風力発電所からの送電には自励式直流送電による接続例が多くある。接続距離が 100 km を超える場合はこの方式がただ一つの選択肢となる。利点としては事故があった際に交流側と直流側互いに波及しないこと、各国のグリッドコードを準拠できること、洋上風車の要求仕様を緩和できること、将来の直流グリッドに組み込めることなどである。また、欧州では直流送電によるグリッドの相互接続も多く、直流送電は環境負荷への配慮、長距離接続、非同期系統接続、異なるグリッド規定やグリッドコードへの解決策となるなどのメリットが直流送電にはある。

ヨーロッパの将来構想

2009 年 7 月にドイツの企業が中心になり、Desertec foundation が設立された。この構想は、2050 年までにヨーロッパの電力需要の 15%をサハラ砂漠や北海からの再生可能エネルギーからの発電電力で賄おうとするアイデアである。構想全体図を図 5 に示す。

発電には Solar Thermal Power Plant(太陽熱発電)とあるが、一般には CSP が使われる。これは、Concentrated Solar Power の略である。太陽光発電(Photovoltaics, PV)、風力(Wind)、水力(Hydro)、バイオマス(Biomass)、地熱(Geothermal)が想定されている。当初の見積もりでは 550 Billion 米ドルであった。現在では 1000 Billion 米ドルとも言われている。これは当初建設費の 90%が発電設備に投入し、10%を送電設備に投入する予定であったが、ヨーロッパ内での送電投資が大きくなることが分かったため急遽予算を大きくなった。このため、全体として必ずしも予算が確保されているわけではないようである。部分的に 2020 年の送電開始を目指している。さて、送電は鉄塔架空線を利用した超高圧直流送電(super grid と呼ばれる)となっている。本構想の理由は以下のようである。

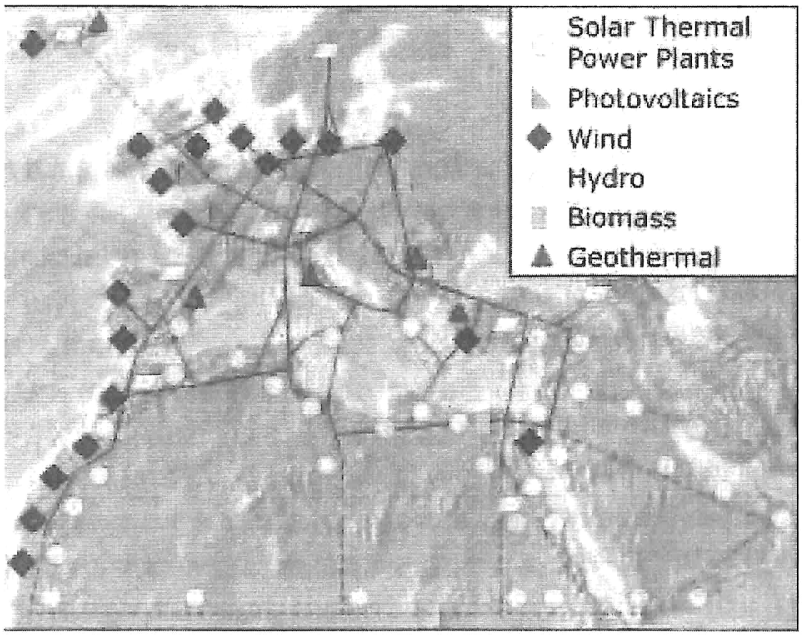

図 5.　Desertec 構想（http://www.desertec.org/）

1)　気候変動への対処
2)　増大する電力需要への対応
3)　老朽化が進む電力網への対応
4)　新しい技術の取込
5)　エネルギー安全保障
6)　マグレブ諸国及びアフリカの経済開発

既に、ドイツでは企業、大学、政府のチームがあり、マグレブ諸国との交流が始まっている。特に、日本の 311 震災の後、2022 年までにドイツは原子力発電所の全廃を行うことをメルケル首相が公表し、その実現のために、検討を加速させている。その中には、ドイツの IASS(Institute of Advanced Sustainability Studies)を中心に送電に直流超伝導送電を利用する検討も進んでいる。これは高温超伝導技術の進展が著しく、架空線を利用する HVDC を超長距離送電には以下の課題があるからである。

1)　エネルギー輸送の安全確保
2)　地中海をどのように渡るか？
3)　送電ロスの低減とコスト削減

架空線はガイシを利用して電気絶縁を取っているので、比較的安価に建設できるが、ガイシを射撃すれば容易に送電を止めることができる。つまり、テロに弱い。さらに、中国などでは冬季の強風や雪などによって送電線鉄塔の倒壊があり、ケーブルを用いた地中化が必要と言われている。一方、超長距離を低損失で送電するための超高圧(UHV)送電にケーブルを用いると、電気絶縁に高度な技術が要請され、著しくケーブルが高価になる。そして、海中を通す UHV ケーブルはさらにコストが上昇するので、低電圧(≦200 kV)でも損失が少ない超伝導直流送電が期待される。電圧が低くなると、電力変換器への技術的要請も低減し、コスト低減につながる。

一方、アルジェリア等の産油国でも再生可能エネルギー開発に強い期待を寄せている。その主な理由は下記のようである。

1)　産油国は、原油の枯渇に備えた産業育成が最大の長期的国家戦略の柱になっている
2)　マグレブ諸国では失業率が高く、社会不安の要因となる一方、産油国は手持ち資金がある

3) ヨーロッパに地理的に近い

現在、ヨーロッパでは2050年での再生可能エネルギーの割合が40%から80%程度で色々なシナリオが検討されていて、上記に述べたようにその中には「超伝導直流送電」も重要な技術としてドイツでは複数の国立研究所でプロジェクトが始まった。そして、北海やバルティック海での洋上風力開発を精力的に進めている。前節でも述べたように、この電力は直流送電で陸上まで送るだけでなく、スイスまで送電されて、これから建設される揚水発電所で安定化される予定である。つまり、再生可能エネルギーの大規模な利用は、広域連携を行うために必然的に長距離送電を必要とし、送電ロスを下げることが求められる。このため、超伝導送電技術の応用範囲は極めて広汎と言えよう。

《会議報告》

11th International Symposium on High Temperature Superconductors in High Frequency Field, [HTSHFF2012] (2012.5/29-6/1@宮城県松島町　ホテル松島大観荘：主催 HTSHFF2012 実行委員会)

HTSHFF は 2 年に 1 度欧米で開かれてきた、高温超伝導体の高周波領域に関するコンパクトな国際シンポジウムである。11 回目にして初めてアジア(日本)で開かれることが、2010 年の米国サンディエゴの大会で決定された。日本で開くにあたり、震災の復興のサポートになることを念じて松島で開くことにした。この会議は、参加者全員が同じホテルに宿泊し、朝から夜までディスカッションを繰り広げ、研究の情報交換と親睦を深めることを目的としている。今回は約 70 名の参加者があり、講演数は４９であった。海外からは、米国、中国、韓国、ニュージーランド等から 12 名の参加があった。今回のシンポジウムでは主に、①高温超伝導薄膜のマイクロ波の基礎と応用、②HTS-SQUID の基礎と応用、③超伝導 THz 発信とその応用、④日本の超伝導エレクトロニクスプロジェクトの紹介、に分類される内容を集めた。その中で、印象に残った講演を幾つか紹介したい。①では、オーストラリアの James Cook 大学の Mazierska 教授が移動体通信基地局に超伝導フィルタを設置した場合の有効性をシミュレーションで示し、応用の可能性を示した。また、東芝の加屋野氏は気象レーダに用いる超狭帯域フィルタに超伝導フィルタを利用する応用例を紹介し、注目された。②では豊橋技科大の田中教授が High- T_c SQUID を用いた金属異物検査技術について、ISTEC の波頭博士は High-T_c SQUID を用いた地下資源探索の実例を紹介した。様々な分野で SQUID が実用化されつつあることが印象付けられた。③の分野では、NIMS の Wang 博士が高温超伝導の固有ジョセフソン接合から狭帯域のテラヘルツ波が発信されることを紹介し、また阪大の斗内教授は高温超伝導薄膜からのテラヘルツ波発振について発表した。④については、現在進行している４つの超伝導プロジェクトを紹介していただいた。名大の藤巻教授より単一磁束量子デバイスについて、名大の生田教授より鉄系

図 1.　HTSHFF2012 の参加者写真

超伝導ビームラインとして2008年末に完成した。2009年からのビーム運転では2011年3月11日の東日本大震災による約10ヶ月の中断を除けば、安定的に運転が行われ、J-PARCでのニュートリノ振動実験に貢献している。

参考文献

[1] M. Furusaka, et al., “The joint project for high-intensity proton accelerators”, *KEK Report 99-1; JAERI-Tech 99-056; JHF-99-3*, 1999.

[2] Y. Itow et al., “The JHF-Kamioka neutrino project”, *hep-ex/0106019*.

[3] T. Ogitsu, et al., “Superconducting Magnet System at the 50 GeV Proton Beam Line for the J-PARC Neutrino Experiment”, IEEE Trans. on Appl. Spercond. **14** (2004) 604-607.

[4] T. Nakamoto, et al., “Development of Superconducting Combined Function Magnets for the J-PARC Beam Line”, 第 3 回加速器学会年会プロシーディングス, (2006) 67-69.

[5] Y. Makida, et al., “Cryogenic system for J-PARC neutrino superconducting magnet beam line – Design, construction and performance test”, Advances in Cryogenic Engineering. AIP Conference Proceedings, **1218** (2010) 531-538.

[6] 木村 誠宏, その他; 技術ノート “超伝導磁石システム用作動圧力可変型クエンチ放出弁の開発”,低温工学 第 45 巻 (2010) 199-203.

[7] K. Sasaki, et al., “Commissioning Results of Superconducting Magnet System for the Neutrino Beam Line”, *IEEE Trans. on Appl. Supercond.* **20** (2010) 242-245.

(6)直流超伝導送配電システムの研究開発とその役割

Development of DC Superconducting Power Transmission and Distribution System and Its Role in Society

中部大学・超伝導センター
山口 作太郎, 浜辺 誠, 渡邉 裕文, 河原 敏男
Center for Applied Superconductivity and Sustainable Energy Research (CASER), Chubu University
S. Yamaguchi, M. Hamabe, H. Watanabe and T. Kawahara

1. はじめに

高温超伝導体(HTS)が発見される前から金属系超伝導体を利用し、冷媒に液体ヘリウムを利用する超伝導マグネットは加速器や医療用では利用されていた。これは「直流」で利用され、ヘリウムを利用するシステムでも十分に経済性があることや、他技術の置換えが不可能であったためである。このため、金属系材料を使った超伝導ケーブルの開発は直流、交流を問わず複数の国で行われたが、何れも計画が中止された。理由は低温保持の電力が大きいことや資源としてのヘリウムの希少性と高価格のためと思われる。このため、HTSが発見され、液体窒素(LN_2)で超伝導が利用できる可能性が高まると、かかる問題が容易に解決されると多くの研究者が考え、多くの国ですぐに超伝導ケーブルの開発計画が再開された。そこでは、冷凍機の消費電力の軽減と、液体窒素利用が前提となった。

HTS発見後の超伝導ケーブルの研究開発は交流ケーブルからはじまった。これはほとんどの送電ケーブルが「交流」であったことが理由である。つまり「交流」ケーブルでないと、使い道が無いか、大きな開発費を投じることができないという側面があった。

2. 中部大学での応用超伝導研究開始について

中部大学では2000年から文部科学省の援助を受けて応用超伝導研究がはじまった。その当時、山口は核融合科学研究所に所属をしていたが、飯吉厚夫学長(現在は理事長)から、中部大学の計画を手伝うようにといわれて、超伝導送電の研究を行うための予備研究から始めた。計画がスタートした後の2001年からは山口は中部大に移籍し、計画に加わった。この計画では、端末での熱損失低減をペルチェ効果によって実現する「ペルチェ電流リード」の実験から始めることにした。同時に、直流超伝導送配電の検討を本格的に

始めた。直流を選択した理由は下記のようである。

1) 既に多くの研究者が交流ケーブル研究に関与し、山口等が新たに交流ケーブルを初めても「特徴」を出すのが困難と思われた。
2) 技術上、超伝導ケーブルは原理的に「直流」が得意である。
3) 今後利用が進む再生可能エネルギーの主体となる太陽電池や風力発電は「直流」送電との親和性が高い。
4) 大電力長距離送電は既に「直流」がヨーロッパや中国で広く使われていて、今後も導入が増えることが予定されていた。
5) ハイブリッド車が日本で開発され、交流・直流を変換する電力変換器コストが急激に下がった。
6) 家庭、オフィス及び工場での電力最終需要のほとんどが「直流」である。

等である。

そして、2005年から文部科学省の援助を新たに得て、HTSテープ線材を利用した20 mケーブル実験装置を建設した。これは、前年には住友電工のビスマス系線材臨界電流が100 Aを超し、工業利用の可能性が急激に高まったことも技術的な背景となる。

3. 20 mケーブル実験装置について

中部大学では2005年から文部科学省の援助を得て、20 m級直流ケーブル実験装置を建設した。図1に装置写真を示す。浜辺は「装置建設」の頃に研究グループに加わった。この装置では次の項目の検討を主に行った。

1) ペルチェ電流リードの組み込みによる熱侵入量低減を実験 [1, 2]
2) HTSテープ線材の偏流防止を電流リード抵抗法によって実現し、その効果の計測を行う[2]
3) 断熱2重管にストレート管を利用し、ベローズ管で熱収縮を吸収する[3]
4) ケーブルの臨界電流測定だけでなく、HTSテープ線材単体の臨界電流測定を単独で行うこと[2]
5) ケーブルの熱収縮への対応 [4]

などである。

以上の目標の設定には、山口が夏にMITに滞在して構想を練った。

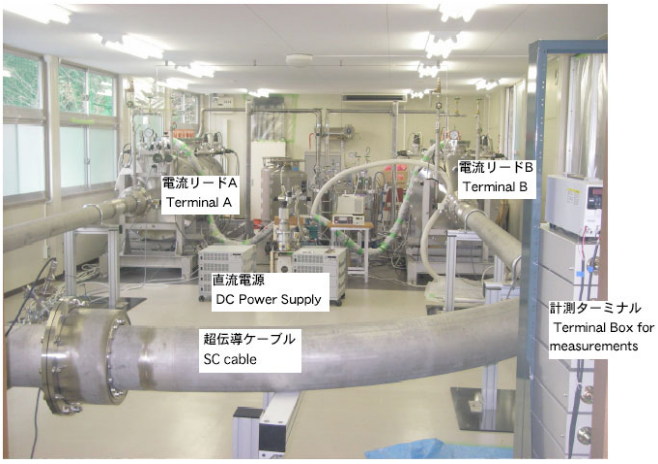

図1. 20 mケーブル実験装置写真（2006年10月）

これらの実験結果は既に論文発表で説明しているが、今後ケーブルが長くなるにつれて偏流問題[5]が顕在化する可能性があるので、説明を以下に行う。図2はケーブルを構成するHTSテープ線材と端末部での電流リードの素線との接続を模式的に示している。

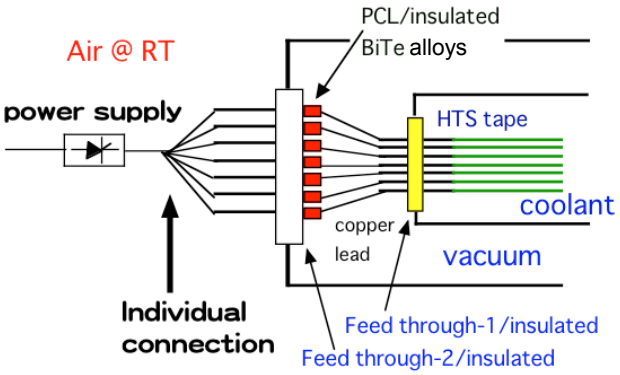

図2. 電流リードでの接続方法

偏流問題とは、多くの並列接続された超伝導素線に流れる電流が均一にはならないことを指す。大電流が流れる素線は常伝導転移しやすく、常伝導になると電流が著しく減少するため、他の素線電流が急激に上昇し、最終的には超伝導マグネット全体がクエンチすることがある。このため、今までに多くの研究が行われてきた。偏流は超伝導素線の電気回路での抵抗が極めて低く、その値のバラツキがあると直流でも発生する。つまり、超伝導素線は電気抵抗がゼロであるが、素線接続部の有限電気抵抗が存在し、それは極めて低いが半田などによって接続すると、接続抵抗は1桁以上変動する。一般に接続部の抵抗は低い方が良いので、ある値以下とするのが工業的基準である。しかし、それぞれの素線電流は接続抵抗比で分配されるので10倍以上の違いが生じる。素線電流に大きな差が生じることは、超伝導機器の安定性には好ましくなく、で

きるだけ均一にすることが望ましいが極めて小さな接続抵抗を均一に制御することは困難である。しかし、図2のように電流リード素線とHTS素線をそれぞれ接続すると、HTSテープ線材の接続抵抗に比べて電流リード素線の抵抗は数桁以上大きいので、それぞれの超伝導素線電流は電流リード素線の抵抗比で決まる。このため、偏流が生じない。今後ケーブルが長くなると接続部が増えるため、このような対策は必要不可欠になろう。尚、この偏流問題は交流ではより起こりやすい。

4. 200 mケーブル実験装置について

20 mケーブル実験装置では短尺ケーブルで可能な実験を行った。特に、電気的特性は接続部を除けば短尺ケーブルでも十分な場合が多いが、熱・機械的な特性は長尺ケーブルで実験を行う必要がある。幸いナノオプト・エナジー社（藤原洋社長）から中部大学に資金提供があり、200 mケーブル実験装置を建設が可能になった。実験装置写真を図3に示す。

図3. 200 mケーブル実験装置写真

200 mケーブル実験装置では下記の事項が主な検討項目として、研究開発を進めている。

1) 超伝導ケーブルの熱収縮の吸収方法 [3]
2) 液体窒素循環についてのスケール則 [6]
3) 液体窒素循環でのサイホン効果 [7]
4) 断熱2重管の真空排気方法と真空保持 [8]
5) 断熱2重管での鉄管利用 [3, 9]
6) 断熱2重管での熱侵入量の更なる低減 [10]
7) 鉄管利用による電力貯蔵 [9]

などである。

ここでは1), 2) の研究課題について簡単に触れる。超伝導ケーブルの熱収縮率は0.3%程度されている。このため、200 mケーブルでは60 cmほど縮む。もし、ケーブルが一様に縮むのであれば大きな問題は生じないであろうが、現状構造では長尺ケーブルが一様に縮むことは無いであろう。このため、200 mケーブル実験装置では端末クライオスタット方式を可動式にして、ケーブルの熱応力ができるだけ発生しない方式をとった。この課題は今後も改善する必要がある。それは、もし10 kmのケーブルを考えると、熱収縮は30 mにも及び、可動式端末だけでは吸収が不可能となるからである。

次の課題は冷媒循環のための動力に関連する。ケーブルに流すことができる電流は冷媒の温度で決まるため、ケーブルが1桁長くなると、温度上昇を同じにするためには流速は1桁早くなる必要がある。すると、ポンプ圧は同じ長さで2桁上昇する。ケーブルは1桁長くなっているため、最終的にポンプ圧は3桁上昇する。大都市での利用が想定されているとすると、変電所間の距離は数 kmであり、その間にはcooling stationを置くことは超伝導ケーブル利用の経済的メリットをほぼ完全に消し去るため、冷媒循環のための圧力損がどの程度まで低くできるかを実機で確かめる必要がある。このため、流体力学的なスケール則を得て、それを長尺ケーブルに適用し、装置建設の可能性を探ることが重要な課題である。また、スケール則は長さのほぼ3乗に比例するため、一度に長くすることは実験誤差があるため工学的には危険である。したがって、実証を重ねて順次延長することが必要となる。幸い実験データとその解析から、2 km程度までは現存機器で対応できることが分かった。

5. 今後の展望

以上述べたように、2 km程度までなら現状機器で対応できるので、次のステップは、実際の現場で~2 kmの装置を建設し、運転を通じて経験を積みながら開発を続けることが重要であると考えている。日本国内にそのような施設があれば幸せであるが、現時点では不明である。米国ではTres Amigas計画がそれに相当し、~2マイル長の高圧直流送電に超伝導ケーブルを用いた5 GW送電を検討している。これは米国内の3つの電力系統間での調整に用いられる予定であり、超伝導以外の部分では計画はスタートした。また、中国ではアルミ精錬工場での利用が本年には行われると言われている。更に、ロシア、ドイツなどでも同程度の超伝導直流送電のプロジェクトが走ろうとしている。

中部大学・超伝導センターは東京大学・鯉沼秀臣先生のサハラ・ソーラーブリーダー計画（SSB）[11]に参画し、超伝導直流送電を担当している。サハラ砂漠で発電した電力を都市部に長距離送電を行うためである。今までに何度かアルジェリア、チェニジアを訪問し、研究交流を進めると同時に今後の新しい国作りも

議論してきた。ドイツでもDESERTECと称する、国家レベルのプロジェクトがあり、2050年には~50 GWを北アフリカから導入する計画がある。このような計画では、超伝導を利用して長距離を低損失で送電するだけでなく、現在のインターネットのように双方向送電することがエネルギーセキュリティーにとって重要である。そして、超伝導直流送電が世界平和に貢献し、エネルギー問題の解決につながることが筆者等の夢である。

参考文献

[1] M. Hamabe, A. Sasaki, T. Kasukabe, M. Oue, K. Nakamura, S. Yamaguchi, A. Ninomiya, H. Okumura, K. Kawamura, and I. Aoki: IEEE Trans Appl. Supercond. **16** (2006) 465-468.

[2] S. Yamaguchi, M. Hamabe, I. Yamamoto, T. Famakinwa, A. Sasaki, A. Iiyoshi, J. Schultz, J. Minervini, T. Hoshino, Y. Ishiguro, and K. Kawamura: J. Appl. Phys.: Conf. Ser. **97** (2008) 012290.

[3] S. Yamaguchi, T. Kawahara, M. Hamabe, H. Watanabe, Yu. Ivanov, J. Sun, and A. Iiyoshi: Proc. of ICEC23 and ICMC2010 (2011) Wroclaw, Poland, 1041-1047.

[4] S. Yamaguchi, T. Kawahara, M. Hamabe, H. Watanabe, Yu. Ivanov, J. Sun, and A. Iiyoshi: Physica C **471** (2011) 1300-1303.

[5] S. Yamaguchi, K. Seo, M. Morita, Cryogenics **38** (1998) 875-880.

[6] S. Yamaguchi, Yu. Ivanov, J. Sun, H. Watanabe, M. Hamabe, T. Kawahara, A. Iiyoshi, M. Sugino, and H. Yamada: Proc. of SCC 2011 (to be published).

[7] Yu.V. Ivanov, H. Watanabe, M. Hamabe, J. Sun, T. Kawahara, and S. Yamaguchi: Physica C **471** (2011) 1308-1312.

[8] H. Watanabe, M. Hamabe, T. Kawahara, S. Yamaguchi: Proc. of ICEC23 and ICMC2010 (2011) Wroclaw, Poland, 649-652.

[9] S. Yamaguchi, T. Fujii, M. Sugino, M. Hamabe, H.Watanabe, T. Kawahara, and A. Iiyoshi: IEEE Trans Appl. Supercond., **21** (2011) 1046-1049.

[10] M. Sugino, M. Hamabe, H. Watanabe, T. Kawahara, S. Yamaguchi, Y. Ishiguro, and O. Shinshi: Proc. of ICEC23 and ICMC2010 (2011) Wroclaw, Poland, 639-643.

[11] http://spectrum.ieee.org/green-tech/solar/a-green-energy-dream-grows-in-the-sahara

＜会議報告 1＞

第 3 回 超伝導と磁性に関する国際会議報告

Report on the III. International Conference on Superconductivity and Magnetism (ICSM2012)

（独）産業技術総合研究所
伊豫 彰
National Institute of Advanced Industrial Science and Technology
A. Iyo

イスタンブール（トルコ共和国）にて、2012年4月29日~5月4日の日程で開催されたIII. International Conference on Superconductivity and Magnetism (ICSM2012) に参加した。手元にある小冊子によると、この会議はアンカラ大学を中心に設立された超伝導研究のCOE (CESUR) の主要な活動の一環として、2年毎にトルコ国内で開催されているようである。2008年、2010年に次いで3回目となる今回の会議には、世界各国から約1300名の登録があったと発表された。内訳は、トルコ国内からの登録が約170名と最多であり、日本は、ロシア、アメリカ合衆国、インド、ドイツに次いで6番目に参加者の多い国であった（約65名）。その他、アルジェリアやイランなど周辺諸国からの登録も多かったのが特徴的である。

会議場となったのは、イスタンブール中心部からバスで1時間程の場所（ヨーロッパ側）にある美しい砂浜に面したホテルである。夏はバカンスの客で賑わうのであろうが、会議の期間中は、気温10~25℃程度と涼しく過ごしやすかった。会議初日に、会議の主催者であるアンカラ大学のGencer教授は、会議を紹介する動画などを用いてオープニングの挨拶を行った。その後、銅酸化物超伝導の発見によりノーベル賞を受賞したMüller氏（University of Zurich）による基調講演が行われた。講演に先だって85歳の誕生日をお祝いするケーキが出されるという演出があった（写真）。Müller氏は、銅酸化物超伝導発見の指導原理となった電子-格子相互作用の重要性について述べた。

会議のプログラムは、毎朝の基調講演の後、約7ヶ所の部屋で平行してオーラルセッションが行われ、その後ポスターセッションが行われるという構成であった。約半分が超伝導に関するセッション（残りは磁性など）であり、理論などの基礎から大規模応用まで幅広いテーマが扱われた。また、ジョセフソン効果発見50周年を記念して“50 Years of Josephson Effect”と題するパネルセッションが夜に行われた。以下に、筆者の印象に残った幾つかの講演について報告を行う。

未踏科学技術

平成24年度夏号

目　次

ページ

● 巻頭言 ●

科学技術の信頼性回復と超伝導

中部大学教授　超伝導・持続可能エネルギー研究センター長
山口作太郎

昨年3月11日の東日本大震災（311震災）とそれに伴う福島第一原子力発電所の事故（原発事故）から、日本のエネルギー需給に関して広い議論がされるようになった。エネルギー問題は社会基幹に係わり、社会の各種課題と関連しており、議論は過去にも遡りつつ、日本国内のほとんど全ての分野を巻き込んで行われている。しかし、これらの議論は却って「混迷を深めている」面も多々あるように見える。この原因として、マスコミなどで広く指摘されている理由の一つに「政治家のリーダーシップ不在」がある。この指摘はそれなりに正しい面もあろうが、政治家だけが問題のようには見えない。例えば、「福島原発事故独立検証委員会」報告書や「国会東京電力福島原子力発電所事故調査委員会」の活動の最近のマスコミ報道を見れば、「原子力分野の科学技術者の無責任やリーダーシップのなさ」なども重要なファクターと考えられる。

更に遡れば、単に「原子力の科学技術者」と限定することは不適当で、広く科学技術者の「信用」が落ちているように感じられる。例えば、ローレンス・D・フィンク「不安定な新世界、動かない資金　ー長期ビジョンとコンフィデンスの喪失」（*Foreign Affairs Report*, p. 15, No. 4, 2012）などを読むと、エネルギー問題だけでなく社会的広汎な課題は極めて切迫していて、それを解決するための資金も社会はため込んでいるが、将来へのコンフィデンスがないため、投資が出来ない状況が指摘されている。実際、日本は世界一お金を貯め込んでいるが、そのお金が将来の課題を解決するために効果的に運用されているかについては疑問に思われる。現在の日本の年金積立金は100兆円を超しているが、現行制度を維持するには全く不足している。これは年金利回りが低かったことが直接の理由である。このため、将来大きく伸びる産業への投資が必要であるが、例えば「原子力発電所に投資して良いか？」という設問を立てると、「分からない」というのが日本の現況であると思う。311震災の前には2050年までに世界各国で原子力発電所を合計ー2000基作る計画となっていて（現在は約450基）、単純に考えれば原子力産業は伸びることを意味し、本来なら大変よい良い投資先のはずである。しかし、多くの年金運用者は311震災前からそのようには考えなかったのではないか？　そして、311震災により、そのような「将来（技術）に対する漠然とした不安」が直観として正しかったと感じ、この認識（直観）が他の将来技術も含んでコンフィデンス喪失を助長している状況、つまり「科学技術全般に対する漠然とした不安・不信」に拍車をかけているように見える。

また、小中学生から若者の理科系離れが言われて長いが、その原因の一つに「科学技術への不信・不安」があるのではないかと考えている。もし、そうなら科学技術の「面白さ」を教えるだけでは、十分な解決方法になっていないと思われる。そして、その底には、科学技術全般への「不信・不安」があるのではないかと思っている。つまり、「科学技術の進展は本当に人類社会を進歩させ、地球環境を保全したか？」という設問を若い人向けに立てると、それほど肯定的な説明できるほど、大学教員は十分な自信を持っていないように感じられる。特に、社会科学系を専門とされる方と話していて、それを強く感じることがある。

話を超伝導技術に転じよう。高温超伝導体が発見されてから25年以上が経過し、各国で多大な研究資金が投じられた。このため、多くの人たちは今にも超伝導技術が多くの人類共通課題を解決することに期待をかけている。しかし、現状は、高温超伝導技術は目に見える形で社会に提供されてなく、期待に応えていないのではないか？　もしそうなら、「高温超伝導技術」も科学技術全般への「漠然とした不安（不信）」を助長しているのではないかと思う。

このような観点に立ったときに、超伝導技術の研究者としてなすべき研究開発は何か、あるいは、研究者が社会的責任を自覚した上で開発すべき技術とは何か。そして、研究者が本音と建て前を一致できるような技術とは何かを考えざるを得ない。つまり、近未来に使われると同時に社会貢献が大きい技術とは何かを探す努力が必要になる。

手前味噌になるが、この日本の現状の中で「直流超伝導送電システムの開発」は上記の問への一つの回答であるとの思いを強くしている。超伝導分野が民生で使われるようになると、不断の技術改良が多くの分野で行われるようになり、技術波及を通じて産業として自立できるようになると期待している。超伝導送電による超長距離送電の実現によって、人類社会が安全で、より安定的な平和社会を築くことができれば、社会の「将来への漠然とした不安・不信」の低減を図ることができるであろう。このためには、研究者が再度強い矜持を持ち、上記の問題意識を持ち、科学技術の課題の解決を図ることが必要と考えている。

J. Plasma Fusion Res. Vol.87, No.12 (2011) 830-834

小特集 熱電変換技術の現状と展望

4．核融合分野における熱電変換技術の応用

山口作太郎，河原敏男
中部大学　超伝導センター

（原稿受付：2011年8月29日）

核融合炉の設計では，低温の超電導マグネットから始まり高温のダイバータおよび核反応プラズマまで極めて温度範囲が広い．これが10m程度の大きさ内に含まれているため，装置内に大きな温度差がある．さらに，いくつかの機器やプラズマ自身には電流が流れる．その意味で熱電変換（温度差と電流が流れる機器でのエネルギー変換を行う研究）は広い応用範囲があると考えている．ここでは，超伝導マグネットに使うペルチェ電流リード，電力変換器で用いられるパワー半導体への応用（自己冷却素子），熱電ダイバータについて筆者等の最近の研究結果を中心に述べる．

Keywords:
nuclear fusion reactor, Peltier current lead (PCL), self-cooling semiconductor device, thermoelectric divertor

4.1　はじめに

筆者（山口）は1996年および2002年に熱電変換研究の核融合への応用についてプラズマ・核融合学会誌にいくつかの案を書いている[1,2]．そこでは超伝導マグネットで利用する電流リードおよび高温熱電材料を利用した応用について述べると共に，磁場中での熱電変換（ネルンスト効果）について核融合科学研究所で行った実験データを元に展望を述べた．その後，山口は中部大学に移籍して主に直流超伝導送電に関する研究[3,4]を行ってきたため，超伝導機器向けの電流リードへの熱電材料の応用（ペルチェ電流リードと言っている）については新しいアイデアや実験結果が集積されてきた．そして，実用化に向けての開発が進んだ．したがって，本論文では最初に2002年以降の主に中部大学で行われたペルチェ電流リード研究のまとめを行う．これは以下に河原によって起稿された．

また，中部大学では，直流超伝導送電のために交直電力変換器についての検討も行ってきた．交直変換器は半導体スイッチング素子を利用するため，半導体素子の性能が交直変換器の性能を左右する．このため，パワー半導体素子の高性能化検討を行ってきた．この分野は1990年代には研究としては飽和したと考えられ，企業の再編成も行われた．しかしその後，電気自動車やハイブリッド車などの車応用が広がり，2000年代に入り研究開発が広がった．そして，2008年に米国でオバマ政権が発足してから「スマート・グリッド」と呼ばれる技術体系が広く議論されるようになり，そこでは電力網に「直流」を持ち込むことが議論され，特に311震災以降重要性を増している．このために，2つめの話題として半導体スイッチング素子の研究開発について述べる．

そして，最後に核融合炉での熱電発電について新しい提案を述べる．「石油後（After Oil）」のことが広く議論されるようになり，ほぼ21世紀の中頃にはeasy oil（安価で入手しやすい石油）は新興国の経済発展もあり，不足する事態が懸念されている．このような中で「再生可能エネルギー」の大規模利用が広く行き渡り，人類が利用するエネルギーの大部分を今世紀中に生産することになれば，「核融合」の地位がどのようになるかを議論することは重要であろう．

4.2　ペルチェ電流リード

超伝導は大電流がロスなく流せることから強磁場磁石の線材としての応用が期待され，既に，核融合応用や加速器応用のための大型超伝導磁石が開発されている．また，低損失・高電流密度の省エネルギー技術として送配電システムへの応用研究も進められ，中部大学でも直流超伝導送配電システムの実証実験装置として20 m級のCASER-1[3]，200 m級のCASER-2の研究開発[4]を行ってきている．しかし，超伝導状態は低温で発現するため，室温の機器との接続を担う電流リードでの熱侵入に伴う損失を下げるのは重要な課題である．銅電流リードでは伝導熱とジュール熱のバランスをとった最適形状が求められているが（**図1**），熱電材料を用いた新しい原理で断熱性能を向上させことが可能なペルチェ電流リード（PCL）について，その原理と応用展開[5]に関してまとめる．

4.2.1　ペルチェ電流リードの原理

PCLでは，電流リードの一部に熱電素子を直接挿入し，電流リードを流れる電流によるペルチェ効果をヒートポンプとして利用することで，直接低温機器からの熱をくみ上げる．その原理は，熱伝導率が低くゼーベック係数の高い熱電素子を電流リードの一部に使用することで，

(1) 低い熱伝導率（通常電流リードに使われる銅の0.3%

4. Thermoelectric Conversion in Fusion Reactor and the Related Fields
YAMAGUCHI Sataro and KAWAHARA Toshio

corresponding author's e-mail: yamax@isc.chubu.ac.jp

程度）により電流リードの室温側からの伝導熱を低下させ，

(2) 通電時には，電流に比例したペルチェ熱が低温側から高温側へ熱をくみ上げる（ただし，電流リード上では通電によるジュール熱も発生する），

という2つの効果で低温側への熱侵入を低減させるというものである（**図1**）．

4.2.2 PCLの各種応用

電流リードではその熱分布を計算し最適形状を決める．そこで，PCLの熱分布に関する計算機コードが初期のころから開発され[6]，数値シミュレーションと超伝導磁石への適用が実験的に検討された．そして，無冷媒超伝導磁石での実験的な研究から（**図2**）熱電材料の両端で大きな温度差が存在することが示され，この結果から**図3**のようにPCLによる熱侵入の低減が可能であることがわかった[7]．

熱電材料をn型，p型を独立に用いるPCLでは，電流方向が一方向となるDC応用が最適である．しかし，ACシステム応用や，電磁石応用では電流方向の反転も必要な場合もある．そのため，スイッチング素子と組み合わせたPCLが提案され（**図4**），数値的な検討が行われた[8]．磁石の極性反転応用の際には，**図5**に示すようにFETを用いた実験が行われた[9]．

また，マルチステージ熱電素子構成モジュールによる電流リード（**図6**）の検討も行われ[10]，超伝導磁石への応用の際に有用であることが示された．さらに，超伝導送電システムでの実証結果[11]や中部大学ではこのPCLを用

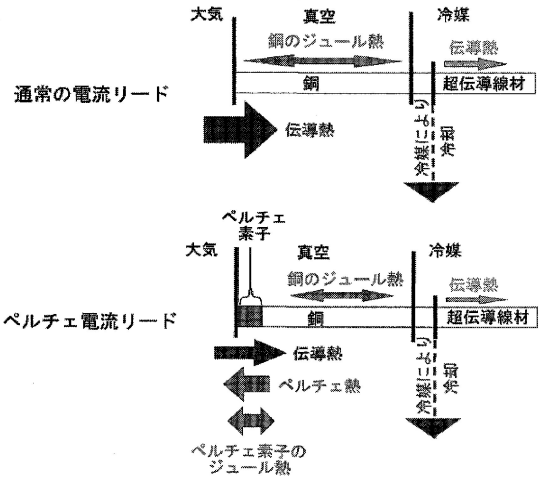

図1　ペルチェ電流リード(PCL)の原理．

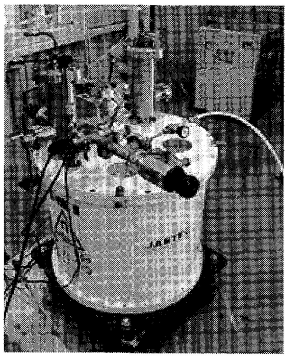

図2　PCL組み込み実験での無冷媒磁石．

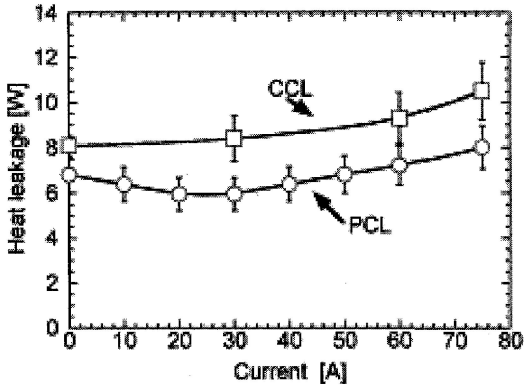

図3　電流リードの温度分布から見積もった熱侵入の通電電流依存性．

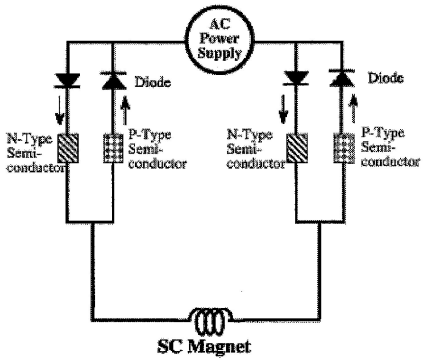

図4　AC-PCLの概念図．

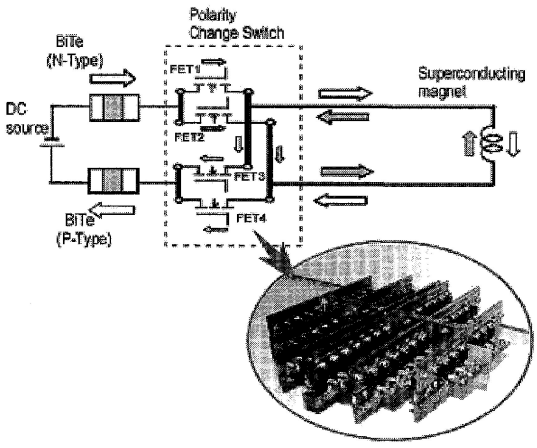

図5　磁石極性反転回路を組み込んだPCL．

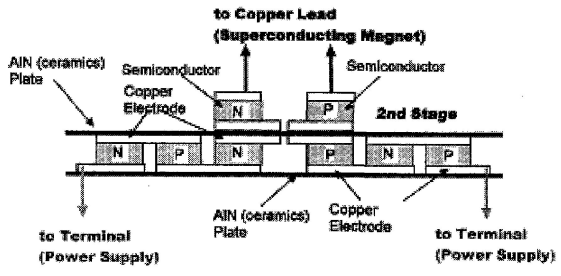

図6　マルチステージ構成のPCL．

Journal of Plasma and Fusion Research Vol.87, No.12 December 2011

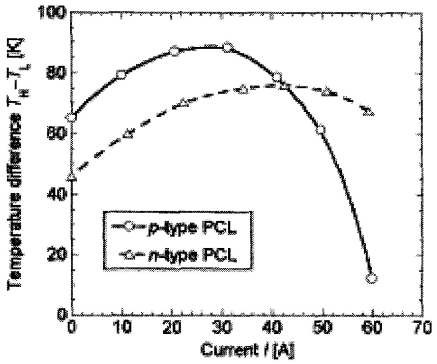

図7 PCL上の熱電素子部の両端温度差の電流依存性(CASER-1).

いることで，端末からの熱侵入を実験的に26 W/kA程度まで低減できた．そして，**図7**のように熱電素子両端の温度差が100 Kに近くなった．PCL性能向上には常温以下の低温熱電材料開発が必要である．これによって，端末熱侵入のより低下が可能である．また，システムからの蒸発冷媒ガスの利用も検討がなされ，15 W/kA以下の熱侵入量が可能であろう[12]．CASER-2でも冷却試験が行われ，銅の電流リードでは氷がつく状況でPCLでは氷がつかず断熱がよいことが示されている（**図8**）．

4.3 自己冷却素子

電力変換器にパワー半導体素子を利用する場合の技術的な問題点は，要約すると2つある．一つは以下に発熱を下げること．もう一つは冷却することである．発熱は素子の損失であり，低い方が望ましい．発熱によって素子温度が上昇するとスイッチングができなくなるため冷却が行われる．発熱や利用温度範囲は半導体材料によって決まり，最近では新しい材料研究[13,14]が行われている．例えば，SiCがある．Siに比べて発熱が1/10になることが期待されている．一方，冷却は素子からの発熱量が回路条件などで決まると，除熱の方法やシステムを考えることになるが，現状のSi素子では素子より遙かに大きな冷却フィン（体積にして100倍以上）や液体冷却システムが用いられる．

自己冷却素子とは，半導体素子に流れる電流を利用して半導体部の熱を除去する素子である．**図9**に原理を示す[15,16]．縦型MOSFETではドレイン側に銅板が貼り付けてあり，上部に，ゲートおよびソース電極がある．そして，電流は矢印の方向に流れる．その銅板をn型熱電半導体にする．すると，電流によってペルチェ熱がシリコンチップ側から矢印のように外に排出される．

そして，このような材料は以下の性質が望ましい．

1）高いゼーベック係数（α）
2）低い電気抵抗率（η）
3）高い熱伝導率（κ）

である．従来からの熱電材料は，下記で定義される性能指数Zが高いことが求められる．

$$Z=\frac{\alpha^2}{\eta\kappa} \tag{1}$$

しかし，求められる性質は必ずしも高い性能指数の材料が良いとは限らない．一般に電気抵抗率の低い材料は高い熱伝導率を持つため，この傾向は材料探求の点からはむしろ望ましい．銅板では熱伝導による冷却だけであるが，n型熱電材料を使うと熱伝導にペルチェ効果が付加される．したがって，この2つの物理プロセスで冷却能力が上回れば良いことになる．方程式で書けば，下記のようになる．

$$Q_P \geq Q_C \tag{2}$$

ここでQ_P，Q_Cはそれぞれペルチェ効果を入れた熱流束および熱伝導のみの熱流束を表し，以下のように定義される．

$$\begin{aligned} Q_P &= \kappa\frac{s}{d}\Delta T+\alpha\cdot T_h\cdot I-\eta\frac{d}{S}\cdot\frac{I^2}{2} \\ Q_C &= \kappa_C\frac{S}{d}\Delta T \end{aligned} \tag{3}$$

ここで，Sはペルチェ部の断面積，dは厚さ，T_hは高温側温度，ΔTは温度差，κ_Cは銅の熱伝導率である．そして，高いゼーベック係数と高い熱伝導率を持つ材料としてSiCが最初の候補材料として検討された[16,17]．そして，現在色々な材料の探求が行われている段階であり，有望な材料も見つかりつつある状況と考えている．もし，銅より冷却

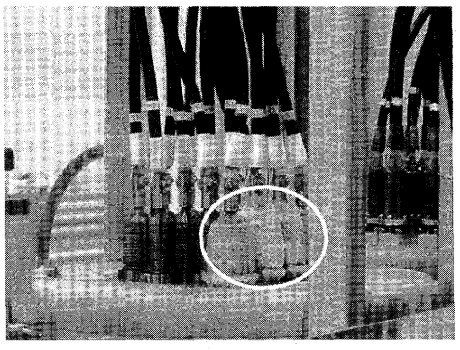

図8 CASER-2の冷却試験中のPCL．銅リードには氷が成長(丸部).

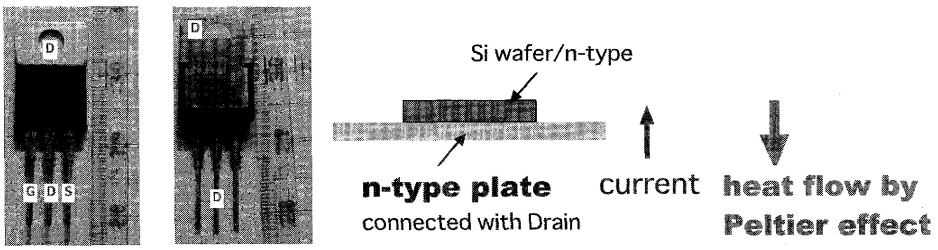

図9 パワーMOSFET（写真，左図，G：ゲート，D：ドレイン，S：ソース）と自己冷却素子原理構造図（左）.

能率の高い材料が見つかれば，電力変換器にとっては大きな福音であり，現在一般に利用されているほとんどの電気・電子機器で広く応用されるであろう．

4.4 熱電ダイバータ

筆者の一人の山口は1996年のプラズマ・核融合学会誌に熱電ダイバータを提案した[1]．これは，ダイバータへの熱流を利用して発電を行うアイデアである．**図10**に概念図を示す．プラズマからの熱をダイバータは受けるが，これを水やガス冷却で熱除去しているため，大きな温度差が第1壁と冷却水が流れる部分（多くは熱伝導率の良い銅を利用するようであるが）に発生する．したがって，この部分に熱電材料を組み込み，発電を行うのである．発電は熱除去でもあるので，冷却にも寄与するからである．

残念なことに，現在まで核融合炉が実現していないこともあり，その後，研究開発は進まなかった．さらに，当初は熱電材料としてカーボンや炭化ボロンなどを熱電材料として考えた．あいにく，これらは性能指数があまり高くなく，冷却効果も期待できない理由もあった．しかし，ITER向けのダイバータ開発[18-20]はその後急速に進み，異なった材料も出てきたので，再度このアイデアの適用可能性を考えても良い時期になっているのではないかと考えている．**表1**に想定される材料についてまとめた．第1壁として利用されるタングステンは金属であるためゼーベック係数はそれほど高くない．カーボン材料はタングステン第1壁と組み合わせて利用が想定されて，高い熱伝導率材料も開発されつつあるが，やはりゼーベック係数は高くない．高温での熱電変換利用では炭化ボロン材料が研究され，高いゼーベック係数が報告[21]されている．そして，この材料は核分裂炉で制御棒材料として広く利用されているため，耐放射線性能も良いが，熱伝導率はカーボンほど良くない．一方，炭化ケイ素はカーボンよりは低い温度になるが，炭化ボロンより高い温度まで利用できる．更に，熱伝導率は一般のカーボンより高く，ゼーベック係数も極めて大きい．そして，電気抵抗率も低い[22]．但し，高温での測定はあまり報告されていないようである．したがって，SiCは熱電ダイバータの候補材料となろう．尚，この表でMPは融点を指し，SPは昇華温度を指す．このため，**表1**の値を利用してSiCの発電能力の見積もりを行い，結果を**図11**に示す．横軸は性能指数であり，縦軸は変換効率である．

SiC性能指数は300－400 Kで$10^{-4}(K^{-1})$のオーダーであり，一般に利用されている熱電材料に比べて1桁以上低い．しかし，温度差を1500 K（冷却水温度350 K，SiC第1壁側温度2000 K程度を想定）以上取ることによって15%に近い変換効率を得ることができる．このような高い変換効率は熱電材料では今までに実現されたことない値である．

SiCを利用する場合，放射線性能は構成元素から推測するに，炭化ボロン並みであろう．したがって，熱電ダイバータだけでなく，他の高熱伝導率材料として核融合炉で利用できよう．ただし，高温での物性値の測定が今後必要になろう．特に，SiCでは単結晶は極めて高い熱伝導率であるが，焼結体はカーボン並みであり，製法によってかなり熱伝導率は異なる．一方，SiC単結晶はほとんどがn型である．このため，p型材料の開発が必要になるが，高温p型材料は比較的多くあるので，熱電素子ペアを構成しやす

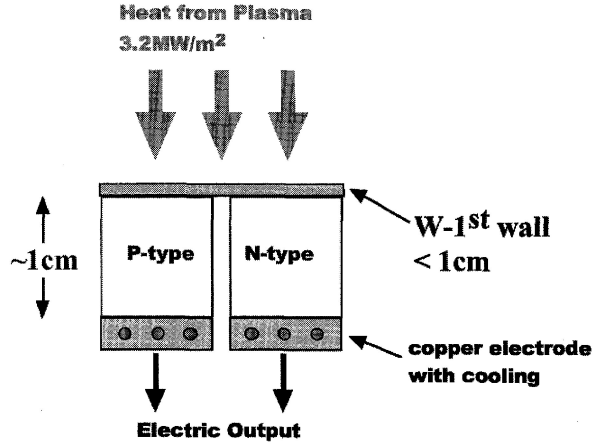

図10　プラズマ核融合装置で利用する熱電ダイバータ原理構造．

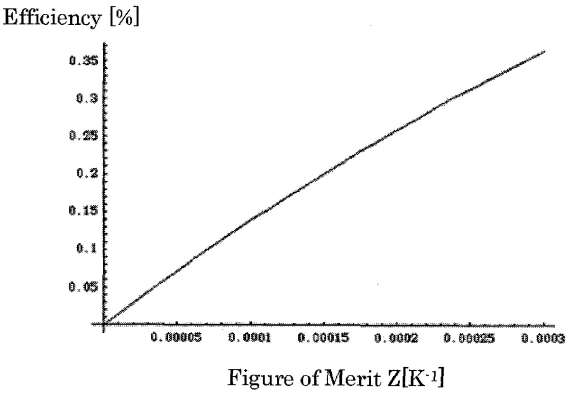

図11　発電効率と性能指数（温度差1500 K）．

表1　熱電ダイバータで利用される候補材料

Material	MP/SP [K]	κ [W/km]	α [μV/K]	η [Ω/m]	comments
W (tungsten)	3695 MP	~170 @300K	< 10	5.2×10^{-8} @300K	For 1st wall
Carbon	3915 SP	**100**~300	< 10	10^{-6}~10^{-2}	κ>2000 for Diamond
B_xC	2763 MP	30-42 @300K	~120 @1000K	~0.006 @1000K	used in fission reactor
SiC	3003 SP	~490	>400	~0.0001	

Journal of Plasma and Fusion Research Vol.87, No.12 December 2011

いであろう．また，プラズマからの熱流束は周辺部の磁場構造によって制御できるので，プラズマ電場を利用しての熱電子発電や冷却も想定される[23]．このプロセスは，熱電変換プロセスだけでないであろう．何れにしても，核融合炉でSiC利用は広範囲に及ぼう．

4.5 まとめ

核融合炉を人類が研究開発することを「地上に太陽を！」と言うキャッチフレーズで呼ばれてきた．太陽の熱源が水素の核融合反応であるためであろう．しかし，地上の「太陽」は高温プラズマを閉じ込めるために高い磁場を用いる．そして，その磁場は超伝導マグネットによって発生していて，超伝導マグネットは～4Kの低温で保持されている．このため，ITERでは低温の超伝導マグネットからプラズマ表面までの距離は2m程度である．一方，宇宙背景輻射測定によって宇宙の平均温度が測定され，～3Kと言われているので，超伝導マグネット温度に近い．つまり，核融合炉はその内部に宇宙の平均温度から核融合反応が生じる高温プラズマまでを含んでいる．その意味で核融合炉とは「地上に宇宙を」と言った方が適切であろう．

この認識に立つと，熱電変換は温度差を利用して発電や冷却などの機能を発現することを考える学術分野であり，核融合炉は温度差がもっとも大きな機器システムであるため，熱電変換が広く応用できる対象と見ることができる．更に，核融合炉では色々な種類の巨大な電力変換器を使う．即ち，マグネット電源，加熱関係の電源などがある．これらはどれも半導体スイッチング素子を利用している．以上の状況を考えると，ここで述べた応用以外にも核融合分野では熱電変換応用を新たに発見できるであろう．この記事を読んでいただいたプラズマ・核融合の研究者から熱電変換研究への多くの新しい提案があれば筆者の喜びとするものである．

最後になるが，防衛大学校の岡本庸一，横浜国立大学の中津川博，島根大学の北川裕之，産業技術総合研究所の加藤智久，荒井和雄，奥村元の先生方には研究を進める議論および実験データ評価およびサンプル提供などでお世話になりました．また，中部大学・超伝導センターの浜辺誠，渡邊裕文，ユーリ・イワノフ，孫建の各氏には日常的に多くの協力があります．大学院生であった福田君は自己冷却素子の実験を進めてくれました．さらに，ソニーの佐飛裕一様，みずほ情報総研の石原範之様にもサンプルの提供や計算機実験などでお世話になりました．さらに，核融合科学研究所の相良明男氏には最新のダイバータの状況を教えていただきました．最後に，中部大学・理事長（総長）の飯吉厚夫先生には研究環境を整えていただくことなどで多くの援助をいただいています．以上，名前を記して感謝を表す次第であります．

参考文献

[1] 山口作太郎：プラズマ・核融合学会誌 **72**, 1283 (1996).
[2] 山口作太郎：プラズマ・核融合学会誌 **78**, 19 (2002).
[3] S. Yamaguchi, M. Hamabe, I. Yamamoto, T. Famakinwa, A. Sasaki, A. Iiyoshi, J. Schultz, J. Minervini, T. Hoshino, Y. Ishiguro and K, Kwamura, J. Phys. Conf. Series **97**, 012290 (2008).
[4] S. Yamaguchi, T. Kawahara, M. Hamabe, H. Watanabe, Yu. Ivanov, J. Sun and A. Iiyoshi, Physica C *in print.*
[5] S. Yamaguchi, T. Yamaguchi, K. Nakamura, Y. Hasegawa, H. Okumura and K. Sato, Rev. Sci. Instrum. **75**, 207 (2004).
[6] H. Okumura and S. Yamaguchi, IEEE Trans. Appl. Supercond. **7**, 715 (1997).
[7] M. Hamabe, A. Sasaki, T. Kasukabe, M. Oue, K. Nakamura, S. Yamaguchi, A. Ninomiya, H. Okumura, K. Kawamura and I. Aoki, IEEE Trans. Appl. Supercond. **16**, 465 (2006).
[8] T. Yamaguchi T. Yamaguchi, H. Okumura, K. Nakamura and S. Yamaguchi, IEEE Trans. Appl. Supercond. **13**, 1910 (2003).
[9] M. Moriguchi, S. Mizutani, S. Miwa, T. Famakinwa, T. Yamaguchi, M. Hamabe, H. Takahashi, K. Nakamura, S. Yamaguchi, H. Okumura and Y. Hasegawa, IEEE Trans. Appl. Supercond. **14**, 1786 (2004).
[10] T. Yamaguchi, H. Okumura, K. Nakamura and S. Yamaguchi, IEEE Trans. Appl. Supercond. **13**, 1914 (2003).
[11] M. Hamabe, T. Fujii, I. Yamamoto, A. Sasaki, Y. Nasu, S. Yamaguchi, A. Ninomiya, T. Hoshino, Y. Ishiguro and K. Kawamura, IEEE Trans. Appl. Supercond. **19**, 1778 (2009).
[12] T. Kawahara, T. Fujii, M. Emoto, M. Hamabe, J. Sun, H. Watanabe and S. Yamaguchi, Physica C **470**, S1011 (2010).
[13] 荒井和雄，吉田貞史共編：SiC素子の基礎と応用（オーム社，2003）．
[14] S. Yamaguchi, T. Noro, H. Takahashi, H. Majima, Y. Nagao, K. Ishikawaand Y. Zhou, T. Kato, Mat. Sci. Forum, **600-603**, 851 (2009).
[15] 山口作太郎：熱電変換技術ハンドブック（NTS，2008）p. 484.
[16] H. Nakatsugawa, K. Nagasawa, Y. Okamoto, S. Yamaguchi, S. Fukuda and H. Kitagawa, J. Electronic Materials **38**, 1387 (2009).
[17] S. Fukuda, T. Kato, Y. Okamoto, H. Nakatsugawa, H. Kitagawa and S. Yamaguchi, Jpn J. Applied Phys. **50**, 031301 (2011).
[18] R. Tivey, T. Ando, A. Antipenkov, V. Barabash, S. Chiocchio, G. Federici, C. Ibbott, R. Jakeman, G. Janeschitz, R. Raffray, M. Akiba, I. Mazul, H. Pacher, M. Ulrickson and G. Vieider, Fusion Eng. Des. **46**, 207 (1999).
[19] A.S. Kukushkin, H.D. Pacher, G. Federici, G. Janeschitz, A. Loarte and G.W. Pacher, Fusion Eng. Des. **65**, 355 (2003).
[20] M.S. Tillack, A.R. Raffray, X.R. Wang, S. Malang, S. Abdel-Khalik, M. Yoda and D. Youchison, Fusion Eng. Design **86**, 71 (2011).
[21] 河本邦仁，関　務，Chul Hoon，柳田博明：J. Ceramic Soc. Japan 100, 853 (1992).
[22] 松波弘之：半導体SiC技術と応用（日刊工業新聞社，2003）．
[23] S. Yamaguchi, S. Ohyabu and O. Motojima, *Proc. 1996 Int. Conf. Plasma Phys.* (ICPP96) 1394 (1996).

電力供給と再生可能エネルギーの普及

中部大学超伝導・持続可能エネルギー研究センター長

山口 作太郎 〈やまぐち さたろう〉

■略　歴／三菱電機エネルギー開発部、文部省核融合科学研究所助教授、中部大学工学部教授、同大学先進技術連携研究センター長を経て、現職。著書に『はじめての電気磁気』など多数。超伝導科学技術賞受賞（2013）。

次の五十年ほどを考えてみると、一番大きな課題は日本の人口が大きく減少することであろう。次の課題は色々あろうが、エネルギー供給をどのように確保するかであると思われる。特に、後者は日本だけの課題ではなくて、世界で今後最も重要になってくると考えている。現実には、東日本大震災・津波及びそれに伴う原子炉の水素爆発などによって、日本の原子力発電所での発電が止まり、火力発電所での発電量が急増し、これによって日本の燃料輸入代金が大きくなり、貿易収支が赤字になると同時に電気料金が上がり始めている。しかし、米国で非従来型の資源であるシェールガス・タイトオイルの生産によって天然ガス価格は逆に下落しているので、日本の燃料費の支払いの急増は単に原子力発電所の停止だけではなくて、日本固有の契約上の問題も絡んでいる。そして、世界の発展途上国では電力供給が常に不足している状況が続いている。そして、今後の世界規模の経済発展を考えると、電力・エネルギー供給を上手く行うことが戦争を回避し、人類全体の福祉の向上につながる蓋然性は高いであろう。

エジソンが電力会社を興してから百年以上が経過しているが、その間に一次エネルギーに占める電力の割合は上昇を続け、日本では四〇パーセントを超し、世界的には二〇パーセントほどとなった。この傾向は今後五十年間続くと思われる。例えば、自動車の電気化（ハイブリッド車、電気自動車、燃料電池車など）は今後も進むであろうし、家庭や工場、オフィスでのエコキュートなどの普及は電力の割合を増やすであろう。このため、今後もインフラとしての電力への大規模な投資は日本だけでなく、世界的にも五十年以上長く続くであろう。このため、東日本大震災の前には二〇五〇年までに世界で稼動する原子力発電所の原子炉数は二千基を超すと思われていた。現状が四百五十基程度であるため、原子力は大きな

成長が期待できる分野であった。

さて、筆者は民間電機会社に勤めていたときに、一九四五年の第二次世界大戦の敗戦から一九七三年の第一次石油ショックまでに日本の民間設備投資の半分が電力投資であったと聞いた。つまり、戦後建設された多くの民間工場や道路、鉄道などへの投資より大きいと言うのである。したがって、世界的にも電力投資が一番大きな割合を占めると思っている。アベノミクスは発展途上国へのインフラ輸出を目指しているが、この意味で主な狙いは電力投資かと思って見ている。

以上の状況の中で再生可能エネルギーの将来を考えてみる。これは炭酸ガスを発生し有限な資源の化石燃料を必要としなく、核技術を使わない発電装置となるため、現在普及が急速に進んでいる。例えば、太陽電池（ＰＶ）である。日本での稼働率は一二・五パーセントであり、日本の電力消費は一〇〇〇テラワット時（TWh）程度なので、全量をＰＶで賄うには、

$$\frac{1000\times10^{12}}{0.125\times365\times24}=1.14\times10^{12}=1140GW$$

となる。

一方、日本での電力消費ピークは八月上旬の日中にあり、一八〇ギガワット（GW）程度であるため、ＰＶ発電能力はその六倍以上の値になる。つまり、ＰＶ以外の全ての発電所を止めてもまだ五倍以上の電力を貯蔵するか、他に送電することが必要になる。尚、現在の日本では揚水発電所が電力貯蔵を行う施設としては最大で有り、二五ギガワット程度あるとされている。したがって、全く不足である。このため、ＰＶで全ての電力を賄うことは無理である。つまり、他の電源と組み合わせて利用することが必要になる。この状況は他の国でも同じである。但し、ＰＶは電力需要の大きい昼間に発電するので、当面の導入はより良い電源構成につながるであろう。

また、ヨーロッパや北米では長距離送電が直流を利用して広く用いられていて、電力貯蔵が高価であるので、長距離送電が整備されると、ＰＶの導入量が多くなろう。実際、ヨーロッパでは主に風力発電の出力安定化が他の電源の運転制御及び長距離送電と合わせて使われている。

再生可能エネルギーは高価であることが大きな問題とされている。日本のＰＶの固定価格買い取り制度（ＦＩＴ）の価格は現在三十二円～三十七円／キロワット時(kWh)であるが、これはＰＶが高価であり、稼働率が低いためである。稼働率は天候で決まるため、価格を安くすることが普及の決め手となる。しかし、ドイツでのＰＶ価格と日本との価格を比較すると、最近の五年間程度ではドイツでの価格は日本の半分程度である。家庭の屋根などに取り付けるとほとんど維持費は掛からないので、半分の価格で購入できるとするとＦＩＴの価格は半分で済むことになり、十六円～十八・五円／キロワッ

ト時となる。この価格はドイツでも日本でも電力会社から購入する電力が二十四円／キロワット時程度であるため、より安価である。実際、ドイツでは家庭の電気代が膨らんでいるが、ＰＶの普及が現時点でも進んでいる。これは電力会社から購入するよりＰＶからの電力の方が安価であるためである。家庭の屋根で発電した電力は自家消費に回され、電力網に接続して販売されない傾向が強くなってきている。つまり、家庭で利用する電力でＰＶ発電では不足分のみを電力会社から購入するのである。この問題について、筆者は色々な人に「何故、日本のＰＶは高いか?」と聞いているが、まだ納得できる回答を得たことはない。

しかしながら、現時点でもＰＶからの電力コストは他の電源に比べて高めではあるが、屋根で発電し、その家で利用することは経済的な合理性が高い。つまり、高価な電力網を利用しないからである。同時に、給配電系を利用して一軒の家だけではなく小さいコミュニティにＰＶで電力を供給することは良い答えがあると筆者は思っている。

筆者はＰＶシステムが家電製品のようにコモディティ化して、現在のドイツの価格よりもう少し下がると思っている。そして、家庭や小さなコミュニティでの電力コストは十五円／キロワット時を割るであろうと思っている。実際米国エネルギー省の発表では二〇一三年の電力コストは十二円／キロワット時を割っている。このような安価で高性能なシステムが日本で生産できると、今後発展が期待できるアフリカなどへのインフラ輸出にも迫力が出てこよう。テレビなどの報道を見ると、ケニアではマサイ族の七五パーセント以上が携帯電話を利用しているが、その充電電源はＰＶである。これは携帯電話が牛の放牧管理にはとても便利であることと電力網が整備されてないからである。テレビや蛍光灯、白熱灯などの普及より先に携帯電話がＰＶと一緒に普及するのである。多分、次はインターネットに接続するＰＣやタブレット端末機器が普及するのであろう。

発展途上国の方が案外スムーズにＰＶが普及するのであろうか。

50周年後の発展への礎 ⑧

武道体育館建設（平成23年）

第6章　電力ロスを低減する技術シーズからの研究開発テーマの発掘

第1節　超伝導機器の電流リード損失低減と熱電プロセスによるLNG冷熱回収

山口　作太郎
中部大学　超伝導センター　教授　センター長　理学博士

(株)技術情報協会

2013年7月発刊「技術シーズを活用した研究開発テーマの発掘」抜刷

第１節　超伝導機器の電流リード損失低減と熱電プロセスによるLNG冷熱回収

●このシーズが狙い目の企業	●想定される応用先
・熱電材料のコア技術を保有している	・超伝導マグネット機器及び超伝導ケーブル
・LNG輸入を行っている電力，ガス会社	・電力生産機器
・LNGプラントを手がけている企業	

はじめに

2011年3月11日の東日本大震災とそれに伴う福島第一原子力発電所での事故によって電力供給のために液化天然ガス（LNG）輸入が大きく増えている。LNG主成分はメタンであり，産地によって成分は少し違うが，メタンの沸点温度程度であり，－160℃とされる。これはガスタービンと蒸気タービンを利用した高効率の複合火力発電所（効率は55%を超したとされ従来からの汽水火力発電所の40%程度に比べて著しく高い）の燃料に利用されるため，米国でのシェールガス革命と相まって益々LNG輸入は増えるであろう。

しかしながら，LNGの生産には莫大な電力を必要とする。つまり，地中からの常温より温度の高い天然ガスを得た後，それを液化するために冷凍機を使うからである。この時，冷凍機は890kJ/kg[1]の熱量を吸収する必要がある。冷凍機は電力で運転されるため，生産地では発電所が必要になるこの発電機及びモーター系の総合効率を40%とし，冷凍機の%カルノー効率を30%[2]とし，カルノー効率ε_cは低温T_cと常温T_hで式（1）のように表されるので，

$$\varepsilon_c = \frac{T_c}{T_h - T_c} \tag{1}$$

19%程度となり，生産地では11.7MJ/kgのエネルギーを消費することになる。日本に輸入される天然ガスの総発熱量は54.6MJ/kg[3]とされるため，発熱量の21.4%がLNG生産時に消費されることになる。このため，低温のLNG冷熱回収は地球全体を考えると極めて重要であり，今までに色々な検討がなされている。しかし，日本に輸入されるLNG冷熱の90%以上が利用されていないと言われている。このため，新しい利用方法の開発が望まれている。

一方，超伝導機器は損失が極めて少なく究極の省エネルギー機器と言われるが，低温に保持するために冷凍機が必要となり，最終的には冷凍機の電力消費が損失になる。これを最小にするためには超伝導機器などの低温系への熱侵入量を最小にする必要がある。このため，機器を納める容器は断熱真空容器（クライオスタット）が広く利用されている。一方，低温の超伝導機器に電力を供給するためには，常温端から低温端までを電気的に接続された「電流リード」[4]と呼ばれる機器が利用される。つまり，ここでは電気回路に大きな温度差が発生する。電流リードの材料は通常は銅が利用され，断面と長さについての最適設計がされる。簡単な解析から通電時には合金よりも高純度銅（アルミ）の熱侵入量が少ないことがわかる。銅は熱伝導率が高いので，常温側から低温系への熱侵入量は小さくなく，50W/kA程度とされる。このため，大電流機器では大きな熱侵入となり，冷凍機の電力消費が大きくなる。実際，大型超伝導マグネットでは，マグネットより大きな冷凍機が設置されることが多い。そして，冷凍機能力は電流リードからの熱侵入でほぼ決まっている。したがって，超伝導分野では電流リードからの熱侵入低減が重要な研究課題であり，材料的には「電気は通すが，熱は通さない」材料が求められる。この問題は物理的に矛盾した要請であるため，解決方法を見つけるのは容易ではないが，筆者は長くこの問題解決について検討を行っていて，一つのアイデアとしてペルチェ電流リード[5-9]（PCL）を提案し，研究開発を進めてきた。これは熱電効果であるペルチェ効果を利用して熱侵入を低減する原理である。

一方，熱電半導体（ペルチェ）材料に大きな温度差を付けると発電するため，熱電発電の研究が世界各国で行われている。したがって，このPCLで利用される熱電半導体は温度的にも同じ範囲であるため，LNG冷熱回収を原理的にできる。以下では，今までのPCLの研究開発状況の簡単なレビューを行うと同時にLNG冷熱回収についての提案を行う。

1. ペルチェ電流リードの研究開発

ペルチェ電流リードの解説は複数[10]ある。図1にPCLの原理構成図と電流リード導体に沿った温度分布の模式図を示す。電流リードの常温側に熱電半導体を設置し，これに銅リードを接続し，最後に高温超伝導部（HTS部）を接続して電流リードとする。但し，高温超伝導を利用する機器の場合には必ずしもHTS部は必要ではない。

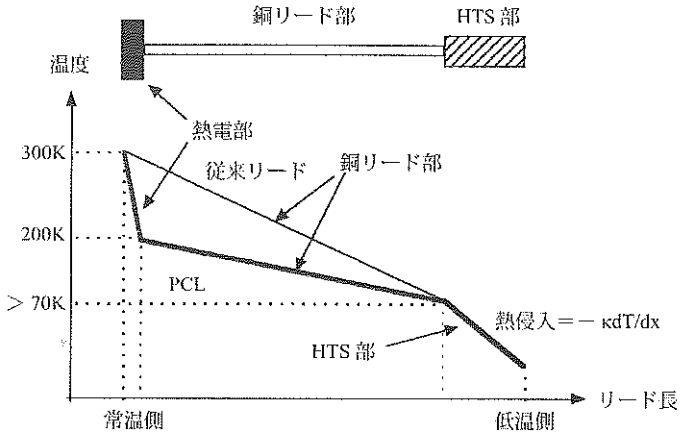

図1　ペルチェ電流リード（PCL）の原理構成図と模式的温度分析

熱電（ペルチェ）材料は現時点ではビスマス・テルル合金（BiTe）を用いる。これは，一般商用で販売されている唯一の材料であり，常温付近での性能指数が大きい。また，熱は常温部から入るため，BiTeは電流リードの常温側に取り付ける。BiTeの熱伝導率は銅の0.3％ほどであり，電流によって熱輸送を行うため（これをペルチェ効果という），熱流束の方向を低温側から高温側にすれば大きな熱絶縁が期待できるからである。性能指数の大きな材料が求められる。性能指数Zは式（2）で表される。

$$Z=\frac{\alpha^2}{\eta\kappa} \tag{2}$$

ここでαはゼーベック係数であり，ηは電気抵抗率，κは熱伝導率である。このため，熱伝導率は小さく，電気抵抗率は低く，ゼーベック係数は大きいことが望ましい。しかし，この要請は物理的に矛盾しているため，材料の開発には現象論的な大きな努力が払われているのが実情である。尚，実験ではペルチェ部と銅リード部からなるため，熱侵入量を最小にするために材料特性に合わせた最適設計を行っている。

図2はPCLと通常の銅を用いた電流リード（CCL）の実験中の写真[8]を示す。計測線ポート（measurement cable port）及び電気絶縁のためのFRPフランジが示されている。この実験は筆者の研究室で行っている直流超伝導送電システムの開発の一環であり，超伝導ケーブルは冷却して超伝導状態になっている。この写真はステンレス製クライオスタット上部に取り付けてあるケーブルを接続するための電極部分である。電極は銅で作られ，電気絶縁のためのFRP製フランジに取り付けてある。

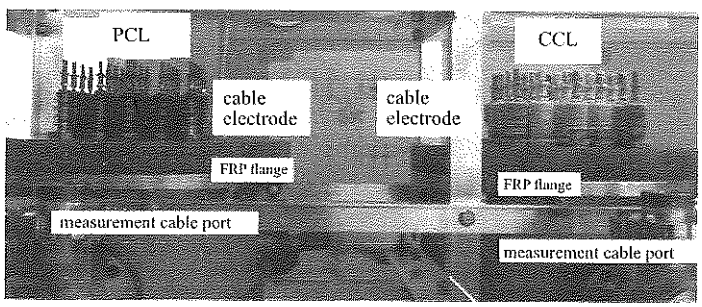

図2　PCLと従来型電流リード（CCL）の比較写真

CCL 側の電極（cable electrode と表示）は表面に霜が付いているが，PCL 側には霜が付いていない。これは PCL 側電極の温度が高いことを意味していると同時に，PCL 側からの熱侵入が少ないことの写真による直接的な証明である。図 2 の実験では BiTe の厚さは 8mm，非通電時には BiTe の両端温度差は 75K 以上であり，30A 程度の通電を行うと温度差は拡大し 100K を越した。常温との温度差は 230K 程度であるため，熱侵入が半分程度になっている。

一方，ペルチェ材料は電気抵抗率が銅より高いので，この部分の発熱損失を考える必要があるが，冷凍機 COP が低いため現状ではネットで損失を大幅に減らしている。また，ここでの損失は超伝導マグネットやケーブルの性能改善につながることもあり，ペルチェ材料を電流リードに利用することは今後汎用化するであろう。そして，現時点（2013 年）では，大学の実験室での機器だけではなくて，実用に供されようとしている。

2. 現状の LNG 冷熱回収システムと新たな提案

LNG は主に海水を用いた熱交換器に導かれ，温度が上がり気化する。これを気化器と言う。このため，気化したガスの圧力は極めて高いので，ポンプ動力を用いないで長距離（数十 km）の輸送が可能である。これは一つの冷熱回収であるが，それほど回収率は高くない。このため，気化時のこの圧力を利用して膨張タービンを使い，電力生産も行っている[10]。文献 1）によると，膨張タービンの熱サイクルは 250K ～ 280K なので，エクセルギー回収としては 10%ほどになり，それほど大きくはない。また，タービン出口圧力は配送時のポンプ動力節約のためにある程度高くしたいため，タービン効率も高くなりにくい。このため，色々な冷熱回収や冷熱利用が提案されている。例えば，プラスチックを破砕するときに低温にすれば小さく破砕しやすいとか，空気分離器の予冷に使うことなどである。空気分離器は空気から酸素，窒素，アルゴンを液化して分離を行うため，LNG で予備冷却を行うと，冷凍機の消費電力が節約されるからである。酸素は病院や石炭火力発電所の需要があり，アルゴンは Tig 溶接に使うなどの用途があるが，窒素用途はあまり無いようである。このため，液体窒素をアイスクリーム製造にも利用することがあると聞いている。但し，これらのガスの液化温度は LNG 温度よりも低いため，消費電力の節約は半分程度であるとされている。しかし，高温超伝導利用が広がれば，空気分離器からの液体窒素は広く利用される可能性があり，その意味で超伝導応用技術は LNG 冷熱利用の大きなポテンシャルを持っていると言える。

さて，現状のシステムでは冷熱利用には LNG を気化することが何れにしても必要なので，気化器に何らかの工夫をすれば，現状システムとの整合性がよく，ほとんど変更無く今までの冷熱回収も変更なく利用できる。そこで図 3 に示すように気化器に熱電半導体を用い，熱電発電を行うシステムを提案する。

現行の気化器はアルミパイプ内部に LNG を導き，外部から組み上げた常温の海水を流すような構造になっている。これによって，あるパイプを通じて熱交換が行われ，LNG が気化する。したがって，アルミ管内側と外側には大きな温度差が発生している。この温度差を利用して発電するように，アルミ管を 2 重にして間に熱電素子を入れる構造である。これによって，熱電半導体に大きな温度差が発生し，電力を生み出す。

設計上検討を要する事項は，熱電半導体を導入することによって熱交換器としての熱抵抗が増大することである。したがって，此に応じて気化器のサイズが大きくなる。熱抵抗を減らすには，熱電半導体を温度差方向に薄くすればよい。薄くすると単位面積当たりの出力電力

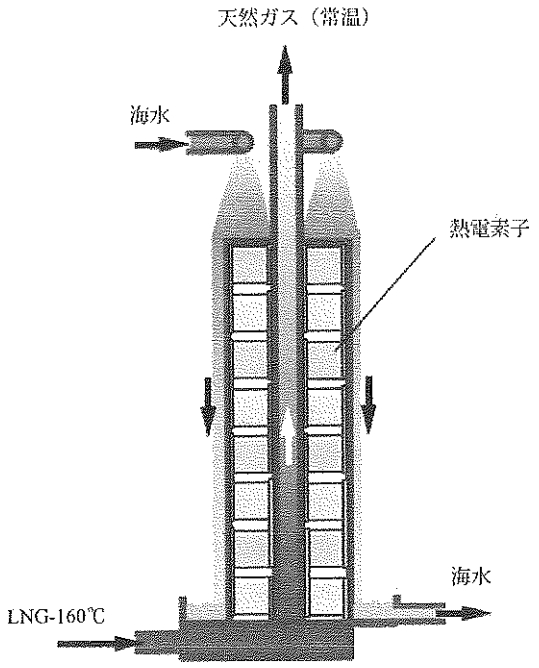

図 3　熱電 LNG 気化器構想図

は大きくなり，利用する半導体材料も減らすことができる。しかし，薄い材料に大きな温度差が発生するため，熱応力が大きくなる。このため，電極との接合や材料強度を考慮して開発を進めるべきである。市販の BiTe を利用するとすれば，気化器サイズ（熱交換を行う面積）は 50%程度大きくする必要がある。したがって，経済性は発生する電力を考慮して研究開発を進めることになろう。

3. 今後の研究課題と展望

現在，常温付近で性能指数が高い市販の熱電材料は BiTe である。しかし，現状では常温より少し温度の高い側で性能が大きくなるように材料開発が行われている。一方，LNG 冷熱回収のためには，低温側で性能指数が高くなることが望ましい。その意味で低温用 BiTe の開発が求められている。更に，より低温ではビスマス・アンチモン合金（BiSb）[12] が高い性能指数を持つとの古い報告がある。今までの報告では n-type のみであるが，p-type 材料の探求も含めて実用化研究が必要と思われる。

材料としては，他に磁場効果の一つであるネルンスト効果[13]を利用した検討もあろう。図 3 のような気化器であれば，ネルンスト効果を使いやすいシステムを構築できることや，高い移動度を持つ材料が候補材料になるが，一般に低温では移動度が高くなりやすいので変換効率が高くなるため，基礎研究の段階であるが，有望であろう。

文　　献

1）相山義道章主査，超伝導・低温工学ハンドブック，低温工学協会編，オーム社，（1993 年），第 7 章，p. 944

2）P. Kittel, *Cryocooler 14*, p. 563 (2007)

3）経済産業省資源エネルギー庁,「2005 年度以降に適用する標準発熱量の検討結果と改定値について」, 平成 19 年 5 月, http://www.enecho.meti.go.jp/info/statistics/jukyu/resource/pdf/070601.pdf

4）M. N. Wilson, Superconducting Magnets, Oxford University Press, (1983), p. 256

5）S. Yamaguchi et al, Proc. 16th Int. Cryogenic Eng./Int. Cryogenic Material Conf. (ICEC/ICMC1996), p. 1159(1996)

6）H. Okumura and S. Yamaguchi, *IEEE Trans. Applied Supercond.*, vol. 7, p. 715 (2001)

7）S. Yamaguchi et al, *Rev. Scientific Instruments*, vol. 75, p. 207 (2004)

8）S. Yamaguchi et al, J. Physics: Conference Series vol. 97, p. 012290 (2008)

9）T. Kawahara et al, *Physica C*, vol. 470, p. S1011 (2010)

10）山口作太郎，熱電変換技術ハンドブック，梶川武信，（株）エヌ・ティー・エス，（2008），p. 508

11）例えば，三井化学，大阪石油化学，大阪ガスによる堺・泉北コンビナートの例 http://www.nedo.go.jp/content/100510445.pdf

12）G. E. Smith and R. Wolfe, *J. Appl. Physics*, vol. 7, p. 841 (1960)

13）山口作太郎，熱電変換－基礎と応用－，坂田 亮編，裳華房（2005 年），p. 69